THE IMPORTANCE OF INTERNEURONS IN NEURONAL CIRCUITRY

EDITED BY: Maria Gutierrez-Mecinas, Joshua Singer and Eduardo Weruaga

PUBLISHED IN: Frontiers in Neural Circuits and Frontiers in Integrative Neuroscience

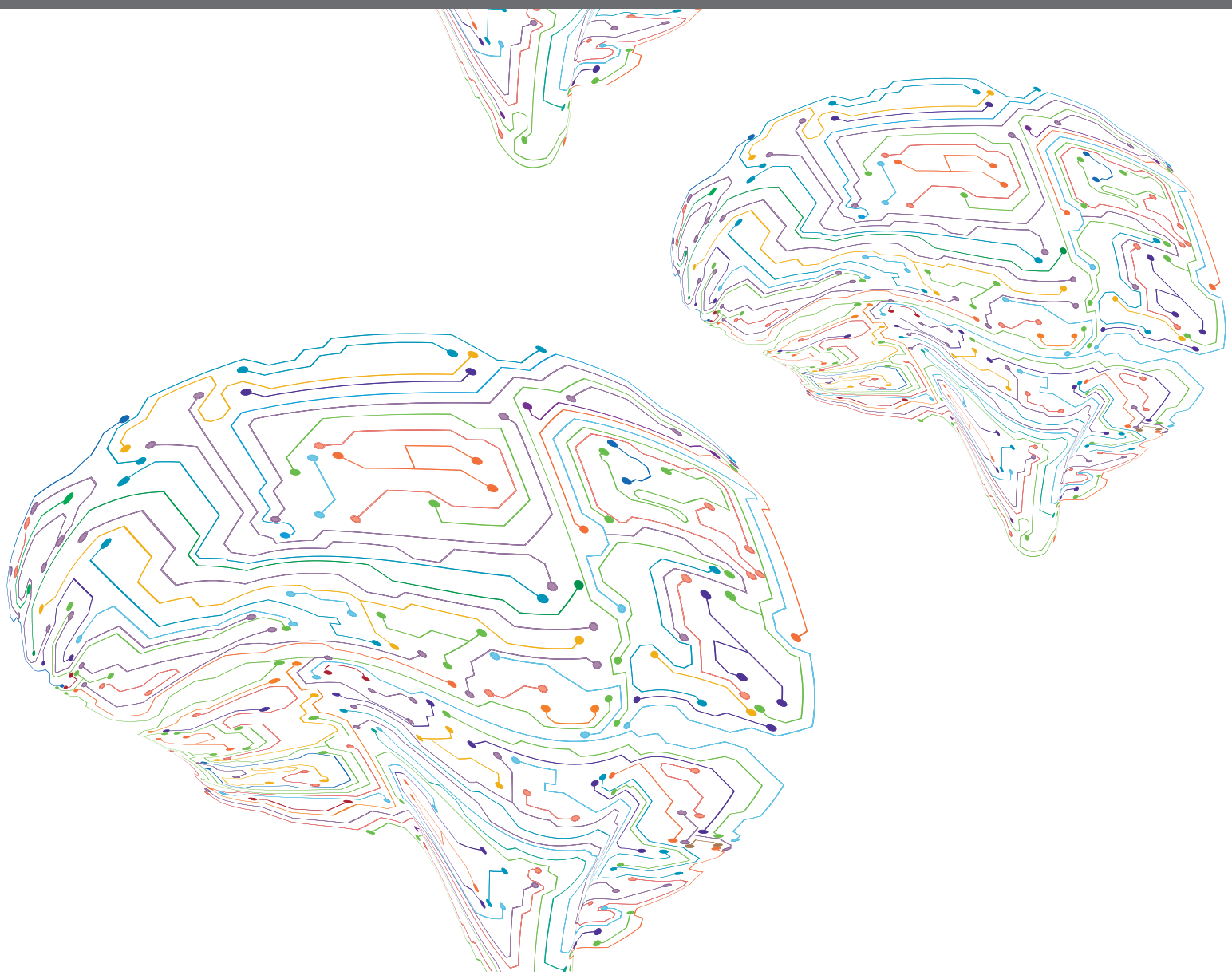

frontiers Research Topics

ISSN 1664-8714
ISBN 978-2-88974-166-3
DOI 10.3389/978-2-88974-166-3

About Frontiers

Frontiers is more than just an open-access publisher of scholarly articles: it is a pioneering approach to the world of academia, radically improving the way scholarly research is managed. The grand vision of Frontiers is a world where all people have an equal opportunity to seek, share and generate knowledge. Frontiers provides immediate and permanent online open access to all its publications, but this alone is not enough to realize our grand goals.

Frontiers Journal Series

The Frontiers Journal Series is a multi-tier and interdisciplinary set of open-access, online journals, promising a paradigm shift from the current review, selection and dissemination processes in academic publishing. All Frontiers journals are driven by researchers for researchers; therefore, they constitute a service to the scholarly community. At the same time, the Frontiers Journal Series operates on a revolutionary invention, the tiered publishing system, initially addressing specific communities of scholars, and gradually climbing up to broader public understanding, thus serving the interests of the lay society, too.

Dedication to Quality

Each Frontiers article is a landmark of the highest quality, thanks to genuinely collaborative interactions between authors and review editors, who include some of the world's best academicians. Research must be certified by peers before entering a stream of knowledge that may eventually reach the public - and shape society; therefore, Frontiers only applies the most rigorous and unbiased reviews.
Frontiers revolutionizes research publishing by freely delivering the most outstanding research, evaluated with no bias from both the academic and social point of view. By applying the most advanced information technologies, Frontiers is catapulting scholarly publishing into a new generation.

What are Frontiers Research Topics?

Frontiers Research Topics are very popular trademarks of the Frontiers Journals Series: they are collections of at least ten articles, all centered on a particular subject. With their unique mix of varied contributions from Original Research to Review Articles, Frontiers Research Topics unify the most influential researchers, the latest key findings and historical advances in a hot research area! Find out more on how to host your own Frontiers Research Topic or contribute to one as an author by contacting the Frontiers Editorial Office: frontiersin.org/about/contact

THE IMPORTANCE OF INTERNEURONS IN NEURONAL CIRCUITRY

Topic Editors:
Maria Gutierrez-Mecinas, University of Glasgow, United Kingdom
Joshua Singer, University of Maryland, College Park, United States
Eduardo Weruaga, University of Salamanca, Spain

Citation: Gutierrez-Mecinas, M., Singer, J., Weruaga, E., eds. (2022). The Importance of Interneurons in Neuronal Circuitry. Lausanne: Frontiers Media SA. doi: 10.3389/978-2-88974-166-3

Table of Contents

frontiers in Integrative Neuroscience

ORIGINAL RESEARCH
published: 24 January 2020
doi: 10.3389/fnint.2019.00075

Afterdischarges of Spinal Interneurons Following a Brief High-Frequency Stimulation of Ia Afferents in the Cat

Abraham Méndez-Fernández, Mayra Moreno-Castillo, Nayeli Huidobro, Amira Flores and Elias Manjarrez**

Instituto de Fisiología, Benemérita Universidad Autónoma de Puebla, Puebla, México

Spinal motoneurons exhibit sustained afterdischarges and plateau potentials following a brief high-frequency stimulation of Ia afferents. Also, there is evidence that spinal cord interneurons exhibit plateau potentials. However, to our knowledge, there are no reports about the possible afterdischarge behavior of lumbar spinal interneurons activated by Ia afferents. Given that there are spinal interneurons receiving monosynaptic inputs from Ia afferents, these cells could then be activated in parallel to motoneurons after repetitive muscle stretch. We explored this possibility in cats with a precollicular-postmammillary decerebration. We found that a brief high-frequency stimulation of Ia afferents produces afterdischarges that are highly correlated to a DC slow potential recorded at the cord dorsum. We conclude that in the cat spinal cord, not only the motoneurons but also the interneurons from the superficial and deep dorsal horn produce sustained afterdischarges, thus highlighting the importance of interneurons in the spinal neuronal circuitry. The significance of our finding is that it opens the possibility that the spinal cord interneurons activated by Ia afferents could also exhibit bistability, a relevant phenomenon well-characterized in the motoneurons.

Keywords: interneuros, bistability, afterdischarges, DC shift, spinal cord

OPEN ACCESS

Edited by:
Maria Gutierrez-Mecinas, University of Glasgow, United Kingdom

Reviewed by:
Tuan Vu Bui, University of Ottawa, Canada
Marin Manuel, Université Paris Descartes, France
Peter Szucs, University of Debrecen, Hungary

****Correspondence:***
Amira Flores
amira.flores@correo.buap.mx
Elias Manjarrez
eliasmanjarrez@gmail.com

Received: *30 October 2019*
Accepted: *16 December 2019*
Published: *24 January 2020*

Citation:
Méndez-Fernández A, Moreno-Castillo M, Huidobro N, Flores A and Manjarrez E (2020) Afterdischarges of Spinal Interneurons Following a Brief High-Frequency Stimulation of Ia Afferents in the Cat. Front. Integr. Neurosci. 13:75. doi: 10.3389/fnint.2019.00075

INTRODUCTION

The firing pattern of a spinal motoneuron can alternate between two stable states depending on the immediate previous history of such motoneuron; this is called bistability (Hounsgaard and Kiehn, 1985; Hounsgaard et al., 1988). Functionally, this property allows a motor unit to self-sustain its activity during the performance of long-lasting tonic motor tasks, such as postural tone maintenance (Eken and Kiehn, 1989; Gorassini et al., 1998). Also, under certain pathological circumstances, this ability gets anomalously increased in the motoneurons as it is believed to occur during spasticity after chronic spinal injury (Harvey et al., 2006a,b). A shift into a high-frequency firing state in the motoneurons can be achieved through the high-frequency stimulation of the homonymous muscle stretch receptors and specific brainstem nuclei (Granit et al., 1957; Mori et al., 1982; Crone et al., 1988; Bennett et al., 1998). The integrity of monoaminergic descendent pathways is fundamental for the activation of motoneuron bistable properties (Conway et al., 1988; Kiehn et al., 1996; Perrier and Delgado-Lezama, 2005; Perrier et al., 2013).

The capability to generate afterdischarges is shared by different neurons in the spinal cord. For instance, similarly to motoneurons, a class of spinal interneurons can exhibit sustained

discharges after a brief exposure to electrical stimulation to the sensory pudendal nerve of female cats (Cueva-Rolón et al., 2002; Muñoz-Martínez and Delgado-Lezama, 2007). Also, interneuron afterdischarges can be related to the persistence of secondary pain (Price et al., 1978) and the triggering of the scratch pattern (Currie and Stein, 1990). In the same way, the capability to generate plateau potentials is shared by many neurons in the spinal cord (Abbinanti et al., 2012; Husch et al., 2014). For example, motoneurons and interneurons exhibit the property to generate plateau potentials (Russo and Hounsgaard, 1994, 1996; Abbinanti et al., 2012; Husch et al., 2014). Furthermore, the mechanisms that underlie plateau generation in both sets of spinal neurons are substantially similar (Hounsgaard and Kjaerulff, 1992; Svirskis and Hounsgaard, 1997; Abbinanti et al., 2012; Husch et al., 2014).

The present study aimed to examine whether a brief high-frequency stimulation of Ia afferents produces afterdischarges in spinal interneurons as was previously found for the spinal motoneurons (Hounsgaard et al., 1988; Lee and Heckman, 1998). Since there are spinal interneurons receiving monosynaptic and polysynaptic contacts from Ia afferents (Kanda, 1972; Brown, 1981; Harrison and Jankowska, 1985; Bannatyne et al., 2009), it is feasible that these cells are recruited in parallel to motoneurons after repetitive muscle stretch. Our results will highlight the importance of interneurons in the spinal neuronal circuitry.

MATERIALS AND METHODS

Preparation

Experiments were performed in seven adult cats whose weights ranged between 2.3 and 4.5 kg. We performed two types of experiments: (1) recording of the spinal cord dorsum in four cats; and (2) multiunit recording of spinal interneurons in four cats. In one cat, we performed both experimental paradigms. The protocol was approved by the ethics committee (CICUAL-Proyecto-00489) of the Benemérita Universidad Autónoma de Puebla. The guidelines stipulated in the Guide for the Care and Use of Laboratory Animals (Eighth Edition, revised in 2011) and the Mexican regulations (NOM-062-ZOO-1999) were carefully followed. Before surgery, anesthesia was induced by a volatile mix of isoflurane (3%–4%) and oxygen (96%–97%). After tracheostomy, anesthesia was maintained *via* a tracheal cannula until decerebration. Atropine (0.05 mg kg^{-1}) and dexamethasone (2 mg kg^{-1}) were administered at the beginning of the procedures. The radial vein and the common carotid artery were cannulated for liquid administration and blood pressure monitoring, respectively. We maintained the blood pressure between 80 and 120 mmHg by the administration of Dextran and glucose (5%) isotonic solution. Bicarbonate (100 mM) and glucose (5%) solution were delivered at a constant flux (5 ml h^{-1}) throughout the whole experiment *via* the common carotid artery. The temperature was kept inside a physiological range through a heating pad over which the animal was laid and a radiant heat lamp. The decerebration method consisted of a precollicular-postmammillary transection. After the decerebration, anesthesia was gradually suspended. At the end of the experimental procedures, a lethal dose of pentobarbital sodium was administered intravenously.

Recording of the Spinal Cord Dorsum

In four cats, a laminectomy was performed to expose the lumbosacral spinal enlargement. We recorded the activity of the spinal cord dorsum using an array of 32 Ag-AgCl spherical electrodes (diameter of 200 μm), positioned over the surface of the lumbosacral spinal cord (**Figure 1A**). Such activity was acquired with the Synamps 2 amplifier (CompuMedics NeuroScan) at a sampling rate of 10 kHz and filters in DC mode. Simultaneously, the electroneurographic (ENG) activity was recorded from the *gastrocnemius lateralis* (GL) nerve, employing a bipolar hook silver wire electrode. GL activity was rectified and integrated. Pools were made at the hind limb exposed areas and filled with mineral oil.

Multiunit Recording of Spinal Interneurons

We also recorded the multiunit activity (MUA) of the superficial and deep dorsal horn interneurons of the L7 segment in four cats. These neurons did not respond to antidromic stimulation of the ventral roots. For this purpose, we employed quartz/platinum-tungsten fiber microelectrodes (1–2 MΩ) coupled with the Minimatrix system (Thomas Recording). Signals were acquired by a Digidata system (Molecular Devices, San Jose, CA, USA) at a sampling rate of 250 kHz. We used the "WaveClus" spike-sorting algorithm (Quiroga et al., 2004) to obtain unitary spikes from the raw signals.

Mechanical Stimulation of Stretch Receptors

The Achilles tendon of the left hind limb was dissected and coupled to a mechanical stimulator (Chubbuck, 1966). In this form, the mechanical stimulator administered vibrating stimuli to the *triceps surae* muscle. The stimulus consisted of high-frequency (200 Hz) and low-amplitude (200 μm) brief vibration (0.85–1.2 s). The stimulus characteristics ensured activation of the total amount of *triceps surae* Ia afferents (Lucas and Willis, 1974).

Statistical Analysis

The instantaneous firing rate of the sorted units was measured and grouped into three intervals: "before," "during," and "after" the stimulus presentation. Time zero was defined as the instance of the beginning of stimulus presentation. The rates were compared by applying the nonparametric Friedman test and a *post hoc* Wilcoxon signed-rank test (R version 3.3.0, The R Project for Statistical Computing). The Pearson correlation coefficient between the DC signal and the relative counts of interneuronal spike times was computed. In all cases, the threshold for a type I error was set at 0.05.

RESULTS

Spinal cord dorsum activity was recorded in response to a brief high-frequency repetitive stretch of the Achilles tendon. After the stimulus presentation, the baseline cord dorsum potential

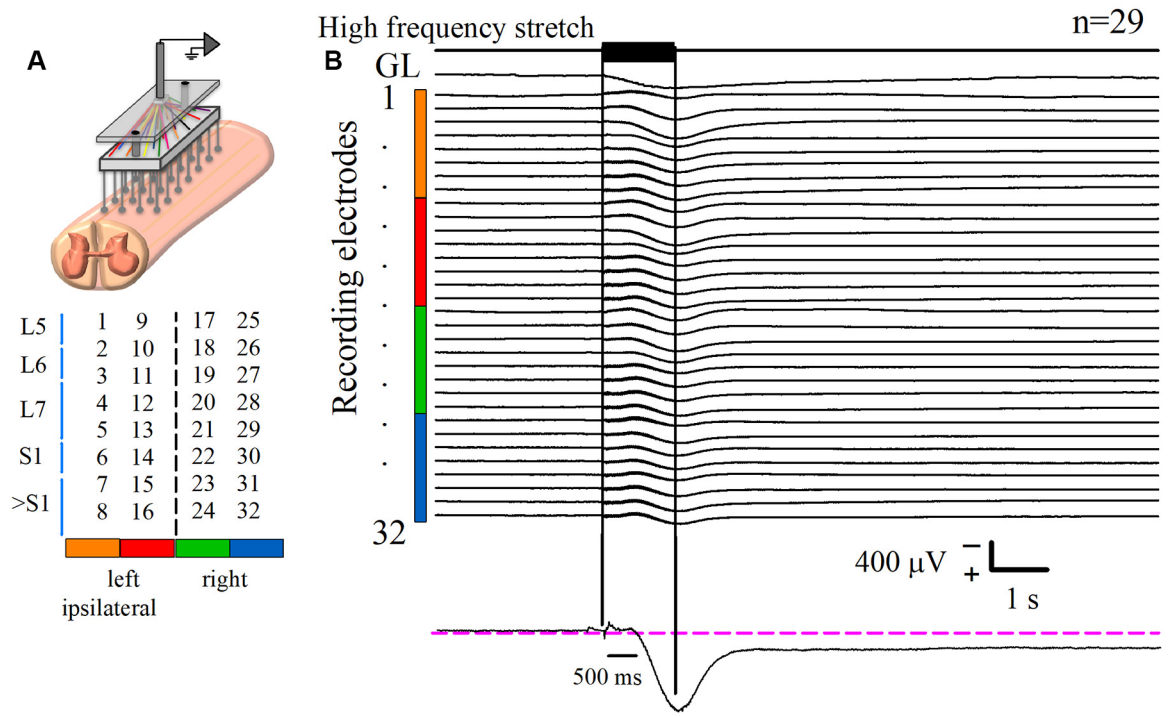

FIGURE 1 | Recording of the DC potential on the spinal cord dorsum in response to a high-frequency stretch stimulus applied to the Achilles tendon. **(A)** Scheme of the recording paradigm, which consisted of an array of 32 (8 × 4) Ag-AgCl spherical electrodes positioned over the surface of the lumbosacral spinal cord. The array was coupled to a Synamps amplifier system in DC mode. The midline is represented by the dashed line that divides the two halves of the array. Spinal segments are specified at the left, according to Marcoux and Rossignol (2000). **(B)** The first upper trace is the high-frequency stretch stimulus applied on the left Achilles tendon. The two vertical black lines indicate the duration of such stimulus. The trace labeled with *gastrocnemius lateralis* (GL) is the rectified and integrated electroneurographic (ENG) signal recorded from the *GL* nerve. See how the GL activity experiences a sustained rise following the stimulus. The next 32 traces are the averaged DC potentials recorded from the spinal cord dorsum after several trials (n = 29) of stimulation. Such signals were obtained from the electrode array represented in **(A)**; see color code. Note the marked positive DC shift that outlasts the mechanical stimulus duration for 6.4 ± 0.3 s (mean ± standard error). Observe that the sustained slow DC potential in the cord dorsum occurs concomitantly with the GL ENG activity. The recording in the lower panel is a zoom of a slow DC potential.

recorded over the bilateral lumbosacral spinal cord exhibited a positive and slow DC shift. This slow DC potential was observed with a peak latency of 0.96 ± 0.004 s after the beginning of the stimulation. **Figure 1B** shows the averaged traces of 29 trials obtained from one cat. To characterize the slow DC potential, a double exponential model was fitted to these signals. A decay of 0.95 of the maximum amplitude was the criterion to determine the end of the DC potential. We found that the slow DC potential outlasted the duration of the stimulus by 6.4 ± 0.3 s (four cats, 108 trials); that is, we observed an "afterdischarge" in the cord dorsum activity due to the Ia afferent activation. More interestingly, this phenomenon occurred during the ENG sustained activity of the GL nerve (**Figure 1B**). This co-activation of spinal cord dorsum and motor output (GL) activity was seen in four animals.

We also found that the DC potential amplitude depended markedly on the recording site. The spatial distribution of the mean amplitude of the slow DC potential is presented in **Figure 2**. Each map of **Figure 2A** was obtained from one animal (four cats), whereas the map of **Figure 2B** is the grand average of the normalized maps shown in **Figure 2A** (four cats, 108 trials). In these maps, the dashed line represents the midline. We can observe that the amplitude of the DC potential was higher at the L6–L7 spinal segments ipsilateral to the stimulus presentation. This result was expected in accordance with the reported Ia afferent branching pattern, as discussed later.

The MUA was recorded at the L7 spinal segment from the sites drawn as white and black circles in **Figure 3A**. The distribution of the depth of recording sites is roughly bimodal, with the first mode around 2,000 μm and the second one about 2,800 μm (**Figure 3B**). In such locations, we found 37 interneurons that responded with unitary firing activity to muscle stretch. We recorded 20 superficial neurons (see white circles in **Figure 3A**) whose firing activity exhibited a low firing rate (**Figure 3C**) and 17 deep interneurons (see black with circles in **Figure 3A**) whose firing activity exhibited a high firing rate (**Figure 3C**). The pooled activity of both classes of interneurons is displayed in **Figures 4A,B**, in which each dot represents a single spike and the rows stand for different interneurons. The two black vertical lines indicate the stimulus duration. Sustained afterdischarges were observed after

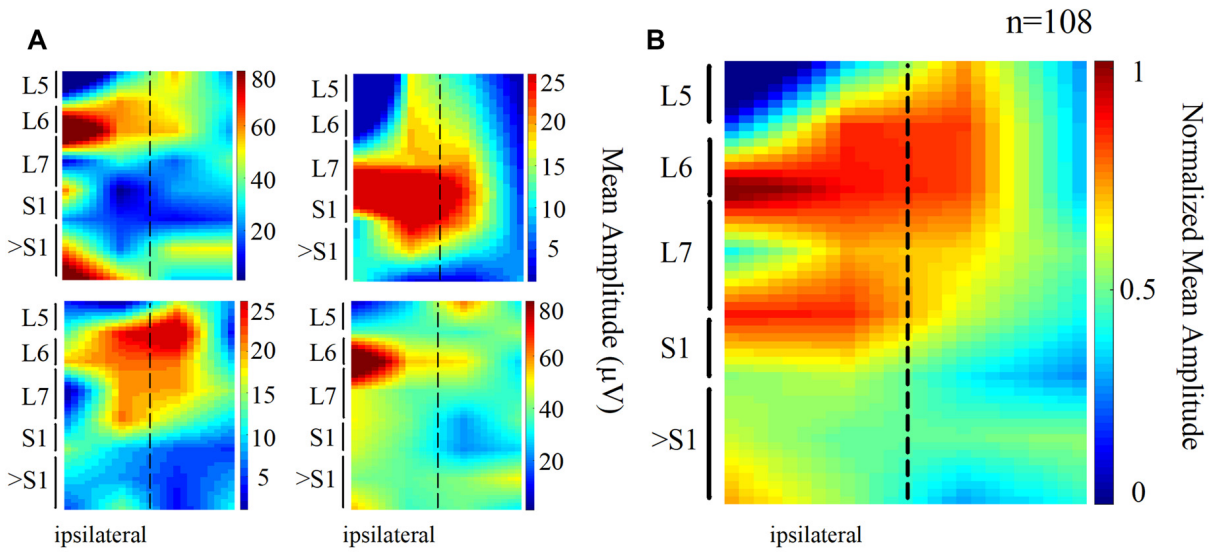

FIGURE 2 | Topographic maps obtained from the spatial distribution of the DC potentials recorded from the cord dorsum. **(A)** Each map was obtained from one animal. Again, the dashed line represents the midline. Larger amplitudes tend to focus at the ipsilateral (left) L6 and L7 segments. **(B)** Grand average of the four normalized maps in **(A)** n = 108 trials, four cats.

the cessation of the stimulus for up to 7 s; see the rasters of firing activity following the stimulation compared to the basal activity. Also, see the yellow bars in the histograms of **Figure 4** in comparison to the blue bars; note that the height of the yellow bars remains well above the basal activity (dashed horizontal line). To quantify these changes, the instantaneous firing rate was measured and compared between the following intervals: "before" (−7 to 0 s), "during" (0–0.93 s), and "after" (0.93–7.93 s). For all of the neurons (37), the mean firing rate was calculated considering the values of all interneurons throughout the corresponding time window. The instantaneous firing rates were time-averaged to obtain mean values of 22.2 ± 0.6 Hz, 27.2 ± 1.2 Hz, and 26.15 ± 0.74 Hz, respectively. We found statistical differences among these intervals (Friedman test, $p = 0.012$). Additionally, a *post hoc* comparison yielded statistical differences when applied to "before" vs. "during" ($p = 0.002$) and to "before" vs. "after" ($p = 0.014$) intervals. Finally, we found a strong correlation between the grand average of the DC potential recorded on the cord dorsum and the relative counts of the interneuronal spikes (Pearson correlation coefficient $r = 0.78$, $p = 2.9 \times 10^{-12}$).

We compared the firing rate for both the superficial and the deep dorsal horn neurons. **Figure 5A** shows a graph of the depth vs. the firing rate (frequency) of such neurons before and after the vibratory stimuli. Note that the superficial neurons exhibit a slower firing rate and less frequency dispersion than the deep neurons. **Figure 5B** illustrates significant differences in the mean firing rate between the superficial and deep dorsal horn neurons for both conditions before and after the vibratory stimuli. **Figure 5C** shows that both groups of neurons exhibit a similar dispersion in the after/before ratio of their firing rate, irrespective of their depth.

Figure 6 shows the firing activity of other neurons, not exhibiting afterdischarges. We found 18 neurons that did not respond to the Ia stimulation. Moreover, we found three neurons responding to the Ia stimulation but not exhibiting sustained firing and two other neurons that were inhibited during the Ia stimulation.

DISCUSSION

We found interneurons in the superficial and deep dorsal horn exhibiting afterdischarges following a brief high-frequency stimulation of Ia afferents. The superficial dorsal horn neurons exhibited a significantly lower firing rate compared with the deep dorsal horn neurons. The sustained interneuronal activity of both classes of neurons was correlated to the DC potential recorded on the lumbosacral spinal cord. However, although similar stimulation schemas have been used before, in mammals (Crone et al., 1988; Hounsgaard et al., 1988; Lee and Heckman, 1998) as well as in reptiles (Hounsgaard and Kjaerulff, 1992; Russo and Hounsgaard, 1996), attention was mainly focused on the motoneuron response.

Slow DC Potential

The amplitude of the slow DC potential distributed spatially was consistent with anatomical data about the Ia afferent branching pattern. The Ia afferents of the soleus and *gastrocnemius medialis* muscles are mainly distributed through the ipsilateral spinal segment L7 but also give numerous branches to the L6 and S1 segments (Brown and Fyffe, 1978; Ishizuka et al., 1979).

Other slow waves, as the DC potential (also termed DC shift), can be recorded in other contexts. For instance, after the pudendal nerve stimulation in the female cat, it is

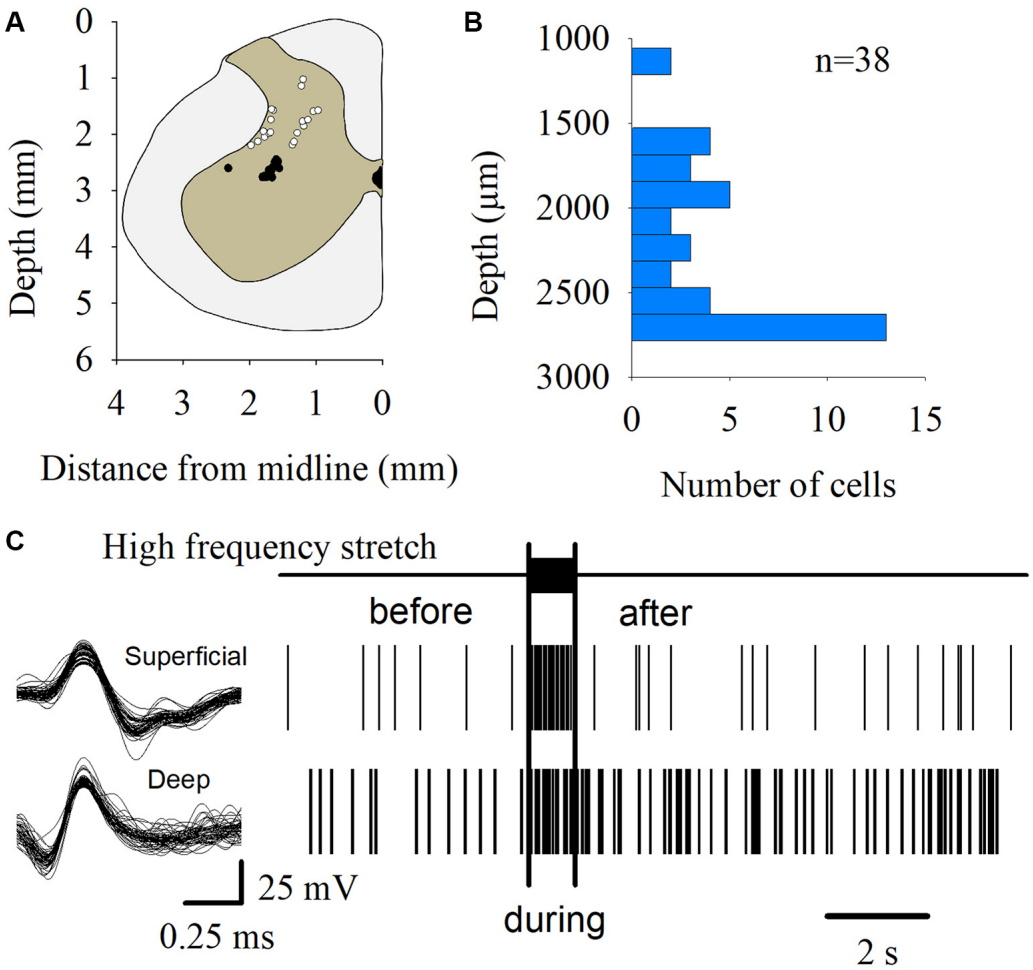

FIGURE 3 | Multiunit recording of lumbar interneurons from the superficial and deep dorsal horn. **(A)** The white and black circles represent the sites from which the multiunit recordings of the spinal neurons were performed. The white circles represent the superficial dorsal horn neurons. The black circles represent the deep dorsal horn neurons. **(B)** Distribution of the depth of the recorded interneurons (n = 37) shown in **(A)**. **(C)** Scheme representing the spike-sorting for both the superficial and deep dorsal horn neurons, as indicated. Note that the superficial dorsal horn neurons exhibited a slower firing rate than the deep dorsal horn neurons. The signals from single interneurons were obtained from the raw multiunit activity (MUA). The waveforms illustrated in the left panel are superimposed traces of two interneurons from two different animals. The right panel shows the raster plots of such neurons in response to the high-frequency stretch of the Achilles tendon (uppermost trace and vertical bars).

possible to record a "delayed depolarization" in the hind limb motoneurons that outlasted the stimulus by up to 6 s. This is consistent with our observation of a DC shift in the cord dorsum potential that also outlasted the stimulus up to 6 s (Muñoz-Martínez and Delgado-Lezama, 2007). In other studies, it was found that previous to the alternating flexor-extensor activity during scratching, a positive DC shift occurs in the hind limb enlargement of decerebrate cats (Bayev and Kostyuk, 1981). Such DC shift is correlated to the tonic activity of interneurons from the deep dorsal horn and to the postural stage that precedes scratching (Cuellar et al., 2018). As stated in our "Results" section, we recorded a similar positive DC shift correlated to interneuron activity from the deep dorsal horn. It is possible that under certain circumstances (e.g., throughout the scratch postural stage or due to high-frequency muscle spindle stimulation), interneurons could exhibit shifts in their membrane potential in a bistable-like manner. In accordance with this idea, intermediate zone neurons located in the hind limb enlargement of an *in vivo* turtle preparation go into alternating shifts in their membrane potential in a phase-dependent manner during the scratch cycle (Berkowitz et al., 2006).

Recently, it was demonstrated that in mammals, intraspinal DC stimulation leads to the facilitation of several phenomena that outlasts the period of stimulation, including the monosynaptic reflex and the rise in excitability of cutaneous afferents (Bolzoni and Jankowska, 2015; see also Jankowska, 2017). Interestingly, in our *in vivo* preparation, both the GL-ENG activity and slow DC potential also exhibited facilitation after the brief high-frequency stimulation of Ia afferents. Therefore,

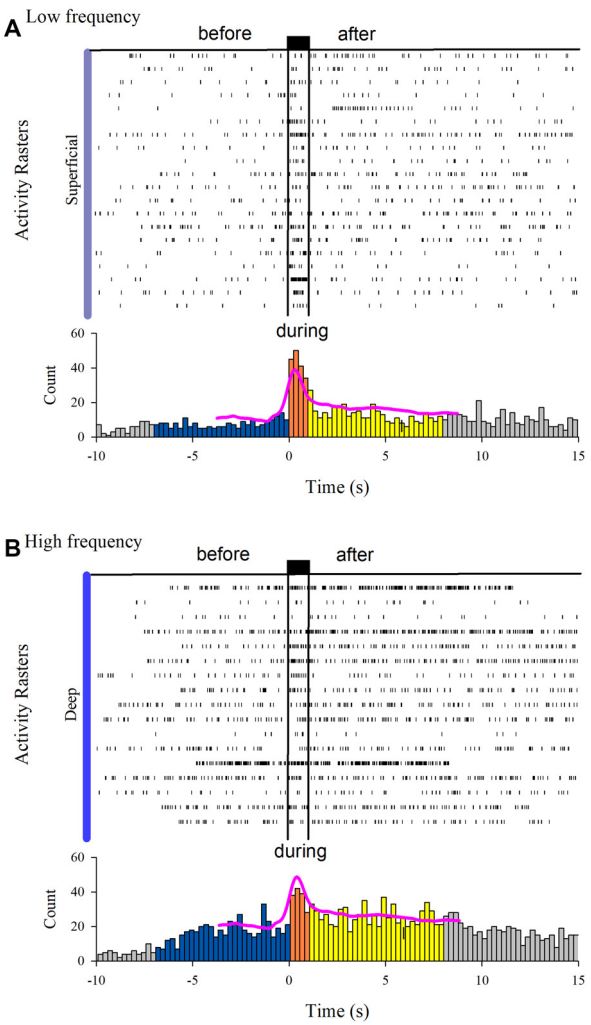

FIGURE 4 | Interneuron afterdischarges of superficial and deep dorsal horn neurons. **(A)** Rasters of spiking activity from 20 superficial dorsal horn interneurons. Note the increase in the activity during and after the stimulation compared to the basal activity before stretch. The uppermost trace depicts the high-frequency stretch stimulus applied to the Achilles tendon. The duration of the stimulus is indicated by the two vertical bars. **(B)** The same as **(A)** but for 17 deep dorsal horn interneurons. The relative count histograms from the activity rasters are illustrated with the superimposed recording of the DC cord dorsum potential.

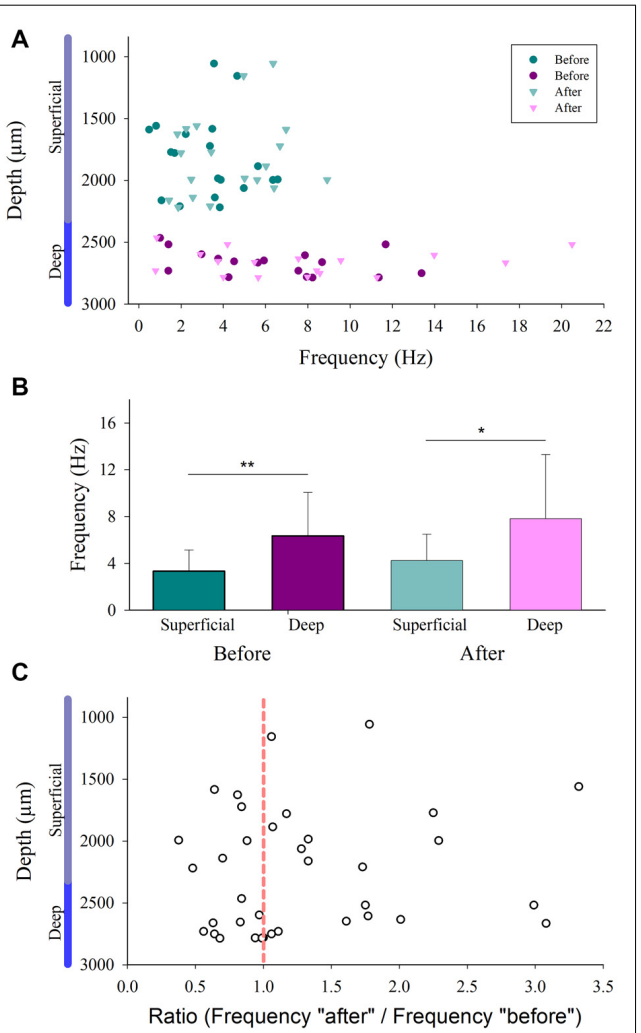

FIGURE 5 | Firing rate distribution for the superficial and the deep dorsal horn neurons. **(A)** The depth vs. the firing rate (frequency in Hz) of superficial and the deep dorsal horn neurons before and after the vibratory stimuli. **(B)** Mean firing rate of the superficial and deep dorsal horn neurons for both conditions before and after the vibratory stimuli. **(C)** The after/before ratio of firing rate for the superficial and the deep dorsal horn neurons vs. the depth in which they were recorded.

we cannot exclude that the observed responses are due in part to the rise in excitability of muscle afferents or to the associated K+ release, among other factors, as potentially suggested by the DC potentials. In this context, it is essential to mention some limitations of our study.

Limitations

The phenomenon described here is a first necessary step to highlight the importance of the afterdischarges in interneurons in spinal circuits. However, several elements will need to be addressed. First, we do not know the identity of these spinal interneurons other than that they receive Ia afferent inputs and that they are distributed in the superficial and deep dorsal horn. However, they may belong to a class of neurons exhibiting plateau potentials, which could be modulated by neuromodulators, as seen in motoneurons. This could be possible because there is a wide plethora of evidence suggesting that a plateau potential is a typical process inherent to afterdischarges in spinal motoneurons and interneurons (Russo and Hounsgaard, 1996; Svirskis and Hounsgaard, 1997; Abbinanti et al., 2012; Reali and Russo, 2013; Husch et al., 2014) and in other cell types of the nervous system (Llinás and Sugimori, 1980; Flatman et al., 1983). Also, there is evidence of the postnatal emergence of serotonin-induced plateau potentials in commissural interneurons of the mouse

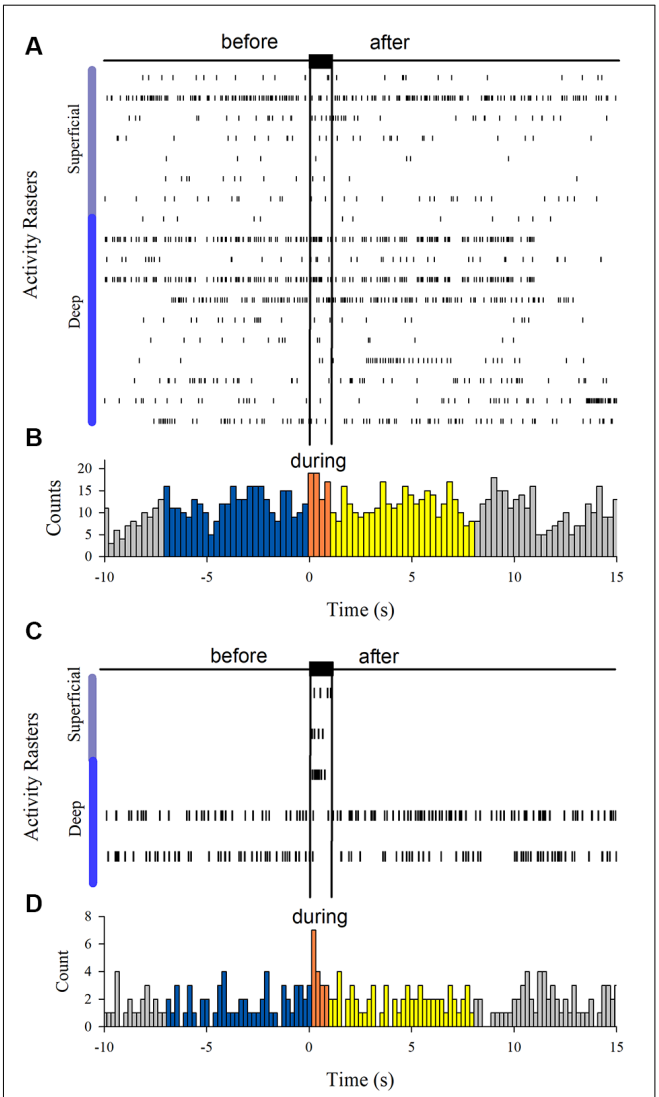

FIGURE 6 | (A) Spiking activity of neurons not responding during the vibratory stimuli (n = 18). **(C)** Spiking activity of other neurons that only were excited (n = 3) or inhibited (n = 2) by the vibratory stimuli. **(B,D)** Histograms obtained from the raster displays in **(A,C)**.

spinal cord (Abbinanti et al., 2012) and in adult spinal V2a interneurons (Husch et al., 2014). However, more experimental evidence is needed for unveiling the electrophysiological and pharmacological nature of the dorsal horn neurons exhibiting afterdischarges. Second, we do not know the underlying mechanisms in the relationship between the DC potential in the cord dorsum vs. the possible plateau potentials in interneurons. We can only speculate in this respect based on results from other animal preparations. For instance, turtle ventral horn interneurons seem not to depend on neuromodulator actions since neither serotonin receptor agonists nor other modulators need to be added to *in vitro* cord preparations to promote plateau potentials in these cells (Hounsgaard and Kjaerulff, 1992). Similarly, dorsal horn interneurons do not rely on neuromodulators for afterdischarge generation (Russo and Hounsgaard, 1996) as opposed to motoneurons in comparable settings (Perrier and Hounsgaard, 2003). Plateaus in both interneurons and motoneurons are highly sensitive to dihydropiridines, a phenomenon that suggests common mechanisms (Russo and Hounsgaard, 1996; Morisset and Nagy, 1999; Perrier and Hounsgaard, 2003).

Unitary Interneuronal Activity

We found that both the slow DC potential and the afterdischarge spiking activity of the spinal interneurons from the superficial and deep dorsal horn outlasted the duration of the brief high-frequency stimulation of Ia afferents around 6 s. We can compare this long-lasting activity with the activity of other cell types activated by sensory stimulation. For instance, spinal interneurons and motoneurons can exhibit similar sustained discharges after a brief exposure to electrical stimulation to the sensory pudendal nerve of female cats that outlasted the stimulus by up to 6 s (Muñoz-Martínez and Delgado-Lezama, 2007). Also, there is evidence that several types of interneurons can sustain long-lasting activity in the dorsal and ventral horns (Currie and Stein, 1990; Russo and Hounsgaard, 1994, 1996). Compared to other cell types, spinal neurons exhibit afterdischarges during especially prolonged periods: even in the tens of seconds scale. In the rodent cerebellar cortex, Purkinje cells undergo down-to-up transitions in their simple spike firing rate either spontaneously (Llinás and Sugimori, 1980) or in response to climbing fiber input. In this last case, after such an abrupt increase, the firing rate decays smoothly during a narrow 1 s time window (Loewenstein et al., 2005). In the cat, a neuronal population from the reticular nucleus of the thalamus exhibits plateau potentials during the occurrence of sleep spindles, about 1–2 s (Fuentealba et al., 2005). Cat hind limb motoneurons are said to be "fully bistable" whenever self-sustained firing lasts at least 3 s (Lee and Heckman, 1998), although there are reports of afterdischarges lasting as long as 1 min (Crone et al., 1988).

Functionally, particular interest has been paid to the so-called wide dynamic range (WDR) neurons. In the cat, WDR cells respond to low- as well as to high-threshold afferent stimulation (Salter and Henry, 1990). It is believed that WDR afterdischarges produce both secondary pain and non-nociceptive aftersensations (Price et al., 1978; Morisset and Nagy, 1998, 1999). The Ia information also reaches WDR neurons; however, its influence over these cells is mainly inhibitory (Pomeranz et al., 1968; Le Bars, 2002). Thus, we could exclude the involvement of this kind of cell in the phenomenon exposed here.

Other possible candidates that are able to sustain long-lasting activity are the diverse types of interneurons that reside in the intermediate zone, which respond to muscle stretch (Harrison and Jankowska, 1985), and laminae V–VII interneurons that establish direct excitatory and inhibitory contacts with ipsilateral motoneurons (Bannatyne et al., 2009; Jankowska, 2015). We can speculate that the afterdischarges of excitatory interneurons would reinforce the effect of motoneuron intrinsic properties to keep active the already

recruited units. It must be mentioned that a reverberating loop of interneuronal activity was proposed early besides the motoneuron intrinsic properties to explain sustained motor activity (Hultborn et al., 1975). Contrarily, afterdischarges of inhibitory interneurons would tend to finish plateau in motoneurons. Additionally, inhibitory input would contribute to reverse the "normal" order of the recruitment of motor units (Heckman and Binder, 1993).

Also, in *in vitro* turtle preparations, interneurons have been found within laminae VII and VIII with plateau potentials, which emit contralateral projections (Hounsgaard and Kjaerulff, 1992). In this last case, a role during alternating motor activities was suggested. Further characterization is needed to understand whether the cat interneurons exhibiting afterdischarges also emit contralateral projections.

In conclusion, interneurons of the superficial and deep dorsal horn in the cat remain active in a parallel manner to motoneurons after ipsilateral hind limb Ia stimulation. These neurons could be characterized by the stimulation of different segmental and descending afferents, as well as by the intrinsic properties measured from intracellular recordings; however, such types of experiments are challenging in our *in vivo* preparation in cats and are out of the scope of the present manuscript. We can only show the phenomenon of afterdischarges in dorsal horn neurons that are highly correlated to a DC slow potential at the cord dorsum. Morphological and physiological characterization of these cells would be of paramount importance for a deeper understanding of the functional role of the present phenomenon.

DATA AVAILABILITY STATEMENT

The raw data supporting the conclusions of this article will be made available by the authors, without undue reservation, to any qualified researcher.

ETHICS STATEMENT

The animal study was reviewed and approved by Ethics committee (CICUAL) from the Benemérita Universidad Autónoma de Puebla.

AUTHOR CONTRIBUTIONS

EM and AF conceived and designed the experiments. EM and AM-F wrote the article. AM-F, MM-C and EM performed the experiments. AM-F, MM-C, NH, AF and EM performed the analysis. All of the authors revised and approved the manuscript.

FUNDING

This work was supported by Consejo Nacional de Ciencia y Tecnología (CONACYT) grant under projects F1–153583, 229866, and PIFI-PROMEP-VIEP-Cátedra-Marcos Moshinsky (Fundación Marcos Moshinsky; EM).

ACKNOWLEDGMENTS

We thank John Reid for proofreading the English manuscript.

REFERENCES

Abbinanti, M. D., Zhong, G., and Harris-Warrick, R. M. (2012). Postnatal emergence of serotonin-induced plateau potentials in commissural interneurons of the mouse spinal cord. *J. Neurophysiol.* 108, 2191–2202. doi: 10.1152/jn.00336.2012

Bannatyne, B. A., Liu, T. T., Hammar, I., Stecina, K., Jankowska, E., and Maxwell, D. J. (2009). Excitatory and inhibitory intermediate zone interneurons in pathways from feline group I and II afferents: differences in axonal projections and input. *J. Physiol.* 587, 379–399. doi: 10.1113/jphysiol.2008.159129

Bayev, K. V., and Kostyuk, P. G. (1981). Primary afferent depolarization evoked by the activity of spinal scratching generator. *Neuroscience* 6, 205–215. doi: 10.1016/0306-4522(81)90056-7

Bennett, D. J., Hultborn, H., Fedirchuk, B., and Gorassini, M. (1998). Synaptic activation of plateaus in hindlimb motoneurons of decerebrate cats. *J. Neurophysiol.* 80, 2023–2037. doi: 10.1152/jn.1998.80.4.2023

Berkowitz, A., Yosten, G. L., and Ballard, R. M. (2006). Somato-dendritic morphology predicts physiology for neurons that contribute to several kinds of limb movements. *J. Neurophysiol.* 95, 2821–2831. doi: 10.1152/jn.01246.2005

Bolzoni, F., and Jankowska, E. (2015). Presynaptic and postsynaptic effects of local cathodal DC polarization within the spinal cord in anaesthetized animal preparations. *J. Physiol.* 593, 947–966. doi: 10.1113/jphysiol.2014.285940

Brown, A. G. (1981). "Afferent fibres from primary endings in muscle spindles," in *Organization in the Spinal Cord*, (New York, NY: Springer), 154–171.

Brown, A. G., and Fyffe, R. E. (1978). The morphology of group Ia afferent fibre collaterals in the spinal cord of the cat. *J. Physiol.* 274, 111–127. doi: 10.1113/jphysiol.1978.sp012137

Chubbuck, J. G. (1966). Small motion biological stimulator. *Johns Hopkins APL Tech. Digest.* 5, 18–23.

Conway, B. A., Hultborn, H., Kiehn, O., and Mintz, I. (1988). Plateau potentials in alpha-motoneurones induced by intravenous injection of L-dopa and clonidine in the spinal cat. *J. Physiol.* 405, 369–384. doi: 10.1113/jphysiol.1988.sp017337

Crone, C., Hultborn, H., Kiehn, O., Mazieres, L., and Wigström, H. (1988). Maintained changes in motoneuronal excitability by short-lasting synaptic inputs in the decerebrate cat. *J. Physiol.* 405, 321–343. doi: 10.1113/jphysiol.1988.sp017335

Cuellar, C. A., De La Torre Valdovinos, B., Huidobro, N., Delgado-Lezama, R., Ornelas-Kobayashi, R., and Manjarrez, E. (2018). The spinal neurons exhibit an ON-OFF and OFF-ON firing activity around the onset of fictive scratching episodes in the cat. *Front. Cell. Neurosci.* 12:68. doi: 10.3389/fncel.2018.00068

Cueva-Rolón, R., Delgado-Lezama, R., Raya, J. G., Raya, M., Tecuanhuey, R., and Muñoz-Martínez, E. J. (2002). Sustained firing of alpha and gamma hind limb motoneurons induced by stimulation of the pudendal nerve. *J. Neurophysiol.* 88, 3232–3242. doi: 10.1152/jn.00157.2002

Currie, S. N., and Stein, P. S. (1990). Cutaneous stimulation evokes long-lasting excitation of spinal interneurons in the turtle. *J. Neurophysiol.* 64, 1134–1148. doi: 10.1152/jn.1990.64.4.1134

Eken, T., and Kiehn, O. (1989). Bistable firing properties of soleus motor units in unrestrained rats. *Acta Physiol. Scand.* 136, 383–394. doi: 10.1111/j.1748-1716.1989.tb08679.x

Flatman, J. A., Schwindt, P. C., Crill, W. E., and Stafstrom, C. E. (1983). Multiple actions of N-methyl-D-aspartate on cat neocortical neurons *in vitro*. *Brain Res.* 266, 169–173. doi: 10.1016/0006-8993(83)91323-9

Fuentealba, P., Timofeev, I., Bazhenov, M., Sejnowski, T. J., and Steriade, M. (2005). Membrane bistability in thalamic reticular neurons during spindle oscillations. *J. Neurophysiol.* 93, 294–304. doi: 10.1152/jn.00552.2004

Gorassini, M. A., Bennett, D. J., and Yang, J. F. (1998). Self-sustained firing of human motor units. *Neurosci. Lett.* 247, 13–16. doi: 10.1016/s0304-3940(98)00277-8

Granit, R., Phillips, C. G., Skoglund, S., and Steg, G. (1957). Differentiation of tonic from phasic alpha ventral horn cells by stretch, pinna and crossed extensor reflexes. *J. Neurophysiol.* 20, 470–481. doi: 10.1152/jn.1957.20.5.470

Harrison, P. J., and Jankowska, E. (1985). Sources of input to interneurones mediating group I non-reciprocal inhibition of motoneurones in the cat. *J. Physiol.* 361, 379–401. doi: 10.1113/jphysiol.1985.sp015651

Harvey, P. J., Li, X., Li, Y., and Bennett, D. J. (2006a). 5-HT2 receptor activation facilitates a persistent sodium current and repetitive firing in spinal motoneurons of rats with and without chronic spinal cord injury. *J. Neurophysiol.* 96, 1158–1170. doi: 10.1152/jn.01088.2005

Harvey, P. J., Li, Y., Li, X., and Bennett, D. J. (2006b). Persistent sodium currents and repetitive firing in motoneurons of the sacrocaudal spinal cord of adult rats. *J. Neurophysiol.* 96, 1141–1157. doi: 10.1152/jn.00335.2005

Heckman, C. J., and Binder, M. D. (1993). Computer simulations of the effects of different synaptic input systems on motor unit recruitment. *J. Neurophysiol.* 70, 1827–1840. doi: 10.1152/jn.1993.70.5.1827

Hounsgaard, J., Hultborn, H., Jespersen, B., and Kiehn, O. (1988). Bistability of alpha-motoneurones in the decerebrate cat and in the acute spinal cat after intravenous 5-hydroxytryptophan. *J. Physiol.* 405, 345–367. doi: 10.1113/jphysiol.1988.sp017336

Hounsgaard, J., and Kiehn, O. (1985). Ca^{++} dependent bistability induced by serotonin in spinal motoneurons. *Exp. Brain Res.* 57, 422–425. doi: 10.1007/bf00236551

Hounsgaard, J., and Kjaerulff, O. (1992). Ca^{2+}-mediated plateau potentials in a subpopulation of interneurons in the ventral horn of the turtle spinal cord. *Eur. J. Neurosci.* 4, 183–188. doi: 10.1111/j.1460-9568.1992.tb00865.x

Hultborn, H., Wigström, H., and Wängberg, B. (1975). Prolonged activation of soleus motoneurones following a conditioning train in soleus Ia afferents—a case for a reverberating loop? *Neurosci. Lett.* 1, 147–152. doi: 10.1016/0304-3940(75)90030-0

Husch, A., Dietz, S. B., Hong, D. N., and Harris-Warrick, R. M. (2014). Adult spinal V2a interneurons show increased excitability and serotonin-dependent bistability. *J. Neurophysiol.* 113, 1124–1134. doi: 10.1152/jn.00741.2014

Ishizuka, N., Mannen, H., Hongo, T., and Sasaki, S. (1979). Trajectory of group Ia afferent fibers stained with horseradish peroxidase in the lumbosacral spinal cord of the cat: three dimensional reconstructions from serial sections. *J. Comp. Neurol.* 186, 189–211. doi: 10.1002/cne.901860206

Jankowska, E. (2015). On the distribution of information from muscle spindles in the spinal cord; how much does it depend on random factors? *J. Anat.* 227, 184–193. doi: 10.1111/joa.12331

Jankowska, E. (2017). Spinal control of motor outputs by intrinsic and externally induced electric field potentials. *J. Neurophysiol.* 118, 1221–1234. doi: 10.1152/jn.00169.2017

Kanda, K. (1972). Contribution of polysynaptic pathways to the tonic vibration reflex. *Jpn. J. Physiol.* 22, 367–377. doi: 10.2170/jjphysiol.22.367

Kiehn, O., Erdal, J., Eken, T., and Bruhn, T. (1996). Selective depletion of spinal monoamines changes the rat soleus EMG from a tonic to a more phasic pattern. *J. Physiol.* 492, 173–184. doi: 10.1113/jphysiol.1996.sp021299

Le Bars, D. (2002). The whole body receptive field of dorsal horn multireceptive neurones. *Brain Res. Rev.* 40, 29–44. doi: 10.1016/s0165-0173(02)00186-8

Lee, R. H., and Heckman, C. J. (1998). Bistability in spinal motoneurons *in vivo*: systematic variations in rhythmic firing patterns. *J. Neurophysiol.* 80, 572–582. doi: 10.1152/jn.1998.80.2.572

Llinás, R., and Sugimori, M. (1980). Electrophysiological properties of *in vitro* Purkinje cell dendrites in mammalian cerebellar slices. *J. Physiol.* 305, 197–213. doi: 10.1113/jphysiol.1980.sp013358

Loewenstein, Y., Mahon, S., Chadderton, P., Kitamura, K., Sompolinsky, H., Yarom, Y., et al. (2005). Bistability of cerebellar Purkinje cells modulated by sensory stimulation. *Nat. Neurosci.* 8, 202–211. doi: 10.1038/nn1393

Lucas, M. E., and Willis, W. D. (1974). Identification of muscle afferents which activate interneurons in the intermediate nucleus. *J. Neurophysiol.* 37, 282–293. doi: 10.1152/jn.1974.37.2.282

Marcoux, J., and Rossignol, S. (2000). Initiating or blocking locomotion in spinal cats by applying noradrenergic drugs to restricted lumbar spinal segments. *J. Neurosci.* 20, 8577–8585. doi: 10.1523/jneurosci.20-22-08577.2000

Mori, S., Kawahara, K., Sakamoto, T., Aoki, M., and Tomiyama, T. (1982). Setting and resetting of level of postural muscle tone in decerebrate cat by stimulation of brain stem. *J. Neurophysiol.* 48, 737–748. doi: 10.1152/jn.1982.48.3.737

Morisset, V., and Nagy, F. (1998). Nociceptive integration in the rat spinal cord: role of non-linear membrane properties of deep dorsal horn neurons. *Eur. J. Neurosci.* 10, 3642–3652. doi: 10.1046/j.1460-9568.1998.00370.x

Morisset, V., and Nagy, F. (1999). Ionic basis for plateau potentials in deep dorsal horn neurons of the rat spinal cord. *J. Neurosci.* 19, 7309–7316. doi: 10.1523/jneurosci.19-17-07309.1999

Muñoz-Martínez, E. J., and Delgado-Lezama, R. (2007). Pudendal nerve stimulation, interneurons post-discharge and delayed depolarization in hind limb motoneurons of the female cat. *Brain Res.* 1143, 126–131. doi: 10.1016/j.brainres.2007.01.064

Perrier, J. F., and Delgado-Lezama, R. (2005). Synaptic release of serotonin induced by stimulation of the raphe nucleus promotes plateau potentials in spinal motoneurons of the adult turtle. *J. Neurosci.* 25, 7993–7999. doi: 10.1523/jneurosci.1957-05.2005

Perrier, J. F., and Hounsgaard, J. (2003). 5-HT2 receptors promote plateau potentials in turtle spinal motoneurons by facilitating an L-type calcium current. *J. Neurophysiol.* 89, 954–959. doi: 10.1152/jn.00753.2002

Perrier, J. F., Rasmussen, H. B., Christensen, R. K., and Petersen, A. V. (2013). Modulation of the intrinsic properties of motoneurons by serotonin. *Curr. Pharm. Des.* 19, 4371–4384. doi: 10.2174/1381612811319990341

Pomeranz, B., Wall, P. D., and Weber, W. V. (1968). Cord cells responding to fine myelinated afferents from viscera, muscle and skin. *J. Physiol.* 199, 511–532. doi: 10.1113/jphysiol.1968.sp008666

Price, D. D., Hayes, R. L., Ruda, M., and Dubner, R. (1978). Spatial and temporal transformations of input to spinothalamic tract neurons and their relation to somatic sensations. *J. Neurophysiol.* 41, 933–947. doi: 10.1152/jn.1978.41.4.933

Quiroga, R. Q., Nadasdy, Z., and Ben-Shaul, Y. (2004). Unsupervised spike detection and sorting with wavelets and superparamagnetic clustering. *Neural Comput.* 16, 1661–1687. doi: 10.1162/089976604774201631

Reali, C., and Russo, R. E. (2013). Neuronal intrinsic properties shape naturally evoked sensory inputs in the dorsal horn of the spinal cord. *Front. Cell. Neurosci.* 7:276. doi: 10.3389/fncel.2013.00276

Russo, R. E., and Hounsgaard, J. (1994). Short-term plasticity in turtle dorsal horn neurons mediated by L-type Ca^{2+} channels. *Neuroscience* 61, 191–197. doi: 10.1016/0306-4522(94)90222-4

Russo, R. E., and Hounsgaard, J. (1996). Plateau-generating neurones in the dorsal horn in an *in vitro* preparation of the turtle spinal cord. *J. Physiol.* 493, 39–54. doi: 10.1113/jphysiol.1996.sp021363

Salter, M. W., and Henry, J. L. (1990). Physiological characteristics of responses of wide dynamic range spinal neurones to cutaneously applied vibration in the cat. *Brain Res.* 507, 69–84. doi: 10.1016/0006-8993(90)90524-f

Svirskis, G., and Hounsgaard, J. (1997). Depolarization-induced facilitation of a plateau-generating current in ventral horn neurons in the turtle spinal cord. *J. Neurophysiol.* 78, 1740–1742. doi: 10.1152/jn.1997.78.3.1740

Conflict of Interest: The authors declare that the research was conducted in the absence of any commercial or financial relationships that could be construed as a potential conflict of interest.

frontiers in Neural Circuits

ORIGINAL RESEARCH
published: 12 June 2020
doi: 10.3389/fncir.2020.00036

Broadband Entrainment of Striatal Low-Threshold Spike Interneurons

*Juan C. Morales[1], Matthew H. Higgs[1], Soomin C. Song[2] and Charles J. Wilson[1]**

[1] Department of Biology, University of Texas at San Antonio, San Antonio, TX, United States, [2] Skirball Institute of Biomolecular Medicine and Neurosciences Institute, New York University School of Medicine, New York, NY, United States

Striatal interneurons and spiny projection (SP) neurons are differentially tuned to spectral components of their input. Previous studies showed that spike responses of somatostatin/NPY-expressing low threshold spike (LTS) interneurons have broad frequency tuning, setting these cells apart from other striatal GABAergic interneurons and SP neurons. We investigated the mechanism of LTS interneuron spiking resonance and its relationship to non-spiking membrane impedance resonance, finding that abolition of impedance resonance did not alter spiking resonance. Because LTS interneurons are pacemakers whose rhythmic firing is perturbed by synaptic input, we tested the hypothesis that their spiking resonance arises from their phase resetting properties. Phase resetting curves (PRCs) were measured in LTS interneurons and SP neurons and used to make phase-oscillator models of both cell types. The models reproduced the broad tuning of LTS interneurons, and the differences from SP neurons. The spectral components of the PRC predicted each cell's sensitivity to corresponding input frequencies. LTS interneuron PRCs contain larger high-frequency components than SP neuron PRCs, providing enhanced responses to input frequencies above the cells' average firing rates. Thus, LTS cells can be entrained by input oscillations to which SP neurons are less responsive. These findings suggest that feedforward inhibition by LTS interneurons may regulate SP neurons' entrainment by oscillatory afferents.

Keywords: oscillations, phase-resetting, basal ganglia, resonance, interneuron

Edited by:
Joshua Singer, University of Maryland, College Park, United States

Reviewed by:
Zayd Khaliq, National Institute of Neurological Disorders and Stroke (NINDS), United States
Tim Jarsky, Allen Institute for Brain Science, United States

***Correspondence:**
Charles J. Wilson
Charles.Wilson@utsa.edu

Received: *04 March 2020*
Accepted: *19 May 2020*
Published: *12 June 2020*

Citation:
Morales JC, Higgs MH, Song SC and Wilson CJ (2020) Broadband Entrainment of Striatal Low-Threshold Spike Interneurons. Front. Neural Circuits 14:36. doi: 10.3389/fncir.2020.00036

INTRODUCTION

Oscillatory synaptic inputs can entrain spiking in neurons, but in each cell type some input frequencies are more effective than others. Frequency-selectivity is one way in which cell types within a local circuit can specialize in the processing of complex input patterns. This phenomenon, called spiking resonance, applies not only to oscillatory signals that are large and easily distinguished from other components of the input, but also to the multiple frequency components embedded in a broadband synaptic input (e.g., Wilson et al., 2018). All signals can be decomposed into a set of constituent sinusoids, so frequency-selectivity affects the responses of neurons to all input patterns. Spiking resonance can be measured as entrainment to experimentally applied sinusoidal input, or as selective entrainment to frequency components in a noisy input.

Cells vary in spiking resonance according to cell type, some showing very sharp frequency selectivity and others broad sensitivity. Some have a relatively fixed frequency sensitivity and in others the frequency sensitivity can be altered flexibly (Beatty et al., 2015). These differences are frequency signatures of cell types and determine the rate and timing of their responses to

specific patterns of synaptic input. In a circuit like the mammalian striatum, in which there are diverse cell types sharing synaptic input from the same set of afferents, cells of different types may respond preferentially to different frequency components in the shared input. In the striatum, spiny projection (SP) neurons are tunable, being very selective for input frequencies matching their individual firing rates (Wilson, 2017). In contrast, somatostatin/neuropeptide-Y containing low-threshold spiking (LTS) interneurons are sensitive to a broad range of input frequencies that depends less the cell's firing rate (Beatty et al., 2015). LTS interneurons provide feedforward inhibition to SP neurons, and their broad frequency sensitivity might oppose SP cell entrainment over a range of input frequencies, altering their effective frequency tuning.

Two different cellular mechanisms can produce spiking resonance: membrane impedance resonance and spike-induced resonance. Membrane impedance resonance is a property of a cell's constituent subthreshold voltage-dependent ion channels, increasing the subthreshold voltage response to periodic input currents at some frequencies. Membrane impedance resonance is independent of spiking (e.g., Hutcheon and Yarom, 2000) and is best measured in its absence. In cells that have a stable resting membrane potential it can be measured in current clamp recordings by applying sinusoidal currents at various frequencies and determining the amplitude of voltage changes as a function of frequency. In cells that fire spontaneously this approach is not available, but spiking can be controlled in voltage clamp, and impedance is measured as the inverse of current generated by the membrane in response to sinusoids of applied voltage (e.g., Beatty et al., 2015). The second mechanism of spiking resonance arises from ion channels triggered by action potentials; this mechanism is not operational when the cell is silent. Spike-triggered currents vary in sign and in time course, producing a sequence of changes in sensitivity to inputs following each action potential (e.g., Yarom et al., 1985; Higashi et al., 1993). Periodic synaptic inputs that are properly aligned with the sequence of spike-induced intrinsic currents gain an advantage in entraining firing. Theoretical and simulation studies have explored the relative strength of these two mechanisms of spiking resonance and possible interactions between them (e.g., Richardson et al., 2003; Rotstein, 2017) and suggest that they might interact to produce the spiking resonance phenomena observed in neurons. Of course, subthreshold-activated ion channels contribute to the trajectory of the neuron between action potentials, and so membrane impedance resonance and spike-dependent mechanisms are not easily separable in experiments when cells are firing.

Striatal SP neurons have no membrane impedance resonance, so their spiking resonance arises solely from spike-dependent mechanisms. That explains why their frequency sensitivity follows their own firing rate (Beatty et al., 2015; Wilson, 2017). Striatal LTS interneurons do have a membrane impedance resonance, and so it is possible that their spiking resonance depends on an interaction between spike-induced and spike-independent resonance mechanisms. The mechanism of membrane impedance resonance in striatal LTS interneurons is known (Song et al., 2016), and it depends on calcium influx through Cav2 channels. This offers the opportunity to remove membrane impedance resonance by blocking those channels and determine the contribution of this mechanism to spiking resonance. In the work reported here we show that membrane impedance resonance has no measurable contribution to the spiking resonance of striatal LTS interneurons or their entrainment by periodic current waveforms. The characteristic features of the LTS cell's spiking resonance can all be traced to spike-induced changes in input-sensitivity that can be measured using phase resetting.

MATERIALS AND METHODS

All experimental procedures were in accordance with the National Institutes of Health *Guidelines for the Care and Use of Laboratory Animals* and were approved by the Institutional Animal Care and Use Committee of the University of Texas at San Antonio.

Brain Slice Preparation

Transgenic mice (B6.FVB-Tg(Npy-hrGFP)1Lowl/J) expressing the green fluorescent protein (GFP) reporter under the control of the neuropeptide-Y (NPY) promoter (Jackson Laboratories, stock no. 006417) were deeply anesthetized with isoflurane and perfused intracardially with a sodium-free, chilled solution containing (in mM) 2.5 KCl, 1.25 NaH_2PO_4, 0.5 $CaCl_2$, 10 $MgSO_4$, 10 D-glucose, 26 $NaHCO_3$, and 202 sucrose at pH 7.4. Immediately after perfusion, mice were decapitated and their brains extracted for the slicing procedure. 300 μm parasagittal slices containing the striatum were cut in the chilled solution used for perfusion (described above) using a vibrating slicer. Slices were collected in bubbled (95% O_2–5% CO_2) artificial cerebrospinal fluid (ACSF), which consisted of (in mM) 126 NaCl, 2.5 KCl, 1.25 NaH_2PO_4, 2 $CaCl_2$, 2 $MgSO_4$, and kept at room temperature for at least 1 h before transfer to the recording chamber for perforated patch recordings.

Electrophysiological Recordings

Slices were bathed continuously with oxygenated ACSF at a rate of 2–3 mL/min and kept at 35°C. We used the perforated patch method to reduce cell dialysis and prevent rundown of spontaneous firing. Micropipettes with 4–8 MΩ tip resistances were filled with a solution containing 140.5 mM $KMeSO_4$, 7.5 mM NaCl, 10 mM HEPES, and 0.5 μg/ml gramicidin. Gramicidin was mixed in DMSO (0.5 mg/ml) and diluted (1:1000) in filtered electrode solution. Synaptic transmission was not blocked, as injected currents were applied to single neurons. Blockade of GABAergic transmission was considered unnecessary, as other spiny neurons were mostly inactive in our slices, and LTS interneurons have been reported not to be strongly interconnected (Gittis et al., 2010).

Striatal LTS cells and spiny neurons were targeted with an Olympus BX50WI upright microscope using the water-immersion 40x objective. Data were acquired using a Multiclamp 700B amplifier (Molecular Devices, Union City, CA, United States), filtered at 10 kHz, digitized at 20 kHz by a HEKA

ITC-18 analog-to-digital converter, and collected using Igor Pro (WaveMetrics, Lake Oswego, OR, United States). All data analysis was done offline using *Mathematica* (Wolfram Research, Champaign, IL, United States).

Measuring Entrainment of Spiking

To measure entrainment, cells of both types were stimulated with a sequence of sine wave currents varying in frequency with amplitude of 20 pA. The frequency of the sine wave was varied from 1 Hz to 25 Hz, in 1 Hz steps. Spike times were detected offline. For each sine wave frequency (f), each spike time (t_i) was converted to phase ($0 \leq \theta < 1$) relative to the period of the sine wave using the Mod operator:

$$\theta_{f,i} = Mod(f \cdot t_i, 1),$$

The phase probability distribution for each frequency was then calculated using 100 bins to represent phases from 0 to 1. We then calculated the entropy of each phase distribution, normalized by the expected entropy of a sample of the same size drawn from the uniform phase distribution, $E(H_u)$,

$$H = \frac{-\sum_{i=1}^{N} p_i log_2(p_i)}{E(H_u)}.$$

This entropy measure removes any bias from differences in the number of spikes collected in each sample. Perfect entrainment (i.e., all phases falling within one of the 100 bins of the phase distribution) would produce an entropy value of zero. At the other extreme, sampling from a uniform distribution of spike phases would produce an expected entropy value of one.

Measuring Spiking Resonance

To measure spiking resonance, LTS cells were stimulated for 160 s with a barrage of contiguous brief (0.5 ms) current pulses, whose amplitudes were drawn from a Gaussian distribution (mean = 0 pA and standard deviation = 40 pA). For some experiments we substituted a 1000/s Poisson-triggered barrage of artificial synaptic currents with 20 pA amplitudes and 2.5 ms time constants, as described in Beatty et al. (2015). These two stimulus waveforms differ only at high frequencies, and they produced the same results. In either case, each injected current waveform was Fourier transformed in *Mathematica* and filtered in the frequency domain by multiplying the frequency-domain waveform by Tukey filters ($\alpha = 0.25$) with bandwidths of 10 Hz, centered at every 5 Hz from 5 to 110 Hz. This resulted in 22 filtered signals which were then transformed back into the time domain. Spikes were assigned phases on these waveforms by finding the zero-crossings of the signal, finding the time of each spike from the left positive-slope zero-crossing, and dividing by the length of that cycle (see **Figure 1**). The vector strength was then calculated for phases corresponding to each of the 22 filtered signals by:

$$vs(f) = |\frac{1}{N}\sum_{j=1}^{N}(cos(2\pi\phi_j) + isin(2\pi\phi_j))|,$$

which is the magnitude of the normalized vector sum. This resulted in a value ranging from zero to one, with one indicating perfect phase locking and zero meaning no locking.

Measuring Phase Resetting Curves

The method used for experimentally measuring phase resetting curves (PRCs) has been described previously (Netoff et al., 2011; Wilson et al., 2014). A sequence of contiguous 0.5 ms current pulses whose amplitudes were independently drawn from a Gaussian distribution (mean = 0 pA and standard deviation = 40 pA) was injected into repetitively firing LTS or spiny cells through the recording electrode for 160 s. This stimulus was the same as one of the two used to measure spiking resonance, so it was possible to measure spiking resonance and PRCs from the same cell. Phase within each interspike interval was estimated by interpolation (i.e., the estimated phase ramped linearly from 0 to 1 between spikes) and was discretized into 50 bins. The charge delivered during each bin was calculated by integration of the noise waveform for each bin in each interspike interval during the noise stimulus. Because the charge delivered in each phase bin was different on each ISI, it was possible to calculate linear regressions between charge and ISI length by multiple linear regression. The slopes of these regressions, normalized by the average ISI, produced the 50 values that make up the PRC. The standard errors for each of the estimates of Z were also calculated and are shown as error bars around the PRC values.

We measured the duration of individual inter-spike intervals (ISI_n), the average inter-spike interval ($\overline{ISI}$), and the charge (Q) delivered per phase bin (in all cases $m = 50$), to solve for the PRC values (Z_m) at m phase bins using multiple regression, minimizing the mean squared value of the residual ξ_n:

$$\frac{ISI_n - \overline{ISI}}{\overline{ISI}} = \sum_{i=1}^{m} Q_{n,i}Z_i + \xi_n$$

Calculation of the PRC was done in *Mathematica* using the built-in function, *LinearModelFit*.

Phase Modeling

We implemented a version of the phase model containing intrinsic noise and an external stimulus (either pulsed noise current or sinusoidal current). The phase model describes the temporal evolution of phase and is governed by the differential equation:

$$\frac{d\varphi}{dt} = F_{cell} + [I_{\text{stim}}(t) + \eta(t)]Z(\varphi)$$

$$\varphi(0) = \varphi_0$$

where φ is the cell's intrinsic phase, F_{cell} is the cell's measured unperturbed firing rate, I_{stim} the stimulus current delivered through the recording electrode, η is the cell's estimated intrinsic noise, and Z is the PRC measured using multiple regression (outlined above). Phase is only defined from zero to one, with one indicating a spike, so when phi reached one, it was reset back to zero.

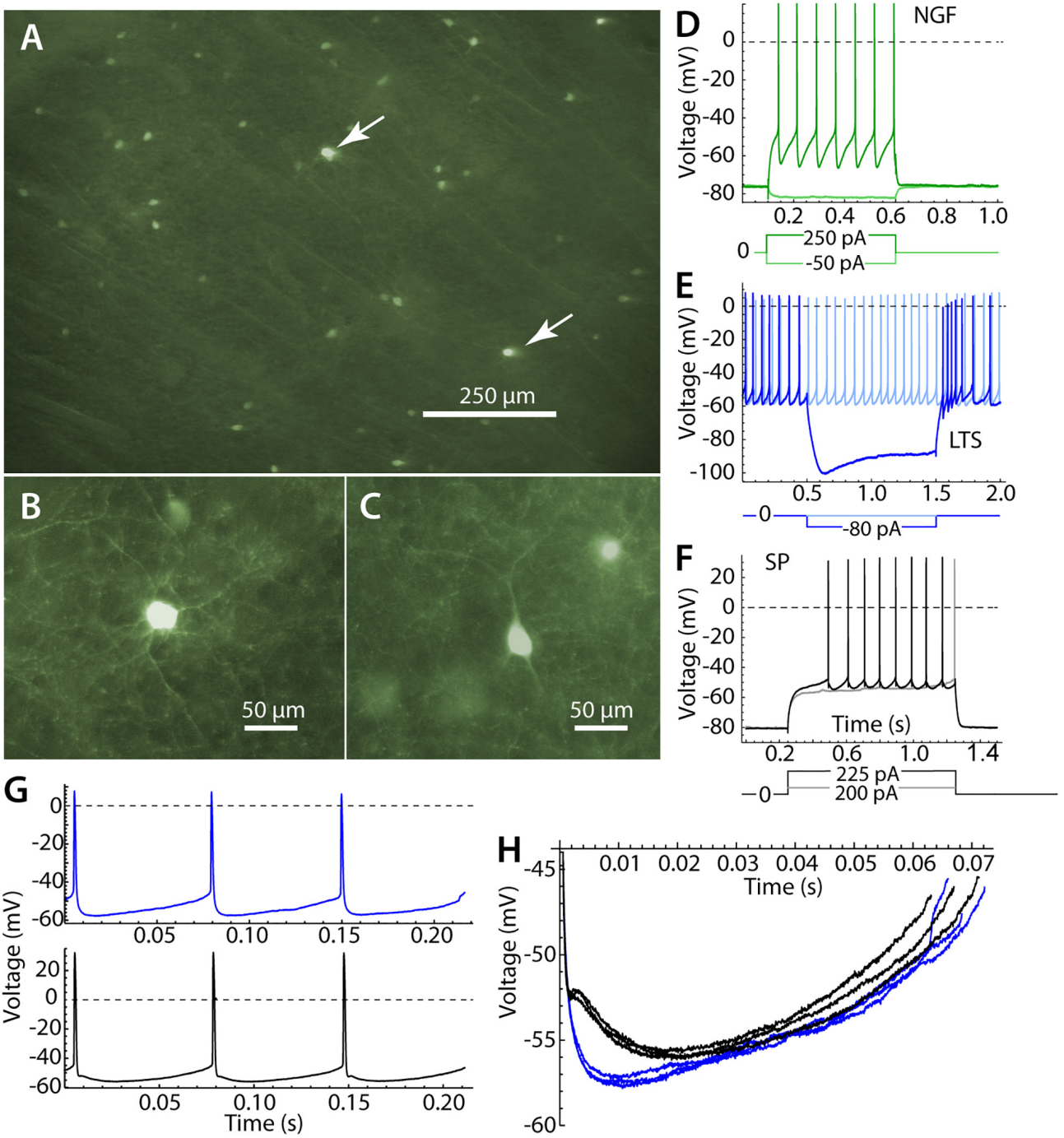

FIGURE 1 | Identification of striatal neurons. **(A)** Panoramic view of the striatum in parasagittal section. Most labeled cells are LTS interneurons, but there are a few neurogliaform (NGF) cells, which are brighter (arrows). **(B)** A NGF cell at higher magnification, characterized by many primary dendrites that branch frequently. **(C)** An LTS interneuron, with fewer and straighter dendrites. **(D)** Responses of an NGF cell to hyperpolarizing and depolarizing current pulses. Note the stable hyperpolarized membrane potential in the absence of current. **(E)** An LTS interneuron, with continuous autonomous firing in the absence of current, and a prominent rebound burst at the offset of a hyperpolarizing current pulse. **(F)** A SP neuron, with characteristic long delay to first spike in response to depolarizing currents. **(G)** Repetitive firing of an LTS interneuron in the absence of injected current (blue) and an SP neuron, firing repetitively (black) when depolarized to approximately match the firing rate of the LTS interneuron. **(H)** The interspike membrane potential trajectory of the same LTS interneuron (blue) and SP neuron (black) shown in **(G)**. SP neurons show separate fast and medium afterhyperpolarizations, whereas LTS interneurons have a single afterhyperpolarization.

RESULTS

Cell Identification

Striatal LTS interneurons were identified by fluorescence microscopy in brain slices from NPY-GFP mice at the time of recording. We were careful not to include recordings from neurogliaform (NGF) cells, which are also fluorescent in the mouse line used in our study (Ibáñez-Sandoval et al., 2011). NGF cells were identifiable by their brighter fluorescence and their characteristic morphological and physiological properties (Ibáñez-Sandoval et al., 2011). Examples of the morphology and responses of LTS and NGF cells are shown in **Figure 1**. All LTS cells used in the sample had the morphology and responses to current steps characteristic of striatal LTS cells (Kawaguchi, 1993; Tepper et al., 2010; Beatty et al., 2012). These include sustained autonomous rhythmic firing and rebound bursts following hyperpolarizing current steps, neither of which were seen in NGF cells. LTS cells in the persistent depolarized state (Song et al., 2016) were not included in our sample.

Recordings of SP neurons were taken from a previous dataset (Wilson, 2017). Half of the SP cells were identified as either direct or indirect pathway neurons in mice expressing tdTomato or GFP under control of the D1 or D2 receptor promoter, respectively. The remainder were SP neurons identified by their characteristic physiological properties: low input resistance, hyperpolarized resting potential, fast inward rectification, and late first spike in response to a near-threshold depolarizing pulse. Entrainment of SP cells by sine wave currents was reported in the previous paper (Wilson, 2017) and is included here only for comparison to LTS cells. The spiking resonance results reported here have not been presented previously, but a similar measurement in a different sample of SP cells was reported in Beatty et al. (2015). D1R and D2R neurons did not differ in spiking resonance and so results from all SP cells of both types were pooled.

Low threshold spike interneurons are autonomously active in slices and measurements of sinusoidal entrainment and spiking resonance were made at their spontaneous firing rates. Spiking resonance was measured in 18 LTS interneurons with firing rates ranging from 6.9 to 23.8 spikes/s (mean = 15.4, sd = 5.7). Because striatal SP neurons are silent in slices, we used constant current to evoke repetitive firing in these cells. The current was adjusted to achieve firing rates in the same range as those of LTS interneurons. Firing rates in 18 SP cells ranged from 11.1 to 19.8 spikes/s, mean = 14.0, sd = 2.6). When firing at comparable rates, the interspike membrane potential trajectories of LTS interneurons and SP neurons traversed a similar range, but LTS interneurons had deeper and faster spike afterhyperpolarizations (**Figures 1G,H**).

Spiking Resonance

The measurement of spiking resonance is illustrated in **Figure 2**. Cells were recorded in the perforated patch configuration, and electrode capacitance was compensated to ensure accurate delivery of charge to the cell membrane. In some cells, the stimulus was a Poisson-timed 1000/s barrage of synaptic-like currents averaging 20 pA in amplitude, with decay time constants of 2.5 ms (see **Figure 4**). In the rest of the cells (as shown in **Figure 2**), contiguous pulses of current 0.5 ms in duration with amplitudes drawn from a Gaussian distribution with a mean of zero and a standard deviation of 40 pA were injected through the somatic recording electrode. These two stimulus waveforms both have constant spectra over most of the frequency range of interest, and they yielded similar spiking resonance measurements. An example showing the appearance of the current waveform, and its effect on the firing pattern of a repetitively firing cell is shown in **Figure 2A**. To analyze spiking resonance, the current waveform was digitally filtered into 22 frequency bands, each 10 Hz wide, centered on frequencies from 5 to 110 Hz in 5 Hz intervals. These were chosen to cover the range of membrane and spiking resonances previously reported for LTS interneurons, with resolution sufficient to characterize the broad resonance peaks of those cells (Beatty et al., 2015; Song et al., 2016). Examples of the filtered current waveforms for selected frequency bands are shown in **Figure 2A**. Like the original stimulus waveform, each filtered waveform had a mean of zero. The stimulus altered the timing of spikes, with no consistent effect on average firing rate. The spike times were converted to phases on each of the filtered waveforms. Spike phase was defined as the proportion of the cycle between positive-slope zero crossings of the filtered waveform bracketing the spike, as shown in **Figure 2B**. The phases of all spikes were vector-summed to make a resultant vector, as shown in **Figure 2C**. The lengths of the resultant vectors (vector strengths) potentially range from zero (meaning phases are uniformly distributed with respect to the filtered stimulus waveform) to one (if every spike is at exactly the same phase on the filtered stimulus). The vector strengths for all the filtered waveforms were used to make a spectrum of spiking resonance, as shown in **Figure 2D**. The peak frequency and half-width (bandwidth **Figure 2D**) were measured from the spiking resonance spectrum.

Spiking resonance spectra for an example LTS interneuron and SP neuron, and the average spectra for both cell types, are shown in **Figure 3**. The spectra for the two cell types differed in overall amplitude, the peak frequency, and the bandwidth, as defined in **Figure 2**. Example spectra are shown in **Figures 3A,B**. Spiking resonance spectra for all cells in each group are superimposed with the group means in **Figures 3C,D**. On average, LTS interneurons showed larger vector strengths at all frequencies. That is, spike timing was more coherent with all frequency components of the stimulus waveform. The maximum value of each spiking resonance spectrum for both cell types is shown in **Figure 3E**. This difference between cell types was statistically significant (Mann–Whitney U, $p = 0.0005$). We have previously shown (Wilson, 2017) that D2R-expressing SP neurons have greater sensitivity to periodic inputs than D1R-expressing ones, and this accounts for some of the variation among SP neurons in overall vector strength. The peak of the spiking resonance spectrum occurred at a lower frequency for the SP neurons (**Figure 3F**, Mann–Whitney U, $p = 0.0004$). In SP neurons, the peak frequency for spiking resonance varies with firing rate (Beatty et al., 2015). In LTS interneurons firing at the

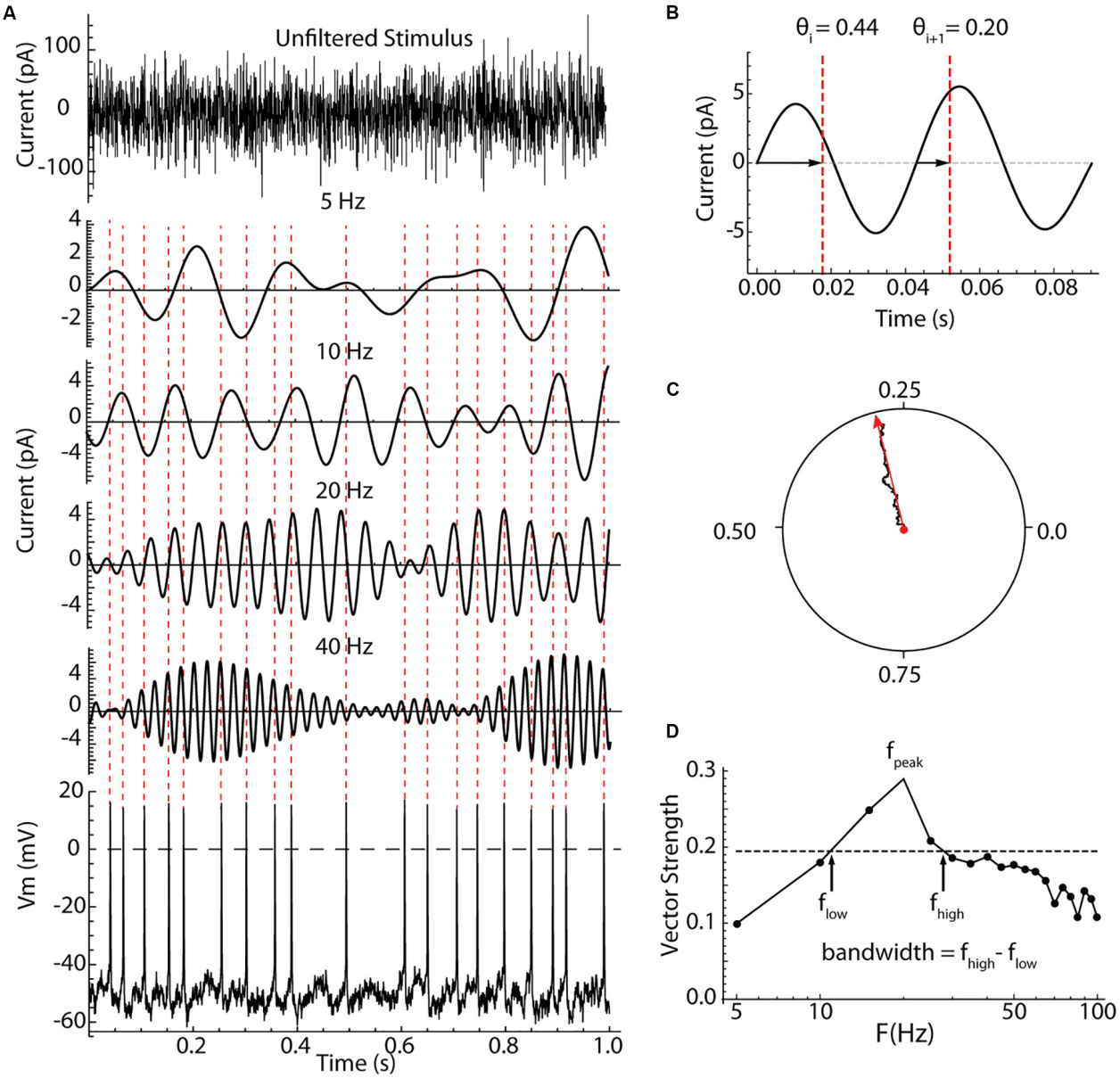

FIGURE 2 | Measurement of spiking resonance. **(A)** An example 1 s of the injected current (top), bandpass filtered components of the same current centered on different frequencies, and the resulting voltage waveform and perturbed spiking in a striatal LTS interneuron. The spike times are indicated with dotted lines crossing the filtered current waveforms. **(B)** Measurement of spike phases on the filtered waveform. Phase was measured between positive-slope zero crossings. **(C)** The summation of phase measurements from many action potentials as a vector sum. The resultant vector in red, points in the direction of the average phase, and its length is the vector strength. **(D)** A spectrum of vector strength measurements from an example LTS interneuron taken for a range of bandpass center frequencies. The frequency producing the peak resonance, f_{peak}, and the half-width of the spectrum (bandwidth) were measured as shown using the half-height taken between the maximum and minimum vector strengths.

same average rate as the SP neurons, the peak frequency was at a higher frequency, usually higher than the cell's average rate (**Figure 3D**). Because the peak frequency of resonance in both cell types depended to some degree on firing rate, we measured the difference between the firing rate and the peak in the spiking resonance spectrum for each cell. This measure was significantly different between the two cell types (**Figure 3G**, Mann–Whitney U, $p = 0.009$). The resonance bandwidth (measured as shown in **Figure 2D**) was broader for LTS interneurons than SP neurons, as also evident in **Figure 3H** (Mann–Whitney U, $p = 0.0008$).

No Contribution From Membrane Impedance Resonance

It was proposed previously that the enhanced sensitivity of LTS interneurons to input frequency components higher than their

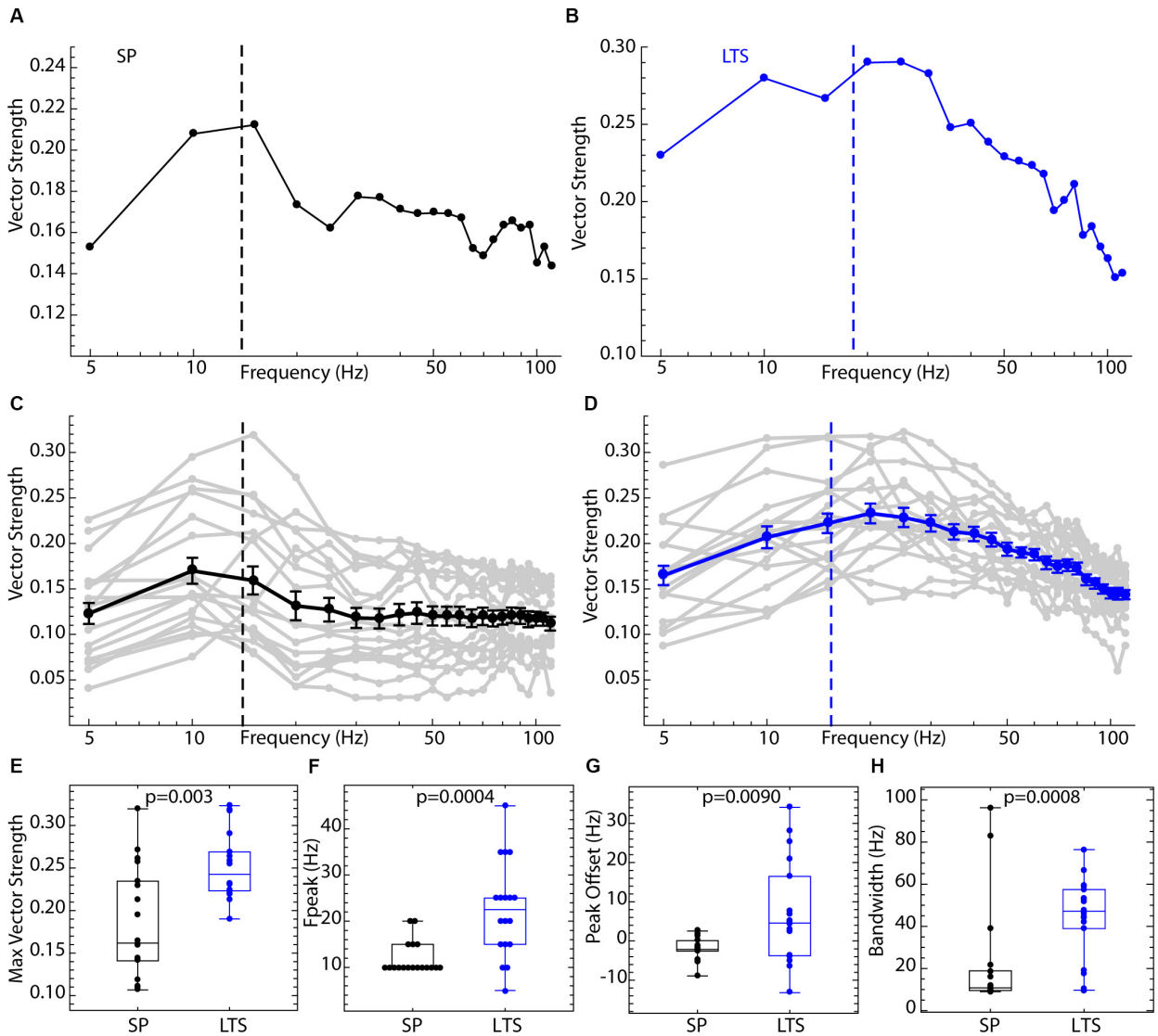

FIGURE 3 | Comparison of spiking resonance in SP neurons and LTS interneurons. **(A)** An example spiking resonance spectrum from an SP neuron. The cell's firing rate is indicated by the dotted line. **(B)** An example LTS interneuron shown the same way. **(C)** Superimposed spiking resonance spectra (gray) and the average spiking resonance (black) for 18 SP neurons. **(D)** Superimposed individual spectra (gray) and average spectrum (blue) for 18 LTS interneurons. Error bars are standard errors of the mean at each frequency. The dotted lines indicate the average firing rates for the two groups of cells. **(E)** LTS interneurons showed a higher vector strength overall than SP neurons. **(F)** The frequency at the peak resonance was higher in LTS interneurons. **(G)** The difference between the firing rate and peak frequency for each cell was greater in LTS interneurons. **(H)** The bandwidth of resonance (measured as shown in **Figure 2**) was greater in LTS interneurons.

firing rates might represent a contribution from their membrane impedance resonance (Beatty et al., 2015). Unlike SP neurons, LTS interneurons have a substantial membrane resonance, which is generated by a calcium-dependent chloride current that is active only when the cell is depolarized (Song et al., 2016). It was previously shown that the membrane impedance resonance is abolished by blockade of Cav2 channels by 1 μM ω-conotoxin GVIA (Song et al., 2016). To determine whether the peculiar features of spiking resonance in LTS interneurons arose from their impedance resonance, we measured spiking resonance in nine LTS interneurons before and after application of 1 μM ω-conotoxin GVIA. For this experiment, spiking resonance was measured using a barrage of artificial synaptic currents like those used in Beatty et al. (2015) (see the section "Materials and Methods"). Examples of this current waveform, and its effects on membrane potential and spiking in control ACSF and in conotoxin are shown in **Figures 4A,B**. The corresponding spiking resonance spectra for an example cell are shown in **Figure 4C**. All spectra are superimposed in **Figure 4D**, along with the average spectra for both conditions. Because this was a paired comparison, the appropriate test for an effect of conotoxin is the difference spectrum for each cell. These are shown in **Figure 4E**. There was no statistically significant frequency trend in the difference curve (ANOVA, F = 0.68, df = 8,21,

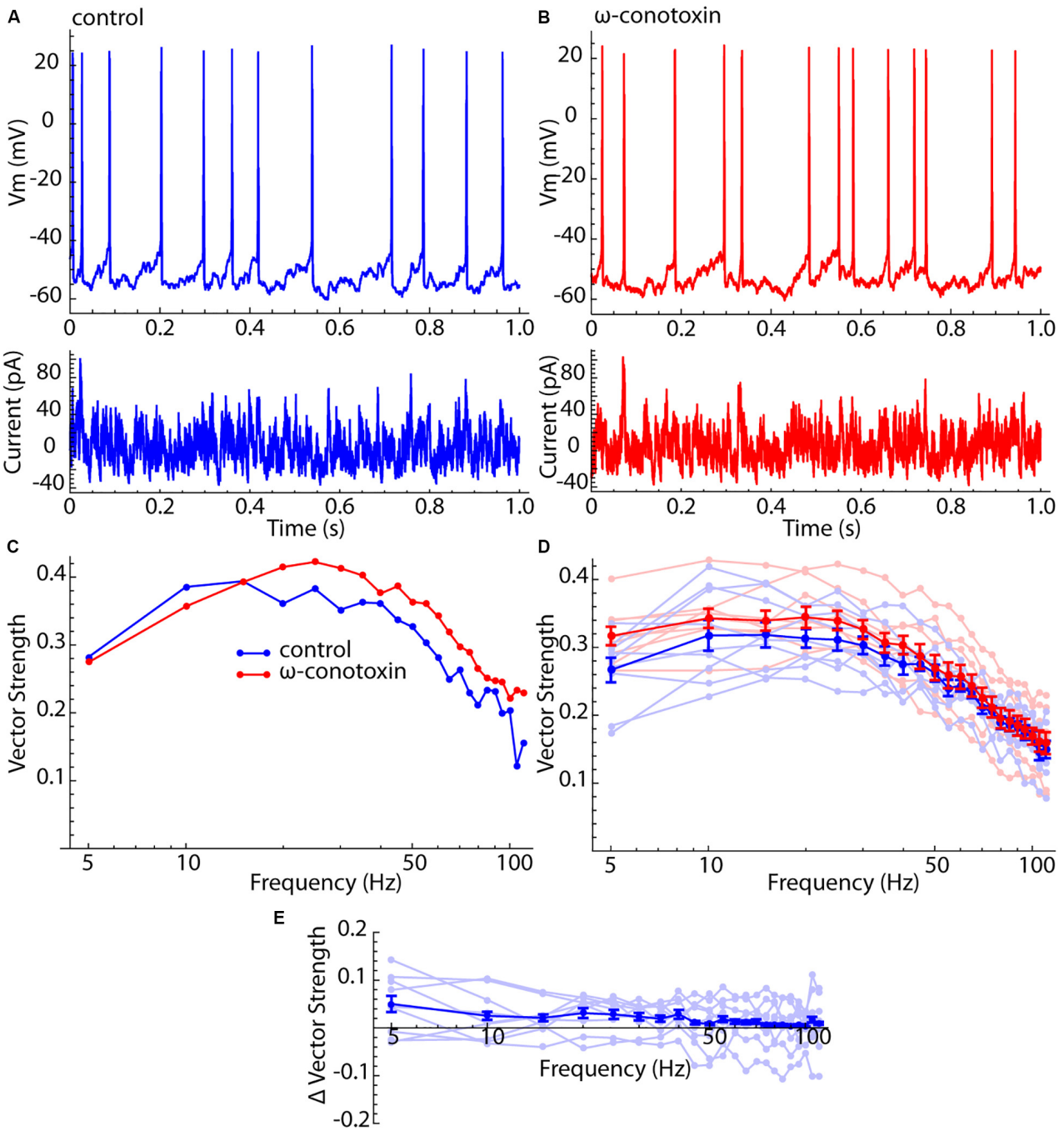

FIGURE 4 | Lack of effect of Cav2 channel blockade on spiking resonance in LTS interneurons. **(A)** Current waveform, membrane potential, and firing pattern for an example LTS interneuron. **(B)** The same example neuron after treatment with 1 μM ω-conotoxin GVIA. **(C)** Spiking resonance spectra for an example LTS interneuron before (blue) and after (red) conotoxin treatment. **(D)** Superimposed spectra for all cells before (light blue) and after (light red) conotoxin treatment, and the mean spectra. Error bars are standard errors of the mean. **(E)** Difference spectra (conotoxin – control) for each cell before and after conotoxin treatment (light blue) and the mean difference spectrum. There was no significant frequency trend for the difference spectra (F = 0.68, df = 8,21, p = 0.85).

p = 0.85). Blockade of Cav2 channels with conotoxin also had no statistically significant effect on the overall sensitivity (signed rank test, p = 0.19), the position of the peak in the spiking resonance curve (signed rank test, p = 0.86), or the resonance bandwidth (signed rank test, p = 0.95). It also had no effect on the firing rates of LTS cells; the average rate for the sample was 12.3 ± 2.7 spikes/s, and 12.3 ± 1.7 for the same cells after conotoxin treatment.

The result shown in **Figure 4** fails to support the idea that the difference between the spiking resonance spectra of SP neurons

and LTS interneurons might result from the LTS interneuron's membrane impedance resonance.

LTS Interneurons Are Entrained Over a Broad Frequency Range

The broad range of spiking resonance in LTS interneurons suggests that they might also be entrained by sinusoidal inputs over a broad range of frequencies. In SP neurons, there is a strong correspondence between spiking resonance measured using broadband stimuli and the entrainment profile to single-frequency sine wave inputs. Like the spiking resonance, entrainment to single sine waves in SP neurons is strong only for stimulus frequencies close to the cell's unperturbed firing rate (Wilson, 2017). Does the broadband spiking resonance of LTS interneurons mean that they have a broader frequency range of entrainment?

We compared the entrainment frequency selectivity of six striatal LTS interneurons to that of seven SP neurons. As in the spiking resonance measurements LTS interneurons were allowed to fire at their natural rates. Repetitive firing in SP neurons was evoked by constant current adjusted to achieve firing rates comparable to those of LTS cells. In both cell types, 20 pA sine wave currents from 1 Hz to 25 Hz at 1 Hz steps were applied for 8 s each. Spike times were converted to phases relative to the stimulus sine wave, and phase histograms were constructed as in the examples shown in **Figures 5A–C**. To quantify entrainment, we estimated the deviation of the spike phase distribution from the uniform distribution expected in the absence of any entrainment by calculating the entropy of the histograms. Entropy measures depend on the sample size (number of action potentials) and on the number of bins in the histogram, so to correct for these factors we calculated the expected entropy for a uniform phase distribution for each sample and normalized the measured entropy by that value. This normalized entropy varies from 0, meaning all spikes occurred in the same phase bin, to 1, indicating no entrainment at all.

Low-frequency sinusoidal current modulated firing rate in phase with the stimulus in both cell-types (**Figure 5A**). As reported previously (e.g., Kawaguchi, 1993), LTS cells have a prominent calcium-dependent rebound (low-threshold) spike when released from constant hyperpolarization. The sine waves used here were too weak to remove the low-threshold calcium current inactivation and did not evoke a rebound spike (e.g., **Figure 5A**). At stimulus frequencies low enough to produce rate modulation, spike timing during the cycle was not reproducible, and the entropy of the phase distribution was only moderately reduced. At higher frequencies, both SP neurons and LTS interneurons fired fewer action potentials per cycle, and these preferentially occurred at specific phases, so the entropy of the phase distribution was reduced further. The precision of spike timing was maximal when the stimulus frequency matched the unperturbed firing rate of the neuron (**Figure 5B**). Some neurons showed another minimum of entropy at frequencies about twice their unperturbed rate (e.g., the SP neuron in **Figure 5D**). At frequencies between the cell's unperturbed rate and twice that rate, the entrainment was minimal, often (in SP neurons) approximating random firing with respect to the sine wave. LTS interneurons showed stronger entrainment than SP neurons at frequencies both lower and higher than the 1:1 locking frequency (**Figure 5D**). At frequencies for which SP neurons showed almost no entrainment by the stimulus, LTS interneurons were still substantially entrained (**Figure 5C**). There was no specific second frequency of entrainment for LTS interneurons corresponding to their membrane impedance resonance. In contrast with the spiking resonance spectra, entrainment of both LTS interneurons and SP neurons was maximal at their unperturbed firing rates (**Figure 5E**). The only exception was one LTS interneuron that showed stronger entrainment to a sine wave at twice its firing rate (1:2 entrainment in **Figure 5E**). To compare cell types, we rescaled the stimulus frequencies by each cell's firing rate (**Figure 5F**). LTS interneurons showed substantial entrainment to all stimulus frequencies, whereas SP neurons were very selective, responding especially weakly to stimulus frequencies above the cell's own rate (**Figure 5C**). The overall mean normalized entropy of LTS interneurons was significantly lower than that of SP neurons (**Figure 5F**, $t = 2.9346$, df = 11, $p = 0.014$).

For the SP neuron, which lacks membrane impedance resonance, frequency selectivity arises directly from the cell's PRC (Wilson, 2017). If the fundamental mechanism of entrainment in SP neurons and LTS interneurons is the same kind of phase resetting, then the wider frequency range of entrainment to sine waves and the broad spiking resonance curves of LTS cells might be explained by the features of their PRCs.

Phase Resetting Curves of LTS Interneurons and SP Neurons

We compared the infinitesimal PRCs of the same 18 LTS interneurons and 18 SP neurons whose spiking resonances are compared in **Figure 3**. The PRC was estimated from the same pulsed noise stimulus used for the spiking resonance measurement. Example PRCs from both cell types are shown in **Figure 6**. The PRC is quantified as phase change per picocoulomb (pA-s) of charge injected. The PRC represents the sensitivity of the cell's spike timing to current perturbations applied at any time between action potentials. The shape of the PRC is determined by the sequence of both spike-triggered and spike-independent currents that are active during the ISI (e.g., Farries and Wilson, 2012). From the PRC, one can predict the cell's response to any waveform of input current that may be imposed during the ISI, including artificial current or synaptic inputs (Wilson, 2017; Simmons et al., 2018).

SP neurons and LTS interneurons showed substantial differences in PRC size and shape. Examples of LTS interneuron PRCs are shown in **Figure 6A**, and the average for LTS interneurons is shown in **Figure 6B**. SP neuron PRCs have a more symmetric shape, peaking at phases near 0.75, and decreasing thereafter, with an extremely brief peak at the end, just before the next action potential. Examples are shown in **Figure 6C**, and the average PRC for SP neurons is shown in **Figure 6D**. On average PRC integrals of LTS interneurons were larger than those of SP neurons (0.74 cycles/pA-s for SP neurons and 1.210 for LTS neurons, Mann–Whitney U, $p = 0.00084$).

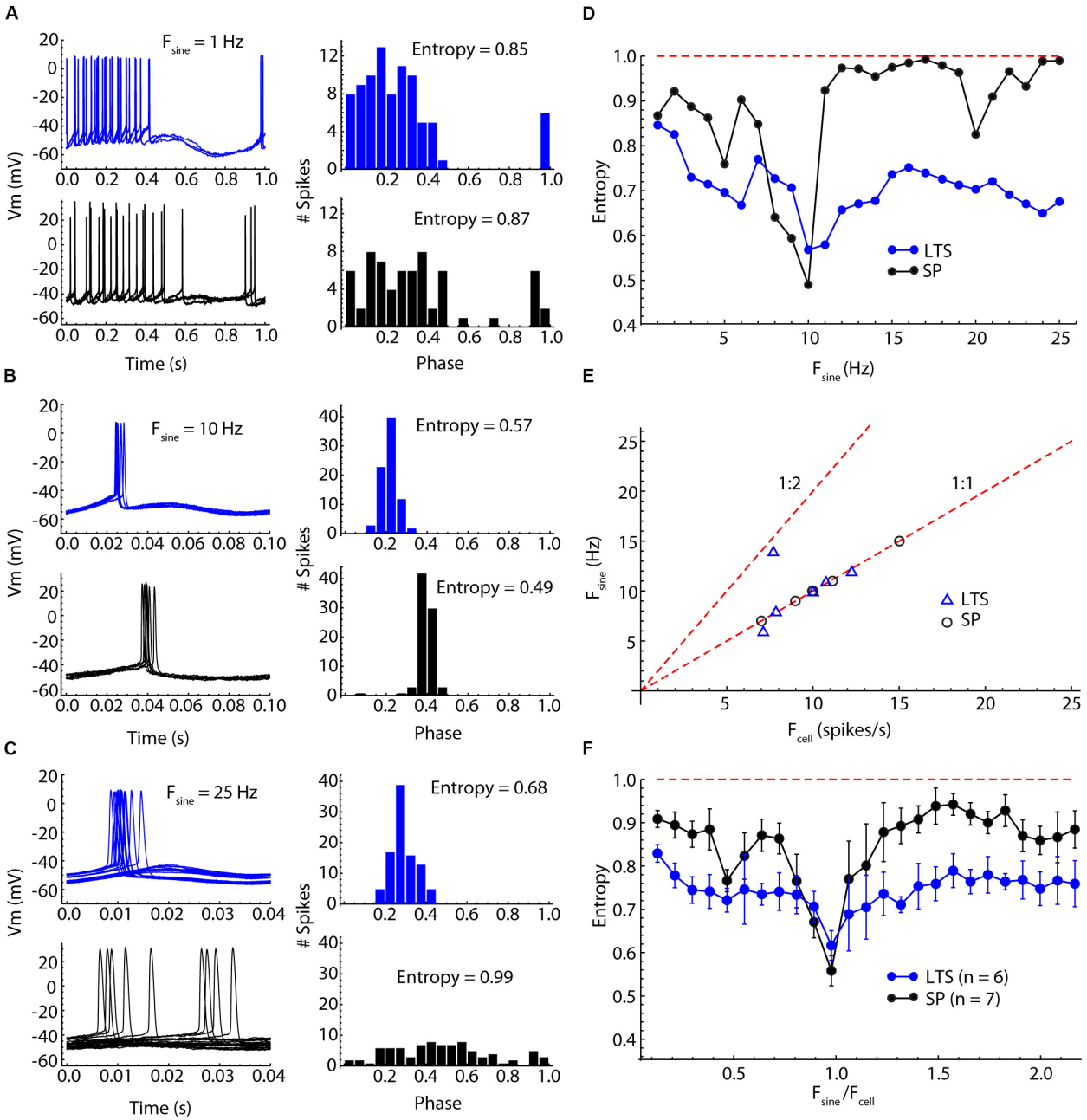

FIGURE 5 | Comparison of SP neuron and LTS interneuron entrainment by injected sinusoidal currents of frequencies between 1 and 25 Hz. **(A)** Low-frequency (1 Hz) sine wave stimulation produced firing rate modulation in both cell types, with neurons firing throughout the positive phase of the stimulus but with little spike time reliability. Example traces for one cycle of the stimulus are shown on the left, and a histogram of spike phases on the stimulus is shown on the right. The peak of the sine wave is phase 0.25, and the trough is phase 0.75. The degree of entrainment is measured as the entropy of the histogram, with low entropies meaning better entrainment. **(B)** Sinusoidal current waveforms at a frequency near the cells' unperturbed firing rates (about 10 Hz in both cells) evoke 1:1 entrainment of firing at a reliable phase of the stimulus in both cell types. **(C)** At frequencies higher than the cell's firing rate, 1:1 entrainment failed, but LTS interneurons continued to be more entrained than SP neurons, whose spike times were almost completely unrelated to the stimulus sine wave. **(D)** Entrainment spectra for the example neurons used in **(A–C)**. Entrainment was better in the LTS interneuron at all frequencies except for those close to the cells' unperturbed firing rates. The difference is especially clear at frequencies near 1.5 times the unperturbed firing rates, at which the SP neurons showed almost no entrainment. The expected entropy for zero entrainment is indicated by the dotted line. **(E)** The sine wave frequency producing peak entrainment (F_{sine}) was close to the cells' unperturbed firing rate (F_{cell}) in both cell types. One exception is an LTS interneuron that had slightly stronger entrainment at twice the unperturbed firing rate. **(F)** Mean entrainment profile for a sample of six LTS interneurons and seven SP neurons. F_{sine} is plotted as a proportion of F_{cell}. Note the absence of any second entrainment peak corresponding to the membrane impedance resonance. Compared to SP neurons, LTS neurons are much less frequency-selective, showing substantial entrainment over the entire frequency range.

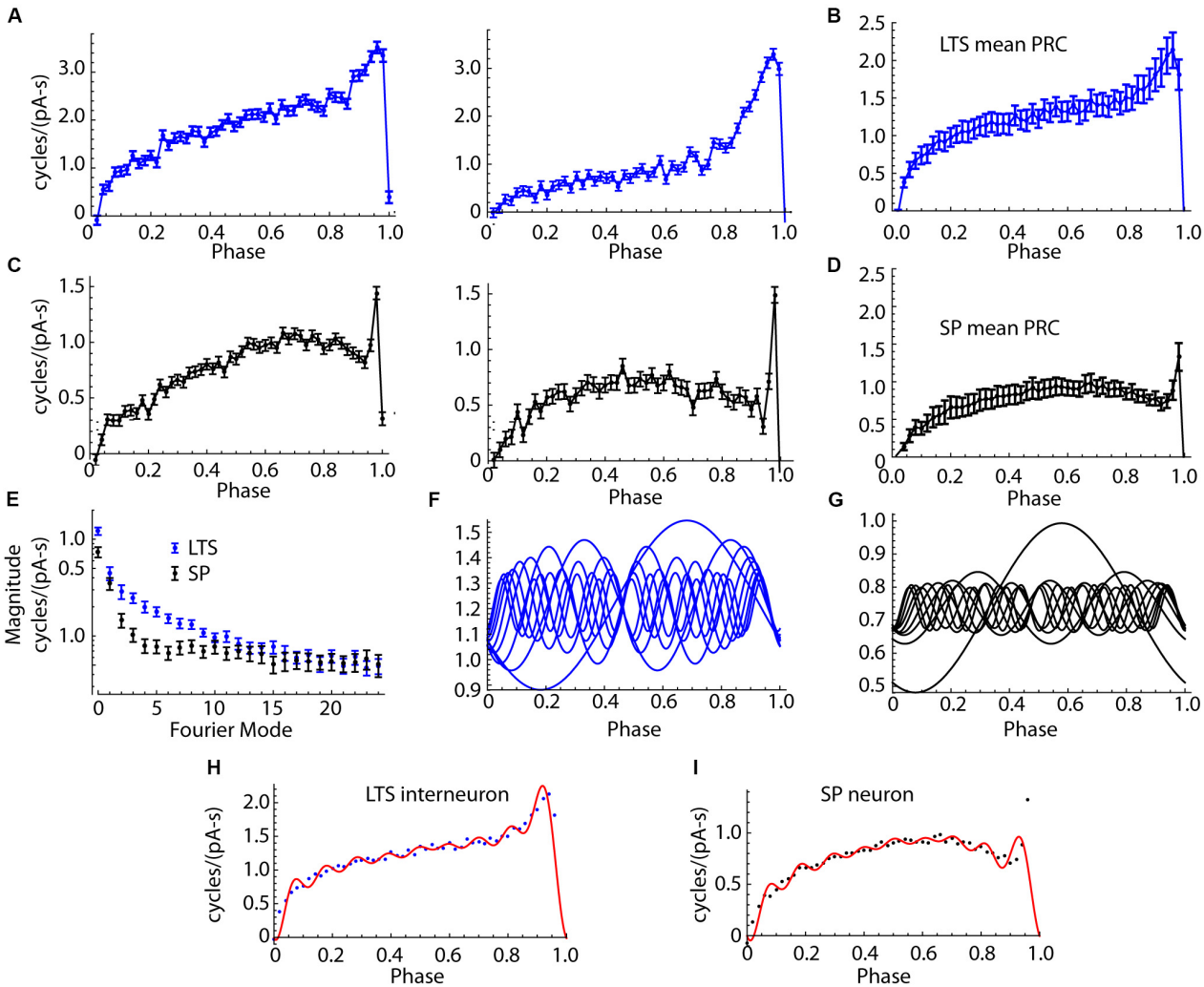

FIGURE 6 | Comparison of PRCs of SP neurons and LTS interneurons. **(A)** Two example LTS interneuron PRCs. **(B)** The mean PRC for the sample of 18 LTS interneurons. Error bars are standard errors of the means. **(C)** Examples PRCs from two SP neurons. **(D)** Mean PRC for the group of SP neurons. The consistent differences in shape include the more pronounced skew in the LTS interneuron PRC and its broader late peak. SP neurons' PRCs were more symmetrical, except for a very narrow late peak, only one or two bins wide, at the end of the ISI. **(E)** Amplitudes of the Fourier modes of the PRCs of LTS interneurons and SP neurons. 26 modes are shown, calculated from the 50 points in the PRC. Mode 0 is the DC component, which is the average amplitude of the PRC. The differences between cell types are confined to the first 10 modes. **(F)** Modes 0–9 of the average LTS interneuron PRC. **(G)** Modes 0–9 of the average SP neuron PRC. **(H)** Mean LTS interneuron PRC, assembled from the modes shown in **(F)**. Points shown are the original mean PRC. **(I)**. SP neuron average PRC (points) and PRC reassembled from modes shown in **(G)** (red line).

In repetitively firing neurons, sinusoidal inputs alter spike timing by interacting with a corresponding (same frequency) mode in the cells' PRCs (Goldberg et al., 2013). To understand how PRC shape determines the response to sinusoidal current inputs, we decomposed each neuron's PRC into sinusoidal components using the discrete Fourier transform. Because the PRC was composed of 50 points, this produced one DC component and 25 sinusoidal components whose sum could reproduce the original PRC. The components (modes) are calculated relative to each cell's mean ISI, so that the frequency of mode 1 is the cell's mean firing rate, mode 2 is twice that rate, etc. The amplitudes and phases of the modes determines the size and shape of the PRC. The PRC mode amplitudes of LTS interneurons and SP neurons are compared in **Figure 6E**. The amplitudes for LTS interneurons were higher than those of SP neurons overall [mixed-design ANOVA, F(cell type) = 13.9, df = 1,34, p = 0.0007]. The difference was large for mode 0, smallest for mode 1, and large again for modes 2–7. Beyond mode 10, there was little difference between cell types. The first 10 components of the average PRCs from the LTS interneurons and SP neuron are shown in **Figures 6F,G**, respectively. Reconstruction of the average PRCs of each cell type from their first 10 modes is compared to the original average PRCs in **Figures 6H,I**. The first 10 modes are sufficient to account for the major features of the PRCs and the differences between cell types. The most

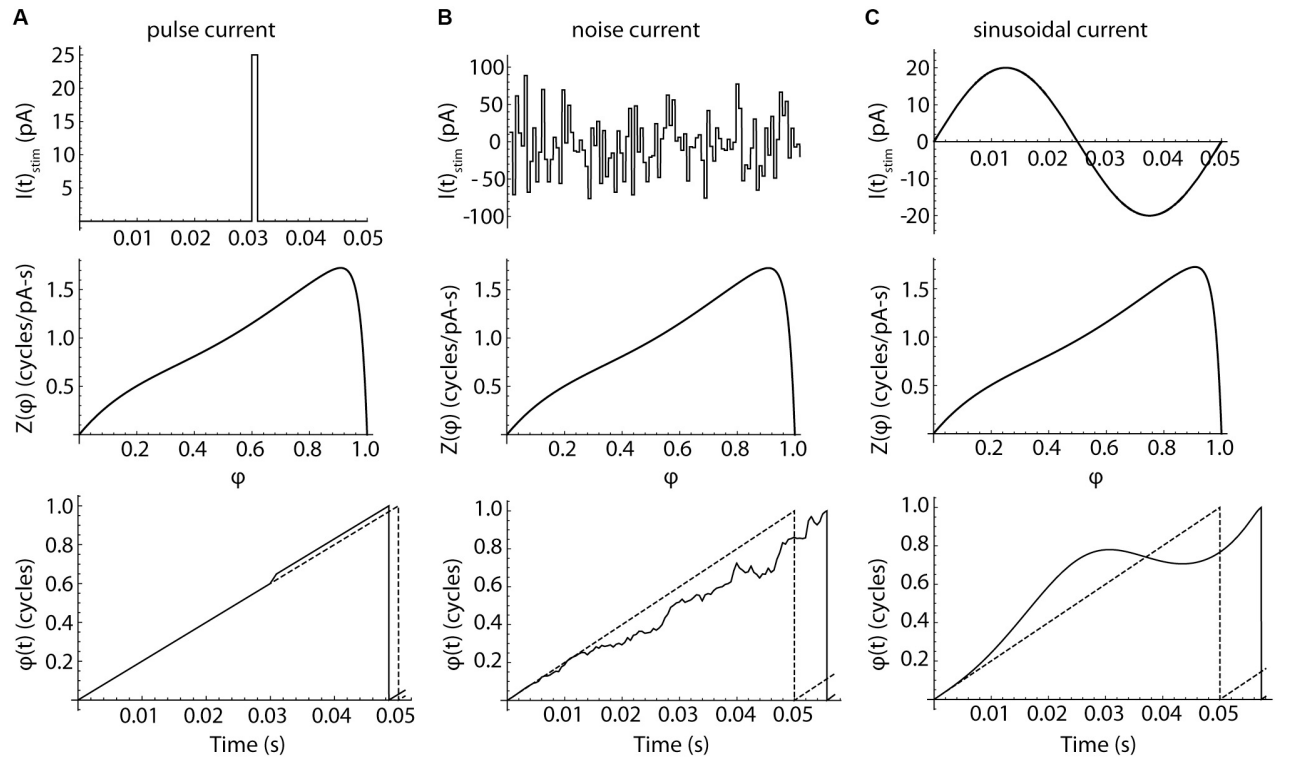

FIGURE 7 | The responses of phase neurons. **(A)** Response to a brief current pulse. Charge delivered by a current pulse (top) causes a phase shift in a noise-free neuron, whose phase otherwise advances at a constant rate F_{cell}. The cell fires when its phase reaches a value of 1. The depolarizing pulse produces a change in spike time. The size of the phase shift and the change in the spike time are determined by the value of the phase resetting curve at the time of the stimulus. The evolution of phase over time in the absence of any perturbation is indicated by the dotted line. **(B)** Pulsed noise, like that used to measure spiking resonance, produces a sequence of phase shifts. Each pulse arrives at a phase determined by the entire sequence of preceding pulses. Pulses arriving at phases near the peak of the PRC are more influential than others, but the time of firing is determined by the entire waveform of input current. **(C)** Sinusoidal current produces a smoothly accumulating change in the time-evolution of phase. A sine wave stimulus can advance or delay the next action potential, depending on the phase of the stimulus relative to each spike.

notable exception is the extremely narrow peak near phase 1 in the SP neuron.

Constructing the Phase Models

To determine whether differences in the PRCs could account for the differential entrainment of SP neurons and LTS interneurons, we constructed phase models from the individual PRCs of each neuron, and from the mean PRCs of the two cell types. This allowed us to simulate the entrainment and spiking resonance experiments using phase-model cells, and compare the simulation with experimental results from the same cells. The phase model is governed by a single differential equation,

$$\frac{d\varphi}{dt} = F_{Cell} + (I_{Stim}(t) + \eta(t))Z(\varphi)$$

in which φ is the model cell's phase, F_{Cell} is the cell's unperturbed firing rate, $I_{\mathrm{Stim}}(t)$ is the stimulus current, $\eta(t)$ is the cell's intrinsic membrane noise, and $Z(\varphi)$ is the infinitesimal PRC measured experimentally. The evolution of phase in the model is illustrated in **Figure 7** (bottom row). In the absence of any stimulus current, the cell's phase evolves at a constant rate, F_{Cell}. In this stimulus-free and noise-free configuration, phase and time co-evolve and the model fires rhythmically. Application of a brief current pulse produces a sudden shift in phase, the magnitude of which is determined by the amplitude and duration of the pulse and the value of the PRC at the phase of stimulus application, $Z(\varphi)$. Because the stimulus alters the cell's phase, later stimuli would arrive at phases that could not be predicted from their timing alone. Complex stimuli, like the sequence of random pulses shown in the center column, produce a correspondingly complex walk of phase through time, with each stimulus pulse altering the phase at which all subsequent stimulus pulses arrive. This disconnect between phase and time separates the phase model used here from those employing the weak-coupling approximation, in which the phase of any applied stimulus is assumed to be equal to its time of application normalized by the cell's unperturbed period (e.g., Schwemmer and Lewis, 2011). All neurons have some intrinsic noise, caused by the stochastic opening of ion channels (White et al., 2000), and this limits the use of the weak-coupling approximation for predicting firing in real neurons, even for very simple inputs like single pulses (Ermentrout et al., 2011). The weak coupling approximation is more severely challenged by complex input waveforms like sinusoids, which cause a systematic deviation

between phase and time, as shown in the right column of **Figure 7**. Accurate prediction of neuronal activity in response to these stimuli requires the more general version of the phase model used here, in which phase may evolve non-linearly in time. However, the general form is not amenable to closed-form mathematical solution and must be evaluated numerically.

A Model of Entrainment

The experimental results showed that LTS interneurons can be entrained by oscillatory inputs over a wider range of frequencies than SP neurons, but do not have a second frequency preference determined by their membrane impedance resonance. Possibly, this difference in entrainment arises from a difference in the shape or size of their PRCs. We used phase models based on the average PRCs of the SP neuron and LTS interneuron samples (the PRCs in **Figures 6B,D**) and repeated the experiments shown for real neurons in **Figure 5** using these two neuron models. The unperturbed firing rate was set at 15 spikes/s in both cases, which was near the sample average for both cell types. The models included an estimate of the intrinsic noise of each cell type. On each time step of the integration, intrinsic noise was implemented by applying a current drawn from a normal distribution with a mean of zero. The standard deviation of the noise input was adjusted to reproduce the average coefficient of variation for our samples of SP neurons and LTS interneurons (0.10 and 0.12, respectively) in the absence of any stimulus using the method of Ermentrout et al. (2011). The results are shown in **Figure 8A**. Like the real neurons, the phase model of the SP neuron and the LTS neuron showed entrainment peaks at their unperturbed firing rates. They also showed smaller peaks near half and twice their firing rates, which were sometimes visible but less prominent in the real neurons. Also like the real neurons, the model LTS interneuron showed a much higher level of entrainment than SP neurons at all frequencies. As in real SP neurons, entrainment in the SP model was practically absent for input frequencies about 1.5 times the cell's unperturbed rate. In this phase model, all differences in entrainment must be attributable to differences in the two cells' PRCs.

Some of the difference in entrainment should result from the mean amplitude, rather than the shape of the PRC. The integral of the PRC (the amplitude of mode 0) is a measure of the response to the average current delivered during the interspike interval. It contributes to the response to sine waves of all periods except those that are integer multiples of the cell's firing rate (for which the stimulus averaged over the interspike interval is zero). The overall larger PRC of the LTS cell (larger mode 0) is therefore expected to affect entrainment at nearly all stimulus frequencies. To determine the influence of mode 0, we shifted the SP neuron PRC by a constant value to equalize its average to that of the LTS interneuron (**Figure 8A**). Equalizing mode 0 reduced the difference in entrainment between LTS and SP models at all frequencies, and eliminated most of the differences between cell types at frequencies less than the cells' firing rate. However, after equalizing mode 0, a substantial and consistent difference between LTS and SP models persisted at higher frequencies.

To dissect the contributions of PRC shape, we systematically eliminated frequency components of both cells' PRCs. **Figure 8B** shows the result of eliminating all PRC modes except modes 0 and 1, while equalizing mode 0 as in **Figure 8A** so that the only difference remaining is in mode 1. Mode 1 is only slightly different in the two PRCs, and the remaining difference between the models was also small and restricted to frequencies near the cells' firing rates. LTS interneuron and SP neuron PRCs differ greatly in the magnitude of mode 2. When each cell's mode 2 was restored, the entrainment at twice the cells' rates (about 30 Hz) returned, as did most of the difference in entrainment over the entire range above their firing rates. Additional replacement of mode 3 restored most of the remaining differences between models, especially at higher frequencies. Examination of the PRCs produced by reconstruction from modes 0–3 shows that these are not accurate reproductions of the original PRC shapes, but they do capture the large difference in the PRC skew between the cell types, including the LTS interneuron's increase in the PRC at late phases. The similarity between the results from the phase model in **Figure 8** and those from the real neurons in **Figure 5** suggests that the entrainment of LTS interneurons may be fully explained by their phase resetting properties without reference to membrane impedance resonance.

Spiking Resonance for Broadband Input in the Phase Model

The difference in entrainment of LTS interneurons and SP neurons by sine wave input is attributable to differences in their PRCs, which could be reduced to the differences in the modes shown in **Figures 6**, **8**. The differences between cell types in spiking resonance for broadband input share some resemblance to the frequency profile of entrainment by sine wave currents, as LTS interneurons showed much wider bandwidth of resonance and overall higher vector strength at all frequencies. To determine whether the differences in PRCs could explain these results, we repeated the spiking resonance experiment shown in **Figure 3** using phase models generated for each of the cells. Current pulse noise was applied to phase models with firing rates and PRCs from the experimental sample, and spiking resonance spectra were calculated for each model cell. Examples are shown in **Figures 9A,B**, and the spectra for each cell and the mean spectrum are superimposed for each cell type in **Figures 9C,D**. The phase models reproduced all the differences between LTS interneurons and SP cells, including the differences in maximal amplitude, frequency at the peak, peak offset, and bandwidth, seen in the corresponding neurons as shown in **Figures 9E–H**. These results indicate that the cell type differences in frequency-selectivity were all attributable to differences in the size and shape of the PRCs.

DISCUSSION

The input to striatal neurons from the cortex and other areas contains oscillatory components, and cells in the striatum often fire in a consistent phase relationship with that input (Courtemanche et al., 2003; Kalenscher et al., 2010; Howe et al., 2011; Leventhal et al., 2012). Phase-locking depends on cell type, with fast-spiking interneurons usually locking to high or low

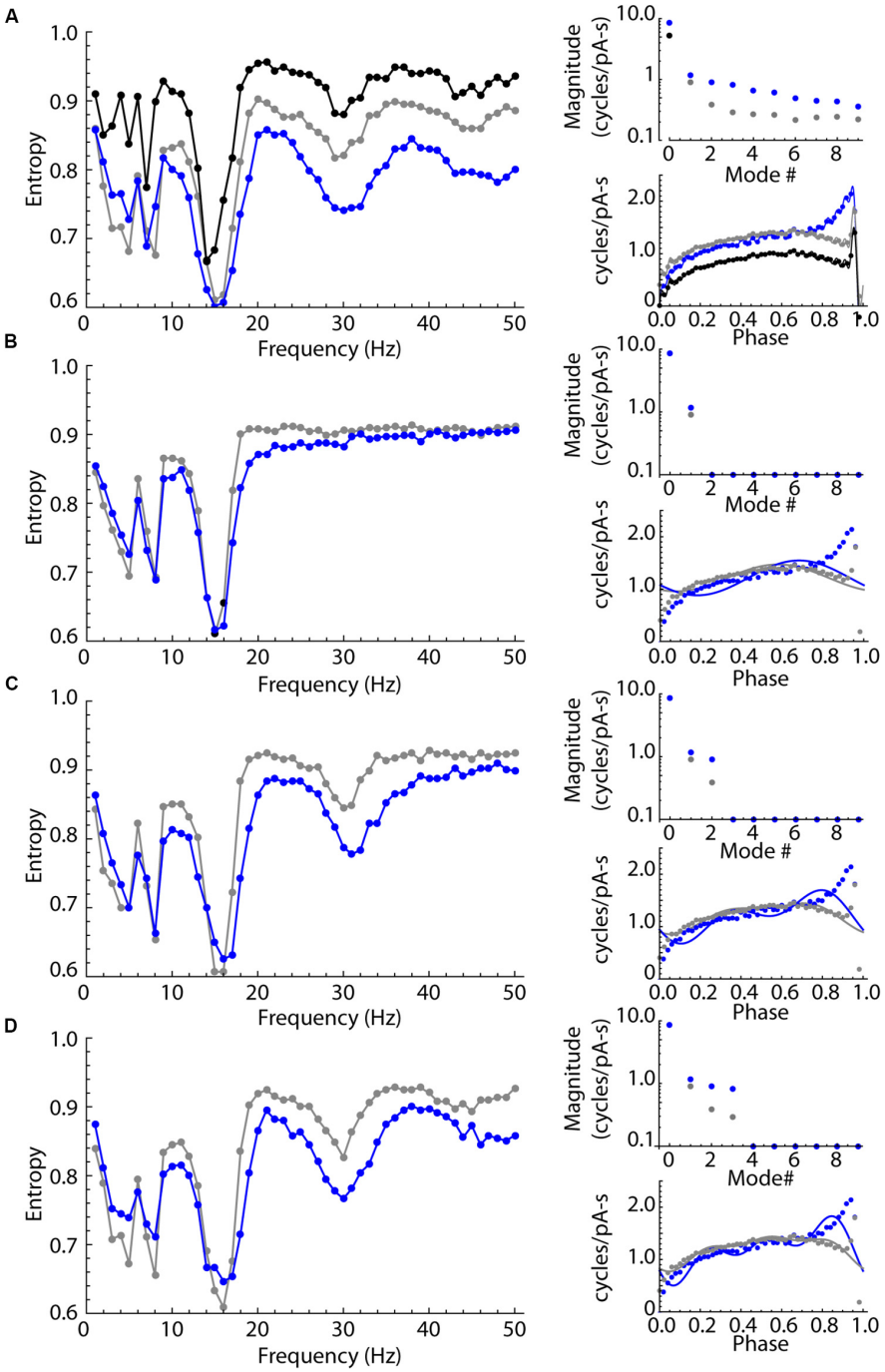

FIGURE 8 | Sinusoidal entrainment in phase models of the LTS interneuron (in blue) and the SP neuron (in black and gray). **(A)** Entrainment spectra from 1 to 50 Hz for the phase model LTS interneuron (blue) and the SP neuron (black) using a phase model with all modes present. To test for the influence of the DC component mode 0, the SP neuron PRC was shifted to have the same mode 0 as the LTS interneuron, and the spectrum for that version of the SP neuron model is shown in gray. This mode 0 equalization brought the entrainment spectra mostly into alignment for frequencies at and below the cells' unperturbed rate (15 spikes/s). The entrainment at higher frequencies continued to be different, with the SP neuron showing consistently higher entropy (less entrainment). The amplitudes of the first 10 modes in both PRCs are shown at right, including the shift in mode zero between the measured value for SP neurons (black), LTS neurons (blue) and the mode 0-equalized SP neuron (gray). The PRCs used in these simulations are shown at lower right in **(A)**. **(B)** The effect of equalizing mode 0 as above, and removing all modes higher than mode 1, which corresponds to the cell's firing rate. At right are shown the amplitudes of modes and the synthetic PRCs (lines) superimposed on the original PRCs (points). The only difference between PRCs is the difference in amplitude and phase of mode 1. The cell type difference in entrainment at high frequencies is absent, except for a small range of frequencies near the cells' firing rate. **(C)**. The same comparison except including differences in modes 1 and 2. The secondary (1:2) entrainment at twice the cells' frequencies is returned and the difference in entrainment in that frequency range is restored. **(D)** Restoring modes 1 through 3 reproduces most of the original differences in high-frequency entrainment between the cell types.

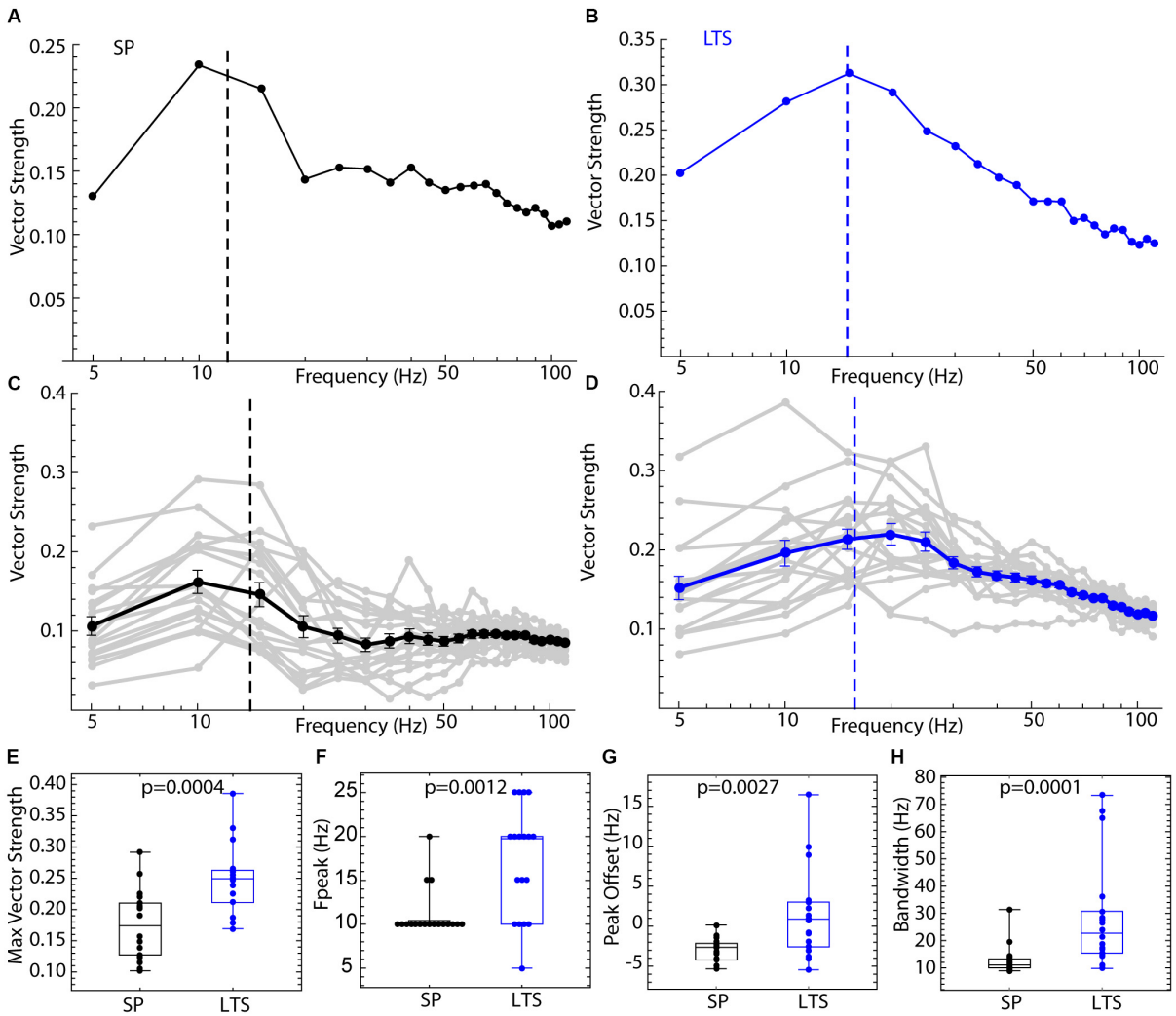

FIGURE 9 | Spiking resonance for broadband input in the phase model. For each of the 18 LTS interneurons and 18 SP neurons, the experimental PRC and unperturbed firing rate were used to generate spike trains in response to pulsed noise stimuli like those used to measure spiking resonance in the real cells. **(A)** An example spiking resonance spectrum from a phase model based on an SP neuron. The cell's firing rate is indicated by the dotted line. **(B)** An example phase model LTS interneuron shown the same way. **(C)** Superimposed spiking resonance spectra (gray) and the average spiking resonance (black) for 18 SP phase model neurons. **(D)** Superimposed individual spectra (gray) and average spectrum (blue) for phase models based on all 18 LTS interneurons. Error bars are standard errors of the mean at each frequency. The dotted lines indicate the average firing rates for the two groups of cells. **(E)** Model LTS interneurons showed a higher vector strength overall than model SP neurons. **(F)** The frequency at the peak resonance was higher in model LTS interneurons. **(G)** The difference between the firing rate and peak frequency for each cell was greater in model LTS interneurons. **(H)** The bandwidth of resonance (measured as shown in **Figure 2**) was greater in model LTS interneurons.

parts of the gamma frequency range, and SP neurons usually related to lower frequencies (Berke et al., 2004; Sharott et al., 2009; van der Meer and Redish, 2009). The frequency selectivity of each interneuron type may be a key to its circuit function, at least in the feed-forward configuration in which interneurons and principal cells receive the same input. In that case, inhibition may reduce the response of principal cells to specific frequency components in the shared input, but not others.

The usefulness of frequency-based measurements is not restricted to understanding responses to periodic inputs. All realizable input waveforms, even noise, can be decomposed into sine wave components. If cells have a greater sensitivity to some frequencies than others, their responses to complex input waveforms are colored by that sensitivity. The frequency sensitivity of neurons is also a measure of how fast they respond to changes in the stimulus. Cells that can entrain to very high frequencies respond strongly and quickly to brief stimuli or abrupt changes in input.

The Origin of Frequency Selectivity

Of course, the frequency selectivity of spike generation is not the only process imposing frequency selectivity on neurons in the striatal circuit. The frequency content of the input spike trains, synaptic current time course, dendritic filtering of synaptic

input and frequency dependent short term synaptic plasticity all determine the frequency content of the current delivered to the spike generation mechanism. In our experiments, a broad range of frequencies were present and equally represented in the stimuli delivered to the soma, to isolate the frequency sensitivity of the spiking mechanism. In the real circuits, some frequencies will be represented more than others.

What determines the frequency selectivity of a neuron's spiking response? Striatal SP cells have no subthreshold membrane resonance that could contribute to spiking resonance. Their spiking resonance and entrainment are the consequence of spike-triggered currents. Striatal LTS interneurons do have a membrane impedance resonance, but our results here show no influence of it on spiking resonance or entrainment when the cells are firing repetitively. Why does it not influence spiking? One possibility is that the membrane resonance of LTS neurons is engaged only at more depolarized membrane potentials. The calcium mechanism discovered by Song et al. (2016) to underlie membrane impedance resonance is engaged by ion channels that are not normally activated during the interspike interval. It is possible that membrane resonance could be influential in resumption of firing after a cell's autonomous firing has been blocked in the persistent depolarized state (Song et al., 2016). This function would be consistent with known instances of spike patterning by membrane impedance resonance, in which firing is triggered on peaks of a noisy input applied to a cell near, but below the current threshold for repetitive firing (e.g., Kispersky et al., 2012; Linaro et al., 2018). In contrast, during repetitive firing, the responses of the non-resonant SP neuron and the resonant LTS interneuron could both be predicted using a phase-resetting model that includes no explicit subthreshold dynamics.

Of course, not all neurons *in vivo* are firing repetitively at any one time. In the basal ganglia there are several cell types that fire repetitively most or all of the time, because their firing is driven autonomously. Neurons in the output nuclei, the GPi and SNr, are all autonomously active, as are the neurons in the middle structures, the subthalamic nucleus and GPe (Surmeier et al., 2005; Wilson, 2015). In the striatum, the somatostatin positive LTS interneurons are autonomously active (Beatty et al., 2012), as are the cholinergic interneurons (Bennett and Wilson, 1999) and a class of burst-firing GABAergic interneurons (Assous et al., 2018). Other cells, including the SP neurons and fast-spiking interneurons, are not autonomously active but fire repetitively in brief episodes in response to stimuli or during movements. During those responses, firing rates transiently go well into the range of frequencies at which the cells fire repetitively (e.g., Kimura, 1990). When a neuron is firing repetitively, even for brief periods, it is possible to characterize input-driven changes in spiking using the phase resetting method (Wilson, 2017; Higgs and Wilson, 2019). The phase model of the neuron is not completely general and it is possible to force a repetitively firing neuron out of the range of its applicability (Kogh-Madsen et al., 2012). A host of experimental and environmental conditions might alter repetitive firing and the phase resetting process. The most obvious example would be an input that abolishes repetitive firing altogether. Neurons must be depolarized above rheobase to satisfy the assumptions of the phase model. However, it is not required that neurons fire rhythmically. A neuron that would fire rhythmically in the absence of perturbing stimuli but is densely perturbed by inputs and so fires irregularly may still be predicable by phase methods (Wilson et al., 2014).

In the phase resetting formulation, the unique properties of each neuron are encapsulated in its PRC. The results presented here show that differences in PRC shape can contribute to the characteristic frequency sensitivity differences between neurons. PRCs come in a variety of shapes, and there are a variety of ways to parameterize their shapes. Fourier components are not fundamentally better than any other method, but they are best suited for describing the responses to sinusoidal inputs or sinusoidal components of complex inputs (Goldberg et al., 2013). The results reported here show that the first few modes of the PRC are directly responsible for frequency sensitivity differences between LTS interneurons and SP neurons. For a neuron to respond to input frequencies higher than its own firing rate, its PRC must contain correspondingly high frequency components.

Frequency-Selective Feed-Forward Inhibition

Striatal LTS interneurons provide feed-forward inhibition to the SP neurons, which are the striatal output cells. There is no recurrent excitation of interneurons by SP neurons, which are themselves GABAergic and inhibitory. SP neurons' narrow frequency sensitivities are centered on their individual firing rates, and thus are easily tuned by rate (Wilson, 2017). At any one moment, there are SP neurons firing at a wide variety of rates, and so there are cells poised to respond differentially to a variety of frequency components in the synaptic input. SP neurons are also very numerous, so fragmenting the frequency sensitivities among the population of SP neurons by firing rate does not cause a great loss of representational capacity. LTS interneurons, on the other hand, are outnumbered by SP neurons by a factor of 100 or more (Tepper et al., 2010), and single LTS interneurons provide feed-forward inhibition to many SP neurons. The ability of LTS neurons to phase-lock to a wide range of frequencies may allow them to provide phase-locked inhibition to the much more numerous SP neurons a broad frequency range.

Compared to SP neurons, LTS interneurons are more sensitive to synaptic input, as indicated by the overall larger amplitude of their PRCs, and their firing is more phase-locked to periodic inputs at frequencies higher than their own firing rate as indicated by the higher magnitudes of their PRC modes above mode 1. The only exception to the LTS interneurons superiority is the SP neuron's phase-locking to input frequencies near its own firing rate. The LTS interneuron is positioned to disrupt phase-locked firing in the SP neuron, by providing an inhibitory signal in phase with periodic excitatory inputs shared by both cell types. Because of its broadband response, the LTS neuron's firing is most entrained by the largest-amplitude periodic signal in the input, and its inhibition of entrainment of SP neurons will be most effective for that frequency. This inhibition could further suppress the entrainment of SP neurons whose firing rates differ

from the frequency of the dominant periodic input. Thus, the LTS interneuron could provide a broad surround inhibition to SP neurons, not in space, but in the frequency domain.

DATA AVAILABILITY STATEMENT

The datasets generated for this study are available on request to the corresponding author.

ETHICS STATEMENT

The animal study was reviewed and approved by Institutional Animal Care and Use Committee of the University of Texas at San Antonio.

AUTHOR CONTRIBUTIONS

JM, MH, SS, and CW designed the experiments and formulated the analysis. JM, SS, and CW collected the data and performed the analysis. JM, MH, SS, and CW wrote the manuscript.

FUNDING

This study was supported by NIH/NINDS grant NS097185 (to CW) and NIH/NIGMS R25GM060655 (to JM).

ACKNOWLEDGMENTS

Thanks to Sharmon Lebby for excellent technical help.

REFERENCES

Assous, M., Faust, T. W., Assini, R., Shah, F., Sidibe, Y., and Tepper, J. M. (2018). Identification and characterization of a novel spontaneously active bursty GABAergic interneuron in the mouse striatum. *J. Neurosci.* 38, 5688–5699. doi: 10.1523/jneurosci.3354-17.2018

Beatty, J. A., Song, S. C., and Wilson, C. J. (2015). Cell-type-specific resonances shape the responses of striatal neurons to synaptic input. *J. Neurophysiol.* 113, 688–700. doi: 10.1152/jn.00827.2014

Beatty, J. A., Sullivan, M. A., Morikawa, H., and Wilson, C. J. (2012). Complex autonomous firing patterns of striatal low-threshold spike interneurons. *J. Neurophysiol.* 108, 771–781. doi: 10.1152/jn.00283.2012

Bennett, B. D., and Wilson, C. J. (1999). Spontaneous activity of neostriatal cholinergic interneurons in vitro. *J. Neurosci.* 19, 5586–5596. doi: 10.1523/jneurosci.19-13-05586.1999

Berke, J. D., Okatan, M., Skurski, J., and Eichenbaum, H. B. (2004). Oscillatory entrainment of striatal neurons in freely moving rats. *Neuron* 43, 883–896. doi: 10.1016/j.neuron.2004.08.035

Courtemanche, R., Fujii, N., and Graybiel, A. M. (2003). Synchronous, focally modulated β-band oscillations characterize local field potential activity in the striatum of awake behaving monkeys. *J. Neurosci.* 23, 11741–11752. doi: 10.1523/jneurosci.23-37-11741.2003

Ermentrout, G. B., Beverlin, B., Troyer, T., and Netoff, T. I. (2011). The variance of phase-resetting curves. *J. Comput. Neurosci* 31, 185–197. doi: 10.1007/s10827-010-0305-9

Farries, M. A., and Wilson, C. J. (2012). Biophysical basis of the phase response curve of subthalamic neurons. *J. Neurophysiol.* 108, 1838–1855. doi: 10.1152/jn.00054.2012

Gittis, A. H., Nelson, A. B., Thwin, M. T., Palop, J. J., and Kreitzer, A. C. (2010). Distinct roles of GABAergic interneurons in the regulation of striatal output pathways. *J. Neurosci.* 30, 2223–2234. doi: 10.1523/jneurosci.4870-09.2010

Goldberg, J. A., Atherton, J. F., and Surmeier, D. J. (2013). Spectral reconstruction of phase response curves reveals the synchronization properties of mouse globus pallidus neurons. *J. Neurophysiol.* 110, 2497–2506. doi: 10.1152/jn.00177.2013

Higashi, H., Tanaka, E., Inokuchi, H., and Nishi, S. (1993). Ionic mechanisms underlying the depolarizing and hyperpolarizing afterpotentials of single spike in guinea-pig cingulate cortical neurons. *Neuroscience* 55, 129–138. doi: 10.1016/0306-4522(93)90460-w

Higgs, M. H., and Wilson, C. J. (2019). Frequency-dependent entrainment of striatal fast-spiking interneurons. *J. Neurophysiol.* 122, 1060–1072. doi: 10.1152/jn.00369.2019

Howe, M. W., Atallah, H. E., McCool, A., Gibson, D. J., and Graybiel, A. M. (2011). Habit learning is associated with major shifts in frequencies of oscillatory activity and synchronized spike firing in striatum. *Proc. Natl. Acad. Sci. U.S.A.* 108, 16801–16806. doi: 10.1073/pnas.1113158108

Hutcheon, B., and Yarom, Y. (2000). Resonance, oscillation and the intrinsic frequency preferences of neurons. *Trends Neurosci.* 23, 216–222. doi: 10.1016/s0166-2236(00)01547-2

Ibáñez-Sandoval, O., Tecuapetla, F., Unal, B., Shah, F., Koós, T., and Tepper, J. M. (2011). A novel functionally distinct subtype of striatal neuropeptide interneuron. *J. Neurosci.* 31, 16757–16769. doi: 10.1523/jneurosci.2628-11.2011

Kalenscher, T., Lansink, C. S., Lankelma, J. V., and Pennarts, C. M. A. (2010). Reward-associated gamma oscillations in ventral striatum are regionally differentiated and modulate local firing activity. *J. Neurophysiol.* 103, 1658–1672. doi: 10.1152/jn.00432.2009

Kawaguchi, Y. (1993). Physiological, morphological and histochemical characterization of three classes of interneurons in rat neostriatum. *J. Neurosci.* 13, 4908–4923. doi: 10.1523/jneurosci.13-11-04908.1993

Kimura, M. (1990). Behaviorally contingent property of movement-related activity of the primate putamen. *J. Neurophysiol.* 63, 1277–1296. doi: 10.1152/jn.1990.63.6.1277

Kispersky, T. J., Fernandes, F. R., Economo, M. N., and White, J. A. (2012). Spike resonance properties in hippocampal O-LM cells are dependent on refractory dynamics. *J. Neurosci.* 32, 3637–3651. doi: 10.1523/jneurosci.1361-11.2012

Kogh-Madsen, T., Butera, R., Ermentrout, G. B., and Glass, L. (2012). "Phase resetting neural oscillators: Topological theory versus the real world," in *Phase Response Curves in Neuroscience*, eds N. W. Schultheiss, A. A. Prinz, and R. J. Butera (New York, NY: Springer), 33–52.

Leventhal, D. K., Gage, G. J., Schmidt, R., Pettibone, J. R., Case, A. C., and Berke, J. D. (2012). Basal ganglia beta oscillations accompany cue utilization. *Neuron* 73, 523–536. doi: 10.1016/j.neuron.2011.11.032

Linaro, D., Biro, I., and Giugliano, M. (2018). Dynamical response properties of neocortical neurons to conductance-driven time-varying inputs. *Eur. J. Neurosci.* 47, 17–32. doi: 10.1111/ejn.13761

Netoff, T., Schwemmer, M. A., and Lewis, T. J. (2011). "Experimentally estimating phase response curves of neurons: theoretical and practical issues," in *Phase Response Curves in Neuroscience: Theory, Experiment and Analysis*, eds N. W. Schultheiss, A. A. Prinz, and R. J. Butera (New York, NY: Springer), 95–130.

Richardson, M. J., Brunel, N., and Hakim, V. (2003). From subthreshold to firing-rate resonance. *J. Neurophysiol.* 89, 2538–2554. doi: 10.1152/jn.00955.2002

Rotstein, H. G. (2017). Spiking resonances in models with the same slow resonant and fast amplifying currents but different subthreshold dynamic properties. *J. Comput. Neurosci.* 43, 243–271. doi: 10.1007/s10827-017-0661-9

Schwemmer, M. A., and Lewis, T. J. (2011). "The theory of weekly coupled oscillators," in *Phase Response Curves in Neuroscience: Theory, Experiment and Analysis*, eds N. W. Schultheiss, A. A. Prinz, and R. J. Butera (New York, NY: Springer), 3–32.

Sharott, A., Moll, C. K. E., Engler, G., Denker, M., Grün, S., and Engel, A. K. (2009). Different subtypes of striatal neurons are selectively modulated by cortical oscillations. *J. Neurosci.* 29, 4571–4585. doi: 10.1523/jneurosci.5097-08.2009

Simmons, D. V., Higgs, M. H., Lebby, S., and Wilson, C. J. (2018). Predicting responses to inhibitory synaptic input in substantia nigra pars reticulata neurons. *J. Neurophysiol.* 120, 2679–2693. doi: 10.1152/jn.00535.2018

Song, S. C., Beatty, J. A., and Wilson, C. J. (2016). The ionic mechanism of membrane potential oscillations and membrane resonance in striatal LTS interneurons. *J. Neurophysiol.* 116, 1752–1764. doi: 10.1152/jn.00511.2016

Surmeier, D. J., Mercer, J. N., and Chan, C. S. (2005). Autonomous pacemakers in the basal ganglia: who needs excitatory synapses anyway? *Curr. Opin. Neurobiol.* 15, 312–318. doi: 10.1016/j.conb.2005.05.007

Tepper, J. M., Tecuapetla, F., Koós, T., and Ibáñez-Sandoval, O. (2010). Heterogeneity and diversity of striatal GABAergic interneurons. *Front. Neuroanatomy* 4:150. doi: 10.3389/fnana.2010.00150

van der Meer, A. M., and Redish, A. D. (2009). Low and high gamma oscillations in rat ventral striatum have distinct relationships to behavior, reward, and spiking activity on a learned spatial decision task. *Front. Integr. Neurosci.* 3:9. doi: 10.3389/neuro.07.009.2009

White, J. A., Rubinstein, J. T., and Kay, A. R. (2000). Channel noise in neurons. *Trends Neurosci.* 23, 131–137. doi: 10.1016/s0166-2236(99)01521-0

Wilson, C. J. (2015). Oscillators and oscillations in the basal ganglia. *Neuroscientist* 21, 530–539. doi: 10.1177/1073858414560826

Wilson, C. J. (2017). Predicting the response of striatal spiny neurons to sinusoidal input. *J. Neurophysiol.* 118, 855–873. doi: 10.1152/jn.00143.2017

Wilson, C. J., Barraza, D., Troyer, T., and Farries, F. A. (2014). Predicting the responses of repetitively firing neurons to current noise. *PLoS Comput. Biol.* 10:e1003612. doi: 10.1371/journal.pcbi.1003612

Wilson, C. J., Higgs, M. H., Simmons, D. V., and Morales, J. C. (2018). Oscillations and spike entrainment. *F1000Res.* 7:F1000FacultyRev–1960. doi: 10.12688/f1000research.16451.1

Yarom, Y., Sugimori, M., and Llinás, R. (1985). Ionic currents and firing patterns of mammalian vagal motoneurons in vitro. *Neuroscience* 16, 719–737. doi: 10.1016/0306-4522(85)90090-9

Conflict of Interest: The authors declare that the research was conducted in the absence of any commercial or financial relationships that could be construed as a potential conflict of interest.

frontiers in Neural Circuits

ORIGINAL RESEARCH
published: 23 July 2020
doi: 10.3389/fncir.2020.00045

Auditory Long-Range Parvalbumin Cortico-Striatal Neurons

*Alice Bertero, Hector Zurita, Marc Normandin and Alfonso Junior Apicella**

Department of Biology, Neurosciences Institute, The University of Texas at San Antonio, San Antonio, TX, United States

Previous studies have shown that cortico-striatal pathways link auditory signals to action-selection and reward-learning behavior through excitatory projections. Only recently it has been demonstrated that long-range GABAergic cortico-striatal somatostatin-expressing neurons in the auditory cortex project to the dorsal striatum, and functionally inhibit the main projecting neuronal population, the spiny projecting neuron. Here we tested the hypothesis that parvalbumin-expressing neurons of the auditory cortex can also send long-range projections to the auditory striatum. To address this fundamental question, we took advantage of viral and non-viral anatomical tracing approaches to identify cortico-striatal parvalbumin neurons (**CS-Parv inhibitory projections → auditory striatum**). Here, we describe their anatomical distribution in the auditory cortex and determine the anatomical and electrophysiological properties of layer 5 CS-Parv neurons. We also analyzed their characteristic voltage-dependent membrane potential gamma oscillation, showing that intrinsic membrane mechanisms generate them. The inherent membrane mechanisms can also trigger intermittent and irregular bursts (stuttering) of the action potential in response to steps of depolarizing current pulses.

Keywords: long-range, gabaergic neurons, interneurons, parvalbumin-expressing, auditory cortex, excitation, inhibition, connectivity patterns

OPEN ACCESS

Edited by:
Eduardo Weruaga,
University of Salamanca, Spain

Reviewed by:
Paul George Anastasiades,
University of Bristol, United Kingdom
Shaowen Bao,
University of Arizona, United States

***Correspondence:**
Alfonso Junior Apicella
alfonso.apicella@utsa.edu

Received: *20 April 2020*
Accepted: *29 June 2020*
Published: *23 July 2020*

Citation:
Bertero A, Zurita H, Normandin M and Apicella AJ (2020) Auditory Long-Range Parvalbumin Cortico-Striatal Neurons. Front. Neural Circuits 14:45. doi: 10.3389/fncir.2020.00045

INTRODUCTION

Since the late 19th century, the Spanish neuroanatomist Santiago Ramon y Cajal postulated the importance of interneurons in the neocortex (Ramon y Cajal et al., 1988; Benavides-Piccione and DeFelipe, 2007). After observing and studying the neuronal diversity and anatomy in several mammalian species, he concluded that "*the functional excellence of the human brain is intimately linked to the prodigious abundance and unwonted wealth of forms of the so-called neurons with short axon*" (i.e., GABAergic interneurons; Cajal, 1897). Since then, the local connectivity and neuronal computations of GABAergic "interneurons" in the cerebral cortex, which comprise 15–20% of the whole neuronal population (Xu et al., 2010; Rudy et al., 2011), has been extensively studied. This leading to the overall principle that excitation is both local and long-range, while inhibition is described as being exclusively local (for review see: Isaacson and Scanziani, 2011; Tremblay et al., 2016). The existence of long-range GABAergic neurons in rats, cats and monkey has been proven anatomically since the 80s (Seress and Ribak, 1983; Ribak et al., 1986; Toth and Freund, 1992; McDonald and Burkhalter, 1993; Toth et al., 1993; Freund and Buzsaki, 1996; Tomioka et al., 2005, 2015; Higo et al., 2007, 2009; Tomioka and Rockland, 2007; Tamamaki and Tomioka, 2010; for review see: Caputi et al., 2013; Tremblay et al., 2016). However, only recent investigation

has been engaged to understand the functional significance of long-range GABAergic neurons and how different subtypes play distinct roles in cortical processing according to their differences in morphology, electrophysiology, molecular content, and synaptic connectivity patterns (Melzer et al., 2012, 2017; Lee et al., 2014; Rock et al., 2016, 2018; Zurita et al., 2018a; Bertero et al., 2019).

Evidence from our lab and others showed a direct inhibitory projection from the cortex to the striatum (Rock et al., 2016; Melzer et al., 2017), a basal ganglia area that is involved in the movement, reward-learning, and action selection behavior (Znamenskiy and Zador, 2013; Bahuguna et al., 2015; Xiong et al., 2015; Melzer et al., 2017; Guo et al., 2019). Melzer et al. (2017) demonstrated that locomotion could be modulated through direct stimulation of long-range GABAergic neuron terminals in the motor striatum. Moreover, Rock et al. (2016) found that long-range GABAergic somatostatin-expressing neurons in the auditory cortex control the spike timing/generation in both direct and indirect pathway spiny projection neurons of the auditory striatum. Overall this suggests that the balance of direct excitation/inhibition can promote the transformation of the acoustic signal into reward-learning and action-selection behaviors. However, no evidence of long-range GABAergic parvalbumin-expressing neurons from the auditory cortex to the auditory striatum has been shown yet. The present study focused on three main goals: (1) determine the laminar and areal distribution of cortico-striatal parvalbumin-expressing (CS-Parv neurons) neurons in the auditory cortex; (2) describe the anatomical and electrophysiological properties of these neurons; and (3) determine the impact that the voltage-dependent membrane potential resonance has on the spiking pattern of layer 5 CS-Parv neurons.

We addressed this fundamental question using both anterograde and retrograde anatomical methods in conjunction with *in vitro* electrophysiology. Using these techniques, we demonstrate, for the first time, the existence of parvalbumin-expressing GABAergic neurons in the auditory cortex with projections to the auditory striatum. We found that steps of depolarizing current pulses in layer 5 CS-Parv neurons can trigger intermittent and irregular bursts (stuttering) of action potentials. Also, our data suggest that while the first action potential of layer 5 CS-Parv neurons is triggered by an oscillation, whose frequency is in the gamma frequency, the second action potential was maintained by a different membrane mechanism. In sum, we describe a previously unknown long-range parvalbumin-expressing cortico-striatal projection (**CS-Parv inhibitory projections → auditory striatum**) that is engaged in cortico-striatal communication.

MATERIALS AND METHODS

All animal procedures were approved by the Institutional Animal Care and Use Committee at the University of Texas at San Antonio. Procedures followed animal welfare guidelines set by the National Institutes of Health. Mice used in this experiment were housed in a vivarium with a 12 h light/dark schedule and *ad libitum* access to mouse chow and water.

Transgenic Mouse Lines

The following mouse lines were used in this study:

C57BL/6: (Charles river, strain code#027); Parv-Cre: B6.129P2-Pvalbtm1(cre)Arbr/J (The Jackson Laboratory, stock #017320); ROSA-tdTomato reporter: B6.CG.Gt(ROSA)26Sortm14 (CAG-tdTomato)Hze/J (The Jackson Laboratory, stock #007914); ROSA-eYFP reporter: B6.129X1-Gt(ROSA)26Sortm1(EYFP)Cos/J (The Jackson Laboratory, stock #006148); Parv-Cre homozygous mice were crossed with ROSA-tdTomato or ROSA-eYFP reporter homozygous mice to generate Parv-Cre/tdTomato and Parv-Cre/YFP parvalbumin-containing neurons expressing both Cre and tdTomato/eYFP lines, respectively.

Viral Vectors

AAV1-CAG-FLEX-EGFP-WPRE, titer 3.1×10^{13} VG/ml (Addgene viral prep # 51502-AAV1).

Stereotaxic Injections

Basic Surgical Procedures

As described in our previous studies (Rock and Apicella, 2015; Rock et al., 2016, 2018; Zurita et al., 2018a,b; Bertero et al., 2019), mice were initially anesthetized with isoflurane (3%; 1 L/min O_2 flow) in preparation for the stereotaxic injections detailed in the next section. Mice were head-fixed on a stereotaxic frame (model 1900, Kopf Instruments) using non-rupture ear bars, and anesthesia was maintained at 1–1.5% isoflurane for the duration of the surgery. Injections were performed using a pressure injector (Nanoject III, Drummond Scientific) mounted on the stereotaxic frame and were delivered through a borosilicate glass injection pipette (Wiretrol II, Drummond Scientific) with a taper length of ∼30 mm and a tip diameter of ∼50 μm. The pipette remained in place for 5 min before to start injecting at 4 nl/min rate and was left in place for 5 min after the injection to avoid viral backflow along the injection tract. Both male and female mice, P35–P40 at the time of the infusion, were used in these experiments.

Retrograde Labeling

CS-Parv neurons in the auditory cortex were retrogradely labeled by injecting 30 nl of Red Retrobeads (lumafluor) in the right striatum of C57BL/6 (n = 3 animals from 1 litter) or Parv-Cre/YFP (n = 3 animals from 1 litter). Stereotaxic coordinates: 1.4 mm posterior and 3.4 mm lateral to bregma at a depth of 2.8 mm below the surface of the brain. Mice were transcardially perfused 14–21 days post injections and brain fixed and sliced for immunofluorescence and antibody staining.

Thirty nanolitre of AAV1-flex-GFP were injected in the right striatum of Parv-Cre/tdTomato (n = 7 animals, from 4 litters). Stereotaxic coordinates: 1.4 mm posterior and 3.35 mm lateral to bregma at a depth of 2.8 mm below the surface of the brain. Mice were processed for electrophysiology 21–28 days post-injection.

In vitro Slice Preparation and Recordings

As described in our previous studies (Rock and Apicella, 2015; Rock et al., 2016, 2018; Zurita et al., 2018a,b; Bertero et al., 2019), mice were anesthetized with isoflurane and

decapitated. Coronal slices (300 μm) containing the area of interest were obtained on a vibratome (VT1200S, Leica) in a chilled cutting solution containing the following (in mM): 100 choline chloride, 25 $NaHCO_3$, 25 D-glucose, 11.6 sodium ascorbate, 7 $MgSO_4$ 3.1 sodium pyruvate, 2.5 KCl, 1.25 NaH_2PO_4, 0.5 $CaCl_2$. Slices were then incubated in oxygenated artificial cerebrospinal fluid (ACSF) in a submerged chamber at 35–37°C for 30 min and then room temperature (21–25°C) until recordings were performed. ACSF contained the following (in mM): 126 NaCl, 26 $NaHCO_3$, 10 D-glucose, 2.5 KCl, 2 $CaCl_2$, 1.25 NaH_2PO_4, 1 $MgCl_2$; osmolarity was ∼290 Osm/L.

Whole-cell recordings were performed in 31–33°C ACSF. Thin-walled borosilicate glass pipettes (Warner Instruments) were pulled on a vertical pipette puller (PC-10, Narishige). They typically were in the range of 3–5 MΩ resistance. Intrinsic properties were recorded in the current-clamp configuration using a potassium-based intracellular solution which contained the following (in mM): 120 potassium gluconate, 20 KCl, 10 HEPES, 10 phosphocreatine, 4 ATP, 0.3 GTP, 0.2 EGTA, and 0.3–0.5% biocytin).

Signals were sampled at 10 kHz and filtered (lowpass filter) at 4 kHz. Pharmacological blockers used were as follows: CPP (5 μM; Tocris Bioscience), NBQX (10 μM; Abcam), and gabazine (25 μM; Abcam). Hardware control and data acquisition were performed with the Matlab-based Ephus package[1] (Suter et al., 2010). The resting membrane potential (V_m) was calculated in current-clamp mode ($I = 0$) immediately after breaking in. Series (R_s) and input resistance (R_{in}) were calculated in voltage-clamp mode ($V_{hold} = -70$ mV) by giving a −5 mV step, which resulted in transient current responses. R_s was determined by dividing the voltage step amplitude by the peak of the capacitive current generated by the voltage step. The difference between baseline and steady-state hyperpolarized current (ΔI) was used to calculate R_{in} using the following formula: $R_{in} = -5\ mV/\Delta I - R_s$. Subthreshold and suprathreshold membrane responses in current-clamp were elicited by injecting −100 to +500 pA in 50 pA increments at V_{rest}. The first resulting AP at rheobase (the minimal current of infinite duration (experimentally limited to 1 s) required to generate an AP) was analyzed for AP width. The adaptation ratio was measured at the current step that gave the closest APs firing rate to 20 Hz. The adaptation ratio was calculated, dividing the first instantaneous frequency by the last (f_2/f_{last}) or dividing the third instantaneous frequency by the fifth (f_3/f_5). Afterhyperpolarization (AHP) was calculated as the difference between the threshold and minimum membrane potential after an action potential. For the analysis of oscillations and action potential bursts, we used 20 s long steps of depolarizing current pulses. These current pulses were able to trigger intermittent and irregular bursts (stuttering) of action potential while holding the membrane potential at −70 mV. The analysis of membrane potential oscillations and relation with action potential generation was performed as described in Bracci et al. (2003). Briefly, the oscillation threshold was defined as the level of membrane potential at which spontaneous depolarizing and hyperpolarizing fluctuations of the membrane potential were larger than 1 mV. The cycle period of each oscillation was designated as the interval between two consecutive peaks. The inverse of the period was used to determine the frequency of the oscillation.

Spectral analysis of the oscillations was performed by using a Fast Fourier transform (FFT) custom MATLAB (MathWorks) routine. For oscillation analysis, $T_{Osc.Peak2\text{-}Osc.Peak1}$ was defined as the time interval between the last two consecutive peaks of oscillations before a burst of APs. $T_{SpikeOsc.Peak2}$ was defined as the interval between the last peak before an AP burst and the time when the last oscillation peak was higher than that of the preceding membrane potential. Oscillation slope (expressed in mV ms^{-1}) was calculated as the slope of the line connecting an oscillation trough to the next oscillation peak. The pre-spike slope was defined as the slope of a line connecting the trough of the last oscillation before a spike burst and the point where the last peak oscillation amplitude was greater than the membrane potential amplitude. In each neuron analyzed a comparison between $T_{Osc.Peak2\text{-}Osc.Peak1}$ and $T_{SpikeOsc.Peak2}$ and between the oscillation slope and the pre-spike slope was performed by analyzing each of the pause and bursts obtained during 20 s of long of near-threshold current steps. In each cell, at least five spike bursts (preceded by oscillations) were used for analysis. The histogram of the values of $T_{SpikeOsc.Peak2}/T_{Osc.Peak2\text{-}Osc.Peak1}$ and pre-spike slope/oscillation slope were obtained by calculating these ratios for each spike burst from different CS-Parv neurons.

Immunohistochemistry and Histology

As described in our previous studies (Rock and Apicella, 2015; Rock et al., 2016, 2018; Zurita et al., 2018a,b; Bertero et al., 2019), mice were transcardially perfused with 4% paraformaldehyde, brains were dissected, postfixed overnight at 4°C, and coronal sections (100 μm thick) were obtained with a vibratome (VT1200S, Leica). Immunohisto-chemical procedures were performed on free-floating sections using: rabbit anti-GFP (for YFP, 1:500; Abcam, catalog #ab13970), rabbit anti-parvalbumin (1:1,000, Abcam, catalog #ab11427), primary antibodies, followed by AlexaFluor 633 goat anti-rabbit IgG (1:500; Life Technologies) and AlexaFluor 488 goat anti-chicken IgG (1:500; Abcam) secondary antibodies.

During whole-cell recordings, neurons were filled with an internal solution containing 0.3–0.5% biocytin. Filled neurons were held for at least 20 min, and then the slices were fixed in a formalin solution (neutral buffered, 10% solution; Sigma-Aldrich) for 1–7 days at 4°C. Fixed slices were then thoroughly washed in PBS, incubated overnight in a 4% streptavidin (AlexaFluor 680 conjugate; Life Technologies) solution, washed in PBS, and mounted with Fluoromount-G (Southern Biotech) on a glass microscope slide.

Quantification of Laminar Distribution of CS-Parv Neurons in the AC

The mice, previously injected with a retrograde tracer into the auditory striatum (see "Materials and Methods" section

[1]https://www.janelia.org/open-science/ephus

above), were deeply anesthetized with 5% isoflurane, perfused, and the brain was fixed using the same procedures as previously described in Bertero et al. (2019). The fixed brain was then sectioned into 100 μm thick slices on a vibrating microtome. After washing in PBS, the slices were mounted on microscope slides, and images were taken with an Olympus SZX7 microscope. Images of 100 μm thick slices expressing the retrograde label GFP were rotated, cropped, and the brightness/contrast was adjusted in ImageJ. Using Adobe Illustrator, epifluorescence images were overlaid onto images from the Allen Mouse Brain Reference Atlas for coronal slices (Allen Institute for Brain Science) and aligned using anatomical landmarks such as the rhinal fissure and subcortical structures. Dorsal, primary, and ventral areas of the AC were identified using the overlaid reference images. A similar approach was used to determine the laminar distribution of the CS-Parv neurons. The distance from the pia to the white matter was normalized to 1,000 μm. Auditory cortex layer boundaries were determined as described in Ji et al. (2016) and Zurita et al. (2018b), as normalized depth from pia: layer 1 = 0–158 μm; layer 2/3 = 159–368 μm, layer 4 = 369–526 μm, layer 5 = 527–789 μm; layer 6 = 790–1,000 μm.

Data Analysis

Figure error bars represent SEM. Data analysis was performed offline using custom MATLAB (MathWorks) routines. Group comparisons were made using the rank-sum test, and one-way *ANOVA*, with significance defined as $^{*}p < 0.05$, and $^{**}p < 0.01$.

RESULTS

Anatomical Identification of CS-Parv Neurons in the Auditory Cortex

To visualize long-range GABAergic projection originating in the auditory cortex (AC) and terminating in the ipsilateral striatum, we conditionally expressed GFP in parvalbumin-expressing neurons (from this point forward referred to as CS-Parv neurons) by injecting AAV1-Flex-GFP into the right striatum of Parv-Cre/tdTomato transgenic mice (animals: $n = 7$; litter $n = 6$; **Figure 1**). GFP was colocalized with Parv/tdTomato-expressing neurons in the AC (**Figures 1B,C**). We used this viral approach because data from our study and others (Rothermel et al., 2013; Rock et al., 2016, 2018; Zurita et al., 2018a; Bertero et al., 2019) demonstrated that AAV1-Flex. Flex viral vectors exhibited both anterograde and retrograde transfection capabilities. From the center of the injection, the spread of the viral tracer was estimated at around 600 μm anteroposterior, and 900 μm dorsal-ventral/medial-lateral, with negligible or no evidence of tracer spillover in the somatosensory cortex above the injection site (**Figure 1B**). This approach allowed us to identify transfected somata in the ipsilateral AC and to highlight long-range cortico-striatal parvalbumin-expressing neurons (**Figure 1C**).

In a different set of experiments, to visualize long-range parvalbumin projections originating in the AC and terminating in the striatum, we injected a well-established non-viral retrograde tracer, such as red Retrobeads, into the right auditory striatum of Parv-Cre/eYFP transgenic mice (animals: $n = 3$; litters: $n = 1$) and analyzed retrogradely labeled neurons in the AC (**Figure 1D**). The injection site was centered primarily in the posterior region of the dorsal striatum. From the center of the injection, the spread of the tracer was estimated at around 500 μm anteroposterior, 900 μm dorsal-ventral, and 500 μm medial-lateral. For all our injections (animals: $n = 3$; litters: $n = 1$), there was no evidence and/or negligible of tracer spillover or deposit in the somatosensory cortex above the injection site. Using this method, we found that, in CS-Parv neurons' thin optical slices (1 μm thick optical slices, 1–3 slices z projection), YFP was colocalized with red RetroBeads of the AC in the hemisphere ipsilateral to the injection site (**Figure 1E**, middle panels). We further characterized the CS-Parv neurons by confirming their expression of the calcium-binding protein parvalbumin (Parv; **Figure 1E**, right panels). To further corroborate our findings, we injected wild type C57BL/6 mice (animals: $n = 3$; litter $n = 1$), the genetic background of Parv-Cre, and derived reporter lines, with red Retrobeads in the right striatum (**Figure 2A**). Again, we were able to confirm the presence of double-positive Parv/Red beads neurons in the hemisphere of the AC ipsilateral to the injection site (**Figure 2B**). Our results demonstrate that, independently of the mouse strain and reporter used, long-range CS-Parv neurons can be detected in the AC with well-established retrograde tracing techniques. The red beads retrogradely methods further validated our viral retrograde approach, which exhibits high labeling efficiency of CS-Parv neurons in the auditory cortex of injected mice.

Areal and Laminar Characterization of CS-Parv Neurons in the Auditory Cortex

We first determined the areal distribution of CS-Parv neurons. Double labeled tdtomato/GFP neurons were observed in both the dorsal-ventral and anteroposterior extent of the AC, including the dorsal, primary, and ventral auditory cortex (**Figure 3A**), as quantified in **Figure 3B** ($n = 6$ animals, $n = 9$ slices, 300 μm thick). The distribution of the retrogradely labeled neurons is indicated in **Figure 3** by overlapping coronal epifluorescence images with reference images from the online mouse atlas provided by the Allen Institute for Brain Science[2] (coronal atlas). Next, we determine the laminar distribution of the CS-Parv neurons in the AC. Using the same method described above, we found that cortical CS-Parv neurons were spanning all layers of the AC in the hemisphere ipsilateral to the injection site (**Figure 3C**: $n = 140$ neurons, six animals from 5 litters, average depth 0.549 ± 0.018 mm from pia). Interestingly, as already shown for the auditory cortical excitatory projections (Znamenskiy and Zador, 2013), the majority (50.79%; Layer 5 and 6 CS-Parv neurons: $n = 71/140$ neurons) of the long-range CS-Parv neurons were located in the infragranular region of the AC (L1, 0.33 ± 0.30 neurons; L2/3, 4.33 ± 2.19 neurons; L4, 6.83 ± 1.77 neurons; L5, 8.33 ± 3.15 neurons; L6, 3.5 ± 0.94 neurons). These multiple complementary data sets confirm that, in the entire AC, long-range CS-Parv GABAergic neurons send a direct projection to the posterior region of the dorsal striatum (**CS-Parv inhibitory projections → striatum**).

[2]http://mouse.brain-map.org/static/atlas

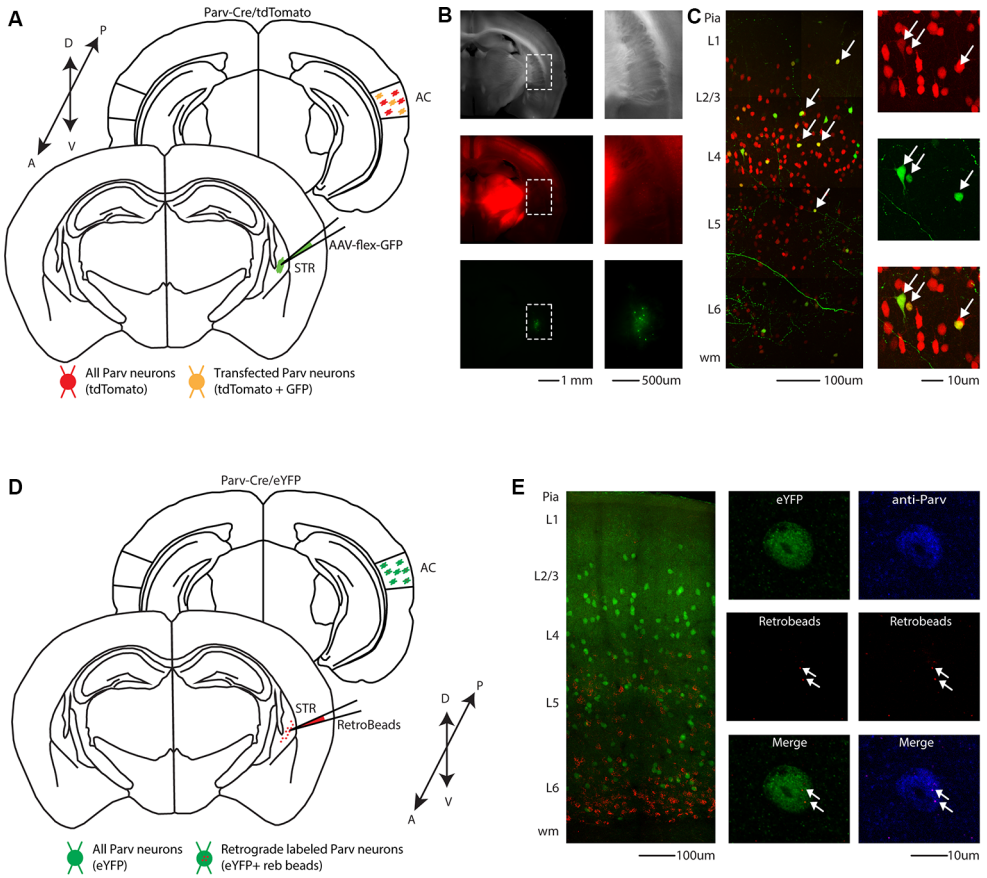

FIGURE 1 | Cre-dependent identification of CS-Parv neurons in the mouse auditory cortex. **(A)** Schematic depicting injection site using the Parv-Cre-tdTomato transgenic mouse line to identify CS-Parv neurons in the auditory cortex. Bottom, striatum: green AAV1-Flex-GFP injection site; yellow Parv somata were coexpressing GFP and tdTomato; red Parv-tdTomato-positive interneurons. Top, auditory cortex: yellow CS-Parv somata coexpressing GFP and tdTomato; red Parv-tdTomato-positive "interneurons." **(B)** Epifluorescence images of Parv tdTomato-positive neurons. Left, top: bright-field image of a slice containing the striatum injection site of AAV1-Flex-GFP in the Parv-Cre.tdTomato transgenic mouse line. Left, middle: tdTomato-expressing Parv neurons in the Parv-Cre-tdTomato transgenic mouse line. Left, bottom: GFP-positive Parv neurons in the dorsal striatum containing the viral injection of AAV1-Flex-GFP in the Parv-Cre-tdTomato transgenic mouse line. The dashed line indicates the striatum boundaries containing the striatum injection site of AAV1-Flex-GFP. Right, top: higher magnification of the bright-field image of a slice containing the striatum injection site of AAV1-Flex-GFP in the Parv-Cre.tdTomato transgenic mouse line. Right, middle: higher magnification image of tdTomato-expressing Parv neurons in the Parv-Cre-tdTomato transgenic mouse line. Right, bottom: higher magnification image of GFP-positive Parv neurons in dorsal striatum containing the viral injection of AAV1.GFP.Flex in the Parv-Cre-tdTomato transgenic mouse line. **(C)** Left: overlay image of GFP-positive Parv neurons in the auditory cortex identified by viral injection of AAV1.GFP.Flex and Parv neurons in the Parv-Cre-tdTomato transgenic mouse line. The dashed box and the arrows indicate the location of the somata of CS-Parv neurons. Top, right: tdTomato-expressing Parv neurons in the Parv-Cre-tdTomato transgenic mouse line. Middle, right: GFP-positive CS-Parv neurons in the auditory cortex retrogradely identified by viral injection of AAV1.GFP.Flex in the dorsal striatum of the Parv-Cre-tdTomato transgenic mouse line. Bottom right: overlay of GFP and tdTomato images. The arrow indicates the location of the CS-Parv neurons. **(D)** Schematic depicting the injection site of red RetroBeads using the Parv-Cre/eYFP transgenic mouse line to identify CS-Parv neurons in the auditory cortex. Bottom, striatum: red RetroBeads injection site; Top: auditory cortex: red beads retro-labeled CS-Parv neurons identified by YFP expression (green). **(E)** Left: overlay image of red-positive neurons in the auditory cortex identified by injection of retrograde beads in the dorsal striatum and Parv eYFP neurons in the Parv-Cre/eYFP transgenic mouse line. Middle: high magnification epifluorescence images of Parv red-beads-positive neurons. Middle, top: eYFP-positive Parv neurons in the auditory cortex in the Parv-Cre-tdTomato transgenic mouse line. Middle, center: CS-Parv neurons identified by anatomical retrograde labeling in the Parv-Cre-eYFP transgenic mouse line. Middle, bottom: overlay of eYFP and retrograde beads labeled CS-Parv neurons. The arrows indicate the location of the red beads in the CS-Parv neurons. Top, right: CS-Parv neurons immunostained with anti-Parv. Middle, right: CS-Parv neurons identified by anatomical retrograde labeling in the Parv-Cre-eYFP transgenic mouse line. Bottom, right: overlay of CS-Parv neurons immunostained with anti-parv and retrograde beads labeled CS-Parv neurons. The arrows indicate the location of the red beads in the CS-Parv neuron.

Morphological and Electrophysiological Characterization of Layer 5 CS-Parv Neurons

Given the higher abundance of CS-Parv in layer 5 of the auditory cortex, and the high heterogeneity of GABAergic neurons, especially across different cortical layers, we decided to focus our study on layer 5 CS-Parv neurons that were retrogradely labeled by injecting the AAV1-Flex-GFP virus in the right striatum. This approach allowed us to visually identify and record from layer 5 CS-Parv neurons using whole-cell patch-clamp (**Figure 1C**).

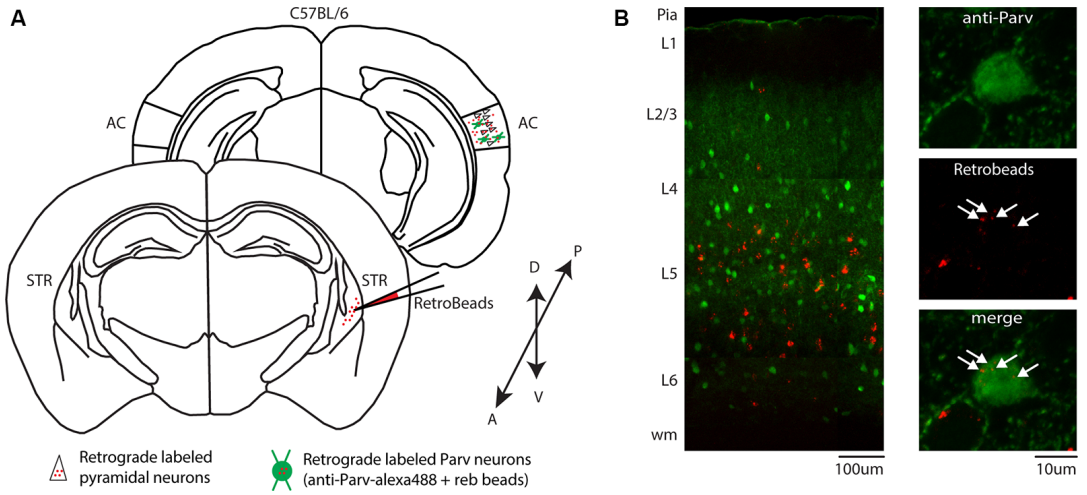

FIGURE 2 | Identification of CS-Parv neurons in the auditory cortex of wild-type C57BL/6 mice. **(A)** Schematic depicting the injection site of red RetroBeads using the wild-type C57BL/6 mouse line to identify CS-Parv neurons in the auditory cortex. Bottom, striatum: red RetroBeads injection site; Top, auditory cortex: red beads retrolabeled pyramidal and CS-Parv neurons identified by immunostaining with anti-Parv. **(B)** Left: overlay image of red-positive retrograde labeled neurons in the auditory cortex identified by injection of retrograde beads in the dorsal striatum and anti-Parv in the wild-type C57BL/6 mouse line. Top, right: anti-Parv immunostained Parv neurons in the auditory cortex in the wild-type C57BL/6 mouse line. Middle, right: CS-Parv neurons identified by anatomical retrograde labeling in the wild-type C57BL/6 mouse line. The arrow indicates the location of the red beads in the CS-Parv neurons. Bottom, right: overlay of CS-Parv neurons immunostained with anti-Parv and retrograde beads labeled CS-Parv neurons. The arrow indicates the location of the red beads in the CS-Parv neurons.

Confocal images of biocytin filled layer 5 CS-Parv neurons (12 out of 15 recorded neurons) showed that they are similar to Parv basket-like GABAergic neurons in their cortical axonal morphology (**Figure 4A**), aspiny and multipolar dendritic arbor (**Figure 5**), and send collaterals towards the subcortical white matter. In addition to the basket-like axonal morphology, a small fraction (4 out of 15 recorded neurons) exhibit a translaminar axonal distribution (data not shown). Electrophysiological characterization (n = 15 neurons, animals n = 8, litters n = 5) showed that layer 5 CS-Parv neurons display common fast-spiking properties, including a high rheobase (the smallest current step evoking an action potential: 306.7 ± 20.04 pA), a narrower action potential compared to somatostatin-expressing GABAergic neurons in the AC (**Figure 4B**, inset, showing a representative layer 5 CS-Parv action potential in black and a representative somatostatin-expressing neuron action potential in red; layer 5 CS-Parv action potential half-width: 0.26 ± 0.01 ms), large fast afterhyperpolarization (fAHP: −17.6 ± 0.6 mV), and no synaptic integration (data not shown; **Table 1**). Basic electrophysiology properties include: resting membrane potential, −74.7 ± 0.89 mV; input resistance, 96.4 ± 6.8 MΩ; membrane time constant, 0.54 ± 0.04 ms (**Figure 4C**). The sustained current injection also showed that the majority of layer 5 CS-Parv neurons exhibit a suprathreshold stuttering firing pattern (Li and Huntsman, 2014), and continuous firing of action potential under a further increase of current injection that can reach up to 150 Hz (F/I summary plot: F/I slope: 0.56 ± 0.04 Hz/pA; **Figure 4D**, left and middle panels) with no spike frequency adaptation (SFA ratio: 0.97 ± 0.03 third/fifth, 0.84 ± 0.04 s/last; **Figure 4D**, right panel). Near-threshold, the initial instantaneous frequency was 47.16 ± 4.95 Hz, remained constant in time and increased in responses to higher depolarizing current steps (**Figure 4E**). Further characterization of membrane potential in response to depolarizing currents also showed that the frequency content of membrane oscillations shifted towards the gamma band with increasing steps of depolarizing current pulses (see representative membrane potential oscillations and frequency content analysis in **Figure 4F**). We, therefore, analyzed the frequency content for each cell to the near-threshold current steps and three consecutive steps of less depolarizing current pulses (minus 50 pA each, **Figure 4G**). This allowed us to demonstrate that the gamma band frequency content of membrane oscillation was correlated to the membrane potential increase. As shown in **Figure 4G**, no gamma oscillations are detected up to 100 pA below threshold, and the gamma content significantly increased at 50 pA below threshold (column factor $p = 1.36 \times 10^{-11}$, f = 34.32 one-way *ANOVA*; multiple comparisons: step 1 vs. step 2 p = 0.97, step 2 vs. step 3 p = 0.0014, step 3 vs. step 4 $p < 0.00001$, step 2 vs. step 3 p = 0.005, step 2 vs. step 4 $p < 0.00001$, step 3 vs. step 4 p = 0.0001). This increase in gamma-range oscillation was also correlated to the increase in membrane potential (**Figure 4G**). These data show that layer 5 CS-Parv neuronal morphology and intrinsic electrophysiological properties resemble those of the Parv basket-like "interneurons."

Relationship Between Membrane Near-Threshold Oscillations and Action Potentials

We then characterized the relationship between membrane oscillations and action potentials train generation at

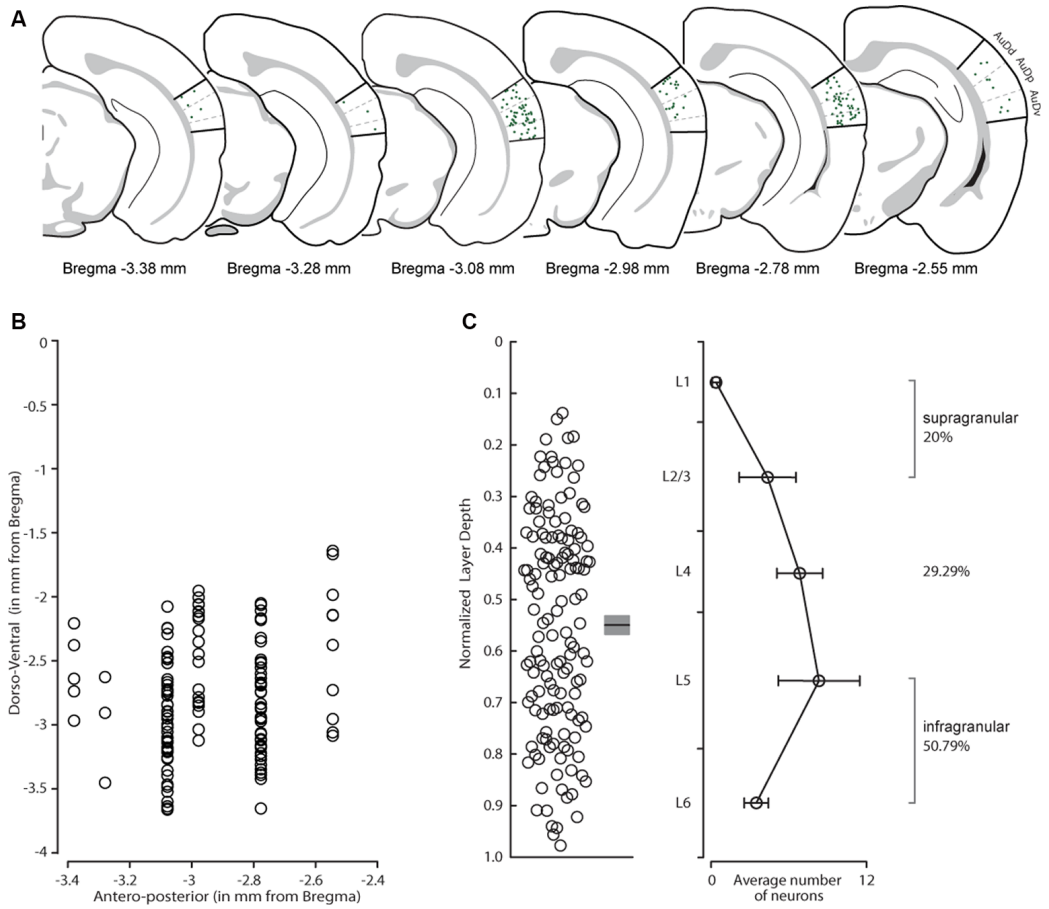

FIGURE 3 | Distribution of CS-Parv neurons in the mouse auditory cortex. **(A)** Anatomical distribution of CS-Parv neurons in serial coronal sections. **(B)** The plot shows the anteroposterior and dorso-ventral soma location of CS-Parv neurons. **(C)** Left: plot shows the group average soma location (±SEM) of CS-Parv neurons. The black circles mark the absolute distances from the pia to the soma (CS-Parv: n = 140 neurons, n = 6 animals). Right: laminar distribution of CS-Parv neurons. For the quantification of SC-Parv neurons coexpressing GFP and tdTomato, the distance between the pia and white matter was normalized to 1,000 μm, and the cortex was divided into layers based on the following thicknesses: L1, 0–158 μm; L2/3, 159–368 μm; L4, 369–526 μm; L5, 501–750 μm; and L6, 790–1,000 μm. Average neuron number per layer was calculated among n = 6 animals: L1, 0.33 ± 0.30 neurons; L2/3, 4.33 ± 2.19 neurons; L4, 6.83 ± 1.77 neurons; L5, 8.33 ± 3.15 neurons; L6, 3.5 ± 0.94 neurons.

near-threshold current steps. Since standard 1 s depolarizing current pulses were not suitable to describe the firing pattern of layer 5 CS-Parv neurons, we studied their (n = 11 neurons) response to long (20 s) current pulses, which evoked sequences of bursts (stuttering) and pauses (**Figure 6A**).

The striking feature of the layer 5 CS-Parv neurons was that their firing pattern during long positive current steps was mostly unpredictable. A typical profile of the layer 5 CS-Parv neurons behavior and instantaneous firing rate during these repeated bursts is shown in **Figures 6A,B**. The duration of the action potential bursts and the pauses varied from 100 ms to up to 10 s when a near-threshold current was injected at the same resting membrane potential, reaching up to 193 spikes per burst and ranging from 16.8 Hz to 101.6 Hz spiking rate, in a visible random fashion (**Figure 6C**). Before the first burst, two out of 10 neurons showed an initial single action potential at the start of the pulse, followed by a long pause. In comparison, three out of 10 neurons displayed a long delay before the first burst with no previous action potential. High-frequency repetitive firing following this pause exhibited a non-adaptation through the entire duration of the burst. The instantaneous firing frequency of each burst was nearly constant across them, as shown in **Figure 6D** in which the firing rate of the first 10 bursts was normalized on the first burst firing rate and, on average, no difference was found between the first and subsequent bursts firing rate (p = 0.9705, f = 0.31 one-way *ANOVA*).

In the period between the bursts, the membrane potential showed a near-threshold oscillation in the gamma frequency range (**Figure 6E**). The amplitude of these oscillations varied between 1 and 4 mV, and the frequency range was voltage-dependent and was completely absent at the resting membrane potential (data not shown). The presence of synaptic blockers during our recording [NBQX (10 μM), CPP (5 μM), and gabazine (25 μM)] and the observation that the oscillation frequencies are voltage-dependent

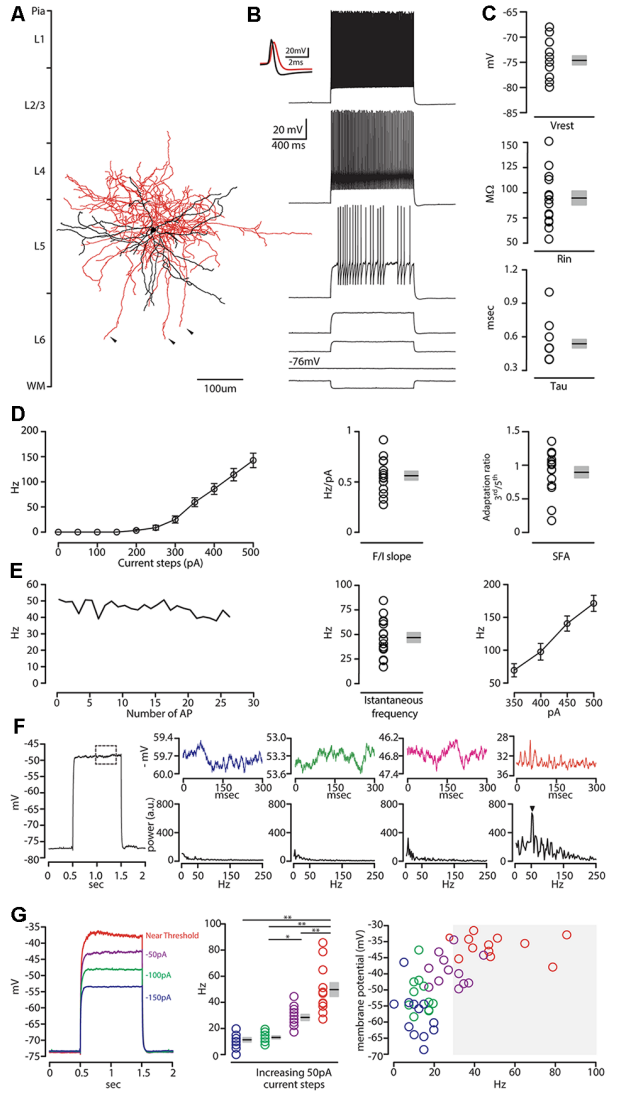

FIGURE 4 | Morphological and electrophysiological characterization of layer 5 CS-Parv neurons. **(A)** Morphological reconstruction of one CS-Parv neuron (dendrites, black; axons, red). **(B)** Train of action potentials recorded in a layer 5 GFP/tdTomato-positive CS-Parv neuron during step current injection (1.0 s, 100 pA pulse). Top left inset, single action potential from layer 5 GFP/tdTomato-positive CS-Parv neuron (black); compare to an action potential from a corticostriatal somatostatin-expressing GABAergic neuron (red). **(C)** Top: summary plot of V_{rest}: resting membrane potential; Middle: R_i: input resistance; Bottom: Tau: membrane time constant; from CS-Parv neurons (neurons $n = 15$, animals $n = 8$; including group average ± SEM). **(D)** Left: summary plot of averaging firing rate per current step amplitude recorded from layer 5 CS-Parv neurons (black circles, $n = 15$ neurons, animals $n = 8$), including group averages (± SEM). Middle: same as in panel **(D)** for F/I slope. Right: same as in panel **(D)**, for *spike frequency adaptation (SFA; f*3rd/*f*5th). **(E)** Left: representative instantaneous frequency near-threshold as a function of the number of AP from layer 5 CS-Parv. Middle: summary plot of instantaneous frequency near-threshold from layer 5 CS-Parv neurons (black circles, $n = 15$ neurons, animals $n = 8$), including group averages (± SEM). Right: summary plot of instantaneous firing frequency in response to increasing depolarizing current (350–500 pA, 50 pA increments) for layer 5 CS-Parv neurons (black circles, $n = 15$ neurons, animals $n = 8$) including group averages (± SEM). **(F)** Left: example

(*Continued*)

FIGURE 4 | Continued

trace in response to depolarizing 1 s current. The dashed box represents the region analyzed in the left section of the panel. Top row: representative membrane potential oscillation at four increasing 50 pA increasing current steps to reach near-threshold membrane potential (blue trace: −150 pA; green trace: −100 pA; magenta trace: −50 pA of the near-threshold current; red trace: membrane potential near-threshold defined as 0 pA current injection from near-threshold). Bottom row: corresponding frequency contents of the four different membrane potentials. The arrow indicates the peak in the gamma range (52 Hz) of membrane oscillation at the near-threshold potential. **(G)** Left: representative membrane potential changes in response to 1 s long 50 pA increasing current steps (blue, green, and purple traces) to reach near-threshold (red trace). Middle: frequency content of membrane oscillation in response to increasing current steps, color code as in panel **(G)** (left, $n = 12$ neurons, including group average ± SEM, $^*p < 0.05$; $^{**}p < 0.001$). Right: membrane potential in response to increasing current steps [color code as in panel **(G)** (left as a function of the frequency content of membrane oscillation]. Gray box: gamma frequency range (30–100 Hz, $n = 12$ neurons).

suggested that this phenomenon is generated by intrinsic properties of the layer 5 CS-Parv neurons and was not preferentially reliant on the cortical connectivity patterns of these neurons.

We then investigated the relationship between layer 5 CS-Parv neurons oscillations and action potential (AP) generation. One clear aspect in the sequence of bursts and membrane potential oscillations was that the first spike of the burst was almost consistently preceded by oscillations and appeared to be triggered by the depolarizing phase of the oscillations. To test this quantitively, we used the same method used by Bracci et al. (2003). The Bracci's method allowed us to investigate: (1) if the depolarizing membrane potential between the one that preceded the first spike of the burst with the preceding oscillation had a similar phase relationship; and (2) if the slope of the rising phase between them was comparable. To test the first point, we quantified the time interval between three consecutive oscillation peaks. $T_{Osc.Peak2\text{-}Osc.Peak1}$ was defined as the time interval between the last two consecutive oscillation peaks before a burst of action potentials (**Figure 7A**); and $T_{SpikeOsc.Peak2}$ as the interval between the last peak before an action potential burst and the time when the last oscillation peak amplitude was greater than the membrane potential amplitude (**Figure 7A**). As illustrated in **Figure 7A**, this allowed us to quantify the two-time intervals between the three oscillation peaks ($T_{Osc.Peak2\text{-}Osc.Peak1}$; $T_{Spike\text{-}Osc.Peak2}$).

The values of $T_{Spike\text{-}Osc.Peak2}$ were not statistically significant form $T_{Osc.Peak2\text{-}Osc.Peak1}$ (rank-sum test, $p = 0.9$), as shown by the summary histogram ($n = 11$ neurons), and their ratio was distributed around unity (Summary plot: **Figure 7A**, right). This suggests that the first AP of the burst was triggered by near-threshold oscillation potential that has the same peak-time intervals. To test the second point, we compared the slope of the depolarizing phase of the spike oscillation to that of the oscillation preceding the spike (**Figure 7B**, left). Again, the ratio of the spike and the oscillation slope was distributed around unity (Summary plot: **Figure 7B**, right). The slope data are consistent with the idea that the spike oscillation and the

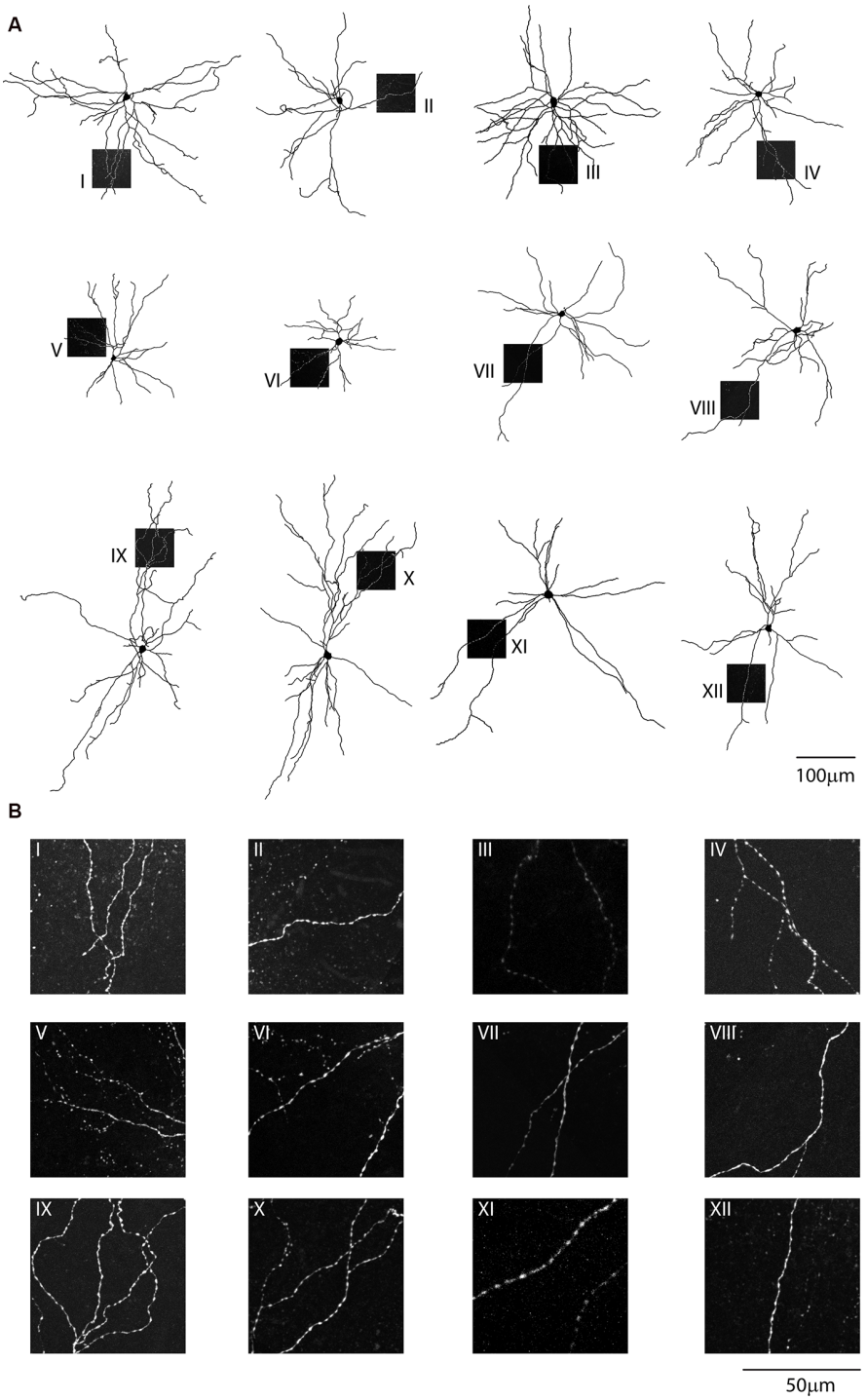

FIGURE 5 | Single-cell reconstruction of the dendritic arborization of biocytin-filled retrograde labeled CS-Parv neurons. **(A)** All neurons are oriented towards pia and the dashed boxes indicate the location of the dendritic confocal images for each neuron. **(B)** Each neuron displays no dendritic spines, as shown in the corresponding high-resolution confocal images.

oscillation preceding the spike are characterized by the same kinetics. Altogether, these data suggest that the first action potential of the burst in the layer 5 CS-Parv neurons is caused by an oscillation in the gamma range that was sufficiently large to take the neuron above the firing threshold. Our data also indicated that the spike frequency was always higher than the near-threshold oscillation frequency (data not shown), suggesting that the second action potential of the burst is not

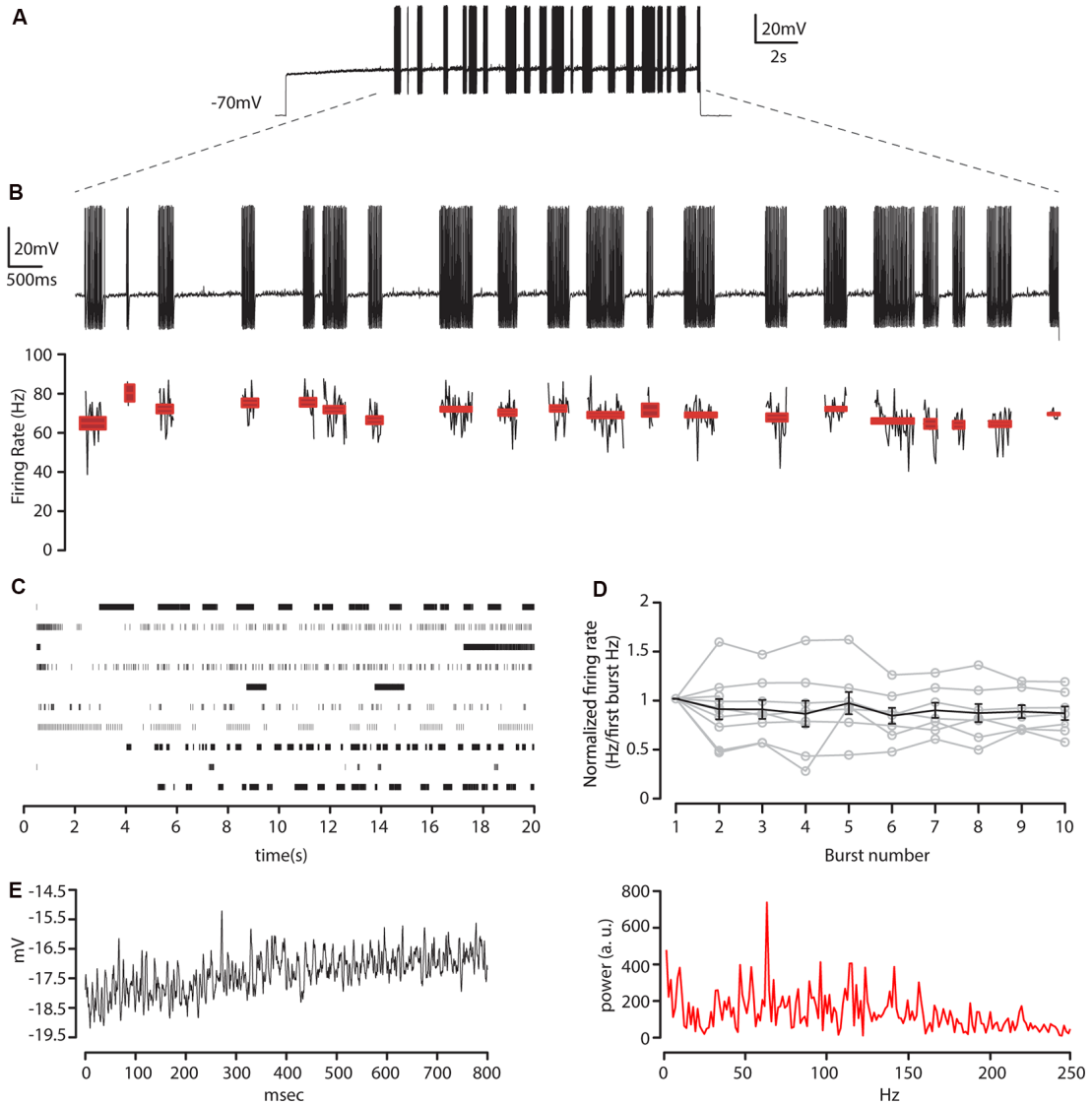

FIGURE 6 | Membrane resonance in response to near-threshold sustained current steps. **(A)** Train of action potentials recorded at −70 mV from layer 5 CS-Parv neurons in response to a step of depolarizing current pulse (20 s, pA = near-threshold). **(B)** Top: enlargement of bursts in **(A)**. Bottom: instantaneous firing rate for each burst and spike count for each burst, including average ± SEM **(C)** Raster plot for each neuron recorded in response to steps of depolarizing current pulses near-threshold (n = 10 neurons). **(D)** The average plot of firing rate for the first 10 bursts normalized to the average firing rate of the first burst of action potentials (gray traces: n = 11 neurons), including average ± SEM (black trace). **(E)** Left: an example of a membrane potential trajectory between bursts of action potentials. Right: corresponding frequency spectrum of the near-threshold oscillations during the pause. The peak of the spectrum corresponds to the gamma-band frequency (63.2 Hz).

triggered by the same oscillatory mechanism of the first action potential in the burst. To test this hypothesis, we compared the slope of the first and second action potential (**Figure 7C**). The summary plot shows that the slope of the second action potential is statistically faster than the first action potential (first spike slope: 0.52 ± 0.04 mV/ms; second spike slope: 29.95 ± 7.62 mV/ms; n = 11, rank-sum test, $p = 2.1 \times 10^{-4}$). The second actional potential differed from the first action potential also in the membrane threshold (first spike threshold: −27.84 ± 1.54 mV; second spike threshold: −32.99 ± 1.25 mV; rank-sum test, p = 0.0265) and amplitude (first spike amplitude: 39.46 ± 1.25 mV; second spike amplitude: 46.29 ± 1.08 mV; rank-sum test, 3.8×10^{-5}; **Figure 7D**).

These data suggest that while the first AP of the layer 5 CS-Parv neuron burst is triggered by an oscillation, whose frequency is in the gamma range, the second action potential was maintained by a potential different membrane mechanism.

DISCUSSION

In this study, we tested the hypothesis that parvalbumin-expressing neurons in the AC project to the ipsilateral dorsal

TABLE 1 | Layer 5 cortico-striatal Parvalbumin neurons intrinsic properties.

Parameter	Mean ± SEM
Resting potential (mV)	−74.66 ± 0.88
Input resistance (MΩ)	96.4 ± 6.77
Membrane time constant Tau (ms)	0.54 ± 0.03
Rheobase (pA)	306.66 ± 20.03
After hyperpolarization (mV)	−17.60 ± 0.64
After depolarization (mV)	14.011 ± 0.57
Action potential threshold (mV)	−33.58 ± 1.34
Action potential height (mV)	43.20 ± 1.96
Action potential halfwidth (ms)	0.25 ± 0.01
F/I slope (Hz/pA)	0.56 ± 0.04
Spike frequency adaptation (third/fifth)	0.96 ± 0.03
Spike frequency adaptation (second/last)	0.84 ± 0.04

striatum. Here, we identify a previously unknown auditory cortico-striatal long-range parvalbumin-expressing projection (**CS-Parv inhibitory projections → auditory striatum**; **Figure 8**) with two complementary labeling techniques and in different mouse lines.

As we described previously (Rock et al., 2016, 2018; Zurita et al., 2018a; Bertero et al., 2019), the employed viral and non-viral labeling approaches (restricted injection volume (focal injection) and variability in transfection leading to incomplete coverage of the cortical region) prevents us from determining the absolute number of CS-Parv neurons. Despite these caveats, our viral retrograde labeling approach allowed us to routinely determine the cortical distribution, axonal morphology, and electrophysiological properties of layer 5 long-range CS-Parv neurons and establish the presence of voltage-dependent membrane potential oscillations. We also showed that the layer distribution of CS-Parv neurons, with higher concentrations in the infragranular layer, is not reflecting the overall Parv neurons distribution, which generally shows higher abundancy in layer IV (Tremblay et al., 2016), paralleling the distribution of excitatory auditory cortico-striatal projections (Znamenskiy and Zador, 2013).

Layer 5 CS-Parv Neurons: From Anatomical-Electrophysiological Properties to Circuits

Previous data from our lab highlighted that another class of long-range parvalbumin-expressing neurons projecting from the left auditory cortex to the contralateral one (corticocortical-Parv, CC-Parv neurons) can be distinguished from local Parv neurons based on their intrinsic properties (Zurita et al., 2018a). In particular, layer 5 CC-Parv neurons are characterized by a lower input resistance, a higher rheobase, a larger AHP, and lower instantaneous frequency at threshold compared to layer 5 non-callosal projecting Parv neurons (Zurita et al., 2018a), all features comparable to the hereby described layer 5 CS-Parv neurons. This observation lead to ask whether long-range Parv neurons sharing common electrophysiological properties can also share their projection pattern (i.e., can CC-Parv neurons also project to the ipsilateral striatum?) or constitute two segregate classes of long-range inhibitory neurons (i.e., are CC-Parv neurons only engaged in cortico-cortical circuitry while CS-Parv neurons only in corticofugal circuits)? These are only a few of the numerous questions that still need to be addressed concerning

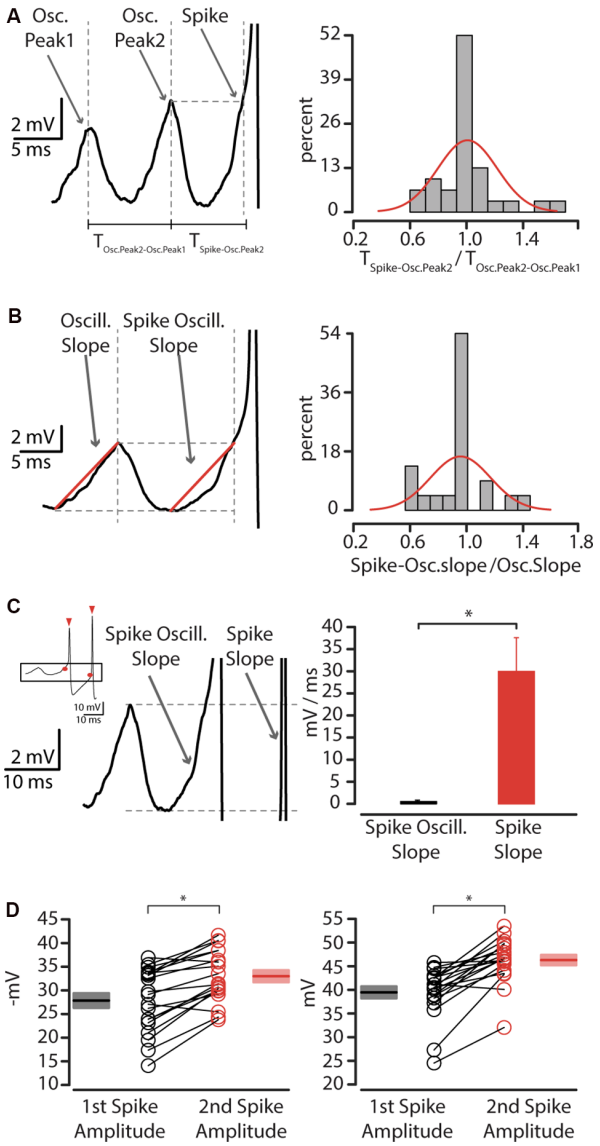

FIGURE 7 | The relation between membrane oscillations and action potentials. **(A)** Left: the interpeak interval between oscillations preceding action potential. Right: quantification of the ratio between the interpeak interval of the last oscillation peak and spike, and the interpeak interval between second to last and last oscillation peak before an action potential, showing unitary distribution (mu = 1.007, sigma = 0.210). **(B)** Left: oscillation slope and spike-oscillation slope before first action potential. Right: quantification of the ratio between spike-oscillation slope and oscillation slope, showing unitary distribution (mu = 0.953, sigma = 0.213). **(C)** Left: spike-oscillation slope compared to spike slope. The inset shows a representative trace of action potentials thresholds (red circle) and amplitude (red triangles) Right: summary plot of the spike-oscillation slope, expressed in mV/ms ± SEM, $*p < 0.05$. **(D)** Left: plot of first ($n = 35$, black circles) and second ($n = 35$, red circles) AP threshold recorded from layer 5 CS-Parv neurons, including group average (±SEM, $*p < 0.05$). Right: Plot of first ($n = 35$, black circles) and second ($n = 35$, red circles) AP amplitude recorded from layer 5 CS-Parv neurons, including group average (±SEM, $*p < 0.05$).

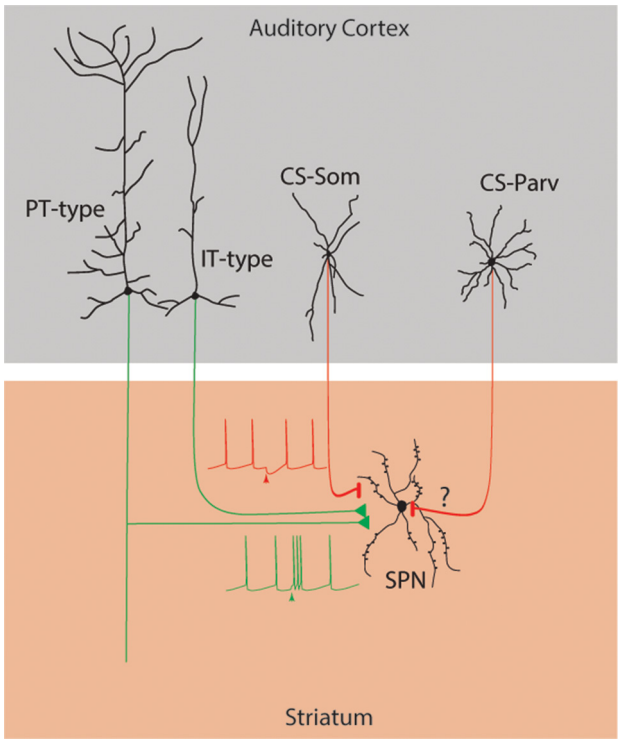

FIGURE 8 | Summary diagram: Long-range cortico-striatal CS-Parv neurons. Green lines: excitatory inputs from intratelencephalic (IT-type) and projecting-type (PT-type) layer 5 pyramidal neurons. Red lines: inhibitory input from long-range GABAergic CS-Som and CS-Parv neurons.

long-range GABAergic circuits in the neocortex. A crucial line of investigation will be to characterize how CS-Parv neurons may differ from local parvalbumin-expressing "short-axons interneurons." For example, are the excitatory and inhibitory connectivity patterns of CS-Parv neurons similar and/or different to those with local short-axons parvalbumin-expressing "interneurons" (Xu and Callaway, 2009; Apicella et al., 2012; Pfeffer and Beltramo, 2017)? Do CS-Parv neurons modulate network oscillation (Buzsáki and Draguhn, 2004; Buzsáki and Wang, 2012)? Do CS-Parv neurons have different embryonic development as already demonstrated for the long-range GABAergic hippocampal neurons (Picardo et al., 2011; Christenson Wick et al., 2019)? Do CS-Parv neurons have different gene expression profiles (for review see Huang and Paul, 2019)? Do CS-Parv neurons form depressing inhibitory synapses as reported for parvalbumin-expressing basket-like "interneurons" (Reyes et al., 1998; Silberberg, 2008)? Does electrical synapse couple CS-Parv neurons, and if so, are they only electrically-coupled with the neurons expressing the similar molecular markers (for review see Connors, 2017)? Do CS-Parv co-release GABA and other neurotransmitters (Burnstock, 1976)? Do cortico-striatal long-range GABAergic neurons modulate cognition and behavior? Further studies will be fundamental to address all these numerous questions regarding long-range GABAergic circuits in the cortex.

Layer 5 CS-Parv Neurons: From Circuits to Auditory Response Selectivity

Our results on layer 5 CS-Parv neurons demonstrate that these neurons morphologically resembled basket-like neurons, with massive axonal arborization in layer 5 that can span through layer IV and VI, and send collaterals towards the white matter and subcortical target(s). This suggests that layer 5 CS-Parv neurons are not only involved in long-range corticofugal circuits (together with excitatory neurons) but can also be embedded in local circuits involved in cortical sound processing as their short-range counterparts (Sun et al., 2013). Previous studies have shown that parvalbumin-expressing neurons receive input from different pathways (Helmstaedter et al., 2009; Xu and Callaway, 2009; Bagnall et al., 2011; Kubota et al., 2011; Tukker et al., 2013; Pfeffer and Beltramo, 2017), and have examined the dynamics of the membrane potential and mapped the sensory space of GABAergic "interneurons" (Niell and Stryker, 2008; Liu et al., 2009, 2010; Gentet et al., 2010; Kerlin et al., 2010; Runyan et al., 2010; Runyan and Sur, 2013; Li et al., 2015; Resnik and Polley, 2017) describing the existence of neurons that are characterized by broad and high tuned responses.

Also, studies in both motor and sensory cortex have characterized different connectivity patterns between subtypes of layer 5 pyramidal neurons and GABAergic "interneurons" (Markram, 1997; Morishima and Kawaguchi, 2006; Brown and Hestrin, 2009a,b; Dani and Nelson, 2009; Morishima et al., 2011; Apicella et al., 2012). Particularly, Sakata and Harris (2009) observed that, during a sound presentation, layer 5 thick-tufted neurons (such as layer 5 cortico-striatal excitatory/glutamatergic projecting-type (PT-type) neurons) received weaker inhibition than slender neurons [such as layer 5 cortico-striatal excitatory/glutamatergic intratelencephalic-type (IT-type) neurons]. More recently, Sun et al. (2013) suggested that intrinsic bursting pyramidal neurons (such as PT-type cortico-striatal neurons) have mechanisms of synaptic integration that are broader than pyramidal neurons with regular spiking properties (such as IT-type cortico-striatal neurons). Moreover, Sun et al. (2013) speculated the parvalbumin-expressing neurons are capable of providing feedforward inhibitory input preferentially to the PT-type neurons.

In this view, our finding of the existence of layer 5 CS-Parv neurons requires further experiments focused to better characterize the local synaptic connectivity partners of long-range CS-Parv neurons, and their activity in response to sensory stimuli. This will be crucial for the understanding of connectivity patterns of these neurons and their role in cortical auditory processing.

Layer 5 CS-Parv Neurons: Cortical Oscillations

The anatomical and electrophysiological properties underlying different cell-types of long-range GABAergic neurons, as well as their connectivity patterns within the cortex is virtually unknown. A crucial goal is to determine the differences

between CS-Parv neurons and local parvalbumin-expressing "short-axons interneurons" in the generation of locally cortical oscillations and the propagation along the cortico-striatal pathway. Cortical rhythms are a well-established feature of cortical neuronal activity that has been observed across a wide range of cortical regions (Buzsáki and Wang, 2012). The growing body of evidence that long-range GABAergic and glutamatergic/excitatory neurons, across different cortical areas, innervate the same target region (Tomioka et al., 2005, 2015; Tomioka and Rockland, 2007; Lee et al., 2014; Rock et al., 2016; Melzer et al., 2017; Zurita et al., 2018a; Bertero et al., 2019) invite to speculate that these two opposing forces can dynamically contribute to oscillations between different brain areas.

In the cortex, neuronal activity synchronization, especially in the gamma-frequency (30–100 Hz), has been supposed to enable communication between pyramidal neurons across areas of the brain to facilitate learning, attention, and cognitive behavior. Particularly, the circuits underlying gamma oscillations are thought to depend entirely on Parv neurons with local axonal arborization (Buzsáki and Wang, 2012). Buzsáki et al. (2004), using a computational model of excitatory and inhibitory neurons, demonstrated that by adding long-range GABAergic neurons to the neuronal model increased the synchronization of the entire network as was showed by the emergence of a clear oscillation. Despite theoretical and computer modeling studies showing that long-range GABAergic neurons are crucial for cortical oscillations, there is no study yet that has resolute the function of these neurons in cortical oscillation across multiple brain areas. The intrinsic oscillatory properties of CS-Parv neurons mirror the characteristics of striatal fast-spiking neurons, as described by Bracci et al. (2003). Their study revealed that such voltage-dependent oscillations were generated by an intrinsic membrane mechanism that did not require fast synaptic transmission and depended on sodium but not calcium conductance. They also showed how a small additional injected current during the rising phase of oscillation was able to trigger a new burst of an action potential that largely outlasted the current pulse, suggesting that the correct timing of synaptic input on near-threshold membrane potential oscillation can result in long-lasting effects. This result invites to speculate that sodium conductance can be the underlying mechanism of CS-Parv intrinsic generation of gamma-oscillations in membrane potential, and the triggering of the fast-spiking burst. However, an additional study from the cortex (Golomb et al., 2007) and striatum (Sciamanna and Wilson, 2011) showed that not only sodium but also potassium conductance (Kv1 Channels) contributes to both gamma resonance and stuttering properties of the parvalbumin-expressing neurons.

Further experiments aiming at understanding the ionic mechanism and circuit involved in the triggering and termination of CS-Parv action potential bursts, and the channel composition of their subcellular compartments, will be fundamental better to understand their role in long-range GABAergic oscillatory mechanisms. Also, it has been demonstrated striatal local field potentials (LFPs) are characterized by gamma oscillations that are differentially modulated during behavior (e.g., DeCoteau et al., 2007; Berke, 2009). Particularly, Cowan and Wilson (1994) and Stern et al. (1997) have established that some of these striatal LFPs are generated from cortico-striatal excitatory inputs that are also locked in the gamma frequency. Here, we have shown that the striatum receives not only glutamatergic excitatory inputs from the auditory cortex but also inhibitory inputs from parvalbumin-expressing neurons (**CS-Parv inhibitory projections → auditory striatum**). Further investigations focusing on the role of striatal partners of auditory CS-Parv neurons will be fundamental. Can these long-range projections target the direct and/or indirect pathway? Can they exert their functions through direct inhibition on spiny projection neurons or cause disinhibition by targeting local interstriatal GABAergic neurons? How can CS-Parv neurons modulate local and long-range circuits during auditory processing?

Although beyond the target of the present study, it is intriguing to speculate that layer 5 CS-Parv neurons could play a role, through gamma oscillation, in the synchronization between the auditory cortex and striatum. Mainly, layer 5 CC-Parv neurons will provide temporal windows in which active neural assemblies can interact coherently and effectively, therefore acting as high pass filter of concerted network activity not only locally but also in their long-range target(s).

We are proposing that future experiments will provide further insight into the role of the CS-Parv neurons in timing and ratio of excitation and inhibition, two opposing forces in the mammalian cerebral cortex, that can dynamically affect the cortico-striatal dynamic. The new studies will provide a general mechanism of cortico-striatal oscillation involved in reward-learning, and action-selection behavior driven by the auditory stimuli.

DATA AVAILABILITY STATEMENT

The raw data supporting the conclusions of this article will be made available by the authors, without undue reservation.

ETHICS STATEMENT

The animal study was reviewed and approved by LARC, University of Texas at San Antonio.

AUTHOR CONTRIBUTIONS

All authors designed the experiments, performed the experiments, analyzed the data, and wrote the manuscript.

FUNDING

AA was supported by two NIH grants: GM122645 and MH123260.

ACKNOWLEDGMENTS

We thank G. Gaufo for help with confocal imaging. We thank Isabel Muzzio for comments on the manuscript.

REFERENCES

Apicella, A. J., Wickersham, I. R., Seung, H. S., and Shepherd, G. M. (2012). Laminarly orthogonal excitation of fast-spiking and low-threshold-spiking interneurons in mouse motor cortex. *J. Neurosci.* 32, 7021–7033. doi: 10.1523/jneurosci.0011-12.2012

Bagnall, M. W., Hull, C., Bushong, E. A., Ellisman, M. H., and Scanziani, M. (2011). Multiple clusters of release sites formed by individual thalamic afferents onto cortical interneurons ensure reliable transmission. *Neuron* 71, 180–194. doi: 10.1016/j.neuron.2011.05.032

Bahuguna, J., Aertsen, A., and Kumar, A. (2015). Existence and control of Go/No-Go decision transition threshold in the striatum. *PLoS Comput. Biol.* 11:e1004233. doi: 10.1371/journal.pcbi.1004233

Benavides-Piccione, R., and DeFelipe, J. (2007). Distribution of neurons expressing tyrosine hydroxylase in the human cerebral cortex. *J. Anat.* 211, 212–222. doi: 10.1111/j.1469-7580.2007.00760.x

Berke, J. D. (2009). Fast oscillations in cortical-striatal networks switch frequency following rewarding events and stimulant drugs. *Eur. J. Neurosci.* 30, 848–859. doi: 10.1111/j.1460-9568.2009.06843.x

Bertero, A., Feyen, P. L. C., Zurita, H., and Apicella, A. J. (2019). A non-canonical cortico-amygdala inhibitory loop. *J. Neurosci.* 39, 8424–8438. doi: 10.1523/jneurosci.1515-19.2019

Bracci, E., Centonze, D., Bernardi, G., and Calabresi, P. (2003). Voltage-dependent membrane potential oscillations of rat striatal fast-spiking interneurons. *J. Physiol.* 549, 121–130. doi: 10.1113/jphysiol.2003.040857

Brown, S. P., and Hestrin, S. (2009a). Intracortical circuits of pyramidal neurons reflect their long-range axonal targets. *Nature* 457, 1133–1136. doi: 10.1038/nature07658

Brown, S. P., and Hestrin, S. (2009b). Cell-type identity: a key to unlocking the function of neocortical circuits. *Curr. Opin. Neurobiol.* 19, 415–421. doi: 10.1016/j.conb.2009.07.011

Burnstock, G. (1976). Do some nerve cells release more than one transmitter? *Neuroscience* 1, 239–248. doi: 10.1016/0306-4522(76)90054-3

Buzsáki, G., and Draguhn, A. (2004). Neuronal oscillations in cortical networks. *Science* 304, 1926–1929. doi: 10.1126/science.1099745

Buzsáki, G., Geisler, C., Henze, D. A., and Wang, X. J. (2004). Interneuron Diversity series: circuit complexity and axon wiring economy of cortical interneurons. *Trends Neurosci.* 27, 186–193. doi: 10.1016/j.tins.2004.02.007

Buzsáki, G., and Wang, X. J. (2012). Mechanisms of gamma oscillations. *Annu. Rev. Neurosci.* 35, 203–225. doi: 10.1146/annurev-neuro-062111-150444

Cajal, S. R. Y. (1897). Las células de cilindro-eje corto de la capa molecular del cerebro. *Revista Trimestral Micrográfica* 2, 153–162.

Caputi, A., Melzer, S., Michael, M., and Monyer, H. (2013). The long and short of GABAergic neurons. *Curr. Opin. Neurobiol.* 23, 179–186. doi: 10.1016/j.conb.2013.01.021

Christenson Wick, Z., Tetzlaff, M. R., and Krook-Magnuson, E. (2019). Novel long-range inhibitory nNOS-expressing hippocampal cells. *Elife* 8:e46816. doi: 10.7554/eLife.46816

Connors, B. W. (2017). Synchrony and so much more: diverse roles for electrical synapses in neural circuits. *Dev. Neurobiol.* 77, 610–624. doi: 10.1002/dneu.22493

Cowan, R. L., and Wilson, C. J. (1994). Spontaneous firing patterns and axonal projections of single corticostriatal neurons in the rat medial agranular cortex. *J. Neurophysiol.* 71, 17–32. doi: 10.1152/jn.1994.71.1.17

Dani, V. S., and Nelson, S. B. (2009). Intact long-term potentiation but reduced connectivity between neocortical layer 5 pyramidal neurons in a mouse model of Rett syndrome. *J. Neurosci.* 29, 11263–11270. doi: 10.1523/jneurosci.1019-09.2009

DeCoteau, W. E., Thorn, C., Gibson, D. J., Courtemanche, R., Mitra, P., Kubota, Y., et al. (2007). Oscillations of local field potentials in the rat dorsal striatum during spontaneous and instructed behaviors. *J. Neurophysiol.* 97, 3800–3805. doi: 10.1152/jn.00108.2007

Freund, T. F., and Buzsaki, G. (1996). Interneurons of the hippocampus. *Hippocampus* 6, 347–470. doi: 10.1002/(sici)1098-1063(1996)6:4<347::aid-hipo1>3.0.co;2-i

Gentet, L. J., Avermann, M., Matyas, F., Staiger, J. F., and Petersen, C. C. (2010). Membrane potential dynamics of GABAergic neurons in the barrel cortex of behaving mice. *Neuron* 65, 422–435. doi: 10.1016/j.neuron.2010.01.006

Golomb, D., Donner, K., Shacham, L., Shlosberg, D., Amitai, Y., and Hansel, D. (2007). Mechanisms of firing patterns in fast-spiking cortical interneurons. *PLoS Comput. Biol.* 3:e156. doi: 10.1371/journal.pcbi.0030156.eor

Guo, L., Weems, J. T., Walker, W. I., Levichev, A., and Jaramillo, S. (2019). Choice-selective neurons in the auditory cortex and in its striatal target encode reward expectation. *J. Neurosci.* 39, 3687–3697. doi: 10.1523/jneurosci.2585-18.2019

Helmstaedter, M., Sakmann, B., and Feldmeyer, D. (2009). L2/3 interneuron groups defined by multiparameter analysis of axonal projection, dendritic geometry and electrical excitability. *Cereb. Cortex* 19, 951–962. doi: 10.1093/cercor/bhn130

Higo, S., Akashi, K., Sakimura, K., and Tamamaki, N. (2009). Subtypes of GABAergic neurons project axons in the neocortex. *Front. Neuroanat.* 3:25. doi: 10.3389/neuro.05.025.2009

Higo, S., Udaka, N., and Tamamaki, N. (2007). Long-range GABAergic projection neurons in the cat neocortex. *J. Comp. Neurol.* 503, 421–431. doi: 10.1002/cne.21395

Huang, Z. J., and Paul, A. (2019). The diversity of GABAergic neurons and neural communication elements. *Nat. Rev. Neurosci.* 20, 563–572. doi: 10.1038/s41583-019-0195-4

Isaacson, J. S., and Scanziani, M. (2011). How inhibition shapes cortical activity. *Neuron* 72, 231–243. doi: 10.1016/j.neuron.2011.09.027

Ji, X. Y., Zingg, B., Mesik, L., Xiao, Z., Zhang, L. I., and Tao, H. W. (2016). Thalamocortical innervation pattern in mouse auditory and visual cortex: laminar and cell-type specificity. *Cereb. Cortex* 26, 2612–2625. doi: 10.1093/cercor/bhv099

Kerlin, A. M., Andermann, M. L., Berezovskii, V. K., and Reid, R. C. (2010). Broadly tuned response properties of diverse inhibitory neuron subtypes in mouse visual cortex. *Neuron* 67, 858–871. doi: 10.1016/j.neuron.2010.08.002

Kubota, Y., Karube, F., Nomura, M., Gulledge, A. T., Mochizuki, A., Schertel, A., et al. (2011). Conserved properties of dendritic trees in four cortical interneuron subtypes. *Sci. Rep.* 1:89. doi: 10.1038/srep00089

Lee, A. T., Vogt, D., Rubenstein, J. L., and Sohal, V. S. (2014). A class of GABAergic neurons in the prefrontal cortex sends long-range projections to the nucleus accumbens and elicits acute avoidance behavior. *J. Neurosci.* 34, 11519–11525. doi: 10.1523/JNEUROSCI.1157-14.2014

Li, L. Y., Xiong, X. R., Ibrahim, L. A., Yuan, W., Tao, H. W., and Zhang, L. I. (2015). Differential receptive field properties of parvalbumin and somatostatin inhibitory neurons in mouse auditory cortex. *Cereb. Cortex* 25, 1782–1791. doi: 10.1093/cercor/bht417

Li, P., and Huntsman, M. M. (2014). Two Functional Inhibitory Circuits Are Comprised of a Heterogeneous Population of Fast-Spiking Cortical Interneurons. *Neuroscience* 265, 60–71. doi: 10.1016/j.neuroscience.2014.01.033

Liu, B. H., Li, P., Li, Y. T., Sun, Y. J., Yanagawa, Y., Obata, K., et al. (2009). Visual receptive field structure of cortical inhibitory neurons revealed by two-photon imaging guided recording. *J. Neurosci.* 29, 10520–10532. doi: 10.1523/JNEUROSCI.1915-09.2009

Liu, B. H., Li, P., Sun, Y. J., Li, Y. T., Zhang, L. I., and Tao, H. W. (2010). Intervening inhibition underlies simple-cell receptive field structure in visual cortex. *Nat. Neurosci.* 13, 89–96. doi: 10.1038/nn.2443

Markram, H. (1997). A network of tufted layer 5 pyramidal neurons. *Cereb. Cortex* 7, 523–533. doi: 10.1093/cercor/7.6.523

McDonald, C. T., and Burkhalter, A. (1993). Organization of long-range inhibitory connections with rat visual cortex. *J. Neurosci.* 13, 768–781. doi: 10.1523/jneurosci.13-02-00768.1993

Melzer, S., Gil, M., Koser, D. E., Michael, M., Huang, K. W., and Monyer, H. (2017). Distinct corticostriatal gabaergic neurons modulate striatal output neurons and motor activity. *Cell Rep.* 19, 1045–1055. doi: 10.1016/j.celrep.2017.04.024

Melzer, S., Michael, M., Caputi, A., Eliava, M., Fuchs, E. C., Whittington, M. A., et al. (2012). Long-range-projecting GABAergic neurons modulate inhibition in hippocampus and entorhinal cortex. *Science* 335, 1506–1510. doi: 10.1126/science.1217139

Morishima, M., Morita, K., Kubota, Y., and Kawaguchi, Y. (2011). Highly differentiated projection-specific cortical subnetworks. *J. Neurosci.* 31, 10380–10391. doi: 10.1523/jneurosci.0772-11.2011

Morishima, M., and Kawaguchi, Y. (2006). Recurrent connection patterns of corticostriatal pyramidal cells in frontal cortex. *J. Neurosci.* 26, 4394–4405. doi: 10.1523/JNEUROSCI.0252-06.2006

Niell, C. M., and Stryker, M. P. (2008). Highly selective receptive fields in mouse visual cortex. *J. Neurosci.* 28, 7520–7536. doi: 10.1523/jneurosci.0623-08.2008

Pfeffer, C. K., and Beltramo, R. (2017). Correlating anatomy and function with gene expression in individual neurons by combining *in vivo* labeling, patch clamp, and single cell RNA-seq. *Front. Cell. Neurosci.* 11:376. doi: 10.3389/fncel.2017.00376

Picardo, M. A., Guigue, P., Bonifazi, P., Batista-Brito, R., Allene, C., Ribas, A., et al. (2011). Pioneer GABA cells comprise a subpopulation of hub neurons in the developing hippocampus. *Neuron* 71, 695–709. doi: 10.1016/j.neuron.2011.06.018

Ramon y Cajal, S., DeFelipe, J., and Jones, E. G. (1988). *Cajal on the Cerebral Cortex: An Annotated Translation of the Complete Writings.* New York, NY: Oxford University Press.

Resnik, J., and Polley, D. B. (2017). Fast-spiking GABA circuit dynamics in the auditory cortex predict recovery of sensory processing following peripheral nerve damage. *Elife* 6:e21452. doi: 10.7554/eLife.21452

Reyes, A., Lujan, R., Rozov, A., Burnashev, N., Somogyi, P., and Sakmann, B. (1998). Target-cell-specific facilitation and depression in neocortical circuits. *Nat. Neurosci.* 1, 279–285. doi: 10.1038/1092

Ribak, C. E., Seress, L., Peterson, G. M., Seroogy, K. B., Fallon, J. H., and Schmued, L. C. (1986). A GABAergic inhibitory component within the hippocampal commissural pathway. *J. Neurosci.* 6, 3492–3498. doi: 10.1523/jneurosci.06-12-03492.1986

Rock, C., and Apicella, A. J. (2015). Callosal projections drive neuronal-specific responses in the mouse auditory cortex. *J. Neurosci.* 35, 6703–6713. doi: 10.1523/jneurosci.5049-14.2015

Rock, C., Zurita, H., Lebby, S., Wilson, C. J., and Apicella, A. J. (2018). Cortical circuits of callosal GABAergic neurons. *Cereb. Cortex* 28, 1154–1167. doi: 10.1093/cercor/bhx025

Rock, C., Zurita, H., Wilson, C., and Apicella, A. J. (2016). An inhibitory corticostriatal pathway. *Elife* 5:e15890. doi: 10.7554/eLife.15890

Rothermel, M., Brunert, D., Zabawa, C., Diaz-Quesada, M., and Wachowiak, M. (2013). Transgene expression in target-defined neuron populations mediated by retrograde infection with adeno-associated viral vectors. *J. Neurosci.* 33, 15195–15206. doi: 10.1523/jneurosci.1618-13.2013

Rudy, B., Fishell, G., Lee, S., and Hjerling-Leffler, J. (2011). Three groups of interneurons account for nearly 100% of neocortical GABAergic neurons. *Dev. Neurobiol.* 71, 45–61. doi: 10.1002/dneu.20853

Runyan, C. A., Schummers, J., Van Wart, A., Kuhlman, S. J., Wilson, N. R., Huang, Z. J., et al. (2010). Response features of parvalbumin-expressing interneurons suggest precise roles for subtypes of inhibition in visual cortex. *Neuron* 67, 847–857. doi: 10.1016/j.neuron.2010.08.006

Runyan, C. A., and Sur, M. (2013). Response selectivity is correlated to dendritic structure in parvalbumin-expressing inhibitory neurons in visual cortex. *J. Neurosci.* 33, 11724–11733. doi: 10.1523/jneurosci.2196-12.2013

Sakata, S., and Harris, K. D. (2009). Laminar structure of spontaneous and sensory-evoked population activity in auditory cortex. *Neuron* 64, 404–418. doi: 10.1016/j.neuron.2009.09.020

Sciamanna, G., and Wilson, C. J. (2011). The ionic mechanism of gamma resonance in rat striatal fast-spiking neurons. *J. Neurophysiol.* 106, 2936–2949. doi: 10.1152/jn.00280.2011

Seress, L., and Ribak, C. E. (1983). GABAergic cells in the dentate gyrus appear to be local circuit and projection neurons. *Exp. Brain Res.* 50, 173–182. doi: 10.1007/bf00239181

Silberberg, G. (2008). Polysynaptic subcircuits in the neocortex: spatial and temporal diversity. *Curr. Opin. Neurobiol.* 18, 332–337. doi: 10.1016/j.conb.2008.08.009

Stern, E. A., Kincaid, A. E., and Wilson, C. J. (1997). Spontaneous subthreshold membrane potential fluctuations and action potential variability of rat corticostriatal and striatal neurons *in vivo*. *J. Neurophysiol.* 77, 1697–1715. doi: 10.1152/jn.1997.77.4.1697

Sun, Y. J., Kim, Y. J., Ibrahim, L. A., Tao, H. W., and Zhang, L. I. (2013). Synaptic mechanisms underlying functional dichotomy between intrinsic-bursting and regular-spiking neurons in auditory cortical layer 5. *J. Neurosci.* 33, 5326–5339. doi: 10.1523/jneurosci.4810-12.2013

Suter, B. A., O'Connor, T., Iyer, V., Petreanu, L. T., Hooks, B. M., Kiritani, T., et al. (2010). Ephus: multipurpose data acquisition software for neuroscience experiments. *Front. Neural Circuits* 4:100. doi: 10.3389/fnins.2010.00053

Tamamaki, N., and Tomioka, R. (2010). Long-range GABAergic connections distributed throughout the neocortex and their possible function. *Front. Neurosci.* 4:202. doi: 10.3389/fnins.2010.00202

Tomioka, R., Okamoto, K., Furuta, T., Fujiyama, F., Iwasato, T., Yanagawa, Y., et al. (2005). Demonstration of long-range GABAergic connections distributed throughout the mouse neocortex. *Eur. J. Neurosci.* 21, 1587–1600. doi: 10.1111/j.1460-9568.2005.03989.x

Tomioka, R., and Rockland, K. S. (2007). Long-distance corticocortical GABAergic neurons in the adult monkey white and gray matter. *J. Comp. Neurol.* 505, 526–538. doi: 10.1002/cne.21504

Tomioka, R., Sakimura, K., and Yanagawa, Y. (2015). Corticofugal GABAergic projection neurons in the mouse frontal cortex. *Front. Neuroanat.* 9:133. doi: 10.3389/fnana.2015.00133

Toth, K., Borhegyi, Z., and Freund, T. F. (1993). Postsynaptic targets of GABAergic hippocampal neurons in the medial septum-diagonal band of broca complex. *J. Neurosci.* 13, 3712–3724. doi: 10.1523/jneurosci.13-09-03712.1993

Toth, K., and Freund, T. F. (1992). Calbindin D28k-containing nonpyramidal cells in the rat hippocampus: their immunoreactivity for GABA and projection to the medial septum. *Neuroscience* 49, 793–805. doi: 10.1016/0306-4522(92)90357-8

Tremblay, R., Lee, S., and Rudy, B. (2016). GABAergic interneurons in the neocortex: from cellular properties to circuits. *Neuron* 91, 260–292. doi: 10.1016/j.neuron.2016.06.033

Tukker, J. J., Lasztoczi, B., Katona, L., Roberts, J. D., Pissadaki, E. K., Dalezios, Y., et al. (2013). Distinct dendritic arborization and *in vivo* firing patterns of parvalbumin-expressing basket cells in the hippocampal area CA3. *J. Neurosci.* 33, 6809–6825. doi: 10.1523/jneurosci.5052-12.2013

Xiong, Q., Znamenskiy, P., and Zador, A. M. (2015). Selective corticostriatal plasticity during acquisition of an auditory discrimination task. *Nature* 521, 348–351. doi: 10.1038/nature14225

Xu, X., and Callaway, E. M. (2009). Laminar specificity of functional input to distinct types of inhibitory cortical neurons. *J. Neurosci.* 29, 70–85. doi: 10.1523/JNEUROSCI.4104-08.2009

Xu, X., Roby, K. D., and Callaway, E. M. (2010). Immunochemical characterization of inhibitory mouse cortical neurons: three chemically distinct classes of inhibitory cells. *J. Comp. Neurol.* 518, 389–404. doi: 10.1002/cne.22229

Znamenskiy, P., and Zador, A. M. (2013). Corticostriatal neurons in auditory cortex drive decisions during auditory discrimination. *Nature* 497, 482–485. doi: 10.1038/nature12077

Zurita, H., Feyen, P. L. C., and Apicella, A. J. (2018a). Layer 5 callosal parvalbumin-expressing neurons: a distinct functional group of GABAergic neurons. *Front. Cell. Neurosci.* 12:53. doi: 10.3389/fncel.2018.00053

Zurita, H., Rock, C., Perkins, J., and Apicella, A. J. (2018b). A layer-specific corticofugal input to the mouse superior colliculus. *Cereb. Cortex* 28, 2817–2833. doi: 10.1093/cercor/bhx161

Conflict of Interest: The authors declare that the research was conducted in the absence of any commercial or financial relationships that could be construed as a potential conflict of interest.

frontiers in Neural Circuits

ORIGINAL RESEARCH
published: 06 January 2021
doi: 10.3389/fncir.2020.607391

Calcium Imaging and the Curse of Negativity

Gilles Vanwalleghem, Lena Constantin and Ethan K. Scott*

Neural Circuits and Behavior Laboratory, Queensland Brain Institute, The University of Queensland, St Lucia, QLD, Australia

The imaging of neuronal activity using calcium indicators has become a staple of modern neuroscience. However, without ground truths, there is a real risk of missing a significant portion of the real responses. Here, we show that a common assumption, the non-negativity of the neuronal responses as detected by calcium indicators, biases all levels of the frequently used analytical methods for these data. From the extraction of meaningful fluorescence changes to spike inference and the analysis of inferred spikes, each step risks missing real responses because of the assumption of non-negativity. We first show that negative deviations from baseline can exist in calcium imaging of neuronal activity. Then, we use simulated data to test three popular algorithms for image analysis, CaImAn, suite2p, and CellSort, finding that suite2p may be the best suited to large datasets. We also tested the spike inference algorithms included in CaImAn, suite2p, and Cellsort, as well as the dedicated inference algorithms MLspike and CASCADE, and found each to have limitations in dealing with inhibited neurons. Among these spike inference algorithms, FOOPSI, from CaImAn, performed the best on inhibited neurons, but even this algorithm inferred spurious spikes upon the return of the fluorescence signal to baseline. As such, new approaches will be needed before spikes can be sensitively and accurately inferred from calcium data in inhibited neurons. We further suggest avoiding data analysis approaches that, by assuming non-negativity, ignore inhibited responses. Instead, we suggest a first exploratory step, using k-means or PCA for example, to detect whether meaningful negative deviations are present. Taking these steps will ensure that inhibition, as well as excitation, is detected in calcium imaging datasets.

Keywords: calcium imaging, zebrafish, GCaMP, baseline fluorescence, data analysis, cerebellar circuitry, segmentation, spike inference

OPEN ACCESS

Edited by:
Maria Gutierrez-Mecinas, University of Glasgow, United Kingdom

Reviewed by:
Guillaume Etter, McGill University, Canada
Yoshikazu Isomura, Tokyo Medical and Dental University, Japan

****Correspondence:***
Gilles Vanwalleghem
g.vanwalleghem@uq.edu.au

Received: *17 September 2020*
Accepted: *02 December 2020*
Published: *06 January 2021*

Citation:
Vanwalleghem G, Constantin L and Scott EK (2021) Calcium Imaging and the Curse of Negativity. Front. Neural Circuits 14:607391. doi: 10.3389/fncir.2020.607391

INTRODUCTION

The advent of Genetically Encoded Calcium Indicators (GECI) has transformed the field of neuroscience by allowing the imaging of activity across large populations of neurons (Nakai et al., 2001; Pologruto et al., 2004; Tian et al., 2009), and these methods are now being integrated in other fields of biology (Balaji et al., 2017; Shannon et al., 2017; Stevenson et al., 2020). A concurrent boom in microscopy techniques has allowed the rapid volumetric imaging of these populations, *in vivo*, in models including larval zebrafish (Wyart et al., 2009; Ahrens et al., 2012; Constantin et al., 2020; Vanwalleghem et al., 2020); flies (Wang et al., 2003; Suh et al., 2004), and rodents (Chen et al., 2012; Cai et al., 2016; Klioutchnikov et al., 2020). The vast datasets produced by this approach have driven the development of computational tools designed to extract and process

activity information from populations of neurons (Mukamel et al., 2009; Freeman et al., 2014; Pachitariu et al., 2017; Giovannucci et al., 2019; Stringer and Pachitariu, 2019). A common assumption in most of these modern computational tools is the non-negativity of the GECI's signal.

However, negative deviations from the fluorescence baselines have been observed, and assumptions of non-negativity may cause the omission or misinterpretation of GECI data from populations with such negative deviations (Galizia et al., 2010; Munch and Galizia, 2017; Favre-Bulle et al., 2018; Marquez-Legorreta et al., 2019; Zimmerman et al., 2019). With the slow rise and decay of GECI probes, on the order of hundreds of milliseconds, a long-term average firing rate above 1 Hz would be convolved as a high fluorescence baseline. Such tonic activity can be found in vestibular neurons, even at rest (Shimazu and Precht, 1965; Cullen and McCrea, 1993), and in the primary visual cortex neurons (Baddeley et al., 1997) among a great many others. Notably, inhibition of tonically active neurons has been observed with electrophysiology in vestibular neurons (Shimazu and Precht, 1966), Purkinje cells (Tian et al., 2013), and distributed across the brain in response to stimulus-driven decisions (Steinmetz et al., 2019). Such inhibition of tonic neurons, convolved by the slow GECI kernels, translate to negative deviations from baseline as we and others have observed (Favre-Bulle et al., 2018; Zimmerman et al., 2019).

Many tools for GECI analysis include methods for inferring the spike train that generated the observed fluorescence signal, and again most of these spike deconvolution algorithms assume non-negativity (Vogelstein et al., 2010; Pachitariu et al., 2018). For example, the spikefinder online challenge had this implicit assumption in the datasets offered to the community (Theis et al., 2016), and their best performing algorithms were based on convolutional neural networks. This supervised approach, however, would miss inhibited response profiles as they have been trained on datasets with no negative deviation in the fluorescent traces.

Finally, this non-negative assumption is built into popular approaches for interpreting the patterns of activity across populations of neurons. For example, Non-negative Matrix Factorization (NMF), not to be confused with CNMF that is used to extract fluorescent traces from the videos (Pnevmatikakis et al., 2016), has been used as a dimensionality reduction or clustering tool on the fluorescent traces of individual neurons (Freeman et al., 2014; Mu et al., 2019; Torigoe et al., 2019). The NMF approach, when applied on extracted neuronal activity data normalized with z-scoring or $\Delta F/F_0$, discards negative deviations from the baseline fluorescent signal. Another approach that we and others have used, the binarization of the data based on a threshold of activity to generate "bar codes" of the brain activity, also has an intrinsic non-negative assumption (Kubo et al., 2014; Naumann et al., 2016; Heap et al., 2018; Daviu et al., 2020; Etter et al., 2020). Other threshold-based approaches, or even data cleaning steps, run the risk of discarding all negative deviations from baseline, biasing conclusions drawn from the dataset to exclude inhibition from the modeled system.

In summary, we find this non-negative assumption at all levels of calcium imaging analysis, from the extraction of fluorescence traces to spike inference and analyses of populations' dynamics. Our goal here was to assess how the most popular calcium imaging analyses responded to negative deviations from the baseline, including whether or not each approach was sensitive to traces that were typical of inhibitory signals in neural networks. We also hope to spark a discussion on how these assumptions may have biased past studies, and may continue to bias future work using GECIs.

TABLE 1 | Parameters used for the simulation of calcium datasets.

Frame rate	Simulated volume	Radius nuclei	τ of GECI	Time points
5 Hz	90 × 90 × 50	5.9 m	1.5	1,000

MATERIALS AND METHODS

The imaging data came from Favre-Bulle et al. (2018). Briefly, experiments were carried on 6 day post-fertilization (dpf) *nacre* mutant zebrafish (Danio rerio) larvae of the Tüpfel long fin strain carrying the transgene *elavl3:H2B-GCaMP6s* (Chen et al., 2013). The larvae were immobilized in 2% low melting point agarose (Progen Biosciences, Australia) and imaged using a diffuse digitally scanned light-sheet microscope (Taylor et al., 2018) while an optical trap was applied to the otolith to simulate acceleration (Favre-Bulle et al., 2017, 2018, 2019, 2020). All procedures were performed with approval from the University of Queensland Animal Welfare Unit in accordance with approval SBMS/378/16/ARC.

Artificial datasets were generated using the Neural Anatomy and Optical Microscopy simulation toolbox (Charles et al., 2019). We used the parameters for nuclear simulation with GCaMP6f default (see **Table 1**). To simulate inhibited neuronal responses, we randomly attributed a spike number from a Poisson distribution (λ of 1, based on; Baddeley et al., 1997) to each 200 ms time window of 10 to 20 percent of all simulated neurons (since ∼20% of neurons were inhibited when observed by Steinmetz et al., 2019). We then set a time frame of 0.2 to 5 s of inhibition (0 spikes), which was used to simulate the neuronal activity and generate movies that were processed with the tools below. For the mixed activity, we used a similar approach on the second half from the time series of 20% of the neurons in the simulated dataset.

For fluorescence extraction and spike inference, we benchmarked the most cited calcium imaging toolboxes: suite2p (suite2p, version 0.8.0, RRID:SCR_016434) (Pachitariu et al., 2017), CaImAn version 1.8 (Giovannucci et al., 2019), and the PCA/ICA approach CellSort (Mukamel et al., 2009). We did not simulate motion, and as such did not use the registration algorithms included in either suite2p or CaImAn. The parameters used for each of these approaches can be found in the github repository. Briefly, for suite2p we used the sourcery roi extraction, with a τ of 2, frame rate of 5, diameter of neurons (4,6), threshold scaling of 0.5 and a high pass of 50. For CaImAn, we used the CNMFe implementation which shows a better accuracy for background estimation than CNMF and should

avoid the risks of spurious negative deviations due to background subtraction (Zhou et al., 2018). The parameters for CaImAn were a τ of 2, frame rate of 5, a gSig of 4 and autoregressive order of 2. For the deep-learning spike inference method CASCADE, we used the Universal_5Hz_smoothing200ms pretrained model to infer the spikes on our dataset (Rupprecht et al., 2020). For MLspike, we used $\tau = 2$, dt = 0.2, pnonlin = [0.55 0.03] as suggested for GCaMP6f in Deneux et al. (2016).

For the analysis of the responses, we used MATLAB (R2018b, RRID: SCR_001622). $\Delta F/F_0$ was computed as in Akerboom et al. (2012). We used the non-negative matrix factorization function nnmf with 15 factors to reanalyze the data from Favre-Bulle et al. (2018). We used the correlation coefficients tools from MATLAB to compute the 2-dimensional correlation between the regions of interest (ROIs) and the ideal components, as well as between the traces or spikes and the ideal traces or spikes.

Statistical tests and plotting were done in Graphpad Prism (8.4.3, RRID:SCR_002798), using ordinary ANOVA with Tukey's multiple comparison test.

All the code used to generate and analyze the data can be found on github.com/Scott-Lab-QBI/NegativeCalciumResponses.

RESULTS

Real Data

First, we reanalyzed a zebrafish dataset from our previous study of vestibular processing in which we identified inhibited responses in hundreds of neurons across the thalamus and cerebellum (Favre-Bulle et al., 2018). For the analysis presented here, we focus on two representative neurons from the cerebellum and hindbrain of a larval zebrafish (**Figure 1A**) as larvae were subjected to vestibular stimuli (**Figure 1B**, shaded areas). As seen in the raw data (**Figure 1B**, arrows), we observe negative deviations from baseline during stimulation (**Figure 1B**, magenta traces), as well as positive responses (**Figure 1B**, green).

Our first observation was that the classical $\Delta F/F_0$ approach with a moving baseline window (Akerboom et al., 2012) creates positive artifacts following negative deviation from baseline as seen in **Figure 1B** (arrows). These positive artifacts could be construed as actual responses by some approaches, since they peak at the same level as the actual responses (magenta traces with arrows vs. adjacent green traces in **Figure 1B**). In the $\Delta F/F_0$ trace, the results do not correlate as well for the (magenta) inhibited neuron ($\rho = 0.599$) when compared to the (green) activated neuron ($\rho = 0.979$). However, the z-scored trace was perfectly correlated to the raw trace ($\rho = 1$) for both neurons. As such, we recommend the use of z-score as a normalization of calcium traces, and we will use this normalization in the following analysis.

Beyond these artifacts, there was the concern that popular data analysis methods could miss inhibited response profiles. NMF has been used to analyze larval zebrafish calcium imaging data (Mu et al., 2019; Torigoe et al., 2019), so we tested this method on the same vestibular dataset from our group (Favre-Bulle et al., 2018). As can be seen (**Supplementary Figure 1**), the NMF approach failed to identify responses resembling the inhibited cluster identified by k-means while the other (non-negative) clusters were found with a high correlation ($\rho = 0.92$, $\rho = 0.94$, respectively, **Figure 1C**).

The major limitation of this analysis was that it lacked a ground truth, making it impossible to judge whether outputs from apparently successful approaches actually reflected physiology. To solve this problem, we turned to simulated data for which we control the ground truth.

Simulated Data

We used the Neural Anatomy and Optical Microscopy (NAOMi) Simulation toolbox (Charles et al., 2019) to generate 10 datasets of simulated nuclear-targeted GCaMP6f data, as described in the Materials and Methods. Briefly, each dataset contained about 90 neurons, and for each, we randomly selected either 10 or 20% of the neurons to be inhibited. For each inhibited neuron, we simulated tonic firing, based on an observed Poisson distribution (Baddeley et al., 1997), which was randomly interrupted for 0.2 to 5 s to simulate inhibition (**Figure 2A**). We chose a random inhibition pattern as both suite2p and CaImAn depend on the correlation between pixels to generate the ROIs, and we wanted to make the inhibited neurons as easy to identify as possible, since most methods depend on local correlations to identify the neurons. The simulated spiking (**Figure 2A**) was then convolved with a GCaMP6f kernel to simulate neural activity (**Figure 2B**), which was then used to generate movies using NAOMi (**Figure 2C**). As most simulated neurons would be below the detection threshold, we used NAOMi to output the ideal responses corresponding to what would be detected with a microscope. While other algorithms occasionally identified additional neurons, the effect was marginal (<1%), so we decided to use the ideal responses as ground truth for the sake of simplicity (Charles et al., 2019).

Each fluorescence dataset was processed through suite2p (Pachitariu et al., 2017), CaImAn (Giovannucci et al., 2019), or CellSort (Mukamel et al., 2009), and the outputs for each approach were then analyzed in the same manner. We did not investigate whether the suite2p default classifier or the CaImAn components evaluation would exclude inhibited neurons, and as such, we kept all the ROIs either algorithm identified. The raster plots of the ten datasets (**Figure 3A**) show that CaImAn identifies the highest number of ROIs, with CellSort and suite2p identifying a similar number of ROIs (Ideal = 94.3 ± 4.7, CaImAn = 84.7 ± 14.4, CellSort = 55.5 ± 3.8, suite2p = 56.1 ± 4.7).

The segmentation of the simulated fluorescent movies gave good results for all three algorithms, with well-defined regions of interest that correlated well with the ideal ROIs (**Figures 3B,C**, $\rho_{CaImAn} = 0.74 \pm 0.06$, $\rho_{CellSort} = 0.80 \pm 0.02$, $\rho_{suite2p} = 0.79 \pm 0.03$). We then correlated the ideal traces of activated or inhibited simulated neurons to the traces extracted by each algorithm, and for each dataset, we averaged the maximum correlations to each ideal trace (**Figure 3D**). All three algorithms succeeded in extracting the relevant traces for the activated neurons (**Figure 3D**, left, indicated by green bar), but CellSort and suite2p outperformed CaImAn for the inhibited traces

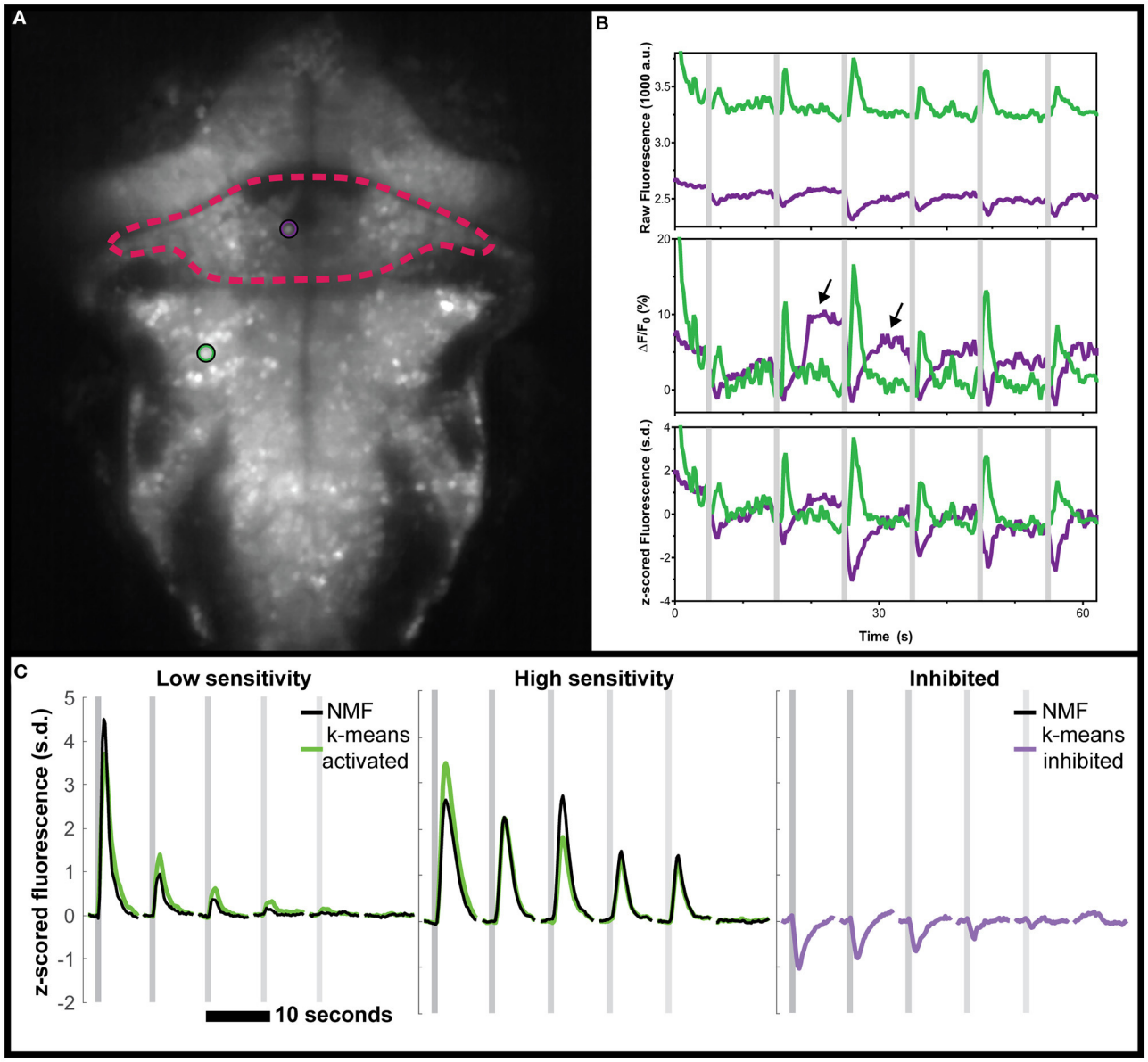

FIGURE 1 | Negative deviations from baseline in real data from the cerebellum of zebrafish, and performance of various analysis tools. **(A)** Mean fluorescence image of a 6 dpf zebrafish expressing nuclear-targeted GCaMP6s (Chen et al., 2013). The cerebellum is outlined in red, and an inhibited neuron is indicated with a magenta circle. The green circle indicates an activated neuron in the hindbrain. **(B)** Time traces of the raw (top), $\Delta F/F_0$ (middle), or z-scored (bottom) fluorescence for these two neurons, in their respective colors. Arrows indicate positive deviation artifacts resulting from the cessation of inhibition on the inhibited neuron. **(C)** Comparisons between the clusters identified using k-means (green for activated, magenta for inhibited) and those identified with NMF (black). No inhibited cluster was identified by NMF. Gray shaded areas indicate the time of vestibular stimulation (Favre-Bulle et al., 2018), with a progression from strong to weak stimuli across the stimulus train.

($\rho_{\text{CaImAn}} = 0.43 \pm 0.09$, $\rho_{\text{CellSort}} = 0.82 \pm 0.07$, $\rho_{\text{suite2p}} = 0.83 \pm 0.08$, **Figure 3D**, right, magenta).

To assess the proportion of true positives, we identified the ideal fluorescent trace to which each ROI's fluorescent trace best correlated. We only counted the unique ROIs that passed a 0.5 correlation cut-off, as all algorithms over-segment some of the sources in duplicated fluorescent traces (Charles et al., 2019). When comparing the proportions of identified ideal activated neurons, CellSort outperformed suite2p slightly, followed by CaImAn (proportions of $0.38 \pm 0.05_{\text{CaImAn}}$, $0.58 \pm 0.06_{\text{CellSort}}$, and $0.54 \pm 0.04_{\text{suite2p}}$, **Figure 3E** left). For inhibited neurons, CellSort outperformed suite2p slightly again, but the divide with CaImAn grew (proportions of $0.34 \pm 0.19_{\text{CaImAn}}$, $0.86 \pm 0.10_{\text{CellSort}}$ and $0.82 \pm 0.10_{\text{suite2p}}$, **Figure 3E**, right). All algorithms seemed insensitive to the ratio of inhibited neurons presented, as we saw no difference in those metrics between datasets with 10 vs. 20% inhibited neurons.

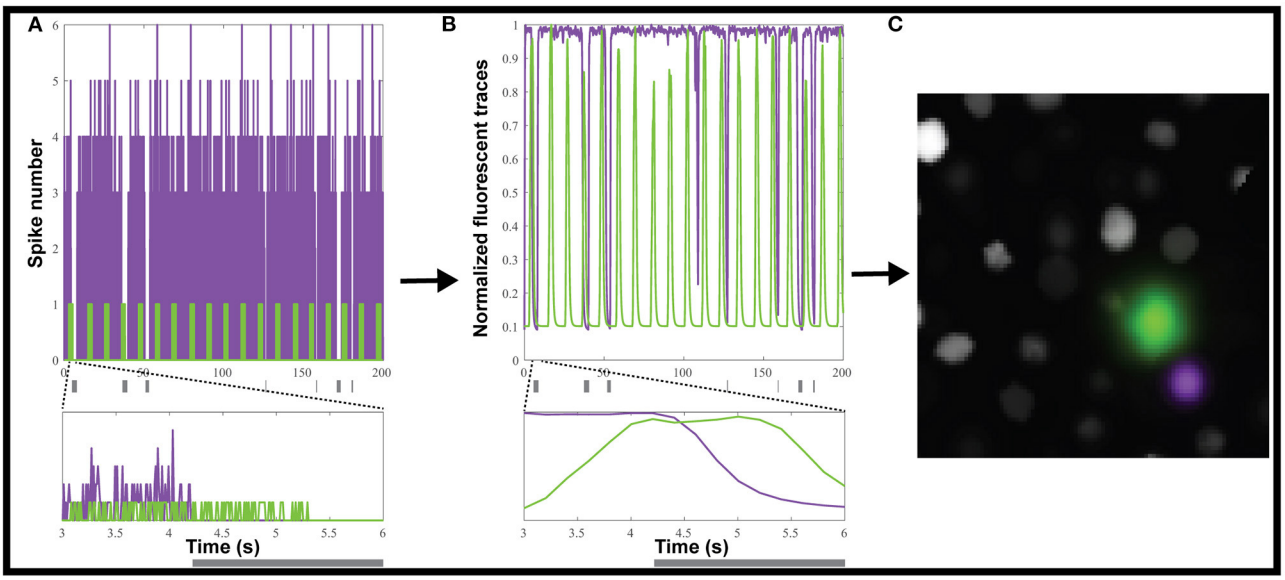

FIGURE 2 | Creating simulated calcium imaging datasets. **(A)** An example dataset of simulated activity, showing spike numbers for one neuron (green) activated and one (magenta) inhibited by a hypothetical stimulus (gray rectangles). **(B)** The spike trains are convolved with a GCaMP6f kernel and noise to generate fluorescence traces. **(C)** The simulated neuronal activity was used to create an artificial movie as captured by a microscope.

These results are lower than the results from Charles et al. (2019), who found that both CaImAn and suite2p outperformed CellSort (proportions of 0.71, 0.69 and 0.33, respectively). One possible explanation for the difference is that our use of nuclear-targeted GCaMP simulations, like our real datasets, may favor CellSort.

Spike Inference From Simulated Calcium Traces

In theory, inferring the spike trains responsible for calcium traces is one way to improve the temporal resolution, as you get rid of the convolved GCaMP kernel, but the frame rate of acquisition often makes such deconvolution impractical and unreliable. Each of the above algorithms offers some form of spike inference (**Figure 4A**), and multiple other approaches have been proposed during an online challenge (Berens et al., 2018). CaImAn offers multiple options for spike inference, among which we selected their fast non-negative deconvolution (FOOPSI) method (Vogelstein et al., 2010). For suite2p, we used the Online Active Set method to Infer Spikes (OASIS) (Friedrich et al., 2017). We also tested a recent spike inference method based on deep learning, CASCADE, which offers universal pre-trained models (Rupprecht et al., 2020) and a maximum likelihood approach to the probable spiked train, MLspike (Deneux et al., 2016).

Using this approach, we tested how accurate each spike detection algorithm was on our datasets. To avoid any confounding issues from the detection algorithm, we used the ideal calcium responses as the basis for the spike detection. Based on our results with the moving baseline of $\Delta F/F_0$ (**Figure 1B**), we also did not pre-process the data for the spike inference with suite2p, and used a global minimum to normalize for CASCADE and MLspike. The CellSort deconvolution approach had limited success with both activated and inhibited neurons ($\rho_{CellSort} = 0.08 \pm 0.08$, and $\rho_{CellSort} = 0.003 \pm 0.013$ respectively, **Figure 4B**, **Supplementary Figure 2**). The more recent CaImAn and suite2p did well for the activated neurons, ($\rho_{CaImAn} = 0.53 \pm 0.04$, $\rho_{suite2p} = 0.55 \pm 0.03$), but CaImAn outperformed suite2p for inhibited neurons ($\rho_{CaImAn} = 0.60 \pm 0.05$, $\rho_{suite2p} = 0.37 \pm 0.03$). The universal model of CASCADE performed better than the rest on the activated neurons ($\rho_{CASCADE} = 0.66 \pm 0.03$), but worse on the inhibited neurons ($\rho_{CASCADE} = 0.03 \pm 0.03$). MLspike performed slightly worse than the above algorithms on the activated neurons ($\rho_{MLspike} = 0.53 \pm 0.03$), but was intermediate on the inhibited neurons ($\rho_{MLspike} = 0.28 \pm 0.02$).

Those performances were also tested in a scenario containing neurons with a mixture of activation and inhibition (**Supplementary Figure 3**). In that scenario there was little difference between the activated neurons and the mixed activity neurons with the different algorithms for ROI detections. The spike inference results were slightly worse across the board, but not as strongly as in **Figure 4**.

DISCUSSION

In this study, we show that the often implicit assumption of non-negativity for calcium imaging data can lead to missing real responses from inhibited neurons. Current approaches run the risk of missing a significant fraction of responses at every step of the analysis pipeline, including cleaning the data, processing, feature extraction, dimensionality reduction, and clustering.

We have shown these negative deviations exist in real data from zebrafish, as we previously observed (**Figure 1**; Favre-Bulle

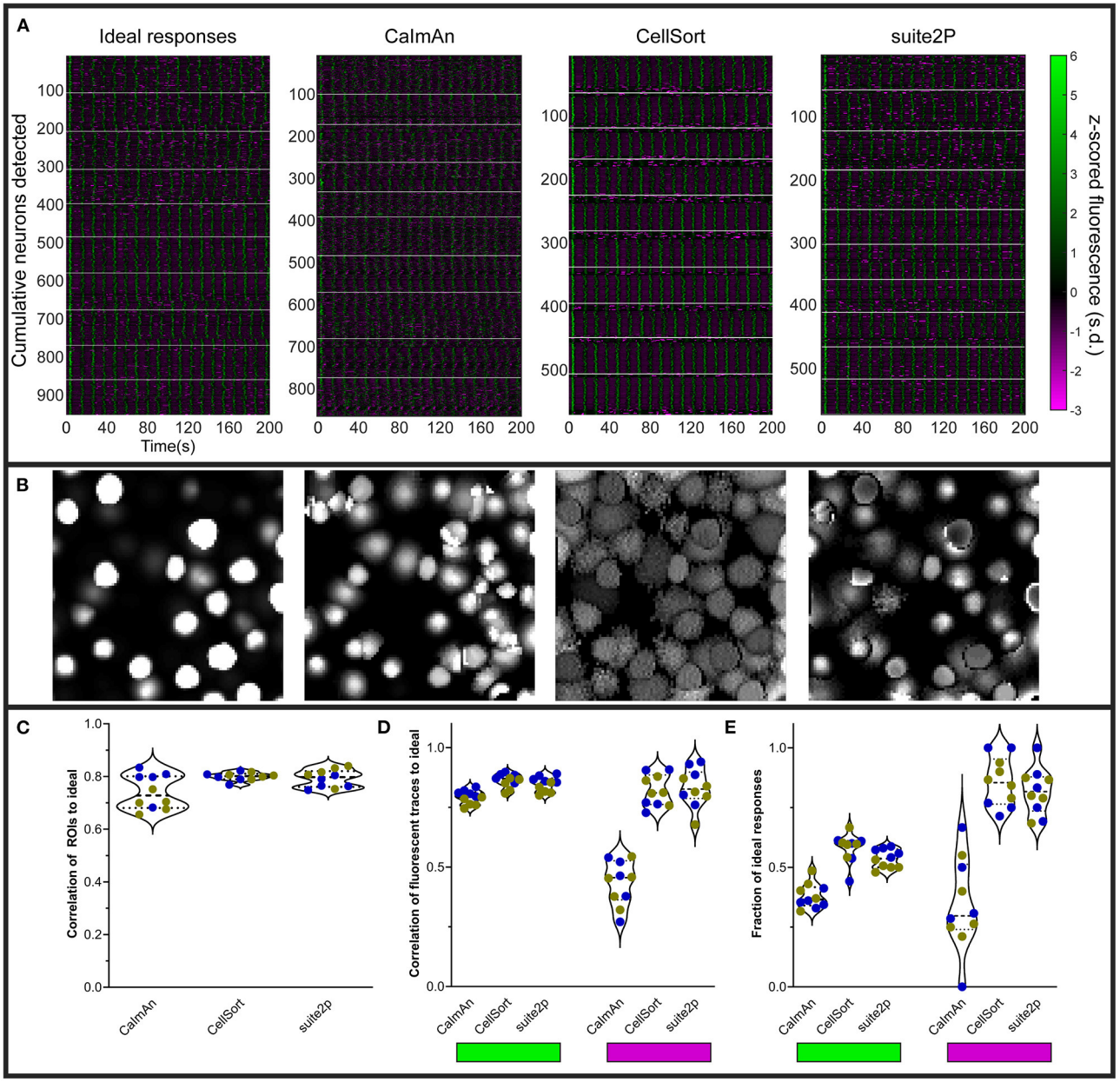

FIGURE 3 | Various analyses' performances on simulated data. **(A)** Raster plots of ideal responses from NAOMi, and extracted fluorescence traces from CaImAn, CellSort, and suite2p. All the fluorescent traces were z-scored from−3 to 6 s.d. White horizontal lines separate the individual datasets. **(B)** Segmentation of the regions of interest (ROIs) by each algorithm, as for the raster plots in **(A)**, for one representative dataset. **(C)** Quantification of the correlation between the ROIs identified by each of the three algorithms and the ideal ROIs. Symbol color indicate the percentage of inhibited neurons ($n = 5$ datasets with 10% inhibited neurons in blue, and $n = 5$ datasets with 20% inhibited neurons in yellow). **(D)** Average maximum correlations between the traces identified by each algorithm and the ideal responses for the activated neurons (left, green rectangle) and the inhibited neurons (right, magenta rectangle). **(E)** Fraction of the ideal responses identified with a correlation above 0.5 by the three algorithms for the activated neurons (left) and the inhibited neurons (right).

et al., 2018), and as observed in mice (Steinmetz et al., 2019) and flies (Galizia et al., 2010; Munch and Galizia, 2017).

Hyperpolarization is well-known to decrease GCaMP signals in cells that are partially active at resting potential and that can be further inactivated by hyperpolarization (Zhao et al., 2018). We speculate that the negative deflections that we observed in GCaMP6 signals of our real dataset (**Figure 1**) are, based on the spatial location and activity of the ROIs, Purkinje cells. In zebrafish, Purkinje cells receive excitatory inputs from granule cells and climbing fibers, and inhibitory inputs from stellate interneurons. Their cell bodies are located within one of the most superficial layers of the cerebellum, and hence would

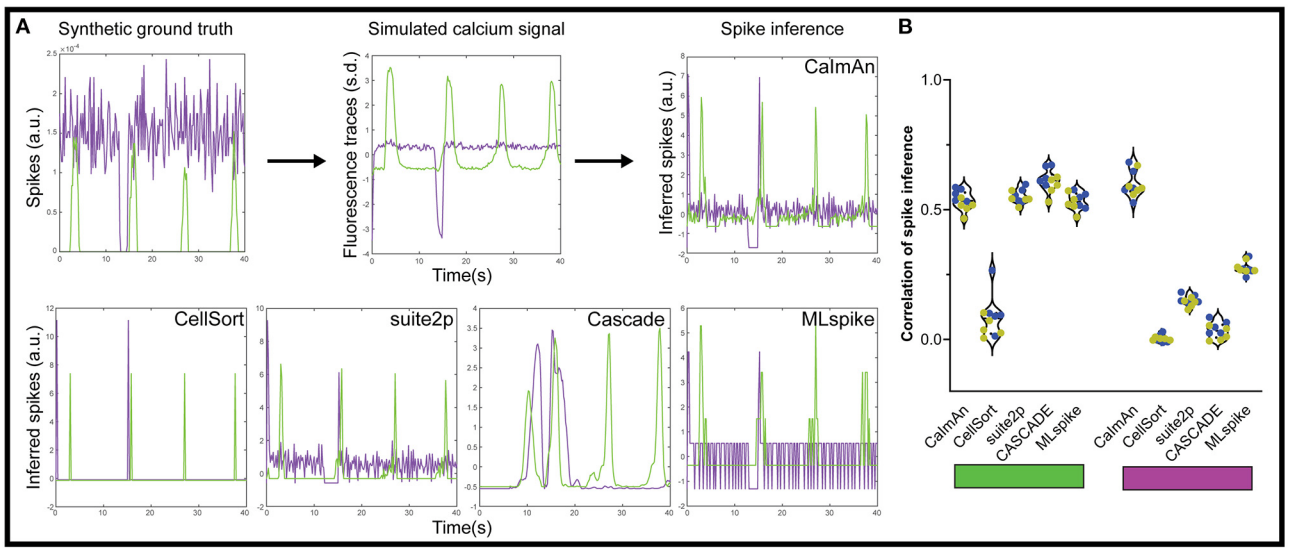

FIGURE 4 | Spike inference from simulated calcium traces. **(A)** We applied each of the five spike inference algorithm on simulated GECI fluorescence data generated from a synthetic ground truth. The inferred spikes were then compared to the synthetic ground truth using a correlation. We show example inferred spikes from each algorithm, as well as the synthetic ground truth and simulated fluorescence. **(B)** Correlation between the inferred spikes from the simulated calcium traces and the actual spikes for the activated neurons (left, green rectangle) and the inhibited neurons (right, magenta rectangle). Each datapoint represents the performance on one simulated dataset ($n = 5$ datasets with 10% inhibited neurons in blue, and $n = 5$ datasets with 20% inhibited neurons in yellow).

be the first cells to be optically sectioned from the dorsal orientation. Purkinje cells display bistable spontaneous activity, where they switch between the steady production of tonic or depolarising "up" spikes and short bursts of intermittent activity or hyperpolarizing "down" states (Sengupta and Thirumalai, 2015). Therefore, the negative defections in GCaMP6 signals that we observed in our real dataset in **Figure 1** could be tonically-active Purkinje cells in the superficial layers of cerebellum that have toggled to their climbing-fiber induced bursting or "down" state (Engbers et al., 2013), which would produce negative voltages.

We have demonstrated that a moving baseline, such as for $\Delta F/F_0$, may create artifacts in inhibited neurons, which may lead to the generation of spurious positive signals. Finally, inhibited responses, when normalized, can also be lost when using NMF or thresholding approaches to analyze and visualize the data (**Figure 1C**). Even pixel-wise NMF approaches such as Thunder could miss inhibited responses, if they include a preprocessing step such as $\Delta F/F_0$ (Freeman et al., 2014). It would be interesting to revisit the data from studies that used these approaches (Mu et al., 2019; Torigoe et al., 2019) to see whether inhibited neurons are present in the datasets. We suggest that an initial unbiased step of data exploration of the dataset should be performed to ensure that no inhibited responses are present before pursuing steps including the above methods that assume non-negativity. Principal component analysis, or other dimensionality reduction tools, could be used to explore the data in the case of spontaneous activity or complex stimuli. Alternatively, for stimulus-driven activity, a correlation or linear regression should reveal any neuronal activity that deviates negatively from baseline.

By using simulated data (**Figure 2**), we tested how reliably CellSort, suite2p, and CaImAn could detect inhibited neurons in a calcium imaging dataset. CellSort was the best algorithm in our specific analysis of nuclear-targeted GCaMP (**Figure 3**), which is at odds with other comparisons (Charles et al., 2019). However, both CaImAn and suite2p are better suited to larger datasets of thousands of neurons. Between these two approaches, suite2p outperformed CaImAn for the detection of activated responses both in terms of the fidelity of the extracted response (**Figure 3D**, mean difference of 0.056 and $p = 0.0006$) and the fraction of responses identified (**Figure 3E**, mean difference of 0.16 and $p < 0.0001$). For inhibited responses, suite2p largely outperformed CaImAn with more than twice the fraction of ideal inhibited responses recovered (mean difference $= 0.47$ and $p < 0.0001$). CellSort is a good option for smaller datasets as it requires an *a priori* estimate of the number of components (neurons) and does not perform as well at low SNR typical of endoscopic recordings (Resendez et al., 2016; Zhou et al., 2018). Among the currently available approaches, we therefore favor suite2p, or CellSort for smaller datasets, in order to recover the most inhibited responses from calcium imaging of neuronal activity.

As for the spike inference, the algorithm included with CellSort did poorly on both activated and inhibited neurons. MLspike was outperformed by suite2p and CaImAn performed similarly to one another with activated neurons, in line with published results (Pachitariu et al., 2018). However, for inhibited responses, suite2p's performance collapsed when using OASIS. CASCADE performed well on the activated neurons, but the lack of inhibited neurons in the training datasets mean it performed poorly when detecting our inhibited responses, as such the use of a more varied training dataset could improve its performance. Overall CaImAn, using FOOPSI, presents the best approach to infer spikes from inhibited neurons (Vogelstein et al., 2010). Several other methods of spike inference have been benchmarked

(Berens et al., 2018), and it would be interesting to benchmark these with simulated inhibited neurons. Finally, we want to point out that all the spike inference algorithms mistakenly inferred a strong spiking probably/rate when the inhibition ended (**Figure 4A**, bottom), this would need to be accounted for in any downstream analysis of these inferences.

We saw no significant differences between simulated datasets with 10 or 20% inhibited neurons in any of the above metrics, showing that the proportion of inhibited neurons should not affect the detection of the activated neurons.

Overall, we suggest that the PCA/ICA approach, such as implemented in CellSort should be favored when dealing with smaller datasets, where the number of ROIs can be estimated before processing, and nuclear-targeted GECIs. For larger datasets however, we suggest using suite2p, which has worked well both with nuclear-targeted simulations in this study, and with a cytoplasmic GECI simulation (Charles et al., 2019). With regard to spike inference, the FOOPSI approach gave the best results, so we would favor this method when inferring spikes. In terms of data analysis, NMF or thresholding based on activity should be avoided before an unbiased analysis such as PCA, or k-means can be used to ensure the absence of relevant inhibited neurons.

Another way to address the issue of negative deviations is to change the calcium indicator used. For example, an inverse-response GECI (Zhao et al., 2018) has been specifically designed to easily visualize neuronal inhibition in flies, but then the activated neurons would be the ones deviating negatively from the baseline. A powerful alternative is the use of Genetically Encoded fluorescent Voltage Indicators (GEVIs), which directly report membrane potential (Akemann et al., 2010; Gong et al., 2015; Bando et al., 2019). Those GEVIs can be used to visualize action potentials with millisecond time resolution, their signal to noise ratio are constantly improving and they would offer an accurate measure of the actual spikes of the imaged neurons. However, the requirement of ∼kHz imaging speed precludes their use for volumetric or whole-brain imaging with the current technologies.

Finally, GECIs allow the genetic targeting of the calcium indicator to subtypes of neuronal cells, providing information on the expected firing rate and behavior of the neurons (Scott et al., 2007; Forster et al., 2017). Alternatively, imaged neurons can be identified *post-hoc* using fixation and labeling (Lovett-Barron et al., 2017), which can be used to choose an analysis method that would be more appropriate if one expects negative deviations.

In summary, we have shown that assumptions of non-negativity can lead to the omission of real and simulated inhibited responses, and can produce spurious positive signals during the analysis of neural calcium imaging datasets. We have tested three popular and readily available approaches for analyzing such data, and provide recommendations for the best approaches to use when analyzing calcium imaging data that may contain inhibited signals.

DATA AVAILABILITY STATEMENT

The datasets generated for this study can be found in online repositories. The names of the repository/repositories and accession number(s) can be found at: doi: 10.14264/63584b3.

ETHICS STATEMENT

The animal study was reviewed and approved by SBMS/378/16/ARC.

AUTHOR CONTRIBUTIONS

GV, LC, and ES contributed conception and design of the study and wrote sections of the manuscript. GV performed the statistical analysis. GV and LC wrote the first draft of the manuscript. All authors contributed to manuscript revision, read, and approved the submitted version.

FUNDING

Support was provided by NHMRC Project Grants APP1066887 and APP1165173, a Simons Foundation Pilot Award (399432), a Simons Foundation Research Award (625793), and two ARC Discovery Project Grants (DP140102036 and DP110103612) to ES, and the Australian National Fabrication Facility (ANFF), QLD node. The research reported in this publication was supported by the National Institute of Neurological Disorders and Stroke of the National Institutes of Health under Award Number R01NS118406 to ES. The content is solely the responsibility of the authors and does not necessarily represent the official views of the National Institutes of Health. GV was supported by an EMBO Long-term Fellowship.

ACKNOWLEDGMENTS

We thank Itia A. Favre-Bulle for data and the Vulcans who remind us "Challenge your preconceptions, or they will challenge you". We thank Carsen Stringer, Peter Rupprecht, and Eftichyos A. Pnevmatikakis for helpful discussions and comments on the manuscript.

SUPPLEMENTARY MATERIAL

The Supplementary Material for this article can be found online at: https://www.frontiersin.org/articles/10.3389/fncir.2020.607391/full#supplementary-material

REFERENCES

Ahrens, M. B., Li, J. M., Orger, M. B., and Robson, D. (2012). Brain-wide neuronal dynamics during motor adaptation in zebrafish. *Nature* 485, 471–477. doi: 10.1038/nature11057

Akemann, W., Mutoh, H., Perron, A., Rossier, J., and Knopfel, T. (2010). Imaging brain electric signals with genetically targeted voltage-sensitive fluorescent proteins. *Nat. Methods* 7, 643–649. doi: 10.1038/nmeth.1479

Akerboom, J., Chen, T. W., Wardill, T. J., and Tian, L. (2012). Optimization of a GCaMP calcium indicator for neural activity

imaging. *J. Neurosci.* 32, 13819–13840. doi: 10.1523/JNEUROSCI.2601-12.2012

Baddeley, R., Abbott, L. F., Booth, M. C., and Sengpiel, F. (1997). Responses of neurons in primary and inferior temporal visual cortices to natural scenes. *Proc. Biol. Sci.* 264, 1775–1783. doi: 10.1098/rspb.1997.0246

Balaji, R., Bielmeier, C., Harz, H., Bates, J., Stadler, C., Hildebrand, A., et al. (2017). Calcium spikes, waves and oscillations in a large, patterned epithelial tissue. *Sci. Rep.* 7:42786. doi: 10.1038/srep42786

Bando, Y., Sakamoto, M., Kim, S., Ayzenshtat, I., and Yuste, R. (2019). Comparative evaluation of genetically encoded voltage indicators. *Cell Rep.* 26, 802–813.e804. doi: 10.1016/j.celrep.2018.12.088

Berens, P., Freeman, J., Deneux, T., Chenkov, N., McColgan, T., Speiser, A., et al. (2018). Community-based benchmarking improves spike rate inference from two-photon calcium imaging data. *PLoS Comput. Biol.* 14:e1006157. doi: 10.1371/journal.pcbi.1006157

Cai, D. J., Aharoni, D., Shuman, T., Shobe, J., Biane, J., Song, W., et al. (2016). A shared neural ensemble links distinct contextual memories encoded close in time. *Nature* 534, 115–118. doi: 10.1038/nature17955

Charles, A. S., Song, A., Gauthier, J. L., and Pillow, J. W. (2019). Neural anatomy and optical microscopy (NAOMi) simulation for evaluating calcium imaging methods. *bioRxiv [Preprint]*. doi: 10.1101/726174

Chen, Q., Cichon, J., Wang, W., Qiu, L., and Lee, S. J. (2012). Imaging neural activity using Thy1-GCaMP transgenic mice. *Neuron* 76, 297–308. doi: 10.1016/j.neuron.2012.07.011

Chen, T. W., Wardill, T. J., Sun, Y., and Pulver, S. R. (2013). Ultrasensitive fluorescent proteins for imaging neuronal activity. *Nature* 499, 295–300. doi: 10.1038/nature12354

Constantin, L., Poulsen, R. E., Scholz, L. A., and Favre-Bulle, I. (2020). Altered brain-wide auditory networks in a zebrafish model of fragile X syndrome. *BMC Biol.* 18:125. doi: 10.1186/s12915-020-00857-6

Cullen, K. E., and McCrea, R. A. (1993). Firing behavior of brain stem neurons during voluntary cancellation of the horizontal vestibuloocular reflex. I. Secondary vestibular neurons. *J. Neurophysiol.* 70, 828–843. doi: 10.1152/jn.1993.70.2.828

Daviu, N., Fuzesi, T., Rosenegger, D. G., and Rasiah, N. P. (2020). Paraventricular nucleus CRH neurons encode stress controllability and regulate defensive behavior selection. *Nat. Neurosci.* 23, 398–410. doi: 10.1038/s41593-020-0591-0

Deneux, T., Kaszas, A., Szalay, G., Katona, G., Lakner, T., Grinvald, A., et al. (2016). Accurate spike estimation from noisy calcium signals for ultrafast three-dimensional imaging of large neuronal populations *in vivo*. *Nat. Commun.* 7:12190. doi: 10.1038/ncomms12190

Engbers, J. D., Fernandez, F. R., and Turner, R. W. (2013). Bistability in purkinje neurons: ups and downs in cerebellar research. *Neural. Netw.* 47, 18–31. doi: 10.1016/j.neunet.2012.09.006

Etter, G., Manseau, F., and Williams, S. (2020). A probabilistic framework for decoding behavior from *in vivo* calcium imaging data. *Front. Neural. Circuits* 14:19. doi: 10.3389/fncir.2020.00019

Favre-Bulle, I. A., Stilgoe, A. B., Rubinsztein-Dunlop, H., and Scott, E. K. (2017). Optical trapping of otoliths drives vestibular behaviours in larval zebrafish. *Nat. Commun.* 8:630. doi: 10.1038/s41467-017-00713-2

Favre-Bulle, I. A., Stilgoe, A. B., Scott, E. K., and Rubinsztein-Dunlop, H. (2019). Optical trapping *in vivo*: theory, practice, and applications. *Nanophotonics* 8, 1023–1040. doi: 10.1515/nanoph-2019-0055

Favre-Bulle, I. A., Taylor, M. A., Marquez-Legorreta, E., Vanwalleghem, G., Poulsen, R., Rubinsztein-Dunlop, H., et al. (2020). Sound generation in zebrafish with bio-opto-acoustics (BOA). *bioRxiv [Preprint]*. doi: 10.1101/2020.06.09.143362

Favre-Bulle, I. A., Vanwalleghem, G., Taylor, M. A., Rubinsztein-Dunlop, H., and Scott, E. (2018). Cellular-resolution imaging of vestibular processing across the larval zebrafish brain. *Curr. Biol.* 28, 3711–3722.e3713. doi: 10.1016/j.cub.2018.09.060

Forster, D., Arnold-Ammer, I., Laurell, E., Barker, A. J., and Fernandes, A. (2017). Genetic targeting and anatomical registration of neuronal populations in the zebrafish brain with a new set of BAC transgenic tools. *Sci. Rep.* 7:5230. doi: 10.1038/s41598-017-04657-x

Freeman, J., Vladimirov, N., Kawashima, T., Mu, Y., and Sofroniew, N. J. (2014). Mapping brain activity at scale with cluster computing. *Nat. Methods* 11, 941–950. doi: 10.1038/nmeth.3041

Friedrich, J., Zhou, P., and Paninski, L. (2017). Fast online deconvolution of calcium imaging data. *PLoS Comput. Biol.* 13:e1005423. doi: 10.1371/journal.pcbi.1005423

Galizia, C. G., Munch, D., Strauch, M., Nissler, A., and Ma, S. (2010). Integrating heterogeneous odor response data into a common response model: a DoOR to the complete olfactome. *Chem. Senses.* 35, 551–563. doi: 10.1093/chemse/bjq042

Giovannucci, A., Friedrich, J., Gunn, P., Kalfon, J., and Brown, B. L. (2019). CaImAn an open source tool for scalable calcium imaging data analysis. *Elife* 8:e38173. doi: 10.7554/eLife.38173

Gong, Y., Huang, C., Li, J. Z., and Grewe, B. F. (2015). High-speed recording of neural spikes in awake mice and flies with a fluorescent voltage sensor. *Science* 350, 1361–1366. doi: 10.1126/science.aab0810

Heap, L. A. L., Vanwalleghem, G., Thompson, A. W., and Favre-Bulle, I. A. (2018). Luminance changes drive directional startle through a thalamic pathway. *Neuron* 99, 293–301.e294. doi: 10.1016/j.neuron.2018.06.013

Klioutchnikov, A., Wallace, D. J., Frosz, M. H., and Zeltner, R. (2020). Three-photon head-mounted microscope for imaging deep cortical layers in freely moving rats. *Nat. Methods* 17, 509–513. doi: 10.1038/s41592-020-0817-9

Kubo, F., Hablitzel, B., Dal Maschio, M., Driever, W., Baier, H., Arrenberg, A., et al. (2014). Functional architecture of an optic flow-responsive area that drives horizontal eye movements in zebrafish. *Neuron* 81, 1344–1359. doi: 10.1016/j.neuron.2014.02.043

Lovett-Barron, M., Andalman, A. S., Allen, W. E., and Vesuna, S. (2017). Ancestral circuits for the coordinated modulation of brain state. *Cell* 171, 1411–1423.e1417. doi: 10.1016/j.cell.2017.10.021

Marquez-Legorreta, E., Constantin, L., Piber, M., Favre-Bulle, I. A., and Taylor, M. (2019). Brain-wide visual habituation networks in wild type and & zebrafish. *bioRxiv [Preprint]*. doi: 10.1101/722074

Mu, Y., Bennett, D. V., Rubinov, M., Narayan, S., and Yang, C. (2019). Glia accumulate evidence that actions are futile and suppress unsuccessful behavior. *Cell* 178, 27–43.e19. doi: 10.1016/j.cell.2019.05.050

Mukamel, E. A., Nimmerjahn, A., and Schnitzer, M. J. (2009). Automated analysis of cellular signals from large-scale calcium imaging data. *Neuron* 63, 747–760. doi: 10.1016/j.neuron.2009.08.009

Munch, D., and Galizia, C. G. (2017). Take time: odor coding capacity across sensory neurons increases over time in Drosophila. *J. Comp. Physiol. A Neuroethol. Sens. Neural. Behav. Physiol.* 203, 959–972. doi: 10.1007/s00359-017-1209-1

Nakai, J., Ohkura, M., and Imoto, K. (2001). A high signal-to-noise Ca(2+) probe composed of a single green fluorescent protein. *Nat. Biotechnol.* 19, 137–141. doi: 10.1038/84397

Naumann, E. A., Fitzgerald, J. E., Dunn, T. W., and Rihel, J. (2016). From whole-brain data to functional circuit models: the zebrafish optomotor response. *Cell* 167, 947–960.e920. doi: 10.1016/j.cell.2016.10.019

Pachitariu, M., Stringer, C., Dipoppa, M., Schröder, S., and Rossi, L. F. (2017). Suite2p: beyond 10,000 neurons with standard two-photon microscopy. *bioRxiv [Preprint]*. doi: 10.1101/061507

Pachitariu, M., Stringer, C., and Harris, K. D. (2018). Robustness of spike deconvolution for neuronal calcium imaging. *J. Neurosci.* 38, 7976–7985. doi: 10.1523/JNEUROSCI.3339-17.2018

Pnevmatikakis, E. A., Soudry, D., Gao, Y., Machado, T. A., Merel, J., Pfau, D., et al. (2016). Simultaneous denoising, deconvolution, and demixing of calcium imaging data. *Neuron* 89, 285–299. doi: 10.1016/j.neuron.2015.11.037

Pologruto, T. A., Yasuda, R., and Svoboda, K. (2004). Monitoring neural activity and [Ca2+] with genetically encoded Ca2+ indicators. *J. Neurosci.* 24, 9572–9579. doi: 10.1523/JNEUROSCI.2854-04.2004

Resendez, S. L., Jennings, J. H., Ung, R. L., Namboodiri, V. M., Zhou, Z. C., Otis, J. M., et al. (2016). Visualization of cortical, subcortical and deep brain neural circuit dynamics during naturalistic mammalian behavior with head-mounted microscopes and chronically implanted lenses. *Nat. Protoc.* 11, 566–597. doi: 10.1038/nprot.2016.021

Rupprecht, P., Carta, S., Hoffmann, A., Echizen, M., Kitamura, K., Helmchen, F., et al. (2020). A deep learning toolbox for noise-optimized, generalized spike inference from calcium imaging data. *bioRxiv [Preprint]*. doi: 10.1101/2020.08.31.272450

Scott, E. K., Mason, L., Arrenberg, A. B., Ziv, L., Gosse, N. J., Xiao, T., et al. (2007). Targeting neural circuitry in zebrafish using GAL4 enhancer trapping. *Nat. Methods* 4, 323–326. doi: 10.1038/nmeth1033

Sengupta, M., and Thirumalai, V. (2015). AMPA receptor mediated synaptic excitation drives state-dependent bursting in purkinje neurons of zebrafish larvae. *Elife* 4:e09158. doi: 10.7554/eLife.09158.020

Shannon, E. K., Stevens, A., Edrington, W., Zhao, Y., Jayasinghe, A. K., Page-McCaw, A., et al. (2017). Multiple mechanisms drive calcium signal dynamics around laser-induced epithelial wounds. *Biophys. J.* 113, 1623–1635. doi: 10.1016/j.bpj.2017.07.022

Shimazu, H., and Precht, W. (1965). Tonic and kinetic responses of cat's vestibular neurons to horizontal angular acceleration. *J. Neurophysiol.* 28, 991–1013. doi: 10.1152/jn.1965.28.6.991

Shimazu, H., and Precht, W. (1966). Inhibition of central vestibular neurons from the contralateral labyrinth and its mediating pathway. *J. Neurophysiol.* 29, 467–492. doi: 10.1152/jn.1966.29.3.467

Steinmetz, N. A., Zatka-Haas, P., Carandini, M., and Harris, K. D. (2019). Distributed coding of choice, action and engagement across the mouse brain. *Nature* 576, 266–273. doi: 10.1038/s41586-019-1787-x

Stevenson, A. J., Vanwalleghem, G., Stewart, T. A., Condon, N. D., Lloyd-Lewis, B., Marino, N., et al. (2020). Multiscale activity imaging in the mammary gland reveals how oxytocin enables lactation. *Proc Natl Acad Sci USA* 117, 26822–26832. doi: 10.1101/657510

Stringer, C., and Pachitariu, M. (2019). Computational processing of neural recordings from calcium imaging data. *Curr. Opin. Neurobiol.* 55, 22–31. doi: 10.1016/j.conb.2018.11.005

Suh, G. S., Wong, A. M., Hergarden, A. C., Wang, J. W., Simon, A. F., Benzer, S., et al. (2004). A single population of olfactory sensory neurons mediates an innate avoidance behaviour in Drosophila. *Nature* 431, 854–859. doi: 10.1038/nature02980

Taylor, M. A., Vanwalleghem, G. C., Favre-Bulle, I. A., and Scott, E. K. (2018). Diffuse light-sheet microscopy for stripe-free calcium imaging of neural populations. *J. Biophoton.* 11:e201800088. doi: 10.1002/jbio.201800088

Theis, L., Berens, P., Froudarakis, E., Reimer, J., Roman Roson, M., Baden, T., et al. (2016). Benchmarking spike rate inference in population calcium imaging. *Neuron* 90, 471–482. doi: 10.1016/j.neuron.2016.04.014

Tian, J., Tep, C., Zhu, M. X., and Yoon, S. O. (2013). Changes in Spontaneous firing patterns of cerebellar purkinje cells in p75 knockout mice. *Cerebellum* 12, 300–303. doi: 10.1007/s12311-012-0439-6

Tian, L., Hires, S. A., Mao, T., Huber, D., Chiappe, M. E., Chalasani, S. H., et al. (2009). Imaging neural activity in worms, flies and mice with improved GCaMP calcium indicators. *Nat. Methods* 6, 875–881. doi: 10.1038/nmeth.1398

Torigoe, M., Islam, T., Kakinuma, H., Fung, C. C. A., Isomura, T., Shimazaki, H., et al. (2019). Future state prediction errors guide active avoidance behavior by adult zebrafish. *bioRxiv [Preprint]*. doi: 10.2139/ssrn.3345551

Vanwalleghem, G., Schuster, K., Taylor, M. A., Favre-Bulle, I. A., and Scott, E. K. (2020). Brain-wide mapping of water flow perception in zebrafish. *J. Neurosci.* 40, 4130–4144. doi: 10.1523/JNEUROSCI.0049-20.2020

Vogelstein, J. T., Packer, A. M., Machado, T. A., Sippy, T., Babadi, B., Yuste, R., et al. (2010). Fast nonnegative deconvolution for spike train inference from population calcium imaging. *J. Neurophysiol.* 104, 3691–3704. doi: 10.1152/jn.01073.2009

Wang, J. W., Wong, A. M., Flores, J., Vosshall, L. B., and Axel, R. (2003). Two-photon calcium imaging reveals an odor-evoked map of activity in the fly brain. *Cell* 112, 271–282. doi: 10.1016/S0092-8674(03)00004-7

Wyart, C., Del Bene, F., Warp, E., Scott, E. K., Trauner, D., Baier, H., et al. (2009). Optogenetic dissection of a behavioural module in the vertebrate spinal cord. *Nature* 461, 407–410. doi: 10.1038/nature08323

Zhao, Y., Bushey, D., Zhao, Y., Schreiter, E. R., Harrison, D. J., Wong, A. M., et al. (2018). Inverse-response Ca(2+) indicators for optogenetic visualization of neuronal inhibition. *Sci. Rep.* 8:11758. doi: 10.1038/s41598-018-30080-x

Zhou, P., Resendez, S. L., Rodriguez-Romaguera, J., Jimenez, J. C., Neufeld, S. Q., Giovannucci, A., et al. (2018). Efficient and accurate extraction of *in vivo* calcium signals from microendoscopic video data. *Elife* 7:e28728. doi: 10.7554/eLife.28728

Zimmerman, C. A., Huey, E. L., Ahn, J. S., Beutler, L. R., Tan, C. L., Kosar, S., et al. (2019). A gut-to-brain signal of fluid osmolarity controls thirst satiation. *Nature* 568, 98–102. doi: 10.1038/s41586-019-1066-x

Conflict of Interest: The authors declare that the research was conducted in the absence of any commercial or financial relationships that could be construed as a potential conflict of interest.

frontiers in Integrative Neuroscience

ORIGINAL RESEARCH
published: 11 January 2021
doi: 10.3389/fnint.2020.616778

Correlated Sensory and Sympathetic Innervation Between the Acupoint BL23 and Kidney in the Rat

Zhiyun Zhang[1,2], Dongsheng Xu[2], Jia Wang[2], Jingjing Cui[2], Shuang Wu[2], Ling Zou[2], Yi Shen[2], Xianghong Jing[1,2] and Wanzhu Bai[2]**

[1]*Key Laboratory of Acupuncture and Neurology of Zhejiang Province, Department of Neurobiology and Acupuncture Research, The Third Clinical Medical College, Zhejiang Chinese Medical University, Hangzhou, China,* [2]*Institute of Acupuncture and Moxibustion, China Academy of Chinese Medical Sciences, Beijing, China*

Objective: To investigate the sensory and sympathetic innervations associated with both acupoint "Shenshu" (BL23) and kidney in the rat for insight into the neuronal correlation between the Back-Shu Point and its corresponding visceral organ.

Methods: The BL23 and kidney were selected as the representative acupoint and visceral organ in this study, in which their local nerve fibers were examined by using double fluorescent immunohistochemistry with calcitonin gene-related peptide (CGRP) and tyrosine hydroxylase (TH). Meanwhile, their neuronal correlation in the dorsal root ganglia (DRGs), spinal cord, and sympathetic (paravertebral) chain were investigated using a double fluorescent neural tracing technique with Alexa Fluor 488 and 594 conjugates with cholera toxin subunit B (AF488/594-CTB).

Results: The local tissue of acupoint BL23 and the fibrous capsule of kidney distributed abundantly with CGRP- and TH-positive nerve fibers, corresponding to their sensory and sympathetic innervation. On the other hand, the sensory neurons associated with acupoint BL23 and kidney were labeled with AF488/594-CTB and distributed from thoracic (T) 11 to lumbar (L) 3 DRGs and from T10 to L2 DRGs, respectively, in which some of them in T12-T13 DRGs were simultaneously labeled with both AF488/594-CTB. Also, postganglionic neurons associated with both acupoint BL23 and kidney were found in the sympathetic chain at the same spinal segments but separately labeled with AF488-CTB and AF594-CTB.

Conclusion: Our study demonstrates the neural characteristics of the acupoint BL23 and kidney in the rat from the perspective of neurochemistry and neural pathways, providing an example for understanding the neuronal correlation between the Back-Shu Points and their corresponding visceral organs. These results suggest that the stimulation of the Back-Shu Points may regulate the activities of the target-organs *via* the periphery sensory and sympathetic pathways.

Keywords: kidney, Shenshu (BL23), double fluorescent neural tracing technique, sensory neuron, postganglionic neuron

OPEN ACCESS

Edited by:
Eduardo Weruaga, University of Salamanca, Spain

Reviewed by:
Elias Manjarrez, Meritorious Autonomous University of Puebla, Mexico
Raul Aguilar-Roblero, National Autonomous University of Mexico, Mexico

****Correspondence:***
Xianghong Jing
jxhtjb@263.net
Wanzhu Bai
wanzhubaisy@hotmail.com

Received: *13 October 2020*
Accepted: *15 December 2020*
Published: *11 January 2021*

Citation:
Zhang Z, Xu D, Wang J, Cui J, Wu S, Zou L, Shen Y, Jing X and Bai W (2021) Correlated Sensory and Sympathetic Innervation Between the Acupoint BL23 and Kidney in the Rat. Front. Integr. Neurosci. 14:616778. doi: 10.3389/fnint.2020.616778

INTRODUCTION

Back-Shu Points are the specific acupoints on the back, which are named as per their anatomical locations adjacent to visceral organs (in terms of Zang-Fu in Traditional Chinese Medicine; Cao et al., 2017). Although this kind of acupoints is commonly used for regulating the disorders of their corresponding visceral organs following the vicinal principle of acupoint selection, there is a lack of clear understanding of their inherent links (Cheng, 2011; Tu et al., 2019; Dai et al., 2020; Shou et al., 2020). Considering the diagnostic and therapeutic roles of Back-Shu Points playing in visceral diseases, viscerocutaneous reflexes have been paid more attention in this field. However, their neuronal correlation remains unclear (Cabioglu and Arslan, 2008; da Silva, 2010; Liu et al., 2010).

To reveal the inherent links between the Back-Shu Points and their corresponding visceral organs in detail, the acupoint "Shenshu" (BL23) and kidney were selected as the representative targets and examined with neuroanatomical approaches in the present study.

First, a double fluorescent immunohistochemistry with calcitonin gene-related peptide (CGRP) and tyrosine hydroxylase (TH) was employed to observe the sensory and sympathetic innervation in the local tissues of acupoint BL23 and the fibrous capsule of the kidney, respectively (Benarroch, 2011; Chakrabarty et al., 2013; Cui et al., 2015; Wang et al., 2019b). Second, the neural elements associated with acupoint BL23 and kidney were traced by using a double fluorescent neural tracing technique with Alexa Fluor 488 and 594 conjugates of cholera toxin subunit B (AF488/594-CTB) for figuring out the neuronal correlation between the acupoint BL23 and kidney. Through the injection of different neural tracers, sensory, sympathetic and motor neurons associated with BL23 and kidney can be observed. These two kinds of effective tools have been successfully applied in the field of acupuncture research (Xu et al., 2016; Wang et al., 2018b; Cui J. J. et al., 2019). By taking their advantages, we expect not only to determine the innervated characteristics of acupoint BL23 and kidney individually but also to outline the neuronal correlation between them *via* the sensory and sympathetic pathways. From the perspectives of neurochemistry and neural pathways, this research could provide valuable references for understanding the inherent links of Back-Shu Points and their corresponding visceral organs at the cellular level.

MATERIALS AND METHODS

Animals

A total of eight young adult male Sprague–Dawley rats (8–10 weeks, weight 180–210 g) were used in the present study. Animals [license number SCXK(JING) 2017-0005] were provided by the National Institutes for Food and Drug Control. All animals were maintained with free access to water and food under controlled conditions with a 12 h light and dark cycle at a temperature of 24 ± 2°C. This study was approved by the ethics committee of the Institute of Acupuncture and Moxibustion, China Academy of Chinese Medical Sciences (reference number 20160011). All surgical procedures were performed following guidelines for animal experiments by the National Institutes of Health Guide for the Care and Use of Laboratory Animals (National Academy Press, Washington, DC, USA, 1996).

Surgical Procedures and Tracer Injection

The BL23 and kidney were selected as the representative acupoint and visceral organ in this study. The corresponding site of BL23 on the rat was determined by relative anatomy (Xu et al., 2019). The BL23 locates at the same level as the inferior border of the spinous process of the second lumbar vertebra, 1.5 B-cun lateral to the posterior median line on the human (Huang and Huang, 2007). Under the respiratory anesthesia (1.5% isoflurane), a total of 4 μl 1% AF488-CTB (Invitrogen-Molecular Probes, Eugene, OR, USA) was injected subcutaneously and muscularly into the left side of BL23, while 2 μl 1% AF594-CTB was also injected into the left side of the fibrous capsule of the kidney that was exposed by local surgery. Hamilton micro-syringe was used for the injection. To prevent leakage of the solution, the syringe was left in place for an additional 5 min after injection and then withdrawn slowly.

Perfusion

Three days after injection, the rats were transcardially perfused with 100 ml of 0.9% saline followed by 300 ml of 4% paraformaldehyde in 0.1 M phosphate-buffered solution (PB, pH = 7.4). The local tissues of BL23 (at length of 5 mm and width of 3 mm) and the fibrous capsule of the kidney on the right side were taken for examining the nerve fibers in the regional distribution, while the spinal cord, dorsal root ganglia (DRGs), and sympathetic (paravertebral) chain on the left side were dissected out and stored in 25% sucrose in 0.1 M PB at 4°C for 2 days.

Section

Serial transverse sections of the skin tissue of BL23 and longitudinal sections of the sympathetic chain were cut at a thickness of 20 μm on a cryostat (Thermo, Microm International FSE, Germany) and mounted on silane-coated glass slides, while the sections of the spinal cord and DRGs were cut in the transverse and sagittal pattern, respectively on a freezing microtome (Microm International HM 430, Thermo, Germany). Also, the fibrous capsule of the kidney was mounted on silane-coated glass slides in a whole-mount pattern.

Double Fluorescent Immunohistochemistry

The mounted sections of skin tissue of BL23 and the fibrous capsule of the kidney were simultaneously stained by using double fluorescent immunohistochemistry with CGRP and TH. First, the tissues were incubated in a blocking solution containing 3% normal donkey serum and 0.5% Triton X-100 in 0.1 M PB for 30 min and then transferred to mouse anti-CGRP monoclonal antibody (1:1,000, Abcam, Hong Kong) and rabbit anti-TH antibody (1:1,000, Abcam, Hong Kong) for overnight at 4°C. On the following day, after washing three times with 0.1 M PB, the tissues were exposed to donkey anti-mouse Alexa Fluor 594, donkey anti-rabbit Alexa Fluor 488 secondary antibodies (1:500,

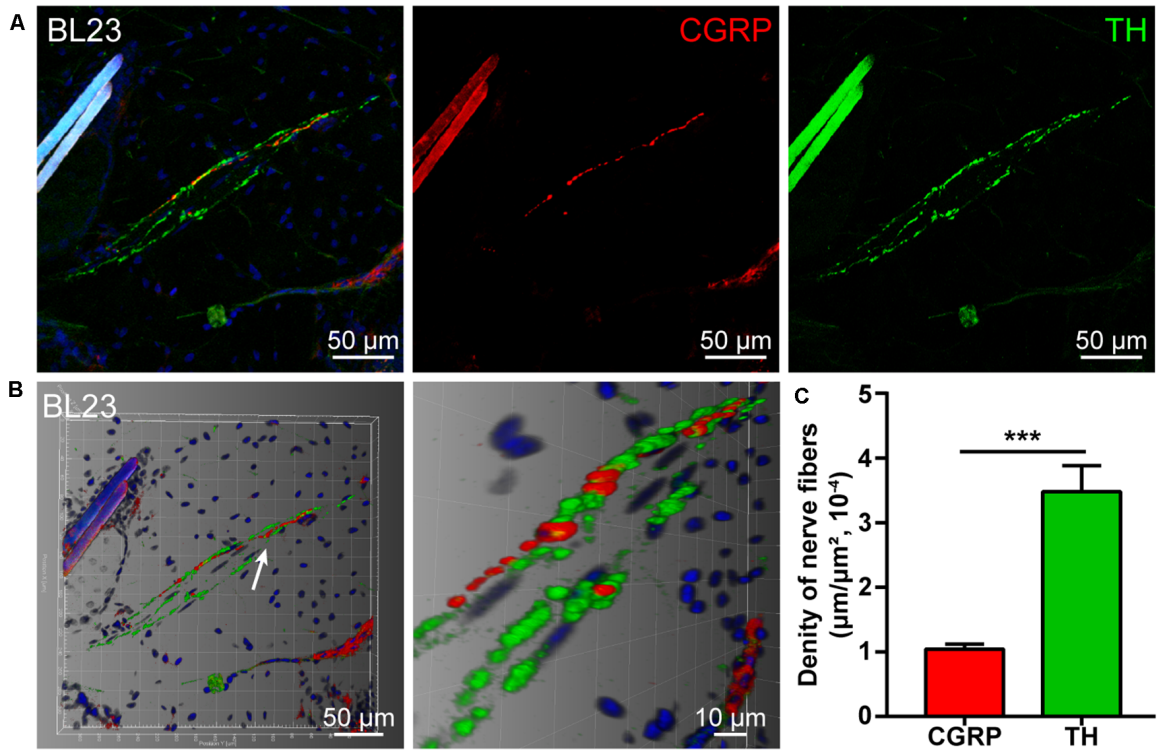

FIGURE 1 | Distribution of the calcitonin gene-related peptide (CGRP)- and tyrosine hydroxylase (TH)-positive nerve fibers in the local tissue of BL23. **(A)** Representative images of CGRP- and TH-positive nerve fibers in the local tissue of BL23. **(B)** Adjusted images from **(A)** with three-dimensional reconstruction in a sloping pattern showing the CGRP- and TH-labeling, respectively. **(C)** The density of CGRP- and TH-positive nerve fibers distributed in the local tissue of BL23 ($\bar{x} \pm$ SEM, $n = 6$). ***$p < 0.001$.

Molecular Probes, Eugene, OR, USA), and 4′,6-diamidino-2-phenylindole dihydrochloride (DAPI, 1:40,000; Molecular Probes, Eugene, OR, USA) for 2 h of incubation. After washing, the tissues were coverslipped with 50% glycerin for observation. In contrast, the neuronal labeling with AF488/594-CTB in the sections of the spinal cord, DRGs, and sympathetic chain can be directly observed without further staining.

Observation and Three-Dimensional Reconstruction

The anatomical structure of tissue sections from the spinal cord was based on Paxinos and Watson (2006). Samples were viewed and analyzed under a fluorescent microscope equipped with a digital camera (DP73, Olympus, Japan) or a laser scanning confocal microscope (FV1200, Olympus, Tokyo, Japan) equipped with a digital camera (DP70, Olympus, Tokyo, Japan). Three-dimensional reconstruction of CGRP- and TH-positive nerve fibers were performed using Imaris 7.7.1 software. Final images were processed with Adobe Photoshop/Illustrator CS5 (Adobe Systems, San Jose, CA, USA). The illustration was drawn with Adobe Illustrator CS5.

Statistical Analysis

Twenty images captured by fluorescent microscope (10× magnification) were randomly selected to measure the length of nerve fibers in the local tissue of BL23 and the fibrous capsule of the kidney by cellSens dimension software. The density of CGRP- and TH-positive nerve fibers were compared according to the ratio of the length of nerve fibers to the local area. Data was expressed with mean ± standard error of the mean. The statistical analysis was performed by two-tailed Student's *t*-test using the GraphPad Prism software 7.0.

RESULTS

The Distribution of CGRP- and TH-Positive Nerve Fibers

By using double fluorescent immunohistochemistry with CGRP and TH, there were abundant CGRP- and TH-positive nerve fibers observed in acupoint BL23 and the fibrous capsule of the kidney (**Figures 1A**, **2A**). These two kinds of nerve fibers ran together or separately. Although some of them are located closely in an intermingling pattern, by three-dimensional analysis, these two types of nerve fibers are distributed independently of each other (**Figures 1B**, **2B**). Furthermore, the length of nerve fibers was quantitatively analyzed within the same twenty areas (2,790 μm × 2,091 μm). As a comparison, the density of TH-positive nerve fibers was significantly higher than that of CGRP-positive nerve fibers in both regions (**Figures 1C**, **2C**).

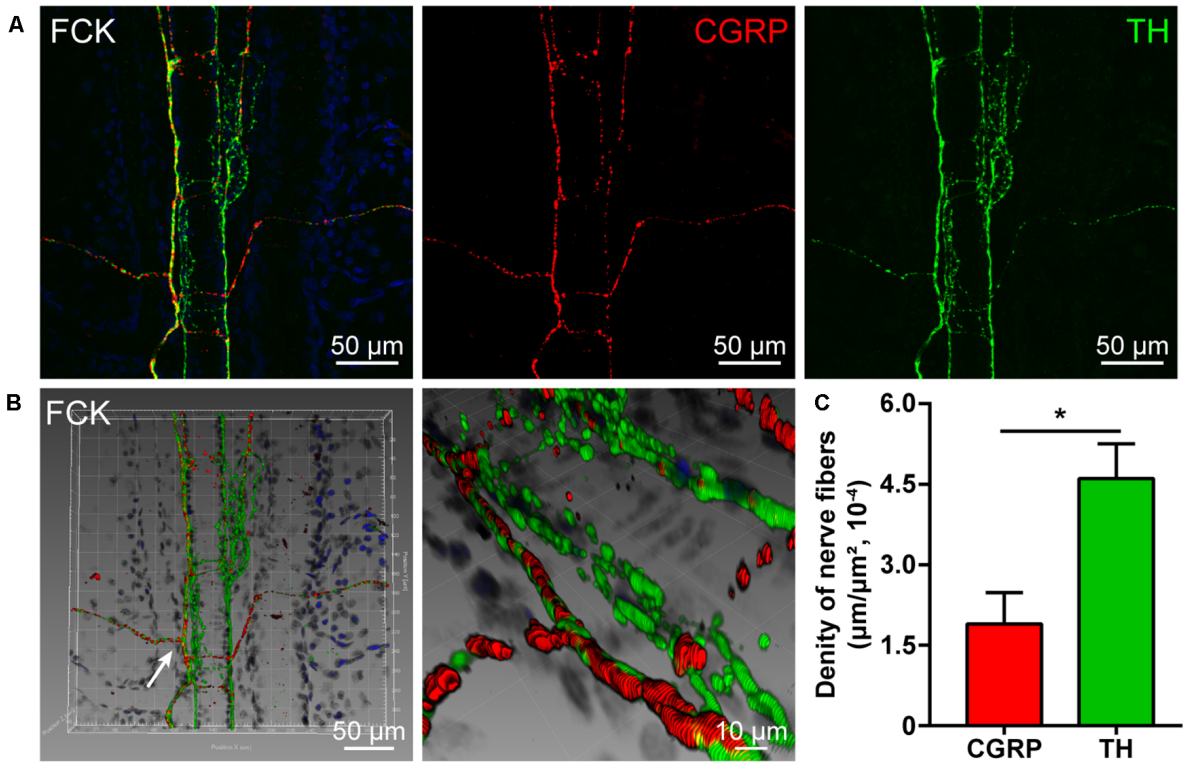

FIGURE 2 | Distribution of the CGRP- and TH-positive nerve fibers in the fibrous capsule of the kidney. **(A)** Representative images of CGRP- and TH-positive nerve fibers in the fibrous capsule of the kidney. **(B)** Adjusted images from panel **(A)** with three-dimensional reconstruction in a sloping pattern showing the CGRP- and TH-labeling, respectively. **(C)** The density of CGRP- and TH-positive nerve fibers distributed in the fibrous capsule of the kidney ($\bar{x} \pm$ SEM, $n = 6$). $^*p < 0.05$. FCK refers to the fibrous capsule of the kidney.

The Distribution of the Labeled Neurons With AF488/594-CTB

The sensory neurons associated with acupoint BL23 were labeled with AF488-CTB and observed from thoracic (T) 10 to lumbar (L) 2 DRGs with a higher concentration in T12-T13 DRGs. While the sensory neurons related to the kidney were labeled with AF594-CTB and detected from T10 to L1 DRGs with a higher concentration in T13 DRG. Comparatively, some sensory neurons were simultaneously labeled with AF488/594-CTB in T12-T13 DRGs (**Figures 3A,B**).

Also, postganglionic neurons associated with acupoint BL23 and kidney were found in the sympathetic chain at the same lumbar segments, but they were separately labeled with AF488-CTB or AF594-CTB (**Figure 4A**). By counting the labeled neurons, the number of the postganglionic neurons associated with the kidney was higher than that of BL23 (**Figure 4B**).

Besides the sensory and sympathetic innervation, the motor innervation was also examined. The motor neurons associated with the acupoint BL23 were also observed in the spinal ventral horn at cervical, thoracic, and lumbar segments, respectively (**Figure 5**). The number of labeled motor neurons was not further counted in the present study. As a technical limitation, parasympathetic innervation was not demonstrated in the present study.

DISCUSSION

By applying the immunohistochemical and neural tracing techniques, we provide detailed information to insight into the sensory and sympathetic innervation associated with acupoint BL23 and kidney, including the nerve fibers in local tissues, sensory neurons in the DRGs, and sympathetic neurons in the paravertebral chain.

Technical Consideration

From a technical point of view, the double fluorescent immunohistochemistry and neural tracing techniques have been effectively used in the field of acupuncture research (Wu et al., 2015b; Wang et al., 2018a, 2019a). Taking the advantages of double fluorescent immunohistochemistry, it makes a sharp contrast between the CGRP- and TH-positive nerve fibers on the local tissue of acupoint BL23 and the fibrous capsule of the kidney. Since the innervations of both the kidney and its fibrous capsule come from the same origin by way of the renal plexus (Mulder et al., 2013; Mompeo et al., 2016; van Amsterdam et al., 2016), the nerve fibers in the kidney were not further examined in the present study. A previous study has shown that CGRP- and TH-positive nerve fibers were distributed widely in the renal parenchymal (Mulder et al., 2013).

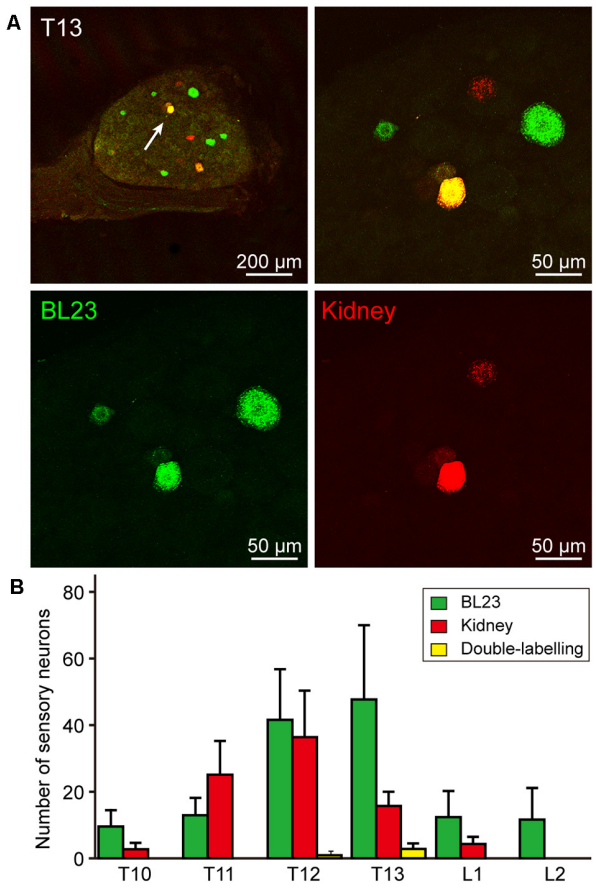

FIGURE 3 | Sensory neurons associated with the acupoint BL23 and kidney in the dorsal root ganglia (DRGs). **(A)** A representative and magnified (arrowhead) photomicrograph showing the distribution of AF488/594-CTB labeled sensory neurons in T13 DRG. The double-labeled neurons with AF488/594-CTB presenting in yellow. **(B)** The number of labeled sensory neurons in the thoracic (T) and lumbar (L) DRGs ($\bar{x} \pm$ SEM, $n = 8$).

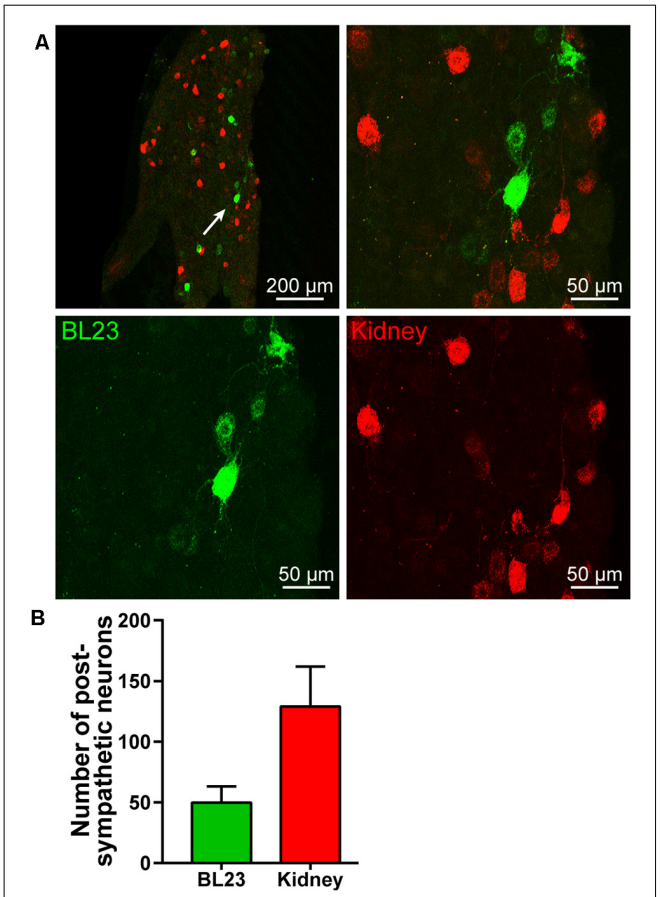

FIGURE 4 | Postsympathetic neurons associated with the acupoint BL23 and kidney in the sympathetic chain. **(A)** A representative and magnified (arrowhead) photomicrograph showing the distribution of AF488/594-CTB labeled post sympathetic neurons in the sympathetic chain at the lumbar segments. **(B)** The number of labeled post sympathetic neurons in the sympathetic chain ($\bar{x} \pm$ SEM, $n = 8$).

For the neural tracing approach, AF488/594-CTB have been frequently used to compare the sensory and motor innervations of the different acupoints as well as the sensory and sympathetic innervations of visceral organs (Cui et al., 2013; Wu et al., 2015a; Zhang et al., 2015, 2018). Using the same approach, we further revealed the innervated characteristics of acupoint BL23 and kidney individually, and also outlined the neuronal correlation between them *via* the sensory and sympathetic pathways.

It should be noted here that the labeled neurons with AF594/488-CTB belong to the first-order neurons associated with the acupoint BL23 and kidney. Although numerous studies have shown that the neurons in the nucleus tractus solitarius can be activated by acupuncture stimulation (Fang et al., 2017; Xiao et al., 2018), these higher-order neurons cannot be traced in this study, which might be transsynaptically traced with neurotropic viruses (Wyss and Donovan, 1984; Weiss and Chowdhury, 1998; Holt et al., 2019). The other limitation of this study should be also emphasized here that, since non-acupoints are still a controversial issue, a control group of non-acupoints was not included in our study (Kim et al., 2017; Liu, 2019).

CGRP- and TH-Positive Nerve Fibers Associated With the Acupoint BL23 and Kidney

By this study, it is clearly shown that the chemical innervation of the local tissue of acupoint BL23 and the fibrous capsule of the kidney includes the CGRP- and TH-positive nerve fibers. As a comparison, CGRP and TH are expressed separately on different kinds of nerve fibers running in a parallel or individual pattern.

As a sensitive bio-marker, CGRP expresses on the sensory nerve fibers that are widely distributed in the skin and visceral tissues (Eftekhari et al., 2013; Carr and Frings, 2019; Li et al., 2019; Smolilo et al., 2020). Previous studies have shown that CGRP-positive nerve fibers originate from the sensory neurons in DRGs and distribute widely in the local skin tissues of acupoints and the visceral tissues (Ha et al., 2014; Fan et al., 2018; De Logu et al., 2019). Growing evidence indicates that upregulated CGRP can cause vasodilatation and neurogenic inflammation during the pain and plays a critical role in the development of peripheral and central sensitization through

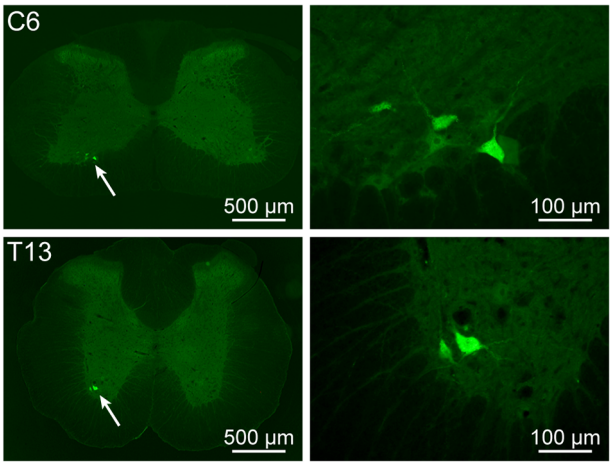

FIGURE 5 | Motor neurons associated with the acupoint BL23 in the spinal ventral horn. The representative and magnified (arrowhead) photomicrographs showing the distribution of AF488-CTB labeled motor neurons at cervical (C) 6 and thoracic (T) 13 segments.

the nociceptive signaling pathway (Russell et al., 2014; Iyengar et al., 2017). For the TH, it is the rate-limiting enzyme in the biosynthesis of the catecholamines dopamine, noradrenaline (NA, also known as norepinephrine), and adrenaline (Briggs et al., 2013; Dickson and Briggs, 2013). In the sympathetic nervous system, NA stores in the postganglionic neurons and their nerve fibers with TH-positive expression, serving as the main neurotransmitter released from the sympathetic nerve endings for controlling vasoconstriction (Mukouyama, 2014; Connolly et al., 2015). Accordingly, TH-positive nerve fibers distribute extensively in cutaneous tissues and internal organs (Rodionova et al., 2016; Enríquez-Pérez et al., 2017; Zhang et al., 2020).

Taken together, it indicates that NA and CGRP are a pair of opposite messengers for regulating the vasoconstriction and vasodilatation in response to the local stimulation of the peripheral sensory and sympathetic nerve fibers in the skin (Hodges and Johnson, 2009; Thomas, 2011; Zhang et al., 2020). Although both NA and CGRP play significant roles in maintaining the balance of homeostasis, how the stimulation of the acupoint to affect the release of these chemical messengers in its corresponding visceral organ remains to be studied under the physiological and pathological conditions.

Neuronal Correlation Between the Acupoint BL23 and Kidney

In parallel to observing the distribution of the sensory and sympathetic nerve fibers, the origins of sensory and postganglionic neurons associated with the acupoint BL23 and kidney were further determined with the neural tracing approach in this study. Even though most of the neurons were separately labeled with AF488-CTB or AF594-CTB, they locate adjacently in the DRGs and sympathetic chain at the same spinal segments, and some of the sensory neurons were simultaneously labeled with both AF488/594-CTB (**Figure 6**). These results indicate that there are a direct sensory correlation and an indirect sympathetic relationship between the acupoint BL23 and the kidney. Considering the sensory and sympathetic correlation, it is reasonable to speculate that stimulating signals from the acupoint BL23 area could be either directly or indirectly transported along the sensory and sympathetic pathways to the kidney,

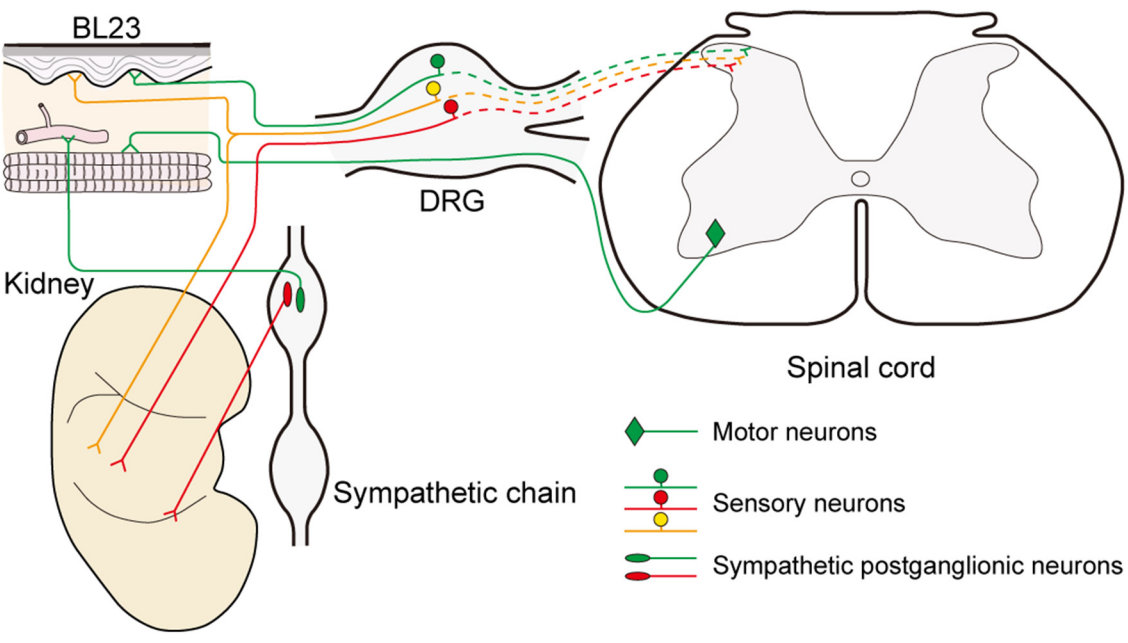

FIGURE 6 | Illustration of the sensory, sympathetic, and motor correlation between the acupoint BL23 and kidney.

conversely, the disorders of the kidney might also be reflected on the body surface through the same routines. A similar neuronal correlation was also observed between the acupoint BL23 and the adrenal gland in our previous study (Zhang et al., 2018). In the present research, we provide another example to explain the neuronal correlation between the Back-Shu points and their corresponding visceral organs *via* the sensory and sympathetic pathways.

Besides the sensory and sympathetic innervations, we also observed the motor neurons that are relative to acupoint BL23 only, and not to the kidney. Additionally, other parasympathetic elements, such as the vagal dorsal motor nucleus and nodose ganglion were not examined in the present study, but it is an important issue to be solved in the future study.

Clinical Implication

In general, the selection of acupoints along the course of meridians is the basic principle in the treatment of acupuncture. Unlike acupoints on the extremities to be orderly arranged in twelve meridians, it is an exception for the application of Back-Shu Points, because all of them belong to the bladder meridian of Foot-Taiyang, but each of them is responsible for reflecting and treating the disorder of visceral organs in corresponding to its name (Jia and Zhao, 2005). As it is known, certain areas of the skin sensitively responding to visceral diseases has been recorded in ancient Chinese medical texts (Cui X. et al., 2019), while the similar phenomenon has also been systematically investigated by the English neurologist Head (1861–1940) basing on the clinical findings of visceral disease associated with cutaneous manifestations as hyperalgesia or allodynia, and termed these areas as "Head zones" (Head, 1893). A recent study indicated that Back-Shu Points coincide spatially and functionally with the "maximum points" as described within the Head zones (Beissner et al., 2011; Beltrán Molano et al., 2014). According to the anatomo-functional correlation between the Back-Shu Points or the maximum points with their corresponding visceral organs, the most often considered explanation for their interactions is the viscerocutaneous reflexes (Gao et al., 2010; Rong et al., 2011). Although the exact mechanism behind viscerocutaneous reflexes is far from being fully understood, our neuroanatomical evidence supports the idea that viscerocutaneous reflexes could be an important approach for the neuronal interactions between the acupoint BL23 and kidney, which might be started as early as at the level of DRGs and sympathetic chain.

Coincidently, the "stimulating peripheral activity to relieve conditions (SPARC)" program to be funded by the National Institutes of Health is also aimed to investigate the complex pathways of nerve-organ interactions for ultimately promoting the precise treatment of diseases and conditions through peripheral electro-stimulation. Both acupuncture and SPARC are established by way of stimulating the peripheral nervous system. Therefore, figuring out the correlation between two types of peripheral nerves, somatic and visceral, could serve as a great source of inspiration for modern acupuncture research. As representative targets of acupoint and visceral organs, our study in the neuronal correlation of BL23 and kidney may provide an example to examine the interconnection between somatic and visceral nerves.

Increasing evidence shows that visceral diseases can induce the referred pain or sensitization on the body surface at their corresponding spinal segments in patients and experimental rats, which were closely correlated with the locations of traditional acupoints (Chen et al., 2014; Shi et al., 2018). In facing the sophisticated neuronal interconnection between the acupoints and visceral organs, from the viewpoint of the neural pathway, Back-Shu Points could be an important starting for observing the neuronal correlation with their corresponding visceral organs. The precise neural network how to serve the signal communication between the Back-Shu Points and their corresponding visceral organs might be a new issue in future studies.

In summary, by using the double fluorescent immunohistochemistry and neural tracing techniques, we have provided histological evidence to benefit the understanding of the sensory and sympathetic innervation of the acupoint BL23 and kidney. Considering the chemical characteristics and neural pathways, the acupoint BL23 and kidney establish a close sensory and sympathetic correlation between each other. Although present data cannot explain how the acupoint BL23 works on the kidney, this neuroanatomical connectivity may provide clues for exploring the mechanism of the role of neural pathways between the acupoint BL23 and kidney, which might also provide insights into the general rules underlying the other Back-Shu Points and their corresponding visceral organs.

DATA AVAILABILITY STATEMENT

The original contributions presented in the study are included in the article, further inquiries can be directed to the corresponding author/s.

ETHICS STATEMENT

The animal study was reviewed and approved by ethics committee of the Institute of Acupuncture and Moxibustion, China Academy of Chinese Medical Sciences.

AUTHOR CONTRIBUTIONS

The manuscript presented here was carried out in collaboration between all authors. ZZ, DX, SW, YS, and LZ carried out the experiments. ZZ, DX, JW, and JC analyzed the data. XJ and WB designed the study. ZZ, JW, and WB wrote the article. All authors read and approved the final version of the manuscript accepted for publication.

FUNDING

This study was supported by the project of the National Key R&D Program of China (No. 2019YFC1709103 and 2019YFC1709002) and the National Natural Science Foundation of China (No. 81774211, 81774432, 81801561, and 82004492).

REFERENCES

Beissner, F., Henke, C., and Unschuld, P. U. (2011). Forgotten features of head zones and their relation to diagnostically relevant acupuncture points. *Evid. Based Complement. Alternat. Med.* 2011:240653. doi: 10.1093/ecam/nen088

Beltrán Molano, M. L., Pinilla Bonilla, L. B., Beltrán Dussan, E. H., and Vasquez Londono, C. A. (2014). Anatomo-functional correlation between head zones and acupuncture channels and points: a comparative analysis from the perspective of neural therapy. *Evid. Based Complement. Alternat. Med.* 2014:836392. doi: 10.1155/2014/836392

Benarroch, E. E. (2011). CGRP: sensory neuropeptide with multiple neurologic implications. *Neurology* 77, 281–287. doi: 10.1212/WNL.0b013e31822550e2

Briggs, G. D., Nagy, G. M., and Dickson, P. W. (2013). Mechanism of action of salsolinol on tyrosine hydroxylase. *Neurochem. Int.* 63, 726–731. doi: 10.1016/j.neuint.2013.09.016

Cabioglu, M. T., and Arslan, G. (2008). Neurophysiologic basis of back-shu and huatuo-jiaji points. *Am. J. Chin. Med.* 36, 473–479. doi: 10.1142/S0192415X08005916

Cao, B. Y., Zhu, S. P., and Liu, T. (2017). Discussion on locating of back-shu points. *Zhongguo Zhen Jiu* 37, 851–855. doi: 10.13703/j.0255-2930.2017.08.013

Carr, R., and Frings, S. (2019). Neuropeptides in sensory signal processing. *Cell Tissue Res.* 375, 217–225. doi: 10.1007/s00441-018-2946-3

Chakrabarty, A., Liao, Z. H., and Smith, P. G. (2013). Angiotensin II receptor type 2 activation is required for cutaneous sensory hyperinnervation and hypersensitivity in a rat hind paw model of inflammatory pain. *J. Pain.* 14, 1053–1065. doi: 10.1016/j.jpain.2013.04.002

Chen, S. P., Wang, S. B., Rong, P. J., Wang, J. Y., Qiao, L. N., Feng, X. M., et al. (2014). Acupuncture for visceral pain: neural substrates and potential mechanisms. *Evid. Based Complement. Alternat. Med.* 2014:609594. doi: 10.1155/2014/609594

Cheng, K. J. (2011). Neuroanatomical characteristics of acupuncture points: relationship between their anatomical locations and traditional clinical indications. *Acupunct. Med.* 29, 289–294. doi: 10.1136/acupmed.2011.010056

Connolly, K., Jackson, D., Pullen, C., and Fenning, A. (2015). Alpha-adrenoceptor antagonism by Crassostrea gigas oyster extract inhibits noradrenaline-induced vascular contraction in Wistar rats. *J. Integr. Med.* 13, 194–200. doi: 10.1016/S2095-4964(15)60167-4

Cui, J. J., Ha, L. J., Zhu, X. L., Wang, F. C., Jing, X. H., and Bai, W. Z. (2013). Specificity of sensory and motor neurons associated with BL40 and GB30 in the rat: a dual fluorescent labeling study. *Evid. Based Complement. Alternat. Med.* 2013:643403. doi: 10.1155/2013/643403

Cui, J. J., Wang, J., and Bai, W. Z. (2019). Innervated properties of acupuncture points LI 4 and LR 3 in the rat: neural pathway tracing with cholera toxin subunit B. *Med. Acupunct.* 31, 169–175. doi: 10.1089/acu.2019.1334

Cui, J. J., Zhu, X. L., Shi, H., Su, Y. S., Jing, X. H., and Bai, W. Z. (2015). The expression of calcitonin gene-related peptide on the neurons associated Zusanli (ST 36) in rats. *Chin. J. Integr. Med.* 21, 630–634. doi: 10.1007/s11655-015-2111-8

Cui, X., Zhang, W., Sun, J. H., He, X., Fu, Y., Wang, J., et al. (2019). Correlation between referred pain distribution and acupoint sensitization in patients with intestinal diseases. *Zhongguo Zhen Jiu* 39, 1193–1198. doi: 10.13703/j.0255-2930.2019.11.016

da Silva, M. A. H. (2010). A neurosegmental perspective of the classical Back Shu points. *Med. Acupunct.* 22, 257–264. doi: 10.1089/acu.2010.0762

Dai, L., Ooi, V. V., Zhou, W. J., and Guang, J. (2020). Acupoint embedding therapy improves nonalcoholic fatty liver disease with abnormal transaminase: a PRISMA-compliant systematic review and meta-analysis. *Medicine* 99:e18775. doi: 10.1097/MD.0000000000018775

De Logu, F., Nassini, R., Landini, L., and Geppetti, P. (2019). Pathways of CGRP release from primary sensory neurons. *Handb. Exp. Pharmacol.* 255, 65–84. doi: 10.1007/164_2018_145

Dickson, P. W., and Briggs, G. D. (2013). Tyrosine hydroxylase: regulation by feedback inhibition and phosphorylation. *Adv. Pharmacol.* 68, 13–21. doi: 10.1016/B978-0-12-411512-5.00002-6

Eftekhari, S., Warfvinge, K., Blixt, F. W., and Edvinsson, L. (2013). Differentiation of nerve fibers storing CGRP and CGRP receptors in the peripheral trigeminovascular system. *J. Pain* 14, 1289–1303. doi: 10.1016/j.jpain.2013.03.010

Enríquez-Pérez, I. A., Galindo-Ordoñez, K. E., Pantoja-Ortíz, C. E., Martínez-Martínez, A., Acosta-González, R. I., Muñoz-Islas, E., et al. (2017). Streptozocin-induced type-1 diabetes mellitus results in decreased density of CGRP sensory and TH sympathetic nerve fibers that are positively correlated with bone loss at the mouse femoral neck. *Neurosci. Lett.* 655, 28–34. doi: 10.1016/j.neulet.2017.06.042

Fan, Y., Kim, D. H., Ryu, Y., Chang, S., Lee, B. H., Yang, C. H., et al. (2018). Neuropeptides SP and CGRP underlie the electrical properties of acupoints. *Front. Neurosci.* 12:907. doi: 10.3389/fnins.2018.00907

Fang, J. F., Du, J. Y., Shao, X. M., Fang, J. Q., and Liu, Z. (2017). Effect of electroacupuncture on the NTS is modulated primarily by acupuncture point selection and stimulation frequency in normal rats. *BMC Complement Altern. Med.* 17:182. doi: 10.1186/s12906-017-1690-7

Gao, J. H., Wang, Y. M., Cui, J. J., Ma, S. H., Cui, H. F., Fu, W. X., et al. (2010). On the scientific foundation that the tissue structure of acupoints can decide and affect specificity of acupoints-organs effects. *Zhongguo Zhen Jiu* 30, 293–295. doi: 10.13703/j.0255-2930.2010.04.010

Ha, L. J., Cui, J. J., Wang, F. C., Jing, X. H., and Bai, W. Z. (2014). The expression of calcitonin gene-related peptide in the sensory and motor neurons associated with "hegu" (LI 4) in the rat. *Zhen Ci Yan Jiu* 39, 112–116. doi: 10.13702/j.1000-0607.2014.02.005

Head, H. (1893). On disturbances of sensation with especial reference to the pain of visceral disease. *Brain* 16, 1–133. doi: 10.1093/brain/16.1-2.1

Hodges, G. J., and Johnson, J. M. (2009). Adrenergic control of the human cutaneous circulation. *Appl. Physiol. Nutr. Metab.* 34, 829–839. doi: 10.1139/H09-076

Holt, M. K., Pomeranz, L. E., Beier, K. T., Reimann, F., Gribble, F. M., and Rinaman, L. (2019). Synaptic inputs to the mouse dorsal vagal complex and its resident preproglucagon neurons. *J. Neurosci.* 39, 9767–9781. doi: 10.1523/JNEUROSCI.2145-19.2019

Huang, L. X., and Huang, Y. M. (2007). *Evidence-Based Surface Anatomy for Acupuncture-Acupuncture Integrated With Surface Anatomy and Imaging.* Beijing: People's Medical Publishing House.

Iyengar, S., Ossipov, M. H., and Johnson, K. W. (2017). The role of calcitonin gene-related peptide in peripheral and central pain mechanisms including migraine. *Pain* 158, 543–559. doi: 10.1097/j.pain.0000000000000831

Jia, J., and Zhao, J. S. (2005). Relation of indications of back-shu points of zang- and fu-organs with the bladder channel of foot-taiyang. *Zhongguo Zhen Jiu* 25, 414–416.

Kim, D. H., Ryu, Y., Hahm, D. H., Sohn, B. Y., Shim, I., Kwon, O. S., et al. (2017). Acupuncture points can be identified as cutaneous neurogenic inflammatory spots. *Sci. Rep.* 7:15214. doi: 10.1038/s41598-017-14359-z

Li, Y. Z., Miao, R. P., Yu, T. Y., Bai, W. Z., Cui, J. J., Lu, M. Q., et al. (2019). Mild mechanic stimulate on acupoints regulation of CGRP-positive cells and microglia morphology in spinal cord of sciatic nerve injured rats. *Front. Integr. Neurosci.* 13:58. doi: 10.3389/fnint.2019.00058

Liu, B. (2019). Non-acupoint effects: based on the analysis of traditional acupuncture-moxibustion theory. *Zhong Guo Zhen Jiu* 39, 161–165. doi: 10.13703/j.0255-2930.2019.02.014

Liu, J. L., Wang, J. Y., Chen, S. P., Gao, Y. H., Qiao, L. N., and Han, Y. J. (2010). Progress in the study on the mechanism underlying the correlation between acupoints/meridians and Zangfu organs. *Zhen Ci Yan Jiu* 35, 71–77. doi: 10.13702/j.1000-0607.2010.01.003

Mompeo, B., Maranillo, E., Garcia-Touchard, A., Larkin, T., and Sanudo, J. (2016). The gross anatomy of the renal sympathetic nerves revisited. *Clin. Anat.* 29, 660–664. doi: 10.1002/ca.22720

Mukouyama, Y. S. (2014). Vessel-dependent recruitment of sympathetic axons: looking for innervation in all the right places. *J. Clin. Invest.* 124, 2855–2857. doi: 10.1172/JCI76622

Mulder, J., Hökfelt, T., Knuepfer, M. M., and Kopp, U. C. (2013). Renal sensory and sympathetic nerves reinnervate the kidney in a similar time-dependent fashion after renal denervation in rats. *Am. J. Physiol. Regul. Integr. Comp. Physiol.* 304, R675–R682. doi: 10.1152/ajpregu.00599.2012

Paxinos, G., and Watson, C. (2006). *The Rat Brain in Stereotaxic Coordinates: Hard Cover Edition.* Amsterdam, Netherlands: Elsevier.

Rodionova, K., Fiedler, C., Guenther, F., Grouzmann, E., Neuhuber, W., Fischer, M. J., et al. (2016). Complex reinnervation pattern after unilateral

renal denervation in rats. *Am. J. Physiol. Regul. Integr. Comp. Physiol.* 310, R806–R818. doi: 10.1152/ajpregu.00227.2014

Rong, P. J., Zhu, B., Li, Y. Q., Gao, X. Y., Ben, H., Li, Y. H., et al. (2011). Mechanism of acupuncture regulating visceral sensation and mobility. *Front. Med.* 5, 151–156. doi: 10.1007/s11684-011-0129-7

Russell, F. A., King, R., Smillie, S. J., Kodji, X., and Brain, S. D. (2014). Calcitonin gene-related peptide: physiology and pathophysiology. *Physiol. Rev.* 94, 1099–1142. doi: 10.1152/physrev.00034.2013

Shi, J., Wang, J., Wang, Y., Liu, K., Fu, Y., Sun, J. H., et al. (2018). Correlation between referred pain region and sensitized acupoints in patients with stable angina pectoris and distribution of sensitized spots in rats with myocardial ischemia. *Zhen Ci Yan Jiu* 43, 277–284. doi: 10.13702/j.1000-0607.180123

Shou, Y., Hu, L., Zhang, C. H., Xu, S. F., Jin, Q., Huang, L., et al. (2020). Efficacy of acupuncture at three nasal acupoints plus acupoint application for perennial allergic rhinitis: a multicenter, randomized controlled trial protocol. *Trials* 21:110. doi: 10.1186/s13063-019-4039-3

Smolilo, D. J., Hibberd, T. J., Costa, M., Wattchow, D. A., De Fontgalland, D., and Spencer, N. J. (2020). Intrinsic sensory neurons provide direct input to motor neurons and interneurons in mouse distal colon *via* varicose baskets. *J. Comp. Neurol.* 528, 2033–2043. doi: 10.1002/cne.24872

Thomas, G. D. (2011). Neural control of the circulation. *Adv. Physiol. Educ.* 35, 28–32. doi: 10.1152/advan.00114.2010

Tu, Q., Gan, J. H., Shi, J. L., Yu, H., He, S. L., and Zhang, J. (2019). Effect of transcutaneous electrical acupoint stimulation on postoperative analgesia after ureteroscopic lithotripsy: a randomized controlled trial. *Urolithiasis* 47, 279–287. doi: 10.1007/s00240-018-1056-8

van Amsterdam, W. A. C., Blankestijn, P. J., Goldschmeding, R., and Bleys, R. L. A. W. (2016). The morphological substrate for renal denervation: nerve distribution patterns and parasympathetic nerves. A post-mortem histological study. *Ann. Anat.* 204, 71–79. doi: 10.1016/j.aanat.2015.11.004

Wang, J., Cui, J. J., Ha, L. J., She, C., Xu, D. S., Jing, X. H., et al. (2019a). Review on application of neural tracing technique to experimental research of acupuncture. *Zhen Ci Yan Jiu* 44, 926–931. doi: 10.13702/j.1000-0607.180522

Wang, Y. L., Su, Y. S., He, W., and Jing, X. H. (2019b). Electroacupuncture relieved visceral and referred hindpaw hypersensitivity in colitis rats by inhibiting tyrosine hydroxylase expression in the sixth lumbar dorsal root ganglia. *Neuropeptides* 77:101957. doi: 10.1016/j.npep.2019.101957

Wang, J., Cui, J. J., She, C., Xu, D. S., Zhang, Z. Y., Wang, H., et al. (2018a). Differential innervation of tissues located at traditional acupuncture points in the rat forehead and face. *Acupunct. Med.* 36, 408–414. doi: 10.1136/acupmed-2017-011595

Wang, J., Gao, Q., Xu, D. S., Zhang, Z. Y., Cui, J. J., and Bai, W. Z. (2018b). Application of laser scanning confocal microscope to morphologic research of acupuncture and moxibustion. *Zhen Ci Yan Jiu* 43, 581–584. doi: 10.13702/j.1000-0607.171003

Weiss, M. L., and Chowdhury, S. I. (1998). The renal afferent pathways in the rat: a pseudorabies virus study. *Brain Res.* 812, 227–241. doi: 10.1016/s0006-8993(98)00950-0

Wu, M. L., Cui, J. J., Xu, D. S., Zhang, K., Jing, X. H., and Bai, W. Z. (2015a). Neuroanatomical characteristics of deep and superficial needling using LI11 as an example. *Acupunct. Med.* 33, 472–477. doi: 10.1136/acupmed-2015-010882

Wu, M. L., Xu, D. S., Bai, W. Z., Cui, J. J., Shu, H. M., He, W., et al. (2015b). Local cutaneous nerve terminal and mast cell responses to manual acupuncture in acupoint LI4 area of the rats. *J. Chem. Neuroanat.* 68, 14–21. doi: 10.1016/j.jchemneu.2015.06.002

Wyss, J. M., and Donovan, M. K. (1984). A direct projection from the kidney to the brainstem. *Brain Res.* 298, 130–134. doi: 10.1016/0006-8993(84)91154-5

Xiao, L. Y., Wang, X. R., Yang, Y., Yang, J. W., Cao, Y., Ma, S. M., et al. (2018). Applications of acupuncture therapy in modulating plasticity of central nervous system. *Neuromodulation* 21, 762–776. doi: 10.1111/ner.12724

Xu, D. S., She, C., Wang, J., Cui, J. J., Cai, H., and Bai, W. Z. (2016). Characteristics of distribution of blood vessels and nerve fibers in the skin tissues of acupoint "taichong" (LR 3) in the rat. *Zhen Ci Yan Jiu* 41, 486–491. doi: 10.13702/j.1000-0607.2016.06.002

Xu, D. S., Zhao, S., Cui, J. J., Ma, T. M., Xu, B., Yu, X. C., et al. (2019). A new attempt of re-mapping acupoint atlas in the rat. *Zhen Ci Yan Jiu* 44, 62–65. doi: 10.13702/j.1000-0607.180396

Zhang, B., Ma, S., Rachmin, I., He, M., Baral, P., Choi, S., et al. (2020). Hyperactivation of sympathetic nerves drives depletion of melanocyte stem cells. *Nature* 577, 676–681. doi: 10.1038/s41586-020-1935-3

Zhang, K., Xu, D. S., Cui, J. J., Zhang, Z. Y., Jing, X. H., and Bai, W. Z. (2015). The expression of substance P in sensory neurons and nerve fibers associated with "sanyinjiao" (SP 6) region in the rat. *Zhen Ci Yan Jiu* 40, 449–454. doi: 10.13702/j.1000-0607.2015.06.004

Zhang, Z. Y., Xu, D. S., Wang, H., She, C., Wang, J., Cui, J. J., et al. (2018). Neuronal correlation between acupoint BL 23 and the adrenal gland in rats. *Zhen Ci Yan Jiu* 43, 414–418. doi: 10.13702/j.1000-0607.170609

Conflict of Interest: The authors declare that the research was conducted in the absence of any commercial or financial relationships that could be construed as a potential conflict of interest.

frontiers in Neural Circuits

REVIEW
published: 15 January 2021
doi: 10.3389/fncir.2020.611841

Origins, Development, and Compartmentation of the Granule Cells of the Cerebellum

G. Giacomo Consalez[1†], Daniel Goldowitz[2†], Filippo Casoni[1†] and Richard Hawkes[3†]*

[1]Division of Neuroscience, San Raffaele Scientific Institute, San Raffaele University, Milan, Italy, [2]Department of Medical Genetics, Centre for Molecular Medicine and Therapeutics, University of British Columbia, Vancouver, BC, Canada, [3]Department of Cell Biology and Anatomy, Hotchkiss Brain Institute, Cumming School of Medicine, University of Calgary, Calgary, AB, Canada

Granule cells (GCs) are the most numerous cell type in the cerebellum and indeed, in the brain: at least 99% of all cerebellar neurons are granule cells. In this review article, we first consider the formation of the upper rhombic lip, from which all granule cell precursors arise, and the way by which the upper rhombic lip generates the external granular layer, a secondary germinal epithelium that serves to amplify the upper rhombic lip precursors. Next, we review the mechanisms by which postmitotic granule cells are generated in the external granular layer and migrate radially to settle in the granular layer. In addition, we review the evidence that far from being a homogeneous population, granule cells come in multiple phenotypes with distinct topographical distributions and consider ways in which the heterogeneity of granule cells might arise during development.

Keywords: granule cell, upper rhombic lip, external granular layer, radial migration, Bergmann glial fibers, compartmentation, cerebellum

OPEN ACCESS

Edited by:
Eduardo Weruaga, University of Salamanca, Spain

Reviewed by:
Mitsuhiro Hashimoto, Fukushima Medical University, Japan
Tetsushi Sadakata, Gunma University, Japan

***Correspondence:**
Richard Hawkes
rhawkes@ucalgary.ca

†These authors have contributed equally to this work and share first authorship

Received: *29 September 2020*
Accepted: *17 December 2020*
Published: *15 January 2021*

Citation:
Consalez GG, Goldowitz D, Casoni F and Hawkes R (2021) Origins, Development, and Compartmentation of the Granule Cells of the Cerebellum. Front. Neural Circuits 14:611841. doi: 10.3389/fncir.2020.611841

INTRODUCTION

In this review article, we address how granule cells (GCs) develop: their origins in the upper rhombic lip (URL: also known as the anterior or rostral rhombic lip) and the elaborate migrations and amplifications that lead GCs to become the most populous neurons in the brain, and secondly the embryological origins of granular layer (GL) heterogeneity. Given the space constraints we do not review synaptogenesis and circuit formation; recent reviews may be found in Leto et al. (2015) and Lackey et al. (2018). This aspect has been covered in several excellent reviews (inter alia Yuzaki, 2011) and in recent research articles that suggest there is much to find out about this critical process (Toledo et al., 2019; Yang et al., 2019; **Table 1**).

Abbreviations: AZ, Anterior Zone; CZa/p, Central Zone, anterior and posterior; EGL, External Granular Layer (oEGL/iEGL: outer and inner laminae); GC, Granule Cell; GCP, Granule Cell Progenitors; GL, Granular Layer; NZ, Nodular Zone; PC, Purkinje Cell; PZ, Posterior Zone; UBC, Unipolar Brush Cell; URL, Upper Rhombic Lip (eURL/iURL: exterior and interior laminae).

TABLE 1 | Summary of genes cited in this review that are involved in granule cell development.

Symbol	Name	Chromosome	Start	End	cM	strand GRCm38	MGI ID
Astn1	astrotactin 1	1	158362273	158691781	68.35	+	MGI:1098567
Astn2	astrotactin 2	4	65380803	66404537	34.31	-	MGI:1889277
Atoh1	atonal bHLH transcription factor 1	6	64729125	64731245	30.03	+	MGI:104654
Bmpr1a	bone morphogenetic protein receptor, type 1A	14	34411061	34503336	20.81	-	MGI:1338938
Bmpr1b	bone morphogenetic protein receptor, type 1B	3	141837136	142169425	66.11	-	MGI:107191
Ccnd1	cyclin D1	7	144929931	144939831	88.92	-	MGI:88313
Ccne1	cyclin E1	7	38097984	38107490	25.35	-	MGI:88316
Cdh2	cadherin 2	18	16588877	16809246	10.1	-	MGI:88355
Cdkn1b	cyclin-dependent kinase inhibitor 1B	6	134920401	134925513	65.77	+	MGI:104565
Cep131	centrosomal protein 131	11	120064430	120086827	83.96	-	MGI:107440
Cep290	centrosomal protein 290	10	100487558	100574840	51.48	+	MGI:2384917
Chrna3	cholinergic receptor, nicotinic, alpha polypeptide 3	9	55010117	55026562	29.84	-	MGI:87887
Cntn1	contactin 1	15	92051165	92341967	46.39	+	MGI:105980
Cntn2/Tag1	contactin 2	1	132509425	132543251	57.42	-	MGI:104518
Cxcr4	chemokine (C-X-C motif) receptor 4	1	128588199	128592293	56.43	-	MGI:109563
Cxcl3	chemokine (C-X-C motif) ligand 3	5	90786101	90788093	44.78	+	MGI:3037818
Cxcl12	chemokine (C-X-C motif) ligand 12	6	117168535	117181367	54.81	+	MGI:103556
Dab1	disabled 1	4	103619500	104744844	47.79	+	MGI:108554
Dcc	deleted in colorectal carcinoma	18	71253634	72351069	45.24	-	MGI:94869
Ebf2	early B cell factor 2	14	67233292	67430918	34.63	+	MGI:894332
Ebf3	early B cell factor 3	7	137193673	137314445	82.26	-	MGI:894289
Efnb2	ephrin B2	8	8617434	8661242	3.42	-	MGI:105097
En1	engrailed 1	1	120602487	120607991	52.74	+	MGI:95389
En2	engrailed 2	5	28165694	28172166	13.94	+	MGI:95390
Mapk3/Erk1	mitogen-activated protein kinase 3	7	126759626	126765816	69.25	+	MGI:1346859
Mapk1/Erk2	mitogen-activated protein kinase 1	16	16983382	17047453	10.53	+	MGI:1346858
Mapk7/Erk5	mitogen-activated protein kinase 7	11	61488812	61494267	37.96	-	MGI:1346347
Fgf8	fibroblast growth factor 8	19	45736798	45742915	38.75	-	MGI:99604
Foxc1	forkhead box C1	13	31806646	31810635	13.52	+	MGI:1347466
Fzr1	fizzy and cell division cycle 20 related 1	10	81366879	81378370	39.72	-	MGI:1926790
Gbx2	gastrulation brain homeobox 2	1	89927962	89931176	45.06	-	MGI:95668
Gdf7	growth differentiation factor 7	12	8297918	8301954	3.85	-	MGI:95690
Gli1	GLI-Kruppel family member GLI1	10	127329882	127341579	74.5	-	MGI:95727
Gli2	GLI-Kruppel family member GLI2	1	118834132	119053619	52.17	-	MGI:95728
Gli3	GLI-Kruppel family member GLI3	13	15463723	15730026	5.43	+	MGI:95729
Hes1	hes family bHLH transcription factor 1	16	30065357	30067796	21.09	+	MGI:104853
Hif1a	hypoxia inducible factor 1, alpha subunit	12	73901375	73947530	31.99	+	MGI:106918
Hoxa2	homeobox A2	6	52162417	52164831	25.4	-	MGI:96174
Ift88	intraflagellar transport 88	14	57424064	57517936	30.1	+	MGI:98715
Itgb1	integrin beta 1 (fibronectin receptor beta)	8	128685654	128733200	76.09	+	MGI:96610
Lmx1a	LIM homeobox transcription factor 1 alpha	1	167689237	167848741	75.08	+	MGI:1888519
Jag1	jagged 1	2	137081451	137116520	67.73	-	MGI:1095416
Jam3	junction adhesion molecule 3	9	27097384	27155421	12.27	-	MGI:1933825
Kcnj6	potassium inwardly-rectifying channel, subfamily J, member 6	16	94748636	94997701	55.44	-	MGI:104781
Kif3a	kinesin family member 3A	11	53567379	53601967	31.97	+	MGI:107689
Meis1	Meis homeobox 1	11	18879817	19018985	11.11	-	MGI:104717
Mycn	v-myc avian myelocytomatosis viral related oncogene, neuroblastoma derived	12	12936093	12941836	6.14	-	MGI:97357
Ntf3	neurotrophin 3	6	126101412	126166772	60.45	-	MGI:97380
Neurod1	neurogenic differentiation 1	2	79452637	79456636	47.58	-	MGI:1339708
Neurod2	neurogenic differentiation 2	11	98325415	98329645	61.75	-	MGI:107755
Ntn1	netrin 1	11	68209364	68386826	41.45	-	MGI:105088
Notch2	notch 2	3	98013538	98150367	42.42	+	MGI:97364
Otx1	orthodenticle homeobox 1	11	21994764	22001651	14.1	-	MGI:97450
Otx2	orthodenticle homeobox 2	14	48656781	48667644	25.36	-	MGI:97451
Pard6a	par-6 family cell polarity regulator alpha	8	105701148	105703494	53.04	+	MGI:1927223
Pard3	par-3 family cell polarity regulator	8	127063893	127612286	74.66	+	MGI:2135608
Ptch1	patched 1	13	63508328	63573460	32.8	-	MGI:105373
Ptafr	platelet-activating factor receptor	4	132564067	132582683	65.56	+	MGI:106066
Pax2	paired box 2	19	44756045	44837871	38.09	+	MGI:97486
Pax5	paired box 5	4	44524757	44710487	23.55	-	MGI:97489
Pax6	paired box 6	2	105668900	105697364	55.31	+	MGI:97490
Plxna2	plexin A2	1	194619791	194816869	98.27	+	MGI:107684
Ptf1a	pancreas specific transcription factor, 1a	2	19445663	19447501	13.37	+	MGI:1328312
Reln	reelin	5	21884454	22344702	9.98	-	MGI:103022
Sema6a	sema domain, transmembrane domain (TM), and cytoplasmic domain, (semaphori	18	47245254	47371200	25.08	-	MGI:1203727
Ptpn11/Shp2	protein tyrosine phosphatase, non-receptor type 11	5	121130533	121191397	61.72	-	MGI:99511
Slit2	slit guidance ligand 2	5	47983138	48307733	26.05	+	MGI:1315205
Smad1	SMAD family member 1	8	79338395	79399428	37.56	-	MGI:109452
Smad5	SMAD family member 5	13	56703010	56742377	30.12	+	MGI:1328787
Shh	sonic hedgehog	5	28456840	28467101	14.39	-	MGI:98297
Smo	smoothened, frizzled class receptor	6	29735503	29761365	12.36	+	MGI:108075
Sufu	SUFU negative regulator of hedgehog signaling	19	46396896	46488804	38.85	+	MGI:1345643

(Continued)

TABLE 1 | Continued

Talpid3/KIAA0856	RIKEN cDNA 2700049A03 gene	12	71136848	71243303	29.39	+	MGI:1924217
Tbr1	T-box brain transcription factor 1	2	61802930	61814114	35.56	+	MGI:107404
Tbr2/Eomes	eomesodermin	9	118478212	118486132	70.21	+	MGI:1201683
Btg2/Tis21	BTG anti-proliferation factor 2	1	134075170	134079120	58.1	-	MGI:108384
Tlx3	T cell leukemia, homeobox 3	11	33200752	33203588	19.21	-	MGI:1351209
Unc5c	unc-5 netrin receptor C	3	141465564	141834924	65.57	+	MGI:1095412
Wnt3	wingless-type MMTV integration site family, member 3	11	103774150	103817957	67.5	+	MGI:98955
Wls	wntless WNT ligand secretion mediator	3	159839672	159938664	82.65	+	MGI:1915401
Zeb1	zinc finger E-box binding homeobox 1	18	5591860	5775467	4.42	+	MGI:1344313
Zic1	zinc finger protein of the cerebellum 1	9	91358058	91365810	48.26	-	MGI:106683
Zic2	zinc finger protein of the cerebellum 2	14	122475435	122479852	65.97	+	MGI:106679
Zic4	zinc finger protein of the cerebellum 4	9	91365631	91389351	48.26	+	MGI:107201
Znf423/Zfp423	zinc finger protein 423	8	87661810	87959595	42.29	-	MGI:1891217

The "Symbol" and "Name" columns list the symbols and full names of genes, respectively. The "Chromosome" column lists on which chromosome each gene is located. The "Start" and "End" columns list in base pairs along a chromosome at which a gene begins and ends, respectively. The "cM" column gives the length of each gene in centiMorgans (cM). The "strand GRCm38" column reveals whether a gene is located on the positive or negative strand. Finally, the "MGI ID" column provides the ID of each gene on the JAX Mouse Genome Informatics (MGI) website (http://www.informatics.jax.org/). To find out more about cerebellar-specific phenotypes when a gene is perturbed, first copy the MGI ID into the JAX MGI website. Then, on the Gene Summary page, under the "Mutations, Alleles, and Phenotypes" tab, click on the shaded "Nervous System" box. Under the "Mouse Phenotypes" heading, a list of nervous system-related phenotypes is provided, including those that are specific to the cerebellum.

A Brief Overview of the Adult Cerebellar Cortex

The adult cerebellar cortex has four distinct layers. Superficially lies the molecular layer, a cell-poor structure rich in GC axons, Purkinje cell (PC) dendrites, and their synapses. Next is the narrow PC layer comprising a monolayer of PC somata. Beneath the PC layer is the GL, densely packed with GC somata. Each of these three cellular layers also has distinct populations of inhibitory interneurons. The three cellular layers overlie the white matter tracts, which comprise the cortical afferent and efferent axon pathways (sketched in **Figure 1**). Within these layers, all neurons and some glial cells show restriction to a common cerebellar map (e.g., reviewed in Apps and Hawkes, 2009; Apps et al., 2018). Traditionally, the cerebellum has been subdivided into lobes (e.g., anterior, posterior, and flocculonodular; **Figure 1**), but generally deemed extremely regular (e.g., Marr, 1969). However, on closer inspection, a highly stereotyped pattern of transverse boundaries and parasagittal stripes is revealed, in particular in the distributions of PC phenotypes and afferent terminal fields (recently reviewed in Apps and Hawkes, 2009; Cerminara et al., 2015; Apps et al., 2018). First, the PC layer is comprised of at least five molecularly defined transverse zones—the anterior (AZ), central [CZ: anterior (CZa) and posterior (CZp)], posterior (PZ), and nodular (NZ) zones (Ozol et al., 1999). Each transverse zone is further subdivided into parasagittal stripes, which can be identified by molecular markers (e.g., zebrin II/Aldolase C—Brochu et al., 1990; Ahn et al., 1994); phospholipase Cβ4 (Sarna et al., 2006); heat shock protein 25 (HSP25; Armstrong et al., 2000) and the effects of mutations [rostral cerebellar malformation (rcm) Eisenman and Brothers, 1998; e.g., cerebellar deficient folia (cdf) Beierbach et al., 2001; Niemann Pick disease type C1 (NPC1) Sarna and Hawkes, 2003]. This architecture is reproducible between individuals and conserved across species (e.g., Lannoo et al., 1991; Meek et al., 1992; e.g., reviewed in Marzban et al., 2011). The PC zone-and-stripe array is the ground plan around which other elements are organized. For example, basket and stellate cells (e.g., reviewed in Consalez and Hawkes, 2013), Golgi cells (Sillitoe et al., 2008), unipolar brush cells (UBCs; Chung et al., 2009) and radial glial cells (Eisenman and Hawkes, 1989) all show restriction at PC stripe boundaries, in the sense that either the somata of interneuron subtypes are restricted to particular zones or stripes, or that interneuron neurites do not cross PC stripe boundaries (reviewed in Consalez and Hawkes, 2013). Similarly, afferents are also confined to specific PC stripes (reviewed in Apps et al., 2018) and different stripes exhibit different functional properties (Zhou et al., 2014; Valera et al., 2016). In "Patterning of the Adult Granular Layer" section we describe how this cerebellar compartmentation is reflected in the final arrangement of GCs.

A Brief Overview of Cerebellar Development

Cerebellar development (sketched in **Figure 2**) has been summarized in many reviews (inter alia Leto et al., 2015). The map of the cerebellar anlage is established at early stages [embryonic day (E)8.0–8.5] thanks to extracellular signals released by the isthmic organizer and roof plate and transcription factors expressed rostral and caudal to the isthmus (see **Figure 1**, Leto et al., 2015). All cerebellar neurons arise from the interplay of two germinal epithelia: the ventricular zone (VZ) and the URL. From ∼E9 a small patch in the wall of the VZ of the 4th ventricle (**Figure 2**), identified by *Ptf1a* expression, is specified to generate all GABAergic neurons—the PCs and multiple classes of inhibitory interneurons (Hoshino et al., 2005; unless otherwise noted all timings refer to mice, with the beginning of embryogenesis designated as E0). The postmitotic PCs migrate dorsally *via* the cerebellar plate (E10–E13) to form physically separate and molecularly distinct clusters by ∼E18 (reviewed in Dastjerdi et al., 2012). This stereotyped array is the scaffold around which cerebellar architecture is patterned. The inhibitory interneuron precursors, also derived from the

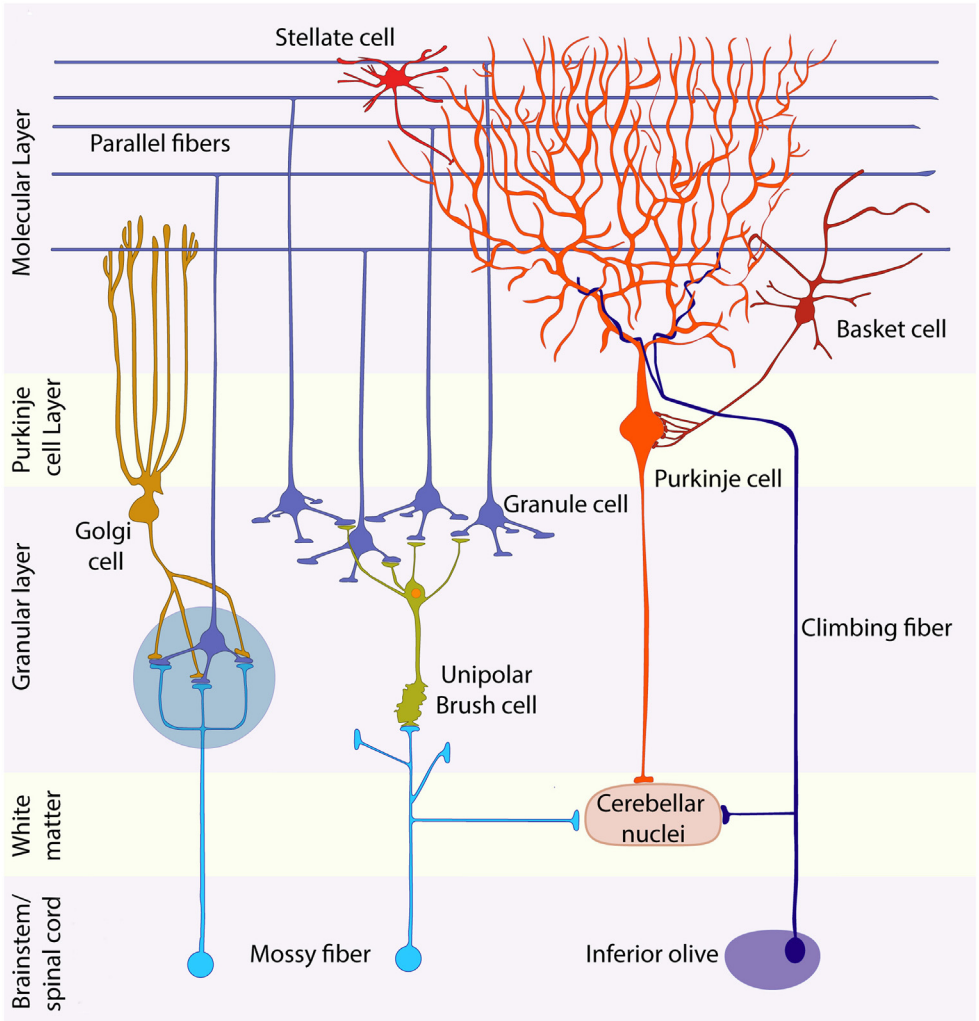

FIGURE 1 | Schematic representation of the cerebellar cytoarchitecture. The cerebellar cortex is organized in three laminae: molecular layer, Purkinje cell (PC) layer, and granular layer (GL). Purkinje, Golgi, stellate, and basket cells are inhibitory neurons; granule and unipolar brush cells are excitatory. Granule cells project their axons into the molecular layer, giving rise to the parallel fibers, which synapse with the dendrites of all inhibitory neurons of the molecular layer and with those of Golgi cells. Afferents are of two main types: mossy and climbing fibers. Both are excitatory. The former originate from brainstem nuclei and the spinal cord, whereas climbing fibers come from the contralateral inferior olive. Most mossy fibers synapse directly on the dendrites of four to five granule cells in specialized synaptic glomeruli (blue-gray circle), which also receive inhibitory feedback from Golgi cell axons. A small mossy fiber subset, first synapses on unipolar brush cells that then relay amplified excitatory signals to granule cells. Each PC receives a connection from a single climbing fiber. Purkinje cell axons carry inhibitory signals to the cerebellar nuclei, whereas mossy and climbing fiber collaterals provide the cerebellar nuclei with excitatory afferents. The large glutamatergic neurons of the CN project their axons to nuclei located in the brainstem and diencephalon.

4th ventricle, migrate *via* the white matter, undergoing further cell divisions *en route*, and then settle in association with the PC clusters (∼E18: Leto and Rossi, 2012). Perinatally, the PC clusters and associated interneurons disperse longitudinally to form a monolayer of parasagittal stripes by ∼P20 (reviewed in Leto et al., 2015).

In parallel, GC progenitors (GCPs), together with excitatory cerebellar nuclei neuron progenitors and glutamatergic UBC progenitors, are generated dorsally in the upper rhombic lip (**Figure 3A**), where they proliferate and migrate to form a secondary germinal epithelium, the external granular layer (EGL), that completely covers the embryonic cerebellar surface [also often called the "external germinal layer." The original term—due to Ramón Y Cajal (1911)—is "granular" ("*couche granulaire externe*"): fortunately, either way, it abbreviates as EGL. The EGL was first described thoroughly by Hess (1858) and then by Obersteiner (1869), and was known for many years as "Obersteiner's layer". GCPs proliferate for 3 weeks in the outer EGL (oEGL; **Figure 3B**) to generate the postmitotic GCs that invade the inner EGL (iEGL) and migrate radially through the molecular layer to eventually settle in the maturing granular layer (GL; **Figures 3B,C**). As they migrate they leave behind trailing axons that bifurcate and extend mediolaterally as parallel fibers,

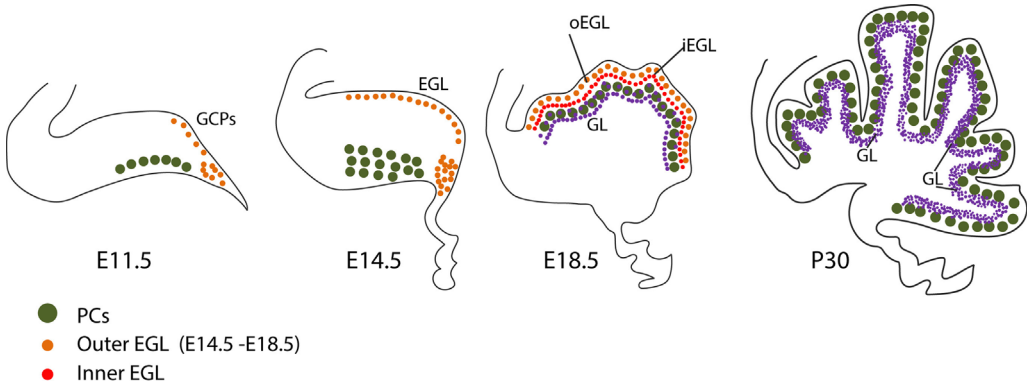

FIGURE 2 | Granule cell development. Schematic representation of granule cell development between E11 and P30. See text for discussion. Abbreviations: EGL, external granular layer; GCPs, granule cell progenitors; GL, granular layer; iEGL, inner lamina of the EGL; oEGL, outer lamina of the EGL; PCs, Purkinje cells; URL, upper rhombic lip.

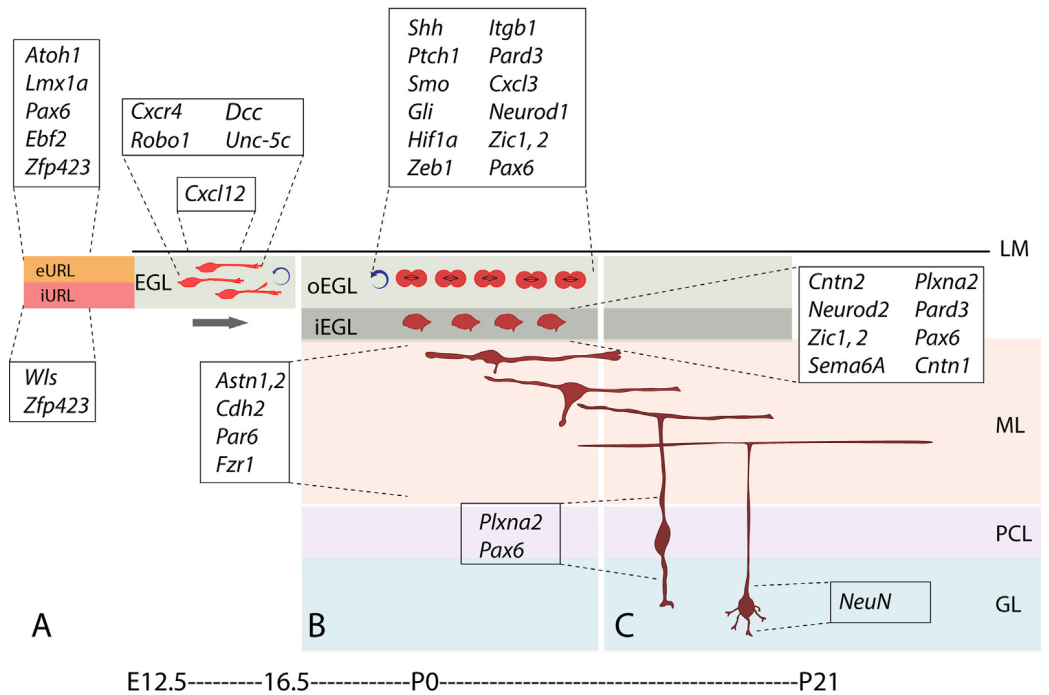

FIGURE 3 | Stages and stage-specific genes of granule cell development. Schematic representation of some genes playing roles in granule cell birth, proliferation, differentiation, and migration. **(A)** *Atoh1*+ granule cell progenitors of the external upper rhombic lip (eURL) derive from ill-defined stem cells of the interior URL (iURL) and migrate to give rise to the EGL thanks to a combination of attractive and repulsive cues (see also **Figure 4C**), and expand in number between E12.5 and E16.5. **(B)** After populating the oEGL, GCPs start dividing mostly symmetrically in a process called clonal expansion, promoted by Purkinje cell-secreted sonic hedgehog. Postmitotic GCs form the interior EGL (iEGL) and undertake tangential and radial migration (see text) after extending two axons in the frontal plane (prospective parallel fibers). **(C)** As they begin their descent into the molecular layer (ML), GC somata extend a radially oriented axon and dendrite, and once in the granular layer, stack with an inside-out progression such that the early-born GCs occupy deeper locations in the GL and project their axons to deeper locations in the ML. Abbreviations: eURL, exterior upper rhombic lip; iURL, interior upper rhombic lip; EGL, external granular layer; oEGL, outer lamina of the EGL; iEGL, inner lamina of the EGL; LM, leptomeninges; ML, molecular layer; PCL, Purkinje cell layer; GL, granular layer.

which synapse with the PC dendritic arbors (see also **Figure 2**, Leto et al., 2015).

In the adult, GC somata located in the GL send out four to five short dendrites that receive excitatory (glutamatergic) input from incoming mossy fiber afferents (**Figure 1**), and long axons that extend through the molecular layer, bifurcate giving rise to parallel fibers (**Figure 3C**) and form excitatory (glutamatergic) synapses on PC dendrites. The circuit is thus: mossy fiber afferent input is relayed *via* GC axons to the PCs, which are the sole efferent projection of the cerebellar cortex

(**Figure 1**). While the mossy fiber ⇛ GC ⇛ PC pathway appears straightforward, it has two remarkable features. Cerebellar GCs are the most numerous neurons in the brain: in mice, there are estimated to be 70,000,000, which constitute well over 99% of all neurons in the cerebellum (Herculano-Houzel et al., 2006)! It is noteworthy that large numbers of GCs are a highly conserved feature of the cerebellar cortex (the GC/PC ratio goes up during evolution: Ito, 1984). Therefore, large numbers matter. It is less clear why such an enormous number of GCs is needed (e.g., the "combinatorial coding" theory of Marr, 1969).

ORIGINS AND FORMATION OF THE RHOMBIC LIP

The GC lineage arises at around E8.75 from the URL, an ephemeral structure located atop the 4th ventricle at the intersection of the roof plate and the cerebellar anlage. A two-step process formats the cerebellum and the future GCs: first, arealization of rhombomere 1 of the dorsal neural tube forms the initial cerebellar territory, which includes the URL, and second signaling from the adjacent roof plate assists in cell specification. Innovative techniques have been applied to the analysis of the origins of the primordium—from the classical chick-quail chimera technique of LeDouarin and colleagues (e.g., Pourquié et al., 1992) to the creative use of transgenic mouse lines. These studies defined rhombomere 1 as the territory that produces the anlage. The application of molecular techniques, whether *in situ* hybridization (Hallonet and Le Douarin, 1993) or mouse knockouts (McMahon and Bradley, 1990; Millet et al., 1996), further refined the URL to an anterior rhombencephalic region bounded by the isthmic organizer (*Otx2+*) rostrally and rhombomere 2 (*Hoxa2+)* caudally. In the arealization of the URL, *Gbx2* plays an important role through the antagonism of *Otx2* expression (Hashimoto and Hibi, 2012). The isthmic organizer resembles a Spemann–Mangold-like inducer in that its secreted signals can induce cerebellar-like structures when transplanted to ectopic sites and if it is eliminated no cerebellum is produced (e.g., FGF8 Chi et al., 2003). Other molecules documented to play a role in specifying this region as future cerebellum include the Paired-box transcription factor genes *Pax2* and *Pax5* (Bouchard et al., 2000), and *En1* and *En2* of the engrailed family (Hanold, 1986; Hanks et al., 1995).

While not contributing to the cells that come to populate the parenchyma of the cerebellum, the roof plate expresses molecules that are key to URL development. Important insights arise from the study of the *Dreher* mutant mouse (*Lmx1adr-J)* whose mutated gene was found to be *Lmx1a* (Millonig et al., 2000). Studies by Chizhikov et al. (2006) led to an appreciation of this extra-cerebellar signaling center. The loss of LMX1A expression from roof plate cells results in both a major loss of GCs (Sekiguchi et al., 1992) and the ablation of the vermis (Millonig et al., 2000; Sillitoe et al., 2014). *Lmx1a* is also expressed in a subset of rhombic lip progenitors that produce GCs predominantly restricted to the cerebellar posterior vermis. In the absence of *Lmx1a*, these cells precociously exit the rhombic lip and overmigrate into the anterior vermis. This overmigration is associated with premature regression of the rhombic lip and posterior vermis hypoplasia in *Lmx1a* null mice (Chizhikov et al., 2010). LMX1A acts downstream to signaling *via* bone morphogenetic protein receptors (BMPRs) and this pathway is likely involved in the production of the crucial progenitor gene *Atoh1* (*Atonal homolog 1*; a.k.a *Math1*, Alder et al., 1999; Krizhanovsky and Ben-Arie, 2006). Genetic destruction of the roof plate by using diphtheria toxin driven by the roof plate specific gene *Gdf7* resulted in the near-total loss of *Atoh1* cells of the URL (Chizhikov et al., 2006). BMPRs assemble into a heterotetramer and phosphorylate members of the SMAD family (Smad1, 5, 8; signaling pathway reviewed in Waite and Eng, 2003). Double knockouts of *Bmpr1a; Bmpr1b* and *Smad1; Smad5* result in a dramatic loss of GCPs that is attended by loss of *Atoh1* and other critical genes in the GC lineage including *Zic1* and *Zic2* (Qin et al., 2006; Tong and Kwan, 2013). Interestingly, BMP signaling has also been implicated in the degradation of ATOH1 (Zhao et al., 2008), an effect promoted by *Meis1* and *Pax6* (Owa et al., 2018).

Atoh1 (**Figure 5A**) is currently viewed as the definitive marker of the GC lineage, as well as of the other glutamatergic cells that arise from the URL (Akazawa et al., 1995; Ben-Arie et al., 1996). This opened up the molecular analysis of GC development by using transgenesis for gene knockouts and lineage tracing. Of note, evidence was brought to bear on possible upstream genes to *Atoh1*, for example, *Hes1* (Akazawa et al., 1995). This issue is still relatively unexplored although the downstream targets of ATOH1 have been well characterized. Critical genes in the pathway to a glutamatergic phenotype (GCs, glutamatergic projection neurons of the cerebellar nuclei, and UBCs) include *Pax6*, *Tbr1*, and *Tbr2*. *Atoh1* deletion results in the elimination of the entire population of GCs in addition to related populations that derive from the full rhombic lip (Ben-Arie et al., 1997; Wang et al., 2005). This dramatic loss places *Atoh1* in the headwaters of the GC lineage. The examination of downstream targets of ATOH1 has identified a set of genes that suggest a broad developmental impact of *Atoh1* on GC development (Klisch et al., 2011; Machold et al., 2011).

With the identification of *Atoh1* as key to GC development, it became important to map the timing of the cells that emerge from the *Atoh1* lineage by using site-specific recombinase genetic fate mapping (Dymecki and Tomasiewicz, 1998; Zinyk et al., 1998). The earliest cells to emerge from the URL—between E10.5 and E12.5—are fated to become neurons of the cerebellar nuclei, and give rise to the so-called nuclear transitory zone. They migrate anteriorly over the cerebellar surface as the "rostral rhombic-lip migratory stream" (Wang et al., 2005) or "subpial stream" (Altman and Bayer, 1997; sketched in **Figures 4A,B**). The GCPs follow the same path from the URL to the EGL. Altman and Bayer's careful analysis of the rat URL at E10.5 showed two distinct cellular organizations—one tangentially oriented in the exterior lamina of the URL (eURL), and a second with a columnar organization in the interior lamina of the URL (iURL), possibly corresponding to apical radial glial progenitors). We do not know if these laminae are a transitional

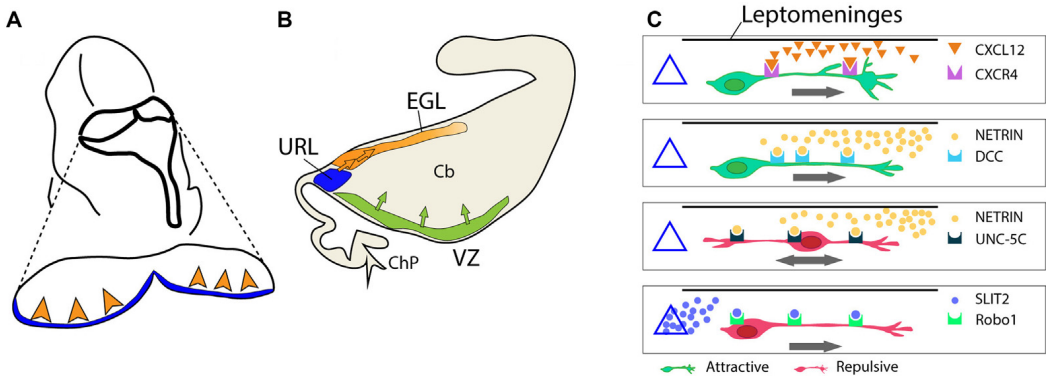

FIGURE 4 | Formation of the external granular layer. **(A)** Schematic representation of the embryonic hindbrain (dorsal view, *circa* E12.5). The view illustrates the departure of GCPs from the URL and the invasion of the EGL (arrowheads). **(B)** The same process is seen in a sagittal view to show the formation of the EGL. **(C)** A sketch of extracellular signals and their receptors controlling GCP migration from the URL into the EGL. The URL is represented as a triangle on the left. The location of the isthmic organizer and mesencephalon is on the right side of each box. CXCL12 is released by the leptomeninges (horizontal black line); SLIT2 is released by the URL (triangle); netrin is secreted by the mesencephalic ventral midline. Abbreviations, URL, upper rhombic lip; EGL, external granular layer; VZ, ventricular zone; ChP, choroid plexus; Cb, cerebellar anlage.

phase of URL development, but it is clear that they comprise distinct subpopulations based upon the analysis of the *Atoh1* null mouse, where the cells of the eURL are absent while the iURL persists in a normal proliferative state (Jensen et al., 2004). Developmental analysis of the *Wnt* pathway gene *Wntless* (*Wls*; signaling cascade reviewed in Clevers and Nusse, 2012), which processes *Wnt* for its extracellular signaling role, confirms this heterogeneity with the identification of a population of *Wls*+ cells in the iURL that are both *Atoh1*-independent [i.e., they persist in the Atoh1 knockout and do not express Atoh1 or the corresponding protein (Yeung et al., 2014)]. In the wildtype, an examination of the two URL laminae suggests that the transition from *Wls*+ to *Atoh1*+ in the iURL serves as a reservoir for the production of ATOH1+ cells and cells of the glutamatergic lineage generally. Genetic fate-mapping of the *Wls*+ population would provide insights into this possibility.

The URL as the First Zone of Transit Amplification

The expansion of the GCP population during the formation of the EGL from the URL can be thought of as an example of transit amplification—comparable to the transit amplification of GABAergic interneurons as they migrate from the subventricular zone of the 4th ventricle through the white matter tracts (e.g., Leto and Rossi, 2012). In support of this perspective, Wingate and coworkers have shown GCP transit amplification in teleosts, from which a well-defined EGL is absent (Chaplin et al., 2010). The molecular signals that direct URL progenitor cells to form the EGL include the antagonistic interplay between ATOH1 and LMX1A (Chizhikov et al., 2010). Such a tug-of-war between molecularly distinct compartments—i.e., an interplay between factors that push forward developmental events and those which inhibit that progression—is a common dynamic in CNS development (e.g., Toresson et al., 2000; Yeung et al., 2014; Kullmann et al., 2020). Any quantitative estimate of the initial phase of amplification of the GCP population in the proliferatively-active URL is bound to be uncertain as this population gives rise not only to GCs but also to cerebellar nuclear neurons and UBCs.

From URL to EGL: The Second Stage of Transit Amplification

Once GCPs exit the URL to form the EGL, starting at E13, we estimate that from the time that the EGL covers the cerebellum (∼E15) to the adult population in the GL (∼P25), there is a ∼3,000× amplification! As *Atoh1*+ cells exit the URL, they proliferate and disperse tangentially to cover the entire dorsal surface of the cerebellum as the EGL (**Figure 3B**). Scant information is available about the molecules that guide GCP migration at this stage. One key factor is chemotactic stromal cell-derived factor 1, encoded by the *Cxcl12* gene (**Figures 4C**, **5D**, **6F,G**) expressed by the developing leptomeninges and its receptor, CXCR4 (**Figures 4C**, **5E**, **6H,I**), expressed by migrating progenitors of the EGL and acting through its downstream effector Shp2 (Hagihara et al., 2009). Fetal cerebellar development in *Cxcl12* mutant animals is markedly different from that in wild-type animals, with many proliferating GCs invading the cerebellar anlage (Zou et al., 1998). Mutations in *Cxcl12* and *Cxcr4* have the same effect on GCP migration, pointing to a monogamous relationship between the corresponding proteins: in the mutant, GCPs depart prematurely from the EGL migrating radially and forming large cell clumps in the cerebellar parenchyma (Ma et al., 1998).

During GCP migration into the EGL (**Figures 4A,B**; reviewed in Chédotal, 2010), the repulsive extracellular signal SLIT-2 is expressed in the URL (**Figure 5J**) and probably propels migrating ROBO-expressing GCPs (**Figures 4C** and **5K**) out of the URL (Gilthorpe et al., 2002). GCPs also express the chemoattractant netrin receptor *deleted in colorectal carcinoma* (DCC, Moore et al., 2007). Netrins are a family of laminin-related secreted proteins that direct axon extension and cell migration during neural development. They act as attractants

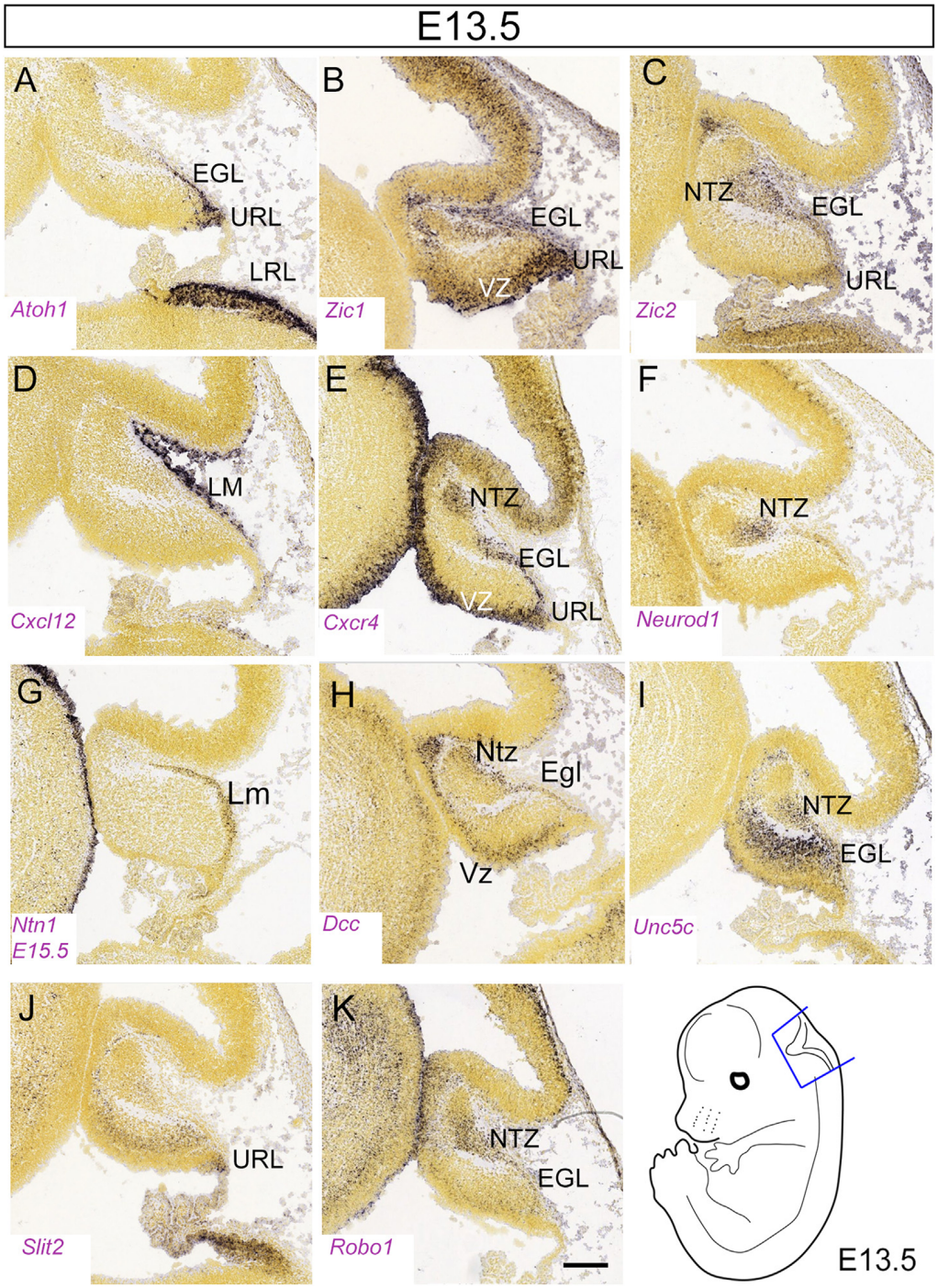

FIGURE 5 | (A–K) Distribution of eleven transcripts in the embryonic cerebellar primordium. Sagittal sections hybridized *in situ* with antisense riboprobes specific for genes, cited in the text, that play important roles in the early stages of cerebellar development. Positive territories are labeled black. All images show E13.5 cerebellar primordia, except **(G)**, which shows an E15.5 section. Image credit: Allen Institute. © 2008 Allen Institute for Brain Science. Allen Developing Mouse Brain Atlas. Available online at: https://developingmouse.brain-map.org/. Abbreviations: Cb, cerebellar primordium; ChP, choroid plexus; EGL, external granular layer; NTZ, nuclear transitory zone; URL, upper rhombic lip; VZ, ventricular zone. Scale Bar in **(K)** = 200 μm and applies to all panels.

for some cell types and as repellents for others, mediated by distinct receptors (**Figure 4C**). Among other expression sites, *Ntn1*, encoding netrin-1, is expressed in the mesencephalic ventral midline (**Figure 5G**). GCPs express the netrin receptor gene *Dcc* (**Figure 5H**), which mediates the attractive response to netrin-1 during EGL formation. Co-expression of the UNC-5C

co-receptor converts the response from attractive to repulsive (**Figure 4C**). GCP migration is confined within the cerebellar anlage by the netrin co-receptor encoded by *Unc5c* (a.k.a *Unc5h3*; **Figure 5I**), which acts cell-autonomously to enact a repulsive response to the netrin-1 ligand (Ackerman et al., 1997; reviewed in Goldowitz et al., 2000), thereby preventing the inappropriate anterior migration of GCPs into the inferior colliculus. Consistent with this, in *Pax6*$^{Sey/Sey}$ mice, in which *Unc5c* is absent, GCPs are not restricted to the cerebellum and migrate ectopically into the inferior colliculus (Engelkamp et al., 1999). Importantly, however, netrin-1 is not expressed at the anterior limit of the cerebellum and it does not repel GC precursors in collagen-gel assays (Alcantara et al., 2000; Gilthorpe et al., 2002). Furthermore, the EGL forms normally in netrin-1 KO mice (Przyborski et al., 1998; Alcantara et al., 2000), possibly suggesting the presence of redundant signals. Another interesting feature of CGPs that migrate to establish the EGL is that they release reelin (D'Arcangelo, 2014), which guides neuronal migration in the cerebellum as it does in the developing telencephalic cortical plate. In this respect, we view the cerebellar GC as equivalent to the Cajal-Retzius neuron of the isocortex.

Clonal Expansion in the EGL

Long before the bulk of clonal expansion, DNA synthesis is detected in the prospective EGL. It is not clear whether GCPs divide after completing their migration or combine migration and proliferation simultaneously, similar to basal progenitors of the cerebral cortex. Prenatal migration of GCPs over the cerebellar primordium (E13–E17.5) and subsequent EGL maintenance (E18–P20) both require contacts with the basement membrane, involving both the basal endfeet of radial glial progenitors and fibroblasts of the pia mater. In 1985 Hausmann and Sievers (1985) identified in the E14 rat (roughly corresponding to E12.5 in the mouse) an EGL cell type oriented tangentially to the cerebellar surface and characterized by persistent contact with the basal lamina *via* an external process with a lamellipodial tip and a cytoskeleton characteristic of migratory cells. They proposed that the basal lamina guides the tangentially migrating GCPs and that persistent contacts with the basal lamina mediate stimuli that maintain GCPs in a proliferative state. The bulk of proliferation starts shortly before birth and continues for about 15 days, peaking around P6 (**Figure 3B**). Clonal expansion requires a mitogenic signal released by neighboring PCs (Smeyne et al., 1995). The nature of this signal is well established—PCs release the morphogen and mitogen sonic hedgehog (SHH) that promotes a massive GCP proliferation (Dahmane and Ruiz-I-Altaba, 1999; Wallace, 1999; Wechsler-Reya and Scott, 1999); accordingly, *Shh* deletion abolishes GCP expansion (Lewis et al., 2004). GCPs are competent to respond to SHH because they express the receptor Patched-1, located near the base of the cell cilium, and the G-protein-coupled transmembrane co-receptor smoothened (SMO; signaling pathway reviewed in Ruiz i Altaba et al., 2002; reviewed in Di Pietro et al., 2017; Lospinoso Severini et al., 2020). SMO activates an inhibitory G protein that in turn activates GLI transcription factors and promotes cell cycle progression. However, the SHH signaling intermediates that regulate GCP proliferation are only just starting to be defined.

GRANULE CELL BIRTH IN THE EGL

Although SHH is available across the thickness of the molecular layer, GCPs only proliferate when they are exposed to the microenvironment of the EGL. GCPs that remain in the EGL because of impaired migration continue to proliferate: thus, the EGL acts as a mitogenic niche and migration away correlates with the transition from a proliferative to a nonproliferative state (Choi et al., 2005). Regulators of the proliferative environment include *Hif1a* (**Figures 6B,C**), *Zeb*, and *Itgb1*; conversely, the Pard gene family promotes cell cycle exit and cell migration (see below and Kullmann et al., 2020).

Symmetric Division of GCPs

Perinatally, GCPs start proliferating rapidly in the EGL and expand clonally over a ∼20-day period. Each GCP undergoes predominantly symmetric divisions, generating two GCPs or two neurons (Legué et al., 2015; Nakashima et al., 2015). Cell divisions are oriented to drive growth along the anteroposterior axis. At the same time, the bases of the fissures act as boundaries for GCP dispersion, allowing each lobe/transverse zone to be a distinct developmental unit and ensuring that appropriate GC numbers are partitioned into each folium (Legué et al., 2015).

As mentioned, clonal expansion of GCPs in the mouse EGL is promoted primarily by SHH secreted by PCs (Dahmane and Ruiz-I-Altaba, 1999; Wallace, 1999; Wechsler-Reya and Scott, 1999). This is also the case in humans (Lewis et al., 2004; Aguilar et al., 2012; Haldipur et al., 2012; Lee et al., 2013). Upon SHH binding, the SHH receptor PTCH1 (Marigo et al., 1996) undergoes a conformational change and releases SMO, which enters the cell cilium triggering the activation of the SHH signaling cascade (reviewed in Hu and Song, 2019). While other factors (codon, brother of codon, and growth arrest-specific 1) also regulate the activation of SHH signal transduction, their role in GCP proliferation has not been fully addressed.

The glioma-associated oncogene homolog (GLI) protein family converts SHH signals into gene expression regulation (Ruiz i Altaba, 1999; Corrales et al., 2004). GLI transcription factors are encoded by three genes: *Gli1*, *Gli2*, and *Gli3* (Ruppert et al., 1988). GLI proteins bind to DNA through zinc finger motifs and activate or repress transcription. SHH signaling promotes GLI-1 accumulation in the nucleus and target gene activation (Mimeault and Batra, 2010). GLI-2 and GLI-3 are transcriptional activators and repressors (Wang et al., 2011; Carballo et al., 2018). Among other GLI target genes, *Mycn*, encoding the N-MYC protein, promotes GCP proliferation (Knoepfler et al., 2002; Kenney et al., 2003; Llinás and Negrello, 2015). Besides regulating the cell cycle progression of GCPs, N-MYC promotes a switch from proliferation to differentiation (Knoepfler et al., 2002; Llinás and Negrello, 2015). Ablation of *Gli3* in *Shh* null mice restores *Mycn* expression (Hu et al., 2006). In addition to *Mycn*, GLI factors activate transcription of *Ccnd*

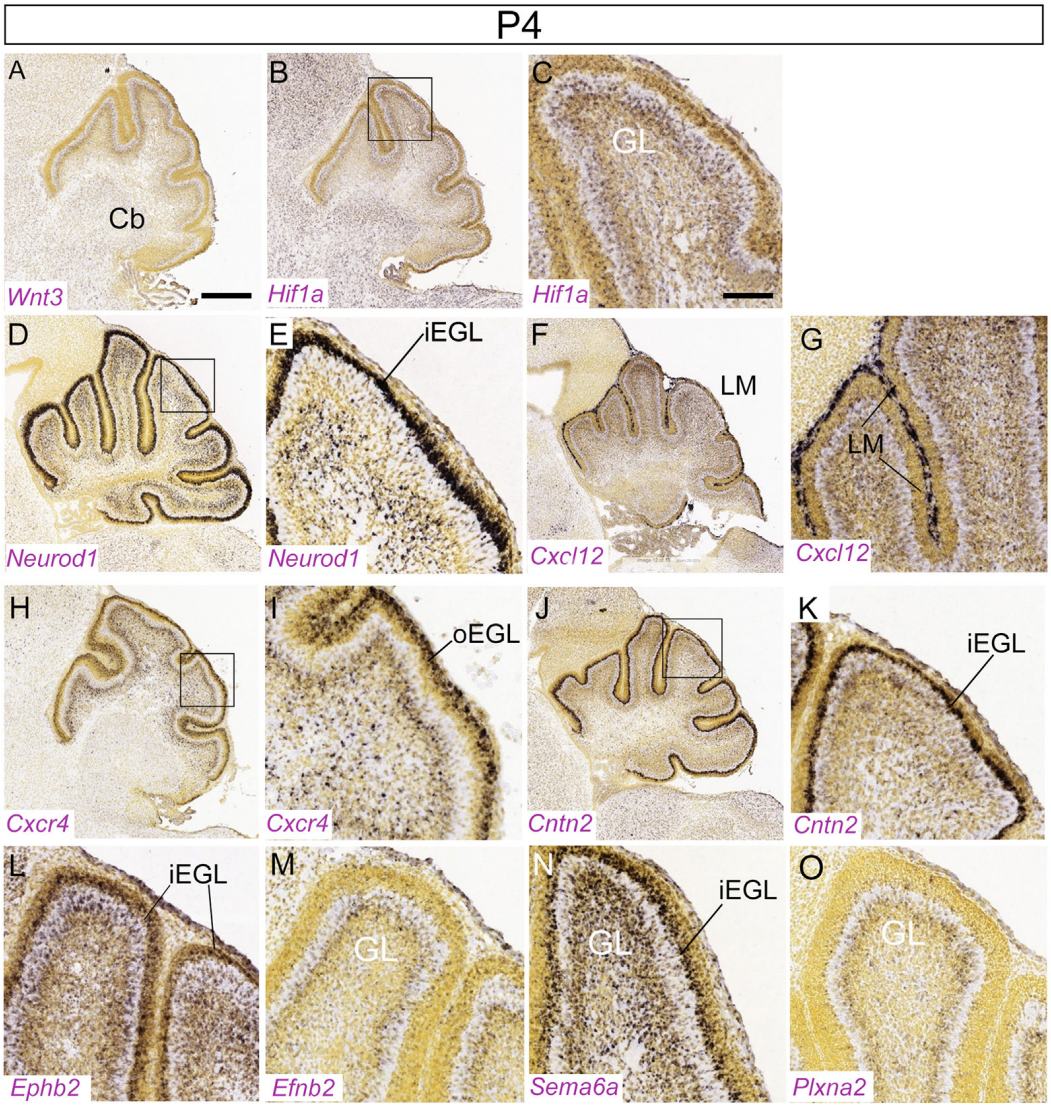

FIGURE 6 | Distribution of nine transcripts in the P4 cerebellum. Sagittal sections hybridized *in situ* with antisense riboprobes specific for genes cited in the text that play important roles at early stages of cerebellar development. Image credit: Allen Institute. ©2008 Allen Institute for Brain Science. Allen Developing Mouse Brain Atlas. Available online at: https://developingmouse.brain-map.org/. Abbreviations: Cb, cerebellum; iEGL, inner EGL; oEGL, outer EGL. **(C,E,J)** are magnifications of areas in panels **(B,D,I)**, respectively. Scale bar in panel (**A**; 400 μm) applies to **(B,D,F,H,J)**; scale bar in panel (**C**; 100 μm) applies to **(E,G,I,K–O)**.

and *Ccne* (encoding cyclin D and E, respectively), and thereby promote GCP proliferation (Hatton et al., 2006).

The notch-2 pathway also promotes the expansion of GCPs. Treatment of GCPs with jagged-1, a Notch-2 ligand, stimulates GCP proliferation, and inhibits GC differentiation (Solecki et al., 2001). Activated notch-2 antagonizes BMP signaling (signaling pathway reviewed in Liu and Niswander, 2005; Zhao et al., 2008) and upregulates *Atoh1* expression (Machold et al., 2007). In neural crest development, WNT signaling negatively regulates SHH and controls cell proliferation and differentiation postnatally (Jacob and Briscoe, 2003; Borday et al., 2012): in GCP development, the WNT-3 ligand may antagonize SHH by post-translationally regulating GLI-3 (Anne et al., 2013). WNT-3 is co-expressed with SHH in the postnatal PC layer (**Figure 6A**) where it suppresses GCP growth through a non-canonical Wnt signaling pathway that activates prototypic mitogen-activated protein kinases (MAPK)—the Ras-dependent extracellular-signal-regulated kinases 1/2 (ERK1/2) and 5 (ERK5) instead of the canonical β-catenin pathway. Inhibition of MAPK activity by using a MAPK kinase inhibitor reversed the inhibitory effect of WNT3 on GCP proliferation (Aguado et al., 2013).

Tis21 is an antiproliferative gene expressed in differentiating apical progenitors throughout the neural tube (Iacopetti et al., 1999). Its deletion causes an increased frequency of medulloblastoma. In the developing cerebellum, *Tis21*, expressed in Bergmann glia, downregulates *Cxcl3*, a gene that maintains

the proliferative niche acting through its receptor expressed in the EGL and delays radial GCP migration from the EGL. Thus, *Tis21* nullisomy may cause GCPs to remain longer in a mitotic state, making them more prone to transformation (Farioli-Vecchioli et al., 2012).

Finally, oxygen tension is a new and complementary pathway to SHH that regulates GCP proliferation. The vascularization of the EGL is reduced in the early postnatal cerebellum and the region is relatively hypoxic resulting in the cells in the EGL expressing the hypoxia-inducing factor 1a gene (*Hif1a*; **Figures 6B,C**), which stimulates GCP proliferation. Perturbation of neither the SHH pathway nor the HIF1A pathway impacts the other's role in driving GCP proliferation (Kullmann et al., 2020). The recent work by Solecki and co-workers identifies a microenvironment in which HIF1A stimulates the expression of the homeobox transcription factor ZEB1, which both enhances restriction to the proliferative niche through *Itgb1* and inhibits the *Pard* family of genes that push cells toward migration (Kullmann et al., 2020). When hypoxia is normalized by vascularization of the EGL, *Hif1a* expression diminishes as does its effect on GCP proliferation.

Primary Cilia and GCP Proliferation

It is now well established that the transduction of SHH signaling starts in the cell cilium. Millen's group showed for the first time in 2007 that CNS-specific inactivation of ciliary genes *Ift88* and *Kif3a* causes severe cerebellar hypoplasia and foliation abnormalities, due to a failure of GCP clonal expansion, demonstrating that cilia proteins are essential for normal development and GCP proliferation (Chizhikov et al., 2007; Spassky et al., 2008). As noted earlier, the SMO receptor translocates to the primary cilium in response to SHH, and cilia are required for SMO activity (Corbit et al., 2005; May et al., 2005). Moreover, GLI1–3 and SUFU, a negative regulator of the pathway and interactor of GLI proteins, all reside in the distal tip of the primary cilium. Consistent with these findings, intraflagellar transport proteins and cilia are required for both the transcriptional activator and repressor functions of the GLI proteins, affecting both the proteolytic processing of full-length GLI-3 to the repressor form and the transcriptional activity of GLI-2 (Haycraft et al., 2005; Huangfu and Anderson, 2005; Liu et al., 2005; May et al., 2005). Thus, the primary cilium contains the machinery required for the reception and transduction of SHH signaling, explaining its key role in GCP proliferation. Consistent with this, several ciliopathies affect cerebellar cortical development. Joubert and Meckel's syndromes are ciliopathies characterized by severe vermis defects, ranging from hypoplasia to aplasia. Joubert syndrome patients exhibit a peculiar brainstem malformation known as the "molar tooth sign." In 2006, Joubert syndrome patients were identified as carrying mutations in *Cep290* (Valente et al., 2006). The homonymous protein is mostly distributed in proliferating GCs and, at the subcellular level, is concentrated in the centrosome and primary cilium. As mentioned previously, cilia control cerebellar morphogenesis by promoting the expansion of the GCP pool (Chizhikov et al., 2007). GCPs possess a primary cilium with CEP290 at its base. The proliferation and the response to SHH are severely impaired in subjects with Joubert or Meckel syndrome (Aguilar et al., 2012). More recently, *ZNF423/Zfp423*, a gene implicated in rare cases of Joubert syndrome, was found to be required for the response to SHH (Hong and Hamilton, 2016), for DNA repair (Chaki et al., 2012; Casoni et al., 2017) and CGP cell cycle progression (Casoni et al., 2017). Likewise, another gene recently implicated in Joubert syndrome, *KIAA0856*, has been shown to encode TALPID3, a centrosomal protein. Mice carrying a conditional *Talpid3* deletion lack primary cilia and show a thinned EGL, presumably due to reduced GCP proliferation (Bashford and Subramanian, 2019). Taken together, Joubert syndrome GCPs exhibit defective or absent primary cilia and have a low proliferative rate throughout the cerebellar cortex.

ATOH1 has been long known to positively regulate the SHH transduction pathway but is also required for the maintenance of primary cilia, which keep GCPs competent to respond to SHH (as mentioned, the loss of primary cilia causes GCPs to exit their proliferative state). ATOH1 activates ciliogenesis by transcriptionally regulating *Cep131*, whose gene product facilitates the clustering of centriolar satellites at the basal body. Importantly, ectopic expression of *Cep131* counteracts the effects of *Atoh1* loss in GCPs by restoring the proper localization of centriolar satellites and consequently ciliogenesis. This pro-proliferative pathway is also conserved in SHH-type medulloblastoma, a pediatric brain tumor arising from GCPs (Chang et al., 2019).

GCP Cell Cycle Exit and the Onset of Differentiation

The basic helix-loop-helix transcription factor gene *Neurod1* (**Figures 5F**; **6D,E**) is required for differentiation of GCs, and its absence results in GC death (Miyata et al., 1999), particularly in the PZ and NZ (populated by the late-born GC subset—see below: Cho and Tsai, 2006). Experiments on chick embryos have shown that NEUROD1 plays a key role in terminating the proliferation of GCPs by downregulating the expression of *Atoh1*, thereby promoting postmitotic GC migration towards the GL. Premature misexpression of NEUROD1 in chick suppresses transit amplification in the URL migratory stream and hence the formation of the EGL. Furthermore, misexpression of *Neurod1* after the establishment of the EGL triggers radial migration and downregulates *Atoh1* (Butts et al., 2014). The structurally-related protein NEUROD2 promotes the postnatal survival of both GCs and molecular layer interneurons (Pieper et al., 2019).

The *Zic* gene family, which encodes zinc finger transcription factors implicated in neural induction in the early embryo (Nagai et al., 1997; Nakata et al., 1997; reviewed in Aruga and Millen, 2018), play multiple roles in GC development. *Zic1/2* is expressed robustly in the EGL from E12 through birth (**Figures 5B,C**). Interestingly, *Zic1* is expressed in the deeper part of the EGL and remains expressed in the GL, supporting the notion that *Zic1* and its paralogs play roles both in GCP differentiation and in regulating their proliferation (Aruga et al., 1994, 2002; Gaston-Massuet et al., 2005; Blank et al., 2011; reviewed in Aruga and Millen, 2018). *Zic* mutants feature variable degrees of patterning defects. Although the lamination

in *Zic1*$^{-/-}$ mice is normal, the pattern of foliation is perturbed (Aruga et al., 1998; Blank et al., 2011). *Zic2* hypomorphs (*Zic2*$^{kd/kd}$) show a medial fusion defect at E16 but no other obvious histological abnormalities (Aruga et al., 2002). Due to cell cycle dysregulation, *Zic1* null mice display hypoplasia of the vermis and hemispheres and reduced GCP proliferation in the EGL. Mechanistically, expression of cyclin D1 (*Ccnd1*) is reduced both in *Zic1*$^{-/-}$ and *Zic1*$^{+/-}$; Zic2$^{+/kd}$ cerebella, and the expression of mitotic inhibitor p27 (*Cdkn1b*), which inhibits GCP proliferation (Miyazawa et al., 2000), is increased in *Zic1*$^{-/-}$ cerebella. Moreover, both ZIC1 and ZIC2 act as critical regulators of GC terminal differentiation by affecting chromatin dynamics (Frank et al., 2015). Finally, patients carrying heterozygous deletions encompassing both *Zic1* and *Zic4*, two genes physically linked on chromosome 3q24, develop Dandy-Walker malformation (DWM; Grinberg et al., 2004; Aruga and Millen, 2018). DWM consists of hypoplasia and upward rotation of the cerebellar vermis and cystic dilation of the fourth ventricle. DWM patients have motor deficits including hypotonia and ataxia; about half have mental retardation and some have hydrocephalus. DWM is a heterogeneous disorder and its family recurrence rate does not match expected Mendelian frequencies.

Cxcl12, a chemokine expressed by the leptomeninges (**Figure 5D**), mentioned previously concerning its role in tangential migration, acts as a chemoattractant during GCP migration from the URL into the EGL (Zhu et al., 2004). Also, GCPs, which express the CXCL12 receptor gene *Cxcr4* (**Figures 5E**, **6G,H**), abnormally invade the cerebellar parenchyma in either *Cxcr4* or *Cxcl12* knockouts (Zhu et al., 2004; Vilz et al., 2005). This suggests that CXCL12/CXCR4-mediated attraction plays a major role in maintaining GCPs at the pial surface. The *Src* homology 2-containing protein tyrosine phosphatase is a crucial downstream signal transducer of *Cxcl12* for GC attraction (Hagihara et al., 2009). Interestingly, *Cxcl12* expression by meningeal cells is positively regulated by the FOXC1 transcription factor expressed by leptomeningeal progenitors (Aldinger et al., 2009). Thus, reduced CXCL12 signaling in the EGL may contribute to the cerebellar malformations observed in Dandy-Walker patients bearing *FOXC1* mutations, and to the severe EGL atrophy in *Foxc1* null mice (Aldinger et al., 2009).

Among other factors known to affect the balance of proliferation and differentiation is neurotrophin-3, which promotes differentiation and exit of GCPs from the EGL (Doughty et al., 1998). Likewise, precocious expression of the migration-associated gene *contactin-1* (*Cntn1*) driven by the *Cntn2* promoter delays but does not arrest GCP proliferation in the EGL (Bizzoca et al., 2003). The two contact-related adhesion molecules, TAG1 (CNTN2; gene expression in **Figures 6J,K**) and F3/contactin (CNTN1) act antagonistically in the response to SHH, promoting GCP expansion and cell cycle exit/differentiation, respectively (Xenaki et al., 2011). Besides adhesion molecules, extracellular matrix glycoproteins also regulate the response to SHH. In particular, laminins and the integrin receptor subunit α6 accumulate in the outermost EGL, where GCP proliferation is greatest. Laminin strongly enhances *in vitro* proliferation of GCPs induced by SHH. Another matrix molecule, vitronectin, and its integrin receptor subunit α(V) are expressed in the inner part of the EGL, where GCPs exit the cell cycle and start to differentiate. Vitronectin promotes phosphorylation of cyclic-AMP responsive element-binding protein (CREB), whose overexpression is sufficient to induce GC differentiation even in the presence of SHH (Pons et al., 2001; also, see above comments regarding Kullmann et al., 2020).

A brief note about the occurrence of normally-occurring cell death in the EGL is appropriate given that such a large expansion of the GCP pool is required to produce the large number of GCs seen in the mature cerebellum. It has been calculated that about 0.12 to 0.37% of EGL cells undergo pyknosis (Smeyne and Goldowitz, 1989). This is a vanishingly small number of cells that leads one to think that the sort of matching mechanisms that drive programmed cell death in other neural structures is not a major sculptor of the final GC number in the adult.

Patterning of the EGL

Despite its seemingly uniform appearance, the EGL is divided into at least three transverse compartments. For example, transverse boundaries between the AZ and the CZ are seen through the expression of the homeobox genes *Otx1/2* (Frantz et al., 1994), fibroblast growth factor-alpha, and protein tyrosine phosphatase rho (McAndrew et al., 1998), and neurotrophin-3 (Tojo et al., 1995). A similar restriction associated with the PZ/NZ transverse boundary (**Figure 7A**) is seen for the HOX homeodomain transcription factor gene *Tlx3* (Logan et al., 2002), shown to have a selector role in glutamatergic subtype specification (Shimomura et al., 2015). *Tlx3*, a gene whose expression is induced by PAX6, is expressed in a highly restricted manner in the iEGL and oEGL plus mature cerebellar granule neurons of the posterior cerebellar lobes, where it is required for the localized expression of the nicotinic cholinergic receptor-α3 subunit (CHRN-α3) and other factors involved in neuronal migration and connectivity (Divya et al., 2016). Other transverse boundaries are seen in birth dating studies. The first GCPs are born around E12.5 and preferentially colonize the anterior EGL. Injection of tamoxifen to promote the precisely timed functional activation of *Atoh1*-driven CreER^{T2} at later times (e.g., E16.5–E17) tag GCs that occupy more caudal territories (Machold and Fishell, 2005). The developmental mechanisms by which different GCP populations preferentially occupy particular transverse zones are not certain. In particular, it is not clear whether different GC populations (e.g., anterior vs. posterior) follow different migration pathways or the early-born cells simply migrate further. However, late-born GCPs (*Lmx1a*+) do not move into the anterior cerebellum in mutants in which the early-born (*Lmx1a*-) GCs are absent, again pointing to the presence of an AZ/CZ restriction boundary (see below). Likewise, in the embryonic primordium, the *Ebf2* gene, encoding a helix-loop-helix transcription factor involved in cerebellar cortical development (Croci et al., 2006, 2011; Chung et al., 2008), is expressed in the eURL and the *Atoh1*+ URL migratory

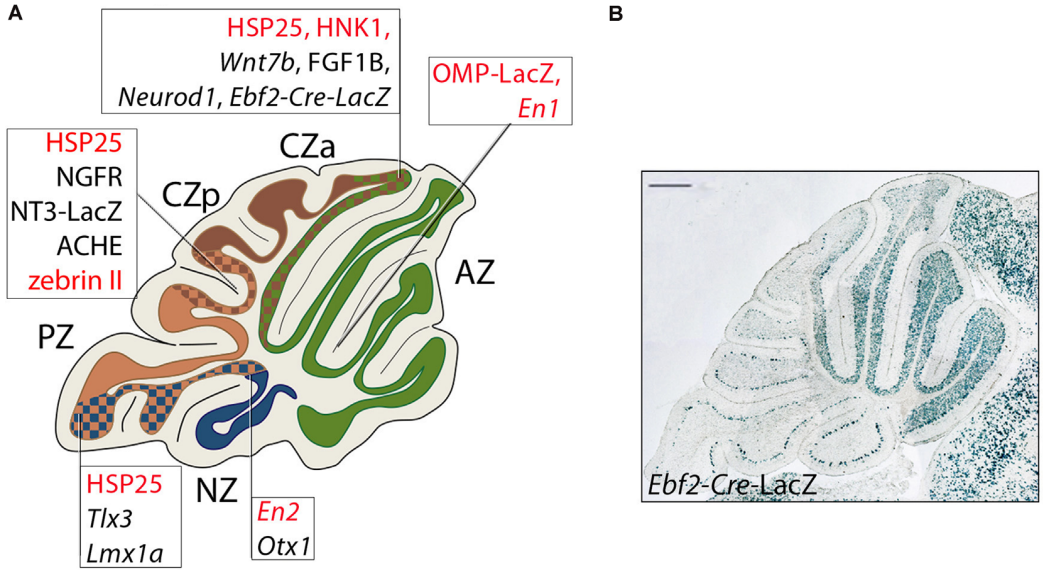

FIGURE 7 | Transverse boundaries established by genes involved in cerebellar development. **(A)** Schematic representation of a midsagittal cerebellar section and its subdivision into PC transverse zones [see text for details: some genes are included that are not expressed in GCs (nor cited in the text) but serve to indicate the locations of transverse boundaries (for a review, see Armstrong and Hawkes, 2013]; PC-specific genes are in red in the text boxes. *Ebf2* is expressed both in GC progenitors and in a PC subset. Lines point to boundaries between adjacent zones identified by the borders of Purkinje cell and granule cell gene expression domains. Abbreviations: AZ, anterior zone; CZa, anterior central zone; CZp, posterior central zone; PZ, posterior zone; NZ, nodular zone. **(B)** An example of the above: a sharp posterior boundary established by GCs derived from *Ebf2*+ GCPs populating from URL at E11.5.

stream at E12.5 and downregulated 1 day later. Genetic fate mapping indicates that GCs derived from *Ebf2*+ GCPs end up in the adult AZ (Badaloni et al., 2019), populated by early-born GCs (Machold and Fishell, 2005; **Figure 7B**). To date it has not been established whether *Ebf2* plays a role in GC development; interestingly, patients carrying mutations of its human paralog *EBF3*, expressed in URL-derivatives of the cerebellar primordium (Croci et al., 2006), exhibit a complex neurodevelopmental syndrome that includes cerebellar ataxia (Sleven et al., 2017).

In like manner, other GCP defects are restricted to the posterior EGL. As hinted above, posterior vermis abnormalities are reported due to mutations in the LIM-homeodomain transcription factor LMX1A, a critical regulator of cell-fate decisions. *Lmx1a* acts downstream of *Atoh1* (Pan et al., 2009) with an expression pattern restricted to a subset of posterior GC progenitors at the border between the URL and the roof plate (Chizhikov et al., 2010). Downregulation of *Lmx1a* is also associated with profound hypoplasia of the choroid plexus (Casoni et al., 2020). These progenitors produce GCs that are predominantly restricted to the posterior EGL and subsequently give rise to the posterior (=NZ; **Figure 7A**) late-born GCs. Consistent with this, the *Lmx1a* recessive mutant *dreher* (*Lmx1a*$^{dr\text{-}J}$) has pronounced GL defects focused on the posterior vermis (Chizhikov et al., 2010). In the absence of *Lmx1a*, mutant CGPs precociously exit the URL and over-migrate into the anterior vermis, leading to a premature regression of the URL and posterior vermis hypoplasia. Finally, the carbohydrate epitope CD15 is transiently expressed in parasagittal stripes in the EGL in both the embryonic human and the developing rabbit cerebellum (Marani and Tetteroo, 1983).

POSTMITOTIC GRANULE CELL RADIAL MIGRATION TO THE GRANULAR LAYER

Postmitotic GCs Go Through a Wave of Tangential Migration

The translocation of EGL cells to the GL begins with the cells becoming postmitotic and occupying the inner lamina of the EGL, where they form neurites and express the adhesion molecule TAG1, encoded by *Cntn2* (Pickford et al., 1989; Furley et al., 1990; **Figure 3B**). Once in the iEGL, the somata of the postmitotic GCs migrate tangentially for up to 2 days after their final mitosis. It is worth mentioning that the term "tangential migration" has been legitimately used to indicate mitotically active GCPs plodding along the subpial region, to invade the secondary germinal zone from the URL (e.g., Gilthorpe et al., 2002) and initiate transit amplification and clonal expansion. However, several studies use the term tangential migration to refer to the movement of postmitotic GCs in the iEGL before initiating their radial migration to the GL. During this period, the GCs alter their polarity to emit an axon at either pole: these axons eventually become parallel fibers. This process starts prenatally and continues through ~P21, by which time the EGL is depleted. Tangential migration slows at the interface of the EGL and the growing molecular layer and stops as the GCs extend a single vertical process—the future ascending GC axon—and switch to radial migration

(Komuro et al., 2001). The purpose of this tangential migration is unclear: perhaps it serves to align descending GC streams with the gaps ("raphes") between embryonic PC clusters, thereby ensuring appropriate GC allocation between stripes and zones of the expanding cerebellar cortex (Komuro et al., 2001). Raphes are prominent in chicken (Feirabend, 1990; Lin and Cepko, 1998) but less so in mammals, save for aberrant conditions such as the *Sey* mutant mouse where they are prominent (Swanson and Goldowitz, 2011).

The switch from tangential migration in the EGL to radial migration along Bergmann glial fibers is mediated non-cell-autonomously *via* semaphorin-6A (SEMA6A; **Figure 6N**) expressed by GCPs (Kerjan et al., 2005) and involves a repulsive interaction with its plexin-A2 receptor (Renaud et al., 2008; gene expression in **Figure 6O**). Plexin A2 binds to SEMA6A and controls GC migration and nucleus-centrosome coupling cell-autonomously: the lack of SEMA6A only affects tangential migration but not radial migration (Renaud and Chédotal, 2014). In *Sema6A* null mice many GCs remain ectopic in the molecular layer where they go through terminal differentiation and are contacted by mossy fibers. Similarly, expression of the repulsive ephrin receptor EPHB2 (**Figure 6L**) is restricted to the iEGL. Through reverse signaling, Ephrin B2, encoded by the *Efnb2* gene (**Figure 6M**) expressed by GCPs of the EGL, inhibits the chemoattractant effect of CXCL12 (Lu et al., 2001), which is expressed in meningeal cells. Finally, as shown by live imaging and functional studies, the SIAH E3 ubiquitin ligase, which controls proteasomal degradation of the PARD3A polarity protein (encoded by the *Pard3* gene), critically regulates GCP adhesion during EGL exit *via* the junctional adhesion molecule JAM-C (Famulski et al., 2010). Additional factors posited to play a role in the switch from tangential to radial migration include: the microtubule-actin crosslinking protein drebrin, interfering with the function of which leads to random movements of both the nucleus and the centrosome and impairs forward motion efficiency (Trivedi et al., 2017); the *Rac* pathway which cell-autonomously controls tangential migration, neurite formation and terminal differentiation of GCPs in the EGL (Nakamura et al., 2017); tenascin (Husmann et al., 1992); tissue plasminogen activator (Seeds et al., 1999); and the platelet-activating factor receptor (Bix and Clark, 1998).

Radial Migration Is Guided by Bergmann Glial Fibers

The modern study of postmitotic GC migration came from research labs in the Boston area using three novel techniques. First, the rapidly developing field of immunohistochemistry identified glial fibrillary acidic protein and raised antibodies that highlighted radial (Bergmann) glial cells and their Bergmann fibers (Bignami et al., 1972). Second, cell culture analysis offered a means to dynamically study GC migration along Bergmann fibers and thus provide an experimental approach to identify molecules that might play an *in vivo* role in the GC-Bergmann fiber interaction (Wolf, 1970; Hatten and Sidman, 1977; Trenkner and Sidman, 1977; Trenkner et al., 1978). Later, Hatten and Liem showed that in a culture system, glial filaments interacted with cerebellar neurons: the interactions were specific to Bergmann fibers and did not occur with parenchymal astrocytes (Hatten and Liem, 1981). Third, electron microscopy revealed the fine detail of the intimate relations between the migrating GCs and the Bergmann glial fibers (Hatten and Sidman, 1977). As GC somata migrate radially through the nascent molecular layer to the GL, the cell somata extend leading processes along the adjacent radial Bergmann glial fibers (Rakic, 1971).

Live imaging experiments have shown that migrating GCs form an extensive junction beneath the cell surface, mediated by the neuron-glial adhesion protein Astrotactin-1 (ASTN1) expressed on migrating GCs (Edmondson et al., 1988; Stitt and Hatten, 1990; Zheng et al., 1996; Adams et al., 2002) and regulates GC migration (Fishell and Hatten, 1991; Zheng et al., 1996). ASTN1 on GCs interacts heterotypically with N-cadherin (CDH2) both in *cis* and in *trans*, to support cell adhesion (Horn et al., 2018), while another family member, Astrotactin-2, regulates ASTN1 trafficking during postmitotic GC locomotion (Wilson et al., 2010). Migrating GCs extend a leading process with short filopodia and lamellipodia that shroud the glial fiber (Edmondson and Hatten, 1987; Gregory et al., 1988). When the neuron-glial adhesion junction beneath the cell body is released the cell soma advances, after which the neuron glides along the glial fiber until a new adhesion forms (Gregory et al., 1988). Migration is coordinated by the PAR-6 polarity complex in the centrosome (Solecki et al., 2004) through a mechanism that includes activation of actomyosin contractile motors in the proximal region of the leading process (Solecki et al., 2009), suggesting that the force needed for the forward movement is provided by contractility in the leading process.

Several ion channels are critical to normal GC radial migration. First is the G-protein coupled, inwardly-rectifying potassium channel GIRK2. A single amino acid mutation in GIRK2 gives rise to the phenotypic picture seen in *weaver* (*Kcnj6*^{wv}) mice (Goldowitz and Smeyne, 1995; Patil et al., 1995). Mice carrying the *weaver* mutation (Sidman et al., 1965) exhibit ataxia, mild locomotor hyperactivity, and, occasionally, tonic-clonic seizures. The failure of migration is accompanied by extensive GC death but the extent to which the two are linked is uncertain. GCs in the *weaver* mutant are born normally (Rezai and Yoon, 1972) but subsequently fail to migrate through the molecular layer to the GL owing to faulty interactions with radial glia (Rakic and Sidman, 1973a,b; Bignami and Dahl, 1974; Sotelo and Changeux, 1974; Sotelo, 1975). The abnormal relationship between GCs that had just begun their migration and Bergmann glial fibers led to the hypothesis that the *weaver* gene targeted the glial cell (Rakic and Sidman, 1973c). However, contrary to the initial hypothesis the homozygous *weaver* mutation does not directly affect migration but rather cell-autonomously promotes GC survival and differentiation (Goldowitz and Mullen, 1982; Gao et al., 1992). This is most dramatically shown by the normal migration of wild-type GCs along *weaver* mutant Bergmann glial fibers (Goldowitz and Mullen, 1982). The death of premigratory *Girk2* null GCs in the EGL prompted further studies of the role played by ion

channels (Surmeier et al., 1996), particularly calcium currents, in GC migration. Studies conducted by Komuro and Rakic in mouse cerebellar slices showed that selective pharmacological blockade of NMDA-subtype calcium channels impairs cell motility (Komuro and Rakic, 1992) and that the amplitude and frequency components of Ca^{2+} fluctuations correlate positively with the rate of GC movement in cerebellar microexplant cultures (Komuro and Rakic, 1996).

As a result of these processes, postmigratory GCs at the interface of the EGL and molecular layer extend axons several millimeters mediolaterally as parallel fibers, which form excitatory glutamatergic synapses on the Purkinje cell dendrites they intersect. The migrating GC somata express TAG1/CNTN2 and its deletion results in disordered parallel fiber extension (Furley et al., 1990; Dang et al., 2012). The elongation of axons projected by inward-migrating GCs is also disrupted by knockdown of *Fzr1*, encoding an adapter for the anaphase-promoting complex/cyclosome (APC/C) E3 ubiquitin-protein ligase complex (Konishi et al., 2004).

As GCs pass through the molecular layer and settle in the nascent GL they accumulate in an inside-out order (albeit not very strictly so—Legué et al., 2015) such that the earliest born settle adjacent to the white matter tracts, and the late-born cohort ends up more superficially, close to the PC somata. This passive stacking has interesting implications. One is that GCs of different molecular phenotypes (NADPH+/−, Hawkes and Turner, 1994; e.g., dystrophin+/−, Sillitoe et al., 2003) form patches that preferentially occupy either the deep or superficial GL. Thus, a superficial GL patch will project to the more distal PC dendritic arbors while parallel fibers from a deeper patch will terminate on dendritic branches more proximal to the PC somata. It is not clear whether proximal parallel fiber inputs are more influential on PC firing (Gundappa-Sulur et al., 1999; Dorgans et al., 2018). Either way, we believe that molecular differences imply functional differences, and focusing mossy fiber inputs to specific PC dendritic subdomains provides an additional subtlety that may serve to enhance the computational capacity of the mossy fiber pathway.

PATTERNING OF THE ADULT GRANULAR LAYER

Granule Cells and Granular Layer Compartmentation

As mentioned, despite its apparent simplicity, it is a mistake to believe that the GL is homogeneous. On the contrary, both expression markers and lineage tracing reveal an intriguing heterogeneity that aligns reliably with the stripe and zone architecture of the PCs, as described briefly in "Introduction" section. For example, consistent lineage restriction boundaries are seen in several models of chimeric mice that express constitutive phenotype markers (sketched in **Figure 7A**, an example in **Figure 7B**). Transverse lineage boundaries are often seen in mouse chimeras, and these boundaries align with the location of boundaries between PC transverse zones. For example, in *M. musculus*⟷*M. caroli* chimeras, two GL lineage boundaries are consistently found—one near the AZ/CZ, the other near the PZ/NZ (Goldowitz, 1989): unfortunately, a direct comparison of lineage and PC boundaries has not been made. Furthermore, transverse PC zones interdigitate such that the boundary line is complex. Similar lineage boundaries are seen in embryonic stem cell chimeras (Hawkes et al., 1999). Similarly, in murine chimeras of the *Pax6* mutation *small eye* ($Pax6^{Sey/Sey}$) and *ROSA26* controls [*Sey/Sey*⟷*Gt(ROSA)26Sor*], the AZ/CZ boundary is apparent, together with the second boundary in lobules VII/VIII (∼CZ/PZ: Swanson and Goldowitz, 2011) such that the *Pax6* mutation preferentially affects the GL of the CZa and CZp. The chimera data are important in that chimeric markers are cell-intrinsic and expression cannot be ascribed to local induction mechanisms. Why do chimera lineages in the GL segregate into discrete transverse zones? One model evokes heterochronicity: autonomous differences in developmental rate between different mouse strains result in one component of the chimera preferentially populating a particular GL compartment (Goldowitz, 1989; e.g., in chimeras the embryonic stem cells develop more quickly and hence end up concentrated in the earlier-born AZ). This view is consistent with the differences in birth dating between GC subtypes.

Many mutations that affect cerebellar development also show GL phenotypes with regional restriction reminiscent of the chimeras, although in these cases it is always a challenge to distinguish intrinsic GC defects from defects in the local environment. For example, in the *meander tail (mea/mea)* mutant the anterior cerebellum is agranular with a transition to normal at the AZ/CZ boundary: the phenotype seems intrinsic to GCPs (Hamre and Goldowitz, 1997) with no loss of PCs (Napieralski and Eisenman, 1993). The same phenotype is seen in *rostral cerebellar malformation* [(Unc5crcm): Ackerman et al., 1997; Eisenman and Brothers, 1998] and, at the same location, physical separation of the GL into anterior and posterior parts, with the two overlapping at the AZ/CZ boundary, is seen in the reelin pathway mouse mutant *disabled* (Dab1: Gallagher et al., 1998). Likewise, deletion of the transcriptional activator *NeuroD1* (expression pattern in **Figures 5F**, **6E**) produces a similar agranular phenotype except that GCs are absent posterior to the AZ/CZ boundary (Miyata et al., 1999). Finally, in the heterozygous *weaver* mutant, numerous defects include PC ectopias restricted to the CZ (Eisenman et al., 1998; Armstrong and Hawkes, 2001) and more pertinent here, substantial GC ectopia is seen in the AZ and a transverse GL discontinuity is present in lobules VIII/IX (= PZ/NZ boundary).

Even more striking than the transverse zone and parasagittal stripe boundaries, expression markers in the adult reveal a much more elaborate division of the GL into thousands of small patches ("hyper-heterogeneity"). This was first described for NADPH/nNOS expression (Hawkes and Turner, 1994; Schilling et al., 1994) and subsequently seen also for anti-dysbindin immunostaining (Sillitoe et al., 2003). In the case of NADPH/nNOS, the evidence suggests that heterogeneous expression by GC patches is likely induced by the local mossy

fiber environment (Schilling et al., 1994). Evidence of hyper-heterogeneity also comes from an elaborate, reproducible pattern of blebs in the GL that is revealed in paraffin-embedded sections on rehydration (Hawkes et al., 1997, 1998) and by the topography of trigeminal mossy fiber terminal fields (Shambes et al., 1978).

As discussed above, there are intrinsic topographic maps in the PC layer, the EGL, and the GL—all are aligned but how this is achieved is not well understood. The data suggest the following scenario: PC embryonic clusters are the prime organizers and restrict the distribution of different GCP subpopulations in the EGL to align with the underlying transverse PC zones. Thus, as GCPs in the URL proliferate and spread over the surface of the cerebellum to form the EGL (Miale and Sidman, 1961; Smeyne and Goldowitz, 1989) the early-born GCPs (from E12.5)—derived from the specific subset of early-born GCPs that do not express *Lmx1a*—give rise to the anterior EGL (AZ; **Figure 7A**). Later-born EGL progenitors subsequently migrate to cover the posterior lobe (the CZ and PZ; **Figure 7A**). The alignment of the PC AZ/CZ boundary with the border between the anterior and posterior EGL compartments—despite their very different embryological origins—suggests that the PC parasagittal architecture restricts GCP dispersal. The EGL transverse boundaries aligned with the CZp/PZ and PZ/NZ presumably arise in similar ways. Perinatally, the EGL boundaries are projected onto the nascent GL as the postmitotic GCs migrate along the radial Bergmann glial fibers and settle. Once the different GC lineages are *in situ*, hyper-heterogeneity appears—as evidenced by expression boundaries, blebs, and trigeminal terminal fields—all reproducible and in register with the overlying PC stripe architecture. It is highly unlikely that GC heterogeneity at this resolution is specified in the URL/EGL so we favor the interpretation that it is secondary to local inductive interactions with PCs and/or mossy fiber afferents (Ozol and Hawkes, 1997). Presumably, GC or PC heterogeneity at the molecular level is a substrate for the fine-tuning of mossy fiber pathways to reflect different input/output requirements and implies the possibility of a much richer mossy fiber input map than is usually appreciated, with up to several thousand parallel afferent pathways (Hawkes and Gravel, 1991).

CONCLUSIONS AND FUTURE DEVELOPMENTS

While much progress has been made in our understanding of GC development, numerous issues remain unclarified. First, the mechanism through which the *Atoh1*+ URL manages to generate multiple cell types—medial, interpositus, and lateral nuclear neurons, early- and late-born GCs, various UBC subtypes—is not clear. Does *Atoh1* label a population of region-specific stem cells or a heterogeneous pool of committed progenitors? In that case, do these committed progenitors originate from "universal" *Sox2*+ apical progenitors or an, as yet undiscovered, URL-specific, asymmetrically dividing stem cell restricted to glutamatergic fates? And if so, what marks this putative stem cell? An attractive candidate is the *Wls* gene, which labels apical progenitors negative for *Atoh1* (Yeung et al., 2014).

Second, not enough is known about the molecular mechanisms, extracellular cues, and cell-matrix interactions regulating the progression of GCPs from the URL into the EGL. Although previous studies have implicated both chemotactic signals and repulsive cues in the fine regulation of GCP migration into the URL, cell-type-specific inactivation or overexpression approaches may be required to obtain a more complete picture of this process. For example, early-born GCPs (E12.5) populate anterior segments of the EGL (Machold and Fishell, 2005; Badaloni et al., 2019) while later-born ones (E13.5–E15.5) spread throughout the AP axis of the cerebellar primordium, and the latest-born ones (E16.5) are mostly restricted to lobule X (Machold and Fishell, 2005). What molecules regulate their migration at each stage? The raw material to address this question has become available through exciting single-cell analyses of RNA expression over early cerebellar development. These data present a rich resource to mine to identify molecular pathways that would be assignable to various developmental events and epochs (Rosenberg et al., 2018; Hovestadt et al., 2019; Vladoiu et al., 2019; Wizeman et al., 2019).

Third, regarding clonal expansion, recent studies have classified pediatric medulloblastoma (MB) into four distinct molecular subgroups—WNT-dependent, SHH-dependent, Group 3, and Group 4 (reviewed in Northcott et al., 2019). WNT-dependent medulloblastoma has the most benign prognosis, while SHH MB is somewhat more severe (reviewed in Northcott et al., 2019). In particular, Group 3 medulloblastomas often metastasize, resulting in a poor prognosis, while Group 4 metastasizes less frequently and has an intermediate prognosis. Group 4 is the most frequent form of medulloblastoma accounting for 35% of all cases (reviewed in Northcott et al., 2019). Thus, recently discovered signaling pathways underlying clonal expansion (Kullmann et al., 2020) may provide new clues to its diagnosis and management.

Finally, the array of parallel fibers is highly conserved through vertebrate evolution and thus is important, but its development remains poorly understood. The mechanisms that restricts the extension of parallel fibers on the frontal plane (e.g., Berglund et al., 1999), their guidance within and across parasagittal domains, and the selection of their targets in the molecular layer are all largely unexplored. Which mechanisms lead parallel fibers to run orthogonal to the PC dendrites? Is the parallel array due to a cell-intrinsic control of cytoskeletal configuration, as is suggested from the parallel fiber disarray in the *Pax6* mutant *small eye* (*Sey*, Engelkamp et al., 1999; Yamasaki et al., 2001)? Parallel fibers also have implications for cerebellar stripe architecture. Parallel fibers extend several millimeters mediolaterally and intersect, and synapse with, multiple PC stripes. This is curious. Why are mossy fiber terminal fields highly topographically organized and aligned with specific PC stripes (Ji and Hawkes, 1994; Apps et al., 2018) if the parallel fibers promptly throw all the specificity away?

In conclusion, we believe that GC development remains a vital research field, not only because it involves the origin of over half of all neurons in the brain but also for its far-reaching implications in developmental biology, human genetics, oncology, and regenerative medicine.

AUTHOR CONTRIBUTIONS

All authors contributed to the article and approved the submitted version.

FUNDING

These studies were supported by the Italian Telethon and Ataxia UK (GC), the Department of Cell Biology and Anatomy, University of Calgary (RH), and the Centre for Molecular Medicine and Therapeutics and the Brain, Behaviour, and Development Themes at the University of British Columbia (DG).

ACKNOWLEDGMENTS

We thank Joanna Yeung, Joshua Wu, Miguel Ramirez, Derek Wu, and Matthew Liu (DG), and Laura Croci (GC) for the helpful discussions.

REFERENCES

Ackerman, S. L., Kozak, L. P., Przyborski, S. A., Rund, L. A., Boyer, B. B., and Knowles, B. B. (1997). The mouse rostral cerebellar malformation gene encodes an UNC-5-like protein. *Nature* 386, 838–842. doi: 10.1038/386838a0

Adams, N. C., Tomoda, T., Cooper, M., Dietz, G., and Hatten, M. E. (2002). Mice that lack astrotactin have slowed neuronal migration. *Development* 129, 965–972.

Aguado, C., Fernández-Alacid, L., Cabañero, M. J., Yanagawa, Y., Schilling, K., Watanabe, M., et al. (2013). Differential maturation of GIRK2-expressing neurons in the mouse cerebellum. *J. Chem. Neuroanat.* 47, 79–89. doi: 10.1016/j.jchemneu.2012.11.001

Aguilar, A., Meunier, A., Strehl, L., Martinovic, J., Bonniere, M., Attie-Bitach, T., et al. (2012). Analysis of human samples reveals impaired SHH-dependent cerebellar development in Joubert syndrome/meckel syndrome. *Proc. Natl. Acad. Sci. U S A* 109, 16951–16956. doi: 10.1073/pnas.1201408109

Ahn, A. H., Dziennis, S., Hawkes, R., and Herrup, K. (1994). The cloning of zebrin II reveals its identity with aldolase C. *Development* 120, 2081–2090.

Akazawa, C., Ishibashi, M., Shimizu, C., Nakanishi, S., and Kageyama, R. (1995). A mammalian helix-loop-helix factor structurally related to the product of *Drosophila* proneural gene atonal is a positive transcriptional regulator expressed in the developing nervous system. *J. Biol. Chem.* 270, 8730–8738. doi: 10.1074/jbc.270.15.8730

Alcantara, S., Ruiz, M., De Castro, F., Soriano, E., and Sotelo, C. (2000). Netrin 1 acts as an attractive or as a repulsive cue for distinct migrating neurons during the development of the cerebellar system. *Development* 127, 1359–1372.

Alder, J., Lee, K. J., Jessell, T. M., and Hatten, M. E. (1999). Generation of cerebellar granule neurons *in vivo* by transplantation of BMP-treated neural progenitor cells. *Nat. Neurosci.* 2, 535–540. doi: 10.1038/9189

Aldinger, K. A., Lehmann, O. J., Hudgins, L., Chizhikov, V. V., Bassuk, A. G., Ades, L. C., et al. (2009). FOXC1 is required for normal cerebellar development and is a major contributor to chromosome 6p25.3 dandy-walker malformation. *Nat. Genet.* 41, 1037–1042. doi: 10.1038/ng.422

Altman, J., and Bayer, S. A. (1997). *Development of the Cerebellar System in Relation to Its Evolution, Structure and Functions.* Boca Raton, FL: CRC Press.

Anne, S. L., Govek, E.-E., Ayrault, O., Kim, J. H., Zhu, X., Murphy, D. A., et al. (2013). WNT3 inhibits cerebellar granule neuron progenitor proliferation and medulloblastoma formation *via* MAPK activation. *PLoS One* 8:e81769. doi: 10.1371/journal.pone.0081769

Apps, R., and Hawkes, R. (2009). Cerebellar cortical organization: a one-map hypothesis. *Nat. Rev. Neurosci.* 10, 670–681. doi: 10.1038/nrn2698

Apps, R., Hawkes, R., Aoki, S., Bengtsson, F., Brown, A. M., Chen, G., et al. (2018). Cerebellar modules and their role as operational cerebellar processing units: a consensus article [corrected]. *Cerebellum* 17, 654–682. doi: 10.1007/s12311-018-0952-3

Armstrong, C., and Hawkes, R. (2001). Selective Purkinje cell ectopia in the cerebellum of the weaver mouse. *J. Comp. Neurol.* 439, 151–161. doi: 10.1002/cne.1339

Armstrong, C. L., and Hawkes, R. (2013). *Pattern Formation in the Cerebellum.* Colloquium digital library of life sciences. San Rafael: Morgan and Claypool.

Armstrong, C. L., Krueger-Naug, A. M., Currie, R. W., and Hawkes, R. (2000). Constitutive expression of the 25-kDa heat shock protein Hsp25 reveals novel parasagittal bands of Purkinje cells in the adult mouse cerebellar cortex. *J. Comp. Neurol.* 416, 383–397. doi: 10.1002/(sici)1096-9861(20000117)416:3<383::aid-cne9>3.0.co;2-m

Aruga, J., and Millen, K. J. (2018). ZIC1 function in normal cerebellar development and human developmental pathology. *Adv. Exp. Med. Biol.* 1046, 249–268. doi: 10.1007/978-981-10-7311-3_13

Aruga, J., Inoue, T., Hoshino, J., and Mikoshiba, K. (2002). Zic2 controls cerebellar development in cooperation with Zic1. *J. Neurosci.* 22, 218–225. doi: 10.1523/JNEUROSCI.22-01-00218.2002

Aruga, J., Minowa, O., Yaginuma, H., Kuno, J., Nagai, T., Noda, T., et al. (1998). Mouse zic1 is involved in cerebellar development. *J. Neurosci.* 18, 284–293. doi: 10.1523/JNEUROSCI.18-01-00284.1998

Aruga, J., Yokota, N., Hashimoto, M., Furuichi, T., Fukuda, M., and Mikoshiba, K. (1994). A novel zinc finger protein, zic, is involved in neurogenesis, especially in the cell lineage of cerebellar granule cells. *J. Neurochem.* 63, 1880–1890. doi: 10.1046/j.1471-4159.1994.63051880.x

Badaloni, A., Casoni, F., Croci, L., Chiara, F., Bizzoca, A., Gennarini, G., et al. (2019). Dynamic expression and new functions of early b cell factor 2 in cerebellar development. *Cerebellum* 18, 999–1010. doi: 10.1007/s12311-019-01051-3

Bashford, A. L., and Subramanian, V. (2019). Mice with a conditional deletion of Talpid3 (KIAA0586)—a model for joubert syndrome. *J. Pathol.* 248, 396–408. doi: 10.1002/path.5271

Beierbach, E., Park, C., Ackerman, S. L., Goldowitz, D., and Hawkes, R. (2001). Abnormal dispersion of a Purkinje cell subset in the mouse mutant cerebellar deficient folia (CDF). *J. Comp. Neurol.* 436, 42–51. doi: 10.1002/cne.1052

Ben-Arie, N., Bellen, H. J., Armstrong, D. L., Mccall, A. E., Gordadze, P. R., Guo, Q., et al. (1997). Math1 is essential for genesis of cerebellar granule neurons. *Nature* 390, 169–172. doi: 10.1038/36579

Ben-Arie, N., Mccall, A. E., Berkman, S., Eichele, G., Bellen, H. J., and Zoghbi, H. Y. (1996). Evolutionary conservation of sequence and expression of the bHLH protein Atonal suggests a conserved role in neurogenesis. *Hum. Mol. Genet.* 5, 1207–1216. doi: 10.1093/hmg/5.9.1207

Berglund, E. O., Murai, K. K., Fredette, B., Sekerkova, G., Marturano, B., Weber, L., et al. (1999). Ataxia and abnormal cerebellar microorganization in mice with ablated contactin gene expression. *Neuron* 24, 739–750. doi: 10.1016/s0896-6273(00)81126-5

Bignami, A., and Dahl, D. (1974). The development of bergmann glia in mutant mice with cerebellar malformations: reeler, staggerer and weaver. Immunofluorescence study with antibodies to the glial fibrillary acidic protein. *J. Comp. Neurol.* 155, 219–229. doi: 10.1002/cne.901550207

Bignami, A., Eng, L. F., Dahl, D., and Uyeda, C. T. (1972). Localization of the glial fibrillary acidic protein in astrocytes by immunofluorescence. *Brain Res.* 43, 429–435. doi: 10.1016/0006-8993(72)90398-8

Bix, G. J., and Clark, G. D. (1998). Platelet-activating factor receptor stimulation disrupts neuronal migration *in vitro*. *J. Neurosci.* 18, 307–318. doi: 10.1523/JNEUROSCI.18-01-00307.1998

Bizzoca, A., Virgintino, D., Lorusso, L., Buttiglione, M., Yoshida, L., Polizzi, A., et al. (2003). Transgenic mice expressing F3/contactin from the TAG-1 promoter exhibit developmentally regulated changes in the differentiation of cerebellar neurons. *Development* 130, 29–43. doi: 10.1242/dev.00183

Blank, M. C., Grinberg, I., Aryee, E., Laliberte, C., Chizhikov, V. V., Henkelman, R. M., et al. (2011). Multiple developmental programs are altered

by loss of zic1 and zic4 to cause dandy-walker malformation cerebellar pathogenesis. *Development* 138, 1207–1216. doi: 10.1242/dev.054114

Borday, C., Cabochette, P., Parain, K., Mazurier, N., Janssens, S., Tran, H. T., et al. (2012). Antagonistic cross-regulation between wnt and hedgehog signaling pathways controls post-embryonic retinal proliferation. *Development* 139, 3499–3509. doi: 10.1242/dev.079582

Bouchard, M., Pfeffer, P., and Busslinger, M. (2000). Functional equivalence of the transcription factors pax2 and pax5 in mouse development. *Development* 127, 3703–3713.

Brochu, G., Maler, L., and Hawkes, R. (1990). Zebrin II: a polypeptide antigen expressed selectively by Purkinje cells reveals compartments in rat and fish cerebellum. *J. Comp. Neurol.* 291, 538–552. doi: 10.1002/cne.902910405

Butts, T., Hanzel, M., and Wingate, R. J. (2014). Transit amplification in the amniote cerebellum evolved *via* a heterochronic shift in neuro D1 expression. *Development* 141, 2791–2795. doi: 10.1242/dev.101758

Carballo, G. B., Honorato, J. R., De Lopes, G. P. F., and Spohr, T. (2018). A highlight on sonic hedgehog pathway. *Cell Commun. Signal.* 16:11. doi: 10.1186/s12964-018-0220-7

Casoni, F., Croci, L., Bosone, C., D'ambrosio, R., Badaloni, A., Gaudesi, D., et al. (2017). *Zfp423/ZNF423* regulates cell cycle progression, the mode of cell division and the DNA-damage response in Purkinje neuron progenitors. *Development* 144, 3686–3697. doi: 10.1242/dev.155077

Casoni, F., Croci, L., Vincenti, F., Podini, P., Riba, M., Massimino, L., et al. (2020). ZFP423 regulates early patterning and multiciliogenesis in the hindbrain choroid plexus. *Development* 147:dev190173. doi: 10.1242/dev.190173

Cerminara, N. L., Lang, E. J., Sillitoe, R. V., and Apps, R. (2015). Redefining the cerebellar cortex as an assembly of non-uniform Purkinje cell microcircuits. *Nat. Rev. Neurosci.* 16, 79–93. doi: 10.1038/nrn3886

Chaki, M., Airik, R., Ghosh, A. K., Giles, R. H., Chen, R., Slaats, G. G., et al. (2012). Exome capture reveals ZNF423 and CEP164 mutations, linking renal ciliopathies to DNA damage response signaling. *Cell* 150, 533–548. doi: 10.1016/j.cell.2012.06.028

Chang, C.-H., Zanini, M., Shirvani, H., Cheng, J.-S., Yu, H., Feng, C.-H., et al. (2019). Atoh1 controls primary cilia formation to allow for SHH-triggered granule neuron progenitor proliferation. *Dev. Cell* 48, 184.e5–199.e5. doi: 10.1016/j.devcel.2018.12.017

Chaplin, N., Tendeng, C., and Wingate, R. J. (2010). Absence of an external germinal layer in zebrafish and shark reveals a distinct, anamniote ground plan of cerebellum development. *J. Neurosci.* 30, 3048–3057. doi: 10.1523/JNEUROSCI.6201-09.2010

Chédotal, A. (2010). Should I stay or should i go? Becoming a granule cell. *Trends Neurosci.* 33, 163–172. doi: 10.1016/j.tins.2010.01.004

Chi, C. L., Martinez, S., Wurst, W., and Martin, G. R. (2003). The isthmic organizer signal FGF8 is required for cell survival in the prospective midbrain and cerebellum. *Development* 130, 2633–2644. doi: 10.1242/dev.00487

Chizhikov, V. V., Davenport, J., Zhang, Q., Shih, E. K., Cabello, O. A., Fuchs, J. L., et al. (2007). Cilia proteins control cerebellar morphogenesis by promoting expansion of the granule progenitor pool. *J. Neurosci.* 27, 9780–9789. doi: 10.1523/JNEUROSCI.5586-06.2007

Chizhikov, V. V., Lindgren, A. G., Currle, D. S., Rose, M. F., Monuki, E. S., and Millen, K. J. (2006). The roof plate regulates cerebellar cell-type specification and proliferation. *Development* 133, 2793–2804. doi: 10.1242/dev.02441

Chizhikov, V. V., Lindgren, A. G., Mishima, Y., Roberts, R. W., Aldinger, K. A., Miesegaes, G. R., et al. (2010). Lmx1a regulates fates and location of cells originating from the cerebellar rhombic lip and telencephalic cortical hem. *Proc. Natl. Acad. Sci. U S A* 107, 10725–10730. doi: 10.1073/pnas.0910786107

Cho, J.-H., and Tsai, M.-J. (2006). Preferential posterior cerebellum defect in BETA2/neuroD1 knockout mice is the result of differential expression of BETA2/neuroD1 along anterior-posterior axis. *Dev. Biol.* 290, 125–138. doi: 10.1016/j.ydbio.2005.11.024

Choi, Y., Borghesani, P. R., Chan, J. A., and Segal, R. A. (2005). Migration from a mitogenic niche promotes cell-cycle exit. *J. Neurosci.* 25, 10437–10445. doi: 10.1523/JNEUROSCI.1559-05.2005

Chung, S.-H., Marzban, H., Croci, L., Consalez, G., and Hawkes, R. (2008). Purkinje cell subtype specification in the cerebellar cortex: ebf2 acts to repress the zebrin II-positive Purkinje cell phenotype. *Neuroscience* 153, 721–732. doi: 10.1016/j.neuroscience.2008.01.090

Chung, S.-H., Sillitoe, R. V., Croci, L., Badaloni, A., Consalez, G., and Hawkes, R. (2009). Purkinje cell phenotype restricts the distribution of unipolar brush cells. *Neuroscience* 164, 1496–1508. doi: 10.1016/j.neuroscience.2009.09.080

Clevers, H., and Nusse, R. (2012). Wnt/β-catenin signaling and disease. *Cell* 149, 1192–1205. doi: 10.1016/j.cell.2012.05.012

Consalez, G. G., and Hawkes, R. (2013). The compartmental restriction of cerebellar interneurons. *Front. Neural Circuits* 6:123. doi: 10.3389/fncir.2012.00123

Corbit, K. C., Aanstad, P., Singla, V., Norman, A. R., Stainier, D. Y., and Reiter, J. F. (2005). Vertebrate smoothened functions at the primary cilium. *Nature* 437, 1018–1021. doi: 10.1038/nature04117

Corrales, J. D., Rocco, G. L., Blaess, S., Guo, Q., and Joyner, A. L. (2004). Spatial pattern of sonic hedgehog signaling through gli genes during cerebellum development. *Development* 131, 5581–5590. doi: 10.1242/dev.01438

Croci, L., Barili, V., Chia, D., Massimino, L., Van Vugt, R., Masserdotti, G., et al. (2011). Local insulin-like growth factor I expression is essential for Purkinje neuron survival at birth. *Cell Death Differ.* 18, 48–59. doi: 10.1038/cdd.2010.78

Croci, L., Chung, S. H., Masserdotti, G., Gianola, S., Bizzoca, A., Gennarini, G., et al. (2006). A key role for the HLH transcription factor EBF2$^{COE2,O/E-3}$ in Purkinje neuron migration and cerebellar cortical topography. *Development* 133, 2719–2729. doi: 10.1242/dev.02437

Dahmane, N., and Ruiz-I-Altaba, A. (1999). Sonic hedgehog regulates the growth and patterning of the cerebellum. *Development* 126, 3089–3100.

Dang, P., Smythe, E., and Furley, A. J. (2012). TAG1 regulates the endocytic trafficking and signaling of the semaphorin3A receptor complex. *J. Neurosci.* 32, 10370–10382. doi: 10.1523/JNEUROSCI.5874-11.2012

D'Arcangelo, G. (2014). Reelin in the years: controlling neuronal migration and maturation in the mammalian brain. *Adv. Neurosci.* 2014:19. doi: 10.1155/2014/597395

Dastjerdi, F. V., Consalez, G. G., and Hawkes, R. (2012). Pattern formation during development of the embryonic cerebellum. *Front. Neuroanat.* 6:10. doi: 10.3389/fnana.2012.00010

Di Pietro, C., Marazziti, D., La Sala, G., Abbaszadeh, Z., Golini, E., Matteoni, R., et al. (2017). Primary cilia in the murine cerebellum and in mutant models of medulloblastoma. *Cell. Mol. Neurobiol.* 37, 145–154. doi: 10.1007/s10571-016-0354-3

Divya, T. S., Lalitha, S., Parvathy, S., Subashini, C., Sanalkumar, R., Dhanesh, S. B., et al. (2016). Regulation of Tlx3 by Pax6 is required for the restricted expression of chrnα3 in cerebellar granule neuron progenitors during development. *Sci. Rep.* 6:30337. doi: 10.1038/srep30337

Dorgans, K., Demais, V., Bailly, Y., Poulain, B., Isope, P., and Doussau, F. (2018). Molecular and functional heterogeneity of cerebellar granule cell terminals expands temporal coding in molecular layer interneurons. *bioRxiv* [Preprint]. doi: 10.1101/338152

Doughty, M. L., Lohof, A., Campana, A., Delhaye-Bouchaud, N., and Mariani, J. (1998). Neurotrophin-3 promotes cerebellar granule cell exit from the EGL. *Eur. J. Neurosci.* 10, 3007–3011. doi: 10.1111/j.1460-9568.1998.00333.x

Dymecki, S. M., and Tomasiewicz, H. (1998). Using Flp-recombinase to characterize expansion of wnt1-expressing neural progenitors in the mouse. *Dev. Biol.* 201, 57–65. doi: 10.1006/dbio.1998.8971

Edmondson, J. C., and Hatten, M. E. (1987). Glial-guided granule neuron migration *in vitro*: a high-resolution time-lapse video microscopic study. *J. Neurosci.* 7, 1928–1934. doi: 10.1523/JNEUROSCI.07-06-01928.1987

Edmondson, J. C., Liem, R. K., Kuster, J. E., and Hatten, M. E. (1988). Astrotactin: a novel neuronal cell surface antigen that mediates neuron-astroglial interactions in cerebellar microcultures. *J. Cell Biol.* 106, 505–517. doi: 10.1083/jcb.106.2.505

Eisenman, L. M., and Brothers, R. (1998). Rostral cerebellar malformation (rcm/rcm): a murine mutant to study regionalization of the cerebellum. *J. Comp. Neurol.* 394, 106–117. doi: 10.1002/(sici)1096-9861(19980427)394:1<106::aid-cne8>3.0.co;2-4

Eisenman, L. M., and Hawkes, R. (1989). 5′-nucleotidase and the mabQ113 antigen share a common distribution in the cerebellar cortex of the mouse. *Neuroscience* 31, 231–235. doi: 10.1016/0306-4522(89)90045-6

Eisenman, L. M., Gallagher, E., and Hawkes, R. (1998). Regionalization defects in the weaver mouse cerebellum. *J. Comp. Neurol.* 394, 431–444.

Engelkamp, D., Rashbass, P., Seawright, A., and Van Heyningen, V. (1999). Role of Pax6 in development of the cerebellar system. *Development* 126, 3585–3596.

Famulski, J. K., Trivedi, N., Howell, D., Yang, Y., Tong, Y., Gilbertson, R., et al. (2010). Siah regulation of pard3A controls neuronal cell adhesion during germinal zone exit. *Science* 330, 1834–1838. doi: 10.1126/science.1198480

Farioli-Vecchioli, S., Ciná, I., Ceccarelli, M., Micheli, L., Leonardi, L., Ciotti, M. T., et al. (2012). Tis21 knock-out enhances the frequency of medulloblastoma in patched1 heterozygous mice by inhibiting the cxcl3-dependent migration of cerebellar neurons. *J. Neurosci.* 32, 15547–15564. doi: 10.1523/JNEUROSCI.0412-12.2012

Feirabend, H. K. (1990). Development of longitudinal patterns in the cerebellum of the chicken (gallus domesticus): a cytoarchitectural study on the genesis of cerebellar modules. *Eur. J. Morphol.* 28, 169–223.

Fishell, G., and Hatten, M. E. (1991). Astrotactin provides a receptor system for CNS neuronal migration. *Development* 113, 755–765.

Frank, C. L., Liu, F., Wijayatunge, R., Song, L., Biegler, M. T., Yang, M. G., et al. (2015). Regulation of chromatin accessibility and zic binding at enhancers in the developing cerebellum. *Nat. Neurosci.* 18, 647–656. doi: 10.1038/nn.3995

Frantz, G. D., Weimann, J. M., Levin, M. E., and Mcconnell, S. K. (1994). Otx1 and Otx2 define layers and regions in developing cerebral cortex and cerebellum. *J. Neurosci.* 14, 5725–5740. doi: 10.1523/JNEUROSCI.14-10-05725.1994

Furley, A. J., Morton, S. B., Manalo, D., Karagogeos, D., Dodd, J., and Jessell, T. M. (1990). The axonal glycoprotein TAG-1 is an immunoglobulin superfamily member with neurite outgrowth-promoting activity. *Cell* 61, 157–170. doi: 10.1016/0092-8674(90)90223-2

Gallagher, E., Howell, B. W., Soriano, P., Cooper, J. A., and Hawkes, R. (1998). Cerebellar abnormalities in the disabled (mdab1-1) mouse. *J. Comp. Neurol.* 402, 238–251.

Gao, W. Q., Liu, X. L., and Hatten, M. E. (1992). The weaver gene encodes a nonautonomous signal for CNS neuronal differentiation. *Cell* 68, 841–854. doi: 10.1016/0092-8674(92)90028-b

Gaston-Massuet, C., Henderson, D. J., Greene, N. D. E., and Copp, A. J. (2005). Zic4, a zinc-finger transcription factor, is expressed in the developing mouse nervous system. *Dev. Dyn.* 233, 1110–1115. doi: 10.1002/dvdy.20417

Gilthorpe, J. D., Papantoniou, E.-K., Chédotal, A., Lumsden, A., and Wingate, R. J. T. (2002). The migration of cerebellar rhombic lip derivatives. *Development* 129, 4719–4728.

Goldowitz, D. (1989). Cell allocation in mammalian CNS formation: evidence from murine interspecies aggregation chimeras. *Neuron* 3, 705–713. doi: 10.1016/0896-6273(89)90239-0

Goldowitz, D., and Mullen, R. J. (1982). Granule cell as a site of gene action in the weaver mouse cerebellum: evidence from heterozygous mutant chimeras. *J. Neurosci.* 2, 1474–1485. doi: 10.1523/JNEUROSCI.02-10-01474.1982

Goldowitz, D., and Smeyne, R. J. (1995). Tune into the weaver channel. *Nat. Genet.* 11, 107–109. doi: 10.1038/ng1095-107

Goldowitz, D., Hamre, K. M., Przyborski, S. A., and Ackerman, S. L. (2000). Granule cells and cerebellar boundaries: analysis of Unc5h3 mutant chimeras. *J. Neurosci.* 20, 4129–4137. doi: 10.1523/JNEUROSCI.20-11-04129.2000

Gregory, W. A., Edmondson, J. C., Hatten, M. E., and Mason, C. A. (1988). Cytology and neuron-glial apposition of migrating cerebellar granule cells *in vitro*. *J. Neurosci.* 8, 1728–1738. doi: 10.1523/JNEUROSCI.08-05-01728.1988

Grinberg, I., Northrup, H., Ardinger, H., Prasad, C., Dobyns, W. B., and Millen, K. J. (2004). Heterozygous deletion of the linked genes ZIC1 and ZIC4 is involved in Dandy-Walker malformation. *Nat. Genet.* 36, 1053–1055. doi: 10.1038/ng1420

Gundappa-Sulur, G., De Schutter, E., and Bower, J. M. (1999). Ascending granule cell axon: an important component of cerebellar cortical circuitry. *J. Comp. Neurol.* 408, 580–596. doi: 10.1002/(sici)1096-9861(19990614)408:4<580::aid-cne11>3.0.co;2-o

Hagihara, K., Zhang, E. E., Ke, Y.-H., Liu, G., Liu, J.-J., Rao, Y., et al. (2009). Shp2 acts downstream of SDF-1alpha/CXCR4 in guiding granule cell migration during cerebellar development. *Dev. Biol.* 334, 276–284. doi: 10.1016/j.ydbio.2009.07.029

Haldipur, P., Bharti, U., Govindan, S., Sarkar, C., Iyengar, S., Gressens, P., et al. (2012). Expression of sonic hedgehog during cell proliferation in the human cerebellum. *Stem Cells Dev.* 21, 1059–1068. doi: 10.1089/scd.2011.0206

Hallonet, M. E., and Le Douarin, N. M. (1993). Tracing neuroepithelial cells of the mesencephalic and metencephalic alar plates during cerebellar ontogeny in quail-chick chimaeras. *Eur. J. Neurosci.* 5, 1145–1155. doi: 10.1111/j.1460-9568.1993.tb00969.x

Hamre, K. M., and Goldowitz, D. (1997). Meander tail acts intrinsic to granule cell precursors to disrupt cerebellar development: analysis of meander tail chimeric mice. *Development* 124, 4201–4212.

Hanks, M., Wurst, W., Anson-Cartwright, L., Auerbach, A., and Joyner, A. (1995). Rescue of the en-1 mutant phenotype by replacement of en-1 with en-2. *Science* 269, 679–682. doi: 10.1126/science.7624797

Hanold, K. C. (1986). Teratogenic potential of valproic acid. *J. Obstet. Gynecol. Neonatal Nurs.* 15, 111–116. doi: 10.1111/j.1552-6909.1986.tb01376.x

Hashimoto, M., and Hibi, M. (2012). Development and evolution of cerebellar neural circuits. *Dev. Growth Differ.* 54, 373–389. doi: 10.1111/j.1440-169X.2012.01348.x

Hatten, M. E., and Liem, R. K. (1981). Astroglial cells provide a template for the positioning of developing cerebellar neurons *in vitro*. *J. Cell. Biol.* 90, 622–630. doi: 10.1083/jcb.90.3.622

Hatten, M. E., and Sidman, R. L. (1977). Plant lectins detect age and region specific differences in cell surface carbohydrates and cell reassociation behavior of embryonic mouse cerebellar cells. *J. Supramol. Struct.* 7, 267–275. doi: 10.1002/jss.400070210

Hatton, B. A., Knoepfler, P. S., Kenney, A. M., Rowitch, D. H., De Alborán, I. M., Olson, J. M., et al. (2006). N-myc is an essential downstream effector of shh signaling during both normal and neoplastic cerebellar growth. *Cancer Res.* 66, 8655–8661. doi: 10.1158/0008-5472.CAN-06-1621

Hausmann, B., and Sievers, J. (1985). Cerebellar external granule cells are attached to the basal lamina from the onset of migration up to the end of their proliferative activity. *J. Comp. Neurol.* 241, 50–62. doi: 10.1002/cne.902410105

Hawkes, R., Beierbach, E., and Tan, S. S. (1999). Granule cell dispersion is restricted across transverse boundaries in mouse chimeras. *Eur. J. Neurosci.* 11, 3800–3808. doi: 10.1046/j.1460-9568.1999.00812.x

Hawkes, R., Gallagher, E., and Ozol, K. (1997). Blebs in the mouse cerebellar granular layer as a sign of structural inhomogeneity: 1. Anterior lobe vermis. *Acta Anat.* 158, 205–214. doi: 10.1159/000147931

Hawkes, R., Gallagher, E., and Ozol, K. (1998). Blebs in the mouse cerebellar granular layer as a sign of structural inhomogeneity: 2. Posterior lobe vermis. *Acta Anat.* 163, 47–55. doi: 10.1159/000046445

Hawkes, R., and Gravel, C. (1991). The modular cerebellum. *Prog. Neurobiol.* 36, 309–327. doi: 10.1016/0301-0082(91)90004-k

Hawkes, R., and Turner, R. W. (1994). Compartmentation of NADPH-diaphorase activity in the mouse cerebellar cortex. *J. Comp. Neurol.* 346, 499–516. doi: 10.1002/cne.903460404

Haycraft, C. J., Banizs, B., Aydin-Son, Y., Zhang, Q., Michaud, E. J., and Yoder, B. K. (2005). Gli2 and gli3 localize to cilia and require the intraflagellar transport protein polaris for processing and function. *PLoS Genet.* 1:e53. doi: 10.1371/journal.pgen.0010053

Herculano-Houzel, S., Mota, B., and Lent, R. (2006). Cellular scaling rules for rodent brains. *Proc. Natl. Acad. Sci. U S A* 103, 12138–12143. doi: 10.1073/pnas.0604911103

Hess, N. (1858). *De Cerebelli Gyrorum Textura Disquisitiones Microscopicae*. Dissertatio inauguralis. Tartu, Russia: Schünmann & Mattiesen.

Hong, C.-J., and Hamilton, B. A. (2016). Zfp423 regulates sonic hedgehog signaling *via* primary cilium function. *PLoS Genet.* 12:e1006357. doi: 10.1371/journal.pgen.1006357

Horn, Z., Behesti, H., and Hatten, M. E. (2018). N-cadherin provides a cis and trans ligand for astrotactin that functions in glial-guided neuronal migration. *Proc. Natl. Acad. Sci. U S A* 115, 10556–10563. doi: 10.1073/pnas.1811100115

Hoshino, M., Nakamura, S., Mori, K., Kawauchi, T., Terao, M., Nishimura, Y. V., et al. (2005). Ptf1a, a bHLH transcriptional gene, defines GABAergic neuronal fates in cerebellum. *Neuron* 47, 201–213. doi: 10.1016/j.neuron.2005.06.007

Hovestadt, V., Smith, K. S., Bihannic, L., Filbin, M. G., Shaw, M. L., Baumgartner, A., et al. (2019). Resolving medulloblastoma cellular architecture by single-cell genomics. *Nature* 572, 74–79. doi: 10.1038/s41586-019-1434-6

Hu, A., and Song, B.-L. (2019). The interplay of patched, smoothened and cholesterol in hedgehog signaling. *Curr. Opin. Cell Biol.* 61, 31–38. doi: 10.1016/j.ceb.2019.06.008

Hu, M. C., Mo, R., Bhella, S., Wilson, C. W., Chuang, P. T., Hui, C.-C., et al. (2006). GLI3-dependent transcriptional repression of gli1, gli2 and kidney patterning genes disrupts renal morphogenesis. *Development* 133, 569–578. doi: 10.1242/dev.02220

Huangfu, D., and Anderson, K. V. (2005). Cilia and hedgehog responsiveness in the mouse. *Proc. Natl. Acad. Sci. U S A* 102, 11325–11330. doi: 10.1073/pnas.0505328102

Husmann, K., Faissner, A., and Schachner, M. (1992). Tenascin promotes cerebellar granule cell migration and neurite outgrowth by different domains in the fibronectin type III repeats. *J. Cell. Biol.* 116, 1475–1486. doi: 10.1083/jcb.116.6.1475

Iacopetti, P., Michelini, M., Stuckmann, I., Oback, B., Aaku-Saraste, E., and Huttner, W. B. (1999). Expression of the antiproliferative gene TIS21 at the onset of neurogenesis identifies single neuroepithelial cells that switch from proliferative to neuron-generating division. *Proc. Natl. Acad. Sci. U S A* 96, 4639–4644. doi: 10.1073/pnas.96.8.4639

Ito, M. (1984). *The Cerebellum and Neural Control*. New York, NY: Raven Press.

Jacob, J., and Briscoe, J. (2003). Gli proteins and the control of spinal-cord patterning. *EMBO Rep.* 4, 761–765. doi: 10.1038/sj.embor.embor896

Jensen, P., Smeyne, R., and Goldowitz, D. (2004). Analysis of cerebellar development in math1 null embryos and chimeras. *J. Neurosci.* 24, 2202–2211. doi: 10.1523/JNEUROSCI.3427-03.2004

Ji, Z., and Hawkes, R. (1994). Topography of Purkinje cell compartments and mossy fiber terminal fields in lobules II and III of the rat cerebellar cortex: spinocerebellar and cuneocerebellar projections. *Neuroscience* 61, 935–954. doi: 10.1016/0306-4522(94)90414-6

Kenney, A. M., Cole, M. D., and Rowitch, D. H. (2003). Nmyc upregulation by sonic hedgehog signaling promotes proliferation in developing cerebellar granule neuron precursors. *Development* 130, 15–28. doi: 10.1242/dev.00182

Kerjan, G., Dolan, J., Haumaitre, C., Schneider-Maunoury, S., Fujisawa, H., Mitchell, K. J., et al. (2005). The transmembrane semaphorin Sema6A controls cerebellar granule cell migration. *Nat. Neurosci.* 8, 1516–1524. doi: 10.1038/nn1555

Klisch, T. J., Xi, Y., Flora, A., Wang, L., Li, W., and Zoghbi, H. Y. (2011). *In vivo* atoh1 targetome reveals how a proneural transcription factor regulates cerebellar development. *Proc. Natl. Acad. Sci. U S A* 108, 3288–3293. doi: 10.1073/pnas.1100230108

Knoepfler, P. S., Cheng, P. F., and Eisenman, R. N. (2002). N-myc is essential during neurogenesis for the rapid expansion of progenitor cell populations and the inhibition of neuronal differentiation. *Genes Dev.* 16, 2699–2712. doi: 10.1101/gad.1021202

Komuro, H., and Rakic, P. (1992). Selective role of N-type calcium channels in neuronal migration. *Science* 257, 806–809. doi: 10.1126/science.1323145

Komuro, H., and Rakic, P. (1996). Intracellular Ca^{2+} fluctuations modulate the rate of neuronal migration. *Neuron* 17, 275–285. doi: 10.1016/s0896-6273(00)80159-2

Komuro, H., Yacubova, E., Yacubova, E., and Rakic, P. (2001). Mode and tempo of tangential cell migration in the cerebellar external granular layer. *J. Neurosci.* 21, 527–540. doi: 10.1523/JNEUROSCI.21-02-00527.2001

Konishi, Y., Stegmuller, J., Matsuda, T., Bonni, S., and Bonni, A. (2004). Cdh1-APC controls axonal growth and patterning in the mammalian brain. *Science* 303, 1026–1030. doi: 10.1126/science.1093712

Krizhanovsky, V., and Ben-Arie, N. (2006). A novel role for the choroid plexus in BMP-mediated inhibition of differentiation of cerebellar neural progenitors. *Mech. Dev.* 123, 67–75. doi: 10.1016/j.mod.2005.09.005

Kullmann, J. A., Trivedi, N., Howell, D., Laumonnerie, C., Nguyen, V., Banerjee, S. S., et al. (2020). Oxygen tension and the VHL-Hif1α pathway determine onset of neuronal polarization and cerebellar germinal zone exit. *Neuron* 106, 607.e5–623.e5. doi: 10.1016/j.neuron.2020.02.025

Lackey, E. P., Heck, D. H., and Sillitoe, R. V. (2018). Recent advances in understanding the mechanisms of cerebellar granule cell development and function and their contribution to behavior. *F1000Res.* 7:F1000. doi: 10.12688/f1000research.15021.1

Lannoo, M. J., Ross, L., Maler, L., and Hawkes, R. (1991). Development of the cerebellum and its extracerebellar Purkinje cell projection in teleost fishes as determined by zebrin II immunocytochemistry. *Prog. Neurobiol.* 37, 329–363. doi: 10.1016/0301-0082(91)90022-s

Lee, S. J., Lindsey, S., Graves, B., Yoo, S., Olson, J. M., and Langhans, S. A. (2013). Sonic hedgehog-induced histone deacetylase activation is required for cerebellar granule precursor hyperplasia in medulloblastoma. *PLoS One* 8:e71455. doi: 10.1371/journal.pone.0071455

Legué, E., Riedel, E., and Joyner, A. L. (2015). Clonal analysis reveals granule cell behaviors and compartmentalization that determine the folded morphology of the cerebellum. *Development* 142, 1661–1671. doi: 10.1242/dev.120287

Leto, K., Arancillo, M., Becker, E. B., Buffo, A., Chiang, C., Ding, B., et al. (2015). Consensus article: cerebellar development. *Cerebellum* 15, 789–828. doi: 10.1007/s12311-015-0724-2

Leto, K., and Rossi, F. (2012). Specification and differentiation of cerebellar GABAergic neurons. *Cerebellum* 11, 434–435. doi: 10.1007/s12311-011-0324-8

Lewis, P. M., Gritli-Linde, A., Smeyne, R., Kottmann, A., and Mcmahon, A. P. (2004). Sonic hedgehog signaling is required for expansion of granule neuron precursors and patterning of the mouse cerebellum. *Dev. Biol.* 270, 393–410. doi: 10.1016/j.ydbio.2004.03.007

Lin, J. C., and Cepko, C. L. (1998). Granule cell raphes and parasagittal domains of Purkinje cells: complementary patterns in the developing chick cerebellum. *J. Neurosci.* 18, 9342–9353. doi: 10.1523/JNEUROSCI.18-22-09342.1998

Liu, A., and Niswander, L. A. (2005). Bone morphogenetic protein signaling and vertebrate nervous system development. *Nat. Rev. Neurosci.* 6, 945–954. doi: 10.1038/nrn1805

Liu, A., Wang, B., and Niswander, L. A. (2005). Mouse intraflagellar transport proteins regulate both the activator and repressor functions of gli transcription factors. *Development* 132, 3103–3111. doi: 10.1242/dev.01894

Llinás, R., and Negrello, M. N. (2015). Cerebellum. *Scholarpedia* 10:4606. doi: 10.4249/scholarpedia.4606

Logan, C., Millar, C., Bharadia, V., and Rouleau, K. (2002). Onset of tlx-3 expression in the chick cerebellar cortex correlates with the morphological development of fissures and delineates a posterior transverse boundary. *J. Comp. Neurol.* 448, 138–149. doi: 10.1002/cne.10234

Lospinoso Severini, L., Ghirga, F., Bufalieri, F., Quaglio, D., Infante, P., and Di Marcotullio, L. (2020). The SHH/GLI signaling pathway: a therapeutic target for medulloblastoma. *Expert Opin. Ther. Targets* 24, 1159–1181. doi: 10.1080/14728222.2020.1823967

Lu, Q., Sun, E. E., Klein, R. S., and Flanagan, J. G. (2001). Ephrin-B reverse signaling is mediated by a novel PDZ-RGS protein and selectively inhibits G protein-coupled chemoattraction. *Cell* 105, 69–79. doi: 10.1016/s0092-8674(01)00297-5

Ma, Q., Jones, D., Borghesani, P. R., Segal, R. A., Nagasawa, T., Kishimoto, T., et al. (1998). Impaired B-lymphopoiesis, myelopoiesis and derailed cerebellar neuron migration in CXCR4- and SDF-1-deficient mice. *Proc. Natl. Acad. Sci. U S A* 95, 9448–9453. doi: 10.1073/pnas.95.16.9448

Machold, R., and Fishell, G. (2005). Math1 is expressed in temporally discrete pools of cerebellar rhombic-lip neural progenitors. *Neuron* 48, 17–24. doi: 10.1016/j.neuron.2005.08.028

Machold, R., Klein, C., and Fishell, G. (2011). Genes expressed in ATOH1 neuronal lineages arising from the r1/isthmus rhombic lip. *Gene. Expr. Patterns* 11, 349–359. doi: 10.1016/j.gep.2011.03.007

Machold, R. P., Kittell, D. J., and Fishell, G. J. (2007). Antagonism between Notch and bone morphogenetic protein receptor signaling regulates neurogenesis in the cerebellar rhombic lip. *Neural Dev.* 2:5. doi: 10.1186/1749-8104-2-5

Marani, E., and Tetteroo, P. A. (1983). A longitudinal band-pattern for the monoclonal human granulocyte antibody B4,3 in the cerebellar external granular layer of the immature rabbit. *Histochemistry* 78, 157–161. doi: 10.1007/BF00489494

Marigo, V., Davey, R. A., Zuo, Y., Cunningham, J. M., and Tabin, C. J. (1996). Biochemical evidence that patched is the hedgehog receptor. *Nature* 384, 176–179. doi: 10.1038/384176a0

Marr, D. (1969). A theory of cerebellar cortex. *J. Physiol.* 202, 437–470. doi: 10.1113/jphysiol.1969.sp008820

Marzban, H., Hoy, N., Aavani, T., Sarko, D. K., Catania, K. C., and Hawkes, R. (2011). Compartmentation of the cerebellar cortex in the naked mole-rat

(*Heterocephalus Glaber*). *Cerebellum* 10, 435–448. doi: 10.1007/s12311-011-0251-8

May, S. R., Ashique, A. M., Karlen, M., Wang, B., Shen, Y., Zarbalis, K., et al. (2005). Loss of the retrograde motor for IFT disrupts localization of SMO to cilia and prevents the expression of both activator and repressor functions of gli. *Dev. Biol.* 287, 378–389. doi: 10.1016/j.ydbio.2005.08.050

McAndrew, P. E., Frostholm, A., Evans, J. E., Zdilar, D., Goldowitz, D., Chiu, I. M., et al. (1998). Novel receptor protein tyrosine phosphatase (RPTPrho) and acidic fibroblast growth factor (FGF-1) transcripts delineate a rostrocaudal boundary in the granule cell layer of the murine cerebellar cortex. *J. Comp. Neurol.* 391, 444–455. doi: 10.1002/(sici)1096-9861(19980222)391:4<444::aid-cne3>3.0.co;2-0

McMahon, A. P., and Bradley, A. (1990). The wnt-1 (int-1) proto-oncogene is required for development of a large region of the mouse brain. *Cell* 62, 1073–1085. doi: 10.1016/0092-8674(90)90385-r

Meek, J., Hafmans, T. G., Maler, L., and Hawkes, R. (1992). Distribution of zebrin II in the gigantocerebellum of the mormyrid fish *Gnathonemus petersii* compared with other teleosts. *J. Comp. Neurol.* 316, 17–31. doi: 10.1002/cne.903160103

Miale, I. L., and Sidman, R. L. (1961). An autoradiographic analysis of histogenesis in the mouse cerebellum. *Exp. Neurol.* 4, 277–296. doi: 10.1016/0014-4886(61)90055-3

Millet, S., Bloch-Gallego, E., Simeone, A., and Alvarado-Mallart, R. M. (1996). The caudal limit of Otx2 gene expression as a marker of the midbrain/hindbrain boundary: a study using *in situ* hybridization and chick/quail homotopic grafts. *Development* 122, 3785–3797.

Millonig, J. H., Millen, K. J., and Hatten, M. E. (2000). The mouse dreher gene lmx1a controls formation of the roof plate in the vertebrate CNS. *Nature* 403, 764–769. doi: 10.1038/35001573

Mimeault, M., and Batra, S. K. (2010). Frequent deregulations in the hedgehog signaling network and cross-talks with the epidermal growth factor receptor pathway involved in cancer progression and targeted therapies. *Pharmacol. Rev.* 62, 497–524. doi: 10.1124/pr.109.002329

Miyata, T., Maeda, T., and Lee, J. E. (1999). NeuroD is required for differentiation of the granule cells in the cerebellum and hippocampus. *Genes Dev.* 13, 1647–1652. doi: 10.1101/gad.13.13.1647

Miyazawa, K., Himi, T., Garcia, V., Yamagishi, H., Sato, S., and Ishizaki, Y. (2000). A role for p27/Kip1 in the control of cerebellar granule cell precursor proliferation. *J. Neurosci.* 20, 5756–5763. doi: 10.1523/JNEUROSCI.20-15-05756.2000

Moore, S. W., Tessier-Lavigne, M., and Kennedy, T. E. (2007). Netrins and their receptors. *Adv. Exp. Med. Biol.* 621, 17–31. doi: 10.1007/978-0-387-76715-4_2

Nagai, T., Aruga, J., Takada, S., Gunther, T., Sporle, R., Schughart, K., et al. (1997). The expression of the mouse Zic1, Zic2 and Zic3 gene suggests an essential role for Zic genes in body pattern formation. *Dev. Biol.* 182, 299–313. doi: 10.1006/dbio.1996.8449

Nakamura, T., Ueyama, T., Ninoyu, Y., Sakaguchi, H., Choijookhuu, N., Hishikawa, Y., et al. (2017). Novel role of rac-mid1 signaling in medial cerebellar development. *Development* 144, 1863–1875. doi: 10.1242/dev.147900

Nakashima, K., Umeshima, H., and Kengaku, M. (2015). Cerebellar granule cells are predominantly generated by terminal symmetric divisions of granule cell precursors. *Dev. Dyn.* 244, 748–758. doi: 10.1002/dvdy.24276

Nakata, K., Nagai, T., Aruga, J., and Mikoshiba, K. (1997). Xenopus zic3, a primary regulator both in neural and neural crest development. *Proc. Natl. Acad. Sci. U S A* 94, 11980–11985. doi: 10.1073/pnas.94.22.11980

Napieralski, J. A., and Eisenman, L. M. (1993). Developmental analysis of the external granular layer in the meander tail mutant mouse: do cerebellar microneurons have independent progenitors? *Dev. Dyn.* 197, 244–254. doi: 10.1002/aja.1001970403

Northcott, P. A., Robinson, G. W., Kratz, C. P., Mabbott, D. J., Pomeroy, S. L., Clifford, S. C., et al. (2019). Medulloblastoma. *Nat. Rev. Dis. Primers* 5:11. doi: 10.1038/s41572-019-0063-6

Obersteiner, H. (1869). Beiträge zur kenntniss vom feineren bau der kleinhirnrinde, mit besonderer berücksichtigung der entwicklung. *S.B. Akad. Wiss. Mien. Bd.* 60, 101–114.

Owa, T., Taya, S., Miyashita, S., Yamashita, M., Adachi, T., Yamada, K., et al. (2018). Meis1 coordinates cerebellar granule cell development by regulating Pax6 transcription, BMP signaling and atoh1 degradation. *J. Neurosci.* 38, 1277–1294. doi: 10.1523/JNEUROSCI.1545-17.2017

Ozol, K., Hayden, J. M., Oberdick, J., and Hawkes, R. (1999). Transverse zones in the vermis of the mouse cerebellum. *J. Comp. Neurol.* 412, 95–111.

Ozol, K. O., and Hawkes, R. (1997). Compartmentation of the granular layer of the cerebellum. *Histol. Histopathol.* 12, 171–184.

Pan, N., Jahan, I., Lee, J., and Fritzsch, B. (2009). Defects in the cerebella of conditional *Neurod1* null mice correlate with effective *Tg (Atoh1-cre)* recombination and granule cell requirements for *Neurod1* for differentiation. *Cell Tissue Res.* 337, 407–428. doi: 10.1007/s00441-009-0826-6

Patil, N., Cox, D. R., Bhat, D., Faham, M., Myers, R. M., and Peterson, A. S. (1995). A potassium channel mutation in weaver mice implicates membrane excitability in granule cell differentiation. *Nat. Genet.* 11, 126–129. doi: 10.1038/ng1095-126

Pickford, L. B., Mayer, D. N., Bolin, L. M., and Rouse, R. V. (1989). Transiently expressed, neural-specific molecule associated with premigratory granule cells in postnatal mouse cerebellum. *J. Neurocytol.* 18, 465–478. doi: 10.1007/BF01474543

Pieper, A., Rudolph, S., Wieser, G. L., Gotze, T., Miessner, H., Yonemasu, T., et al. (2019). NeuroD2 controls inhibitory circuit formation in the molecular layer of the cerebellum. *Sci. Rep.* 9:1448. doi: 10.1038/s41598-018-37850-7

Pons, S., Trejo, J. L., Martinez-Morales, J. R., and Marti, E. (2001). Vitronectin regulates Sonic hedgehog activity during cerebellum development through CREB phosphorylation. *Development* 128, 1481–1492.

Pourquié, O., Hallonet, M. E., and Le Douarin, N. M. (1992). Association of BEN glycoprotein expression with climbing fiber axonogenesis in the avian cerebellum. *J. Neurosci.* 12, 1548–1557. doi: 10.1523/JNEUROSCI.12-04-01548.1992

Przyborski, S. A., Knowles, B. B., and Ackerman, S. L. (1998). Embryonic phenotype of Unc5h3 mutant mice suggests chemorepulsion during the formation of the rostral cerebellar boundary. *Development* 125, 41–50.

Qin, L., Wine-Lee, L., Ahn, K. J., and Crenshaw, E. B. III (2006). Genetic analyses demonstrate that bone morphogenetic protein signaling is required for embryonic cerebellar development. *J. Neurosci.* 26, 1896–1905. doi: 10.1523/JNEUROSCI.3202-05.2006

Rakic, P. (1971). Neuron-glia relationship during granule cell migration in developing cerebellar cortex. A golgi and electronmicroscopic study in macacus rhesus. *J. Comp. Neurol.* 141, 283–312. doi: 10.1002/cne.901410303

Rakic, P., and Sidman, R. L. (1973a). Organization of cerebellar cortex secondary to deficit of granule cells in weaver mutant mice. *J. Comp. Neurol.* 152, 133–161. doi: 10.1002/cne.901520203

Rakic, P., and Sidman, R. L. (1973b). Sequence of developmental abnormalities leading to granule cell deficit in cerebellar cortex of weaver mutant mice. *J. Comp. Neurol.* 152, 103–132. doi: 10.1002/cne.901520202

Rakic, P., and Sidman, R. L. (1973c). Weaver mutant mouse cerebellum: defective neuronal migration secondary to abnormality of Bergmann glia. *Proc. Natl. Acad. Sci. U S A* 70, 240–244. doi: 10.1073/pnas.70.1.240

Ramón Y Cajal, S. (1911). *Histologie Du Système Nerveux De L'homme & Des Vertébrés*. Paris: Maloine.

Renaud, J., and Chédotal, A. (2014). Time-lapse analysis of tangential migration in Sema6A and PlexinA2 knockouts. *Mol. Cell. Neurosci.* 63, 49–59. doi: 10.1016/j.mcn.2014.09.005

Renaud, J., Kerjan, G., Sumita, I., Zagar, Y., Georget, V., Kim, D., et al. (2008). Plexin-A2 and its ligand, Sema6A, control nucleus-centrosome coupling in migrating granule cells. *Nat. Neurosci.* 11, 440–449. doi: 10.1038/nn2064

Rezai, Z., and Yoon, C. H. (1972). Abnormal rate of granule cell migration in the cerebellum of "weaver" mutant mice. *Dev. Biol.* 29, 17–26. doi: 10.1016/0012-1606(72)90039-5

Rosenberg, A. B., Roco, C. M., Muscat, R. A., Kuchina, A., Sample, P., Yao, Z., et al. (2018). Single-cell profiling of the developing mouse brain and spinal cord with split-pool barcoding. *Science* 360, 176–182. doi: 10.1126/science.aam8999

Ruiz i Altaba, A. (1999). Gli proteins encode context-dependent positive and negative functions: implications for development and disease. *Development* 126, 3205–3216.

Ruiz i Altaba, A., Palma, V., and Dahmane, N. (2002). Hedgehog-gli signaling and the growth of the brain. *Nat. Rev. Neurosci.* 3, 24–33. doi: 10.1038/nrn704

Ruppert, J. M., Kinzler, K. W., Wong, A. J., Bigner, S. H., Kao, F. T., Law, M. L., et al. (1988). The GLI-kruppel family of human genes. *Mol. Cell. Biol.* 8, 3104–3113. doi: 10.1128/mcb.8.8.3104

Sarna, J. R., and Hawkes, R. (2003). Patterned Purkinje cell death in the cerebellum. *Prog. Neurobiol.* 70, 473–507. doi: 10.1016/s0301-0082(03)00114-x

Sarna, J. R., Marzban, H., Watanabe, M., and Hawkes, R. (2006). Complementary stripes of phospholipase Cβ3 and Cβ4 expression by Purkinje cell subsets in the mouse cerebellum. *J. Comp. Neurol.* 496, 303–313. doi: 10.1002/cne.20912

Schilling, K., Schmidt, H. H., and Baader, S. L. (1994). Nitric oxide synthase expression reveals compartments of cerebellar granule cells and suggests a role for mossy fibers in their development. *Neuroscience* 59, 893–903. doi: 10.1016/0306-4522(94)90293-3

Seeds, N. W., Basham, M. E., and Haffke, S. P. (1999). Neuronal migration is retarded in mice lacking the tissue plasminogen activator gene. *Proc. Natl. Acad. Sci. U S A* 96, 14118–14123. doi: 10.1073/pnas.96.24.14118

Sekiguchi, M., Shimai, K., Guo, H., and Nowakowski, R. S. (1992). Cytoarchitectonic abnormalities in hippocampal formation and cerebellum of dreher mutant mouse. *Brain Res. Dev.* 67, 105–112. doi: 10.1016/0165-3806(92)90030-z

Shambes, G. M., Gibson, J. M., and Welker, W. (1978). Fractured somatotopy in granule cell tactile areas of rat cerebellar hemispheres revealed by micromapping. *Brain Behav. Evol.* 15, 94–140. doi: 10.1159/000123774

Shimomura, A., Patel, D., Wilson, S. M., Koehler, K. R., Khanna, R., and Hashino, E. (2015). Tlx3 promotes glutamatergic neuronal subtype specification through direct interactions with the chromatin modifier CBP. *PLoS One* 10:e0135060. doi: 10.1371/journal.pone.0135060

Sidman, R. L., Green, M. C., and Appel, S. (1965). *Catalog of the Neurological Mutants of the Mouse.* Cambridge, MA: Harvard University Press.

Sillitoe, R. V., Benson, M. A., Blake, D. J., and Hawkes, R. (2003). Abnormal dysbindin expression in cerebellar mossy fiber synapses in the mdx mouse model of Duchenne muscular dystrophy. *J. Neurosci.* 23, 6576–6585. doi: 10.1523/JNEUROSCI.23-16-06576.2003

Sillitoe, R. V., Chung, S.-H., Fritschy, J.-M., Hoy, M., and Hawkes, R. (2008). Golgi cell dendrites are restricted by Purkinje cell stripe boundaries in the adult mouse cerebellar cortex. *J. Neurosci.* 28, 2820–2826. doi: 10.1523/JNEUROSCI.4145-07.2008

Sillitoe, R. V., George-Jones, N. A., Millen, K. J., and Hawkes, R. (2014). Purkinje cell compartmentalization in the cerebellum of the spontaneous mutant mouse dreher. *Brain Struct. Funct.* 219, 35–47. doi: 10.1007/s00429-012-0482-6

Sleven, H., Welsh, S. J., Yu, J., Churchill, M. E., Wright, C. F., Henderson, A., et al. (2017). *De novo* mutations in EBF3 cause a neurodevelopmental syndrome. *Am. J. Hum. Genet.* 100, 138–150. doi: 10.1016/j.ajhg.2016.11.020

Smeyne, R. J., and Goldowitz, D. (1989). Development and death of external granular layer cells in the weaver mouse cerebellum: a quantitative study. *J. Neurosci.* 9, 1608–1620. doi: 10.1523/JNEUROSCI.09-05-01608.1989

Smeyne, R. J., Chu, T., Lewin, A., Bian, F., Sanlioglu, S., Kunsch, C., et al. (1995). Local control of granule cell generation by cerebellar Purkinje cells. *Mol. Cell. Neurosci.* 6, 230–251. doi: 10.1006/mcne.1995.1019

Solecki, D. J., Liu, X. L., Tomoda, T., Fang, Y., and Hatten, M. E. (2001). Activated notch2 signaling inhibits differentiation of cerebellar granule neuron precursors by maintaining proliferation. *Neuron* 31, 557–568. doi: 10.1016/s0896-6273(01)00395-6

Solecki, D. J., Model, L., Gaetz, J., Kapoor, T. M., and Hatten, M. E. (2004). Par6alpha signaling controls glial-guided neuronal migration. *Nat. Neurosci.* 7, 1195–1203. doi: 10.1038/nn1332

Solecki, D. J., Trivedi, N., Govek, E. E., Kerekes, R. A., Gleason, S. S., and Hatten, M. E. (2009). Myosin II motors and F-actin dynamics drive the coordinated movement of the centrosome and soma during CNS glial-guided neuronal migration. *Neuron* 63, 63–80. doi: 10.1016/j.neuron.2009.05.028

Sotelo, C. (1975). Anatomical, physiological and biochemical studies of the cerebellum from mutant mice: II. Morphological study of cerebellar cortical neurons and circuits in the weaver mouse. *Brain Res.* 94, 19–44. doi: 10.1016/0006-8993(75)90874-4

Sotelo, C., and Changeux, J. P. (1974). Bergmann fibers and granular cell migration in the cerebellum of homozygous weaver mutant mouse. *Brain Res.* 77, 484–491. doi: 10.1016/0006-8993(74)90636-2

Spassky, N., Han, Y.-G., Aguilar, A., Strehl, L., Besse, L., Laclef, C., et al. (2008). Primary cilia are required for cerebellar development and shh-dependent expansion of progenitor pool. *Dev. Biol.* 317, 246–259. doi: 10.1016/j.ydbio.2008.02.026

Stitt, T. N., and Hatten, M. E. (1990). Antibodies that recognize astrotactin block granule neuron binding to astroglia. *Neuron* 5, 639–649. doi: 10.1016/0896-6273(90)90218-5

Surmeier, D. J., Mermelstein, P. G., and Goldowitz, D. (1996). The weaver mutation of GIRK2 results in a loss of inwardly rectifying K^+ current in cerebellar granule cells. *Proc. Natl. Acad. Sci. U S A* 93, 11191–11195. doi: 10.1073/pnas.93.20.11191

Swanson, D. J., and Goldowitz, D. (2011). Experimental Sey mouse chimeras reveal the developmental deficiencies of Pax6-null granule cells in the postnatal cerebellum. *Dev. Biol.* 351, 1–12. doi: 10.1016/j.ydbio.2010.11.018

Tojo, H., Takami, K., Kaisho, Y., Nakata, M., Abe, T., Shiho, O., et al. (1995). Neurotrophin-3 is expressed in the posterior lobe of mouse cerebellum, but does not affect the cerebellar development. *Neurosci. Lett.* 192, 169–172. doi: 10.1016/0304-3940(95)11637-c

Toledo, A., Lang, F., Doengi, M., Morrison, H., Stein, V., and Baader, S. L. (2019). Merlin modulates process outgrowth and synaptogenesis in the cerebellum. *Brain Struct. Funct.* 224, 2121–2142. doi: 10.1007/s00429-019-01897-7

Tong, K. K., and Kwan, K. M. (2013). Common partner Smad-independent canonical bone morphogenetic protein signaling in the specification process of the anterior rhombic lip during cerebellum development. *Mol. Cell. Biol.* 33, 1925–1937. doi: 10.1128/MCB.01143-12

Toresson, H., Potter, S. S., and Campbell, K. (2000). Genetic control of dorsal-ventral identity in the telencephalon: opposing roles for Pax6 and Gsh2. *Development* 127, 4361–4371.

Trenkner, E., Hatten, M. E., and Sidman, R. L. (1978). Effect of ether-soluble serum components *in vitro* on the behavior of immature cerebellar cells in weaver mutant mice. *Neuroscience* 3, 1093–1100. doi: 10.1016/0306-4522(78)90127-6

Trenkner, E., and Sidman, R. L. (1977). Histogenesis of mouse cerebellum in microwell cultures. Cell reaggregation and migration, fiber and synapse formation. *J. Cell. Biol.* 75, 915–940. doi: 10.1083/jcb.75.3.915

Trivedi, N., Stabley, D. R., Cain, B., Howell, D., Laumonnerie, C., Ramahi, J. S., et al. (2017). Drebrin-mediated microtubule-actomyosin coupling steers cerebellar granule neuron nucleokinesis and migration pathway selection. *Nat. Commun.* 8:14484. doi: 10.1038/ncomms14484

Valente, E. M., Silhavy, J. L., Brancati, F., Barrano, G., Krishnaswami, S. R., Castori, M., et al. (2006). Mutations in CEP290, which encodes a centrosomal protein, cause pleiotropic forms of joubert syndrome. *Nat. Genet.* 38, 623–625. doi: 10.1038/ng1805

Valera, A. M., Binda, F., Pawlowski, S. A., Dupont, J.-L., Casella, J.-F., Rothstein, J. D., et al. (2016). Stereotyped spatial patterns of functional synaptic connectivity in the cerebellar cortex. *eLife* 5:e09862. doi: 10.7554/eLife.09862

Vilz, T. O., Moepps, B., Engele, J., Molly, S., Littman, D. R., and Schilling, K. (2005). The SDF-1/CXCR4 pathway and the development of the cerebellar system. *Eur. J. Neurosci.* 22, 1831–1839. doi: 10.1111/j.1460-9568.2005.04378.x

Vladoiu, M. C., El-Hamamy, I., Donovan, L. K., Farooq, H., Holgado, B. L., Sundaravadanam, Y., et al. (2019). Childhood cerebellar tumours mirror conserved fetal transcriptional programs. *Nature* 572, 67–73. doi: 10.1038/s41586-019-1158-7

Waite, K. A., and Eng, C. (2003). From developmental disorder to heritable cancer: it's all in the BMP/TGF-β family. *Nat. Rev. Genet.* 4, 763–773. doi: 10.1038/nrg1178

Wallace, V. A. (1999). Purkinje-cell-derived sonic hedgehog regulates granule neuron precursor cell proliferation in the developing mouse cerebellum. *Curr. Biol.* 9, 445–448. doi: 10.1016/s0960-9822(99)80195-x

Wang, H., Ge, G., Uchida, Y., Luu, B., and Ahn, S. (2011). Gli3 is required for maintenance and fate specification of cortical progenitors. *J. Neurosci.* 31, 6440–6448. doi: 10.1523/JNEUROSCI.4892-10.2011

Wang, V. Y., Rose, M. F., and Zoghbi, H. Y. (2005). Math1 expression redefines the rhombic lip derivatives and reveals novel lineages within the brainstem and cerebellum. *Neuron* 48, 31–43. doi: 10.1016/j.neuron.2005.08.024

Wechsler-Reya, R. J., and Scott, M. P. (1999). Control of neuronal precursor proliferation in the cerebellum by sonic hedgehog. *Neuron* 22, 103–114. doi: 10.1016/s0896-6273(00)80682-0

Wilson, P. M., Fryer, R. H., Fang, Y., and Hatten, M. E. (2010). Astn2, a novel member of the astrotactin gene family, regulates the trafficking of ASTN1 during glial-guided neuronal migration. *J. Neurosci.* 30, 8529–8540. doi: 10.1523/JNEUROSCI.0032-10.2010

Wizeman, J. W., Guo, Q., Wilion, E. M., and Li, J. Y. (2019). Specification of diverse cell types during early neurogenesis of the mouse cerebellum. *eLife* 8:e42388. doi: 10.7554/eLife.42388

Wolf, M. K. (1970). Anatomy of cultured mouse cerebellum: II. Organotypic migration of granule cells demonstrated by silver impregnantion of normal and mutant cultures. *J. Comp. Neurol.* 140, 281–298. doi: 10.1002/cne.901400304

Xenaki, D., Martin, I. B., Yoshida, L., Ohyama, K., Gennarini, G., Grumet, M., et al. (2011). F3/contactin and TAG1 play antagonistic roles in the regulation of sonic hedgehog-induced cerebellar granule neuron progenitor proliferation. *Development* 138, 519–529. doi: 10.1242/dev.051912

Yamasaki, T., Kawaji, K., Ono, K., Bito, H., Hirano, T., Osumi, N., et al. (2001). Pax6 regulates granule cell polarization during parallel fiber formation in the developing cerebellum. *Development* 128, 3133–3144.

Yang, H., Yang, C., Zhu, Q., Wei, M., Li, Y., Cheng, J., et al. (2019). Rack1 controls parallel fiber-purkinje cell synaptogenesis and synaptic transmission. *Front. Cell. Neurosci.* 13:539. doi: 10.3389/fncel.2019.00539

Yeung, J., Ha, T. J., Swanson, D. J., Choi, K., Tong, Y., and Goldowitz, D. (2014). Wls provides a new compartmental view of the rhombic lip in mouse cerebellar development. *J. Neurosci.* 34, 12527–12537. doi: 10.1523/JNEUROSCI.1330-14.2014

Yuzaki, M. (2011). Cbln1 and its family proteins in synapse formation and maintenance. *Curr. Opin. Neurobiol.* 21, 215–220. doi: 10.1016/j.conb.2011.01.010

Zhao, H., Ayrault, O., Zindy, F., Kim, J. H., and Roussel, M. F. (2008). Post-transcriptional down-regulation of Atoh1/Math1 by bone morphogenic proteins suppresses medulloblastoma development. *Genes Dev.* 22, 722–727. doi: 10.1101/gad.1636408

Zheng, C., Heintz, N., and Hatten, M. E. (1996). CNS gene encoding astrotactin, which supports neuronal migration along glial fibers. *Science* 272, 417–419. doi: 10.1126/science.272.5260.417

Zhou, H., Lin, Z., Voges, K., Ju, C., Gao, Z., Bosman, L. W., et al. (2014). Cerebellar modules operate at different frequencies. *eLife* 3:e02536. doi: 10.7554/eLife.02536

Zhu, Y., Yu, T., and Rao, Y. (2004). Temporal regulation of cerebellar EGL migration through a switch in cellular responsiveness to the meninges. *Dev. Biol.* 267, 153–164. doi: 10.1016/j.ydbio.2003.10.037

Zinyk, D. L., Mercer, E. H., Harris, E., Anderson, D. J., and Joyner, A. L. (1998). Fate mapping of the mouse midbrain-hindbrain constriction using a site-specific recombination system. *Curr. Biol.* 8, 665–668. doi: 10.1016/s0960-9822(98)70255-6

Zou, Y. R., Kottmann, A. H., Kuroda, M., Taniuchi, I., and Littman, D. R. (1998). Function of the chemokine receptor CXCR4 in hematopoiesis and in cerebellar development. *Nature* 393, 595–599. doi: 10.1038/31269

Conflict of Interest: The authors declare that the research was conducted in the absence of any commercial or financial relationships that could be construed as a potential conflict of interest.

frontiers in Neural Circuits

REVIEW
published: 30 April 2021
doi: 10.3389/fncir.2021.633235

Inhibitory Circuits in the Basolateral Amygdala in Aversive Learning and Memory

Madhusoothanan B. Perumal[1] *and Pankaj Sah*[1,2,3]*

[1] Queensland Brain Institute, The University of Queensland, Brisbane, QLD, Australia, [2] Joint Center for Neuroscience and Neural Engineering, Southern University of Science and Technology, Shenzhen, China, [3] Department of Biology, Southern University of Science and Technology, Shenzhen, China

Neural circuits in the basolateral amygdala (BLA) play a pivotal role in the learning and memory formation, and processing of emotionally salient experiences, particularly aversive ones. A diverse population of GABAergic neurons present in the BLA orchestrate local circuits to mediate emotional memory functions. Targeted manipulation of GABAergic neuronal subtypes has shed light on cell-type specific functional roles in the fear learning and memory, revealing organizing principles for the operation of inhibitory circuit motifs in the BLA.

Keywords: parvalbumin, somatostatin, chandelier, axo-axonic, fear, GABAergic, anxiety, stress

"*Unfortunately, nature seems unaware of our intellectual need for convenience and unity, and very often takes delight in complication and diversity.*"

Santiago Ramón Y Cajal, Nobel lecture 1901

OPEN ACCESS

Edited by:
Eduardo Weruaga,
University of Salamanca, Spain

Reviewed by:
Haijiang Cai,
University of Arizona, United States
Gabrielle Girardeau,
INSERM U839 Institut du Fer à Moulin (IFM), France

***Correspondence:**
Pankaj Sah
pankaj.sah@uq.edu.au

Received: *25 November 2020*
Accepted: *23 March 2021*
Published: *30 April 2021*

Citation:
Perumal MB and Sah P (2021) Inhibitory Circuits in the Basolateral Amygdala in Aversive Learning and Memory. Front. Neural Circuits 15:633235. doi: 10.3389/fncir.2021.633235

INTRODUCTION

Classical anatomical studies by Cajal and Golgi shed light on the morphological diversity of neurons in the brain. Cajal in particular was intrigued by the increase in number and complexity of "short axon neurons" up the evolutionary scale and concluded "*..functional superiority of the human brain is intimately bound up with the prodigious abundance and the unusual wealth of forms of the so called neurons with short axons*" (Yuste, 2005). These short axon neurons were subsequently found to release gamma-aminobutyric acid (GABA) at their axon terminals, the main inhibitory neurotransmitter in the mammalian brain, establishing these cells as inhibitory interneurons (Krnjevic, 1974). GABAergic neurons only comprise ∼10–20% of the total population of neurons in the cortex, hippocampus and amygdala (McDonald, 1992; Freund and Buzsaki, 1996; Ascoli et al., 2008; Tremblay et al., 2016), but their activity tightly controls local network activity including the generation of large-scale network oscillations, such as gamma oscillations and sharp wave ripples, associated with learning and memory (Buzsaki, 2001; Roux and Buzsaki, 2015).

Information processing in the brain requires temporally organized activity in neural circuits (Harris, 2005). The identification of molecular markers to classify different types of interneurons, is revealing that the GABAergic neurons are an incredibly diverse population of cells, that have distinct physiological properties and form different types of local circuits (Ascoli et al., 2008; Tremblay et al., 2016). As a result, interneurons form specific circuit motifs to precisely control the timing of activity in mammalian circuits, and thus sculpt the temporal structure of network activity (Buzsaki, 2001; Woodruff and Sah, 2007a). Here we review the diversity of GABAergic neurons and their local circuits in the rodent basolateral amygdala (BLA), a mid-temporal lobe structure that

plays a pivotal role in processing emotionally salient experiences, particularly aversive ones. The BLA is a cortical like structure, and similar to other cortical regions, local microcircuits are formed by excitatory glutamatergic neurons that make ∼80% of total neuronal population and GABAergic interneurons (Sah et al., 2003; Tovote et al., 2015). These circuits generate a myriad of oscillatory network activities with distinctive frequency bands that play key roles in the acquisition, storage and consolidation of emotionally salient memories (Pare et al., 2002; Ponomarenko et al., 2003; Paz and Pare, 2013). In the BLA, many glutamatergic neurons resemble their cortical counterparts with a classical pyramidal soma, thicker apical dendrite and a spiny dendritic tree (McDonald, 1982). However, glutamatergic neurons in the lateral amygdala often lack pyramidal shaped soma or clear basal and apical dendrites as in the cortex. As glutamatergic neurons constitute the main neuronal subtype in the amygdala, they are referred as principal neurons (PNs) (Faber et al., 2001; Sah et al., 2003). In contrast, GABAergic neurons comprise of a diverse population of cells with different somatic morphologies such as triangular, oval, round or square shaped somata with bipolar or tuft dendrites that are either aspiny or sparsely spiny (McDonald, 1982). Similar to cortical regions (Kepecs and Fishell, 2014; Huang and Paul, 2019), GABAergic neurons in the BLA have been classified into a number of subtypes based on the expression of cytosolic markers, and their local connectivity (Spampanato et al., 2011; Capogna, 2014) and intrinsic electrophysiological properties (Sosulina et al., 2010). Apart from the presence of cytosolic markers, GABAergic neurons in the cortex and hippocampus, have also been separated based on the distribution of their local connections along organized layers (e.g., double bouquet cells in the cortex). With some principal neurons lacking a distinctive apical dendrite, and the fact that cyto-architectonically, the BLA lacks any recognizable laminar organization, comparison of morphological subtypes with their cortical or hippocampal counterparts is often not straightforward. However, oscillatory network activities in the BLA display similar frequency bands to those in the cortex and hippocampus suggesting functionally similar microcircuits may operate across these brain regions to mediate distinct cognitive functions (Pare et al., 2002). Here we review GABAergic neuronal subtypes in the BLA, their local circuit connectivity and their putative functional roles in aversive learning and memory.

DIVERSITY OF GABAERGIC NEURONS

Immunohistochemically, using expression of calcium binding proteins, GABAergic neurons in the BLA can be firstly be divided into two non-overlapping populations that express either calbindin or calretinin (McDonald and Mascagni, 2002). These neurons cells are then further classified based on the expression of other calcium binding proteins, neuropeptides or transmitter receptors into: (a) parvalbumin (PV), (b) somatostatin (SST), (c) cholecystokinin (CCK), (d) neuropeptide Y, (e) vaso-intestinal peptide (VIP), and (f) neurokinin 1subtypes (Kemppainen and Pitkanen, 2000; McDonald and Mascagni, 2002; Mascagni and McDonald, 2003; Sreepathi and Ferraguti, 2012) (**Figure 1**). To some extent, GABAergic neurons containing distinct cytosolic protein expression also target specific post-synaptic neuronal compartments of principal neurons. For example, PV+ and CCK+ neurons form basket-type synapses on the soma and/or proximal apical dendrites while SOM+ interneurons tend to target the distal dendritic tree of principal neurons (McDonald and Mascagni, 2001; Muller et al., 2006, 2007). However, GABAergic neurons with the same cytosolic marker proteins also display distinctive synaptic targeting. For example, while most PV+ interneurons make somatic basket synapses on principal neurons, a small proportion of PV+ neurons (<5%), named axo-axonic or chandelier neurons, form specialized "cartridge" type axo-axonic synapses at the axon-initial segment (McDonald and Betette, 2001). VIP+ terminals are less specific in their post-synaptic target selection, though this represents a heterogeneous group of CCK+ and CCK- terminals (Muller et al., 2003). In this schema, synaptic targeting distinguishes cells that innervate either the somatic compartment, the dendritic tree or the axon initial segment of principal neurons. In addition, some GABAergic neurons preferentially innervate other GABAergic neurons, some display non-synaptic volume transmission, and some make long range projections to other brain regions (McDonald et al., 2012; Capogna, 2014; McDonald and Zaric, 2015). Below we use the current immunohistochemical classification to review neuronal subsets and known circuit connections in the BLA.

Parvalbumin GABAergic Neurons

Parvalbumin expressing neurons form ∼40–50% of the total interneuron pool and largely target the peri-somatic region of principal neurons (Spampanato et al., 2011). The density of PV+ varicosities is highest in the magnocellular and parvicellular portion of basal nucleus and dorsolateral and ventrolateral regions of the lateral amygdala (McDonald and Betette, 2001). Nearly half these cells also express calbindin (McDonald and Mascagni, 2002). Anatomically, PV+ cells have been divided into three types that target different cellular compartments (McDonald and Mascagni, 2002; Woodruff and Sah, 2007b; Vereczki et al., 2016). The majority (∼50%) of PV+ interneurons are basket cells and they characteristically make synaptic contacts on the soma and proximal dendrites of principal neurons (Woodruff and Sah, 2007b; Vereczki et al., 2016). The second group, called axo-axonic or chandelier cells, although less numerous, form a distinct population that make a characteristic string or "cartridge" of synaptic contacts on the axon initial segment of principal neurons, the key site of action potential initiation (Woodruff et al., 2006; Bienvenu et al., 2012; Veres et al., 2014; Spampanato et al., 2016). The third group target principal neurons and also send axon collaterals to amygdala-striatal region transition zone, named as AStria cells (Bienvenu et al., 2012). Finally, some PV+ interneurons also innervate other PV+ neurons, and SST neurons (Muller et al., 2005; Spampanato et al., 2016). Electrophysiologically, PV+ cells are often described as a single population–called fast spikers (FS cells) with narrow action potentials (half-width of ∼0.5 ms) which can discharge at high frequencies (200–300 Hz) with little to no spike frequency adaptation (Ascoli et al., 2008). However,

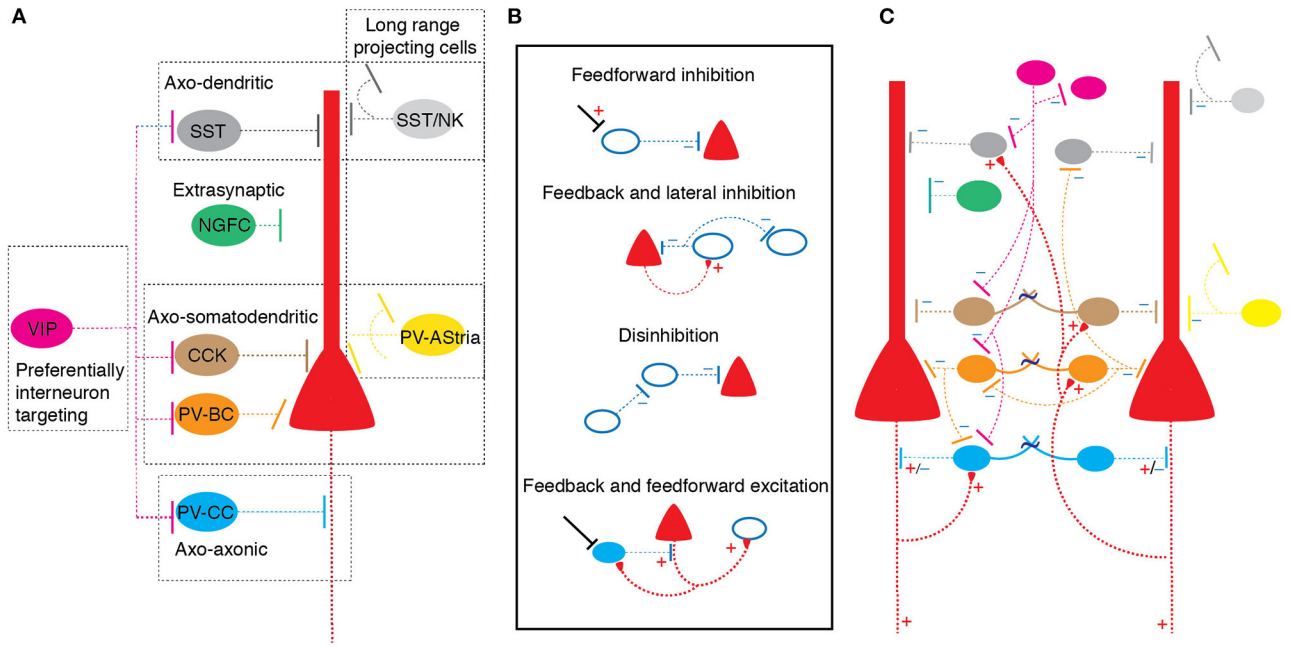

FIGURE 1 | GABAergic neuronal diversity and circuit organization in the basolateral amygdala. **(A)** Types of GABAergic neurons color coded based on cytosolic protein expression: Somatostatin (SST), Neurokinin 1 (NK), Vaso intestinal peptide (VIP), cholecystokinin (CCK), Parvalbumin basket cell (PV-BC) and Parvalbumin chandelier cell (PV-CC) and Neurogliaform (NGFC). Dotted box indicates classification of groups based on synaptic target on principal neurons. Neurons with distinct cytosolic proteins tend to make distinct synaptic connections. **(B)** Schematic showing organization of circuit 'motif's formed on principal neurons and interneurons in the BLA. Bottom filled cell indicate excitatory axo-axonic chandelier interneuron; "+" excitatory connection, "–" inhibitory connection. **(C)** Schematic of a simplified BLA circuit model shows arrangement of different interneuron subtypes and putative circuit motifs shown in **(B)**.

in the BLA, in line with the anatomical separation, they have been divided into several subtypes based on their different patterns of firing to long current injection, and gap-junctional coupling (Rainnie et al., 1991; Woodruff and Sah, 2007b). Of these, cells which show little or no spike frequency adaptation (FS cells) have been proposed to be basket cells targeting the somatic region, while cells with spike frequency adaptation target distal dendrites (Woodruff and Sah, 2007b). Finally, chandelier cells that target axon initial segment, predominantly show a fast-stuttering phenotype (unpublished observations). PV+ interneurons receive excitatory input from both principal neurons, and cortical sources thus forming both feedback and feed-forward inhibitory circuits (Samson et al., 2003).

Although GABAergic transmission in mature neurons is generally thought to be inhibitory, PV chandelier cells in the BLA have been reported to have excitatory action on at least some principal neurons driving both feedback and feedforward excitatory connections (Woodruff et al., 2006; Spampanato et al., 2016). Thus, it has been suggested that in the BLA, some principal neurons are driven to threshold by chandelier neurons (Woodruff et al., 2006). However, the identity of principal neurons excited by chandelier cells, the mechanism of this excitatory drive, or if these cells form a distinct population of principal neurons is not known. Each chandelier cell is estimated to innervate several hundred principal neurons, thus individual cells can powerfully influence glutamatergic drive in the local circuits (Bienvenu et al., 2012; Veres et al., 2014; Spampanato et al., 2016). In addition to chemical synapses, PV+ cells are extensively interconnected with similar types connected by gap junctions, thus are ideally positioned to generate synchronized network activity (Woodruff and Sah, 2007b).

Somatostatin GABAergic Neurons

Somatostatin expressing interneurons predominantly target the distal dendrites and influence the gating of excitatory synaptic input to principal neurons (Muller et al., 2007; Wolff et al., 2014). These cells receive inhibitory input from PV+ basket cells and VIP+ cells (Wolff et al., 2014; Krabbe et al., 2019). A proportion of SST+ neurons, including some that colocalize with neuropeptide Y, send long range axonal projections out of the BLA (McDonald et al., 2012; McDonald and Zaric, 2015). Finally, a small population of SST+ cells have been identified as neurogliaform cells which mediate local slow inhibition by diffuse volume transmission (Manko et al., 2012). Thus, as for PV+ interneurons, SST+ cells show a diversity of different types that likely play distinct functional roles. Electrophysiologically, individual SST+ neurons typically display accommodative action potential discharge. It is interesting that PV+ interneurons that target distal dendrites also have accommodating discharge properties (Woodruff and Sah, 2007b), and these two cells types are electrophysiologically indistinguishable. The computational relevance of distal dendrite targeting interneurons having an accomodating phenotype is not currently clear.

Cholecystokinin/Vasoactive-Intestinal Peptide GABAergic Neurons

Cholecystokinin expressing interneurons have been classified into two subsets: Large (CCK_L) and small (CCK_S) neurons (Mascagni and McDonald, 2003). CCK_L cells co-express calbindin or VGLUT3 and are the only cell type to express cannabinoid receptor 1 (CB1) in the BLA (Katona et al., 2001; Rovira-Esteban et al., 2017), while CCK_S cells co-express calretinin or VIP. Electro-physiologically, CCK cells reported to display three distinct spike discharge patterns and broader action potentials than principal neurons (Rovira-Esteban et al., 2017). Both subtypes form peri-somatic synaptic contacts on the post-synaptic principal neuron and have been reported to drive both fast $GABA_A$ receptor mediated and slow $GABA_B$ mediated inhibitory responses that provide peri-somatic inhibition to principal neurons and form feedback inhibitory circuits (Vereczki et al., 2016; Veres et al., 2017; Krabbe et al., 2019).

VIP+ neurons form a heterogeneous group of cells that are sparsely distributed throughout BLA (Rhomberg et al., 2018) and target principal neurons and other interneurons. Nearly 60% of VIP+ cells co-express calretinin and these cells target PV+, SST+, CCK+, as well as neurogliaform and other VIP interneurons (Rhomberg et al., 2018). Some VIP+ neurons co-express CCK/CB1 and innervate the soma of principal neurons. The remaining population of VIP+ cells do not appear to express any other known markers and target interneurons. Thus, VIP+ interneurons are a complex set of cells that mediate both feedforward and feedback inhibition, and as a result of their strong connections to other interneurons also form local disinhibitory circuits.

FUNCTIONAL ROLE OF GABAERGIC CELL TYPES IN FEAR MEMORY

A large body research over many years has established that cellular activity and synaptic plasticity in the BLA underpin emotional learning and memory, particularly of aversive events (LeDoux, 2003). The neural circuits that underpin emotional memory formation and retrieval has been extensively investigated using cued Pavlovian fear conditioning. In this paradigm, a neutral conditioned stimulus (CS, such as auditory tone) is paired with an aversive unconditioned stimulus (US, typically a mild foot shock), such that after several pairings, the CS elicits a defensive "fear" response with motor, autonomic and neuroendocrine components. However, subsequent repeated unpaired presentation of CS alone leads to reduced conditioned response, known as "fear extinction." Fear extinction is thought to result from the formation of new associative memory representation (Maren and Quirk, 2004; Quirk and Mueller, 2008; Marek et al., 2019). Fear acquisition, storage and extinction engage the amygdala through evolutionarily conserved circuits and provides a robust behavioral paradigm to investigate neurobiological correlates of learning and memory (Fanselow and Poulos, 2005; Fanselow and Wassum, 2015). These studies have established that excitatory inputs from the thalamus and the cortex carrying sensory information encoding the CS converge on principal neurons in the dorsal part of the BLA, the lateral amygdala (Polepalli et al., 2020; Sun et al., 2020). Inputs carrying CS and US information converge on neurons in the BLA (Romanski et al., 1993; Wolff et al., 2014; Windels et al., 2016). The BLA also receives multimodal information from the ventral hippocampus and prefrontal cortex (McDonald, 1998; Sah et al., 2003). Together with the CS and US, this information is processed by local circuits in the BLA and the resultant plasticity of excitatory inputs carrying CS information is thought to underlie this associative learning (Pape and Pare, 2010; Sun et al., 2020). Subsequent presentation of the CS again recruits circuits within the BLA that sends afferents to the central amygdala, from which downstream projections drive the defensive response - fear expression (Tovote et al., 2015). Within the BLA, sensory and multimodal inputs drive potent feedforward inhibition to principal neurons (Lang and Pare, 1997; Windels et al., 2010; Krabbe et al., 2018). Thus, it has been recognized that local GABAergic circuits gate principal neuronal activity during both acquisition and recall of fear memory (Tovote et al., 2015).

Early experiments established the important role of local inhibition in fear learning (Harris and Westbrook, 1998; Ehrlich et al., 2009), and cortical inputs to interneurons in the BLA also show synaptic plasticity (Mahanty and Sah, 1998; Spampanato et al., 2011). The development of transgenic lines to identify selective neural populations (Huang et al., 2014), and molecular tools to temporally control neural activity (Johansen et al., 2012) is now providing rich insight into the functional roles of specific interneuron populations. Thus, Wolff et al. (2014) combined optogenetics with single unit recordings targeted at PV+ and SST+ neurons in the BLA during fear conditioning (Wolff et al., 2014). They found that presentation of an auditory CS drives PV+ interneurons but inhibits SST+ interneurons, while the US (footshock) inhibits both PV+ and SST+ interneurons. Behaviourally, activating PV+ cells during associative fear learning (i.e., CS-US pairing) reduced learning to the CS+, showing that the activity of PV+ interneurons is necessary for effective learning. In support of this, artificially activating PV+ cells were during CS presentation, enhanced learning while inhibition of these cells during the CS reduced fear memory. In contrast, manipulation of SST+ interneurons had the opposite effect. Driving these cells during CS+ presentation reduced learning and inhibiting SST+ cells had the opposite effect. These results show that both PV+ and SST+ interneurons are engaged during associative fear learning. Authors proposed that that during CS-US pairing, there is effective disinhibition of principal neurons firstly by PV+ cells inhibiting SST+ cells during the CS and then by inhibition of both interneuron populations during the US (Wolff et al., 2014).

Targeting a different interneuron population, Krabbe et al. (2019) found that VIP+ cells also modulate fear learning. Targeted expression of the genetically encoded calcium sensor GCaMP to detect spike triggered calcium transients, revealed that either the CS or the US can recruit VIP+ interneurons in the BLA, but the US alone or combined CS+US presentation recruited a substantially larger proportion of VIP+ cells, as compared to CS alone. Unexpectedly, in the BLA, optical activation of VIP+ interneurons enhanced putative principal

neuronal discharge. Behaviourally, inhibition of VIP cells during the US reduced learning with a lower freezing response on fear retrieval, showing that activity of VIP+ cells during learning is needed for optimal learning. Thus, they concluded that VIP cells drive disinhibitory circuit operations in the BLA in the fear conditioning paradigm. Thus, optogenetic targeting of GABAergic subtypes defined by cytosolic proteins revealed putatively distinct functional role for PV+, SST+, and VIP+ neurons in the Pavlovian fear conditioning paradigm. Taken together, these studies propose both PV+ and VIP+ neurons operate through disinhibitory circuit mechanisms during associative learning of CS and US. Based on their synaptic connectivity in the BLA, it is proposed that PV+ gate CS by inhibiting SST+ cells (Wolff et al., 2014) and VIP+ cells mediate disinhibition mainly during US (Krabbe et al., 2019).

These experiments show that PV+, SST+, and VIP+ interneurons are activated differently by the auditory CS and footshock, and have different effects on fear learning. However, as described above, both PV+ and VIP+ cells can be subdivided into several families with distinct circuit functions. To date, SST+ interneurons are less well-studied but may also contain several types. These different types are likely to have different functional roles and raise many questions. For example, PV+ cells have been separated into basket cells, axo-axonic chandelier cells and AStria cells. Juxta-cellular, *in vivo* recordings in anesthetized animals have found that aversive stimuli (hind paw pinch or foot shock) evoke a heterogeneous response in PV basket cells, depress PV+ AStria cells, whilst robustly increase discharge of PV+ chandelier cells (Bienvenu et al., 2012). It is noteworthy that some PV+ chandelier cells have been reported to recruit principal neurons and drive feedback and feedforward circuits *in vitro* (Woodruff and Sah, 2007b; Spampanato et al., 2016). As chandelier cells are preferentially recruited by the US (Bienvenu et al., 2012), whether they operate *in vivo* to recruit PNs for encoding fear memory is not known. Moreover, basket type PV+ cells form the main subtype of GABAergic neurons that provide strong somatic inhibition on principal neurons and tightly control spike discharge (Woodruff and Sah, 2007b; Vereczki et al., 2016). The CS mediated recruitment of PV+ cells is proposed to disinhibit principal neuronal dendrites by inhibition of SST+ cells (Wolff et al., 2014). However, it remains unclear how PV+ basket cell mediated disinhibition of dendrites overcomes direct peri-somatic inhibition of principal neurons by the same cell types to facilitate recruitment and plasticity.

During fear learning, BLA circuits generate oscillatory network activities that entrain local principal neurons (Pare et al., 2002; Harris and Gordon, 2015), which provide output to the hippocampus and prefrontal cortex and generate coherent activities to encode emotional memory (Likhtik et al., 2014). Microcircuit mechanisms for the generation of network oscillations have been extensively studied in the hippocampus. In the hippocampus, feedback and feedforward GABAergic circuit motifs formed PV subset proposed to orchestrate network oscillations (Freund and Buzsaki, 1996; Buzsaki, 2015; Roux and Buzsaki, 2015). While network oscillations in the amygdala are clearly important in fear learning (Pare et al., 2002; Sah et al., 2003), the role of different interneurons in coordinating these different oscillatory bands in the BLA is not currently well-understood. *In vivo,* PNs in the BLA fire rarely even in the presence of extrinsic stimuli and are tightly controlled by local inhibitory circuits (Windels et al., 2016). Incoming inputs to the BLA have been reported to drive feedforward GABAergic neurons during oscillatory network activities and control the spike-timing of PNs (Bazelot et al., 2015). However, how different GABAergic neuronal subtypes and their intricate circuit motifs operate during network oscillations in the BLA remain elusive. Targeted optical manipulation using cytosolic marker proteins in GABAergic subtypes in the BLA has revealed a broad picture of function role of GABAergic cell-types in fear memory. Future studies need to identify functional roles for these GABAergic cell-types and their circuit motifs in the generation of oscillatory network activities in the BLA.

CONCLUSION AND FUTURE DIRECTIONS

The BLA forms a major part of the amygdaloid complex, a region that has a key role in emotional regulation, learning and memory. Dysfunctions within BLA circuits are thought to contribute to a host of anxiety-like disorders such generalized anxiety and post-traumatic stress (Perumal et al., 2018). GABAergic circuits in the BLA play a central role in all aspects of its function and compounds such benzodiazepines that are first line anxiolytics modulate inhibitory synaptic transmission. Thus, understanding GABAergic circuits in the BLA will not only provide insight into learning and memory formation, but also reveal pathological mechanisms associated with dysfunction. The development of genetically driven markers and opto/chemo genetic tools to control and manipulate targeted population of neurons is now rapidly advancing our understanding of processing within the BLA (Janak and Tye, 2015; Mobbs et al., 2019). It is becoming increasingly clear that interneurons are far more diverse and complex than initially thought and our understanding of the roles of GABAergic neuronal subtypes associated with different network functions in the BLA is just scratching the surface. This understanding is pivotal to identify how different circuit motifs operate during physiological network activity and unravel computational principles for emotional memory. A clearer identification of cell types in the BLA, their connections, and the receptors present in different cell-type and sub-cellular compartments will profoundly influence our understanding of the circuits that underpin learning and memory and mediate the different behavioral states in emotional regulation (Perumal et al., 2018).

AUTHOR CONTRIBUTIONS

All authors listed have made a substantial, direct and intellectual contribution to the work, and approved it for publication.

FUNDING

This work was supported by grants from the Australian National Health and Research Council and Australian Research Council (CE140100007).

REFERENCES

Ascoli, G. A., Alonso-Nanclares, L., Anderson, S. A., Barrionuevo, G., Benavides-Piccione, R., Burkhalter, A., et al. (2008). Petilla terminology: nomenclature of features of GABAergic interneurons of the cerebral cortex. *Nat. Rev. Neurosci.* 9, 557–568. doi: 10.1038/nrn2402

Bazelot, M., Bocchio, M., Kasugai, Y., Fischer, D., Dodson, P. D., Ferraguti, F., et al. (2015). Hippocampal theta input to the amygdala shapes feedforward inhibition to gate heterosynaptic plasticity. *Neuron* 87, 1290–1303. doi: 10.1016/j.neuron.2015.08.024

Bienvenu, T. C., Busti, D., Magill, P. J., Ferraguti, F., and Capogna, M. (2012). Cell-type-specific recruitment of amygdala interneurons to hippocampal theta rhythm and noxious stimuli *in vivo*. *Neuron* 74, 1059–1074. doi: 10.1016/j.neuron.2012.04.022

Buzsaki, G. (2001). Hippocampal GABAergic interneurons: a physiological perspective. *Neurochem. Res.* 8/9, 899–905. doi: 10.1023/A:1012324231897

Buzsaki, G. (2015). Hippocampal sharp wave-ripple: a cognitive biomarker for episodic memory and planning. *Hippocampus* 25, 1073–1188. doi: 10.1002/hipo.22488

Capogna, M. (2014). GABAergic cell type diversity in the basolateral amygdala. *Curr. Opin. Neurobiol.* 26, 110–116. doi: 10.1016/j.conb.2014.01.006

Ehrlich, I., Humeau, Y., Grenier, F., Ciocchi, S., Herry, C., and Luthi, A. (2009). Amygdala inhibitory circuits and the control of fear memory. *Neuron* 62, 757–771. doi: 10.1016/j.neuron.2009.05.026

Faber, E. S. L., Callister, R. J., and Sah, P. (2001). Morphological and electrophysiological properties of principal neurons in the rat lateral amygdala *in vitro*. *J. Neurophysiol* 85:714–723. doi: 10.1152/jn.2001.85.2.714

Fanselow, M. S., and Poulos, A. M. (2005). The neuroscience of mammalian associative learning. *Annu. Rev. Psychol.* 56, 207–234. doi: 10.1146/annurev.psych.56.091103.070213

Fanselow, M. S., and Wassum, K. M. (2015). The origins and organization of vertebrate pavlovian conditioning. *Cold Spring Harb. Perspect. Biol.* 8:a021717. doi: 10.1101/cshperspect.a021717

Freund, T. F., and Buzsaki, G. (1996). Interneurons of the hippocampus. *Hippocampus* 6, 347–470. doi: 10.1002/(SICI)1098-1063(1996)6:4<347::AID-HIPO1>3.0.CO;2-I

Harris, A. Z., and Gordon, J. A. (2015). Long-range neural synchrony in behavior. *Annu. Rev. Neurosci.* 38, 171–194. doi: 10.1146/annurev-neuro-071714-034111

Harris, J. A., and Westbrook, R. F. (1998). Evidence that GABA transmission mediates context-specific extinction of learned fear. *Psychopharmacology* 140, 105–115. doi: 10.1007/s002130050745

Harris, K. D. (2005). Neural signatures of cell assembly organization. *Nat. Rev. Neurosci.* 6, 399–407. doi: 10.1038/nrn1669

Huang, Z. J., and Paul, A. (2019). The diversity of GABAergic neurons and neural communication elements. *Nat. Rev. Neurosci.* 20, 563–572. doi: 10.1038/s41583-019-0195-4

Huang, Z. J., Taniguchi, H., He, M., and Kuhlman, S. (2014). Genetic labeling of neurons in mouse brain. *Cold Spring Harb. Protoc.* 2014, 150–160. doi: 10.1101/pdb.top080374

Janak, P. H., and Tye, K. M. (2015). From circuits to behaviour in the amygdala. *Nature* 517, 284–292. doi: 10.1038/nature14188

Johansen, J. P., Wolff, S. B., Luthi, A., and LeDoux, J. E. (2012). Controlling the elements: an optogenetic approach to understanding the neural circuits of fear. *Biol. Psychiatry* 71, 1053–1060. doi: 10.1016/j.biopsych.2011.10.023

Katona, I., Rancz, E. A., Acsady, L., Ledent, C., Mackie, K., Hajos, N., et al. (2001). Distribution of CB1 cannabinoid receptors in the amygdala and their role in the control of GABAergic transmission. *J. Neurosci.* 21, 9506–9518. doi: 10.1523/JNEUROSCI.21-23-09506.2001

Kemppainen, S., and Pitkanen, A. (2000). Distribution of parvalbumin, calretinin, and calbindin-D(28k) immunoreactivity in the rat amygdaloid complex and colocalization with gamma-aminobutyric acid. *J. Comp. Neurol.* 426, 441–467. doi: 10.1002/1096-9861(20001023)426:3<441::AID-CNE8>3.0.CO;2-7

Kepecs, A., and Fishell, G. (2014). Interneuron cell types are fit to function. *Nature* 505, 318–326. doi: 10.1038/nature12983

Krabbe, S., Grundemann, J., and Luthi, A. (2018). Amygdala inhibitory circuits regulate associative fear conditioning. *Biol. Psychiatry* 83, 800–809. doi: 10.1016/j.biopsych.2017.10.006

Krabbe, S., Paradiso, E., d'Aquin, S., Bitterman, Y., Courtin, J., Xu, C., et al. (2019). Adaptive disinhibitory gating by VIP interneurons permits associative learning. *Nat. Neurosci.* 22, 1834–1843. doi: 10.1038/s41593-019-0508-y

Krnjevic, K. (1974). Chemical nature of synaptic transmission in vertebrates. *Physiol. Rev.* 43, 418–540. doi: 10.1152/physrev.1974.54.2.418

Lang, E. J., and Pare, D. (1997). Similar inhibitory processes dominate the responses of cat lateral amygdaloid projection neurons to their various afferents. *J. Neurophysiol.* 77, 341–352. doi: 10.1152/jn.1997.77.1.341

LeDoux, J. (2003). The emotional brain, fear, and the amygdala. *Cell. Mol. Neurobiol.* 23, 727–738. doi: 10.1023/A:1025048802629

Likhtik, E., Stujenske, J. M., Topiwala, M. A., Harris, A. Z., and Gordon, J. A. (2014). Prefrontal entrainment of amygdala activity signals safety in learned fear and innate anxiety. *Nat. Neurosci.* 17, 106–113. doi: 10.1038/nn.3582

Mahanty, N. K., and Sah, P. (1998). Calcium-permeable AMPA receptors mediate long-term potentiation in interneurons in the amygdala. *Nature* 394, 683–687. doi: 10.1038/29312

Manko, M., Bienvenu, T. C., Dalezios, Y., and Capogna, M. (2012). Neurogliaform cells of amygdala: a source of slow phasic inhibition in the basolateral complex. *J. Physiol.* 590, 5611–5627. doi: 10.1113/jphysiol.2012.236745

Marek, R., Sun, Y., and Sah, P. (2019). Neural circuits for a top-down control of fear and extinction. *Psychopharmacology* 236, 313–320. doi: 10.1007/s00213-018-5033-2

Maren, S., and Quirk, G. J. (2004). Neuronal signalling of fear memory. *Nat. Rev. Neurosci.* 5, 844–852. doi: 10.1038/nrn1535

Mascagni, F., and McDonald, A. J. (2003). Immunohistochemical characterization of cholecystokinin containing neurons in the rat basolateral amygdala. *Brain Res.* 976, 171–184. doi: 10.1016/S0006-8993(03)02625-8

McDonald, A. J. (1982). Neurons of the lateral and basolateral amygdaloid nuclei: a golgi study in the rat. *J. Comp. Neurol.* 212, 293–312. doi: 10.1002/cne.902120307

McDonald, A. J. (1992). "Cell types and intrinsic connections of the amygdala," in *The Amygdala: Neurobiological Aspects of Emotion, Memory and Mental Dysfunction*, ed J. P. Aggleton (New York, NY: Wiley Liss).

McDonald, A. J. (1998). Cortical pathways to the mammalian amygdala. *Prog. Brain Res.* 55, 257–332. doi: 10.1016/S0301-0082(98)00003-3

McDonald, A. J., and Betette, R. L. (2001). Parvalbumin-containing neurons in the rat basolateral amygdala: morphology and co-localization of Calbindin-D(28k). *Neurosci.* 102, 413–425. doi: 10.1016/S0306-4522(00)00481-4

McDonald, A. J., and Mascagni, F. (2001). Localization of the CB1 type cannabinoid receptor in the rat basolateral amygdala: high concentrations in a subpopulation of cholecystokinin-containing interneurons. *Neurosci.* 107, 641–652. doi: 10.1016/S0306-4522(01)00380-3

McDonald, A. J., and Mascagni, F. (2002). Immunohistochemical characterization of somatostatin containing interneurons in the rat basolateral amygdala. *Brain Res.* 943, 237–244. doi: 10.1016/S0006-8993(02)02650-1

McDonald, A. J., Mascagni, F., and Zaric, V. (2012). Subpopulations of somatostatin-immunoreactive non-pyramidal neurons in the amygdala and adjacent external capsule project to the basal forebrain: evidence for the existence of GABAergic projection neurons in the cortical nuclei and basolateral nuclear complex. *Front. Neural Circuits* 6:46. doi: 10.3389/fncir.2012.00046

McDonald, A. J., and Zaric, V. (2015). GABAergic somatostatin-immunoreactive neurons in the amygdala project to the entorhinal cortex. *Neuroscience* 290, 227–242. doi: 10.1016/j.neuroscience.2015.01.028

Mobbs, D., Adolphs, R., Fanselow, M. S., Barrett, L. F., LeDoux, J. E., Ressler, K., et al. (2019). Viewpoints: approaches to defining and investigating fear. *Nat. Neurosci.* 22, 1205–1216. doi: 10.1038/s41593-019-0456-6

Muller, J. F., Mascagni, F., and McDonald, A. J. (2003). Synaptic connections of distinct interneuronal subpopulations in the rat basolateral amygdalar nucleus. *J. Comp. Neurol.* 456:217–236. doi: 10.1002/cne.10435

Muller, J. F., Mascagni, F., and McDonald, A. J. (2005). Coupled networks of parvalbumin-immunoreactive interneurons in the rat basolateral amygdala. *J. Neurosci.* 25, 7366–7376. doi: 10.1523/JNEUROSCI.0899-05.2005

Muller, J. F., Mascagni, F., and McDonald, A. J. (2006). Pyramidal cells of the rat basolateral amygdala: synaptology and innervation by parvalbumin-immunoreactive interneurons. *J. Comp. Neurol.* 494, 635–650. doi: 10.1002/cne.20832

Muller, J. F., Mascagni, F., and McDonald, A. J. (2007). Postsynaptic targets of somatostatin-containing interneurons in the rat basolateral amygdala. *J. Comp. Neurol.* 500:513–529. doi: 10.1002/cne.21185

Pape, H. C., and Pare, D. (2010). Plastic synaptic networks of the amygdala for the acquisition, expression, and extinction of conditioned fear. *Physiol. Rev.* 90, 419–463. doi: 10.1152/physrev.00037.2009

Pare, D., Collins, D. R., and Pelletier, J. G. (2002). Amygdala oscillations and the consolidation of emotional memories. *Trends Cogn. Sci.* 6, 306–314. doi: 10.1016/S1364-6613(02)01924-1

Paz, R., and Pare, D. (2013). Physiological basis for emotional modulation of memory circuits by the amygdala. *Curr. Opin. Neurobiol.* 23, 381–386. doi: 10.1016/j.conb.2013.01.008

Perumal, M. B., Lynch, J. W., and Sah, P. (2018). GABA(A) receptors and inhibitory neurotransmission in the amygdalar complex. *Curr. Opin. Physiol.* 2, 58–64. doi: 10.1016/j.cophys.2018.01.003

Polepalli, J. S., Gooch, H., and Sah, P. (2020). Diversity of interneurons in the lateral and basal amygdala. *NPJ Sci. Learn.* 5:10. doi: 10.1038/s41539-020-0071-z

Ponomarenko, A. A., Korotkova, T. M., and Haas, H. L. (2003). High frequency (200 Hz) oscillations and firing patterns in the basolateral amygdala and dorsal endopiriform nucleus of the behaving rat. *Behav. Brain Res.* 141, 123–129. doi: 10.1016/S0166-4328(02)00327-3

Quirk, G. J., and Mueller, D. (2008). Neural mechanisms of extinction learning and retrieval. *Neuropsychopharmacology* 33, 56–72. doi: 10.1038/sj.npp.1301555

Rainnie, D. G., Asprodini, E. K., and Shinnick-Gallagher, P. (1991). Inhibitory transmission in the basolateral amygdala. *J. Neurophysiol.* 66, 999–1009.

Rhomberg, T. L., Rovira-Esteban, A., Vikór, E., Paradiso, C., Kremser, P., Nagy-Pál, O. I., et al. (2018). Vasoactive intestinal polypeptide-immunoreactive interneurons within circuits of the mouse basolateral amygdala. *J. Neurosci.* 38, 6983–7003. doi: 10.1523/JNEUROSCI.2063-17.2018

Romanski, L. M., Clugnet, M. C., Bordi, F., and LeDoux, J. E. (1993). Somatosensory and auditory convergence in the lateral nucleus of the amygdala. *Behav. Neurosci.* 107, 444–450. doi: 10.1037/0735-7044.107.3.444

Roux, L., and Buzsaki, G. (2015). Tasks for inhibitory interneurons in intact brain circuits. *Neuropharmacology* 88, 10–23. doi: 10.1016/j.neuropharm.2014.09.011

Rovira-Esteban, L., Peterfi, Z., Vikor, A., Mate, Z., Szabo, G., and Hajos, N. (2017). Morphological and physiological properties of CCK/CB1R-expressing interneurons in the basal amygdala. *Brain Struct. Funct.* 222, 3543–3565. doi: 10.1007/s00429-017-1417-z

Sah, P., Faber, E. S., Lopez De Armentia, M., and Power, J. (2003). The amygdaloid complex: anatomy and physiology. *Physiol. Rev.* 83, 803–834. doi: 10.1152/physrev.00002.2003

Samson, R. D., Dumont, E. C., and Pare, D. (2003). Feedback inhibition defines transverse processing modules in the lateral amygdala. *J. Neurosci.* 23, 1966–1973. doi: 10.1523/JNEUROSCI.23-05-01966.2003

Sosulina, L., Graebenitz, S., and Pape, H. C. (2010). GABAergic interneurons in the mouse lateral amygdala: a classification study. *J. Neurophysiol.* 104, 617–626 doi: 10.1152/jn.00207.2010

Spampanato, J., Polepalli, J., and Sah, P. (2011). Interneurons in the basolateral amygdala. *Neuropharmacology* 60, 765–773. doi: 10.1016/j.neuropharm.2010.11.006

Spampanato, J., Sullivan, R. K., Perumal, M. B., and Sah, P. (2016). Development and physiology of GABAergic feedback excitation in parvalbumin expressing interneurons of the mouse basolateral amygdala. *Physiol. Rep.* 4:e12664. doi: 10.14814/phy2.12664

Sreepathi, H. K., and Ferraguti, F. (2012). Subpopulations of neurokinin 1 receptor-expressing neurons in the rat lateral amygdala display a differential pattern of innervation from distinct glutamatergic afferents. *Neuroscience* 203, 59–77. doi: 10.1016/j.neuroscience.2011.12.006

Sun, Y., Gooch, H., and Sah, P. (2020). Fear conditioning and the basolateral amygdala. *F1000Research* 9:53. doi: 10.12688/f1000research.21201.1

Tovote, P., Fadok, J. P., and Luthi, A. (2015). Neuronal circuits for fear and anxiety. *Nat. Rev. Neurosci.* 16, 317–331. doi: 10.1038/nrn3945

Tremblay, R., Lee, S., and Rudy, B. (2016). GABAergic interneurons in the neocortex: from cellular properties to circuits. *Neuron* 91, 260–292. doi: 10.1016/j.neuron.2016.06.033

Vereczki, V. K., Veres, J. M., Muller, K., Nagy, G. A., Racz, B., Barsy, B., et al. (2016). Synaptic organization of perisomatic GABAergic inputs onto the principal cells of the mouse basolateral amygdala. *Front. Neuroanat.* 10:20. doi: 10.3389/fnana.2016.00020

Veres, J. M., Nagy, G. A., and Hajos, N. (2017). Perisomatic GABAergic synapses of basket cells effectively control principal neuron activity in amygdala networks. *eLife* 6. doi: 10.7554/eLife.20721

Veres, J. M., Nagy, G. A., Vereczki, V. K., Andrasi, T., and Hajos, N. (2014). Strategically positioned inhibitory synapses of axo-axonic cells potently control principal neuron spiking in the basolateral amygdala. *J. Neurosci.* 34, 16194–16206. doi: 10.1523/JNEUROSCI.2232-14.2014

Windels, F., Crane, J. W., and Sah, P. (2010). Inhibition dominates the early phase of up-states in the basolateral amygdala. *J. Neurophysiol.* 104:3433–3438. doi: 10.1152/jn.00531.2010

Windels, F., Yan, S., Stratton, P. G., Sullivan, R., Crane, J. W., and Sah, P. (2016). Auditory tones and foot-shock recapitulate spontaneous sub-threshold activity in basolateral amygdala principal neurons and interneurons. *PLoS ONE* 11:e0155192. doi: 10.1371/journal.pone.0155192

Wolff, S. B., Grundemann, J., Tovote, P., Krabbe, S., Jacobson, G. A., Muller, C., et al. (2014). Amygdala interneuron subtypes control fear learning through disinhibition. *Nature* 509, 453–458. doi: 10.1038/nature13258

Woodruff, A. R., Monyer, H., and Sah, P. (2006). GABAergic excitation in the basolateral amygdala. *J. Neurosci.* 26, 11881–11887. doi: 10.1523/JNEUROSCI.3389-06.2006

Woodruff, A. R., and Sah, P. (2007a). Inhibition and synchronization of basal amygdala principal neuron spiking by parvalbumin-positive interneurons. *J. Neurophysiol.* 98, 2956–2961. doi: 10.1152/jn.00739.2007

Woodruff, A. R., and Sah, P. (2007b). Networks of parvalbumin-positive interneurons in the basolateral amygdala. *J. Neurosci.* 27, 553–563. doi: 10.1523/JNEUROSCI.3686-06.2007

Yuste, R. (2005). Origin and classification of neocortical interneurons. *Neuron* 48, 524–527.

Conflict of Interest: The authors declare that the research was conducted in the absence of any commercial or financial relationships that could be construed as a potential conflict of interest.

frontiers in Neural Circuits

REVIEW
published: 02 June 2021
doi: 10.3389/fncir.2021.687558

Hippocampal Somatostatin Interneurons, Long-Term Synaptic Plasticity and Memory

*Eve Honoré, Abdessattar Khlaifia, Anthony Bosson and Jean-Claude Lacaille**

Department of Neurosciences, Centre for Interdisciplinary Research on Brain and Learning, Research Group on the Central Nervous System, Université de Montréal, Montreal, QC, Canada

A distinctive feature of the hippocampal structure is the diversity of inhibitory interneurons. These complex inhibitory interconnections largely contribute to the tight modulation of hippocampal circuitry, as well as to the formation and coordination of neuronal assemblies underlying learning and memory. Inhibitory interneurons provide more than a simple transitory inhibition of hippocampal principal cells (PCs). The synaptic plasticity of inhibitory neurons provides long-lasting changes in the hippocampal network and is a key component of memory formation. The dendrite targeting interneurons expressing the peptide somatostatin (SOM) are particularly interesting in this regard because they display unique long-lasting synaptic changes leading to metaplastic regulation of hippocampal networks. In this article, we examine the actions of the neuropeptide SOM on hippocampal cells, synaptic plasticity, learning, and memory. We address the different subtypes of hippocampal SOM interneurons. We describe the long-term synaptic plasticity that takes place at the excitatory synapses of SOM interneurons, its singular induction and expression mechanisms, as well as the consequences of these changes on the hippocampal network, learning, and memory. We also review evidence that astrocytes provide cell-specific dynamic regulation of inhibition of PC dendrites by SOM interneurons. Finally, we cover how, in mouse models of Alzheimer's disease (AD), dysfunction of plasticity of SOM interneuron excitatory synapses may also contribute to cognitive impairments in brain disorders.

Keywords: somatostatin, inhibitory interneuron, hippocampus, network metaplasticity, long-term potentiation, spatial and contextual memory, memory impairment, Alzheimer's disease

OPEN ACCESS

Edited by:
Maria Gutierrez-Mecinas, University of Glasgow, United Kingdom

Reviewed by:
Rebecca Ann Piskorowski, INSERM U1266 Institut de Psychiatrie et Neurosciences de Paris, France
Marco Fuenzalida, Universidad de Valparaiso, Chile

****Correspondence:***
Jean-Claude Lacaille
jean-claude.lacaille@umontreal.ca

Received: *29 March 2021*
Accepted: *30 April 2021*
Published: *02 June 2021*

Citation:
Honoré E, Khlaifia A, Bosson A and Lacaille J-C (2021) Hippocampal Somatostatin Interneurons, Long-Term Synaptic Plasticity and Memory. Front. Neural Circuits 15:687558. doi: 10.3389/fncir.2021.687558

INTRODUCTION

Hippocampal learning and memory emerge from the proper routing of information throughout its networks and the formation of enduring neuronal assemblies encoding a memory (Kandel et al., 2014). These neuronal assemblies, also called engrams, are formed by a discrete population of excitatory glutamatergic principal cells (PCs) between which synaptic transmission is potentiated (Josselyn and Frankland, 2018; Tonegawa et al., 2018).

A distinctive feature of the hippocampal structure is the diversity of inhibitory interneurons. PCs represent the majority of neurons in every hippocampal region. While interneurons

only represent 10 to 20% of the total neuron population, they can be divided into many subgroups based on their laminar position, dendritic and axonal morphology, protein expression, electrophysiological features, and functions (Freund and Buzsáki, 1996; Somogyi and Klausberger, 2005; Tricoire et al., 2011; Kepecs and Fishell, 2014; Pelkey et al., 2017; Booker and Vida, 2018). Interestingly, the different interneuron types have preferred synaptic connections on specific and distinct subcellular domains of the principal cells including the apical and proximal dendrites, cell body, and the axon initial segment. Due to their specific characteristics, inhibitory interneurons play various roles in fine–tuning signal integration and firing of PCs. Additional levels of control of the hippocampal network is achieved by interneurons targeting other interneurons (Katona et al., 1999; Pelkey et al., 2017; Artinian and Lacaille, 2018) along with interneuron-astrocyte interactions (Mederos and Perea, 2019).

These complex inhibitory interconnections largely contribute to the tight modulation of hippocampal circuitry, providing means for the formation and coordination of neuronal assemblies. Hence, hippocampal interneurons also participate in the mechanisms underlying hippocampus-dependent memory. In this review, we aim to shed light on a major subpopulation of GABAergic interneurons specifically inhibiting PC dendrites and characterized by the expression of the peptide somatostatin (SOM). As the morphological and neurochemical profiles of these interneurons have already been reviewed (Pelkey et al., 2017; Booker and Vida, 2018), we will focus on the role of SOM interneuron activity and synaptic plasticity in the regulation of hippocampal networks and memory functions.

SOMATOSTATIN IN THE HIPPOCAMPUS

The peptide SOM, also referred as somatotropin release inhibitory factor (SRIF), was originally discovered in the hypothalamus where it acts as a growth hormone inhibitor (Krulich et al., 1968; Brazeau et al., 1973). In the cerebral cortex, SOM is stored in dense-core vesicles in a specific subset GABAergic interneurons and released by intense neuronal activity (Vezzani et al., 1993; Hou and Yu, 2013; Liguz-Lecznar et al., 2016). SOM can bind to five metabotropic receptors ($SST_{1-5}R$) which are coupled to G protein from the Gi/o and Gq/G11 families. Thus, SSTR activation downregulates adenylyl cyclase activity and activates the phosphoinositide 3-kinase and phospholipase Cβ signaling pathways (Liguz-Lecznar et al., 2016; Günther et al., 2018). $SST_{1-4}R$, but not SST_5R, are present in the hippocampus in PCs and as auto-receptors in SOM interneurons. Although the distribution of SSTRs overlaps within and across hippocampal regions, SSTR subtypes preferentially occupy specific cell compartments. SST_1R are preferentially located pre-synaptically, SST_2R and SST_4R post-synaptically, and SST_3R extra-synaptically. Yet, which cell type expresses the receptors and whether they are pre or postsynaptic remains unclear (Csaba and Dournaud, 2001; Liguz-Lecznar et al., 2016; Cammalleri et al., 2019).

The systematic distribution of SSTRs suggests a precise regulation of hippocampal networks by SOM. However, the mechanisms by which SOM regulates hippocampal networks remain ambiguous. Reports of membrane and synaptic effects are diverse and sometimes contradictory. On the one hand, SOM has an inhibitory effect on pyramidal neurons exhibiting hyperpolarizing effect, decreasing evoked and spontaneous activity, persistently reducing NMDA and AMPA currents, and reducing spine density (Pittman and Siggins, 1981; Tallent and Siggins, 1997; Hou and Yu, 2013). On the other hand, SOM also produces excitatory effects on pyramidal cells inducing membrane depolarization, as well as increasing spontaneous and evoked excitatory postsynaptic potentials (EPSPs; Olpe et al., 1980; Delfs and Dichter, 1983; Scharfman and Schwartzkroin, 1988, 1989).

Many factors may explain these discrepancies. First, in many studies, the effect of SOM is concentration-dependent, and the number of PCs responding to SOM application with a depolarization follows an inverted U-shaped curve between 100 pM and 1 μM, until it reaches potent toxic concentrations over 10 μM (Olpe et al., 1980; Pittman and Siggins, 1981; Delfs and Dichter, 1983; Scharfman and Schwartzkroin, 1988; Tallent and Siggins, 1997). Second, the location of SOM application is also important. In rabbit hippocampal slices, SOM application on the soma of CA1 PCs induces membrane depolarization often accompanied by action potentials. When applied on the dendrites of PCs SOM produces depolarization or hyperpolarization. Larger SOM applications further away from PCs induce membrane hyperpolarization (Scharfman and Schwartzkroin, 1988). Third, inhibitory interneurons also express SSTRs. SOM application at the soma of interneurons at the border between *stratum pyramidale* and *oriens* produces a depolarization accompanied by an action potential in these cells. When applied at their dendrites, SOM produces either depolarization followed by increased action potentials, or hyperpolarization also followed by increased action potentials, or a combination of depolarization and action potential discharge followed by a hyperpolarization (Scharfman and Schwartzkroin, 1988).

The effect of SOM on interneuron output also appears complex. Blocking SST_1R resulted in an increase in SOM concentration but had no effect on GABA concentration *in vivo* (De Bundel et al., 2010). This finding may indicate that SOM release from an interneuron can promote auto-inhibition *via* SST_1R presynaptic activation without interfering with GABA transmission. Bath application of somatostatin did not affect isolated GABAergic inhibitory postsynaptic currents induced by stimulation close to the pyramidal cell layer, nor the density of inhibitory synapses (Tallent and Siggins, 1997; Hou and Yu, 2013). However, earlier research demonstrated persistent reduction or blockade of spontaneous or evoked inhibitory postsynaptic potentials (Pittman and Siggins, 1981; Scharfman and Schwartzkroin, 1988, 1989).

Finally, another level of complexity with SOM effects arises from its long-lasting action. SOM produces long-lasting increases in spontaneous activity and evoked responses of pyramidal cells *via* postsynaptic effects (Delfs and Dichter, 1983; Scharfman and Schwartzkroin, 1988). In addition, transgenic mice with ablation of the SOM gene or mice with pharmacological depletion of

SOM by cysteamine treatment, have normal basal transmission but a deficit in long-term potentiation (LTP) in CA1 (Kluge et al., 2008). Taken altogether this *corpus* of data suggests that SOM has a complex function which is dependent on the location and concentration released, the activated receptor subtype, and experimental conditions (for details see **Table 1**).

Interestingly, at the behavioral level, SOM appears important as a neuromodulator of hippocampal function. Genetic ablation of the SOM gene or SOM depletion by cysteamine impairs contextual fear memory and has no effect on cued fear memory, indicating a specific action on hippocampus-dependent memory (Kluge et al., 2008). Moreover, intracerebroventricular injection of SOM, or a non-hydrolyzable SOM analog, before or after learning, increases active and passive avoidance behaviors 24 h after the acquisition and prevents their extinction (Vécsei and Widerlöv, 1988; Vécsei et al., 1989). However, both treatments have no effect on spatial discrimination learning and reversal learning in the T-maze test (Vécsei et al., 1984). Again, SOM concentration is critical, low concentrations increase passive avoidance memory, while 10-fold higher concentrations have the opposite effect (Vécsei et al., 1984, 1989; Vécsei and Widerlöv, 1988; Schettini, 1991). Pre-training intra-hippocampal injection of SOM or a SST_4R agonist impairs spatial memory in a dose-dependent manner. In addition, the SST_4R agonist decreases cued memory and enhances the retention of bar pressing tasks. Intriguingly, the administration of $SST_{1-3}R$ agonists does not evoke any behavioral change (Gastambide et al., 2008). The timing of SOM treatment is also critical. When injected before the memory acquisition trials in the 8-arm radial maze task, SOM increases acquisition rates. However, when administered before the memory probe test, it impairs performance. Thus, SOM has different effects on acquisition and memory probe tests (Guillou et al., 1993; Lamirault et al., 2001). Finally, it is important to note that hippocampal injections of SOM or agonists of SST_4R and SST_2R have anxiolytic and antidepressant-like effects *via* the inhibition of the hypothalamic-pituitary-adrenal axis. Through this mechanism, SOM also regulates emotions and stress responses which strongly modulate learning and memory (Prévôt et al., 2017; for details see **Table 2**).

Thus, at the behavioral level, SOM is required for proper memory formation. The location, timing, and concentration of SOM release by interneurons appears crucial for SOM functional outcomes, perhaps because of the distribution and types of receptors involved. However, a better understanding of how, where and when SOM is released to fulfill its functions requires new precise tools.

HIPPOCAMPAL SOMATOSTATIN INTERNEURONS

Although hippocampal interneurons release the peptide SOM, in hippocampal research this peptide has largely been regarded as a neurochemical marker for a subset of GABAergic interneurons. Through their GABAergic actions, SOM interneurons provide local inhibition to regulate hippocampal networks, and distal inhibition to synchronize hippocampal activity with other brain areas. Hippocampal SOM interneurons have been the subject of recent comprehensive reviews (Muller and Remy, 2014; Pelkey et al., 2017; Booker and Vida, 2018). Thus, they gate the synaptic inputs of their targets (Katona et al., 1999; Muller and Remy, 2014). SOM interneurons preferentially receive excitatory inputs from local PCs to which they send inhibitory feedback (Lacaille et al., 1987; Blasco-Ibáñez and Freund, 1995). Yet, there is more to SOM interneuron function than negative feedback. SOM interneurons dynamically regulate the input-output transformation and firing of PCs both in slices and during exploration *in vivo* (Lovett-Barron et al., 2012; Royer et al., 2012). In addition, SOM interneurons are diverse, and each type has a different contribution to the regulation of information flow through PCs (**Figure 1**).

Oriens Lacunosum-Moleculare (OLM) Cells

OLM cells are the most extensively studied SOM interneurons in the hippocampus. They are located in CA3 and CA1 along the complete dorso-ventral axis of the hippocampus (Mikulovic et al., 2015). Their designation comes from the location of their soma and dendrites in *stratum oriens* and their rich axonal arborization in *stratum lacunosum-moleculare* (Lacaille et al., 1987; Chittajallu et al., 2013; **Figure 1**). Their main excitatory input comes from local PCs to which they send inhibitory feedback (Lacaille et al., 1987), as well as from cholinergic afferents from the septum and diagonal band of Broca (Lovett-Barron et al., 2012; Sun et al., 2014). They receive inhibition from local inhibitory neurons, mostly vasoactive intestinal peptide (VIP) expressing interneurons, and inhibitory afferents from septal regions (Tyan et al., 2014) and the nucleus incertus (Szonyi et al., 2019).

The main targets of OLM cell axons are the distal dendrites and spines of PCs (Maccaferri et al., 2000). They also target dendrites of other interneurons, such as bistratified cells, basket cells, and interneurons located in *stratum radiatum* (Schaffer collateral associated cells, perforant path associated cells, and neurogliaform cells; Katona et al., 1999; Elfant et al., 2008; **Figure 2**). Consequently, CA1 OLM cells provide differential control of PC excitatory afferents: (1) OLM cell activation directly inhibits the distal excitatory inputs of the temporoammonic pathway (TAP); (2) they also inhibit other interneurons, which themselves inhibit the proximal dendrites of CA1 PCs in *stratum radiatum*, providing indirect disinhibition of the excitatory inputs from the Schaffer collateral pathway (SC). Hence, OLM cells differentially modulate the excitatory synaptic inputs coming from the entorhinal cortex and CA3 onto PCs (Leao et al., 2012; Katona et al., 2014).

Interestingly, OLM cells express a specific set of proteins regulating their excitatory synaptic inputs. They express a high level of the metabotropic glutamate receptor type 1α (mGluR1α; Ferraguti et al., 2004) which localize perisynaptically at their dendritic synapses (Luján et al., 1996). They also express the postsynaptic adhesion molecule, extracellular leucine-rich repeat fibronectin containing 1 (Elfn1) protein, that interacts with the presynaptic receptor mGluR7, expressed specifically at afferent excitatory synapses of OLM cell

TABLE 1 | Effects of somatostatin (SOM) on hippocampal pyramidal cell activity.

Reference	Model	Experiment	Results
Hou and Yu (2013)	Rat hippocampal neuronal-glial culture	1 day SOM application 1 μM.	↘ Spine density (excitatory) and density of pre-post synaptic markers. No effect on inhibitory synapses.
Kluge et al. (2008)	Mouse acute slices	SOM-KO mice or cysteamine application.	SOM KO show normal basal synaptic transmission and ↘ LTP in CA1; same results with cysteamine.
Tallent and Siggins (1997)	Rat, acute slices	1 μM SOM superfusion.	SOM persistently ↘ NMDA and AMPA currents in a time and dose-dependent manner. It has no effect on isolated GABAergic currents elicited by pyramidal layer stimulation.
Scharfman and Schwartzkroin (1989)	Rabbit, acute slices	Pressure application of SOM on distinct CA1 pyramidal cell compartment.	Soma application of SOM depolarizes CA1-PCs and persistently ↘ or blocks IPSPs evoked by *oriens* electrical stimulation.
Scharfman and Schwartzkroin (1988)	Rabbit, acute slices	Pressure application of SOM on distinct CA1 pyramidal cell compartment.	SOM application on pyramidal cell soma elicits depolarization often accompanied by action potentials. On dendrites, it produces depolarization or hyperpolarization. Applied in larger quantities further from the cell it hyperpolarizes CA1-PCs. Potentiation with ↗ spontaneous activity and evoked responses due to postsynaptic effects.
Delfs and Dichter (1983)	Rat cortical neurons in culture	100 pM to 100 μM SOM application just over the studied neuron.	Concentration/response curve inverted U- shaped from 100 pM to 1 μM. 30–50% of the neurons respond ↗ with EPSPs and IPSPs amplitude, and ↗ spontaneous action potentials frequency.
Pittman and Siggins (1981)	Rat, acute slices	Application of 0.12 μM to 1.2 μM SOM superfusion on the slice.	Hyperpolarization of PCs and ↘ evoked and spontaneous activity. Slight ↘IPSPs amplitude. Slight↗ EPSPs amplitude evoked by *radiatum* stimulation.
Olpe et al. (1980)	Rat, *in vivo*, anesthetized	Hippocampal 60 s micro-injection of SOM.	↗ Number of neurons responding with excitation, following ↗ SOM concentration. No alteration of GABA release.

↗ = increase; ↘ = decrease.

(Shigemoto et al., 1996; Sylwestrak and Ghosh, 2012). The Elfn1-mGluR7 interaction facilitates excitatory transmission at these synapses and maximizes excitation in the theta frequency range (4–10 Hz; Sylwestrak and Ghosh, 2012).

The hippocampus displays characteristic oscillatory activities, theta and, gamma oscillations as well as sharp-wave ripples, during exploration and rapid eye movement (REM) sleep (Vanderwolf, 1969; O'Keefe and Nadel, 1978; Buzsaki et al., 1992; Buzsáki, 2002). Thus, the relation of interneuron firing to hippocampal oscillations provides useful functional information (Somogyi et al., 2014). OLM interneurons fire during theta activity at the trough of theta oscillations (Klausberger et al., 2003; Varga et al., 2012; Katona et al., 2014; Somogyi et al., 2014). However, their firing is not coupled to gamma oscillations (Tukker et al., 2007). Also, OLM cell firing is decreased during slow-wave sleep and mostly inhibited during sharp-wave ripples (Klausberger et al., 2003; Varga et al., 2012; Katona et al., 2014). The precise timing of synchronized spikes is crucial for the integration of information because excitatory synapses from CA1 PCs onto SOM interneurons display facilitation on repetitive activation (Ali and Thomson, 1998).

The membrane potential of OLM cells shows intrinsic theta frequency resonance with frequency preferences in theta and low theta ranges (1–5 Hz; Pike et al., 2000). OLM cells display a substantial spike frequency adaptation during sustained discharges (Lacaille and Williams, 1990; Tricoire et al., 2011). These properties constrain OLM cells to delayed low frequency sustained activity (Pouille and Scanziani, 2004). Thus, the facilitation of synaptic activation of SOM interneurons results in gradual recruitment of sustained inhibition of CA1 PCs (Pouille and Scanziani, 2004).

Bistratified Cells (BiC)

BiCs express the peptide SOM as well as the other interneuron-specific marker, parvalbumin (PV; Pelkey et al., 2017). Their somas are located in or around the CA1 pyramidal cell layer (BiCs; **Figure 1**). Their vertical aspinous dendrites arborize in *stratum oriens* and *radiatum* (**Figure 2**; Maccaferri et al., 2000). They receive both feedforward excitation from SC of CA3 PCs and feedback excitation from CA1 PCs (Klausberger et al., 2004). These two major inputs show different short-term dynamics. Repeated stimulation of SC inputs to BiCs show marked and sustained facilitation, whereas similar stimulation of CA1 PCs inputs to BiCs display only an initial transient facilitation (Wierenga and Wadman, 2003; Pouille and Scanziani, 2004). BiCs receive inhibitory synaptic inputs from OLM cells (Leao et al., 2012) and from septal GABAergic neurons (Unal et al., 2018). The designation of BiC comes from the two-layered distribution of their axonal arborizations in the *stratum oriens* and *stratum radiatum* (**Figure 2**). Accordingly, BiCs strongly inhibit the basal and proximal apical dendrites of CA1 PCs, as

TABLE 2 | Effects of somatostatin (SOM) on hippocampus-dependent behavior.

Reference	Model	Experiment	Results
Gastambide et al. (2008)	Mouse	Intra-hippocampal injection of SOM or SSTR agonist at different concentrations before spatial and cued versions of Morris water maze and bar pressing conditioning.	SOM and SST_4R agonist injection ↘ spatial memory dose-dependently. $SST_{1-3}R$ agonist does not affect these behavioral tasks. SST_4R agonist ↘ cued memory but ↗ bar pressing retention.
Kluge et al. (2008)	Mouse	SOM KO mice or cysteamine injection in wild type mice. Contextual fear conditioning and cued fear conditioning.	SOM KO ↘ contextual fear but not cued fear memory. Pre-conditioning cysteamine injection in wild type mice has the same effect, but post-conditioning injection induces unspecific increase of fear response.
Lamirault et al. (2001)	Mouse	Intra-hippocampal injection of SOM or cysteamine prior spatial discrimination eight-arm radial maze task acquisition or test.	SOM injection prior acquisition (0.2 μg/0.2 μl/hippocampus) ↗ acquisition speed but ↘ performances during the test. Injection before the test does not affect memory.
Guillou et al. (1993)	Mouse	Intra hippocampal injection of SOM or cysteamine prior to spatial discrimination eight-arm radial maze task.	SOM injection (0.2 μg/0.2 μl/hippocampus) ↗ acquisition speed, but impairs the ability to change strategies. Cysteamine injection impairs memory.
Vécsei et al. (1989)	Rat	Intra-cerebroventricular SOM or SOM fragments injection in male rats directly after passive avoidance acquisition.	0.6 nM SOM ↗ avoidance latency and 6 nM ↘ it in a passive avoidance task during the test 24 h after. In open field task 6 nM SOM ↘ rearing and 0.6 nM has no effect. Injections above 12 nM are lethal.
Vécsei and Widerlöv (1988)	Rat	Intra-cerebroventricular SOM injection in male rats 30 min before passive avoidance, or active avoidance acquisition.	In passive avoidance: 1 μg of SOM ↗ avoidance latency at 24 h but not 48 h after acquisition. 10 μg ↘ avoidance latency 24 h after acquisition. In active avoidance: 1 μg SOM ↗ learning curve.
Vécsei et al. (1984)	Rat	Intra-cerebroventricular SOM or subcutaneous cysteamine injection in male rats directly after active avoidance and T-maze acquisition.	SOM ↘ extinction of active avoidance but has no effect on T-maze. Cysteamine ↗ extinction in both behavioral tasks. SOM ↗ locomotion in open field 10 min after injection. Cysteamine ↘ locomotion, rearing, and grooming.

↗ = increase; ↘ = decrease.

well as other interneurons (Halasy et al., 1996; Maccaferri et al., 2000).

The action potentials and subsequent after-hyperpolarization of BiCs are fast, enabling these cells to withstand high frequency stimulation with high temporal reliability (Buhl et al., 1996; Pouille and Scanziani, 2004). In relation to hippocampal oscillatory activity, BiCs fire during theta activity in the trough of theta oscillation (Klausberger et al., 2004). In contrast to OLM cells, BiCs show strong modulation of activity during gamma oscillations and fire during the ascending phase of oscillations (Tukker et al., 2007) In addition, BiCs demonstrate high activity during sharp-wave ripples (Katona et al., 2014). BiCs fast-spiking features and the dynamics of their excitatory and inhibitory inputs influence the way they provide recurrent inhibition of PCs. At the beginning of sustained activation of CA1 PC inputs, BiCs respond with reliable time-locked excitation that shows transient facilitation, resulting in onset-transient inhibition of CA1 PCs proximal dendrites (Wierenga and Wadman, 2003; Pouille and Scanziani, 2004). In contrast, OLM cell firing shows a gradual recruitment during sustained activation of CA1 PC inputs, thereby providing a late-persistent type of inhibition (Pouille and Scanziani, 2004). Thus, BiCs and OLM cells provide recurrent inhibition with distinct dynamics, targeting proximal vs. distal CA1 PC dendrites respectively (Wierenga and Wadman, 2003; Pouille and Scanziani, 2004; Muller and Remy, 2014).

Hilar Perforant Path (HIPP) Cells

HIPP cells of the dentate gyrus (DG) have their soma and dendritic arborizations in the hilus (Sik et al., 1997; Yuan et al., 2017). Their axonal projections heavily ramify in the outer two-thirds of the molecular layer (**Figure 1**; Han et al., 1993; Yuan et al., 2017). Although the majority of HIPP axon processes terminate in the DG, some branches traverse the hippocampal fissure and project to the CA1 *stratum lacunosum-moleculare* (Han et al., 1993; Houser, 2007). HIPP cells are mainly excited by granule cell (GC) axons and provide feedback inhibition to distal dendrites of GCs, thereby showing functional similarities with OLM cells (Hosp et al., 2014). HIPPs form functional synapses with GCs, but also with PV interneurons and other HIPP cells. They also rarely connect to CCK hilar commissural associational path (HICAP) interneurons (Savanthrapadian et al., 2014). HIPP provides weak and slow dendritic inhibition (Yuan et al., 2017). However, their inhibition of PV cells is sufficient to regulate their action potential generation and spike timing precision, and hence, control information flow within the DG circuitry (Savanthrapadian et al., 2014).

Radiatum (R) Cells

Other subtypes of SOM cells, that are sparse in number, are found in *stratum radiatum* (**Figure 1**; Oliva et al., 2000; Tricoire et al., 2011). One type of SOM interneuron was

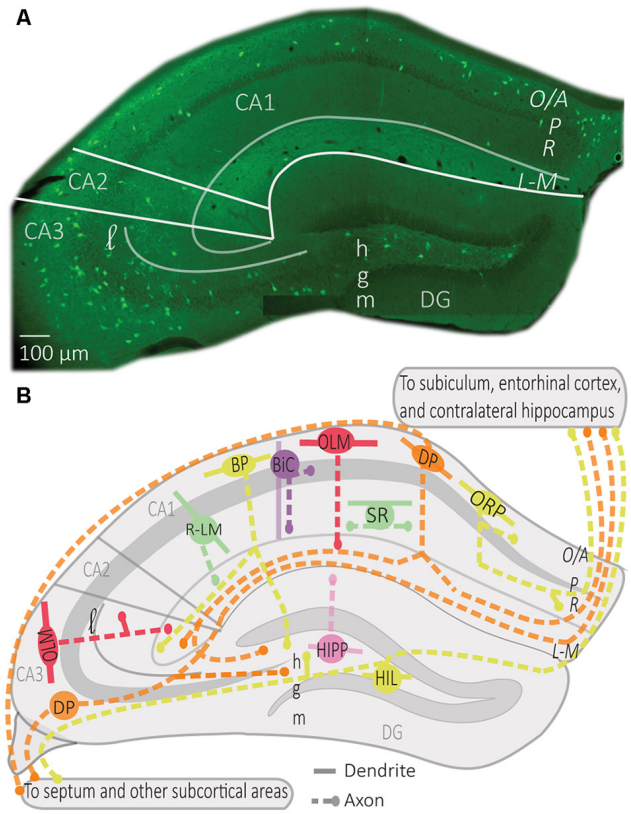

FIGURE 1 | Distribution of somatostatin (SOM) interneurons in hippocampus. **(A)** Representative montage of fluorescence images showing the soma location of SOM interneurons expressing the enhanced yellow fluorescent protein in the dorsal hippocampus of *Sst*$^{Ires\text{-}Cre}$; *Rosa26*$^{lsl\text{-}EYFP}$ mice (Vasuta et al., 2015; Artinian et al., 2019), with indicated anatomical landmarks. **(B)** Simplified diagram illustrating the characteristic position of soma, dendrites, and axons of the different types of SOM interneurons in hippocampus. Abbreviations for hippocampus: CA1–3, *cornu ammonis* 1–3; DG, dentate gyrus; O/A, *oriens/alveus*; P, *pyramidale*; R, *radiatum*; L-M, *lacunosum-moleculare*; l, *lucidum*; h, hilus; g, granule cell layer; m, *moleculare*. Abbreviations for SOM interneuron types: OLM, *oriens/lacunosum-moleculare* cell; ORP, *oriens*-retrohippocampal projecting cell; DP, double projecting cell; BP, back-projecting cell; BiC, bistratified cell; R-LM, *radiatum/lacunosum-moleculare* cell; SR, *stratum radiatum* cell; HIPP, hilar perforant path cell; HIL, hilar cell.

identified in a transgenic mice line (GFP-expressing Inhibitory Neurons, GIN mice; Oliva et al., 2000). These CA1 SOM interneurons have a cell body in *stratum radiatum* and dendrites that span *stratum oriens* and *stratum radiatum*. Their axonal projections ramify in *stratum lacunosum-moleculare* and these cells were designated *radiatum-lacunosum moleculare* (RLM cells; **Figure 1**; Oliva et al., 2000). RLM cells show similar firing properties to OLM cells (Oliva et al., 2000). Hence, RLM cells may provide feedforward inhibition of entorhinal cortex input of PCs (Oliva et al., 2000). Another type of SOM cell was identified with the soma, dendrites and axonal projections restricted to *stratum radiatum* (SR cells; **Figure 1**; Oliva et al., 2000; Tricoire et al., 2011). These SOM cells have similar firing properties to OLM cells and may provide feedforward inhibition of Schaffer collateral input to CA1 pyramidal cells (Oliva et al., 2000; Tricoire et al., 2011).

Projection Cells

Distinct SOM interneurons, in addition to providing local inhibition, have projections to other hippocampal and subcortical areas, where they target many cell types including PCs and GABA interneurons (Gulyas et al., 2003; Katona et al., 2017; Eyre and Bartos, 2019). In CA1, these SOM projecting cells have their soma and dendrites in *stratum oriens*, as well as local axonal arborizations in *stratum oriens* and *stratum radiatum*. Distinct CA1 SOM projection cells are distinguished by their axonal projection targets (**Figure 1**). Back-projecting (BP) cells have axonal projections to CA3 and DG (Goldin et al., 2007; Katona et al., 2017). Oriens-retrohippocampal projecting (ORP) cells project to the subiculum (Jinno et al., 2007; Melzer et al., 2012). Double-projecting (DP) cells have axons projecting to the septum, as well as to CA3 and DG (Gulyas et al., 2003; Katona et al., 2017; Eyre and Bartos, 2019), subiculum (Goldin et al., 2007; Jinno et al., 2007; Melzer et al., 2012) or the medial entorhinal cortex and contralateral hippocampus (Goldin et al., 2007; Jinno et al., 2007; Melzer et al., 2012; Eyre and Bartos, 2019). Much less is known about the physiological properties of these cell types, although *in vivo* recordings indicate that most projection cells discharge during theta activity in the descending slope or at the trough of theta cycles during movement (Jinno et al., 2007; Katona et al., 2017). Some projection cells fire preferentially on the ascending phase of gamma oscillations (Jinno et al., 2007). Most of them also increase their firing during sharp-wave ripples (Jinno et al., 2007; Katona et al., 2017). Thus, SOM projection cells tend to fire similarly to BiC cells during hippocampal oscillations.

In CA3, DP cells were described with soma in *stratum oriens*, *pyramidale*, and *lucidum* (Gulyas et al., 2003; Jinno et al., 2007; **Figure 1**). CA3 DP cells have dendrites in *stratum oriens* and *radiatum*, as well as local axons in *stratum oriens*, *pyramidale* and *radiatum* (Jinno et al., 2007). CA3 DP cells have axonal long-range projections that target the septum, as well as CA1 and subiculum (Jinno et al., 2007) and ventral hippocampal areas (Gulyas et al., 2003). CA3 DP cell axonal long-range projections make synaptic contacts with PCs and GABA interneurons (Gulyas et al., 2003; Jinno et al., 2007).

In DG, another type of SOM cell is the hilar cell (HIL, **Figure 1**). HIL cells have a cell body, dendrites, and local axonal projections in the hilus (Yuan et al., 2017). Their activity is driven by excitatory inputs from GCs and DG mossy cells (Larimer and Strowbridge, 2008; Yuan et al., 2017). HIL cells provide perisomatic inhibition of hilar GABAergic cells and mossy cells and send long-range axonal projections to the medial septum (Gulyas et al., 2003; Larimer and Strowbridge, 2008; Yuan et al., 2017) and contralateral DG (Gulyas et al., 2003; Goldin et al., 2007; Jinno et al., 2007; Eyre and Bartos, 2019). By exerting a powerful inhibition onto local GABAergic and mossy cells, as well as septal neurons, HIL cells can coordinate activities in these

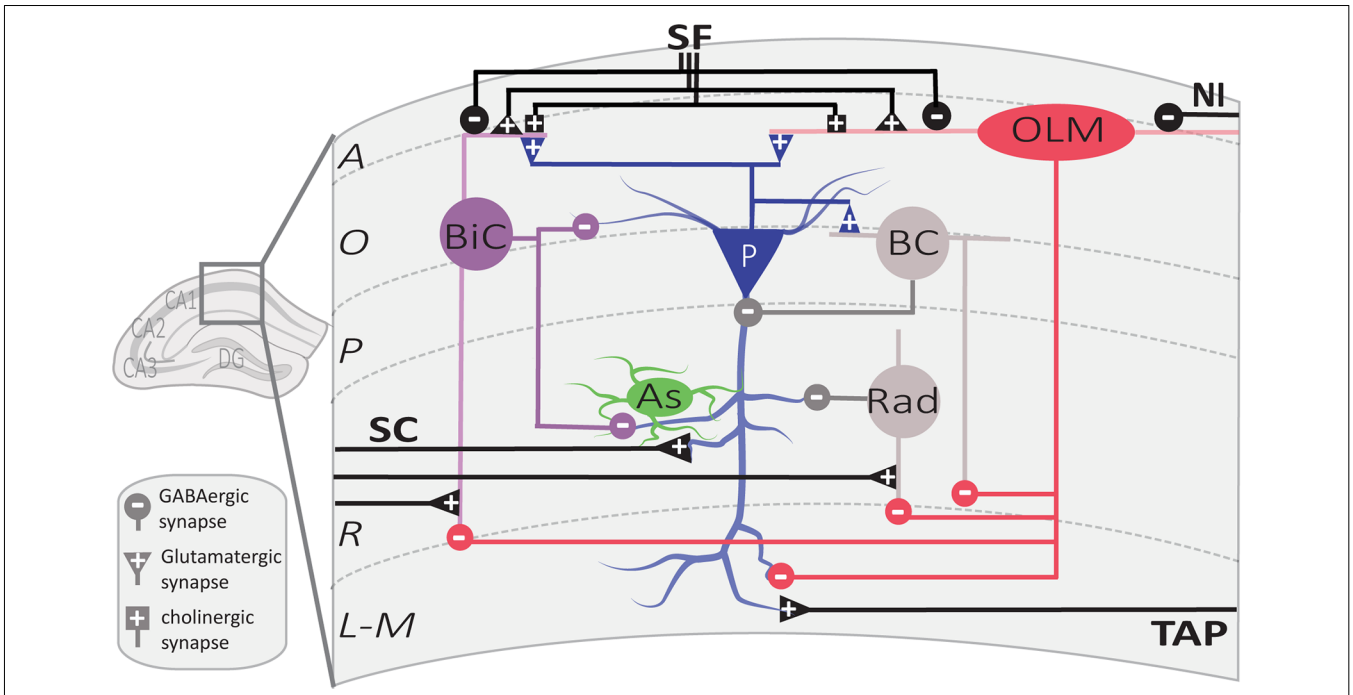

FIGURE 2 | Local circuit of CA1 SOM interneurons. Simplified diagram illustrating the local synaptic circuits of OLM cells and BiCs with other cell types in dorsal CA1 hippocampus. Abbreviations for CA1 layers: A, *alveus*; O, *oriens*; P, *pyramidale*; R, *radiatum*; L-M, *lacunosum-moleculare.* Abbreviations for CA1 afferent inputs: SF, septal fibers; NI, nucleus incertus fibers; SC, Schaffer collateral pathway from CA3 pyramidal cells; TAP, temporo-ammonic pathway from entorhinal cortex. Abbreviations for SOM cell types: (red) OLM, *oriens/lacunosum-moleculare* cell; (violet) BiC, bistratified cell. Abbreviations for other cell types: (blue) P, pyramidal cell; (gray) BC, basket cell; (green) As, astrocyte; (gray) Rad, unidentified *stratum radiatum* interneurons targeted by OLM cells.

areas as a function of GC and mossy cell activation (Larimer and Strowbridge, 2008; Yuan et al., 2017).

SOM INTERNEURONS LONG-TERM SYNAPTIC PLASTICITY

In the central nervous system, two widely studied forms of long-term synaptic plasticity are long-term potentiation (LTP), a long-lasting strengthening of synaptic efficacy, and long-term depression (LTD), a long-lasting weakening of synaptic efficacy (Malenka and Bear, 2004). These forms of synaptic plasticity at hippocampal excitatory synapses are linked to memory storage (Morris, 2003). *In vitro*, several protocols of electrical stimulations, or repetitive pairing of pre- and post-synaptic firing, induce long-term changes of synaptic transmission (Malenka and Bear, 2004; Caporale and Dan, 2008). With electrical stimulation, LTP is generally associated with high frequency afferent stimulation, and LTD with low frequency stimulation. With pre- and post-synaptic pairing, a presynaptic spike preceding the postsynaptic spike within a narrow time window induces LTP, whereas the reverse produces LTD (Feldman, 2012). Although it has been known for some time that blocking GABAergic transmission facilitates the induction of LTP at excitatory synapses (Wigstrom and Gustafsson, 1983) and that afferents of inhibitory interneurons display long-term potentiation (Buzsaki and Eidelberg, 1982), synaptic plasticity at excitatory synapses onto interneurons has recently attracted more attention (Kullmann and Lamsa, 2007; Pelletier and Lacaille, 2008). It is becoming increasingly apparent that hippocampal inhibitory neurons, including SOM interneurons, have highly dynamic activity and express long-lasting changes at their excitatory input synapses and inhibitory output synapses (Maccaferri and McBain, 1996; Perez et al., 2001; Lamsa et al., 2005; Chevaleyre et al., 2006; Kullmann and Lamsa, 2007, 2011; Pelletier and Lacaille, 2008; Vasuta et al., 2015; Udakis et al., 2020). In this section, we will focus on long-term plasticity at excitatory synapses onto hippocampal SOM interneurons (Perez et al., 2001) and later examine its role in hippocampus-dependent memory.

Excitatory Synapses Onto CA1 SOM Interneurons

Plasticity of excitatory synapses onto SOM interneurons has been characterized the most in CA1 OLM cells (Lacaille et al., 1987; Maccaferri and McBain, 1996; Perez et al., 2001; Lamsa et al., 2007). Excitatory synapses made by CA1 PC axons that feedback on CA1 SOM interneurons (notably OLM cells) are composed of Ca^{2+} permeable AMPA receptors (CP-AMPARs). These synapses show inward rectification of their current-voltage (I–V) relationship, display short-term facilitation with repeated stimulation, and are inhibited by mGluR2/3 (Croce et al., 2010). In contrast, excitatory synapses made by axons of CA3 PCs

that feed-forward onto CA1 SOM interneurons (OLM cells) are composed of Ca^{2+} impermeable AMPARs (CI-AMPARs), and these synapses show linear I–V relationships, display short-term depression with repeated stimulation, and are mGluR2/3-insensitive (Croce et al., 2010). These input-specific properties of excitatory synapses differentially control the SOM interneuron output firing, resulting in gradual sustained recruitment of evoked firing with repetitive feedback input activation, and transient evoked firing with repetitive feedforward input activation of SOM cells (Croce et al., 2010). It is interesting to note that input-specific rules of excitatory synapses also occur for other types of interneurons in CA3 *stratum lucidum* (SL) but with the opposite organization (Toth and McBain, 1998). Thus, excitatory synapses onto single SOM cells originate from multiple sources and display afferent-specific mechanisms. In addition, these afferent-specific mechanisms differ from those in other types of interneurons.

Long-Term Potentiation at Excitatory Synapses Onto SOM Interneurons

The synapse between CA1 PC axons and SOM interneurons, notably BiC and OLM cells, express a Hebbian form of LTP that requires the coincident activity of both pre- and postsynaptic neurons for induction (Perez et al., 2001; Lapointe et al., 2004; Vasuta et al., 2015). Multiple lines of evidence indicate that this SOM interneuron LTP is not due to passive propagation of di-synaptic LTP at Schaffer collateral synapses on CA1 pyramidal cells (SC-CA1 synapses; McBain et al., 1999). First, SOM interneuron LTP is insensitive to the NMDA receptor blocker AP-5 (Perez et al., 2001), unlike LTP at SC-CA1 PC synapses (Morris et al., 1986). Second, LTP is induced directly at putative single fiber synapses onto SOM interneurons by using minimal stimulation (Perez et al., 2001; Lapointe et al., 2004; Vasuta et al., 2015). Finally, interfering with Ca^{2+} influx in the postsynaptic SOM interneuron prevents LTP induction (Lapointe et al., 2004).

This LTP is considered Hebbian since it is induced by presynaptic theta-burst stimulation (TBS) paired with postsynaptic depolarization (**Figure 3**), but not by presynaptic stimulation alone nor postsynaptic depolarization alone (Perez et al., 2001). Hebbian LTP is expressed as a decrease in failure rates of EPSCs and an increase in the potency of EPSCs (amplitude of EPSCs excluding failures; Perez et al., 2001; Lapointe et al., 2004). It is also accompanied by a change in paired-pulse facilitation and the coefficient of variation of EPSCs, parameters associated with presynaptic changes (Lapointe et al., 2004). Thus, Hebbian LTP may be expressed by both pre- and post-synaptic mechanisms.

Hebbian LTP in SOM interneurons shows afferent input specificity. Pairing presynaptic TBS with postsynaptic depolarization elicits LTP at synapses between CA1 PCs and SOM interneurons, but not at the synapses between CA3 PCs and SOM interneurons (Croce et al., 2010). Also, it displays cell-type specificity. Pairing presynaptic TBS with postsynaptic depolarization evoked LTP in SOM interneurons (BiC and OLM cells; Perez et al., 2001; Lapointe et al., 2004; Vasuta et al., 2015) but not in PV interneurons (Vasuta et al., 2015) nor in unidentified interneurons in *stratum radiatum* (Perez et al., 2001).

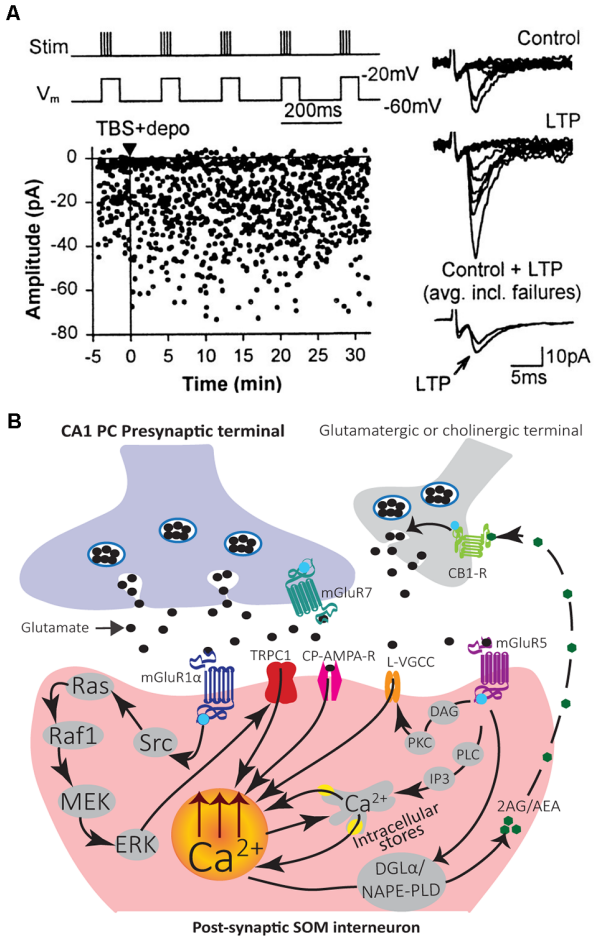

FIGURE 3 | Mechanisms of induction and modulation of Hebbian LTP in SOM interneurons. **(A)** Graph of EPSC amplitude from a representative cell showing LTP after TBS paired with depolarization (TBS + depo; protocol shown above and delivered at time indicated by black triangle and vertical line). Examples of control and potentiated EPSCs (10 consecutive responses) at 30 min after induction (*Right*). Superimposed average EPSCs (bottom traces; n = 64 responses each, failures included) from control and 30 min after induction also show LTP. Adapted from Perez et al. (2001). **(B)** Diagram of LTP induction mechanisms leading to postsynaptic Ca^{2+} elevation in SOM interneurons. Stimulation of the presynaptic terminal releases glutamate that activates postsynaptic CP-AMPAR and mGluR1α. Activation of mGluR1α stimulates the Src signaling cascade leading to ERK activation. ERK leads to postsynaptic Ca^{2+} rise *via* activation of non-selective cationic channels TRPC1 and Ca^{2+} entry, as well as mobilization of Ca^{2+} from intracellular stores. A retrograde signaling mechanism may involve eCBs. Synaptic activation of mGluR1/5 stimulates synthesizing enzymes DGLα and/or NAPE-PLD to produce the eCBs 2-AG and/or AEA. 2-AG/AEA act retrogradely to activate CB1Rs on glutamatergic or cholinergic terminals and potentiate transmission. A potential mechanism of LTP modulation may involve activation of mGluR5 that produces postsynaptic Ca^{2+} rises *via* two pathways. First, mGluR5 activates the PLC/IP3 pathway which leads to Ca^{2+} release from internal stores. Second, mGluR5 activates DAG-PKC pathway to potentiate L-type VGCC function and may regulate LTP induction.

Induction of Hebbian LTP in SOM interneurons involves a very different signaling cascade than LTP in PCs (**Figure 3**). Most

notably, Hebbian LTP in SOM interneurons does not involve NMDA receptors (Perez et al., 2001), but requires the activation of mGluR1α receptors, a glutamate metabotropic receptor highly expressed in SOM interneurons (Perez et al., 2001; Kougioumoutzakis et al., 2020). Pharmacologically blocking mGluR1α, or genetically deleting mGluR1 (mGluR1$^{-/-}$ mice), prevents Hebbian LTP induction, indicating a crucial role of mGluR1α (Perez et al., 2001; Lapointe et al., 2004; Topolnik et al., 2005; Vasuta et al., 2015). During induction of Hebbian LTP, the activation of postsynaptic mGluR1α stimulates Src and extracellular signal-regulated kinase (ERK) pathways, causing the opening of transient receptor potential (TRP) channels and Ca^{2+} influx, as well as Ca^{2+} release from intracellular stores (Topolnik et al., 2006; **Figure 3**). TRPC1 interaction with mGluR1α in SOM interneuron dendrites mediates a mGluR1α-dependent slow EPSC in SOM interneurons, supporting the importance of TRP channels in SOM interneurons LTP (Kougioumoutzakis et al., 2020).

Endocannabinoid (eCB) signaling mainly mediates short- and long-term depression of excitatory and inhibitory transmission (Chevaleyre et al., 2006). In addition, synaptic activation of group I mGluRs (mGluR1/5) is a major pathway for the production of eCBs (Chevaleyre et al., 2006). Interestingly in SOM interneurons, eCBs may be involved as a retrograde messenger in LTP (Friend et al., 2019). SOM interneurons express the endocannabinoid-synthesizing enzyme diacylglycerol lipase α (DGLα) and n-acylphosphatidylethanolamine phospholipase D (NAPE-PLD; Friend et al., 2019). Moreover, inhibition of cannabinoid type 1 receptor (CB1R) prevents LTP in SOM interneurons (Friend et al., 2019). Thus, synaptic activation of mGluR1/5 may lead to the production of eCBs (anandamide, AEA; 2-arachadonyl glycerol, 2-AG) that act retrogradely on presynaptic CB1Rs to potentiate synaptic transmission (**Figure 3**; Friend et al., 2019).

Activation of mGluR5 in SOM interneurons (OLM cells) also elicits postsynaptic Ca^{2+} rises from intracellular stores release, independent of Src-ERK activation (Topolnik et al., 2006). Moreover, this type of Ca^{2+} signaling is not involved directly in Hebbian LTP induction (Topolnik et al., 2006). Pharmacological activation of mGluR5 is sufficient to induce LTP at excitatory synapses onto SOM interneurons (OLM cells), indicating multiple types of LTP linked to mGluRs in SOM interneurons (Le Vasseur et al., 2008). In addition, local mGluR5 activation by agonist application or high frequency synaptic stimulation leads to sustained enhancement of action potential evoked Ca^{2+} transients in dendrites of SOM interneurons (OLM cells; Topolnik et al., 2009). This augmentation of postsynaptic Ca^{2+} transients is expressed as a selective potentiation of L-type voltage-gated calcium channels (VGCCs) function and controlled by mGluR5-mediated intracellular Ca^{2+} release as well as protein kinase C (PKC) activation (**Figure 3**; Topolnik et al., 2009). This activity-dependent regulation of VGCCs by mGluR5 may serve as a mechanism for positively regulating Hebbian synaptic plasticity of SOM interneurons (Topolnik et al., 2009).

In pyramidal cells, $GABA_B$Rs mediate a slow K^+-mediated inhibitory postsynaptic current (sIPSC; Dutar and Nicoll, 1988; Degro et al., 2015) and promote excitatory synapses LTP *via* a presynaptic disinhibition mechanism (Davies et al., 1991; Mott and Lewis, 1991). In SOM interneurons, $GABA_B$Rs are also highly expressed in dendrites. But instead of activating postsynaptic K^+ currents, $GABA_B$Rs inhibit postsynaptic L-type VGCCs in SOM interneurons (Booker et al., 2018). By negatively regulating VGCCs, $GABA_B$Rs inhibit Hebbian LTP in SOM interneurons (Booker et al., 2018). Thus, $GABA_B$R-mediated inhibition of L-type VGCCs provides a mechanism for negative regulation of Hebbian synaptic plasticity of SOM interneurons. Interestingly, excitatory and inhibitory synaptic inputs onto SOM interneurons are inhibited presynaptically by $GABA_B$Rs, as well as SOM interneuron inhibitory synapses onto PCs (Booker et al., 2020). Thus, $GABA_B$R activation may also functionally uncouple SOM interneurons from the CA1 network (Booker et al., 2020).

Persistent Long-Term Potentiation at Excitatory Synapses Onto SOM Interneurons

LTP in principal cells is divided into two phases: an early phase (early LTP, E-LTP) that is induced by brief high frequency stimulation, lasts several minutes to hours and depends on post-translational mechanisms; and a late phase (late LTP, L-LTP) that requires repetitive high frequency stimulation, lasts several hours to days and depends on new gene expression and protein synthesis (Kandel, 2001; Abraham et al., 2019). Although the study of late LTP has mainly focused on excitatory synapses onto principal cells (Malenka and Bear, 2004), recent studies revealed that excitatory synapses onto CA1 SOM interneurons can also undergo L-LTP (Ran et al., 2009, 2012; Artinian et al., 2019).

In hippocampal slice culture, repetitive stimulation of mGluR1, by the repeated application of the mGluR1/5 agonist (RS)-3, 5-dihydroxyphenylglycine (DHPG), in the presence of the mGluR5 antagonist 2-methyl-6-(phenylethynyl) pyridine (MPEP), induces a persistent potentiation of excitatory synapses onto SOM interneurons that can last at least 24 h, termed mGluR1-dependent late LTP (L-LTP_{mGluR1}; **Figure 4**; Ran et al., 2009, 2012; Artinian et al., 2019). L-LTP_{mGluR1} is prevented by inhibitors of transcription and translation, indicating that it is dependent on new gene expression and protein synthesis (**Figure 4**; Ran et al., 2009). L-LTP_{mGluR1} is also induced in acute hippocampal slices by repeated mGluR1 stimulation with DHPG, or by repetitive theta-burst stimulation of afferents (Artinian et al., 2019). Interestingly, using *ex vivo* whole-cell recordings in acute slices 24 h after contextual fear conditioning, training was found to induce mGluR1-mediated, translation-dependent L-LTP at SOM interneuron excitatory synapses, indicating that L-LTP_{mGluR1} may be linked to hippocampus-dependent memory (Artinian et al., 2019).

Mechanistically, L-LTP_{mGluR1} shares many features of Hebbian LTP. Repetitive stimulation of mGluR1 by DHPG during action potentials blockade with tetrodotoxin prevent L-LTP_{mGluR1}, suggesting a Hebbian induction (Ran et al.,

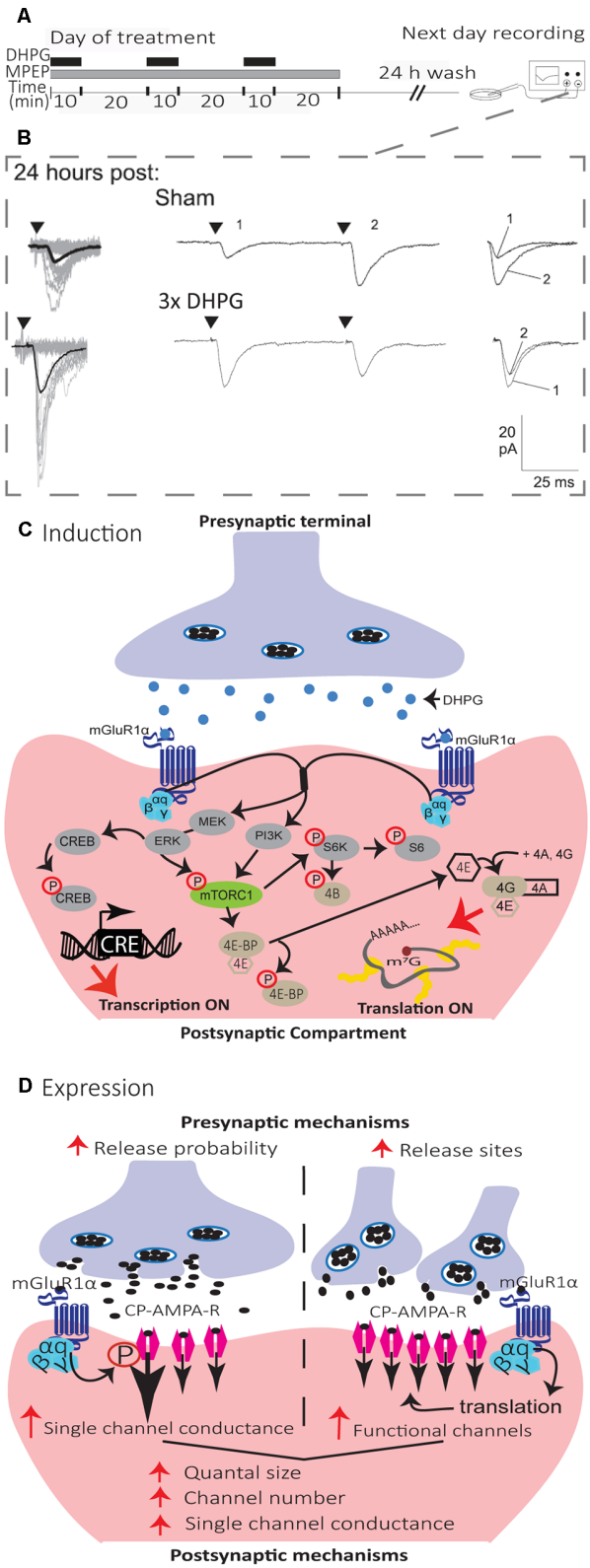

FIGURE 4 | Mechanisms of induction and expression of L-LTP$_{mGluR1}$ in SOM interneurons. **(A)** Schematics of induction and recording protocol. Cultured

(*Continued*)

FIGURE 4 | Continued
hippocampal slices were treated with repetitive (3×) applications of the mGluR1/5 agonist (DHPG, 5 μM, black bars) in the presence of the mGluR5 antagonist (MPEP, 25 μM, gray bar). On the next day, after a 24 h wash-out, whole cell recordings were obtained from visually identified CA1 SOM interneurons in agonist- or sham-treated slices. **(B)** Representative EPSCs evoked by minimal stimulation at 24 h after sham-treatment (top), repetitive (3×; bottom) mGluR1 agonist-stimulation, showing larger responses after repetitive treatment. Left, superimposed 20 successive events (EPSCs + failures; gray) with average EPSC (including failures; solid black line) of 100 events. Middle, average of EPSC pairs (100 events) evoked by paired-pulse stimulation (50 ms interstimulus interval), showing loss of paired-pulse facilitation after repetitive treatment. Right, superimposed first and second EPSCs of average pair. Black triangles indicate the time of stimulation. Adapted from Ran et al. (2009). **(C)** Diagram of L-LTP$_{mGluR1}$ induction mechanisms. Repeated stimulation of mGluR1 by DHPG engages PI3K and MEK/ERK signaling pathways to phosphorylate mTORC1. Activation of mTORC1 leads to initiation of eIF4E-mediated mRNA translation *via* to pathways: (1) ribosomal S6 protein kinase (S6K) stimulation of S6 phosphorylation; and (2) phosphorylation of 4E-BPs repressors proteins which release eIF4E. Subsequently, eIF4E associates with eIF4A and eIF4G to form the cap-binding complex, eIF4F, which initiates translation. Activation of MEK–ERK signaling by repeated mGluR1 stimulation also leads to phosphorylation of CREB to control CRE-dependent gene expression. **(D)** Diagram of L-LTP$_{mGluR1}$ expression mechanisms. The maintenance of L-LTP$_{mGluR1}$ involves both pre- and post-synaptic modifications. At the presynaptic level, transmitter release is increased (increase in release probability and/or addition of functional release site). At the postsynaptic level, postsynaptic responsiveness is increased (recruitment of functional receptors and increase in single-channel conductance).

2012). L-LTP$_{mGluR1}$ is also NMDAR independent, and prior induction of L-LTP$_{mGluR1}$ occludes induction of Hebbian LTP, indicating that they share similar mechanisms (Ran et al., 2012).

The mechanisms of induction of L-LTP$_{mGluR1}$ (**Figure 4**) requires activation of mGluR1α, as it is prevented by the selective antagonist LY367385 (Ran et al., 2009; Artinian et al., 2019). Activation of mGluR1α stimulates both phosphoinositide 3-kinase (PI3K) and mitogen-activated protein kinase kinase (MEK)/extracellular signal-regulated kinase (ERK) pathways resulting in mTORC1 phosphorylation. In turn, mTORC1 activates ribosomal protein S6 kinase (S6K) and S6 phosphorylation, as well as phosphorylation of eIF4E-binding protein (4E-BP), to stimulate eIF4E-dependent translation necessary for L-LTP$_{mGluR1}$ (Ran et al., 2009; Artinian et al., 2019). In addition activation of mGluR1α stimulates phosphorylation of cAMP response element-binding protein (CREB) *via* ERK signaling, to activate CREB-dependent transcription also necessary for L-LTP$_{mGluR1}$ (Ran et al., 2012). A cell-specific conditional knock-out in SOM interneurons of the Regulatory-Associated Protein of mTOR (Raptor) gene, a necessary component of mTORC1, reduces mTORC1 activity and prevents L-LTP$_{mGluR1}$ (Artinian et al., 2019). Conversely, cell-specific conditional heterozygous knock-out in SOM interneurons of the Tuberous Sclerosis Complex 1 (TSC1) gene, a repressor of mTORC1, increases mTORC1 activity in SOM interneurons and facilitates L-LTP$_{mGluR1}$ by lowering the threshold for induction (Artinian et al., 2019). Knock-out of the 4E-BP gene, which removes the repression of eIF4E-dependent

translation, similarly causes a facilitation of L-LTP$_{mGluR1}$ by lowering the threshold for induction (Ran et al., 2009), further highlighting the critical role of mTORC1-dependent translation in L-LTP$_{mGluR1}$ (**Figure 4**).

The mechanisms of expression of synaptic plasticity in central neurons are varied and complex (Citri and Malenka, 2008). In SOM interneurons, L-LTP$_{mGluR1}$ expression may involve both pre- and postsynaptic mechanisms, not occurring necessarily jointly (**Figure 4**; Ran et al., 2009, 2012; Artinian et al., 2019). In slice cultures, L-LTP$_{mGluR1}$ is expressed by an increase in potency of EPSCs evoked by minimal stimulation (Ran et al., 2009; Artinian et al., 2019), and in amplitude of miniature EPSC (mEPSCs; Ran et al., 2009), suggesting postsynaptic mechanisms of expression. L-LTP$_{mGluR1}$ in slice cultures is accompanied by a reduction in the paired-pulse ratio of EPSCs evoked by minimal stimulation (Ran et al., 2009; Artinian et al., 2019) and by an increase in mEPSC frequency (Ran et al., 2009), suggesting presynaptic mechanisms of expression. Moreover, quantal analysis of EPSCs evoked by minimal stimulation in slice culture indicated an increase in quantal content and quantal size during L-LTP$_{mGluR1}$, consistent with coordinated pre- and post-synaptic changes (Ran et al., 2012). The increase in quantal content may result from increased release probability or new release sites (Ran et al., 2012). Conforming with the increase in quantal size, peak-scaled nonstationary fluctuation analysis of mEPSCs indicated that an increase in both single-channel conductance and number of functional receptors contribute to the increase in the postsynaptic response during L-LTP$_{mGluR1}$ (Ran et al., 2012). In acute slices, L-LTP$_{mGluR1}$ induced by DHPG is expressed by an increase in EPSC potency, but no change in paired-pulse ratio, whereas L-LTP$_{mGluR1}$ induced by TBS stimulation is expressed by an increase in EPSC potency and a decrease in paired-pulse ratio (Artinian et al., 2019). Similarly, L-LTP$_{mGluR1}$ induced by contextual fear conditioning is expressed by an increase in spontaneous EPSC amplitude and frequency, as well as an increase in potency of EPSCs evoked by minimal stimulation but no change in the paired-pulse ratio (Artinian et al., 2019), indicating that pre- and post-synaptic expression mechanisms do not always occur jointly during L-LTP$_{mGluR1}$.

Other Types of Synaptic Plasticity in SOM Interneurons

Interestingly, another form of plasticity called anti-Hebbian LTP is induced at excitatory synapses onto CA1 OLM interneurons by pairing presynaptic stimulation with postsynaptic membrane hyperpolarization (Kullmann and Lamsa, 2007). The anti-Hebbian LTP is NMDAR-independent and dependent on CP-AMPARs. This form of LTP is not specific to SOM interneurons and can be induced in fast-spiking PV interneurons (axo-axonic cells and basket cells; Kullmann and Lamsa, 2007). The diversity in types of long-term plasticity at SOM interneuron synapses in the hippocampal CA1 region suggests multiple roles in long-lasting regulation of the CA1 network.

In CA3, excitatory synapses onto interneurons display different types of synaptic plasticity including NMDA-dependent LTP and NMDAR-independent LTD (Laezza et al., 1999; Laezza and Dingledine, 2004). However, whether synaptic plasticity occurs at synapses onto CA3 SOM interneurons remains to be determined.

In DG, however, excitatory synapses onto both types of SOM interneurons, HIPP and HIL cells, show long-term synaptic plasticity (Yuan et al., 2017). In these cases, plasticity is induced by the application of an associative burst frequency stimulation at 30 Hz (aBFS) of afferents paired with postsynaptic action potentials, a stimulation protocol aimed at mimicking fast rhythmic neuronal network activity patterns at gamma (30–100 Hz) frequencies in DG. Remarkably, aBFS induces long-lasting depression (LTD) of excitatory synapses from GC onto HIPP cells, but LTP of excitatory synapses from GC and mossy cells onto HIL cells (Yuan et al., 2017). The increase and the decrease in the failure rate of synaptic transmission accompanying LTD in HIPP cells and LTP in HIL cells, respectively, suggest that both phenomena involve presynaptic expression mechanisms (Yuan et al., 2017). These results indicate that long-term synaptic plasticity in DG HIPP cells differ from that in CA1 OLM cells. Thus, although both cell types provide local dendritic feedback inhibition, their synapses from excitatory inputs display different types of long-term changes, indicating region-specific plasticity properties.

REGULATION OF CA1 NETWORK METAPLASTICITY BY PLASTICITY OF EXCITATORY SYNAPSES OF SOM INTERNEURONS

As mentioned previously, early work established that afferents of inhibitory interneurons express long-term potentiation (Buzsaki and Eidelberg, 1982). Coupled with the finding that pharmacological inhibition of GABAergic transmission facilitated the induction of LTP at PC excitatory synapses (Wigstrom and Gustafsson, 1983), this led to the concept that plasticity at excitatory synapses in interneurons increase inhibition of PCs and dampen LTP at PC excitatory synapses. However, more recent work indicates that multiple types of synaptic plasticity at excitatory synapses onto inhibitory interneurons have more complex actions in hippocampal networks (Kullmann and Lamsa, 2007; Pelletier and Lacaille, 2008).

Long-Term Plasticity of Excitatory Synapses Controls SOM Interneuron Firing and Synaptic Output

Dendrite-projecting SOM interneurons provide efficient suppression of CA1 PC dendritic excitatory synaptic inputs and synaptically-evoked burst firing (Lovett-Barron et al., 2012). *In vivo* during spatial navigation, dendritic inhibition by SOM interneurons suppresses the firing of PCs in their place fields, as well as PC burst firing (Royer et al., 2012). But dendritic inhibition is not static, and the recruitment of recurrent dendritic inhibition in PCs is dynamic during short trains of stimulation (Pouille and Scanziani, 2004). At the onset of a series of stimuli,

soma- and proximal dendrite-targeting recurrent inhibition are elicited. Later in the series of stimuli, recurrent inhibition is evoked in the distant dendritic regions. Thus, during repetitive activation of PCs, recurrent inhibition switches from transient somatic inhibition to late persistent dendritic inhibition (Pouille and Scanziani, 2004). These dynamic changes in dendritic inhibition are due in part to a late and persistent recruitment on SOM interneuron (OLM cell) firing during short trains of CA1 PC stimulation.

Induction of Hebbian LTP during voltage clamp recordings requires the pairing of presynaptic stimulation with postsynaptic depolarization (Perez et al., 2001). However, during current clamp recordings, presynaptic TBS stimulation alone is sufficient to activate mGluR1a and evoke EPSPs that trigger postsynaptic firing of action potentials in SOM interneurons, and thus, induce Hebbian LTP (Vasuta et al., 2015). Using the TBS induction protocol in slices permits the assessment of the functional impact of Hebbian LTP in SOM interneurons. As synaptic efficacy is improved during Hebbian LTP at excitatory synapses in SOM interneurons, the synaptically-evoked firing of SOM interneurons should show long-lasting increases after Hebbian LTP. Indeed, short trains of afferents stimulation in slices elicit two patterns of evoked firing in SOM interneurons (BiC and OLM cells): an onset-transient firing consistent with activation of CA3 afferents; or a late-persistent firing consistent with activation of CA1 afferents (Croce et al., 2010). After application of the TBS induction protocol for Hebbian LTP, onset-transient responses are unchanged but late-persistent firing responses of SOM interneurons show long-term increases (Croce et al., 2010). These long-term changes in synaptically-evoked firing are prevented by the application of the selective mGluR1α antagonist LY367385 during the TBS induction (Croce et al., 2010). These results suggest that Hebbian LTP at excitatory synapses translates into an increase in output firing of SOM interneurons (Croce et al., 2010).

Using a similar approach during the whole-cell recording of inhibitory postsynaptic currents (IPSCs) in CA1 pyramidal cells, the TBS induction protocol for Hebbian LTP produces long-term increases in postsynaptic inhibitory responses in pyramidal cells (Lapointe et al., 2004). The long-term increase in inhibition is not accompanied by any change in excitatory postsynaptic response, and is prevented in mGluR1 knockout mice that lack Hebbian LTP in SOM interneurons (Lapointe et al., 2004). These findings suggest that Hebbian LTP at excitatory synapses of SOM interneurons translates in long-term increases in SOM cell firing and pyramidal cell inhibition (**Figure 5**).

Long-Term Plasticity of SOM Interneuron Excitatory Synapses Controls CA1 Network Metaplasticity

Synaptic plasticity is bidirectionally modulated by prior cellular and/or synaptic activity, a phenomenon called metaplasticity (plasticity of synaptic plasticity; Bear, 1995). In the hippocampus, long-term plasticity at SC-CA1 PC synapses is regulated by multiple metaplastic mechanisms, including both homo- and hetero-synaptic processes (Abraham, 2008). In CA1, the dendrite-projecting SOM interneurons have emerged as central players in the regulation of the local network metaplasticity. Optogenetic activation of CA1 SOM interneurons (OLM cells) dampens information flow from the entorhinal cortex through the TA pathway *via* direct inhibition of CA1 PCs distal dendrites, and facilitates information flow from CA3 through the SC pathway *via* inhibition of other inhibitory interneurons (Leao et al., 2012). In addition, CA1 OLM cells regulate the metaplasticity of TA and SC pathways (**Figure 5**). Optogenetic activation of OLM cells during LTP induction decreases LTP at TA-PC synapses, whereas it facilitates LTP at SC-PC synapses (Leao et al., 2012).

Since Hebbian LTP at excitatory synapses onto SOM interneurons results in long-term changes in their output firing and inhibition of pyramidal cells, it should also result in long-term regulation of plasticity at SC and TA synapses onto PCs (**Figure 5**). Indeed, application of the TBS induction protocol for Hebbian LTP in SOM interneurons does not affect basal transmission at SC-PC synapses, but increases the magnitude of LTP at SC-PC synapses elicited 30 min later (Vasuta et al., 2015). This facilitation of LTP at SC-PC synapses is prevented by optogenetic silencing of SOM interneurons during the TBS induction protocol, or by the mGluR1α antagonist LY367385, suggesting that Hebbian LTP in SOM interneurons result in long-term upregulation of plasticity of SC-PC synapses (Vasuta et al., 2015). Likewise, application of the induction protocol for mGluR1-dependent late LTP (L-LTP$_{mGluR1}$) in SOM interneurons facilitates LTP of SC-PC synapses elicited 2 h later (Artinian et al., 2019). This persistent facilitation of LTP at SC-PC synapses is absent in mice with conditional knock-out of *Rptor* in SOM interneurons that lack L-LTP$_{mGluR1}$, suggesting that long-term upregulation of plasticity of SC-PC synapses lasting hours results from late-LTP at excitatory synapses onto SOM interneurons (Artinian et al., 2019). De-phosphorylation of the eukaryotic initiation factor 2 α subunit (eIF2α) by synaptic activity is a key regulator of mRNA translation and late-LTP in PCs (Costa-Mattioli et al., 2007). Knock-in mice with a mutated non-phosphorylatable eIF2α (eIF2a^{S51A}) show facilitation of late-LTP in CA1 PCs (Costa-Mattioli et al., 2007). Interestingly, conditional knock-in of eIF2α^{S51A} specifically in SOM interneurons, upregulates mRNA translation in SOM interneurons, reduces inhibitory synaptic transmission in CA1 PCs, and facilitates induction of L-LTP at SC-PC synapses (Sharma et al., 2020). Altogether these findings suggest that synaptic plasticity at excitatory synapses of SOM interneurons acts as a long-term metaplasticity switch at SC-PCs synapses *via* disinhibition (**Figure 5**).

Similarly, long-term plasticity at excitatory synapses of SOM interneurons may also regulate metaplasticity of TA synapses of PCs. Application of the TBS induction protocol for Hebbian LTP in SOM interneurons does not affect basal transmission at TA-PC synapses but decreases the magnitude of LTP that is elicited 30 min later at these synapses (Sharma et al., 2020). Importantly, this down-regulation of LTP at TA-PC synapses is increased in mice with conditional knock-in of the non-phosphorylatable eIF2a^{S51A} in SOM interneurons that result

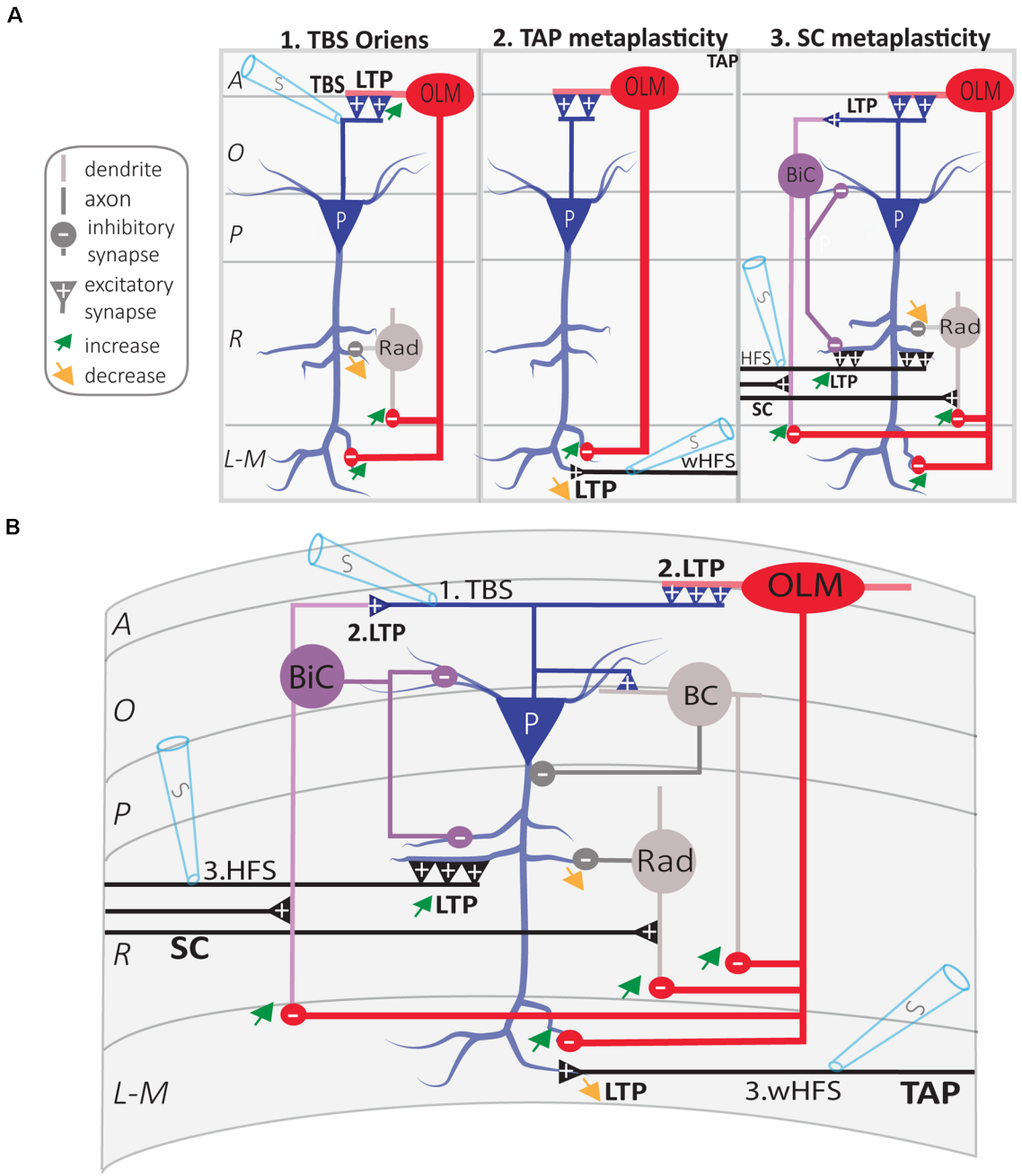

FIGURE 5 | Regulation of CA1 network metaplasticity by plasticity at excitatory synapses of SOM interneurons. **(A)** Diagrams of synaptic plasticity of SOM interneurons and regulation of CA1 network. (A1) Theta burst stimulation (TBS) at the O/A border induces LTP of CA1 PC synapses onto SOM interneurons (OLM cell). LTP at input synapses results in an increased firing of OLM cell, which leads to increased postsynaptic inhibition of (i) PC distal dendrites and (ii) *radiatum* interneurons (rad). This leads to the increased inhibition of distal dendrites in *stratum lacunosum-moleculare* (L-M), and disinhibition of more proximal dendrites in *stratum radiatum* (R). (A2) LTP of excitatory inputs of OLM cell results in TA pathway metaplasticity. Because of distal dendritic inhibition increase, tetanization of the temporoammonic (TA) pathway produces less LTP at TA-PC synapses. (A3) LTP of excitatory inputs of OLM cell results in SC pathway metaplasticity. Because of proximal dendritic disinhibition, tetanization of Schaffer collaterals (SC) produces larger LTP at SC-PC synapses. As electrically induced TBS also produces LTP at PC-BiC synapses, the overall results on BiC inhibition of PCs remain undetermined. **(B)** Integration of synaptic mechanisms described above: 1. TBS of PC axons; 2. LTP at PC-OLM synapses results in more inhibition of distal PC dendrites and disinhibition of proximal PC dendrites; the end-result of LTP at PC-BiC synapses on BiC inhibition of PC remains undetermined. 3. Metaplastic changes of CA1 circuit: increased LTP at SC-PC synapses and decreased LTP at TA-PC synapses. Abbreviations for CA1 layers: A, *alveus*; O, *oriens*; P, *pyramidale*; R, *radiatum*; L-M, *lacunosum-moleculare.* Abbreviations for CA1 afferent inputs: SC, Schaffer collateral pathway; TAP, temporo-ammonic pathway. Abbreviations for SOM cell types: (red) OLM, *oriens/lacunosum-moleculare* cell; (violet) BiC, bistratified cell. Abbreviations for other cell types: (blue) P, pyramidal cell; (gray) BC, basket cell; (gray) Rad, unidentified *stratum radiatum* interneurons. Other Abbreviation: S, stimulation electrode.

in upregulated mRNA translation in these cells and impaired inhibition of PCs (Sharma et al., 2020). Thus, long-term plasticity at excitatory synapses of SOM interneurons may act as a bidirectional long-term metaplasticity switch in the CA1 network to differentially regulate long-term plasticity of SC and TA synapses of PCs (**Figure 5**).

SOM INTERNEURONS IN HIPPOCAMPUS-DEPENDENT LEARNING AND MEMORY

At the behavioral level, the dendritic inhibition mediated by SOM interneurons plays a key role in hippocampus-dependent learning and memory (Lovett-Barron et al., 2014). The contribution of SOM interneurons has been studied particularly in the dorsal part of CA1, in relation to the encoding of spatial and contextual memory by PCs.

A combination of *in vivo* calcium imaging with pharmacogenetic and optogenetic manipulations of SOM interneurons in the CA1 hippocampus of mice revealed that dendritic inhibition by SOM interneurons is necessary for contextual fear memory formation (Lovett-Barron et al., 2014). During contextual conditioning, aversive stimuli activate, *via* septal cholinergic inputs, SOM interneurons that target PC dendrites. The activation of SOM interneurons leads to inhibition of PC distal dendrites that receive aversive sensory excitation from the entorhinal cortex (Lovett-Barron et al., 2014). Inactivating dendrite-targeting SOM interneurons during aversive stimuli increases PC responses and prevents fear learning (Lovett-Barron et al., 2014). Thus, activation of dendritic inhibition by SOM interneurons may be a mechanism for the exclusion of aversive stimuli from hippocampal contextual representations that is necessary during fear learning (Lovett-Barron et al., 2014).

Interestingly, GABAergic cells from the brainstem nucleus incertus (NI) selectively inhibit hippocampal SOM interneurons directly, and indirectly by inhibiting septal excitatory inputs to SOM interneurons (Szonyi et al., 2019). NI GABAergic inputs to the hippocampus are activated by relevant salient environmental stimuli *in vivo* (Szonyi et al., 2019). In addition, optogenetic manipulations of NI GABAergic neurons during contextual fear conditioning modify the strength of contextual fear memory: activation of NI GABA neurons impairs, whereas inhibition improves contextual fear memory (Szonyi et al., 2019). Thus, SOM interneuron gating of PC TA sensory inputs during contextual learning may be regulated by the brainstem NI inhibitory system.

Long-Term Plasticity of SOM Interneuron Excitatory Synapses in Learning and Memory

Cell-specific transgenic mouse approaches were used to test whether there is a functional role of long-term plasticity at SOM interneuron excitatory synapses in hippocampal learning and memory (Artinian et al., 2019). Downregulation of mTORC1 activity was achieved by cell-specific conditional knock-down of the gene for the essential mTORC1 component *Rptor* in SOM interneurons, whereas upregulation of mTORC1 activity was attained by cell-specific conditional knock-down of the mTORC1 repressor *Tsc1* gene. At the behavioral level, loss of mTORC1 function specifically in SOM interneurons impaired contextual fear and spatial long-term memories, but spared sensory-motor gating, hippocampus-dependent short-term contextual memory, and hippocampus-independent long-term auditory-cued fear memory (Artinian et al., 2019). In contrast, upregulation of mTORC1 activity specifically in SOM interneurons augmented spatial and contextual fear memories, and impaired discrimination (Artinian et al., 2019).

As mentioned before, at the cellular level, bidirectional regulation of mTORC1 activity in SOM interneurons differentially regulates mGluR1-mediated late-LTP at SOM interneurons excitatory synapses, whereas at the network level, the SOM interneuron late-LTP induction protocol upregulates metaplasticity of the SC pathway in PCs, in a mTORC1-dependent manner. Moreover, using *ex vivo* whole-cell recordings after training, contextual fear learning was found to persistently increase the efficacy of excitatory synapses of SOM interneurons *via* mGluR1 and mTORC1. These findings link mTORC1 to learning-induced long-term plasticity of SOM interneuron excitatory synapses, regulation of CA1 network metaplasticity, and hippocampal long-term memory consolidation (Artinian et al., 2019). Thus, long-term plasticity at SOM interneuron excitatory synapses may play a role in spatial/contextual information encoding by CA1 PCs, by promoting on a long timescale the internal representations by the hippocampal CA3 pathway while dampening external representations *via* the extrahippocampal entorhinal inputs (Artinian et al., 2019).

Recent work manipulating another pathway to enhance memory, de-phosphorylation of the translation initiation factor eIF2α (Costa-Mattioli et al., 2007), further support the idea that SOM interneurons synaptic plasticity is important for memory formation (Sharma et al., 2020). Contextual fear learning reduces the phosphorylation of eIF2α in hippocampal PCs and SOM interneurons, but not in PV interneurons (Sharma et al., 2020). Moreover, cell-specific conditional knock-in of the non-phosphorylatable $eIF2\alpha^{S51A}$ in PCs or in SOM interneurons upregulates general mRNA translation in these cells and is sufficient to increase long-term contextual fear memory (Sharma et al., 2020). Silencing CA1 SOM interneurons, using the inhibitory designer receptor exclusively activated by designer drug (DREADD), during the consolidation of fear memory, reverses the increase in contextual fear memory in the SOM interneurons conditional knock-in mice (Sharma et al., 2020), indicating that hippocampal CA1 SOM interneurons are pivotal for memory consolidation. As mentioned above, these behavioral changes suggest that a reduction in eIF2α phosphorylation in SOM interneurons promotes memory formation *via* two mechanisms; first, it increases the responsiveness of PCs to SC inputs by disinhibition and thereby facilitates LTP at these synapses; and second, it suppresses LTP in the TA pathway, thereby modulating sensory inputs from the entorhinal cortex

(Sharma et al., 2020). These findings suggest the existence of two autonomous and complementary memory consolidation processes mediated by eIF2α-dependent translational control in PCs and SOM interneurons: (i) translational changes in excitatory PCs help to facilitate memory consolidation by mediating synaptic plasticity in a sparse population of CA1 PCs; and (ii) translational changes in SOM interneurons facilitate memory consolidation by gating synaptic plasticity in the CA1 PCs circuit.

Dorso-Ventral Differences in SOM Interneuron Function

The research reviewed so far on CA1 SOM interneurons and hippocampal function has been mostly concerned with interneurons of the dorsal hippocampus. However, recent work suggests differences in the function of CA1 SOM interneurons along the dorsoventral hippocampal axis (Siwani et al., 2018). Targeted expression of optogenetic tools in CA1 OLM cells expressing the nicotinic receptor α2 subunit (OLMα2) was used to activate or silence these cells in freely moving mice during contextual passive avoidance tasks and novel object recognition (Siwani et al., 2018). Activation of intermediate CA1 OLMα2 interneurons during passive avoidance learning impairs aversive memory, whereas silencing of OLMα2 cells has no effect. In contrast, silencing of dorsal CA1 OLMα2 interneurons impairs aversive memory (Siwani et al., 2018). For object recognition, silencing of intermediate CA1 OLMα2 interneurons during training enhances object memory, while their activation impairs it. In contrast, silencing dorsal CA1 OLMα2 cells has no effect on object memory (Siwani et al., 2018). To summarize, in contrast to dorsal CA1, intermediate CA1 OLMα2 cell activity is not required for contextual fear memory. However, their activation reduces both contextual fear and object memory (Siwani et al., 2018). Thus, intermediate OLMα2 cells can modulate object or fear-related representations. These findings suggest that intermediate OLMα2 cells may be silenced during fear memory formation, meaning that in the intermediate CA1, the inputs from the TAP to CA1 PCs may not be dampened in the learning process. This is consistent with the memory impairment induced by the optogenetic activation of these cells during the aversive stimuli presentation or during object exploration (Siwani et al., 2018). Alternatively, the memory impairment induced by intermediate OLMα2 cell activation may mean that proper memory formation requires the activation of a sparse number of cells and that optogenetic stimulation activates many of them. Interestingly, intermediate OLMα2 cells display increased sensitivity for acetylcholine compared to dorsal CA1 OLMα2 cells which could mean that these cells are more entrained by septal inputs and play a role in timing the inputs onto CA1 PCs. Thus, activating intermediate OLMα2 cells with optogenetics could have disrupted the proper convergence of inputs. Lastly, the increase of object recognition following intermediate OLMα2 cell inhibition during object exploration could indicate that their role is to gate the size of the engram encoding object memory, as seen in other hippocampal areas (see below, Stefanelli et al., 2016), and inhibiting these cells would lead to a stronger but less precise memory.

The role of SOM interneurons in contextual fear memory also appears different in the dentate gyrus (DG) than in the dorsal CA1 hippocampus (Stefanelli et al., 2016). Silencing DG SOM interneurons with inhibitory DREADD, during contextual fear conditioning, increases contextual fear memory and the size of the c-Fos expressing granule cell engram (Stefanelli et al., 2016). Activation of DG SOM interneurons using excitatory DREADD during contextual fear training, impairs contextual fear memory and reduces the number of c-Fos expressing granule cells (Stefanelli et al., 2016). Thus, DG SOM interneurons, most likely HIPP cells, may gate the size of the DG neuronal ensemble encoding contextual memory *via* dendritic lateral inhibition of granule cells (Stefanelli et al., 2016).

SOM Interneurons and Place Cells

During spatial exploration, a subset of dorsal CA1 pyramidal cells progressively displays increased firing when the animal approaches a specific location. Each place cell demonstrates a preference for a different location (place field; O'Keefe and Dostrovsky, 1971). Place cells are characterized by a slow ramp-like depolarization of membrane potential (*Vm*) driving increased AP discharge when the animal passes through the place field (Harvey et al., 2009; Lee et al., 2012; Bittner et al., 2015). The fluctuations in PCs *Vm* drive their output firing, and the formation of place cells is mediated by synaptic potentiation of a specific subset of excitatory inputs (Bittner et al., 2015; Sheffield et al., 2017). In CA1 PCs, dendritic plateau potentials are generated by the coincident activation of CA3 and entorhinal cortex inputs, leading to increased output firing and LTP of perforant path synapses (Takahashi and Magee, 2009), and the induction of place field in PCs (Bittner et al., 2015).

Inhibitory interneurons play a cardinal role in achieving input selectivity necessary to drive place cells output firing (Grienberger et al., 2017). Optogenetic silencing of CA1 SOM or PV interneurons, or both populations, in awake head-fixed mice, performing a spatial navigation task increases PCs output firing in their place fields, without affecting their firing rate out-of-field (Royer et al., 2012; Grienberger et al., 2017). This is consistent with the dendrite-targeting interneurons role in regulating complex spiking and perisomatic-targeting interneurons regulating AP timing (Royer et al., 2012). Thus, inhibitory interneurons may be critical during place cell firing by controlling their excitatory inputs, by limiting dendritic amplification and suppressing out-of-field excitatory inputs (Grienberger et al., 2017). By that mean, SOM interneurons participate in the control of the plasticity of specific relevant inputs (Takahashi and Magee, 2009).

Recent works *in vivo* revealed that CA1 PCs exhibit place field plasticity following the initiation of dendritic plateau potentials occurring naturally in behaving mice or induced artificially by the injection of a depolarizing current through the recording pipette (Bittner et al., 2015, 2017). This synaptic plasticity is termed behavioral timescale synaptic plasticity (BTSP), in which active excitatory inputs within seconds before or after the generation of dendritic plateau potentials are selectively

potentiated, contrary to the classical Hebbian plasticity in which a coincident activation of the presynaptic and the postsynaptic neuron within a narrow time window is required (Bittner et al., 2017; Magee and Grienberger, 2020). BTSP can be induced *ex vivo* in hippocampal acute slices by pairing stimulations of the presynaptic input with dendritic plateau potential in the postsynaptic PC, is pathway-specific, and requires the activation of NMDAR and L-type Ca^{2+} channels (Bittner et al., 2017; Magee and Grienberger, 2020). Interestingly, during spatial navigation, when an animal transits from familiar to a new environment, SOM interneurons-mediated dendritic inhibition transiently decreases which causes a short–lasting increase in PCs dendritic excitability, whereas during the same period, PV interneurons-mediated perisomatic inhibition increases (Sheffield et al., 2017; Sheffield and Dombeck, 2019). Notably, the transient decrease in dendritic inhibition may serve as a time window in which increased dendritic plateau potentials in PCs promotes synaptic potentiation to occur in selective inputs to drive place output firing once the inhibitory system recovers in the familiar environment.

Hence, SOM interneurons have a determining role in place field formation by regulating dendritic plateau potentials and synaptic plasticity induction in selective excitatory inputs necessary for network adaptation to environmental changes.

SOM INTERNEURONS AND ASTROCYTES

In addition to pre- and post-synaptic neurons, glial cells and particularly astrocytes can actively modulate synaptic transmission in hippocampal circuits through bidirectional communication with neurons. The term "tripartite synapse" (Araque et al., 1999) encompasses the structural enwrapping of the synaptic cleft that allows astrocytes to sense neuronal activity through membrane receptors, leading to spatiotemporally coordinated fluctuations of intracellular Ca^{2+} levels and their ability to trigger gliotransmitters release (Araque et al., 2014; Bazargani and Attwell, 2016; Durkee and Araque, 2019). Despite multiple interactions between inhibitory networks and excitatory circuits (Klausberger and Somogyi, 2008), the current understanding of the bidirectional communications between neurons and astrocytes has emerged mainly from studies focusing on excitatory transmission leaving their involvement at inhibitory synapses ill-defined (Losi et al., 2014). However recent studies indicate that astrocytes also interact dynamically with inhibitory interneurons.

Through expression of GABA receptors [$GABA_A$Rs (Egawa et al., 2013; Ishibashi et al., 2019) and $GABA_B$Rs (Kang et al., 1998; Serrano et al., 2006; Ding et al., 2009; Haustein et al., 2014; Ishibashi et al., 2019)] and transporters (GAT-1 and GAT-3; Borden and Caplan, 1996; Ribak et al., 1996; Ishibashi et al., 2019), astrocytes can detect and respond to GABAergic activity with Ca^{2+} oscillations (Nilsson et al., 1993; Lia et al., 2019). Astrocytic GABAergic Ca^{2+} activities are mediated by several mechanisms involving voltage-sensitive Ca^{2+} channels, release from internal stores, G proteins, GATs, and sodium/calcium exchangers (NCXs; Perea et al., 2016; Ishibashi et al., 2019; Mederos and Perea, 2019; Lia et al., 2019). GABAergic activation

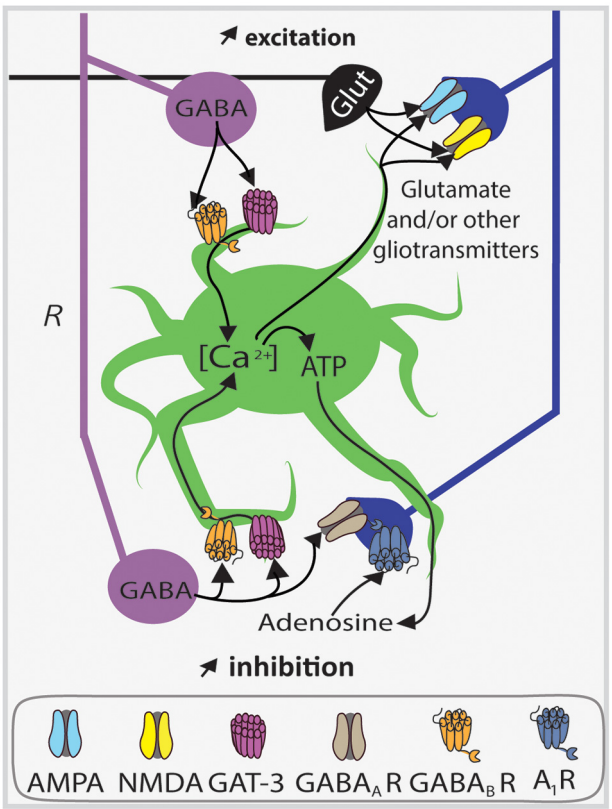

FIGURE 6 | Astrocytes upregulate synaptic inhibition and excitation of PC apical dendrites via SOM interneuron GABA release. Diagram of endogenous astrocyte-mediated positive feedback autoregulation of SOM interneuron (violet) dendritic inhibition of CA1 PCs (blue) and putative regulation of excitatory inputs. Astrocytes (green) sense GABA release through the GABA transporter GAT-3 and $GABA_B$Rs which induce an increase in astrocyte calcium concentration ($[Ca^{2+}]$) leading to the liberation of ATP in the extracellular compartment. After its release, ATP is converted into adenosine, which then activates pyramidal cell adenosine 1 receptors (A_1Rs). Activation of these receptors enhances SOM interneuron synaptic inhibition by a mechanism leading to gain of function of postsynaptic $GABA_A$Rs. Parallel to this mechanism, as a consequence of Ca^{2+} rise, astrocytes can probably release other gliotransmitters like glutamate to coordinate different synapses (black, excitatory synapse). Abbreviations: Glut, Glutamate; R, *radiatum*.

of astrocytes can lead to the release of various gliotransmitters such as glutamate (Kang et al., 1998; Andersson et al., 2007; Mariotti et al., 2016; Perea et al., 2016; Mederos and Perea, 2019), GABA (Lee et al., 2010; Yoon et al., 2011), ATP (Serrano et al., 2006; Boddum et al., 2016; Covelo and Araque, 2018; Matos et al., 2018) or efflux of chloride (Egawa et al., 2013) to modulate both excitatory and inhibitory transmission (**Figure 6**; Perea et al., 2016). While the heterogeneity of interneurons subtypes can give rise to diverse GABAergic signaling, we focus here on the interplay between hippocampal SOM interneurons, PCs, and astrocytes.

Intense depolarization of astrocytes induces Ca^{2+} increases that potentiate miniature inhibitory postsynaptic currents (mIPSCs) in pyramidal cells (Kang et al., 1998), that could originate at least in part from SOM interneurons with axons

in *stratum radiatum* (e.g., BiC). In addition, calcium uncaging in hippocampal astrocytes leads to an increase in spontaneous inhibitory postsynaptic currents (sIPSCs) frequency in *stratum radiatum* interneurons, which is induced by astrocytic glutamate release targeting kainate receptors on PCs (Liu et al., 2004). These studies show that astrocytes are well suited to establish another level of connection and regulation between inhibitory and excitatory networks in the hippocampus. Indeed GABAergic activation of hippocampal astrocytes was found to induce the release of ATP, which is converted extracellularly into adenosine in order to activate presynaptic adenosine A_1 receptors (A_1R) on PCs in the context of heterosynaptic depression at excitatory synapses of CA1 PCs (Serrano et al., 2006). This demonstrated a functional interplay between glial and GABAergic neuronal networks during heterosynaptic plasticity.

More recently, the use of optogenetic tools (Goshen, 2014) allowed the specific stimulation of different subtypes of interneurons to decipher the complex modulatory mechanisms of inhibitory synapses. In acute hippocampal slices, astrocytes specifically upregulate synaptic inhibition of PCs by SOM interneurons but not PV interneurons (Matos et al., 2018). Using the cell-specific expression of channelrhodopsin-2 in SOM or PV interneurons, optogenetic activation of SOM interneurons (evoking one or two action potentials) was found to induce Ca^{2+} activities in astrocyte processes mediated by $GABA_BR$ and GAT-3 (**Figure 6**; Matos et al., 2018). This in turn leads to the astrocytic release of ATP, converted extracellularly into adenosine that acts on postsynaptic A_1R to upregulate SOM interneuron inhibition onto PCs (**Figure 6**). This suggests an endogenous astrocyte-mediated positive feedback autoregulation of SOM interneuron dendritic inhibition of PCs (Matos et al., 2018). Importantly, this mechanism may be specific to SOM interneuron synapses as blockers of A_1R (DPCPX) or GAT-3 (SNAP-5114) failed to affect IPSCs evoked in PCs by optogenetic activation of PV interneurons (Matos et al., 2018). In addition, spontaneous synaptic inhibition (sIPSC) in PCs (which reflects more global inhibition of PCs coming from many interneurons subtypes), was depressed by inhibition of A_1R, GAT-3, or astrocytic Ca^{2+} oscillations (Matos et al., 2018). These findings point toward the possible existence of multiple astrocyte-mediated modulations of synaptic inhibition originating from different interneuron subtypes.

Consistent with this concept, other groups have shown different astrocyte modulation based on interactions with specific interneuron subtypes. Optogenetic activation of CA1 hippocampal astrocytes in slices increases the firing rate of CCK interneurons, but not PV interneurons, dependent on the release of ATP acting on P2Y-1R which leads to inhibition of a two-pore domain potassium channel (K2P; Tan et al., 2017). In contrast, optogenetic activation of astrocytic ATP release induces hyperpolarization of PCs mediated by its conversion into adenosine acting on A_1R (Tan et al., 2017). Interestingly in the neocortex, astrocyte Ca^{2+} elevations are differentially modulated by GABAergic signaling originating from PV or SOM interneurons. Optogenetic activation of PV interneurons induces weak Ca^{2+} elevations whereas SOM interneuron activation results in robust $GABA_B$ receptor-mediated Ca^{2+} elevations (Mariotti et al., 2018). Moreover, these astrocyte Ca^{2+} responses present a form of plasticity, with depression of Ca^{2+} elevations upon repetitive PV interneuron stimulations and enhancement after repetitive SOM interneuron stimulations. The latter relies on somatostatin released by SOM interneurons acting on somatostatin receptors along with astrocytic processes (Mariotti et al., 2018).

Taken together these results show that astrocytes dynamically influence both the input and output of inhibitory interneurons, notably SOM interneurons, and thus, astrocytes do not have only a passive role in inhibitory circuits, similarly to their contribution to excitatory circuits. Astrocytes are at the interface between excitatory and inhibitory synapses, and more detailed and comprehensive studies *in situ* and *in vivo* are required to refine our understanding of the inhibitory-glial-excitatory networks interplay involving SOM interneurons and its role in hippocampal synaptic plasticity and function.

SOM INTERNEURONS IN DISEASE

Given that hippocampal synaptic function and plasticity are impaired in brain disease with cognitive disorder, notably Alzheimer's disease (AD), SOM interneuron dysfunction may also contribute to these cognitive impairments.

In his initial observations after the death of the patient A. Deter suffering from dementia, Alois Alzheimer identified two characteristic cerebral lesions, neurofibrillary tangles made of Tau and senile plaques consisting of Aβ peptide aggregation (Graeber et al., 1997). Accumulation of $Aβ_{1–42}$ oligomers is one of the earliest events leading to direct or indirect synaptic alterations in AD (Huang and Mucke, 2012; Mucke and Selkoe, 2012). Electron microscopy and immunohistochemistry quantifications reported a significant decrease of synaptic density in the hippocampus of AD patients (Davies et al., 1987; Masliah et al., 2001). There is also a strong correlation between Aβ load in the patient brain and the extent of synapse loss (Wang et al., 1999). However, in many animal models of AD, despite cognitive alterations, these dendritic spine losses are not always present or as pronounced as in the human form of the disease (Auld et al., 2002; Elder et al., 2010). Accordingly, previous works have shown that different neuronal populations such as excitatory neurons vs. inhibitory interneurons, are differentially affected (Davies et al., 1980; Ramos et al., 2006). Moreover, inhibitory interneuron damage may occur before principal neuron alterations and the manifestation of symptoms. Focusing on SOM interneurons, a selective and early neurodegeneration of O-LM and HIPP cells was reported (Ramos et al., 2006). In the APP/PS1 transgenic mouse model of AD, several features of these SOM interneurons are altered. Using quantitative RT-PCR, SOM mRNA level is decreased as early as 4 months of age. Quantification of SOM interneurons showed a 60% reduction in cell numbers and the presence of dystrophic SOM interneurons in transgenic compared to wildtype animals (Ramos et al., 2006). Importantly, these alterations precede PC loss. Moreover, SOM interneuron modifications showed a linear relationship with Aβ presence/concentration indicating that SOM interneuron loss

is an early hippocampal neuropathology in this mouse model of AD.

Functional alterations of hippocampal SOM interneurons also accompany the early neuropathological changes in the AD mouse model. In an elegant *in vivo* study taking advantage of Gad1-eGFP mice crossbred with APP/PS1AD mouse model, structural changes consisting of SOM interneuron axon losses were observed at 4 months of age (Schmid et al., 2016). Moreover, chronic imaging of individual eGFP positive O-LM cells revealed that the normal age-dependent increase in the number of SOM interneuron dendritic spines is impaired in APP/PS1 mice. As for excitatory neurons (Koffie et al., 2009; Wei et al., 2010), the reduction in SOM interneuron spine density was correlated with Aβ proximity (<50 μm). Nevertheless, spine stability was impaired in APP/PS1 mice with a greater spine turnover associated with Aβ distance. These structural modifications may represent primary mechanisms to cope with pathological alterations of synapses during AD (Schmid et al., 2016). However, contextual fear learning-associated plasticity of dendritic spines of SOM interneurons is also affected in APP/PS1 mice. *In vivo* imaging showed that, after contextual fear conditioning, the gain of SOM interneuron dendritic spines is impaired in APP/PS1 mice, and this is associated with impaired contextual fear memory, compared to control mice (Schmid et al., 2016). Based on the cholinergic input that O-LM cells receive from the medial septum during aversive stimuli (Lovett-Barron et al., 2014) and the well-documented cholinergic degeneration in AD (Auld et al., 2002; Perez et al., 2007), the reduction in spine formation could be an indirect result of presynaptic cholinergic deficits. Using imaging with GCaMP6m calcium indicator, delivery of aversive air puffs in awake head-fixed mice evoked reduced Ca^{2+} responses in putative O-LM cells of APP/PS1 mice (Schmid et al., 2016). These observations are consistent with the observed reduction of medial septum trans-synaptically labeled monosynaptic afferents to SOM interneurons in APP/PS1 mice. In addition, pharmacological blockade of m1AChR or chemogenetic silencing of SOM interneurons during fear conditioning was sufficient to mimic the spine gain reduction and impair fear memory in control mice. Conversely, application of the m1AChR agonist Cevimeline during fear conditioning restored fear memory in APP/PS1 mice (Schmid et al., 2016). These findings demonstrate that early alterations in SOM interneuron spine plasticity may be linked to behavioral impairment and memory loss in AD. Thus, targeting presynaptic inputs or postsynaptic SOM interneurons may offer complementary therapeutic strategies. Indeed, strategies targeting somatostatin receptor subtype-4 (SST_4R) with agonists have recently been proposed to promote and restore the expression of altered subcortical mRNA genes in AD (Sandoval et al., 2019).

Another key function of SOM interneurons is their involvement in the generation of theta rhythms, which among other hippocampal network oscillations are impaired in AD models (Villette et al., 2010; Palop and Mucke, 2016; Mondragon-Rodriguez et al., 2018). An alternative to transgenic AD models is to inject directly soluble oligomers of Aβ peptide (Aβo). Recently, co-injection of Aβo and AAV5-Ef1a-DIO-hChR2(ET/TC)-mCherry to SST-Cre mice hippocampi was shown to replicate theta oscillations impairments (Villette et al., 2010; Palop and Mucke, 2016), and optogenetic activation of SOM interneurons restored the power of theta oscillations in Aβo injected animals (Chung et al., 2020). In addition, Aβo injection desynchronized SOM interneuron firing relative to theta oscillations, which was restored by optogenetic activation of SOM interneurons (Chung et al., 2020). Finally, in slices from Aβo-injected animals, optogenetic stimulation of SOM interneurons enhances sIPSCs received by CA1 PCs at theta frequencies (Chung et al., 2020). Together with the reported loss of SOM interneurons in the perirhinal cortex of AD patients correlated with Aβ load (Sanchez-Mejias et al., 2020), these findings suggest that targeting SOM interneurons may help restore network oscillations, which are heavily impacted during AD (Palop and Mucke, 2016). Interestingly, transplantation of interneuron progenitors can restore learning and memory in APOE4-KI mice in the presence of Aβ (Tong et al., 2014). Thus, maintaining proper SOM interneurons synaptic function and plasticity could be crucial to reduce the impact of AD on cognitive functions, as soon as Aβ production starts, or even later.

CONCLUSIONS AND FUTURE DIRECTIONS

The rapid pace of development of new experimental tools for cell-specific identification and manipulation of distinct neuron types will likely provide the means to address many interesting questions that remain unresolved about long-term plasticity at excitatory synapses of SOM interneurons and its role in hippocampal memory processes.

As mentioned above, hippocampal SOM interneurons are part of a group composed of many different cell types, even in a specific hippocampal region like CA1 (Pelkey et al., 2017). Presently, studies on synaptic plasticity of SOM interneurons have focused largely on CA1 BiC and OLM cells (Perez et al., 2001; Lamsa et al., 2007). However, other types of SOM interneurons include cells with both local and long-range projections (DP, BP, and ORP cells; Gulyas et al., 2003; Goldin et al., 2007; Jinno et al., 2007). The DP cells that project to the septum, as well as other hippocampal areas, may be particularly interesting to investigate given the crucial role of septal afferents to the hippocampus during spatial and contextual learning (Lovett-Barron et al., 2014; Schmid et al., 2016). Coupling of trans-synaptic monosynaptic labeling with DP cell-specific identification could be used to characterize and manipulate their excitatory synapses and potential long-term plasticity. It would be of interest to determine how the plasticity of DP interneuron excitatory synapses may play a role in coordinating changes across septal and hippocampal areas during hippocampal learning.

Another interesting issue is the regional difference in the function of SOM interneurons in hippocampal learning, and particularly that of OLM cells along the CA1 dorsoventral axis (Lovett-Barron et al., 2014; Siwani et al., 2018). The different roles of OLM cells in hippocampal learning were suggested to

be due to a difference in septal cholinergic inputs along the dorsoventral axis (Siwani et al., 2018). As long-term plasticity of SOM interneuron synapses in hippocampal learning has been examined mostly in the dorsal hippocampus (Artinian et al., 2019), it would be of interest to examine if there is a difference in SOM interneuron long-term synaptic plasticity along the dorsal-ventral axis, and if so, does it parallel the difference in the functional role of SOM interneurons in hippocampal learning.

Much progress has been achieved on characterizing Hebbian and mGluR1-mediated LTP at excitatory synapses of SOM interneurons, and its role in the regulation of hippocampal network and memory (Artinian et al., 2019). However other types of long-term synaptic plasticity occur at excitatory synapses of SOM interneurons, notably anti-Hebbian LTP at BiC and OLM cell synapses (Lamsa et al., 2007), LTP at HIL cell synapses, and LTD at HIPP cell synapses (Yuan et al., 2017). These multiple types of synaptic plasticity may each supports a different function in the formation and consolidation of hippocampus-dependent memory. Therefore, it would be important to demonstrate these roles in hippocampal function using cell-specific manipulations and hippocampal learning tasks.

Another largely unresolved question is the role of the release of the endogenous peptide SOM in SOM interneuron function. Ablation of the SOM gene or depletion of SOM by cysteamine treatment impairs LTP in CA1 PCs and impedes contextual fear memory (Kluge et al., 2008). Similarly, blocking LTP at excitatory synapses of SOM interneurons decreases contextual fear memory and prevents the facilitation of SC-PC LTP by SOM interneuron synaptic plasticity (Artinian et al., 2019). These effects on contextual fear memory and on CA1 PC synaptic plasticity suggest a possible link between the peptide SOM and long-term plasticity at SOM interneuron excitatory synapses. This would be interesting to explore given that endogenous SOM release is considered to be activity-dependent.

Work on astrocyte regulation of SOM interneuron synapses focused largely on astrocyte interactions at inhibitory synapses made by SOM interneurons on PC dendrites (Matos et al., 2018). However, astrocyte interactions are largely documented at excitatory synapses onto PCs and linked to regulation of long-term plasticity at these synapses (Araque et al., 2014). Interestingly, the activity of astrocytic glutamate transporters GLT-1 and GLAST regulate mGluR1-mediated slow EPSCs in CA1 OLM cells, indicating a functional interaction of astrocytes at excitatory synapses onto SOM interneurons (Huang et al., 2004). Thus, it would be interesting to characterize further astrocyte interactions at these excitatory synapses and determine how astrocytes may influence long-term synaptic plasticity of SOM interneurons, and consequently, hippocampal learning and memory.

Astrocytes also display functional heterogeneity, at least in terms of GABAergic-induced Ca^{2+} oscillation and gliotransmitter release. A single astrocyte can be modulated by distinct mechanisms (endocannabinoids and GABA) and can release at least two different gliotransmitters (ATP/adenosine and glutamate; Covelo and Araque, 2018). Given the different astrocytic modulation uncovered with SOM and other interneuron subtypes (Mariotti et al., 2018; Matos et al., 2018), it raises the question whether different subtypes of astrocytes may co-exist within a brain region. Astrocyte heterogeneity has already been reported between brain regions (Chai et al., 2017; Khakh and Deneen, 2019; Kohler et al., 2021). However, given the different firing properties of specific interneurons, do specific firing patterns govern the astrocytic responses or is it another level of modulation? These questions still need to be addressed.

Future progress on these and other questions will likely move forward our understanding of SOM interneuron synaptic plasticity and help uncover how these specific inhibitory cells contribute to hippocampal memory processes.

AUTHOR CONTRIBUTIONS

All authors contributed to the article and approved the submitted version.

FUNDING

This work and research in the laboratory of J-CL were supported by grants from the Canadian Institutes of Health Research (CIHR MOP-125985 and PJT-153311), a Research Centre grant (Centre Interdisciplinaire de Recherche sur le Cerveau et l'Apprentissage; CIRCA) from the Fonds de la Recherche du Québec—Santé (FRQS), and a Group grant from Université de Montréal (Groupe de Recherche sur le Système Nerveux Central; GRSNC). J-CL is the recipient of the Canada Research Chair in Cellular and Molecular Neurophysiology (CRC 950-231066). AK was supported by a fellowship from the Réseau de Médecine Génétique Appliquée (Montréal, Canada).

ACKNOWLEDGMENTS

We thank Drs. Isabel Laplante, François-Xavier Michon, and Darren Clarke for discussions and help with the manuscript.

REFERENCES

Abraham, W. C. (2008). Metaplasticity: tuning synapses and networks for plasticity. *Nat. Rev. Neurosci.* 9, 387–387. doi: 10.1038/nrn2356

Abraham, W. C., Jones, O. D., and Glanzman, D. L. (2019). Is plasticity of synapses the mechanism of long-term memory storage? *NPJ Sci. Learn* 4:9. doi: 10.1038/s41539-019-0048-y

Ali, A. B., and Thomson, A. M. (1998). Facilitating pyramid to horizontal oriens-alveus interneurone inputs: dual intracellular recordings in slices of rat hippocampus. *J. Physiol.* 507, 185–199. doi: 10.1111/j.1469-7793.1998.185bu.x

Andersson, M., Blomstrand, F., and Hanse, E. (2007). Astrocytes play a critical role in transient heterosynaptic depression in the rat hippocampal Ca1 region. *J. Physiol.* 585, 843–852. doi: 10.1113/jphysiol.2007.142737

Araque, A., Carmignoto, G., Haydon, P. G., Oliet, S. H., Robitaille, R., and Volterra, A. (2014). Gliotransmitters travel in time and space. *Neuron* 81, 728–739. doi: 10.1016/j.neuron.2014.02.007

Araque, A., Parpura, V., Sanzgiri, R. P., and Haydon, P. G. (1999). Tripartite synapses: glia, the unacknowledged partner. *Trends Neurosci.* 22, 208–215. doi: 10.1016/s0166-2236(98)01349-6

Artinian, J., and Lacaille, J.-C. (2018). Disinhibition in learning and memory circuits: new vistas for somatostatin interneurons and long-term synaptic plasticity. *Brain Res. Bull.* 141, 20–26. doi: 10.1016/j.brainresbull.2017.11.012

Artinian, J., Jordan, A., Khlaifia, A., Honore, E., La Fontaine, A., Racine, A. S., et al. (2019). Regulation of hippocampal memory by mtorc1 in somatostatin interneurons. *J. Neurosci.* 39, 8439–8456. doi: 10.1523/JNEUROSCI.0728-19.2019

Auld, D. S., Kornecook, T. J., Bastianetto, S., and Quirion, R. (2002). Alzheimer's disease and the basal forebrain cholinergic system: relations to β-amyloid peptides, cognition and treatment strategies. *Prog. Neurobiol.* 68, 209–245. doi: 10.1016/s0301-0082(02)00079-5

Bazargani, N., and Attwell, D. (2016). Astrocyte calcium signaling: the third wave. *Nat. Neurosci.* 19, 182–189. doi: 10.1038/nn.4201

Bear, M. F. (1995). Mechanism for a sliding synaptic modification threshold. *Neuron* 15, 1–4. doi: 10.1016/0896-6273(95)90056-x

Bittner, K. C., Grienberger, C., Vaidya, S. P., Milstein, A. D., Macklin, J. J., Suh, J., et al. (2015). Conjunctive input processing drives feature selectivity in hippocampal Ca1 neurons. *Nat. Neurosci.* 18, 1133–1142. doi: 10.1038/nn.4062

Bittner, K. C., Milstein, A. D., Grienberger, C., Romani, S., and Magee, J. C. (2017). Behavioral time scale synaptic plasticity underlies Ca1 place fields. *Science* 357, 1033–1036. doi: 10.1126/science.aan3846

Blasco-Ibáñez, J. M., and Freund, T. F. (1995). Synaptic input of horizontal interneurons in stratum oriens of the hippocampal Ca1 subfield: Structural basis of feed-back activation. *Eur. J. Neurosci.* 7, 2170–2180. doi: 10.1111/j.1460-9568.1995.tb00638.x

Boddum, K., Jensen, T. P., Magloire, V., Kristiansen, U., Rusakov, D. A., Pavlov, I., et al. (2016). Astrocytic gaba transporter activity modulates excitatory neurotransmission. *Nat. Commun.* 7:13572. doi: 10.1038/ncomms13572

Booker, S. A., and Vida, I. (2018). Morphological diversity and connectivity of hippocampal interneurons. *Cell Tissue Res.* 373, 619–641. doi: 10.1007/s00441-018-2882-2

Booker, S. A., Harada, H., Elgueta, C., Bank, J., Bartos, M., Kulik, A., et al. (2020). Presynaptic gabab receptors functionally uncouple somatostatin interneurons from the active hippocampal network. *eLife* 9:e51156. doi: 10.7554/eLife.51156

Booker, S. A., Loreth, D., Gee, A. L., Watanabe, M., Kind, P. C., Wyllie, D. J. A., et al. (2018). Postsynaptic gababrs inhibit l-type calcium channels and abolish long-term potentiation in hippocampal somatostatin interneurons. *Cell Rep.* 22, 36–43. doi: 10.1016/j.celrep.2017.12.021

Borden, L. A., and Caplan, M. J. (1996). GABA transporter heterogeneity: pharmacology and cellular localization. *Neurochem. Int.* 29, 335–356. doi: 10.1016/0197-0186(95)00158-1

Brazeau, P., Vale, W., Burgus, R., Ling, N., Butcher, M., Rivier, J., et al. (1973). Hypothalamic polypeptide that inhibits the secretion of immunoreactive pituitary growth hormone. *Science* 179, 77–79. doi: 10.1126/science.179.4068.77

Buhl, E. H., Szilágyi, T., Halasy, K., and Somogyi, P. (1996). Physiological properties of anatomically identified basket and bistratified cells in the Ca1 area of the rat hippocampus *in vitro*. *Hippocampus* 6, 294–305. doi: 10.1002/(SICI)1098-1063(1996)6:3<294::AID-HIPO7>3.0.CO;2-N

Buzsáki, G. (2002). Theta oscillations in the hippocampus. *Neuron* 33, 325–340. doi: 10.1016/s0896-6273(02)00586-x

Buzsaki, G., and Eidelberg, E. (1982). Direct afferent excitation and long-term potentiation of hippocampal interneurons. *J. Neurophysiol.* 48, 597–607. doi: 10.1152/jn.1982.48.3.597

Buzsaki, G., Horvath, Z., Urioste, R., Hetke, J., and Wise, K. (1992). High-frequency network oscillation in the hippocampus. *Science* 256, 1025–1027. doi: 10.1126/science.1589772

Cammalleri, M., Bagnoli, P., and Bigiani, A. (2019). Molecular and cellular mechanisms uderlying somatostatin-based signaling in two model neural networks: the retina and the hippocampus. *Int. J. Mol. Sci.* 20:2506. doi: 10.3390/ijms20102506

Caporale, N., and Dan, Y. (2008). Spike timing-dependent plasticity: a hebbian learning rule. *Annu. Rev. Neurosci.* 31, 25–46. doi: 10.1146/annurev.neuro.31.060407.125639

Chai, H., Diaz-Castro, B., Shigetomi, E., Monte, E., Octeau, J. C., Yu, X., et al. (2017). Neural circuit-specialized astrocytes: transcriptomic, proteomic, morphological and functional evidence. *Neuron* 95, 531.e9.–549.e9. doi: 10.1016/j.neuron.2017.06.029

Chevaleyre, V., Takahashi, K. A., and Castillo, P. E. (2006). Endocannabinoid-mediated synaptic plasticity in the cns. *Annu. Rev. Neurosci.* 29, 37–76. doi: 10.1146/annurev.neuro.29.051605.112834

Chittajallu, R., Craig, M. T., McFarland, A., Yuan, X., Gerfen, S., Tricoire, L., et al. (2013). Dual origins of functionally distinct O-LM interneurons revealed by differential 5-HT3AR expression. *Nat. Neurosci.* 16, 1598–1607. doi: 10.1038/nn.3538

Chung, H., Park, K., Jang, H. J., Kohl, M. M., and Kwag, J. (2020). Dissociation of somatostatin and parvalbumin interneurons circuit dysfunctions underlying hippocampal theta and gamma oscillations impaired by amyloid beta oligomers *in vivo*. *Brain Struct. Funct.* 225, 935–954. doi: 10.1007/s00429-020-02044-3

Citri, A., and Malenka, R. C. (2008). Synaptic plasticity: multiple forms, functions and mechanisms. *Neuropsychopharmacology* 33, 18–41. doi: 10.1038/sj.npp.1301559

Costa-Mattioli, M., Gobert, D., Stern, E., Gamache, K., Colina, R., Cuello, C., et al. (2007). Eif2α phosphorylation bidirectionally regulates the switch from short- to long-term synaptic plasticity and memory. *Cell* 129, 195–206. doi: 10.1016/j.cell.2007.01.050

Covelo, A., and Araque, A. (2018). Neuronal activity determines distinct gliotransmitter release from a single astrocyte. *eLife* 7:e32237. doi: 10.7554/eLife.32237

Croce, A., Pelletier, J. G., Tartas, M., and Lacaille, J. C. (2010). Afferent-specific properties of interneuron synapses underlie selective long-term regulation of feedback inhibitory circuits in Ca1 hippocampus. *J. Physiol.* 588, 2091–2107. doi: 10.1113/jphysiol.2010.189316

Csaba, Z., and Dournaud, P. (2001). Cellular biology of somatostatin receptors. *Neuropeptides* 35, 1–23. doi: 10.1054/npep.2001.0848

Davies, C., Mann, D., Sumpter, P., and Yates, P. (1987). A quantitative morphometric analysis of the neuronal and synaptic content of the frontal and temporal cortex in patients with Alzheimers disease. *J. Neurol. Sci.* 78, 151–164. doi: 10.1016/0022-510x(87)90057-8

Davies, C. H., Starkey, S. J., Pozza, M. F., and Collingridge, G. L. (1991). GABA autoreceptors regulate the induction of LTP. *Nature* 349, 609–611. doi: 10.1038/349609a0

Davies, P., Katzman, R., and Terry, R. D. (1980). Reduced somatostatin-like immunoreactivity in cerebral cortex from cases of Alzheimer disease and Alzheimer senile dementa. *Nature* 288, 279–280. doi: 10.1038/288279a0

De Bundel, D., Aourz, N., Kiagiadaki, F., Clinckers, R., Hoyer, D., Kastellakis, A., et al. (2010). Hippocampal SST1 receptors are autoreceptors and do not affect seizures in rats. *NeuroReport* 21, 254–258. doi: 10.1097/WNR.0b013e3283353a64

Degro, C. E., Kulik, A., Booker, S. A., and Vida, I. (2015). Compartmental distribution of GABAB receptor-mediated currents along the somatodendritic axis of hippocampal principal cells. *Front. Synaptic Neurosci.* 7:6. doi: 10.3389/fnsyn.2015.00006

Delfs, J., and Dichter, M. (1983). Effects of somatostatin on mammalian cortical neurons in culture: physiological actions and unusual dose response characteristics. *J. Neurosci.* 3, 1176–1188. doi: 10.1523/JNEUROSCI.03-06-01176.1983

Ding, S., Wang, T., Cui, W., and Haydon, P. G. (2009). Photothrombosis ischemia stimulates a sustained astrocytic calcium signaling *in vivo*. *Glia* 57, 767–776. doi: 10.1002/glia.20804

Durkee, C. A., and Araque, A. (2019). Diversity and specificity of astrocyte-neuron communication. *Neuroscience* 396, 73–78. doi: 10.1016/j.neuroscience.2018.11.010

Dutar, P., and Nicoll, R. A. (1988). A physiological role for gabab receptors in the central nervous system. *Nature* 332, 156–158. doi: 10.1038/332156a0

Egawa, K., Yamada, J., Furukawa, T., Yanagawa, Y., and Fukuda, A. (2013). Choride homeodynamics in gap junction-coupled astrocytic networks on activation of gabaergic synapses. *J. Physiol.* 591, 3901–3917. doi: 10.1113/jphysiol.2013.257162

Elder, G. A., Gama Sosa, M. A., and De Gasperi, R. (2010). Transgenic mouse models of Alzheimers disease. *Mt. Sinai. J. Med.* 77, 69–81. doi: 10.1002/msj.20159

Elfant, D., Pál, B. Z., Emptage, N., and Capogna, M. (2008). Specific inhibitory synapses shift the balance from feedforward to feedback inhibition of hippocampal Ca1 pyramidal cells. *Eur. J. Neurosci.* 27, 104–113. doi: 10.1111/j.1460-9568.2007.06001.x

Eyre, M. D., and Bartos, M. (2019). Somatostatin-expressing interneurons form axonal projections to the contralateral hippocampus. *Front. Neural Circuits* 13:56. doi: 10.3389/fncir.2019.00056

Feldman, D. E. (2012). The spike-timing dependence of plasticity. *Neuron* 75, 556–571. doi: 10.1016/j.neuron.2012.08.001

Ferraguti, F., Cobden, P., Pollard, M., Cope, D., Shigemoto, R., Watanabe, M., et al. (2004). Immunolocalization of metabotropic glutamate receptor 1α (mglur1α) in distinct classes of interneuron in the Ca1 region of the rat hippocampus. *Hippocampus* 14, 193–215. doi: 10.1002/hipo.10163

Freund, T. F., and Buzsáki, G. (1996). Interneurons of the hippocampus. *Hippocampus* 6, 347–470. doi: 10.1002/(SICI)1098-1063(1996)6:4<347::AID-HIPO1>3.0.CO;2-I

Friend, L. N., Williamson, R. C., Merrill, C. B., Newton, S. T., Christensen, M. T., Petersen, J., et al. (2019). Hippocampal stratum oriens somatostatin-positive cells undergo cb1-dependent long-term potentiation and express endocannabinoid biosynthetic enzymes. *Molecules* 24:1306. doi: 10.3390/molecules24071306

Gastambide, F., Viollet, C., Lepousez, G., Epelbaum, J., and Guillou, J.-L. (2008). Hippocampal sstr4 somatostatin receptors control the selection of memory strategies. *Psychopharmacology* 202:153. doi: 10.1007/s00213-008-1204-x

Goldin, M., Epsztein, J., Jorquera, I., Represa, A., Ben-Ari, Y., Crépel, V., et al. (2007). Synaptic kainate receptors tune oriens-lacunosum moleculare interneurons to operate at theta frequency. *J. Neurosci.* 27, 9560–9572. doi: 10.1523/JNEUROSCI.1237-07.2007

Goshen, I. (2014). The optogenetic revolution in memory research. *Trends Neurosci.* 37, 511–522. doi: 10.1016/j.tins.2014.06.002

Graeber, M., Kösel, S., Egensperger, R., Banati, R., Müller, U., Bise, K., et al. (1997). Rediscovery of the case described by alois Alzheimer in 1911: historical, histological and molecular genetic analysis. *Neurogenetics* 1, 73–80. doi: 10.1007/s100480050011

Grienberger, C., Milstein, A. D., Bittner, K. C., Romani, S., and Magee, J. C. (2017). Inhibitory suppression of heterogeneously tuned excitation enhances spatial coding in Ca1 place cells. *Nat. Neurosci.* 20, 417–426. doi: 10.1038/nn.4486

Guillou, J.-L., Micheau, J., and Jaffard, R. (1993). Effects of intrahippocampal injections of somatostatin and cysteamine on spatial discrimination learning in mice. *Psychobiology* 21, 265–271. doi: 10.3758/BF03327144

Gulyas, A. I., Hajos, N., Katona, I., and Freund, T. F. (2003). Interneurons are the local targets of hippocampal inhibitory cells which project to the medial septum. *Eur. J. Neurosci.* 17, 1861–1872. doi: 10.1046/j.1460-9568.2003.02630.x

Günther, T., Tulipano, G., Dournaud, P., Bousquet, C., Csaba, Z., Kreienkamp, H-J., et al. (2018). International union of basic and clinical pharmacology. Cv. Somatostatin receptors: structure, function, ligands and new nomenclature. *Pharmacol. Rev.* 70, 763–835. doi: 10.1124/pr.117.015388

Halasy, K., Buhl, E. H., Lörinczi, Z., Tamás, G., and Somogyi, P. (1996). Synaptic target selectivity and input of gabaergic basket and bistratified interneurons in the Ca1 area of the rat hippocampus. *Hippocampus* 6, 306–329. doi: 10.1002/(SICI)1098-1063(1996)6:3<306::AID-HIPO8>3.0.CO;2-K

Han, Z. S., Buhl, E. H., Lorinczi, Z., and Somogyi, P. (1993). A high degree of spatial selectivity in the axonal and dendritic domains of physiologically identified local-circuit neurons in the dentate gyrus of the rat hippocampus. *Eur. J. Neurosci.* 5, 395–410. doi: 10.1111/j.1460-9568.1993.tb00507.x

Harvey, C. D., Collman, F., Dombeck, D. A., and Tank, D. W. (2009). Intracellular dynamics of hippocampal place cells during virtual navigation. *Nature* 461, 941–946. doi: 10.1038/nature08499

Haustein, M. D., Kracun, S., Lu, X. H., Shih, T., Jackson-Weaver, O., Tong, X., et al. (2014). Conditions and constraints for astrocyte calcium signaling in the hippocampal mossy fiber pathway. *Neuron* 82, 413–429. doi: 10.1016/j.neuron.2014.02.041

Hosp, J. A., Struber, M., Yanagawa, Y., Obata, K., Vida, I., Jonas, P., et al. (2014). Morpho-physiological criteria divide dentate gyrus interneurons into classes. *Hippocampus* 24, 189–203. doi: 10.1002/hipo.22214

Houser, C. R. (2007). Interneurons of the dentate gyrus: an overview of cell types, terminal fields and neurochemical identity. *Prog. Brain Res.* 163, 217–232. doi: 10.1016/S0079-6123(07)63013-1

Hou, Z. H., and Yu, X. (2013). Activity-regulated somatostatin expression reduces dendritic spine density and lowers excitatory synaptic transmission *via* postsynaptic somatostatin reptor 4. *J. Biol. Chem.* 288, 2501–2509. doi: 10.1074/jbc.M112.419051

Huang, Y., and Mucke, L. (2012). Alzheimer mechanisms and therapeutic strategies. *Cell* 148, 1204–1222. doi: 10.1016/j.cell.2012.02.040

Huang, Y. H., Sinha, S. R., Tanaka, K., Rothstein, J. D., and Bergles, D. E. (2004). Astrocyte glutamate transporters regulate metabotropic glutamate receptor-mediated excitation of hippocampal interneurons. *J. Neurosci.* 24, 4551–4559. doi: 10.1523/JNEUROSCI.5217-03.2004

Ishibashi, M., Egawa, K., and Fukuda, A. (2019). Diverse actions of astrocytes in gabaergic signaling. *Int. J. Mol. Sci.* 20:2964. doi: 10.3390/ijms20122964

Jinno, S., Klausberger, T., Marton, L. F., Dalezios, Y., Roberts, J. D., Fuentealba, P., et al. (2007). Neuronal diversity in gabaergic long-range projections from the hippocampus. *J. Neurosci.* 27, 8790–8804. doi: 10.1523/JNEUROSCI.1847-07.2007

Josselyn, S. A., and Frankland, P. W. (2018). Memory allocation: mechanisms and function. *Annu. Rev. Neurosci.* 41, 389–413. doi: 10.1146/annurev-neuro-080317-061956

Kandel, E. R. (2001). The molecular biology of memory storage: a dialogue between genes and synapses. *Science* 294, 1030–1038. doi: 10.1126/science.1067020

Kandel, E. R., Dudai, Y., and Mayford, M. R. (2014). The molecular and systems biology of memory. *Cell* 157, 163–186. doi: 10.1016/j.cell.2014.03.001

Kang, J., Jiang, L., Goldman, S. A., and Nedergaard, M. (1998). Astrocyte-mediated potentiation of inhibitory synaptic transmission. *Nat. Neurosci.* 1, 683–692. doi: 10.1038/3684

Katona, I., Acsády, L., and Freund, T. F. (1999). Postsynaptic targets of somatostatin-immunoreactive interneurons in the rat hippocampus. *Neuroscience* 88, 37–55. doi: 10.1016/s0306-4522(98)00302-9

Katona, L., Lapray, D., Viney, T. J., Oulhaj, A., Borhegyi, Z., Micklem, B. R., et al. (2014). Sleep and movement differentiates actions of two types of somatostatin-expressing gabaergic interneuron in rat hippocampus. *Neuron* 82, 872–886. doi: 10.1016/j.neuron.2014.04.007

Katona, L., Micklem, B., Borhegyi, Z., Swiejkowski, D. A., Valenti, O., Viney, T. J., et al. (2017). Behavior-dependent activity patterns of gabaergic long-range projecting neurons in the rat hippocampus. *Hippocampus* 27, 359–377. doi: 10.1002/hipo.22696

Kepecs, A., and Fishell, G. (2014). Interneuron cell types are fit to function. *Nature* 505, 318–326. doi: 10.1038/nature12983

Khakh, B. S., and Deneen, B. (2019). The emerging nature of astrocyte diversity. *Annu. Rev. Neurosci.* 42, 187–207. doi: 10.1146/annurev-neuro-070918-050443

Klausberger, T., and Somogyi, P. (2008). Neuronal diversity and temporal dynamics: the unity of hippocampal circuit operations. *Science* 321, 53–57. doi: 10.1126/science.1149381

Klausberger, T., Magill, P. J., Márton, L. F., Roberts, J. D. B., Cobden, P. M., Buzsáki, G., et al. (2003). Brain-state- and cell-type-specific firing of hippocampal interneurons *in vivo*. *Nature* 421, 844–848. doi: 10.1038/nature01374

Klausberger, T., Marton, L. F., Baude, A., Roberts, J. D., Magill, P. J., and Somogyi, P. (2004). Spike timing of dendrite-targeting bistratified cells during hippocampal network oscillations *in vivo*. *Nat. Neurosci.* 7, 41–47. doi: 10.1038/nn1159

Kluge, C., Stoppel, C., Szinyei, C., Stork, O., and Pape, H. C. (2008). Role of the somatostatin system in contextual fear memory and hippocampal plasticity. *Learn Mem.* 3, 252–260. doi: 10.1101/lm.793008

Koffie, R. M., Meyer-Luehmann, M., Hashimoto, T., Adams, K. W., Mielke, M. L., Garcia-Alloza, M., et al. (2009). Oligomeric amyloid β associates with postsynaptic densities and correlates with excitatory synapse loss near senile plaques. *Proc. Natl. Acad. Sci. U S A* 106, 4012–4017. doi: 10.1073/pnas.0811698106

Kohler, S., Winkler, U., and Hirrlinger, J. (2021). Heterogeneity of astrocytes in gray and white matter. *Neurochem. Res.* 46, 3–14. doi: 10.1007/s11064-019-02926-x

Kougioumoutzakis, A., Pelletier, J. G., Laplante, I., Khlaifia, A., and Lacaille, J. C. (2020). Trpc1 mediates slow excitatory synaptic transmission in hippocampal oriens/alveus interneurons. *Mol. Brain* 13:12. doi: 10.1186/s13041-020-0558-9

Krulich, L., Dhariwal, A. P. S., and McCann, S. M. (1968). Stimulatory and inhibitory effects of purified hypothalamic extracts on growth hormone release from rat pituitary *in vitro*1. *Endocrinology* 83, 783–790. doi: 10.1210/endo-83-4-783

Kullmann, D. M., and Lamsa, K. P. (2007). Long-term synaptic plasticity in hippocampal interneurons. *Nat. Rev. Neurosci.* 8, 687–699. doi: 10.1038/nrn2207

Kullmann, D. M., and Lamsa, K. P. (2011). Interneurons go plastic. *Neuropharmacology* 60:711. doi: 10.1016/j.neuropharm.2011.02.001

Lacaille, J. C., and Williams, S. (1990). Membrane properties of interneurons in stratum oriens-alveus of the Ca1 region of rat hippocampus *in vitro*. *Neuroscience* 36, 349–359. doi: 10.1016/0306-4522(90)90431-3

Lacaille, J. C., Mueller, A. L., Kunkel, D. D., and Schwartzkroin, P. A. (1987). Local circuit interactions between oriens/alveus interneurons and Ca1 pyramidal cells in hippocampal slices: electrophysiology and morphology. *J. Neurosci.* 7, 1979–1993. doi: 10.1523/JNEUROSCI.07-07-01979.1987

Laezza, F., and Dingledine, R. (2004). Voltage-controlled plasticity at glur2-deficient synapses onto 1319 hippocampal interneurons. *J. Neurophysiol.* 92, 3575–3581. doi: 10.1152/jn.00425.2004

Laezza, F., Doherty, J. J., and Dingledine, R. (1999). Long-term depression in hippocampal interneurons: Joint requirement for pre- and postsynaptic events. *Science* 285, 1411–1414. doi: 10.1126/science.285.5432.1411

Lamirault, L., Guillou, J. L., Micheau, J., and Jaffard, R. (2001). Intrahippocampal injections of somatostatin dissociate acquisition from the flexible use of place responses. *Eur. J. Neurosci.* 14, 567–570. doi: 10.1046/j.0953-816x.2001.01672.x

Lamsa, K., Heeroma, J. H., and Kullmann, D. M. (2005). Hebbian ltp in feed-forward inhibitory interneurons and the temporal fidelity of input discrimination. *Nat. Neurosci.* 8, 916–924. doi: 10.1038/nn1486

Lamsa, K. P., Heeroma, J. H., Somogyi, P., Rusakov, D. A., and Kullmann, D. M. (2007). Anti-hebbian long-term potentiation in the hippocampal feedback inhibitory circuit. *Science* 315, 1262–1266. doi: 10.1126/science.1137450

Lapointe, V., Morin, F., Ratte, S., Croce, A., Conquet, F., and Lacaille, J. C. (2004). Synapse-specific mglur1-dependent long-term potentiation in interneurones regulates mouse hippocampal inhibition. *J. Physiol.* 555, 125–135. doi: 10.1113/jphysiol.2003.053603

Larimer, P., and Strowbridge, B. W. (2008). Nonrandom local circuits in the dentate gyrus. *J. Neurosci.* 28, 12212–12223. doi: 10.1523/JNEUROSCI.3612-08.2008

Le Vasseur, M., Ran, I., and Lacaille, J. C. (2008). Selective induction of metabotropic glutamate receptor 1- and metabotropic glutamate receptor 5-dependent chemical long-term potentiation at oriens/alveus interneuron synapses of mouse hippocampus. *Neuroscience* 151, 28–42. doi: 10.1016/j.neuroscience.2007.09.071

Leao, R. N., Mikulovic, S., Leao, K. E., Munguba, H., Gezelius, H., Enjin, A., et al. (2012). Olm interneurons differentially modulate ca3 and entorhinal inputs to hippocampal Ca1 neurons. *Nat. Neurosci.* 15, 1524–1530. doi: 10.1038/nn.3235

Lee, D., Lin, B. J., and Lee, A. K. (2012). Hippocampal place fields emerge upon single-cell manipulation of excitability during behavior. *Science* 337, 849–853. doi: 10.1126/science.1221489

Lee, S., Yoon, B.-E., Berglund, K., Oh, S.-J., Park, H., Shin, H.-S., et al. (2010). Channel-mediated tonic gaba release from glia. *Science* 330, 790–796. doi: 10.1126/science.1184334

Lia, A., Zonta, M., Requie, L. M., and Carmignoto, G. (2019). Dynamic interactions between gabaergic and astrocytic networks. *Neurosci. Lett.* 689, 14–20. doi: 10.1016/j.neulet.2018.06.026

Liguz-Lecznar, M., Urban-Ciecko, J., and Kossut, M. (2016). Somatostatin and somatostatin-containing neurons in shaping neuronal activity and plasticity. *Front. Neural Circuits* 10:48. doi: 10.3389/fncir.2016.00048

Liu, Q. S., Xu, Q., Arcuino, G., Kang, J., and Nedergaard, M. (2004). Astrocyte-mediated activation of neuronal kainate receptors. *Proc. Natl. Acad. Sci. U S A* 101, 3172–3177. doi: 10.1073/pnas.0306731101

Losi, G., Mariotti, L., and Carmignoto, G. (2014). Gabaergic interneuron to astrocyte signaling: a neglected form of cell communication in the brain. *Philos. Trans. R. Soc. Lond. B Biol. Sci.* 369:20130609. doi: 10.1098/rstb.2013.0609

Lovett-Barron, M., Kaifosh, P., Kheirbek, M. A., Danielson, N., Zaremba, J. D., Reardon, T. R., et al. (2014). Dendritic inhibition in the hippocampus supports fear learning. *Science* 343, 857–863. doi: 10.1126/science.1247485

Lovett-Barron, M., Turi, G. F., Kaifosh, P., Lee, P. H., Bolze, F., Sun, X. H., et al. (2012). Regulation of neuronal input transformations by tunable dendritic inhibition. *Nat. Neurosci.* 15, 423–430. doi: 10.1038/nn.3024

Luján, R., Nusser, Z., Roberts, J. D. B., Shigemoto, R., and Somogyi, P. (1996). Perisynaptic location of metabotropic glutamate receptors mglur1 and mglur5 on dendrites and dendritic spines in the rat hippocampus. *Eur. J. Neurosci.* 8, 1488–1500. doi: 10.1038/s41467-021-22435-2

Maccaferri, G., and McBain, C. J. (1996). Long-term potentiation in distinct subtypes of hippocampal nonpyramidal neurons. *J. Neurosci.* 16, 5334–5343. doi: 10.1523/JNEUROSCI.16-17-05334.1996

Maccaferri, G., David, J., Roberts, B., Szucs, P., Cottingham, C. A., and Somogyi, P. (2000). Cell surface domain specific postsynaptic currents evoked by identified gabaergic neurones in rat hippocampus *in vitro*. *J. Physiol.* 524, 91–116. doi: 10.1111/j.1469-7793.2000.t01-3-00091.x

Magee, J. C., and Grienberger, C. (2020). Synaptic plasticity forms and functions. *Annu. Rev. Neurosci.* 43, 95–117. doi: 10.1146/annurev-neuro-090919-022842

Malenka, R. C., and Bear, M. F. (2004). Ltp and ltd: An embarrassment of riches. *Neuron* 44, 5–21. doi: 10.1016/j.neuron.2004.09.012

Mariotti, L., Losi, G., Lia, A., Melone, M., Chiavegato, A., Gómez-Gonzalo, M., et al. (2018). Interneuron-specific signaling evokes distinctive somatostatin-mediated responses in adult cortical astrocytes. *Nat. Commun.* 9:82. doi: 10.1038/s41467-017-02642-6

Mariotti, L., Losi, G., Sessolo, M., Marcon, I., and Carmignoto, G. (2016). The inhibitory neurotransmitter gaba evokes long-lasting ca(2+) oscillations in cortical astrocytes. *Glia* 64, 363–373. doi: 10.1002/glia.22933

Masliah, E., Mallory, M., Alford, M., DeTeresa, R., Hansen, L., McKeel, D., et al. (2001). Altered expression of synaptic proteins occurs early during progression of Alzheimer's disease. *Neurology* 56, 127–129. doi: 10.1212/wnl.56.1.127

Matos, M., Bosson, A., Riebe, I., Reynell, C., Vallée, J., Laplante, I., et al. (2018). Astrocytes detect and upregulate transmission at inhibitory synapses of somatostatin interneurons onto pyramidal cells. *Nat. commun.* 9, 1–15. doi: 10.1038/s41467-018-06731-y

McBain, C. J., Freund, T. F., and Mody, I. (1999). Glutamatergic synapses onto hippocampal interneurons: Precision timing without lasting plasticity. *Trends Neurosci.* 22, 228–235. doi: 10.1016/s0166-2236(98)01347-2

Mederos, S., and Perea, G. (2019). Gabaergic-astrocyte signaling: a refinement of inhibitory brain networks. *Glia* 67, 1842–1851. doi: 10.1002/glia.23644

Melzer, S., Michael, M., Caputi, A., Eliava, M., Fuchs, E. C., Whittington, M. A., et al. (2012). Long-range-projecting gabaergic neurons modulate inhibition in hippocampus and entorhinal cortex. *Science* 335, 1506–1510. doi: 10.1126/science.1217139

Mikulovic, S., Restrepo, C. E., Hilscher, M. M., Kullander, K., and Leao, R. (2015). Novel markers for olm interneurons in the hippocampus. *Front. Cell. Neurosci.* 9:201. doi: 10.3389/fncel.2015.00201

Mondragon-Rodriguez, S., Salas-Gallardo, A., Gonzalez-Pereyra, P., Macias, M., Ordaz, B., Pena-Ortega, F., et al. (2018). Phosphorylation of tau protein correlates with changes in hippocampal theta oscillations and reduces hippocampal excitability in Alzheimers model. *J. Biol. Chem.* 293, 8462–8472. doi: 10.1074/jbc.RA117.001187

Morris, R. G. (2003). Long-term potentiation and memory. *Philos. Trans. R. Soc. Lond. B Biol. Sci.* 358, 643–647. doi: 10.1098/rstb.2002.1230

Morris, R. G., Anderson, E., Lynch, G. S., and Baudry, M. (1986). Selective impairment of learning and blockade of long-term potentiation by an n-methyl-d-aspartate receptor antagonist, ap5. *Nature* 319, 774–776. doi: 10.1038/319774a0

Mott, D. D., and Lewis, D. V. (1991). Facilitation of the induction of long-term potentiation by gabab receptors. *Science* 252, 1718–1720. doi: 10.1126/science.1675489

Mucke, L., and Selkoe, D. J. (2012). Neurotoxicity of amyloid beta-protein: Synaptic and network dysfunction. *Cold Spring Harb. Perspect. Med.* 2:a006338. doi: 10.1101/cshperspect.a006338

Muller, C., and Remy, S. (2014). Dendritic inhibition mediated by o-lm and bistratified interneurons in the hippocampus. *Front. Synaptic Neurosci.* 6:23. doi: 10.3389/fnsyn.2014.00023

Nilsson, M., Eriksson, P. S., Rönnbäck, L., and Hansson, E. (1993). GABA induces ca^{2+} transients in astrocytes. *Neuroscience* 54, 605–614. doi: 10.1016/0306-4522(93)90232-5

O'Keefe, J., and Dostrovsky, J. (1971). The hippocampus as a spatial map. Preliminary evidence from unit activity in the freely-moving rat. *Brain Res.* 34, 171–175. doi: 10.1016/0006-8993(71)90358-1

O'Keefe, J., and Nadel, L. (1978). *The Hippocampus as a Cognitive Map*. Oxford: Clarendon Press.

Oliva, A. A. Jr., Jiang, M., Lam, T., Smith, K. L., and Swann, J. W. (2000). Novel hippocampal interneuronal subtypes identified using transgenic mice that express green fluorescent protein in gabaergic interneurons. *J. Neurosci.* 20, 3354–3368. doi: 10.1523/JNEUROSCI.20-09-03354.2000

Olpe, H.-R., Balcar, V. J., Bittiger, H., Rink, H., and Sieber, P. (1980). Central actions of somatostatin. *Eur. J. Pharmacol.* 63, 127–133. doi: 10.1016/0014-2999(80)90436-7

Palop, J. J., and Mucke, L. (2016). Network abnormalities and interneuron dysfunction in Alzheimer disease. *Nat. Rev. Neurosci.* 17, 777–792. doi: 10.1038/nrn.2016.141

Pelkey, K. A., Chittajallu, R., Craig, M. T., Tricoire, L., Wester, J. C., and McBain, C. J. (2017). Hippocampal gabaergic inhibitory interneurons. *Physiol. Rev.* 97, 1619–1747. doi: 10.1152/physrev.00007.2017

Pelletier, J. G., and Lacaille, J. C. (2008). Long-term synaptic plasticity in hippocampal feedback inhibitory networks. *Prog. Brain Res.* 169, 241–250. doi: 10.1016/S0079-6123(07)00014-3

Perea, G., Gómez, R., Mederos, S., Covelo, A., Ballesteros, J. J., Schlosser, L., et al. (2016). Activity-dependent switch of gabaergic inhibition into glutamatergic excitation in astrocyte-neuron networks. *eLife* 5:e20362. doi: 10.7554/eLife.20362

Perez, S. E., Dar, S., Ikonomovic, M. D., DeKosky, S. T., and Mufson, E. J. (2007). Cholinergic forebrain degeneration in the appswe/ps1δe9 transgenic mouse. *Neurobiol. Dis.* 28, 3–15. doi: 10.1016/j.nbd.2007.06.015

Perez, Y., Morin, F., and Lacaille, J. C. (2001). A hebbian form of long-term potentiation dependent on mglur1a in hippocampal inhibitory interneurons. *Proc. Natl. Acad. Sci. U S A* 98, 9401–9406. doi: 10.1073/pnas.161493498

Pike, F. G., Goddard, R. S., Suckling, J. M., Ganter, P., Kasthuri, N., and Paulsen, O. (2000). Distinct frequency preferences of different types of rat hippocampal neurones in response to oscillatory input currents. *J. Physiol.* 529, 205–213. doi: 10.1111/j.1469-7793.2000.00205.x

Pittman, Q. J., and Siggins, G. R. (1981). Somatostatin hyperpolarizes hippocampal pyramidal cells *in vitro*. *Brain Res.* 221, 402–408. doi: 10.1016/0006-8993(81)90791-5

Pouille, F., and Scanziani, M. (2004). Routing of spike series by dynamic circuits in the hippocampus. *Nature* 429, 717–723. doi: 10.1038/nature02615

Prévôt, T. D., Gastambide, F., Viollet, C., Henkous, N., Martel, G., Epelbaum, J., et al. (2017). Roles of hippocampal somatostatin receptor subtypes in stress response and emotionality. *Neuropsychopharmacology* 42, 1647–1656. doi: 10.1038/npp.2016.281

Ramos, B., Baglietto-Vargas, D., del Rio, J. C., Moreno-Gonzalez, I., Santa-Maria, C., Jimenez, S., et al. (2006). Early neuropathology of somatostatin/npy gabaergic cells in the hippocampus of a ps1xapp transgenic model of Alzheimers disease. *Neurobiol. Aging* 27, 1658–1672. doi: 10.1016/j.neurobiolaging.2005.09.022

Ran, I., Laplante, I., and Lacaille, J. C. (2012). Creb-dependent transcriptional control and quantal changes in persistent long-term potentiation in hippocampal interneurons. *J. Neurosci.* 32, 6335–6350. doi: 10.1523/JNEUROSCI.5463-11.2012

Ran, I., Laplante, I., Bourgeois, C., Pepin, J., Lacaille, P., Costa-Mattioli, M., et al. (2009). Persistent transcription- and translation-dependent long-term potentiation induced by mglur1 in hippocampal interneurons. *J. Neurosci.* 29, 5605–5615. doi: 10.1523/JNEUROSCI.5355-08.2009

Ribak, C. E., Tong, W. M., and Brecha, N. C. (1996). GABA plasma membrane transporters, gat-1 and gat-3, display different distributions in the rat hippocampus. *J. Comp. Neurol.* 367, 595–606. doi: 10.1002/(SICI)1096-9861(19960415)367:4<595::AID-CNE9>3.0.CO;2-#

Royer, S., Zemelman, B. V., Losonczy, A., Kim, J., Chance, F., Magee, J. C., et al. (2012). Control of timing, rate and bursts of hippocampal place cells by dendritic and somatic inhibition. *Nat. Neurosci.* 15, 769–775. doi: 10.1038/nn.3077

Sanchez-Mejias, E., Nunez-Diaz, C., Sanchez-Varo, R., Gomez-Arboledas, A., Garcia-Leon, J. A., Fernandez-Valenzuela, J. J., et al. (2020). Distinct disease-sensitive gabaergic neurons in the perirhinal cortex of Alzheimers mice and patients. *Brain Pathol.* 30, 345–363. doi: 10.1111/bpa.12785

Sandoval, K., Umbaugh, D., House, A., Crider, A., and Witt, K. (2019). Somatostatin receptor subtype-4 regulates mrna expression of amyloid-beta degrading enzymes and microglia mediators of phagocytosis in brains of 3xtg-ad mice. *Neurochem. Res.* 44, 2670–2680. doi: 10.1007/s11064-019-02890-6

Savanthrapadian, S., Meyer, T., Elgueta, C., Booker, S. A., Vida, I., and Bartos, M. (2014). Synaptic properties of som- and cck-expressing cells in dentate gyrus interneuron networks. *J. Neurosci.* 34, 8197–8209. doi: 10.1523/JNEUROSCI.5433-13.2014

Scharfman, H. E., and Schwartzkroin, P. A. (1988). Further studies of the effects of somatostatin and related peptides in area Ca1 of rabbit hippocampus. *Cell Mol. Biol.* 8, 411–429. doi: 10.1007/BF00711226

Scharfman, H. E., and Schwartzkroin, P. A. (1989). Selective depression of gaba-mediated ipsps by somatostatin in area Ca1 of rabbit hippocampal slices. *Brain Res.* 493, 205–211. doi: 10.1016/0006-8993(89)91155-4

Schettini, G. (1991). Brain somatostatin: receptor-coupled transducing mechanisms and role in cognitive functions. *Pharmacol. Res.* 23, 203–215. doi: 10.1016/s1043-6618(05)80080-5

Schmid, L. C., Mittag, M., Poll, S., Steffen, J., Wagner, J., Geis, H. R., et al. (2016). Dysfunction of somatostatin-positive interneurons associated with memory deficits in an Alzheimers disease model. *Neuron* 92, 114–125. doi: 10.1016/j.neuron.2016.08.034

Serrano, A., Haddjeri, N., Lacaille, J.-C., and Robitaille, R. (2006). Gabaergic network activation of glial cells underlies hippocampal heterosynaptic depression. *J. Neurosci.* 16, 5073–5081. doi: 10.1523/JNEUROSCI.5255-05.2006

Sharma, V., Sood, R., Khlaifia, A., Eslamizade, M. J., Hung, T.-Y., Lou, D., et al. (2020). Eif2α controls memory consolidation *via* excitatory and somatostatin neurons. *Nature* 586, 412–416. doi: 10.1038/s41586-020-2805-8

Sheffield, M. E., and Dombeck, D. A. (2019). Dendritic mechanisms of hippocampal place field formation. *Curr. Opin. Neurobiol.* 54, 1–11. doi: 10.1016/j.conb.2018.07.004

Sheffield, M. E. J., Adoff, M. D., and Dombeck, D. A. (2017). Increased prevalence of calcium transients across the dendritic arbor during place field formation. *Neuron* 96, 490–504.e5.doi: 10.1016/j.neuron.2017.09.029

Shigemoto, R., Kulik, A., Roberts, J. D. B., Ohishi, H., Nusser, Z., Kaneko, T., et al. (1996). Target-cell-specific concentration of a metabotropic glutamate receptor in the presynaptic active zone. *Nature* 381, 523–525. doi: 10.1038/381523a0

Sik, A., Penttonen, M., and Buzsaki, G. (1997). Interneurons in the hippocampal dentate gyrus: an *in vivo* intracellular study. *Eur. J. Neurosci.* 9, 573–588. doi: 10.1111/j.1460-9568.1997.tb01634.x

Siwani, S., França, A. S. C., Mikulovic, S., Reis, A., Hilscher, M. M., Edwards, S. J., et al. (2018). Olmα2 cells bidirectionally modulate learning. *Neuron* 99, 404.e3–412.e3.doi: 10.1016/j.neuron.2018.06.022

Somogyi, P., and Klausberger, T. (2005). Defined types of cortical interneurone structure space and spike timing in the hippocampus. *J. Physiol.* 562, 9–26. doi: 10.1113/jphysiol.2004.078915

Somogyi, P., Katona, L., Klausberger, T., Lasztóczi, B., and Viney, T. J. (2014). Temporal redistribution of inhibition over neuronal subcellular domains underlies state-dependent rhythmic change of excitability in the hippocampus. *Philos. Trans. R. Soc. Lond. B Biol. Sci.* 369:2010518. doi: 10.1098/rstb.2012.0518

Stefanelli, T., Bertollini, C., Lüscher, C., Muller, D., and Mendez, P. (2016). Hippocampal somatostatin interneurons control the size of neuronal memory ensembles. *Neuron* 89, 1074–1085. doi: 10.1016/j.neuron.2016.01.024

Sun, Y., Nguyen, A. Q., Nguyen, J. P., Le, L., Saur, D., Choi, J., et al. (2014). Cell-type-specific circuit connectivity of hippocampal Ca1 revealed through

cre-dependent rabies tracing. *Cell Rep.* 7, 269–280. doi: 10.1016/j.celrep.2014.02.030

Sylwestrak, E. L., and Ghosh, A. (2012). Elfn1 regulates target-specific release probability at Ca1-interneuron synapses. *Science* 338, 536–540. doi: 10.1126/science.1222482

Szonyi, A., Sos, K. E., Nyilas, R., Schlingloff, D., Domonkos, A., Takacs, V. T., et al. (2019). Brainstem nucleus incertus controls contextual memory formation. *Science* 364:eaaw0445. doi: 10.1126/science.aaw0445

Takahashi, H., and Magee, J. C. (2009). Pathway interactions and synaptic plasticity in the dendritic tuft regions of Ca1 pyramidal neurons. *Neuron* 62, 102–111. doi: 10.1016/j.neuron.2009.03.007

Tallent, M. K., and Siggins, G. R. (1997). Somatostatin depresses excitatory but not inhibitory neurotransmission in rat Ca1 hippocampus. *J. Neurophysiol.* 78, 3008–3018. doi: 10.1152/jn.1997.78.6.3008

Tan, Z., Liu, Y., Xi, W., Lou, H. F., Zhu, L., Guo, Z., et al. (2017). Glia-derived atp inversely regulates excitability of pyramidal and cck-positive neurons. *Nat. Commun.* 8:13772. doi: 10.1038/ncomms13772

Tonegawa, S., Mark, D. M., and Kitamura, T. (2018). The role of engram cells in the systems consolidation of memory. *Nat. Neurosci.* 19, 485–498. doi: 10.1038/s41583-018-0031-2

Tong, L. M., Djukic, B., Arnold, C., Gillespie, A. K., Yoon, S. Y., Wang, M. M., et al. (2014). Inhibitory interneuron progenitor transplantation restores normal learning and memory in APOe4 knock-in mice without or with abeta accumulation. *J. Neurosci.* 34, 9506–9515. doi: 10.1523/JNEUROSCI.0693-14.2014

Topolnik, L., Azzi, M., Morin, F., Kougioumoutzakis, A., and Lacaille, J. C. (2006). Mglur1/5 subtype-specific calcium signaling and induction of long-term potentiation in rat hippocampal oriens/alveus interneurones. *J. Physiol.* 575, 115–131. doi: 10.1113/jphysiol.2006.112896

Topolnik, L., Chamberland, S., Pelletier, J. G., Ran, I., and Lacaille, J. C. (2009). Activity-dependent compartmentalized regulation of dendritic ca^{2+} signaling in hippocampal interneurons. *J. Neurosci.* 29, 4658–4663. doi: 10.1523/JNEUROSCI.0493-09.2009

Topolnik, L., Congar, P., and Lacaille, J. C. (2005). Differential regulation of metabotropic glutamate receptor- and ampa receptor-mediated dendritic ca^{2+} signals by presynaptic and postsynaptic activity in hippocampal interneurons. *J. Neurosci.* 25, 990–1001. doi: 10.1523/JNEUROSCI.4388-04.2005

Toth, K., and McBain, C. J. (1998). Afferent-specific innervation of two distinct ampa receptor subtypes on single hippocampal interneurons. *Nat. Neurosci.* 1, 572–578. doi: 10.1038/2807

Tricoire, L., Pelkey, K. A., Erkkila, B. E., Jeffries, B. W., Yuan, X., and McBain, C. J. (2011). A blueprint for the spatiotemporal origins of mouse hippocampal interneuron diversity. *J. Neurosci.* 31, 10948–10970. doi: 10.1523/JNEUROSCI.0323-11.2011

Tukker, J. J., Fuentealba, P., Hartwich, K., Somogyi, P., and Klausberger, T. (2007). Cell type-specific tuning of hippocampal interneuron firing during gamma oscillations *in vivo*. *J. Neurosci.* 27, 8184–8189. doi: 10.1523/JNEUROSCI.1685-07.2007

Tyan, L., Chamberland, S., Magnin, E., Camiré, O., Francavilla, R., David, L. S., et al. (2014). Dendritic inhibition provided by interneuron-specific cells controls the firing rate and timing of the hippocampal feedback inhibitory circuitry. *J. Neurosci.* 34, 4534–4547. doi: 10.1523/JNEUROSCI.3813-13.2014

Udakis, M., Pedrosa, V., Chamberlain, S. E. L., Clopath, C., and Mellor, J. R. (2020). Interneuron-specific plasticity at parvalbumin and somatostatin inhibitory synapses onto Ca1 pyramidal neurons shapes hippocampal output. *Nat. Commun.* 11:4395. doi: 10.1038/s41467-020-18074-8

Unal, G., Crump, M. G., Viney, T. J., Éltes, T., Katona, L., Klausberger, T., et al. (2018). Spatio-temporal specialization of gabaergic septo-hippocampal neurons for rhythmic network activity. *Brain Struct. Funct.* 223, 2409–2432. doi: 10.1007/s00429-018-1626-0

Vanderwolf, C. H. (1969). Hippocampal electrical activity and voluntary movement in the rat. *Electroencephalogr. Clin. Neurophysiol.* 26, 407–418. doi: 10.1016/0013-4694(69)90092-3

Varga, C., Golshani, P., and Soltesz, I. (2012). Frequency-invariant temporal ordering of interneuronal discharges during hippocampal oscillations in awake mice. *Proc. Natl. Acad. Sci. U S A* 109, E2726–E2734. doi: 10.1073/pnas.1210929109

Vasuta, C., Artinian, J., Laplante, I., Hebert-Seropian, S., Elayoubi, K., and Lacaille, J.-C. (2015). Metaplastic regulation of Ca1 schaffer collateral pathway plasticity by hebbian mglur1a-mediated plasticity at excitatory synapses onto somatostatin-expressing interneurons. *eNeuro* 2:ENEURO.0051-15.2015. doi: 10.1523/ENEURO.0051-15.2015

Vécsei, L., and Widerlöv, E. (1988). Effects of intracerebroventricularly administered somatostatin on passive avoidance, shuttle-box behavior and open-field activity in rats. *Neuropeptides* 12, 237–242. doi: 10.1016/0143-4179(88)90061-3

Vécsei, L., Király, C., Bollók, I., Nagy, A., Varga, J., Penke, B., et al. (1984). Comparative studies with somatostatin and cysteamine in different behavioral tests on rats. *Pharmacol. Biochem. Behav.* 21, 833–837. doi: 10.1016/s0091-3057(84)80061-1

Vécsei, L., Pavo, I., Zsigo, J., Penke, B., and Widerlöv, E. (1989). Comparative studies of somatostatin-14 and some of its fragments on passive avoidance behavior, open field activity and on barrel rotation phenomenon in rats. *Peptides* 10, 1153–1157. doi: 10.1016/0196-9781(89)90007-7

Vezzani, A., Ruiz, R., Monno, A., Rizzi, M., Lindefors, N., Samanin, R., et al. (1993). Extracellular somatostatin measured by microdialysis in the hippocampus of freely moving rats: evidence for neuronal release. *J. Neurochem.* 60, 671–677. doi: 10.1111/j.1471-4159.1993.tb03200.x

Villette, V., Poindessous-Jazat, F., Simon, A., Lena, C., Roullot, E., Bellessort, B., et al. (2010). Decreased rhythmic gabaergic septal activity and memory-associated theta oscillations after hippocampal amyloid-beta pathology in the rat. *J. Neurosci.* 30, 10991–11003. doi: 10.1523/JNEUROSCI.6284-09.2010

Wang, J., Dickson, D. W., Trojanowski, J. Q., and Lee, V. M.-Y. (1999). The levels of soluble versus insoluble brain aβ distinguish Alzheimers disease from normal and pathologic aging. *Exp. Neurol.* 158, 328–337. doi: 10.1006/exnr.1999.7085

Wei, W., Nguyen, L. N., Kessels, H. W., Hagiwara, H., Sisodia, S., and Malinow, R. (2010). Amyloid beta from axons and dendrites reduces local spine number and plasticity. *Nat. Neurosci.* 13, 190–196. doi: 10.1038/nn.2476

Wierenga, C. J., and Wadman, W. J. (2003). Excitatory inputs to Ca1 interneurons show selective synaptic dynamics. *J. Neurophysiol.* 90, 811–821. doi: 10.1152/jn.00865.2002

Wigstrom, H., and Gustafsson, B. (1983). Facilitated induction of hippocampal long-lasting potentiation during blockade of inhibition. *Nature* 301, 603–604. doi: 10.1038/301603a0

Yoon, B.-E., Jo, S., Woo, J., Lee, J.-H., Kim, T., Kim, D., et al. (2011). The amount of astrocytic gaba positively correlates with the degree of tonic inhibition in hippocampal Ca1 and cerebellum. *Mol. Brain* 4, 1–7. doi: 10.1186/1756-6606-4-42

Yuan, M., Meyer, T., Benkowitz, C., Savanthrapadian, S., Ansel-Bollepalli, L., Foggetti, A., et al. (2017). Somatostatin-positive interneurons in the dentate gyrus of mice provide local- and long-range septal synaptic inhibition. *eLife* 6:e21105. doi: 10.7554/eLife.21105

Conflict of Interest: The authors declare that the research was conducted in the absence of any commercial or financial relationships that could be construed as a potential conflict of interest.

frontiers in Neural Circuits

REVIEW
published: 10 June 2021
doi: 10.3389/fncir.2021.687257

Interneuron Types and Their Circuits in the Basolateral Amygdala

*Norbert Hájos**

Laboratory of Network Neurophysiology, ELRN Institute of Experimental Medicine, Budapest, Hungary

The basolateral amygdala (BLA) is a cortical structure based on its cell types, connectivity features, and developmental characteristics. This part of the amygdala is considered to be the main entry site of processed and multisensory information delivered *via* cortical and thalamic afferents. Although GABAergic inhibitory cells in the BLA comprise only 20% of the entire neuronal population, they provide essential control over proper network operation. Previous studies have uncovered that GABAergic cells in the basolateral amygdala are as diverse as those present in other cortical regions, including the hippocampus and neocortex. To understand the role of inhibitory cells in various amygdala functions, we need to reveal the connectivity and input-output features of the different types of GABAergic cells. Here, I review the recent achievements in uncovering the diversity of GABAergic cells in the basolateral amygdala with a specific focus on the microcircuit organization of these inhibitory cells.

Keywords: inhibitory, microcircuits, wiring principles, GABAergic, rat, mice

OPEN ACCESS

Edited by:
Eduardo Weruaga,
University of Salamanca, Spain

Reviewed by:
Gianmaria Maccaferri,
Northwestern University,
United States
Andrew MacAskill,
University College London,
United Kingdom

***Correspondence:**
Norbert Hájos
hajos@koki.hu

Received: *29 March 2021*
Accepted: *11 May 2021*
Published: *10 June 2021*

Citation:
Hájos N (2021) Interneuron Types and Their Circuits in the Basolateral Amygdala.
Front. Neural Circuits 15:687257.
doi: 10.3389/fncir.2021.687257

INTRODUCTION TO THE CONNECTIVITY OF THE BASOLATERAL AMYGDALA

Amygdala is the brain region where at least 13 different nuclei are defined with typical neuron types, developmental origin, and connectivity patterns (Pitkanen et al., 1997; Swanson, 2003), playing a role in surprisingly diverse functions, including aversive memory formation, decision-making, social interactions, affective and parental behavior, and homeostatic control, just to list a few (LeDoux, 2000; Phelps et al., 2014). Two different amygdala parts, the lateral (LA) and basal (BA) nuclei, which are often referred to as the basolateral amygdala (BLA), are among the most studied areas. Notably, both nuclei can be further divided into distinct subnuclei (Pitkanen et al., 1997; Swanson and Petrovich, 1998), the functions of which have recently begun to be uncovered using subnucleus-specific manipulations of neural operation (Kim et al., 2016). In spite of a separate role for LA and BA in certain cognitive processes (Janak and Tye, 2015; Manassero et al., 2018), there is no evidence to date of the presence of different cell types or distinct wiring principles in these two amygdalar nuclei. Therefore, I will review the microcircuit organization of the basolateral amygdala as a whole.

Based on the cell types, their connectivity features, and developmental characteristics, the BLA is a cortical structure. Accordingly, glutamatergic excitatory projection cells expressing vesicular glutamate transporter type 1 (VGluT1; Andrasi et al., 2017) are the most numerous neurons in this amygdala region (80–85%; Vereczki et al., 2021). The dendrites of the principal cells (PC) are densely decorated with spines and their axon arborizes within the nucleus, giving rise to local collaterals, but they also project to other amygdala regions and remote cortical and/or subcortical areas (Sah et al., 2003). The BLA, similarly to all cortical structures, is connected to the thalamus and basal ganglia in addition to other cortical networks (McDonald, 1991; Turner and Herkenham, 1991; Sah et al., 2003). VGluT1-expressing glutamatergic axonal varicosities (Fremeau et al., 2001)

originate locally from the amygdala, either from intra- or inter-nuclear sources as well as from cortical areas (Fremeau et al., 2001; Poulin et al., 2008; Andrasi et al., 2017). Numerous cortical regions supply the BLA with excitatory axon terminals, including the prefrontal, insular, higher-order sensory cortices, and ventral hippocampus, all these areas also receive reciprocal projections from the amygdala (Swanson and Petrovich, 1998; Sah et al., 2003). VGluT2-expressing boutons, a vesicular glutamate transporter type, which characterizes subcortical inputs (Fremeau et al., 2001), derive predominantly from various thalamic nuclei (Turner and Herkenham, 1991). Specifically, the LA receives thalamic inputs from the parvocellular part of the ventral posteromedial (VPMpc), the suprageniculate (SG), the medial part of the medial geniculate (MGNm), and posterior intralaminar (PIL) nuclei. In contrast, the BA collects thalamic afferents from the paraventricular (PVT), centromedial (CM), intralaminar (ILM), xiphoid (Xi) and anteriomedial (AM) nuclei. Strictly speaking, the BLA does not receive low-processed sensory inputs, as neither primary thalamic nuclei, nor primary sensory cortices project to this region. In contrast, multisensory and highly processed information is transmitted to the BLA *via* afferents from higher-order thalamic nuclei and secondary or higher-order sensory cortices besides the associative cortices (Sah et al., 2003). These anatomical constraints place the BLA circuits into the position to compare and contrast highly processed information obtained in the past with actual needs, as other cortical areas do (Alexander and Brown, 2018; Keller and Mrsic-Flogel, 2018).

At the output sites, both the LA and BA innervate a substantial part of the basal ganglia, including the nucleus accumbens, olfactory tuberculum, and posterior striatum (McDonald, 1991). Moreover, the LA and BA target the amygdalostriatal transition area (astria) and the dorsomedial striatum, respectively (McDonald, 1992; Barsy et al., 2020). Besides the basal ganglia, the BLA also projects to other striatal structures that are considered to be parts of the amygdala or rather the extended amygdala, namely the central nucleus of amygdala, interstitial nucleus of the posterior limb of the anterior commissure (IPAC), and the bed nucleus of stria terminalis (BNST; Sah et al., 2003).

In summary, distinct thalamic nuclei target the LA and BA, while both nuclei project mainly to overlapping areas of the basal ganglia (with some exceptions). At present, it is not clear if neurons in the LA and BA innervate coinciding or separate circuits within striatal structures. Future studies using advanced techniques should address this important question.

OVERVIEW OF GABAergic CELL TYPES IN THE BLA

Similar to the hippocampus and neocortex, GABAergic cells in the BLA give rise to about 20% of the total neuronal population. Specifically, in the LA 16% of all neurons are inhibitory neurons, whereas in the BA this ratio is significantly higher, 22%, as it has been recently determined (Vereczki et al., 2021). These GABAergic neurons may be categorized into four major functional groups defined by their axonal targets: (1) perisomatic region-targeting inhibitory cells innervate the soma, proximal dendrites, or axon initial segment (AIS) of principal cells and provide the most effective control of spiking activity; (2) dendrite-targeting inhibitory cells innervate primarily the dendrites of principal cells, where they can regulate dendritic computation; (3) interneuron-selective interneurons (ISI) form synaptic contacts specifically with other GABAergic cells, and thus interneurons in this category are in a position to disinhibit principal cells temporarily, permitting their activity to increase in an input-specific manner; and (4) GABAergic projection cells giving rise to both local axonal collaterals and long-range projections can control information flow between the BLA and remote regions they project to. In the listed four major GABAergic cell groups, all cardinal inhibitory cell types of cortical microcircuits have been identified (Fishell and Kepecs, 2020), which will be the subject of the present review (**Figures 1**, **3**). Of note, this review focuses primarily on the microcircuit organization of the BLA, including single-cell features and the connectivity characteristics of individual inhibitory cell types. In addition, I cover the role GABAergic neurons play in circuit operation only in brief by providing updates as this topic has been summarized earlier in detail (Ehrlich et al., 2009; Krabbe et al., 2018). Moreover, it has to be emphasized that the majority of functional studies that aim at elucidating the role of distinct interneuron types in the amygdala use Pavlovian fear conditioning paradigm, as a model of associative learning (Fanselow and LeDoux, 1999; Maren, 2001). In this model, a conditioned stimulus (CS, often a tone) is paired several times with an unconditioned stimulus (US, a mild foot shock) during the conditioning phase. On the subsequent day, CS is presented to test the fear memory formation by monitoring the behavioral response, which is freezing in rodents. If animals are subjected to the CS several times alone, then the CS will not predict the threat anymore, i.e., the fear memory will become extinct. This extinction is likely a combination of new learning of safety and updating the original fear memory (Khalaf et al., 2018; Kida, 2019). As the amygdala plays a role in several other functions on top of fear memory formation and update, upcoming work should shed light on the role of distinct inhibitory neuron types in additional amygdala-related cognitive processes that have not been examined so far.

PERISOMATIC INHIBITION IN CORTICAL REGIONS ORIGINATES FROM THREE INTERNEURON TYPES

Perisomatic inhibition refers to synaptic inputs formed by GABAergic axon terminals targeting the spine-free proximal dendrites, soma, or AIS of postsynaptic principal neurons (**Figure 2A**; Freund and Katona, 2007; Vereczki et al., 2016). In the BA, the functional border of the perisomatic region along the individual dendrites of principal neurons can be labeled with immunostaining against the voltage-gated K^+ channel subunit Kv2.1 (or KCNB1), which visualizes 30 μm-long proximal segments of the dendrites on average. The end of the Kv2.1-immunostained dendritic segments correspond to the steepest increase in spine density along the dendrites, which defines

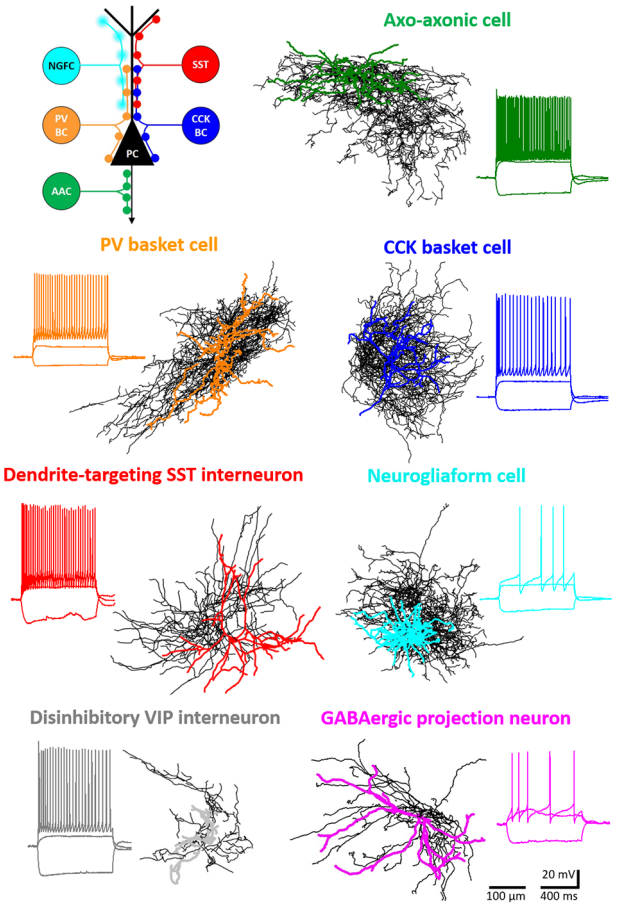

FIGURE 1 | Major inhibitory cell types in the basolateral amygdala (BLA). Intracellularly labeled GABAergic cells were sampled in slice preparations and reconstructed (dendrites in color, axons in black). Voltage responses to depolarizing and hyperpolarizing step current injections are shown for each example cell. Schematic (upper left panel) shows the different membrane domains of principal cells (PC) innervated by distinct interneuron types. NGFC, neurogliaform cells expressing NPY; SST, dendrite-innervating interneurons expressing somatostatin; PVBC, parvalbumin-containing basket cells; CCKBC, cholecystokinin-expressing basket cells; AAC, axo-axonic cells.

the extent of the perisomatic region (Vereczki et al., 2016). Remarkably, the membrane surfaces forming the perisomatic region of cortical principal neurons are predominantly, if not solely covered by GABAergic synapses (Gulyas et al., 1999; McDonald et al., 2002; Muller et al., 2006; Vereczki et al., 2016). With some notable exceptions, perisomatic inhibition in all cortical structures originates from three distinct types of GABAergic interneurons. Namely, axo-axonic cells (or chandelier cells as often called in the neocortex) form synaptic contacts specifically with the AIS of cortical principal, but not GABAergic cells (**Figures 2A,C**; Somogyi, 1977; Somogyi et al., 1985). Basket cells expressing either parvalbumin (PV) or cholecystokinin, and CB1 cannabinoid receptors (CCK/CB1) give rise to the vast majority of inhibitory synapses contacting the soma and the proximal dendrites (**Figures 2A,B**; Freund and Katona, 2007). While cortical principal cells lacking innervation from axo-axonic cells have not been reported, there are some special cases where either PV or CCK/CB1 basket cells are the only sources of GABAergic innervation on the somata and proximal dendrites of excitatory neurons (Bodor et al., 2005; Varga et al., 2010). It is worth mentioning that perisomatic inhibition in non-cortical regions, as in the cerebellum and striatum originates predominantly, if not exclusively from PV basket cells (Ito, 2006; Burke et al., 2017). As axo-axonic cells and CCK/CB1 basket cells have so far been described only in cortical areas, these perisomatic inhibitory cells are likely to be involved in neural processes specific to the cortical operation.

Axo-Axonic Cells

This interneuron type was recognized first in the neocortex by János Szentágothai (Szentágothai and Arbib, 1974), while Péter Somogyi identified their targets as axon initial segments (Somogyi, 1977). In the BLA, the presence of these interneurons has been predicted by showing that the axon initial segments are densely covered with axon terminals forming symmetric synapses (McDonald et al., 2002), a typical feature for GABAergic synaptic junctions in cortical structures. Marco Capogna's group was the first to demonstrate the existence of axo-axonic cells in the rat BLA (Bienvenu et al., 2012), a finding that was followed by the identification of this cell type in the mouse (**Figures 2A,C**; Veres et al., 2014) as well as in the monkey BLA (McDonald and Augustine, 2020). In a recent study, we have estimated that 0.8% and 1.3% of all neurons in the mouse LA and BA belong to axo-axonic cells, respectively (Vereczki et al., 2021). The majority of them (∼70%) express PV, while a small fraction lacks this Ca^{2+} binding protein (Vereczki et al., 2021). Uniformly, axo-axonic cells do not express calbindin (Calb), another Ca^{2+} binding protein (Bienvenu et al., 2012; Vereczki et al., 2016; Andrasi et al., 2017; Rovira-Esteban et al., 2019), which is typically present in PV basket cells (Vereczki et al., 2006; Bienvenu et al., 2012; Andrasi et al., 2017; Rovira-Esteban et al., 2019). Thus, Calb content can be used to distinguish axo-axonic cells from PV basket cells even in the absence of axonal labeling at least in the rodent amygdala circuits.

Axo-axonic cells in the BLA have the shortest dendritic and axonal arborization in comparison to the other two types of perisomatic inhibitory cells (Vereczki et al., 2016). The axon collaterals of axo-axonic cells often display tightly packed varicosities, forming so-called cartridges, which are separated by a longer bouton-free axonal segment. As the directionality of the axon initial segments of amygdalar principal neurons seems to be random, the cartridges of axo-axonic cells do not display a "chandelier" like appearance, which is typical for these interneurons in the neocortex. Axo-axonic cells in the BA innervate their postsynaptic partners with eight-nine boutons on average, ranging between 2 and 16. The axon initial segment of principal neurons in the BA is covered by approximately 50 GABAergic terminals, therefore one may estimate that on an average five-six axo-axonic cells converge on a single principal neuron (Veres et al., 2014). On the other hand, single axo-axonic cells may innervate 600–650 principal neurons in their vicinity. This number roughly corresponds to 18–20% of all principal

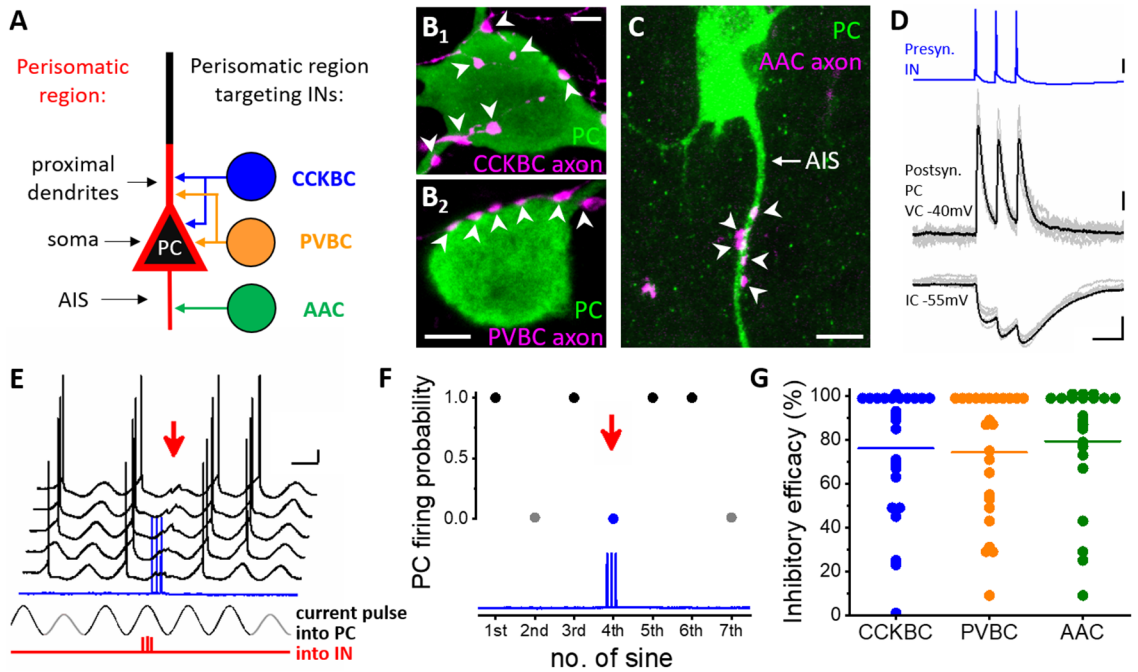

FIGURE 2 | Distinct types of perisomatic region-targeting interneurons provide equally potent synaptic inhibition onto the principal cells in the BLA. **(A)** Persiomatic region is composed of the soma and the spine-free proximal dendrites as well as the axon initial segment (AIS). This region of the principal cells (PC) is innervated by three interneuron (IN) types: cholecystokinin-expressing basket cells (CCKBC), parvalbumin-containing basket cells (PVBC), and axo-axonic cells (AAC). The two basket cell types target overlapping membrane domains of principal cells, whereas their axon initial segments are selectively innervated by axo-axonic cells. **(B_1–B_2)** Axonal varicosities of a basket cell axon (BC, magenta, left) and **(C)** axo-axonic cell axon (AAC, magenta, right) form close appositions with the soma and proximal dendrite (arrowheads, left) and the AIS (arrowheads) of a principal cell (PC), respectively. **(D)** Three action potentials of a presynaptic interneuron (IN, in this case, a CCKBC) evoke postsynaptic responses in a principal cell (PC) recorded in voltage clamp (VC) and current clamp (IC) mode. **(E)** Testing the capacity of a perisomatic region-targeting interneuron (CCKBC) to inhibit spiking in a principal cell. Sinusoidal current trains were injected into the principal cell (PC), and three action potentials were evoked at 30 Hz in the interneuron (red, IN) 30–40 ms before the peak of the fourth cycle. Red arrow indicates the inhibitory postsynaptic potentials and lack of action potential generation in the principal cell caused by the presynaptic interneuron spike train (blue). Voltage traces are offset for clarity. **(F)** Summary plot of the experiment shown in **(D)**. Firing of the PC was prevented when the presynaptic CCKBC spiked three action potentials (red arrow). **(G)** Comparison of the inhibitory efficacy of three interneuron types targeting the perisomatic region. The inhibitory efficacy shows the probability of the suppression of spike generation in the principal cell by interneuron firing. At the population level, there is no difference in the efficacy of synaptic inhibition elicited by three perisomatic region-targeting interneuron types. Each dot represents the inhibitory efficacy obtained in a paired recording, line indicates median. This plot combines data published in (Veres et al., 2014, 2017). Scale bars: **(B_1–B_2,C)**: 5 μm; **(D)**: upper panel: 20 mV, middle panel: 50 pA, lower panel: 2 mV and 50 ms; **(E)**: 10 mV and 200 ms.

neurons that are present in the axon cloud of a single axo-axonic cells (Vereczki et al., 2016).

Action potentials evoked in axo-axonic cells trigger $GABA_A$ receptor-mediated synaptic responses in their postsynaptic partners (Veres et al., 2014). Perforated patch recordings that only minimally alter the intracellular Cl^- concentrations in the recorded neurons have shown that GABA released from the axon terminals of axo-axonic cells causes hyperpolarization in postsynaptic neurons, indicating that these interneurons function as inhibitory cells in the BA (Veres et al., 2014). In line with this finding, it has been estimated that when the membrane potential of postsynaptic principal neurons was adjusted near their firing threshold, GABA release from at least 10–12 axo-axonic cell synapses was required to veto the spiking in the postsynaptic neuron. In addition, axo-axonic cell output could postpone the principal neuron spiking, if the synaptic inhibition arrived 50–150 ms prior to the would-be action potential initiation in the principal neuron. Moreover, axo-axonic cells could suppress excitatory input-driven firing, too (Veres et al., 2014). Taking into account that a single axo-axonic cells give rise to eight-nine contacts onto a given axon initial segment on an average, co-activation of 2–3 axo-axonic cells is likely sufficient to effectively control the spiking of their postsynaptic partners in the BA (Veres et al., 2014).

The analysis of the distribution of GABAergic axon terminals along the axon initial segments in the BA has uncovered that the largest density of boutons irrespective of their PV content peaked at 20–40 μm measured from the soma (Veres et al., 2014; Vereczki et al., 2021). So what is special in that region of the axon initial segment covered by GABAergic terminals with the highest density? Dual electrophysiological recordings have showed that the highest probability for action potential generation in amygdalar principal neurons overlapped with this portion of the axon initial segment. In line with this observation, the density of the immunolabeling for voltage-gated Na^+ channel type 1.6 (Nav1.6) also peaked at 20–40 μm from the beginning

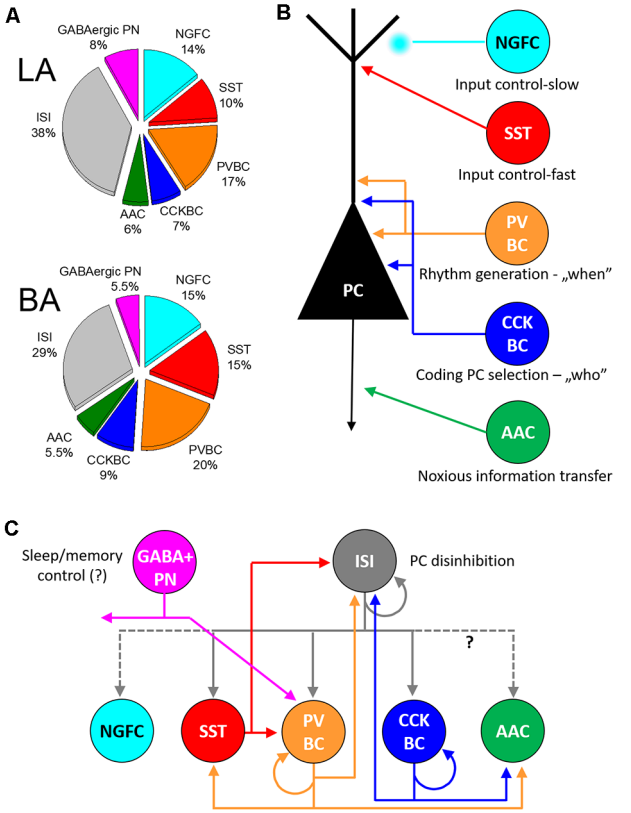

FIGURE 3 | Inhibitory cells, their connectivity, and proposed functions in the circuits of the basolateral amygdala. **(A)** Ratio of distinct types of GABAergic cells in the lateral (LA) and basal amygdala [BA; adopted from (Vereczki et al., 2021)]. **(B)** Five interneuron types innervating the distinct membrane domains of principal cells (PC) may play different roles in circuit operation. **(C)** Connectivity matrix among GABAergic neurons in the basolateral amygdala. Possible functions for GABAergic projection neurons (GABA+ PN) and interneuron-selective interneurons (ISI) are indicated. NGFC, neurogliaform cells expressing NPY; SST, dendrite-innervating interneurons expressing somatostatin; PVBC, parvalbumin-containing basket cells; CCKBC, cholecystokinin-expressing basket cells; AAC, axo-axonic cells.

of the axon initial segments. Remarkably, axo-axonic cells innervated this region with the highest likelihood, irrespective of the number of boutons given by single axo-axonic cells. These results collectively suggest that axo-axonic cells strategically position their GABAergic output synapses onto that portion of the axon initial segment, where the action potential generation has the highest probability. Although the length of axon initial segments is shorter in the LA than in the BA, the relative distance for spike generation site along the axon initial segment (densely covered by GABAergic boutons) in the LA is comparable to that observed in the BA (Vereczki et al., 2021). In summary, axo-axonic cells are in a position to efficiently control the spiking of their postsynaptic partners, as has been demonstrated in paired recordings (Veres et al., 2014).

Whole-cell recordings obtained in slice preparations showed that axo-axonic cells display a fast-spiking phenotype, have low input resistance, and fast membrane time constant (Barsy et al., 2017). *In vivo* electrophysiological recordings showed that these interneurons have narrow spikes recorded extracellularly, a feature based on which one cannot distinguish axo-axonic cells from PV basket cells (or from additional GABAegic cell types; Bienvenu et al., 2012). Axo-axonic cells in the BLA often fire a burst of action potentials at 300 Hz or even at higher rates, a characteristic feature, which distinguishes them from PV basket cells (Barsy et al., 2017). As the maximal firing rate for PV basket cells has been reported to be less than 200 Hz (Woodruff and Sah, 2007; Barsy et al., 2017), the difference in the burst frequency between axo-axonic cells and PV basket cells may be used as a "biomarker" to differentiate between these two narrow spiker interneurons *in vivo* recordings.

Our knowledge is very limited regarding the *in vivo* firing features of axo-axonic cells in the BLA. In a study obtained in anesthetized rats, noxious stimuli like a tail pinch or electrical shock robustly elevated the firing of all axo-axonic cells tested (Bienvenu et al., 2012), similarly to that observed in the medial prefrontal cortex (Massi et al., 2012). These results may suggest that these GABAergic cells can play a role in controlling aversive emotional states evoked by painful stimulation. In another recent study, the role of amygdalar axo-axonic cells in emotional memory formation has been examined by disrupting GABAergic synaptic contacts along the axon initial segments, while sparing those that contacted the soma. This selective manipulation has been achieved by knocking down the cell adhesion molecule neurofascin, which stabilizes axo-axonic GABAergic synapses along the axon initial segment (Kriebel et al., 2011). The results of the neurofascin knockdown have shown that the fear extinction, but not the cued fear conditioning, was impaired upon reducing the number of GABAergic synapses contacting the axon initial segments (Saha et al., 2017). Future research using selective modulation of axo-axonic cell activity may elucidate more precisely the role of these GABAergic interneurons in amygdala operation.

PV Basket Cells

Basket cells in cortical structures were described by Santiago Ramón y Cajal using Golgi impregnation technique (Ramón y Cajal, 1899). The presence of PV in basket cell axon terminals was demonstrated first in the hippocampus (Kawaguchi et al., 1987) and neocortex (Hendry et al., 1989) using immunocytochemistry. In subsequent studies, electron microscopic investigations revealed that in the BLA, axon terminals expressing PV contained GABA and formed synaptic contacts with somata and proximal dendrites of principal cells (**Figures 2A,B**; Sorvari et al., 1996; Smith et al., 1998), distinguishing features of PV basket cells. These interneurons comprise about 2.2% and 4.7% of all neurons in the mouse LA and BA, respectively (Vereczki et al., 2021). At the population level, around 50% of PV basket cell output synapses contact the soma and proximal dendrites, i.e., the perisomatic region. The other half of the axonal varicosities of this basket cell type targets distal dendrites, showing an exponential decrease in the contact number toward the tip of dendrites (Smith et al., 1998; Muller et al., 2005; Vereczki et al., 2016; Veres et al., 2017). Although there is a large variance in the ratio of perisomatic vs. dendritic targets of individual PV basket cells, no dendrite-targeting

PV interneurons, like PV-containing bistratified cells in the CA1 region of the hippocampus (Halasy et al., 1996) have been identified in the BLA, in spite of the fact that some PV interneurons express NPY (Vereczki et al., 2021), a characteristic marker for CA1 bistratified cells (Klausberger et al., 2004). The largest fraction of perisomatic GABAergic inputs (∼40%) received by amygdalar principal neurons originate from PV basket cells, a ratio that corresponds to 90–95 boutons (Vereczki et al., 2016). As single PV basket cells give rise to four-five contacts on the perisomatic region of principal neurons on average, 18–24 PV basket cells should converge on the soma and proximal dendrites of single principal neurons (Vereczki et al., 2016; Veres et al., 2017). On the other hand, a single PV basket cell may innervate 950–1,000 principal neurons, corresponding to roughly 10% of all principal neurons within the area of their axonal arbor. These refined estimates are based on the combined data published recently (Vereczki et al., 2016, 2021; Veres et al., 2017).

PV basket cells have variable soma size, but uniformly give rise to a multipolar dendritic tree (McDonald and Betette, 2001; Mascagni et al., 2009; Vereczki et al., 2016). Their membrane surface is densely covered by synaptic inputs (Smith et al., 1998). The excitatory inputs they receive on their somata and dendrites (McDonald et al., 2005; Andrasi et al., 2017) are more numerous than inhibitory contacts (Smith et al., 1998; in the hippocampus it has been estimated that more than 15,000 excitatory and 3,000 inhibitory synapses contact single PV interneurons; Gulyas et al., 1999). Excitatory synaptic inputs onto PV basket cells are mediated primarily *via* Ca^{2+}-permeable AMPA receptors, the number of which can be increased upon tetanic stimulation causing long-term potentiation (Mahanty and Sah, 1998). These data suggest that the efficacy of excitatory inputs received by PV basket cells in the amygdala can be changed depending on the activity level linked to distinct environmental challenges. Notably, the induction features of long-term potentiation at excitatory synapses studied in fast spiking PV interneurons (the majority of which were likely basket cells) may be different in the LA and BA (Lucas et al., 2016; Polepalli et al., 2020).

Recordings obtained in perforated patch configuration have revealed that PV basket cells are inhibitory cells, as the reversal potential of their $GABA_A$ receptor-mediated postsynaptic responses monitored in amygdalar principal neurons was more hyperpolarized than the resting membrane potential of the postsynaptic neurons (Veres et al., 2017). Interestingly, the reversal potential of postsynaptic potentials from basket cells has more negative values than those originated from axo-axonic cells (Veres et al., 2014). This difference in reversal potentials is in accord with results obtained in hippocampal pyramidal cells using GABA uncaging (Khirug et al., 2008). The reason for the difference in the reversal potentials may be explained, at least in part, by the fact that in the plasma membrane of axon initial segments the neuron-specific potassium-chloride cotransporter 2 (KCC2), a major controller for intracellular Cl^- concentrations (Kaila et al., 2014) is far less abundant than along the soma and dendrites (Baldi et al., 2010).

Paired recordings in acute slice preparations uncovered that 8–12 perisomatic contacts of basket cells are needed to block the spiking in amygdalar principal neurons when their membrane potential is adjusted near the firing threshold. Furthermore, the timing of the firing can be postponed within a 110 ms-long interval by PV basket cells (Veres et al., 2017). These observations indicate that simultaneous activation of two-three PV basket cells is necessary to suppress the postsynaptic spiking. It is important to note that the control of spike generation by basket cells is achieved primarily *via* their perisomatic inputs, while their inputs onto the distal dendrites may have only limited contribution to this effect (Veres et al., 2017). Although, the function of dendritic inhibition provided by basket cells has not been investigated yet, they may play a role in influencing local signaling (Miles et al., 1996; Mullner et al., 2015).

PV basket cells receive innervation both from intra- and extra-amygdalar sources. Intra-amygdalar sources include principal cells and interneurons as well (Smith et al., 2000; McDonald et al., 2005; Muller et al., 2005; Andrasi et al., 2017), with inhibitory input originating from other PV basket cells (Muller et al., 2005; Woodruff and Sah, 2007; Andrasi et al., 2017; Krabbe et al., 2019), and SST and VIP interneurons (Krabbe et al., 2019). Extra-amygdalar input is provided by the frontal, auditory, rhinal and insular cortices, ventral hippocampus, different thalamic nuclei, basal forebrain, dorsal raphe, locus coeruleus, and dopaminergic neurons, uncovered by the use of monosynaptic rabies tracing (Lucas et al., 2016; Krabbe et al., 2019), electron microscopy (Smith et al., 2000; Muller et al., 2007b, 2011; Pinard et al., 2008; McDonald et al., 2011), or optogenetics (Polepalli et al., 2020).

Similarly to axo-axonic cells, PV basket cells show a fast-spiking phenotype, although a substantial variability can be acknowledged in their voltage responses upon depolarizing current step injections (Rainnie et al., 2006; Woodruff and Sah, 2007; Barsy et al., 2017; Polepalli et al., 2020). These interneurons typically have low input resistance and fast membrane time constant, and display a high firing rate in the intact brain (Woodruff and Sah, 2007; Bienvenu et al., 2012; Wolff et al., 2014; Barsy et al., 2017). In contrast to axo-axonic cells, however, PV basket cells show variable responses to noxious stimulations, as some are excited, while others are inhibited or non-responsive in anesthetized rats (Bienvenu et al., 2012). Comparable diverse responses in PV interneuron populations upon both CS and US stimuli during fear conditioning were observed in behaving mice using tracing Ca^{2+} transients (Krabbe et al., 2019). The vast majority of PV interneurons responded to the US: 80% of them were found to elevate their activity, whereas 20% reduced it. Fewer PV interneurons responded to the US-associated CS+ (∼75%) and US-independent CS− (∼50%) presentations. Of the CS-responsive PV interneurons around 2/3 elevated their activity, the others decreased it (Krabbe et al., 2019). Considering that the majority of PV interneurons are basket cells, these results may imply that distinct populations of PV basket cells may belong to various amygdalar sub-circuits acting distinctly, but in concert to fulfill the optimal computation during behavioral challenges. In a different study, optogenetic manipulation of PV interneuron function during associative fear learning revealed that time-locked inhibition of the PV interneuron population

during CS and US stimuli caused improvement or impairment of fear memory formation, respectively (Wolff et al., 2014). Using chemogenetics, it has been shown that PV interneurons may control the number of neurons that participate in memory formation (Morrison et al., 2016), further supporting the role of these interneurons in associative learning. In addition, PV basket cells may also control extinction learning, as "fear" neurons in the amygdala that are activated by associative fear memory formation but are inhibited during extinction training (Herry et al., 2008) received increased innervation from these perisomatic inhibitory cells upon repetitive presentation of CS that no longer signed threat (Trouche et al., 2013).

In summary, PV basket cells are key circuit elements in the BLA complex, where they contribute to fear memory processes. Subsequent studies will likely uncover in the close future how these inhibitory interneurons control other amygdala-linked neural operations.

CCK/CB1 Basket Cells

In addition to GABAergic axon terminals containing PV, other boutons that express CCK were found to form synaptic contacts with the perisomatic region of cortical principal cells (Hendry et al., 1983; Nunzi et al., 1985), demonstrating that two distinct basket cell types participate in perisomatic innervation. CCK basket cells have a unique feature, as their axonal varicosities are decorated with CB1 cannabinoid receptors shown first by István Katona and his colleagues (Katona et al., 1999b). In the BLA, CCK/CB1 basket cells are also present both in the rodent (Katona et al., 2001; McDonald and Mascagni, 2001; Vereczki et al., 2016; Rovira-Esteban et al., 2017) and in the monkey (McDonald, 2021), giving rise to 0.9% of all neurons in the LA and 2.1% in the BA in the mouse BLA (Vereczki et al., 2021). CCK/CB1 basket cells typically have large somata and multipolar dendritic trees both in rodents (Mascagni and McDonald, 2003; Vereczki et al., 2016; Rovira-Esteban et al., 2017) and monkey (McDonald and Mascagni, 2019). The neurochemical content of CCK/CB1 basket cells is variable, as they may express vesicular glutamate transporter type 3 (VGluT3) and Calb in largely non-overlapping subpopulations (Omiya et al., 2015; Rovira-Esteban et al., 2017). In some of these basket cells, VIP may also be expressed (Omiya et al., 2015; Rhomberg et al., 2018). Of note, a recent study has revealed that the Ca^{2+} binding proteins NECAB1 and 2 are expressed in CCK/CB1, but not PV basket cells in cortical structures, including the BLA (Miczan et al., 2021). At the population level, half of the output synapses of CCK/CB1 basket cells target the perisomatic region (similarly to PV basket cells), whereas the other half contacts distal dendrites with a progressive decline in density toward the tip of dendrites (**Figures 2A,B**; Veres et al., 2017). One-third of perisomatic GABAergic inputs onto amygdalar principal neurons originates from CCK/CB1 basket cells, a ratio that corresponds to 65–70 boutons (Vereczki et al., 2016). As single CCK/CB1 basket cells contact the perisomatic region of principal neurons *via* three-four contacts on average, 16–23 CCK/CB1 basket cells should innervate single principal neurons perisomatically (Vereczki et al., 2016; Veres et al., 2017). On the other hand, individual CCK/CB1 basket cells may target 680–730 principal neurons, corresponding to approx. 10% of all principal neurons within the volume of their axonal arbor (Vereczki et al., 2006, 2021; Veres et al., 2017).

CCK/CB1 basket cells receive both excitatory and inhibitory synapses on their membrane surface with a substantially lower density in comparison to PV basket cells (Matyas et al., 2004; Andrasi et al., 2017). Our knowledge regarding the sources of amygdalar CCK/CB1 basket cell inputs is limited. It has been shown that they receive excitatory innervation from amygdalar principal cells, whereas their synaptic inhibition arrives from other CCK/CB1 basket cells and VIP-expressing ISI (Andrasi et al., 2017; Rhomberg et al., 2018). Previous studies obtained in the hippocampus have observed that excitatory synaptic inputs of CCK/CB1 basket cells show no long-term changes using induction protocols in acute slices that readily induced long-term potentiation or long-term depression at glutamatergic afferents recorded from PV basket and axo-axonic cells (Nissen et al., 2010; Szabo et al., 2012). However, environmental challenges may alter excitatory inputs on CCK/CB1 basket cells on a longer time scale, a hypothesis that needs to be tested.

Postsynaptic responses of CCK/CB1 basket cells are mediated *via* $GABA_A$ receptors (Vogel et al., 2016), although their high spiking rates may also cause the activation of $GABA_B$ receptors on the postsynaptic targets (Booker et al., 2013). As revealed by perforated patch recordings, CCK/CB1 basket cell-evoked postsynaptic events in amygdalar principal neurons are inhibitory, similarly to the two other perisomatic inhibitory cell types (Veres et al., 2017). Estimated from whole-cell paired recordings, 8–12 axon terminals of CCK/CB1 basket cells are needed to prevent spiking of amygdalar principal neurons, with membrane potentials set near the firing threshold (**Figures 2D–F**). Similarly to PV basket cells, CCK/CB1 basket cells are also able to postpone the spiking of principal neurons by 110 ms, on average. As individual CCK/CB1 basket cells were assessed to give three-four perisomatic contacts to principal neurons on average, simultaneous discharge of two-four basket cells of this type is necessary to control the spiking of their postsynaptic partners effectively (Veres et al., 2017).

In contrast to the two other perisomatic inhibitory interneurons, the firing of CCK/CB1 basket cells show accommodation, at least at young ages (Jasnow et al., 2009; Barsy et al., 2017), a spiking phenotype that develops to more clustered action potential firing with age (Rovira-Esteban et al., 2019). Typically, these basket cells have higher input resistance, slower membrane time constant, and often display a sag in voltage responses evoked by hyperpolarizing current steps, indicative of the expression of h-current (Jasnow et al., 2009; Vogel et al., 2016; Rovira-Esteban et al., 2017).

The functional role of CCK/CB1 basket cells in neural operation is unclear. The primary reason for this lack of knowledge lies in the fact that currently there is no available tool to manipulate the function of these basket cells without affecting other inhibitory neuron types even by using intersectional viral strategy (Rovira-Esteban et al., 2019). Recent studies, however, provide some hints for the role of CCK/CB1 basket cells in the control of fear memory. For instance, these basket cells can differentially regulate the activity of amygdalar principal

cells that project to distinct parts of the prefrontal cortex. In paired recordings, it has been revealed that CCK/CB1 basket cells evoke comparable unitary inhibitory postsynaptic events in principal neurons irrespective of whether they project to the prelimbic or infralimbic cortex. However, there was a striking difference in the CB1 receptor-mediated inhibition of GABA release from the axon terminals of these basket cells upon the activation of postsynaptic neurons with distinct projections (Vogel et al., 2016). Earlier it has been discovered that endocannabinoids, endogenous ligands of CB1 receptors, are released from the postsynaptic neurons in an activity-dependent manner, causing suppression of neurotransmitter release from presynaptic varicosities (Wilson and Nicoll, 2001). In the BA, those principal neurons that project to the prelimbic cortex could liberate themselves fully from inhibition provided by CCK/CB1 basket cells in an activity- and CB1 receptor-dependent manner, whereas those principal neurons that innervate the infralimbic cortex could reduce this source of synaptic inhibition only partially upon depolarization (Vogel et al., 2016). Thus, CCK/CB1 basket cells can contribute to the dynamic control of the BA output. In addition, other indirect evidence (like correlative changes in bouton numbers and behavior) suggests that these basket cells may critically contribute to extinction learning (Ruehle et al., 2013; Trouche et al., 2013; Rovira-Esteban et al., 2019) and the control of synaptic plasticity demonstrated in slice preparations (Azad et al., 2008). After developing appropriate tools in the future, our knowledge should be substantially advanced regarding the CCK/CB1 basket cell function in amygdala operation.

MICROCIRCUIT ORGANIZATION BY PERISOMATIC INHIBITORY CELLS AND PRINCIPAL NEURONS

By comparing the efficacy of inhibition, i.e., the ability of a principal neuron to fire if a monosynaptically connected perisomatic inhibitory cell discharges action potentials under a given condition, recent investigations have revealed that all three types of perisomatic inhibitory cells can control the spiking of postsynaptic principal neurons in the amygdala microcircuits to a similar extent (**Figure 2G**; Veres et al., 2014, 2017; Andrasi et al., 2017). This surprising observation is in line with the fact that the magnitude of unitary events originating from distinct types of perisomatic inhibitory neurons does not differ substantially in the BA. In contrast, the unitary events CA3 pyramidal cells receive from axo-axonic cells have significantly larger peak amplitude than those arriving from basket cells in the hippocampus (Szabo et al., 2010). In the prefrontal cortex, the peak amplitude of the unitary events between PV basket cells and pyramidal cells was found to be significantly larger in comparison to those recorded in pairs of axo-axonic cells and pyramidal cells or CCK/CB1 basket cells and pyramidal cells (Fekete et al., 2019). These regional differences in the magnitude of unitary inhibitory postsynaptic currents may indicate a more equalized impact for the three perisomatic inhibitory cell types on neural activity in some cortical regions like the BA, while in other regions, one perisomatic inhibitory cell type may have a more profound effect on microcircuit operation at the single-cell level. Clearly, more work is needed to understand the logic and significance of the differences in the efficacy of inhibition provided by the distinct perisomatic inhibitor cell types on neuronal functions.

Consequently, if the synaptic inhibition received by the amygdalar principal neurons from the three perisomatic inhibitory cell types is similar, then the synaptic inputs of these GABAergic cells should differ, otherwise, they cannot fulfill distinct functions in circuit operation as predicted earlier (Freund and Katona, 2007). Indeed, a substantially smaller population of principal neurons can discharge PV basket cells than CCK/CB1 basket cells (Andrasi et al., 2017). Several factors underlie this differential excitation, including the dissimilarity in the peak amplitude of unitary excitatory events and the number of excitatory inputs received by PV basket cells and CCK/CB1 basket cells. Distinct excitation of PV basket cells and CCK/CB1 basket cells may dictate the differential recruitment of these GABAergic cell types during various functions, a necessary prerequisite to fulfill their dedicated roles in amygdala networks.

Another surprising observation is related to the connectivity among these three perisomatic inhibitory cell types. With two independent methods, using paired recordings and immunocytochemistry, it has been uncovered that PV basket cells innervate each other as well as axo-axonic cells with high probability, but avoid CCK/CB1 basket cells. On the other hand, CCK/CB1 basket cells also target each other with a high probability as well as axo-axonic cells, but do not innervate PV basket cells. Axo-axonic cells do not innervate each other or any basket cells (Andrasi et al., 2017). Yet, axo-axonic cells are readily coupled *via* gap junctions, forming a syncytium (Andrasi et al., 2017). Similarly, paired recordings and electron microscopy showed that there is a high probability of finding a gap junction coupling among PV basket cells (Muller et al., 2005; Woodruff and Sah, 2007; Andrasi et al., 2017) or among CCK/CB1 basket cells, but the two basket cell types do not communicate *via* electrical synapses either (Andrasi et al., 2017). Thus, in the amygdala, two independent basket cell networks operate in parallel, which are activated distinctly *via* principal neurons. Notably, this wiring principle of perisomatic inhibitory cells and principal neurons is not unique for the amygdala, as a similar connectivity matrix appears to exist in the CA3 region of the hippocampus (Kohus et al., 2016). At present, it is unknown why this type of wiring diagram is formed at least in two cortical structures, but it may be indicative of a functional dichotomy between the two basket cell types. For instance, PV basket cells may serve as a clock in cortical networks (Freund and Katona, 2007), as together with principal neurons they can generate highly precise oscillatory activities like gamma oscillations without the contribution of axo-axonic cells or CCK/CB1 basket cells (Gulyas et al., 2010). In contrast, CCK/CB1 basket cells can control the spiking of principal neurons by providing profound inhibition on principal neurons that show low activity, while allowing the spiking of those that can release endocannabinoids upon high firing (Zhu and Lovinger, 2005; Vogel et al., 2016), and therefore likely carry important information. Thus, PV

basket cells control "when" to spike, while CCK/CB1 basket cells regulate "who" can fire. The control of principal cell spiking with these two distinct purposes can be achieved with independent networks of basket cells most efficiently.

DENDRITIC INHIBITION

The term dendritic inhibition refers to GABAergic inputs forming synaptic contacts with dendrites (Miles et al., 1996). In cortical regions, two distinct types of GABAergic interneurons target preferentially the dendritic tree of principal neurons. SST (or SOM) interneurons innervate the distal dendrites of pyramidal cells (Katona et al., 1999a; Wang et al., 2004), and are considered to control dendritic information processing in a feedback manner (Miles et al., 1996; Murayama et al., 2009), as these GABAergic cells are primarily excited by the local axon collaterals of principal neurons (Blasco-Ibanez and Freund, 1995; Maccaferri and McBain, 1995). Carlo Martinotti was the first to report an interneuron that had a massive ascending axonal projection reaching even layer 1 (Scarani et al., 1996), a morphology that was clearly distinct from that of basket cells. In the hippocampus, Chris McBain and his colleagues described first an interneuron, the so-called OLM-cell that had an ascending axonal arbor far away from its soma and dendrites (McBain et al., 1994). Both Martinotti cells and OLM cells were found to express SST (Kawaguchi and Kubota, 1996; Katona et al., 1999a). SST interneurons provide $GABA_A$ receptor-mediated postsynaptic responses onto their target neurons (Maccaferri et al., 2000). In contrast, the other source of dendritic inhibition originating from neurogliaform cells, reported first by Ramon y Cajal (Ramón y Cajal, 1899), supplies the microcircuits typically with slow and long-lasting inhibition, composed of both $GABA_A$ and $GABA_B$ receptor-mediated postsynaptic inputs (Tamas et al., 2003; Price et al., 2008). Both types of dendrite-targeting interneurons are present in the BLA in a similar quantity (McDonald, 1985; Amaral et al., 1989; McDonald et al., 1995; McDonald and Mascagni, 2002; Manko et al., 2012). SST interneurons form 1.3% of all neurons in the LA and 4% of all neurons in the BA, whereas neurogliaform cells make up 1.8% and 3.5% of the total neuronal population in the LA and BA, respectively (Vereczki et al., 2021).

Dendrite-Targeting SST Inhibitory Cells

SST interneurons have smooth or sparsely spiny dendrites, give rise to dense local axonal arborization (Vereczki et al., 2021) and often express Calb and/or neuropeptide Y (McDonald, 1989; McDonald and Mascagni, 2002) but lack nNOS (Vereczki et al., 2021). The typical firing of SST interneurons induced by depolarizing current injection shows accommodation and a sag appears in negative voltage responses evoked by hyperpolarizing current steps, indicative of the activation of the h-current (Zemankovics et al., 2010; Unal et al., 2020; Vereczki et al., 2021). These interneurons preferentially innervate small-caliber dendrites, and to a lesser extent, spines of amygdalar principal neurons (Muller et al., 2007a; Vereczki et al., 2021), similarly to that observed in the hippocampus (Katona et al., 1999a) and neocortex (Wang et al., 2004), which explains the slow rising phase of their postsynaptic responses measured at the soma (Wolff et al., 2014; Krabbe et al., 2019; Unal et al., 2020). As amygdalar principal neurons receive their excitatory inputs on their dendrites (Smith and Pare, 1994; Brinley-Reed et al., 1995; Pare et al., 1995; Vereczki et al., 2016; Amir et al., 2019), SST interneurons are in a key position to control the efficacy of excitatory inputs and thus the plastic changes in synaptic strength and dendritic excitability. Indeed, recently it has been demonstrated that the spiking of amygdalar principal neurons evoked by synaptic excitation could be suppressed by activation of SST inhibitory cells (Wolff et al., 2014). This activation can even lead to gating long-term potentiation, at least at excitatory synapses of prefrontal-basal amygdala afferents (Ito et al., 2020).

SST interneurons receive innervation from both intra- and extra-amygdalar sources. Their excitatory inputs from local principal neurons show short-term facilitation (Unal et al., 2020), which ensures a time window for a potential discharge before the feedback inhibition reaches the dendritic tree (Unal et al., 2020), similarly to that observed in other cortical regions (Pouille and Scanziani, 2004). SST interneurons are also part of inhibitory circuits in the BLA, as they innervate and are targeted by both PV and VIP interneurons (Krabbe et al., 2019). In addition to SST interneurons displaying accommodating firing and sag in their voltage responses upon negative step current injections, many SST interneurons showing rather a fast-spiking phenotype and no sag were sampled in transgenic mice generated by crossing Sst-Cre mice with a reporter mouse line (Guthman et al., 2020; Unal et al., 2020). Interestingly, such fast-spiking interneurons were rarely found among SST interneurons if they were visualized by a viral strategy in Sst-Cre mice (2 out of 31; Vereczki et al., 2021). Importantly, such fast-spiking SST interneurons may express PV (Vereczki et al., 2021), raising the possibility that during development Sst gene may be temporarily active in a population of PV interneurons, leading to the expression of reporter proteins in them, if interneurons are labeled by crossing Sst-Cre mice with a reporter mouse line. In line with this hypothesis, fast-spiking SST interneurons were shown to mediate feedforward inhibition in the amygdala (Guthman et al., 2020), a typical trait of PV interneurons (Smith et al., 2000; Hu et al., 2014; Lucas et al., 2016). In contrast, SST interneurons with accommodating firing were readily recruited by amygdalar principal neurons in a feedback manner (Unal et al., 2020), a feature that characterizes dendrite-targeting SST interneurons in cortical structures (Blasco-Ibanez and Freund, 1995; Maccaferri and McBain, 1995; Murayama et al., 2009). Clearly, further investigations are needed to clarify the neurochemical content, postsynaptic targets, and wiring features of fast-spiking SST interneurons in the amygdala.

Using monosynaptic rabies tracing the inputs onto SST inhibitory cells has recently been examined. It has been found that these GABAergic neurons receive innervation both from cortical areas (including the auditory, insular, piriform and medial orbital cortex, and ventral hippocampus) and subcortical regions (including the basal forebrain, thalamus, and dorsal raphe; Krabbe et al., 2019). As this approach does not allow the separation of monosynaptic inputs received by SST interneurons and SST projection cells (see later), more specific investigations

should be conducted in the future to uncover the long-range inputs onto SST GABAergic cell types.

A recent elegant study using imaging techniques for tracking Ca^{2+} transients has investigated the response of SST inhibitory cells in the BA during fear conditioning. The authors observed that 60–70% of these GABAergic neurons changed their Ca^{2+} signals upon presentation of US, CS+, and CS−. Interestingly, half of the responsive SST inhibitory neurons decreased, whereas the other half increased their activity irrespective of the presented stimulus (Krabbe et al., 2019). Furthermore, optogenetic interventions have revealed that SST inhibitory cells in the BA may control associative memory formation bidirectionally. Inhibition and activation of SST inhibitory cell activity accompanied by CS presentation increased and reduced, respectively, the freezing levels during fear memory retrieval. Importantly, CS-evoked principal neuron firing was enhanced by inhibiting SST inhibitory cells, whereas it was suppressed by exciting these GABAergic cells (Wolff et al., 2014). These data strongly support the view that dendrite-targeting SST interneurons effectively control the formation of associative memories at the amygdala level by altering dendritic function. Moreover, SST interneurons in the amygdala may be involved in discriminative learning as well. A very recent study has uncovered that SST inhibitory cells in the amygdala were activated specifically during learned non-threatening cues. This enhanced activity was dependent on the prelimbic cortex and promoted the discrimination of non-threat stimuli. Thus, the prefrontal cortex may control amygdala function during fear discrimination *via* engaging SST interneurons (Stujenske et al., 2021).

However, one has to keep in mind that the use of Sst-Cre mice does not allow to selectively monitor and manipulate the operation of dendrite-targeting SST interneurons exclusively. Although in Sst-Cre mice, the majority of SST GABAergic cells both in the LA and BA likely belong to this interneuron category (60% and 75%, respectively; Vereczki et al., 2021), yet the remaining SST inhibitory cells express neuronal nitric oxide synthase (nNOS) that characterizes GABAergic cells with long-range projections to extra-amygdalar areas (see below). Therefore, further studies using a more selective approach will be needed to unequivocally identify the role of dendrite-targeting SST interneurons in distinct amygdala functions.

Neurogliaform Cells

These interneurons, similarly to that observed in the hippocampus and neocortex, have short, frequently ramifying sparsely spiny dendrites, very dense local axonal arbor, and contain neuropeptide Y (NPY; Manko et al., 2012); in addition, a few of them express CCK (Rovira-Esteban et al., 2019), nNOS at a low level (Vereczki et al., 2021), or even SST (Manko et al., 2012). Similarly to other cortical areas, these GABAergic interneurons in the amygdala generate slow postsynaptic inhibitory responses mediated *via* $GABA_A$ and $GABA_B$ receptors (Manko et al., 2012; Rovira-Esteban et al., 2019), making them very efficient regulators of circuit operation (Tamas et al., 2003; Olah et al., 2009; Abs et al., 2018). Structural features of how neurogliaform cells contact other neurons may explain, at least partially, the typical slow postsynaptic responses. Electron microscopic studies revealed that a significant portion of axon terminals of neurogliaform cells do not form classical tight synaptic contacts with the target elements, instead, the axonal boutons appose the neural profiles from a distance, allowing the released GABA to reach far beyond the potential postsynaptic specialization (Tamas et al., 2003; Manko et al., 2012). This spill-over of GABA for large distances in the extracellular milieu can activate $GABA_B$ receptors located both postsynaptically and presynaptically, even on neighboring axon terminals (Olah et al., 2009). So far, neurogliaform cells have been identified as a main source for evoking pronounced postsynaptic $GABA_B$ receptor-mediated responses in cortical structures (Tamas et al., 2003). They have been shown to be activated in a feedforward manner in the hippocampus (Price et al., 2008), prefrontal cortex (Jackson et al., 2018), or auditory cortex (Abs et al., 2018), yet there is no data available on how these GABAergic interneurons are recruited during microcircuit operation in the amygdala. Neurogliaform cells often display a late-spiking phenotype and a pronounced after-hyperpolarization following the spike that is indistinguishable from the action potential of principal neurons regarding their spike width (Manko et al., 2012; Rovira-Esteban et al., 2019; Vereczki et al., 2021). This latter spike characteristic makes it challenging, if not impossible, to separate extracellularly detected spikes of neurogliaform cells from principal neurons, and on top of it, both types of neurons fire typically with a moderate rate *in vivo* (Bienvenu et al., 2012; Manko et al., 2012). This drawback restrains us from revealing the activity of neurogliaform cells during distinct behaviors without optical tagging or *post hoc* anatomical identification following juxtacellular or intracellular recordings (Manko et al., 2012). As so far no available combination of techniques has made it possible to selectively interfere with the function of neurogliaform cells in the amygdala, their contribution to circuit operation during distinct behaviors remains unknown.

DISINHIBITORY INTERNEURONS EXPRESSING VIP/CR

GABAergic interneurons that specifically innervate other GABAergic cells have been recognized first in the hippocampus and dentate gyrus by the group of Tamás Freund (Acsády et al., 1996; Gulyas et al., 1996; Hájos et al., 1996). Using neuroanatomical techniques, they discovered that GABAergic interneurons expressing VIP and/or CR form synaptic contacts predominantly, if not exclusively on other GABAergic cells, providing the structural basis for the presence of a disinhibitory circuitry in cortical networks. More than 15 years later, Adam Kepecs and his group presented the first functional proof for the existence of such disinhibitory networks (Pi et al., 2013). Since then, numerous studies conducted in several cortical areas have shown that VIP interneurons that lack CB1 expression are fundamental elements of cortical circuits, providing disinhibition of excitatory principal neurons universally in cortical structures (Fishell and Kepecs, 2020). Accordingly, Rhomberg et al. (2018) have shown that in the LA and BA, VIP

interneurons that do not express CB1 specifically target other GABAergic interneurons. These VIP interneurons form the largest fraction among GABAergic cells in the BLA (4.8% and 6.9% of all neurons in the LA and BA, respectively; Vereczki et al., 2021), have short dendrites and their axons are confined to the close vicinity of the soma (Rhomberg et al., 2018). Using optogenetics and viral tracing in VIP-Cre mice combined with confocal microscopy, it has been revealed that VIP interneurons innervate GABAergic cells that express PV or SST in addition to CCK+ basket cells and other VIP interneurons (Rhomberg et al., 2018; Krabbe et al., 2019). Of note, neurogliaform cells are rarely among the targets of VIP interneurons (Rhomberg et al., 2018), similarly to that observed in the auditory cortex (Abs et al., 2018). At present, however, it is not clear how many VIP/CB1-expressing basket cells are labeled among all VIP interneurons in VIP-Cre mice. Based on indirect evidence, it seems safe to assume that the ratio of non-disinhibitory VIP interneurons may not be substantial among viral infected neurons in VIP-Cre mice 4–5 weeks after AAV injection, as no VIP basket cells have been recorded so far using this approach. In contrast, when VIP-Cre mice were crossed with the RCL_ChR2/EYFP mouse line Ai32, CB1 sensitive postsynaptic responses were readily recorded in amygdalar principal neurons (Rhomberg et al., 2018). These observations may imply that a longer time is needed for the virus infection of VIP/CB1 basket cells than of VIP interneuron-specific interneurons.

VIP interneurons receive innervation from distinct extra-amygdalar sources and from local principal neurons, although this has not been demonstrated directly. Using monosynaptic rabies tracing, a wide range of cortical and subcortical areas have been identified as an input region to VIP interneurons. Specifically, neurons located in the auditory, insular, and rhinal cortices, ventral hippocampus, basal forebrain, and also in different thalamic nuclei provide innervation onto VIP interneurons (Krabbe et al., 2019). In addition, local GABAergic afferents also contribute to their inputs: VIP interneurons may innervate each other and receive GABAergic inputs from PV basket cells, SST inhibitory cells, and CCK/CB1 basket cells (Rhomberg et al., 2018; Krabbe et al., 2019). At present, it is unknown whether neurogliaform cells can influence the function of VIP interneuron-selective interneurons.

An already mentioned study has provided insights into the function of VIP interneurons in the amygdala during fear learning as well (Krabbe et al., 2019). Using *in vivo* imaging of Ca^{2+} activity in freely moving mice the authors observed that at the beginning of the conditioning the majority of VIP interneurons increased their activity when the US was delivered. As the conditioning progressed, VIP interneurons responded less to the US, and instead, they began to be activated by the CS. As a proof for the disinhibitory function of VIP interneurons, the activity of principal neurons, which was normally elevated by the US, could be significantly reduced if the elevated activity of VIP interneurons induced by the CS was suppressed by optogenetics. These results clearly show that: (i) VIP interneurons have disinhibitory function in the BLA, (ii) they are strongly activated by salient stimuli and (iii) their activity changes during conditioning in a way that is characteristic for neurons signaling prediction errors. Although this study has not examined the sources of afferents onto VIP interneurons that may excite them during the US presentation, it is tempting to speculate that cholinergic cells in the basal forebrain, neurons that reliably and profoundly discharge upon US presentation (Hangya et al., 2015) can contribute to driving the spiking of VIP interneurons, as these cholinergic connections have been demonstrated experimentally (Krabbe et al., 2019). In addition, thalamic afferents may also contribute to the US-induced excitation of VIP interneurons, as both midline and posterior thalamic neurons are activated by the US (Zhu et al., 2018; Barsy et al., 2020) and innervate these disinhibitory cells (Krabbe et al., 2019). Further studies will be needed to elucidate the role of these disinhibitory cells in other amygdala functions.

GABAergic PROJECTION NEURONS

The last group of inhibitory cells present in cortical structures are not, strictly speaking, interneurons, as in addition to often having local axonal collaterals, they give rise to long-range projections to remote brain regions, as it was demonstrated first in the hippocampus (Alonso and Köhler, 1982; Seress and Ribak, 1983). These GABAergic projection neurons typically have large somata and elongated dendrites, often decorated with spines. Many of them are located close to or within the axonal bundles of cortical principal neurons, i.e., in the alveus/stratum oriens of the hippocampus, in the hilus of the dentate gyrus, or in the sixth layer of the neocortex (Tóth and Freund, 1992; Gulyas et al., 2003; Jinno et al., 2007; Tomioka and Rockland, 2007; Takács et al., 2008; He et al., 2016), where they have the largest chance to be innervated in a feedback manner. The most studied GABAergic projection neurons are the hippocampo-septal GABAergic cells that express SST, Calb, NPY in some cases (Tóth and Freund, 1992; Gulyas et al., 2003; Jinno et al., 2007), and interestingly, even VGluT3 (Pelkey et al., 2020). These GABAergic cells receive a high number of excitatory synapses on their membrane surface (∼20–35,000) and much fewer inhibitory synapses, many of which originate from the medial septum (∼1,000–2,500; Takács et al., 2008), implicating that they are relatively unaffected by interneuronal operation, but are in the position to efficiently monitor the on-going principal neuron activity. Hippocampo-septal inhibitory cells preferentially, if not exclusively target hippocampal interneurons locally (Gulyas et al., 2003), but see (Jinno et al., 2007). Another large group of GABAergic projection neurons expresses muscarinic receptor type 2 (M2; Hajos et al., 1998; Ferraguti et al., 2005). In contrast to hippocampo-septal cells, M2 GABAergic cells can often be found in all layers of the hippocampus and cortex (Hajos et al., 1998; Tomioka and Rockland, 2007), and they prefer to innervate other GABAergic cells (Ferraguti et al., 2005; Katona et al., 2020).

Such GABAergic projection neurons are present also in the amygdala (McDonald et al., 2012; Bienvenu et al., 2015; McDonald and Zaric, 2015). Those GABAergic neurons that project to the basal forebrain (specifically to the substantia innominata and horizontal limb of the diagonal band of Broca, HDB) express SST, Calb, or NPY (McDonald et al., 2012), and nNOS (Vereczki et al., 2021). Interestingly, the

majority of these projecting inhibitory neurons are located either paracapsularly, i.e., on the verge of the LA, BA, and BM, often between these nuclei, or in the external capsule (McDonald et al., 2012; Vereczki et al., 2021), which seems to be equivalent with the alveus of the hippocampus, as it is formed by axonal bundles. In addition, GABAegic neurons projecting to the entorhinal cortex have been also identified in the BLA complex (McDonald and Zaric, 2015). These neurons had a similar location and neurochemical profile as those GABAergic cells that send axon collaterals to the basal forebrain and they also contain nNOS (Vereczki et al., 2021). At present, however, it is not clear whether the same GABAergic projection neurons innervate both the basal forebrain and entorhinal cortex, as suggested by their soma localization within the amygdala and their comparable neurochemical profile. M2 GABAergic neurons have also been described in the amygdala (McDonald and Mascagni, 2011). These neurons, similar to those identified in the hippocampus (Hajos et al., 1998), have large somata and long, sparsely ramified dendrites. Some of these neurons are restricted to the external capsule, displaying elongated morphology, whereas others have a multipolar appearance. It has been verified that some of the M2 GABAergic neurons expressing SST project to the entorhinal cortex (McDonald and Zaric, 2015). In general, GABAergic neurons located in the external capsule are strategically positioned to provide both feedback and feedforward inhibition that can even control synaptic plasticity within amygdalar circuits (Morozov et al., 2011).

Those SST GABAergic cells that express high levels of nNOS belong to GABAergic projection neurons (Vereczki et al., 2021), similarly to those neurons that have been described in the hippocampus (Sik et al., 1994; Christenson Wick et al., 2019) and neocortex (He et al., 2016). In the amygdala, the vast majority of strongly immunopositive nNOS GABAergic cells also show immunoreactivity for SST, NPY, and type 1 neurokinin receptor (NK1, substance P receptor; Bocchio et al., 2016). In the LA and BA, 40 and 25% of all SST GABAergic cells, respectively, were strongly immunopositive for nNOS (Vereczki et al., 2021). These nNOS inhibitory cells were located predominantly in the paracapsular zone of the LA and BA, but some of them were present between these two nuclei (Bocchio et al., 2016), resembling the localization of those SST GABAergic neurons that project outside of the amygdala. Spiking of nNOS inhibitory neurons show accommodation and an h-current-mediated sag decorates their voltage responses upon hyperpolarizing current injection (Bocchio et al., 2016), single-cell properties indistinguishable from SST interneurons (Vereczki et al., 2021). Interestingly, these amygdalar nNOS GABAergic neurons were activated during sleep, an effect that may be linked to their serotonergic receptor expression, as 5-HT application changed their tonic firing to bursting mode measured in acute slices (Bocchio et al., 2016). In line with the potential role for nNOS/SST GABAergic neurons in controlling sleep, a recent study has shown that deleting nNOS from cortical SST inhibitory cells led to changes in slow wave sleep as well as in recognition memory (Zielinski et al., 2019). No doubt, specific modulation of the function of nNOS/NPY/SST GABAergic neurons using an intersectional viral strategy is needed in the future to uncover their contribution to sleep and other cortical operations.

GABAergic projection neurons that lack SST immunoreactivity, but express metabotropic glutamate receptor type 1α (mGluR1α), PV, and $GABA_A$ receptor subunit α1, have been identified in the rat BLA (Bienvenu et al., 2015). Although the authors of this study named mGluR1α GABAergic neurons as large intercalated cells, because their somata and dendrites were preferentially located within the external capsule, often surrounding intercalated cell masses, these inhibitory neurons may belong rather to the amygdala circuits based on their connectivity. The vast majority of the axons of *in vivo* labeled large mGluR1α GABAergic neurons arborized in the LA and BA, while only a negligible portion of their axon terminals was observed in the central amygdala, and no axons were found in the amygdalo-striatal area, the two striatal structures that are the main projection targets of intercalated cells (Pare and Smith, 1993; Busti et al., 2011; Asede et al., 2015). These large mGluR1α GABAergic cells projected to perirhinal, entorhinal, and endopiriform cortices (Bienvenu et al., 2015). Of note, both locally and remotely, the targets of these GABAergic projection neurons were inhibitory cells, preferentially PV interneurons. Furthermore, mGluR1α GABAergic cells were strongly excited by noxious stimuli (Bienvenu et al., 2015). These data collectively imply that, in addition to VIP interneurons, there may be another GABAergic neuronal element within amygdala circuits that disinhibit principal neurons during the presentation of aversive stimuli, and, therefore, promote associative learning.

In summary, GABAergic long-range projections from the BLA to remote areas originate from various inhibitory cell groups. Undoubtedly, more work is needed to understand their role in circuit function.

CONCLUSIONS

Recent studies have elucidated that GABAergic cells in the BLA correspond to those inhibitory neurons, both interneurons and projection neurons that were described in other cortical networks based on their morphology, single-cell features, and connectivity (**Figures 1**, **3**). Overall, these results support the view that there are given circuit motifs universally found in all cortical structures (**Figure 3**). However, there are also notable differences among cortical areas, for instance, the differences in the peak amplitude of postsynaptic responses at the output synapses of perisomatic inhibitory cells relative to each other, a parameter that determines the efficacy of inhibition. Such variabilities along with other inhibitory circuit features likely contribute to distinctive network operations necessary to fulfill the functions of a given cortical region. A better understanding of similarities and differences in microcircuit organizations should help recognize the role of the given cortical area in information processing. To reach this goal, distinct types of interneurons should be manipulated selectively. For instance, at present, PV basket cells and PV axo-axonic cells are impacted simultaneously by using PV-Cre

mice, yet it would be ideal to modulate their functions separately, to which end, novel tools and approaches should be developed. In addition, behavioral manipulations using currently available tools like opto- and chemogenetics should be extended to uncover circuit mechanisms as completely as possible, perhaps by combining research efforts of teams, experts of different methodologies. Finally, rigorous and often labor-intense examinations of wiring principles should be implemented to gain deeper insight into network operations at the cellular, synaptic, and microcircuit levels. Combinations of these approaches with high quality and comprehensive investigations will result in a substantial advance in our knowledge about different GABAergic neuron types and their function in the BLA, a prerequisite for understanding the role of distinct inhibitory circuits in normal and pathological amygdala operation.

AUTHOR CONTRIBUTIONS

The author wrote this review article.

FUNDING

This study was supported by the National Research, Development and Innovation Office (K_119742) and the Hungarian Brain Research Program (2017-1.2.1-NKP-2017-00002).

ACKNOWLEDGMENTS

I would like to thank my past and present colleagues for their enthusiasm and commitment in their research. Specifically, I am grateful for the discussions and for reflecting together on scientific problems. In addition, I would like to express my recognition to Judit Veres for her help in preparation of the figures and her comments on this review together with Tibor Andrási, Zsuzsanna Fekete and Rita Karlócai. I also thank László Barna, the Nikon Microscopy Center at the Institute of Experimental Medicine, Nikon Austria GmbH, and Auro-Science Consulting, Ltd., for kindly providing microscopy support.

REFERENCES

Abs, E., Poorthuis, R. B., Apelblat, D., Muhammad, K., Pardi, M. B., Enke, L., et al. (2018). Learning-related plasticity in dendrite-targeting layer 1 interneurons. *Neuron* 100, e686.684–e686.699. doi: 10.1016/j.neuron.2018.09.001

Acsády, L., Gorcs, T. J., and Freund, T. F. (1996). Different populations of vasoactive intestinal polypeptide- immunoreactive interneurons are specialized to control pyramidal cells or interneurons in the hippocampus. *Neuroscience* 73, 317–334. doi: 10.1016/0306-4522(95)00609-5

Alexander, W. H., and Brown, J. W. (2018). Frontal cortex function as derived from hierarchical predictive coding. *Sci. Rep.* 8:3843. doi: 10.1038/s41598-018-21407-9

Alonso, A., and Köhler, C. (1982). Evidence for separate projections of hippocampal pyramidal and non-pyramidal neurons to different parts of the septum in the rat brain. *Neurosci. Lett.* 31, 209–214. doi: 10.1016/0304-3940(82)90021-0

Amaral, D. G., Avendano, C., and Benoit, R. (1989). Distribution of somatostatin-like immunoreactivity in the monkey amygdala. *J. Comp. Neurol.* 284, 294–313. doi: 10.1002/cne.902840211

Amir, A., Pare, J. F., Smith, Y., and Pare, D. (2019). Midline thalamic inputs to the amygdala: Ultrastructure and synaptic targets. *J. Comp. Neurol.* 527, 942–956. doi: 10.1002/cne.24557

Andrasi, T., Veres, J. M., Rovira-Esteban, L., Kozma, R., Vikor, A., Gregori, E., et al. (2017). Differential excitatory control of 2 parallel basket cell networks in amygdala microcircuits. *PLoS Biol.* 15:e2001421. doi: 10.1371/journal.pbio.2001421

Asede, D., Bosch, D., Luthi, A., Ferraguti, F., and Ehrlich, I. (2015). Sensory inputs to intercalated cells provide fear-learning modulated inhibition to the basolateral amygdala. *Neuron* 86, 541–554. doi: 10.1016/j.neuron.2015.03.008

Azad, S. C., Kurz, J., Marsicano, G., Lutz, B., Zieglgansberger, W., and Rammes, G. (2008). Activation of CB1 specifically located on GABAergic interneurons inhibits LTD in the lateral amygdala. *Learn. Mem.* 15, 143–152. doi: 10.1101/lm.741908

Baldi, R., Varga, C., and Tamas, G. (2010). Differential distribution of KCC2 along the axo-somato-dendritic axis of hippocampal principal cells. *Eur. J. Neurosci.* 32, 1319–1325. doi: 10.1111/j.1460-9568.2010.07361.x

Barsy, B., Kocsis, K., Magyar, A., Babiczky, A., Szabo, M., Veres, J. M., et al. (2020). Associative and plastic thalamic signaling to the lateral amygdala controls fear behavior. *Nat. Neurosci.* 23, 625–637. doi: 10.1038/s41593-020-0620-z

Barsy, B., Szabo, G. G., Andrasi, T., Vikor, A., and Hajos, N. (2017). Different output properties of perisomatic region-targeting interneurons in the basal amygdala. *Eur. J. Neurosci.* 45, 548–558. doi: 10.1111/ejn.13498

Bienvenu, T. C., Busti, D., Magill, P. J., Ferraguti, F., and Capogna, M. (2012). Cell-type-specific recruitment of amygdala interneurons to hippocampal theta rhythm and noxious stimuli *in vivo*. *Neuron* 74, 1059–1074. doi: 10.1016/j.neuron.2012.04.022

Bienvenu, T. C., Busti, D., Micklem, B. R., Mansouri, M., Magill, P. J., Ferraguti, F., et al. (2015). Large intercalated neurons of amygdala relay noxious sensory information. *J. Neurosci.* 35, 2044–2057. doi: 10.1523/JNEUROSCI.1323-14.2015

Blasco-Ibanez, J. M., and Freund, T. F. (1995). Synaptic input of horizontal interneurons in stratum oriens of the hippocampal CA1 subfield:srtructural basis of feed-back activation. *Eur. J. Neurosci.* 7, 2170–2180. doi: 10.1111/j.1460-9568.1995.tb00638.x

Bocchio, M., Fisher, S. P., Unal, G., Ellender, T. J., Vyazovskiy, V. V., and Capogna, M. (2016). Sleep and serotonin modulate paracapsular nitric oxide synthase expressing neurons of the amygdala. *eNeuro* 3:ENEURO.0177-16.2016. doi: 10.1523/ENEURO.0177-16.2016

Bodor, A. L., Katona, I., Nyiri, G., Mackie, K., Ledent, C., Hajos, N., et al. (2005). Endocannabinoid signaling in rat somatosensory cortex: laminar differences and involvement of specific interneuron types. *J. Neurosci.* 25, 6845–6856. doi: 10.1523/JNEUROSCI.0442-05.2005

Booker, S. A., Gross, A., Althof, D., Shigemoto, R., Bettler, B., Frotscher, M., et al. (2013). Differential GABAB-receptor-mediated effects in perisomatic- and dendrite-targeting parvalbumin interneurons. *J. Neurosci.* 33, 7961–7974. doi: 10.1523/JNEUROSCI.1186-12.2013

Brinley-Reed, M., Mascagni, F., and McDonald, A. J. (1995). Synaptology of prefrontal cortical projections to the basolateral amygdala: an electron microscopic study in the rat. *Neurosci. Lett.* 202, 45–48. doi: 10.1016/0304-3940(95)12212-5

Burke, D. A., Rotstein, H. G., and Alvarez, V. A. (2017). Striatal local circuitry: a new framework for lateral inhibition. *Neuron* 96, 267–284. doi: 10.1016/j.neuron.2017.09.019

Busti, D., Geracitano, R., Whittle, N., Dalezios, Y., Manko, M., Kaufmann, W., et al. (2011). Different fear states engage distinct networks within the intercalated cell clusters of the amygdala. *J. Neurosci.* 31, 5131–5144. doi: 10.1523/JNEUROSCI.6100-10.2011

Christenson Wick, Z., Tetzlaff, M. R., and Krook-Magnuson, E. (2019). Novel long-range inhibitory nNOS-expressing hippocampal cells. *eLife* 8:e46816. doi: 10.7554/eLife.46816

Ehrlich, I., Humeau, Y., Grenier, F., Ciocchi, S., Herry, C., and Luthi, A. (2009). Amygdala inhibitory circuits and the control of fear memory. *Neuron* 62, 757–771. doi: 10.1016/j.neuron.2009.05.026

Fanselow, M. S., and LeDoux, J. E. (1999). Why we think plasticity underlying Pavlovian fear conditioning occurs in the basolateral amygdala. *Neuron* 23, 229–232. doi: 10.1016/s0896-6273(00)80775-8

Fekete, Z., Weisz, F., Karlócai, R. M., Andrási, T., and Hájos, N. (2019). Synaptic communication between pyramidal cells and perisomatic inhibitory cells in the mouse prefrontal cortex," in *16th Annual Conference of the Hungarian Neuroscience Society Hungarian Academy of Sciences*, (Debrecen, Hungary). Available online at: https://www.remedicon.hu/tartalmak/fajlok/fajl_poster-abstracts-17v5_20190116091602.pdf.

Ferraguti, F., Klausberger, T., Cobden, P., Baude, A., Roberts, J. D., Szucs, P., et al. (2005). Metabotropic glutamate receptor 8-expressing nerve terminals target subsets of GABAergic neurons in the hippocampus. *J. Neurosci.* 25, 10520–10536. doi: 10.1523/JNEUROSCI.2547-05.2005

Fishell, G., and Kepecs, A. (2020). Interneuron types as attractors and controllers. *Annu. Rev. Neurosci.* 43, 1–30. doi: 10.1146/annurev-neuro-070918-050421

Fremeau, R. T. Jr., Troyer, M. D., Pahner, I., Nygaard, G. O., Tran, C. H., Reimer, R. J., et al. (2001). The expression of vesicular glutamate transporters defines two classes of excitatory synapse. *Neuron* 31, 247–260. doi: 10.1016/s0896-6273(01)00344-0

Freund, T. F., and Katona, I. (2007). Perisomatic inhibition. *Neuron* 56, 33–42. doi: 10.1016/j.neuron.2007.09.012

Gulyas, A. I., Hajos, N., and Freund, T. F. (1996). Interneurons containing calretinin are specialized to control other interneurons in the rat hippocampus. *J. Neurosci.* 16, 3397–3411. doi: 10.1523/JNEUROSCI.16-10-03397.1996

Gulyas, A. I., Hajos, N., Katona, I., and Freund, T. F. (2003). Interneurons are the local targets of hippocampal inhibitory cells which project to the medial septum. *Eur. J. Neurosci.* 17, 1861–1872. doi: 10.1046/j.1460-9568.2003.02630.x

Gulyas, A. I., Megias, M., Emri, Z., and Freund, T. F. (1999). Total number and ratio of excitatory and inhibitory synapses converging onto single interneurons of different types in the CA1 area of the rat hippocampus. *J. Neurosci.* 19, 10082–10097. doi: 10.1523/JNEUROSCI.19-22-10082.1999

Gulyas, A. I., Szabo, G. G., Ulbert, I., Holderith, N., Monyer, H., Erdelyi, F., et al. (2010). Parvalbumin-containing fast-spiking basket cells generate the field potential oscillations induced by cholinergic receptor activation in the hippocampus. *J. Neurosci.* 30, 15134–15145. doi: 10.1523/JNEUROSCI.4104-10.2010

Guthman, E. M., Garcia, J. D., Ma, M., Chu, P., Baca, S. M., Smith, K. R., et al. (2020). Cell-type-specific control of basolateral amygdala neuronal circuits *via* entorhinal cortex-driven feedforward inhibition. *eLife* 9:e50601. doi: 10.7554/eLife.50601

Hájos, N., Acsády, L., and Freund, T. F. (1996). Target selectivity and neurochemical characteristics of VIP- immunoreactive interneurons in the rat dentate gyrus. *Eur. J. Neurosci.* 8, 1415–1431. doi: 10.1111/j.1460-9568.1996.tb01604.x

Hajos, N., Papp, E. C., Acsady, L., Levey, A. I., and Freund, T. F. (1998). Distinct interneuron types express m2 muscarinic receptor immunoreactivity on their dendrites or axon terminals in the hippocampus. *Neuroscience* 82, 355–376. doi: 10.1016/s0306-4522(97)00300-x

Halasy, K., Buhl, E. H., Lorinczi, Z., Tamas, G., and Somogyi, P. (1996). Synaptic target selectivity and input of GABAergic basket and bistratified interneurons in the CA1 area of the rat hippocampus. *Hippocampus* 6, 306–329. doi: 10.1002/(SICI)1098-1063(1996)6:3<306::AID-HIPO8>3.0.CO;2-K

Hangya, B., Ranade, S. P., Lorenc, M., and Kepecs, A. (2015). Central cholinergic neurons are rapidly recruited by reinforcement feedback. *Cell* 162, 1155–1168. doi: 10.1016/j.cell.2015.07.057

He, M., Tucciarone, J., Lee, S., Nigro, M. J., Kim, Y., Levine, J. M., et al. (2016). Strategies and tools for combinatorial targeting of GABAergic neurons in mouse cerebral cortex. *Neuron* 91, 1228–1243. doi: 10.1016/j.neuron.2016.08.021

Hendry, S. H., Jones, E. G., and Beinfeld, M. C. (1983). Cholecystokinin-immunoreactive neurons in rat and monkey cerebral cortex make symmetric synapses and have intimate associations with blood vessels. *Proc. Natl. Acad. Sci. U S A* 80, 2400–2404. doi: 10.1073/pnas.80.8.2400

Hendry, S. H. C., Jones, E. G., Emson, P. S., Lawson, D. E. M., Heizmann, C. W., and Streit, P. (1989). Two classes of cortical GABA neurons defined by differential calcium binding protein immunoreactivities. *Exp. Brain Res.* 76, 467–472. doi: 10.1007/BF00247904

Herry, C., Ciocchi, S., Senn, V., Demmou, L., Muller, C., and Luthi, A. (2008). Switching on and off fear by distinct neuronal circuits. *Nature* 454, 600–606. doi: 10.1038/nature07166

Hu, H., Gan, J., and Jonas, P. (2014). Interneurons. Fast-spiking, parvalbumin(+) GABAergic interneurons: from cellular design to microcircuit function. *Science* 345:1255263. doi: 10.1126/science.1255263

Ito, M. (2006). Cerebellar circuitry as a neuronal machine. *Prog. Neurobiol.* 78, 272–303. doi: 10.1016/j.pneurobio.2006.02.006

Ito, W., Fusco, B., and Morozov, A. (2020). Disinhibition-assisted long-term potentiation in the prefrontal-amygdala pathway *via* suppression of somatostatin-expressing interneurons. *Neurophotonics* 7:015007. doi: 10.1117/1.NPh.7.1.015007

Jackson, J., Karnani, M. M., Zemelman, B. V., Burdakov, D., and Lee, A. K. (2018). Inhibitory control of prefrontal cortex by the claustrum. *Neuron* 99, e4.1029–e4.1039. doi: 10.1016/j.neuron.2018.07.031

Janak, P. H., and Tye, K. M. (2015). From circuits to behaviour in the amygdala. *Nature* 517, 284–292. doi: 10.1038/nature14188

Jasnow, A. M., Ressler, K. J., Hammack, S. E., Chhatwal, J. P., and Rainnie, D. G. (2009). Distinct subtypes of cholecystokinin (CCK)-containing interneurons of the basolateral amygdala identified using a CCK promoter-specific lentivirus. *J. Neurophysiol.* 101, 1494–1506. doi: 10.1152/jn.91149.2008

Jinno, S., Klausberger, T., Marton, L. F., Dalezios, Y., Roberts, J. D., Fuentealba, P., et al. (2007). Neuronal diversity in GABAergic long-range projections from the hippocampus. *J. Neurosci.* 27, 8790–8804. doi: 10.1523/JNEUROSCI.1847-07.2007

Kaila, K., Price, T. J., Payne, J. A., Puskarjov, M., and Voipio, J. (2014). Cation-chloride cotransporters in neuronal development, plasticity and disease. *Nat. Rev. Neurosci.* 15, 637–654. doi: 10.1038/nrn3819

Katona, I., Acsady, L., and Freund, T. F. (1999a). Postsynaptic targets of somatostatin-immunoreactive interneurons in the rat hippocampus. *Neuroscience* 88, 37–55. doi: 10.1016/s0306-4522(98)00302-9

Katona, I., Sperlagh, B., Sik, A., Kafalvi, A., Vizi, E. S., Mackie, K., et al. (1999b). Presynaptically located CB1 cannabinoid receptors regulate GABA release from axon terminals of specific hippocampal interneurons. *J. Neurosci.* 19, 4544–4558. doi: 10.1523/JNEUROSCI.19-11-04544.1999

Katona, I., Rancz, E. A., Acsady, L., Ledent, C., Mackie, K., Hajos, N., et al. (2001). Distribution of CB1 cannabinoid receptors in the amygdala and their role in the control of GABAergic transmission. *J. Neurosci.* 21, 9506–9518. doi: 10.1523/JNEUROSCI.21-23-09506.2001

Katona, L., Hartwich, K., Tomioka, R., Somogyi, J., Roberts, J. D. B., Wagner, K., et al. (2020). Synaptic organisation and behaviour-dependent activity of mGluR8a-innervated GABAergic trilaminar cells projecting from the hippocampus to the subiculum. *Brain Struct. Funct.* 225, 705–734. doi: 10.1007/s00429-020-02029-2

Kawaguchi, Y., Katsumaru, H., Kosaka, T., Heizmann, C. W., and Hama, K. (1987). Fast spiking cells in rat hippocampus (CA1 region) contain the calcium-binding protein parvalbumin. *Brain Res.* 416, 369–374. doi: 10.1016/0006-8993(87)90921-8

Kawaguchi, Y., and Kubota, Y. (1996). Physiological and morphological identification of somatostatin- or vasoactive intestinal polypeptide-containing cells among GABAergic cell subtypes in rat frontal cortex. *J. Neurosci.* 16, 2701–2715. doi: 10.1523/JNEUROSCI.16-08-02701.1996

Keller, G. B., and Mrsic-Flogel, T. D. (2018). Predictive processing: a canonical cortical computation. *Neuron* 100, 424–435. doi: 10.1016/j.neuron.2018.10.003

Khalaf, O., Resch, S., Dixsaut, L., Gorden, V., Glauser, L., and Graff, J. (2018). Reactivation of recall-induced neurons contributes to remote fear memory attenuation. *Science* 360, 1239–1242. doi: 10.1126/science.aas9875

Khirug, S., Yamada, J., Afzalov, R., Voipio, J., Khiroug, L., and Kaila, K. (2008). GABAergic depolarization of the axon initial segment in cortical principal neurons is caused by the Na-K-2Cl cotransporter NKCC1. *J. Neurosci.* 28, 4635–4639. doi: 10.1523/JNEUROSCI.0908-08.2008

Kida, S. (2019). Reconsolidation/destabilization, extinction and forgetting of fear memory as therapeutic targets for PTSD. *Psychopharmacology (Berl)* 236, 49–57. doi: 10.1007/s00213-018-5086-2

Kim, J., Pignatelli, M., Xu, S., Itohara, S., and Tonegawa, S. (2016). Antagonistic negative and positive neurons of the basolateral amygdala. *Nat. Neurosci.* 19, 1636–1646. doi: 10.1038/nn.4414

Klausberger, T., Marton, L. F., Baude, A., Roberts, J. D., Magill, P. J., and Somogyi, P. (2004). Spike timing of dendrite-targeting bistratified cells during hippocampal network oscillations *in vivo*. *Nat. Neurosci.* 7, 41–47. doi: 10.1038/nn1159

Kohus, Z., Kali, S., Rovira-Esteban, L., Schlingloff, D., Papp, O., Freund, T. F., et al. (2016). Properties and dynamics of inhibitory synaptic communication within the CA3 microcircuits of pyramidal cells and interneurons expressing parvalbumin or cholecystokinin. *J. Physiol.* 594, 3745–3774. doi: 10.1038/s41598-021-89378-y

Krabbe, S., Grundemann, J., and Luthi, A. (2018). Amygdala inhibitory circuits regulate associative fear conditioning. *Biol. Psychiatry* 83, 800–809. doi: 10.1016/j.biopsych.2017.10.006

Krabbe, S., Paradiso, E., d'Aquin, S., Bitterman, Y., Courtin, J., Xu, C., et al. (2019). Adaptive disinhibitory gating by VIP interneurons permits associative learning. *Nat. Neurosci.* 22, 1834–1843. doi: 10.1038/s41593-019-0508-y

Kriebel, M., Metzger, J., Trinks, S., Chugh, D., Harvey, R. J., Harvey, K., et al. (2011). The cell adhesion molecule neurofascin stabilizes axo-axonic GABAergic terminals at the axon initial segment. *J. Biol. Chem.* 286, 24385–24393. doi: 10.1074/jbc.M110.212191

LeDoux, J. E. (2000). Emotion circuits in the brain. *Annu. Rev. Neurosci.* 23, 155–184. doi: 10.1146/annurev.neuro.23.1.155

Lucas, E. K., Jegarl, A. M., Morishita, H., and Clem, R. L. (2016). Multimodal and site-specific plasticity of amygdala parvalbumin interneurons after fear learning. *Neuron* 91, 629–643. doi: 10.1016/j.neuron.2016.06.032

Maccaferri, G., and McBain, C. J. (1995). Passive propagation of LTD to stratum oriens-alveus inhibitory neurons modulates the temporoammonic input to the hippocampal CA1 region. *Neuron* 15, 137–145. doi: 10.1016/0896-6273(95)90071-3

Maccaferri, G., Roberts, J. D., Szucs, P., Cottingham, C. A., and Somogyi, P. (2000). Cell surface domain specific postsynaptic currents evoked by identified GABAergic neurones in rat hippocampus *in vitro*. *J. Physiol.* 524, 91–116. doi: 10.1111/j.1469-7793.2000.t01-3-00091.x

Mahanty, N. K., and Sah, P. (1998). Calcium-permeable AMPA receptors mediate long-term potentiation in interneurons in the amygdala. *Nature* 394, 683–687. doi: 10.1038/29312

Manassero, E., Renna, A., Milano, L., and Sacchetti, B. (2018). Lateral and basal amygdala account for opposite behavioral responses during the long-term expression of fearful memories. *Sci. Rep.* 8:518. doi: 10.1038/s41598-017-19074-3

Manko, M., Bienvenu, T. C., Dalezios, Y., and Capogna, M. (2012). Neurogliaform cells of amygdala: a source of slow phasic inhibition in the basolateral complex. *J. Physiol.* 590, 5611–5627. doi: 10.1113/jphysiol.2012.236745

Maren, S. (2001). Neurobiology of Pavlovian fear conditioning. *Annu. Rev. Neurosci.* 24, 897–931. doi: 10.1146/annurev.neuro.24.1.897

Mascagni, F., and McDonald, A. J. (2003). Immunohistochemical characterization of cholecystokinin containing neurons in the rat basolateral amygdala. *Brain Res.* 976, 171–184. doi: 10.1016/s0006-8993(03)02625-8

Mascagni, F., Muly, E. C., Rainnie, D. G., and McDonald, A. J. (2009). Immunohistochemical characterization of parvalbumin-containing interneurons in the monkey basolateral amygdala. *Neuroscience* 158, 1541–1550. doi: 10.1016/j.neuroscience.2008.11.017

Massi, L., Lagler, M., Hartwich, K., Borhegyi, Z., Somogyi, P., and Klausberger, T. (2012). Temporal dynamics of parvalbumin-expressing axo-axonic and basket cells in the rat medial prefrontal cortex *in vivo*. *J. Neurosci.* 32, 16496–16502. doi: 10.1523/JNEUROSCI.3475-12.2012

Matyas, F., Freund, T. F., and Gulyas, A. I. (2004). Convergence of excitatory and inhibitory inputs onto CCK-containing basket cells in the CA1 area of the rat hippocampus. *Eur. J. Neurosci.* 19, 1243–1256. doi: 10.1111/j.1460-9568.2004.03225.x

McBain, C. J., DiChiara, T. J., and Kauer, J. A. (1994). Activation of metabotropic glutamate receptors differentially affects two classes of hippocampal interneurons and potentiates excitatory synaptic transmission. *J. Neurosci.* 14, 4433–4445. doi: 10.1523/JNEUROSCI.14-07-04433.1994

McDonald, A. J. (1985). Immunohistochemical identification of gamma-aminobutyric acid-containing neurons in the rat basolateral amygdala. *Neurosci. Lett.* 53, 203–207. doi: 10.1016/0304-3940(85)90186-7

McDonald, A. J. (1989). Coexistence of somatostatin with neuropeptide Y, but not with cholecystokinin or vasoactive intestinal peptide, in neurons of the rat amygdala. *Brain Res.* 500, 37–45. doi: 10.1016/0006-8993(89)90297-7

McDonald, A. J. (1991). Topographical organization of amygdaloid projections to the caudatoputamen, nucleus accumbens and related striatal-like areas of the rat brain. *Neuroscience* 44, 15–33. doi: 10.1016/0306-4522(91)90248-m

McDonald, A. J. (1992). Projection neurons of the basolateral amygdala: a correlative Golgi and retrograde tract tracing study. *Brain Res. Bull.* 28, 179–185. doi: 10.1016/0361-9230(92)90177-y

McDonald, A. J. (2021). Expression of the type 1 cannabinoid receptor (CB1R) in CCK-immunoreactive axon terminals in the basolateral amygdala of the rhesus monkey (*Macaca mulatta*). *Neurosci. Lett.* 745:135503. doi: 10.1016/j.neulet.2020.135503

McDonald, A. J., and Augustine, J. R. (2020). Nonpyramidal neurons in the primate basolateral amygdala: a golgi study in the baboon (*Papio cynocephalus*) and long-tailed macaque (*Macaca fascicularis*). *J. Comp. Neurol.* 528, 772–786. doi: 10.1002/cne.24785

McDonald, A. J., and Betette, R. L. (2001). Parvalbumin-containing neurons in the rat basolateral amygdala: morphology and co-localization of Calbindin-D(28k). *Neuroscience* 102, 413–425. doi: 10.1016/s0306-4522(00)00481-4

McDonald, A. J., and Mascagni, F. (2001). Localization of the CB1 type cannabinoid receptor in the rat basolateral amygdala: high concentrations in a subpopulation of cholecystokinin-containing interneurons. *Neuroscience* 107, 641–652. doi: 10.1016/s0306-4522(01)00380-3

McDonald, A. J., and Mascagni, F. (2002). Immunohistochemical characterization of somatostatin containing interneurons in the rat basolateral amygdala. *Brain Res.* 943, 237–244. doi: 10.1016/s0006-8993(02)02650-1

McDonald, A. J., and Mascagni, F. (2011). Neuronal localization of M2 muscarinic receptor immunoreactivity in the rat amygdala. *Neuroscience* 196, 49–65. doi: 10.1016/j.neuroscience.2011.08.032

McDonald, A. J., and Mascagni, F. (2019). Cholecystokinin immunoreactive neurons in the basolateral amygdala of the rhesus monkey (*Macaca mulatta*). *J. Comp. Neurol.* 527, 2694–2702. doi: 10.1002/cne.24700

McDonald, A. J., Mascagni, F., and Augustine, J. R. (1995). Neuropeptide Y and somatostatin-like immunoreactivity in neurons of the monkey amygdala. *Neuroscience* 66, 959–982. doi: 10.1016/0306-4522(94)00629-j

McDonald, A. J., Mascagni, F., Mania, I., and Rainnie, D. G. (2005). Evidence for a perisomatic innervation of parvalbumin-containing interneurons by individual pyramidal cells in the basolateral amygdala. *Brain Res.* 1035, 32–40. doi: 10.1016/j.brainres.2004.11.052

McDonald, A. J., Mascagni, F., and Zaric, V. (2012). Subpopulations of somatostatin-immunoreactive non-pyramidal neurons in the amygdala and adjacent external capsule project to the basal forebrain: evidence for the existence of GABAergic projection neurons in the cortical nuclei and basolateral nuclear complex. *Front. Neural Circuits* 6:46. doi: 10.3389/fncir.2012.00046

McDonald, A. J., Muller, J. F., and Mascagni, F. (2002). GABAergic innervation of alpha type II calcium/calmodulin-dependent protein kinase immunoreactive pyramidal neurons in the rat basolateral amygdala. *J. Comp. Neurol.* 446, 199–218. doi: 10.1002/cne.10204

McDonald, A. J., Muller, J. F., and Mascagni, F. (2011). Postsynaptic targets of GABAergic basal forebrain projections to the basolateral amygdala. *Neuroscience* 183, 144–159. doi: 10.1016/j.neuroscience.2011.03.027

McDonald, A. J., and Zaric, V. (2015). GABAergic somatostatin-immunoreactive neurons in the amygdala project to the entorhinal cortex. *Neuroscience* 290, 227–242. doi: 10.1016/j.neuroscience.2015.01.028

Miczan, V., Kelemen, K., Glavinics, J. R., Laszlo, Z. I., Barti, B., Kenesei, K., et al. (2021). NECAB1 and NECAB2 are prevalent calcium-binding proteins of CB1/CCK-positive GABAergic interneurons. *Cereb. Cortex* 31, 1786–1806. doi: 10.1093/cercor/bhaa326

Miles, R., Toth, K., Gulyás, A. I., Hajos, N., and Freund, T. F. (1996). Differences between somatic and dendritic inhibition in the hippocampus. *Neuron* 16, 815–823. doi: 10.1016/s0896-6273(00)80101-4

Morozov, A., Sukato, D., and Ito, W. (2011). Selective suppression of plasticity in amygdala inputs from temporal association cortex by the external capsule. *J. Neurosci.* 31, 339–345. doi: 10.1523/JNEUROSCI.5537-10.2011

Morrison, D. J., Rashid, A. J., Yiu, A. P., Yan, C., Frankland, P. W., and Josselyn, S. A. (2016). Parvalbumin interneurons constrain the size of the lateral amygdala engram. *Neurobiol. Learn. Mem.* 135, 91–99. doi: 10.1016/j.nlm.2016.07.007

Muller, J. F., Mascagni, F., and McDonald, A. J. (2005). Coupled networks of parvalbumin-immunoreactive interneurons in the rat basolateral amygdala. *J. Neurosci.* 25, 7366–7376. doi: 10.1523/JNEUROSCI.0899-05.2005

Muller, J. F., Mascagni, F., and McDonald, A. J. (2006). Pyramidal cells of the rat basolateral amygdala: synaptology and innervation by parvalbumin-immunoreactive interneurons. *J. Comp. Neurol.* 494, 635–650. doi: 10.1002/cne.20832

Muller, J. F., Mascagni, F., and McDonald, A. J. (2007a). Postsynaptic targets of somatostatin-containing interneurons in the rat basolateral amygdala. *J. Comp. Neurol.* 500, 513–529. doi: 10.1002/cne.21185

Muller, J. F., Mascagni, F., and McDonald, A. J. (2007b). Serotonin-immunoreactive axon terminals innervate pyramidal cells and interneurons in the rat basolateral amygdala. *J. Comp. Neurol.* 505, 314–335. doi: 10.1002/cne.21486

Muller, J. F., Mascagni, F., and McDonald, A. J. (2011). Cholinergic innervation of pyramidal cells and parvalbumin-immunoreactive interneurons in the rat basolateral amygdala. *J. Comp. Neurol.* 519, 790–805. doi: 10.1002/cne.22550

Mullner, F. E., Wierenga, C. J., and Bonhoeffer, T. (2015). Precision of inhibition: dendritic inhibition by individual GABAergic synapses on hippocampal pyramidal cells is confined in space and time. *Neuron* 87, 576–589. doi: 10.1016/j.neuron.2015.07.003

Murayama, M., Perez-Garci, E., Nevian, T., Bock, T., Senn, W., and Larkum, M. E. (2009). Dendritic encoding of sensory stimuli controlled by deep cortical interneurons. *Nature* 457, 1137–1141. doi: 10.1038/nature07663

Nissen, W., Szabo, A., Somogyi, J., Somogyi, P., and Lamsa, K. P. (2010). Cell type-specific long-term plasticity at glutamatergic synapses onto hippocampal interneurons expressing either parvalbumin or CB1 cannabinoid receptor. *J. Neurosci.* 30, 1337–1347. doi: 10.1523/JNEUROSCI.3481-09.2010

Nunzi, M. G., Gorio, A., Milan, F., Freund, T. F., Somogyi, P., and Smith, A. D. (1985). Cholecystokinin-immunoreactive cells form symmetrical synaptic contacts with pyramidal and nonpyramidal neurons in the hippocampus. *J. Comp. Neurol.* 237, 485–505. doi: 10.1002/cne.902370406

Olah, S., Fule, M., Komlosi, G., Varga, C., Baldi, R., Barzo, P., et al. (2009). Regulation of cortical microcircuits by unitary GABA-mediated volume transmission. *Nature* 461, 1278–1281. doi: 10.1038/nature08503

Omiya, Y., Uchigashima, M., Konno, K., Yamasaki, M., Miyazaki, T., Yoshida, T., et al. (2015). VGluT3-expressing CCK-positive basket cells construct invaginating synapses enriched with endocannabinoid signaling proteins in particular cortical and cortex-like amygdaloid regions of mouse brains. *J. Neurosci.* 35, 4215–4228. doi: 10.1523/JNEUROSCI.4681-14.2015

Pare, D., and Smith, Y. (1993). The intercalated cell masses project to the central and medial nuclei of the amygdala in cats. *Neuroscience* 57, 1077–1090. doi: 10.1016/0306-4522(93)90050-p

Pare, D., Smith, Y., and Pare, J. F. (1995). Intra-amygdaloid projections of the basolateral and basomedial nuclei in the cat: phaseolus vulgaris-leucoagglutinin anterograde tracing at the light and electron microscopic level. *Neuroscience* 69, 567–583. doi: 10.1016/0306-4522(95)00272-k

Pelkey, K. A., Calvigioni, D., Fang, C., Vargish, G., Ekins, T., Auville, K., et al. (2020). Paradoxical network excitation by glutamate release from VGluT3(+) GABAergic interneurons. *eLife* 9:e51996. doi: 10.7554/eLife.51996

Phelps, E. A., Lempert, K. M., and Sokol-Hessner, P. (2014). Emotion and decision making: multiple modulatory neural circuits. *Annu. Rev. Neurosci.* 37, 263–287. doi: 10.1146/annurev-neuro-071013-014119

Pi, H. J., Hangya, B., Kvitsiani, D., Sanders, J. I., Huang, Z. J., and Kepecs, A. (2013). Cortical interneurons that specialize in disinhibitory control. *Nature* 503, 521–524. doi: 10.1038/nature12676

Pinard, C. R., Muller, J. F., Mascagni, F., and McDonald, A. J. (2008). Dopaminergic innervation of interneurons in the rat basolateral amygdala. *Neuroscience* 157, 850–863. doi: 10.1016/j.neuroscience.2008.09.043

Pitkanen, A., Savander, V., and LeDoux, J. E. (1997). Organization of intra-amygdaloid circuitries in the rat: an emerging framework for understanding functions of the amygdala. *Trends. Neurosci.* 20, 517–523. doi: 10.1016/s0166-2236(97)01125-9

Polepalli, J. S., Gooch, H., and Sah, P. (2020). Diversity of interneurons in the lateral and basal amygdala. *NPJ Sci. Learn.* 5:10. doi: 10.1038/s41539-020-0071-z

Pouille, F., and Scanziani, M. (2004). Routing of spike series by dynamic circuits in the hippocampus. *Nature* 429, 717–723. doi: 10.1038/nature02615

Poulin, J. F., Castonguay-Lebel, Z., Laforest, S., and Drolet, G. (2008). Enkephalin co-expression with classic neurotransmitters in the amygdaloid complex of the rat. *J. Comp. Neurol.* 506, 943–959. doi: 10.1002/cne.21587

Price, C. J., Scott, R., Rusakov, D. A., and Capogna, M. (2008). GABA(B) receptor modulation of feedforward inhibition through hippocampal neurogliaform cells. *J. Neurosci.* 28, 6974–6982. doi: 10.1523/JNEUROSCI.4673-07.2008

Rainnie, D. G., Mania, I., Mascagni, F., and McDonald, A. J. (2006). Physiological and morphological characterization of parvalbumin-containing interneurons of the rat basolateral amygdala. *J. Comp. Neurol.* 498, 142–161. doi: 10.1002/cne.21049

Ramón y Cajal, S. (1899). *Comparative Study of the Sensory Areas of the Human Cortex*. Worcester, MA: Clark University.

Rhomberg, T., Rovira-Esteban, L., Vikor, A., Paradiso, E., Kremser, C., Nagy-Pal, P., et al. (2018). Vasoactive intestinal polypeptide-immunoreactive interneurons within circuits of the mouse basolateral amygdala. *J. Neurosci.* 38, 6983–7003. doi: 10.1523/JNEUROSCI.2063-17.2018

Rovira-Esteban, L., Gunduz-Cinar, O., Bukalo, O., Limoges, A., Brockway, E., Muller, K., et al. (2019). Excitation of diverse classes of cholecystokinin interneurons in the basolateral amygdala facilitates fear extinction. *eNeuro* 6:ENEURO.0220-19.2019. doi: 10.1523/ENEURO.0220-19.2019

Rovira-Esteban, L., Peterfi, Z., Vikor, A., Mate, Z., Szabo, G., and Hajos, N. (2017). Morphological and physiological properties of CCK/CB1R-expressing interneurons in the basal amygdala. *Brain Struct. Funct.* 222, 3543–3565. doi: 10.1007/s00429-017-1417-z

Ruehle, S., Remmers, F., Romo-Parra, H., Massa, F., Wickert, M., Wortge, S., et al. (2013). Cannabinoid CB1 receptor in dorsal telencephalic glutamatergic neurons: distinctive sufficiency for hippocampus-dependent and amygdala-dependent synaptic and behavioral functions. *J. Neurosci.* 33, 10264–10277. doi: 10.1523/JNEUROSCI.4171-12.2013

Sah, P., Faber, E. S., Lopez De Armentia, M., and Power, J. (2003). The amygdaloid complex: anatomy and physiology. *Physiol. Rev.* 83, 803–834. doi: 10.1152/physrev.00002.2003

Saha, R., Knapp, S., Chakraborty, D., Horovitz, O., Albrecht, A., Kriebel, M., et al. (2017). GABAergic synapses at the axon initial segment of basolateral amygdala projection neurons modulate fear extinction. *Neuropsychopharmacology* 42, 473–484. doi: 10.1038/npp.2016.205

Scarani, P., Neroni, S., Giangaspero, F., Orcioni, G. F., and Eusebi, V. (1996). [Carlo martinotti: the real discoverer of martinotti's cells]. *Pathologica* 88, 506–510.

Seress, L., and Ribak, C. E. (1983). GABAergic cells in the dentate gyrus appear to be local circuit and projection neurons. *Exp. Brain Res.* 50, 173–182. doi: 10.1007/BF00239181

Sik, A., Ylinen, A., Penttonen, M., and Buzsaki, G. (1994). Inhibitory CA1-CA3-hilar region feedback in the hippocampus. *Science* 265, 1722–1724. doi: 10.1126/science.8085161

Smith, Y., and Pare, D. (1994). Intra-amygdaloid projections of the lateral nucleus in the cat: PHA-L anterograde labeling combined with postembedding GABA and glutamate immunocytochemistry. *J. Comp. Neurol.* 342, 232–248. doi: 10.1002/cne.903420207

Smith, Y., Pare, J. F., and Pare, D. (1998). Cat intraamygdaloid inhibitory network: ultrastructural organization of parvalbumin-immunoreactive elements. *J. Comp. Neurol.* 391, 164–179. doi: 10.1002/(sici)1096-9861(19980209)391:2<164::aid-cne2>3.0.co;2-0

Smith, Y., Pare, J. F., and Pare, D. (2000). Differential innervation of parvalbumin-immunoreactive interneurons of the basolateral amygdaloid complex by cortical and intrinsic inputs. *J. Comp. Neurol.* 416, 496–508. doi: 10.1002/(SICI)1096-9861(20000124)416:4<496::AID-CNE6>3.0.CO;2-N

Somogyi, P. (1977). A specific 'axo-axonal' interneuron in the visual cortex of the rat. *Brain Res.* 136, 345–350. doi: 10.1016/0006-8993(77)90808-3

Somogyi, P., Freund, T. F., Hodgson, A. J., Somogyi, J., Beroukas, D., and Chubb, I. W. (1985). Identfied axo-axonic cells are immunoreactive for GABA in the hippocampus and visual cortex of the cat. *Brain Res.* 332, 143–149. doi: 10.1016/0006-8993(85)90397-x

Sorvari, H., Miettinen, R., Soininen, H., and Pitkanen, A. (1996). Parvalbumin-immunoreactive neurons make inhibitory synapses on pyramidal cells in the human amygdala: a light and electron microscopic study. *Neurosci. Lett.* 217, 93–96.

Stujenske, J. M., O'Neill, P. K., Nahmmound, I., Goldberg, S., Diaz, L., Labkowich, M., et al. (2021). Prelimbic-dependent activation of amygdala somatostatin interneurons signals non-aversive cues to promote discrimination. *bioRxiv* [Preprint]. doi: 10.1101/2020.06.23.156018

Swanson, L. W. (2003). The amygdala and its place in the cerebral hemisphere. *Ann. N. Y. Acad. Sci.* 985, 174–184. doi: 10.1111/j.1749-6632.2003.tb07081.x

Swanson, L. W., and Petrovich, G. D. (1998). What is the amygdala. *Trends. Neurosci.* 21, 323–331. doi: 10.1016/s0166-2236(98)01265-x

Szabo, A., Somogyi, J., Cauli, B., Lambolez, B., Somogyi, P., and Lamsa, K. P. (2012). Calcium-permeable AMPA receptors provide a common mechanism for LTP in glutamatergic synapses of distinct hippocampal interneuron types. *J. Neurosci.* 32, 6511–6516. doi: 10.1523/JNEUROSCI.0206-12.2012

Szabo, G. G., Holderith, N., Gulyas, A. I., Freund, T. F., and Hajos, N. (2010). Distinct synaptic properties of perisomatic inhibitory cell types and their different modulation by cholinergic receptor activation in the CA3 region of the mouse hippocampus. *Eur. J. Neurosci.* 31, 2234–2246. doi: 10.1111/j.1460-9568.2010.07292.x

Szentágothai, J., and Arbib, M. A. (1974). Conceptual models of neural organization. *Neurosci. Res. Prog. Bull.* 12, 307–510.

Takács, V. T., Freund, T. F., and Gulyas, A. I. (2008). Types and synaptic connections of hippocampal inhibitory neurons reciprocally connected with the medial septum. *Eur. J. Neurosci.* 28, 148–164. doi: 10.1111/j.1460-9568.2008.06319.x

Tamas, G., Lorincz, A., Simon, A., and Szabadics, J. (2003). Identified sources and targets of slow inhibition in the neocortex. *Science* 299, 1902–1905. doi: 10.1126/science.1082053

Tomioka, R., and Rockland, K. S. (2007). Long-distance corticocortical GABAergic neurons in the adult monkey white and gray matter. *J. Comp. Neurol.* 505, 526–538. doi: 10.1002/cne.21504

Tóth, K., and Freund, T. F. (1992). Calbindin D28k-containing nonpyramidal cells in the rat hippocampus: their immunoreactivity for GABA and projection to the medial septum. *Neuroscience* 49, 793–805. doi: 10.1016/0306-4522(92)90357-8

Trouche, S., Sasaki, J. M., Tu, T., and Reijmers, L. G. (2013). Fear extinction causes target-specific remodeling of perisomatic inhibitory synapses. *Neuron* 80, 1054–1065. doi: 10.1016/j.neuron.2013.07.047

Turner, B. H., and Herkenham, M. (1991). Thalamoamygdaloid projections in the rat: a test of the amygdala's role in sensory processing. *J. Comp. Neurol.* 313, 295–325. doi: 10.1002/cne.903130208

Unal, C. T., Unal, B., and Bolton, M. M. (2020). Low-threshold spiking interneurons perform feedback inhibition in the lateral amygdala. *Brain Struct. Funct.* 225, 909–923. doi: 10.1007/s00429-020-02051-4

Varga, C., Lee, S. Y., and Soltesz, I. (2010). Target-selective GABAergic control of entorhinal cortex output. *Nat. Neurosci.* 13, 822–824. doi: 10.1038/nn.2570

Vereczki, V., Martin, E., Rosenthal, R. E., Hof, P. R., Hoffman, G. E., and Fiskum, G. (2006). Normoxic resuscitation after cardiac arrest protects against hippocampal oxidative stress, metabolic dysfunction and neuronal death. *J. Cereb. Blood Flow. Metab.* 26, 821–835. doi: 10.1038/sj.jcbfm.9600234

Vereczki, V. K., Müller, K., Krizsán, E., Máté, Z., Fekete, Z., Rovira-Esteban, L., et al. (2021). Total number and ratio of GABAergic neuron types in the mouse lateral and basal amygdala. *bioRxiv* [Preprint]. doi: 10.1523/JNEUROSCI.2700-20.2021

Vereczki, V. K., Veres, J. M., Muller, K., Nagy, G. A., Racz, B., Barsy, B., et al. (2016). Synaptic organization of perisomatic gabaergic inputs onto the principal cells of the mouse basolateral amygdala. *Front. Neuroanat.* 10:20. doi: 10.3389/fnana.2016.00020

Veres, J. M., Nagy, G. A., and Hajos, N. (2017). Perisomatic GABAergic synapses of basket cells effectively control principal neuron activity in amygdala networks. *eLife* 6:e20721. doi: 10.7554/eLife.20721

Veres, J. M., Nagy, G. A., Vereczki, V. K., Andrasi, T., and Hajos, N. (2014). Strategically positioned inhibitory synapses of axo-axonic cells potently control principal neuron spiking in the basolateral amygdala. *J. Neurosci.* 34, 16194–16206. doi: 10.1523/JNEUROSCI.2232-14.2014

Vogel, E., Krabbe, S., Grundemann, J., Wamsteeker Cusulin, J. I., and Luthi, A. (2016). Projection-specific dynamic regulation of inhibition in amygdala micro-circuits. *Neuron* 91, 644–651. doi: 10.1016/j.neuron.2016.06.036

Wang, Y., Toledo-Rodriguez, M., Gupta, A., Wu, C., Silberberg, G., Luo, J., et al. (2004). Anatomical, physiological and molecular properties of Martinotti cells in the somatosensory cortex of the juvenile rat. *J. Physiol.* 561, 65–90. doi: 10.1113/jphysiol.2004.073353

Wilson, R. I., and Nicoll, R. A. (2001). Endogenous cannabinoids mediate retrograde signalling at hippocampal synapses. *Nature* 410, 588–592. doi: 10.1038/35069076

Wolff, S. B., Grundemann, J., Tovote, P., Krabbe, S., Jacobson, G. A., Muller, C., et al. (2014). Amygdala interneuron subtypes control fear learning through disinhibition. *Nature* 509, 453–458. doi: 10.1038/nature13258

Woodruff, A. R., and Sah, P. (2007). Networks of parvalbumin-positive interneurons in the basolateral amygdala. *J. Neurosci.* 27, 553–563. doi: 10.1523/JNEUROSCI.3686-06.2007

Zemankovics, R., Kali, S., Paulsen, O., Freund, T. F., and Hajos, N. (2010). Differences in subthreshold resonance of hippocampal pyramidal cells and interneurons: the role of h-current and passive membrane characteristics. *J. Physiol.* 588, 2109–2132. doi: 10.1113/jphysiol.2009.185975

Zhu, P. J., and Lovinger, D. M. (2005). Retrograde endocannabinoid signaling in a postsynaptic neuron/synaptic bouton preparation from basolateral amygdala. *J. Neurosci.* 25, 6199–6207. doi: 10.1523/JNEUROSCI.1148-05.2005

Zhu, Y., Nachtrab, G., Keyes, P. C., Allen, W. E., Luo, L., and Chen, X. (2018). Dynamic salience processing in paraventricular thalamus gates associative learning. *Science* 362, 423–429. doi: 10.1126/science.aat0481

Zielinski, M. R., Atochin, D. N., McNally, J. M., McKenna, J. T., Huang, P. L., Strecker, R. E., et al. (2019). Somatostatin+/nNOS+ neurons are involved in delta electroencephalogram activity and cortical-dependent recognition memory. *Sleep* 42:zsz143. doi: 10.1093/sleep/zsz143

Conflict of Interest: The author declares that the research was conducted in the absence of any commercial or financial relationships that could be construed as a potential conflict of interest.

frontiers in Integrative Neuroscience

ORIGINAL RESEARCH
published: 01 September 2021
doi: 10.3389/fnint.2021.728747

Comparison of Sensory and Motor Innervation Between the Acupoints LR3 and LR8 in the Rat With Regional Anatomy and Neural Tract Tracing

*Dongsheng Xu[1†], Ling Zou[1†], Wenjie Zhang[2], Jieying Liao[3], Jia Wang[1], Jingjing Cui[1], Yuxin Su[1], Yuqing Wang[1], Yating Guo[1], Yi Shen[1] and Wanzhu Bai[1]**

[1] Institute of Acupuncture and Moxibustion, China Academy of Chinese Medical Sciences, Beijing, China, [2] South China Research Center for Acupuncture and Moxibustion, Medical College of Acu-Moxi and Rehabilitation, Guangzhou University of Chinese Medicine, Guangzhou, China, [3] School of Traditional Chinese Medicine, Beijing University of Chinese Medicine, Beijing, China

OPEN ACCESS

Edited by:
Eduardo Weruaga,
University of Salamanca, Spain

Reviewed by:
Adrian Rodriguez-Contreras,
City College of New York (CUNY), United States
Raul Aguilar-Roblero,
Universidad Nacional Autónoma de México, Mexico

***Correspondence:**
Wanzhu Bai
wanzhubaisy@hotmail.com

[†] These authors have contributed equally to this work

Received: 22 June 2021
Accepted: 09 August 2021
Published: 01 September 2021

Citation:
Xu D, Zou L, Zhang W, Liao J, Wang J, Cui J, Su Y, Wang Y, Guo Y, Shen Y and Bai W (2021) Comparison of Sensory and Motor Innervation Between the Acupoints LR3 and LR8 in the Rat With Regional Anatomy and Neural Tract Tracing. Front. Integr. Neurosci. 15:728747. doi: 10.3389/fnint.2021.728747

Objective: This study aimed to investigate the sensory and motor innervation of "Taichong" (LR3) and "Ququan" (LR8) in the rat and provide an insight into the neural relationship between the different acupoints in the same meridian.

Methods: The LR3 and LR8 were selected as the representative acupoints from the Liver Meridian and examined by using the techniques of regional anatomy and neural tract tracing in this study. For both acupoints, their local nerves were observed with regional anatomy, and their sensory and motor pathways were traced using neural tract tracing with single cholera toxin subunit B (CTB) and dual Alexa Fluor 594/488 conjugates with CTB (AF594/488-CTB).

Results: Using the regional anatomy, the branches of the deep peroneal nerve and saphenous nerve were separately found under the LR3 and LR8. Using single CTB, the sensory neurons, transganglionic axon terminals, and motor neurons associated with both LR3 and LR8 were demonstrated on the dorsal root ganglia (DRG), spinal dorsal horn, Clarke's nucleus, gracile nucleus, and spinal ventral horn corresponding to their own spinal segments and target regions, respectively. Using dual AF594/488-CTB tracing, it was shown that the sensory and motor neurons associated with LR3 were separated from that of LR8.

Conclusion: This study demonstrates that LR3 and LR8 are innervated by different peripheral nerves, which originated from or terminated in their corresponding spinal segments and target regions independently through the sensory and motor pathways. These results provide an example for understanding the differential innervation between the different acupoints in the same meridian.

Keywords: acupoints, meridian, regional anatomy, neural tract tracing, innervation, nervous system

INTRODUCTION

The two representative acupoints on the hind limbs namely "Taichong" (LR3) and "Ququan" (LR8) are attributed to the Liver Meridian of Foot-Jueyin in the traditional acupuncture theory (Cheng, 1987; Liang, 2005). Although both of the acupoints have been located more precisely at the level of the regional anatomy in modern acupuncture science, their innervation was mainly introduced from the perspective of the peripheral nervous system (PNS) and less involved in the central nervous system (CNS; White and Editorial Board of Acupuncture in Medicine, 2009; Langevin et al., 2010; Cheng, 2011; Dorsher, 2017).

In order to reveal the differential innervation between LR3 and LR8 from the PNS to the CNS, their neural characteristics were systematically examined by the techniques of regional anatomy and neural tract tracing on the experimental rats. The two techniques have been used popularly in acupuncture research (Cui et al., 2013a,b, 2019; Wu et al., 2015; Wang et al., 2018; Lee et al., 2019; Wang H. et al., 2019; Wang J. et al., 2019). Herein, regional anatomy was used to show the peripheral nerves under the regions of LR3 and LR8, and neural tract tracing was applied to trace the origin and termination of the sensory and motor innervation from both acupoints to the CNS. According to our previous studies, single cholera toxin subunit B (CTB) and dual Alexa Fluor 594/488 conjugated with CTB (AF594/488-CTB) were selected for neural tract tracing in this study (Wang et al., 2018; Cui et al., 2019; Wang H. et al., 2019; Zhang et al., 2021). With the peripheral application, the single CTB is capable of retrogradely and transganglionically labeling the sensory and motor neurons and the sensory axon terminals (Cui et al., 2013a, 2019; Wang et al., 2018). Additionally, dual AF594/488-CTB are preferentially used in pair to retrogradely trace the sensory and motor neurons for identifying the neuronal correlation between the different acupoints or between the acupoint and its corresponding visceral organ (Cui et al., 2013b; Wang H. et al., 2019; Zhang et al., 2021).

With both anatomical and histological approaches, this study focused the observation on the nerves under the regions of LR3 and LR8, and their neural components at the cellular level along the sensory and motor pathways. Besides the traditional consideration of the LR3 and LR8 from the perspective of Meridians, this study is expected to provide the neuroanatomical evidence for explaining the differential innervation of different acupoints in the same meridian *via* the neural pathways.

MATERIALS AND METHODS

Animals

This study used nine young adult male Sprague Dawley rats [8–10 weeks old, weight 200–230 g, license no. SCXK (JING) 2019-0010]. All the animals were housed in standard cages on a natural light-dark cycle with controlled temperature and humidity, and free access to food and water. The care and experimental manipulation of rats were approved by the Ethics Committee at the Institute of Acupuncture and Moxibustion, China Academy of Chinese Medical Sciences (reference number 2021-04-15-1).

Microinjection of CTB Into the LR3 and LR8 on the Opposite Side of Hindlimb

Six rats were used for the injection of CTB into the LR3 and LR8 on the opposite sides of hindlimbs. Considering the application of the CTB on the peripheral site only produced neural labeling on the same side of injection, bilateral injections were performed in this study. This is also in order to reduce the number of animals used. Under the anesthesia with 2% isoflurane, 2 μl of 1% CTB solution (List Biological Labs, Inc., Campbell, CA, United States) was injected subcutaneously and muscularly with Hamilton micro-syringe (Hamilton Company, Reno, NV, United States) into the right side of LR3 and the left side of LR8, respectively.

The corresponding sites of LR3 and LR8 in the rat were determined according to the principle of comparative anatomy (Xu et al., 2019). For the human, LR3 is located on the dorsum of the foot, in the depression distal to the junction of the first and second metatarsal bones, while LR8 is located in the depression of the anterior border of the insertions of semimembranosus muscle and semitendinosus muscle, and when the knee is flexed, the point is at the medial end of the transverse popliteal crease (Huang and Huang, 2007; Lim, 2010; **Figure 1**).

Microinjection of AF594/488-CTB Into the LR3 and LR8 on the Same Side of Hindlimb

Besides the application of single CTB on the opposite sides of LR3 and LR8, the injection of dual AF594-CTB/AF488-CTB was also carried out on the ipsilateral side of LR3 and LR8 with the other three rats. In this process, 2 μl of 0.1% AF594-CTB and 2 μl of 0.1% AF488-CTB (Invitrogen, Molecular Probes, Eugene, OR, United States) were separately injected into the LR3 and LR8 on the same hindlimb.

Perfusion

Three days after injection, the rats were anesthetized with an overdose of tribromoethanol solution (250 mg/kg) to induce euthanasia and then transcardially perfused with 100 ml of 0.9% physiological saline followed by 250–300 ml 4% paraformaldehyde in 0.1 M phosphate buffer (PB, pH 7.4).

Regional Anatomy

After perfusion, regional anatomy was performed along the hindlimb to observe the peripheral nerves on the regions of LR3 and LR8 (**Figure 1**). After observation, the brain, spinal cord, and dorsal root ganglia (DRG) were dissected out and cryoprotected in 25% sucrose in 0.1 M PB (pH 7.4) at 4°C for further histological examination.

Slice and Fluorescent Immunohistochemistry

The transverse sections of the brain and spinal cord and sagittal sections of DRG were cut at a thickness of 40 μm on a freezing microtome (Microm International GmbH HM 430, Thermo Fisher Scientific, Germany). Afterward, these were orderly collected in 0.1 M PB (pH 7.4) with the 12-hole Petri dish.

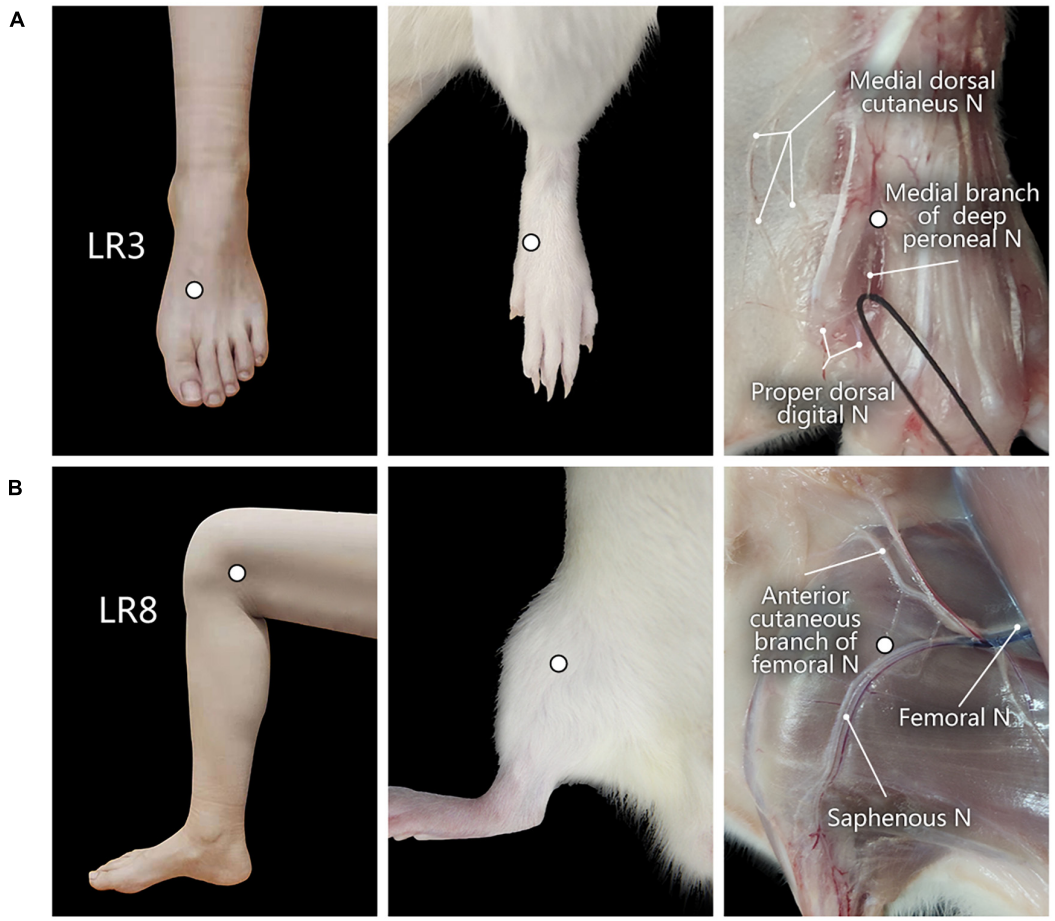

FIGURE 1 | Location of acupoints "Taichong" (LR3) and "Ququan" (LR8) and their regional anatomy. **(A,B)** The sites of LR3 **(A)** and LR8 **(B)** in humans and rats, as well as their regional views of nerves (N) in rats.

The neural labeling with CTB was stained by immunofluorescence. In brief, the slices were incubated in a blocking solution containing 3% normal donkey serum and 0.5% Triton X-100 (Biotopped, China) in 0.1 M PB for 30 min, then removed to goat anti-CTB (1:1000; List Biological Labs, Inc.) in 0.1 M PB containing 1% normal donkey serum and 0.5% Triton X-100 at 4°C for one night. On the next day, the slices were washed thoroughly with 0.1 M PB and exposed to donkey anti-goat Alexa Fluor 488 secondary antibody (Molecular Probes, Eugene, OR, United States) (1:500; Molecular Probes) for 1 h. After that, the slices were washed again and then mounted on slides (Superfrost) (Thermo, MicromInternational FSE, Germany). The slides were cover slipped with 50% glycerin before the observation.

It was noteworthy that the neural labeling with AF594/488-CTB can be directly observed without further staining.

Observation

Tissue samples were scanned with a panoramic tissue slice scanner (VS120; Olympus, Japan). Accordingly, the slices with CTB labeling were further observed and recorded using a fluorescent microscope equipped with a digital camera (DP73, Olympus, Japan) or a laser scanning confocal microscope (FV1200, Olympus, Japan). All images were processed using Adobe Photoshop/Illustration CC2017 (Adobe Systems, San Jose, CA, United States). The anatomical structure of tissue slices from the brain stem and spinal cord was determined according to *The Rat Brain in Stereotaxic Coordinates* (Paxinos and Watson, 2006), and the segments of DRG were marked by the spinal vertebra.

Statistical Analysis

The number of the labeled neurons was obtained from the six rats with the injection of CTB, in which sensory neurons were counted in all the slices of each DRG, and the motor neurons were counted in every 12th slice of the spinal cord. All the data were expressed as mean ± *SE* and processed with the software GraphPad Prism 8.0.2 (La Jolla, CA, United States). Since there is no distinct boundary between the slices of the spinal cord, the number of labeled motor neurons was counted together without further distinguishing their spinal segments.

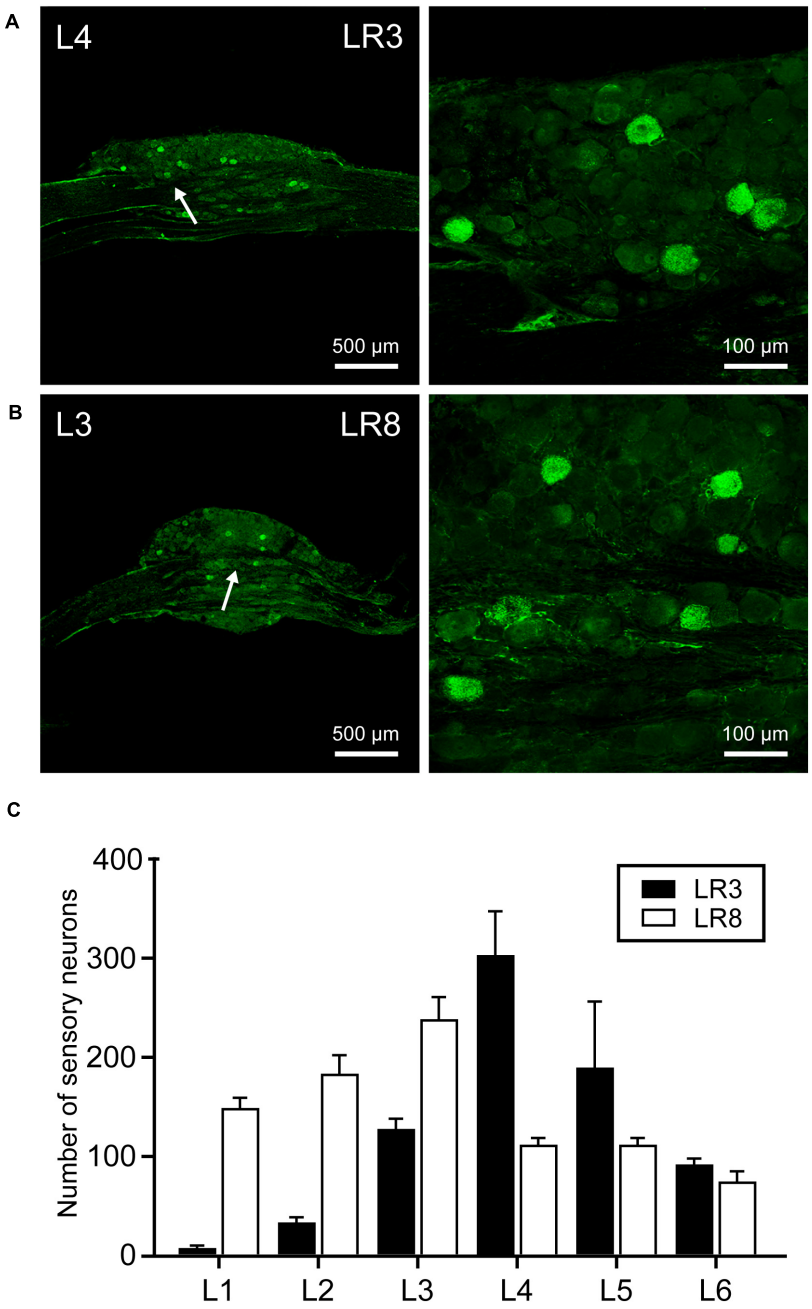

FIGURE 2 | Distribution of the labeled sensory neurons with cholera toxin subunit B (CTB). **(A,B)** Representative photos from lumbar (L) 3 and L4 dorsal root ganglia (DRG) showing the CTB labeled sensory neurons associated with "Taichong" (LR3, **A**) and "Ququan" (LR8, **B**). And their magnified photos (arrowheads) showing the labeling in detail. **(C)** The distribution of CTB labeled sensory neurons for LR3 and LR8 from L1 DRG to L6 DRG in average number (n = 6).

RESULTS

Regional Observation of the LR3 and LR8

With regional anatomy, the peripheral nerves associated with LR3 and LR8 were clearly observed under the naked eyes. The common peroneal nerve branches from the sciatic nerve run down along the leg and further gives out the branch of the deep peroneal nerve toward the region of LR3. The saphenous nerve branches from the femoral nerve run into the region of LR8 (**Figure 1**).

Neural Labeling Associated With LR3 and LR8 by CTB

The neural components associated with LR3 and LR8 were demonstrated with CTB labeling, including the sensory neurons in DRG, transganglionic axon terminals in the spinal dorsal horn,

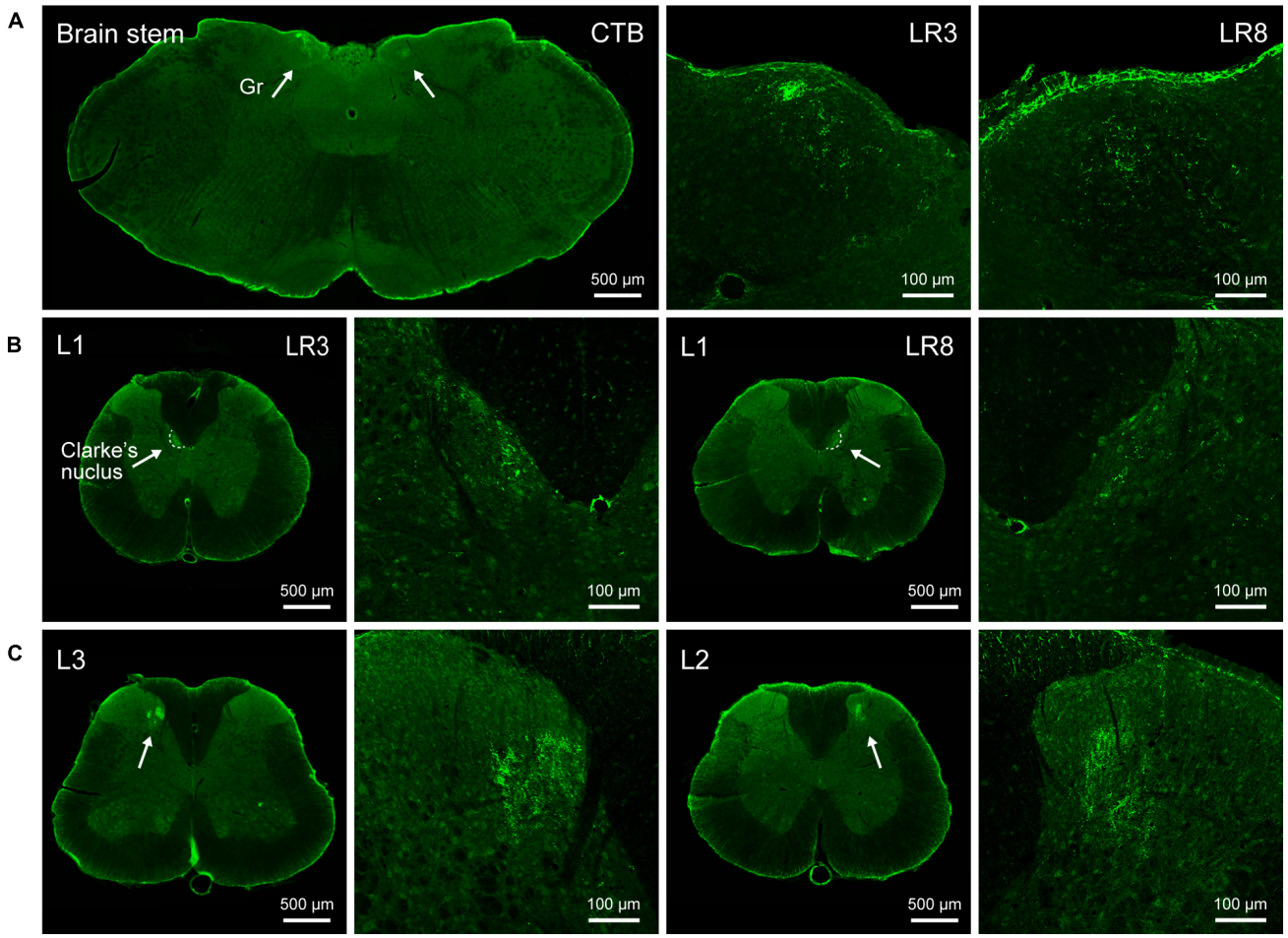

FIGURE 3 | Distribution of the transganglionically labeled axon terminals with cholera toxin subunit B (CTB). **(A–C)** Representative photos from the brain stem **(A)** and spinal cord **(B,C)** showing the CTB labeled axon terminals associated with "Taichong" (LR3, left side) and "Ququan" (LR8, right side) in the gracile nucleus (Gr, **A**), Clarke's nucleus at lumbar (L) 1 segment **(B)**, and spinal dorsal horns at L2 and L3 segments **(C)**, their magnified photos (arrowheads) showing the axon terminals in detail.

Clarke's nucleus, and gracile nucleus, as well as motor neurons in the spinal ventral horn. This labeling is located ipsilaterally corresponding to the side of CTB injection for LR3 and LR8, respectively (**Figures 2–4**).

The sensory neurons for the LR3 were distributed in lumbar (L) 1–6 DRG with higher concentration in L4 DRG (**Figure 2**), and the transganglionic axons were terminated on the dorsal part of the gracile nucleus, Clarke's nucleus, and medial part of the spinal dorsal horn, respectively (**Figure 3**). On the other hand, the motor neurons were present on the lateral part of spinal ventral horns ranging from L3 to L6 segments with a higher concentration on the L4–5 (**Figure 4**). In the cases of LR8, the sensory neurons were also distributed in L1–6 DRG, but with higher concentration in L3 DRG (**Figure 2**), the transganglionic axons terminated on the ventral part of the gracile nucleus, Clarke's nucleus, and central part of the spinal dorsal horn, respectively (**Figure 3**), while the motor neurons were presented on the ventral part of spinal ventral horns in the L2–5 with a higher concentration on the L3–4 (**Figure 4**).

Neural Labeling Associated With LR3 and LR8 by AF594/488-CTB

The differential innervation between LR3 and LR8 was further compared with a dual fluorescent tracing technique (**Figure 5**). Unlike CTB, only sensory and motor neurons associated with LR3 and LR8 were retrogradely labeled with AF594/488-CTB, but the distribution of these labeled neurons was similar to that of CTB. Although some of the sensory and motor neurons associated with LR3 and LR8 intermingled in the certain DRG and spinal ventral horn, these labeling was of separate neurons (**Figure 5**).

DISCUSSION

Traditionally, the meridians were considered as the pathways serving for the circulation of the qi and blood on the human body. They pertain to the zang-fu organs (visceral organs) interiorly and extend over the body exteriorly, forming a network and

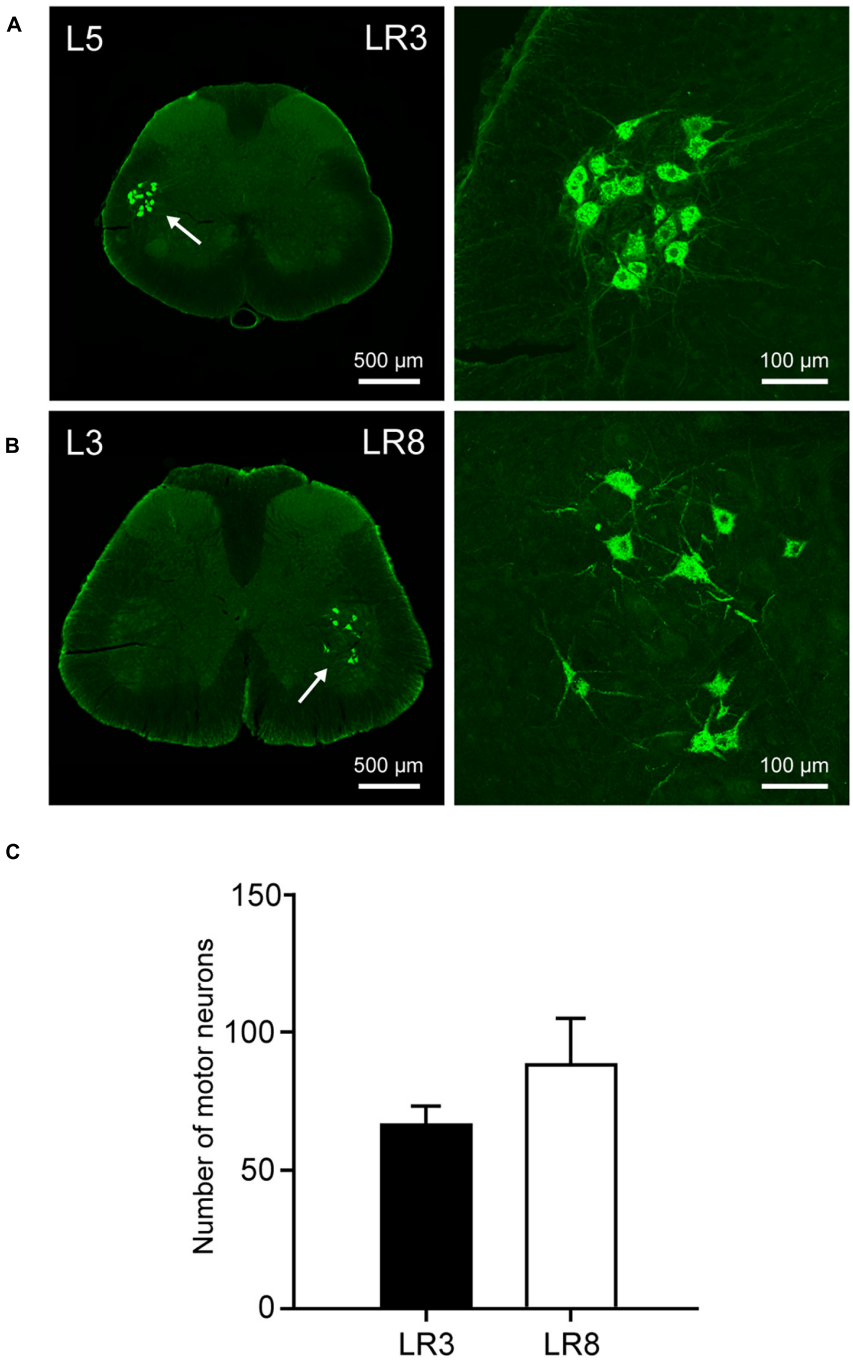

FIGURE 4 | Distribution of the labeled motor neurons with cholera toxin subunit B (CTB). **(A,B)** Representative photos from lumbar (L) 5 and L3 spinal segments showing the CTB labeled motor neurons associated with "Taichong" (LR3, **A**) and "Ququan" (LR8, **B**), their magnified photos (arrowheads) showing the motor neurons in detail. **(C)** The average number of CTB labeled motor neurons for LR3 and LR8 (n = 6).

linking the tissues and organs into an organic whole. This system included the 12 main meridians running longitudinally and interiorly within the body, with each meridian considered to interconnect with its corresponding visceral organ. However, it is absent until now of structural basis to support this discussed interconnection. In our previous study, we have demonstrated the correlated sensory and sympathetic innervations between acupoint BL 23 and kidney in the rat (Zhang et al., 2021). In this study, we focused our observation on the differential innervation between the different acupoints. We demonstrated a detailed view of the neuroanatomical characteristics of LR3 and LR8 with the techniques of regional anatomy and neural tract tracing in

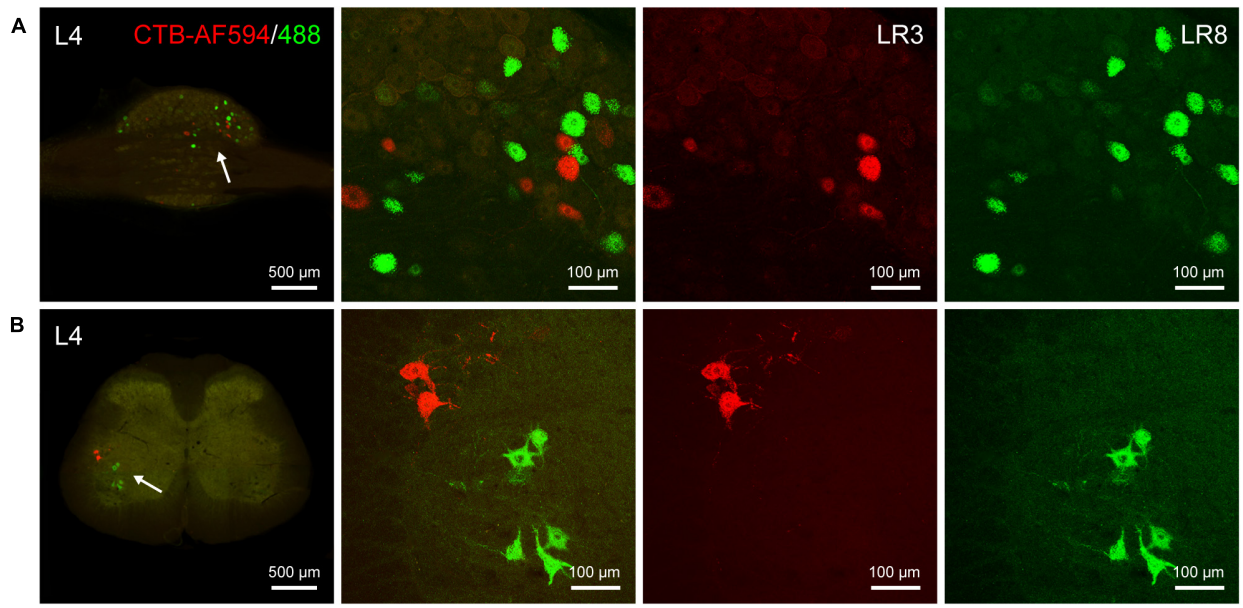

FIGURE 5 | Distribution of the labeled sensory and motor neurons with Alexa Fluor 594 and 488 conjugated cholera toxin subunit B (AF594/488-CTB) in the dorsal root ganglion and spinal cord. **(A,B)** Representative photos from lumbar (L) 4 dorsal root ganglion **(A)** and spinal cord **(B)** showing the labeled sensory and motor neurons associated with "Taichong" (LR3, AF594-CTB, red) and "Ququan" (LR8, AF488-CTB, green), their magnified photos (arrowheads) showing the labeled sensory **(A)** and motor **(B)** neurons in detail.

the rats. Besides the consideration from the traditional theory of meridians, present observation provides new insight into the neuroanatomical difference between the LR3 and LR8 *via* the sensory and motor pathways. From the PNS to the CNS, it is beneficial for understanding the effective routes of the two acupoints by acupuncture stimulation (**Figure 6**).

Neuroanatomical Consideration

The peripheral nerves under the LR3 and LR8 in the rats were demonstrated by the regional anatomy in this study. Similar to the two acupoints on the human body, they are innervated by the peroneal nerve and saphenous nerve, respectively (Cheng, 1987; Liang, 2005; Huang and Huang, 2007). This peripheral difference is further determined with neural tract tracing between the LR3 and LR8 at the cellular level. The sensory neurons, transganglionic axon terminals, and motor neurons associated with LR3 and LR8 are distributed orderly corresponding to their own spinal segments and target regions along the sensory and motor pathways from the PNS to the CNS.

Although the neural components are the same for the innervation of both LR3 and LR8, their segmental and regional distribution is markedly different between each other. For the spinal segments, the concentration of sensory and motor labeling associated with LR3 is obviously one segment lower than that of LR8. For the target regions, it is mainly exhibited on the distribution of the transganglionic axon terminals and motor neurons. The transganglionic axon terminals associated with LR3 locate more medially in the spinal dorsal horn than that of LR8, and the motor neurons associated with LR3 are situated more laterally on the spinal ventral horn than that of LR8. These segmental and regional distribution is accorded with the "somatotopic arrangement" in the CNS of rats, which has been well defined in the previous studies (Swett and Woolf, 1985; Maslany et al., 1991, 1992; Takahashi et al., 2010; Odagaki et al., 2019). Increasing pieces of evidence from the human have proved that "somatotopic arrangement" does not only exist on the cerebral cortices but is also present in the spinal cord (Standring, 2008; Stroman et al., 2012; Willoughby et al., 2021).

According to the distribution of the transganglionically labeled axons in the CNS, our results imply that the acupuncture signals from the LR3 and LR8 can be transported to their corresponding targets in the spinal dorsal horn, Clarke's nucleus, and gracile nucleus, and forwarded *via* these central relay stations to the contralateral side of ventral posterolateral thalamic nucleus and the ipsilateral cerebellum through the spinothalamic, medial lemniscus, and spinocerebellar tracts, respectively (Standring, 2008). Comparatively, the motor innervation of LR3 and LR8 is uncomplicated, originating from the motor neurons in the spinal ventral horn, where the motor neurons associated with LR3 locate more laterally than those of LR8. Taken together, it can be concluded that there is a segmental and regional difference of sensory and motor innervation between LR3 and LR8, which gives out a clue leading to understanding their effective routes of acupuncture stimulation from the perspective of sensory and motor pathways.

Clinical Implication

Since acupoints are considered as the specific sites for acupuncture, how to select a proper acupoint becomes an important issue to be continuously concerned in the clinical

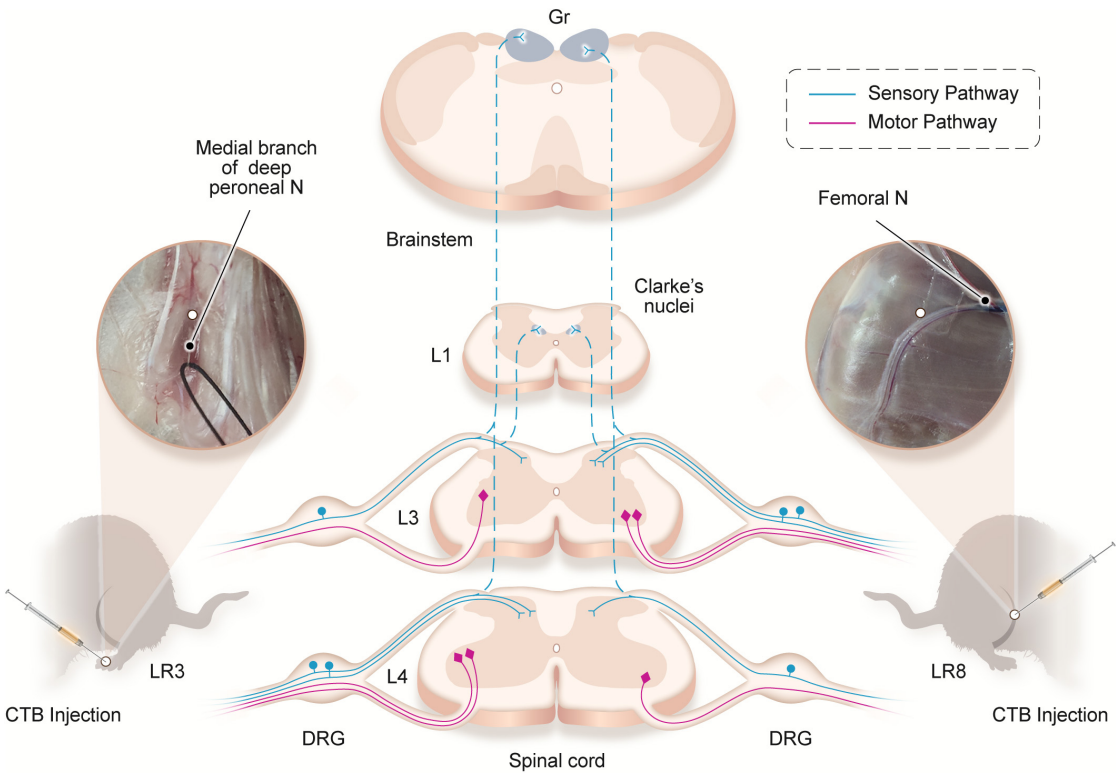

FIGURE 6 | Illustration of the distribution of the neural labeling associated with "Taichong" (LR3) and "Ququan" (LR8) through the sensory and motor pathways. Acupoints LR3 and LR8 establish their sensory and motor connections with the corresponding targets in the dorsal root ganglion (DRG), spinal dorsal horns, Clarke's nucleus, gracile nucleus (Gr), and spinal ventral horns in the segmental and regional pattern.

application (Cheng, 1987; Huang and Huang, 2007; Chiang, 2015). Generally, selecting acupoints along the route of meridians is the basic principle in acupuncture treatment, which is carried out according to the theory that diseases are related to meridians (Liang, 2005; Liu et al., 2010). Despite both LR3 and LR8 belonging to the same meridian, this study suggests that their neuroanatomical specificity should be another important consideration when they are selected as the proper acupoints for acupuncture treatment (Dorsher, 2017; Guo and Ma, 2019).

From the viewpoint of neural pathways, present neuroanatomical findings from the regional anatomy and neural tract tracing suggest that although LR3 and LR8 are directly innervated by the peroneal and saphenous nerves, respectively, they may also involve in their successive parts of sciatic and femoral nerves, even in their corresponding spinal segments and target regions. Accordingly, the acupuncture signals aroused from LR3 and LR8 might be transported along these neural pathways to the CNS for the precise target treatment. Therefore, the results of this study provide valuable references for evaluating the therapeutic roles of LR3 and LR8.

Study Limitations

The primary focus of this study was the identification and characterization of the differential innervation between the LR3 and LR8 at the anatomic and cellular levels. Although our study provides the neuroanatomical pieces of evidence that the sensory and motor pathways may participate in the processes of signal transportation from the LR3 and LR8 to the CNS, their functional effects remain to be established experimentally.

Due to the technical limitation, all the neural labeling with CTB and AF594/488-CTB along the sensory and motor pathways belongs to the first-order neural components associated with the LR3 and LR8. Their successive higher-order neural components remain unclear, which might be transsynaptically traced with neurotropic viruses in the future study (Lanciego and Wouterlood, 2011, 2020; Saleeba et al., 2019). In addition, it is worth noting that besides the nerve fibers, the other cellular components are also distributed in the tissues under the acupoints, which should be an important issue to be tackled in the future study (Zhang et al., 2012; Wu et al., 2015; Xu et al., 2016; She et al., 2018).

CONCLUSION

This study evidently showed the neuroanatomical characteristics of LR3 and LR8. Although both acupoints are attributed to the same meridian, considering their sensory and motor innervation, each of them establishes its own neural connection with corresponding spinal segments and target regions from the PNS to the CNS *via* the sensory and motor pathways. These

results suggest that when we select the proper acupoints for the acupuncture treatment, the neuroanatomical specificity of acupoints should also be taken together as the clinical demands, besides the consideration from the traditional theory of meridians.

DATA AVAILABILITY STATEMENT

The raw data supporting the conclusions of this article will be made available by the authors, without undue reservation.

ETHICS STATEMENT

The animal study was reviewed and approved by the Ethics Committee of the Institute of Acupuncture and Moxibustion, China Academy of Chinese Medical Sciences.

AUTHOR CONTRIBUTIONS

The manuscript presented here was carried out in collaboration between all authors. DX, LZ, WZ, JL, YSu, YG, and YSh carried out the experiments. JW and JC analyzed the data. WB designed the study. DX and WB wrote the article. All authors read and approved the final version of the manuscript.

FUNDING

This study was supported by the project of National Key R&D Program of China (No. 2019YFC1709103); the National Natural Science Foundation of China (Nos. 81801561, 81774211, 81774432, and 82004492); and the Self-Selected Research Program from the Institute of Acupuncture and Moxibustion, China Academy of Chinese Medical Sciences (Nos. ZZ14-YQ-034, ZZ13-YQ-068, and ZZ14-YQ-032).

REFERENCES

Cheng, K. J. (2011). Neuroanatomical characteristics of acupuncture points: relationship between their anatomical locations and traditional clinical indications. *Acupunct. Med.* 29, 289–294. doi: 10.1136/acupmed.2011.010056

Cheng, X. N. (1987). *Chinese Acupuncture and Moxibustion*. Beijing: Foreign Languages Press.

Chiang, P. (2015). What is the point of acupuncture? *Acupunct. Med*. 27, 67–80. doi: 10.1089/acu.2015.1093

Cui, J. J., Ha, L. J., Zhu, X. L., Shi, H., Wang, F. C., Jing, X. H., et al. (2013a). Neuroanatomical basis for acupuncture point PC8 in the rat: neural tracing study with cholera toxin subunit B. *Acupunct. Med*. 31, 389–394. doi: 10.1136/acupmed-2013-010400

Cui, J. J., Ha, L. J., Zhu, X. L., Wang, F. C., Jing, X. H., and Bai, W. Z. (2013b). Specificity of sensory and motor neurons associated with BL40 and GB30 in the rat: a dual fluorescent labeling study. *Evid. Based Complement Alternat. Med.* 2013:643403. doi: 10.1155/2013/643403

Cui, J. J., Wang, J., and Bai, W. Z. (2019). Innervated properties of acupuncture points LI 4 and LR 3 in the rat: neural pathway tracing with cholera toxin subunit B. *Med. Acupunct.* 31, 169–175. doi: 10.1089/acu.2019.1334

Dorsher, P. T. (2017). Neuroembryology of the acupuncture principal meridians: part1. The extremities. *Med. Acupunct*. 29, 10–19. doi: 10.1089/acu.2016.1210

Guo, X., and Ma, T. (2019). Effects of acupuncture on neurological disease in clinical- and animal-based research. *Front. Integr. Neurosci.* 13:47. doi: 10.3389/fnint.2019.00047

Huang, L. X., and Huang, Y. M. (2007). *Evidence-Based Surface Anatomy for Acupuncture-Acupuncture Integrated with Surface Anatomy and Imaging*. Beijing: People's Medical Publishing House.

Lanciego, J. L., and Wouterlood, F. G. (2011). A half century of experimental neuroanatomical tracing. *J. Chem. Neuroanat.* 42, 157–183. doi: 10.1016/j.jchemneu.2011.07.001

Lanciego, J. L., and Wouterlood, F. G. (2020). Neuroanatomical tract-tracing techniques that did go viral. *Brain Struct. Funct*. 225, 1193–1224. doi: 10.1007/s00429-020-02041-6

Langevin, H. M., Wayne, P. M., and Macpherson, H. (2010). Paradoxes in acupuncture research: strategies for moving forward. *Evid. Based Complement Alternat. Med*. 2011:180805. doi: 10.1155/2011/180805

Lee, M., Longenecker, R., Lo, S., and Chiang, P. (2019). Distinct neuroanatomical structures of acupoints kidney 1 to kidney 8: a cadaveric study. *Med. Acupunct*. 31, 19–28. doi: 10.1089/acu.2018.1325

Liang, F. R. (2005). *Acupuncturology*. Beijing: China Press of Traditional Chinese Medicine.

Lim, S. (2010). WHO standard acupuncture point locations. *Evidence-Based Complementary Alternat. Med.* 7, 167–168. doi: 10.1093/ecam/nep006

Liu, J. L., Wang, J. Y., Chen, S. P., Gao, Y. H., Qiao, L. N., and Han, Y. J. (2010). Progress in the study on the mechanism underlying the correlation between acupoints/meridians and Zangfu organs. *Zhen Ci Yan Jiu* 35, 71–77.

Maslany, S., Crockett, D. P., and Egger, M. D. (1991). Somatotopic organization of the dorsal column nuclei in the rat: transganglionic labeling with B-HRP and WGA-HRP. *Brain Res.* 564, 56–65. doi: 10.1016/0006-8993(91)91351-z

Maslany, S., Crockett, D. P., and Egger, M. D. (1992). Organization of cutaneous primary afferent fibers projecting to the dorsal horn in the rat: WGA-HRP versus B-HRP. *Brain Res.* 569, 123–135. doi: 10.1016/0006-8993(92)90378-m

Odagaki, K., Kameda, H., Hayashi, T., and Sakurai, M. (2019). Mediolateral and dorsoventral projection patterns of cutaneous afferents within transverse planes of the mouse spinal dorsal horn. *J. Comparative Neurol.* 527, 972–984. doi: 10.1002/cne.24593

Paxinos, G., and Watson, C. (2006). *The Rat Brain in Stereotaxic Coordinates: Hard Cover Edition*. Amsterdam: Elsevier.

Saleeba, C., Dempsey, B., Le, S., Goodchild, A., and McMullan, S. (2019). A Student's guide to neural circuit tracing. *Front. Neurosci*. 13:897. doi: 10.3389/fnins.2019.00897

She, C., Xu, D. S., Cui, J. J., Wang, J., He, W., Wang, X. Y., et al. (2018). Our considerations about studies on structure of acupuncture points. *Zhen Ci Yan Jiu* 43, 285–289. doi: 10.13702/j.1000-0607.170911

Standring, S. (2008). *Gray's Anatomy: the Anatomical Basis of Clinical Practice*, Vol. 29. London: Churchill Livingstone Elsevier, 260–269.

Stroman, P. W., Bosma, R. L., and Tsyben, A. (2012). Somatotopic arrangement of thermal sensory regions in the healthy human spinal cord determined by means of spinal cord functional MRI. *Magn. Reson. Med*. 68, 923–931. doi: 10.1002/mrm.23292

Swett, J. E., and Woolf, C. J. (1985). The somatotopic organization of primary afferent terminals in the superficial laminae of the dorsal horn of the rat spinal cord. *J. Comp. Neurol.* 231, 66–77. doi: 10.1002/cne.902310106

Takahashi, Y., Ohtori, S., and Takahashi, K. (2010). Somatotopic organization of lumbar muscle–innervating neurons in the ventral horn of the rat spinal cord. *J. Anat.* 216, 489–495. doi: 10.1111/j.1469-7580.2009.01203.x

Wang, J., Cui, J. J., Ha, L. J., She, C., Xu, D. S., Jing, X. H., et al. (2019). Review on application of neural tracing technique to experimental research of acupuncture. *Zhen Ci Yan Jiu* 44, 926–931. doi: 10.13702/j.1000-0607.180522

Wang, H., Wang, J., Cui, J. J., Xu, D. S., She, C., Wu, S., et al. (2019). Neuroanatomical interconnection of the complementary acupoints in the rat hindlimb. *World J. Acupunct.-Moxibustion* 29, 206–209.

Wang, J., Cui, J. J., She, C., Xu, D. S., Zhang, Z. Y., Wang, H., et al. (2018). Differential innervation of tissues located at traditional acupuncture points in the rat forehead and face. *Acupunct. Med*. 36, 408–414. doi: 10.1136/acupmed-2017-011595

White, A., and Editorial Board of Acupuncture in Medicine (2009). Western medical acupuncture: a definition. *Acupunct. Med.* 27, 33–35. doi: 10.1136/aim.2008.000372

Willoughby, W. R., Thoenes, K., and Bolding, M. (2021). Somatotopic arrangement of the human primary somatosensory cortex derived from functional magnetic resonance imaging. *Front. Neurosci.* 14:598482. doi: 10.3389/fnins.2020.598482

Wu, M. L., Cui, J. J., Xu, D. S., Zhang, K., Jing, X. H., and Bai, W. Z. (2015). Neuroanatomical characteristics of deep and superficial needling using LI11 as an example. *Acupunct. Med.* 33, 472–477. doi: 10.1136/acupmed-2015-010882

Xu, D. S., She, C., Wang, J., Cui, J. J., Cai, H., and Bai, W. Z. (2016). Characteristics of distribution of blood vessels and nerve fibers in the skin tissues of acupoint "Taichong" (LR 3) in the rat. *Zhen Ci Yan Jiu* 41, 486–491. doi: 10.13702/j.1000-0607.2016.06.002

Xu, D. S., Zhao, S., Cui, J. J., Ma, T. M., Xu, B., Yu, X. C., et al. (2019). A new attempt of re-mapping acupoint atlas in the rat. *Zhen Ci Yan Jiu* 44, 62–65. doi: 10.13702/j.1000-0607.180396

Zhang, Z. J., Wang, X. M., and McAlonan, G. M. (2012). Neural acupuncture unit: a new concept for interpreting effects and mechanisms of acupuncture. *Evid. Based Complement Alternat. Med.* 2012:429412. doi: 10.1155/2012/429412

Zhang, Z. Y., Xu, D. S., Wang, J., Cui, J. J., Wu, S., Zou, L., et al. (2021). Correlated sensory and sympathetic innervations between acupoint BL 23 and kidney in the rat. *Front. Integr. Neurosci.* 14:616778. doi: 10.3389/fnint.2020.616778

Conflict of Interest: The authors declare that the research was conducted in the absence of any commercial or financial relationships that could be construed as a potential conflict of interest.

Publisher's Note: All claims expressed in this article are solely those of the authors and do not necessarily represent those of their affiliated organizations, or those of the publisher, the editors and the reviewers. Any product that may be evaluated in this article, or claim that may be made by its manufacturer, is not guaranteed or endorsed by the publisher.

frontiers in Neural Circuits

REVIEW
published: 08 October 2021
doi: 10.3389/fncir.2021.718221

Unraveling the Role of Dopaminergic and Calretinin Interneurons in the Olfactory Bulb

Simona Capsoni[1,2], *Alex Fogli Iseppe*[1], *Fabio Casciano*[3,4] *and Angela Pignatelli*[1]*

[1] Department of Neuroscience and Rehabilitation, University of Ferrara, Ferrara, Italy, [2] Bio@SNS Laboratory of Biology, Scuola Normale Superiore, Pisa, Italy, [3] Department of Translational Medicine and LTTA Centre, University of Ferrara, Ferrara, Italy, [4] Interdepartmental Research Centre for the Study of Multiple Sclerosis and Inflammatory and Degenerative Diseases of the Nervous System, University of Ferrara, Ferrara, Italy

The perception and discriminating of odors are sensory activities that are an integral part of our daily life. The first brain region where odors are processed is the olfactory bulb (OB). Among the different cell populations that make up this brain area, interneurons play an essential role in this sensory activity. Moreover, probably because of their activity, they represent an exception compared to other parts of the brain, since OB interneurons are continuously generated in the postnatal and adult period. In this review, we will focus on periglomerular (PG) cells which are a class of interneurons found in the glomerular layer of the OB. These interneurons can be classified into distinct subtypes based on their neurochemical nature, based on the neurotransmitter and calcium-binding proteins expressed by these cells. Dopaminergic (DA) periglomerular cells and calretinin (CR) cells are among the newly generated interneurons and play an important role in the physiology of OB. In the OB, DA cells are involved in the processing of odors and the adaptation of the bulbar network to external conditions. The main role of DA cells in OB appears to be the inhibition of glutamate release from olfactory sensory fibers. Calretinin cells are probably the best morphologically characterized interneurons among PG cells in OB, but little is known about their function except for their inhibitory effect on noisy random excitatory signals arriving at the main neurons. In this review, we will mainly describe the electrophysiological properties related to the excitability profiles of DA and CR cells, with a particular view on the differences that characterize DA mature interneurons from cells in different stages of adult neurogenesis.

Keywords: interneurons, olfactory bulb, dopaminergic cell, calretinin cell, adult neurogenesis

OPEN ACCESS

Edited by:
Eduardo Weruaga, University of Salamanca, Spain

Reviewed by:
Carlos Crespo, University of Valencia, Spain
Markus Rothermel, University of Veterinary Medicine Hannover, Germany

***Correspondence:**
Angela Pignatelli
pnn@unife.it

Received: *31 May 2021*
Accepted: *31 August 2021*
Published: *08 October 2021*

Citation:
Capsoni S, Fogli Iseppe A, Casciano F and Pignatelli A (2021) Unraveling the Role of Dopaminergic and Calretinin Interneurons in the Olfactory Bulb. Front. Neural Circuits 15:718221. doi: 10.3389/fncir.2021.718221

INTRODUCTION

The sense of smell, or olfaction, is one of the oldest senses (Sarafoleanu et al., 2009). In humans, it is believed that in everyday life the sense of smell is less important than hearing or vision. This statement was based on the small size of the olfactory bulb compared to the whole brain and that initially, despite the fact that 1,500 genes encoding for olfactory receptors are found in our genome, thus accounting for the largest part of it (Young and Trask, 2002), only 390 genes were found to be functional and the remaining were considered pseudogenes (Glusman et al., 2001). However, contrary to what it was commonly believed, the human olfactory bulb is in reality quite

large in absolute terms and contains a comparable number of neurons to other mammals (Bushdid et al., 2014; McGann, 2017). In addition, most of the pseudogenes were subsequently found to be functional receptors (Olender et al., 2016; Prieto-Godino et al., 2016). For this reason, humans can distinguish at least 1 trillion of different odors (Bushdid et al., 2014).

In mammals, the olfactory system is capable of odor detection, odor discrimination, and olfactory memory and employs these capabilities in a wide range of behaviors. Indeed, olfaction is essential: (1) to find food and determine the preference for it, (2) in regulating appetite, (3) when exploring the surrounding environment, (4) for social interactions and during behaviors related to courtship and mating; (5) in empathic behaviors (Spinella, 2002; Sarafoleanu et al., 2009; Fine and Riera, 2019). In humans, it plays an important site of integration among different senses such as in the perception of taste (Rolls, 2019) and during eyesight (Gottfried and Dolan, 2003). Moreover, it contributes to the central regulation of gastrointestinal functions (Kitamura et al., 2010) and, thanks to the connections between the olfactory and limbic systems, it is involved in psychosocial interactions (Li and Liberles, 2015; Cherry and Baum, 2020), aggressive behaviors (Ferris et al., 2008), learning and the memory of fear (Mouly and Sullivan, 2010).

Thus, the sense of smell strongly impacts everyday life. Indeed, olfactory dysfunctions significantly worsen physical well-being, quality of life, everyday security, and are associated with increased mortality in older adults and it is among the prodromic symptoms of several neurodegenerative diseases (Attems et al., 2015).

A complex circuitry is the basis of the correct functioning of the sense of smell. In this review, we will focus on the description of two populations of olfactory bulb interneurons, the dopaminergic and calretininergic cells that are important actors in odor discrimination.

NEURONAL CIRCUIT OF THE OLFACTORY SYSTEM

Odors are detected and recognized by odorant receptors expressed on olfactory sensory neurons (OSNs) located in the olfactory epithelium. After binding to the specific receptor, the information is then transduced in an electrical signal that later reaches the olfactory bulb (OB) where the first processing of sensory signals takes place. Indeed, the transmission of sensorial information is not simply conducted by the projection neurons, but the signals are revised and modulated by the local circuitry mainly by the action of interneurons. Then, through projection neurons, the signal reaches higher-order areas of the brain such as the superficial plexiform layer of the accessory olfactory nucleus, the piriform cortex in the temporal lobe, periamygdaloid, and lateral entorhinal cortices, taenia tecta, the anterior hippocampal continuation, indusium griseum, and the olfactory tubercle (Shipley and Ennis, 1996). Additional areas where efferent fibers from the OB can be found are the amygdala (Kang et al., 2011) and the hypothalamus (Scott and Pfaffmann, 1967; Price, 1985; Hatton and Yang, 1989).

In this review, we will focus on the role of the piriform cortex (PCx) in odor processing. The PCx is a three-layer paleocortical structurally different from other neocortical sensory areas and more similar to hippocampal, cerebellar and prefrontal cortical areas (Neville and Haberly, 2004). In the PCx, contrary to the OB, neurons respond to multiple odors (Stettler and Axel, 2009), and thus PCx function does not depend on a spatial order (Miura et al., 2012). Consequently, PCx integrates input coming from different glomeruli. However, PCx neurons can support odor identification, odor discrimination learning and odor value for a complete discussion see (Bekkers and Suzuki, 2013; Blazing and Franks, 2020).

Concerning PCx circuits, it has been found that the piriform cortex can also project directly to prefrontal, amygdaloid, entorhinal, and perirhinal cortex where it can play an associative function, implying that the OB can function similarly to other primary areas of other sensory systems (Johnson et al., 2000; Bekkers and Suzuki, 2013). Here we will briefly focus on the connection between the PCx and the thalamus.

In general, sensory systems use the thalamus as an intermediate step to reach primary cortical areas where other sensory information is processed. In the past it has believed that olfaction is independent from the thalamus but it is now accepted that the odorant information is first processed by the PCx which then projects to the mediodorsal nucleus of the thalamus (Price and Slotnick, 1983; Bay and Cavdar, 2013), giving rise, with the reciprocal connection with the orbitofrontal cortex, to the olfactory trans-thalamic pathway (Krettek and Price, 1977). The role of the mediodorsal thalamus in odor elaboration has not been fully clarified but it is supposed to contribute to odor perception and learning discrimination. A detailed description is beyond the scope of this review and readers can find more information in Courtiol and Wilson (2015).

In this review, we will focus in more detail on the circuitry within the olfactory bulb. In **Figure 1** we illustrate a very schematic pathway of the main connections that concern the transmission of the olfactory signal. The anatomical structure of OB can be described as a sequence of five, concentric layers of cells and fibers. The first one is the olfactory nerve layer, located on the surface of the OB, and it is formed by the afferent projections from the olfactory epithelium. The terminals of these axons enter the second, glomerular layer (GL) which consists of spherical structures called glomeruli from which it takes the name. Within this layer, the axons of OSNs constitute the core of the glomerulus and create synapses with the apical dendrites of projecting neurons (mitral and tufted cells) and at the same time with interneurons surrounding the glomeruli which are called juxtaglomerular cells (JGcs). In a truly surprising way, it has been demonstrated the presence of a very precise mapping for which OSNs expressing the same odorant receptors

Abbreviations: CB, calbindin-28K; CR, calretinin; DA, dopaminergic; eGFP, enhanced green fluorescent protein; EPL, external plexiform layer; EPSCs, excitatory postsynaptic currents; ET, external tufted; GABA, γ-aminobutyric acid; GAD, acid decarboxylase; Gcs, granule cells; GL, glomerular layer; ICa_T, T-type Ca^{2+} current; INa_P, Na^+ persistent current; JGcs, juxtaglomerular cells; KIR, inward rectifier current of potassium; OB, olfactory bulb; OSNs, olfactory sensory neurons; PG, periglomerular; sSA, short axon surface; SVZ, subventricular zone, TH, tyrosine hydroxylase.

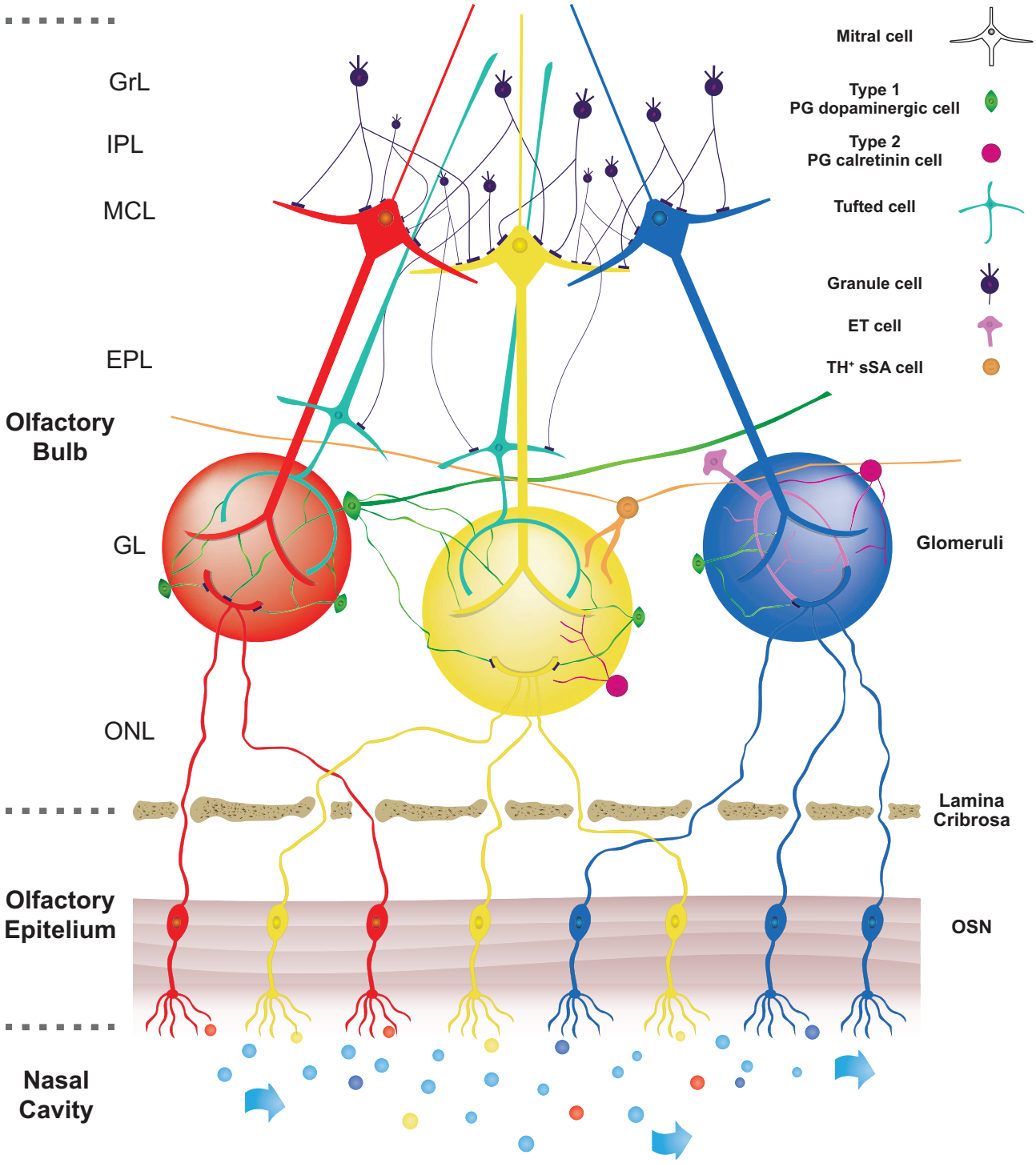

FIGURE 1 | Schematic pathway of the main neuronal connections in OB. In the nasal cavity, airflow transports different odorants (represented by different colours) to specific olfactory receptors expressed on olfactory sensory neurons (OSNs) localized in the olfactory epithelium (OE). Olfactory information is then transduced in an electrical signal to later reach the olfactory bulb (OB). Olfactory sensory neurons send their axons through the lamina cribrosa to reach the core of corresponding glomeruli, which consists of spherical structures located in the olfactory bulb. Axons of OSNs, expressing the same odorant receptors, are projected into the same glomeruli, so each glomerulus is linked to a single odorant receptor. Within the glomerular core, OSNs axons make synapses with apical dendrites of projections corresponding to OB neurons (Mitral and Tufted cells). On the surface of glomeruli are located periglomerular cells (PG). These cells project their dendrite into the glomerulus and make reciprocal synapses with projections neurons and some of them with axons of OSNs. Based on their synaptic connections with axons of OSNs, two subtypes of PG cells are described. Type 1 PG cells, belonging to dopaminergic PG cells, are synaptically connected both with axons of OSNs and dendrites of other neurons in the olfactory bulb. On the other hand, type 2 PG cells, belonging to calretinin PG cells, are not synaptically connected with axons of OSNs. The figure

(Continued)

FIGURE 1 | shows the three subtypes of DA cells present in the glomerulus area according to Nagayama et al. (2014) and Kosaka et al. (2020). The PG-DAs are represented in green. The large ones that have an axon and dendrites that enter more glomeruli and the small ones that in most cases enter one or a few glomeruli and do not have an axon have been represented. The ET cells and those belonging to the subtype of TH^+ sSA were represented too.

project and converge their axons into the same glomeruli (Mori and Sakano, 2011).

The third layer of the OB is the external plexiform layer (EPL), composed of the cell body of tufted cells, the basal dendrites of tufted and mitral cells and the apical dendrites of the principal type of interneurons, the granule cells (Gcs). The cell bodies of mitral cells are found in the fourth layer (mitral layer, MCL) which takes the name from those types of cells.

Mitral and tufted cells are two recognized types of projection neurons. Both types of cells send their axons to the olfactory cortex. However, before exiting the OB, modulation of the signal collected by the mitral and tufted projection neurons occurs in the external plexiform layer where their secondary dendrites are elongated and form reciprocal synapses with the dendrites of the granule cells.

The fifth layer contains axons from mitral, collateral axons from external tufted cells and dendrites of granule cells. It is called internal plexiform layer (IPL).

The sixth layer is formed by the somata of granule cells (granular layer, GrL). The morphology and physiology of granule cells have been thoroughly described in previous reviews (Shepherd et al., 2007; Burton, 2017; Takahashi et al., 2018) and thus we will focus on two types of interneurons expressing dopamine and calretinin found in the glomerular layer.

JUXTAGLOMERULAR INTERNEURONS

In the glomerular layer, the spherical glomeruli are enriched with axons and dendritic processes derived from OSN and cells innervating them. Indeed, glomeruli are surrounded by three main types of interneurons. These cells are overall classified as juxtaglomerular cells but, thanks to their different morphology, they can be divided into three distinct subpopulations which are characterized by the absence of projections outside the olfactory bulb: external tufted (ET) cells, short axon surface (sSA) cells and periglomerular cells (Nagayama et al., 2014).

ET cells can be classified into two subtypes according to their morphology. The first subpopulation is represented by ET without secondary dendrites is the less frequent of the two, while ET neurons with secondary dendrites are generally observed close to the border between the glomerular and the external plexiform layer (Nagayama et al., 2014).

sSA neurons are characterized by long, interglomerular axons connecting a variable number of glomeruli (Kiyokage et al., 2010; Liu et al., 2016) and for this reason, they are believed to be the most frequent origin of interglomerular projections in the OB (Aungst et al., 2003; Kiyokage et al., 2010). These cells express tyrosine hydroxylase (TH) and, due to their long interglomerular projections, they are believed to coincide with the axonic dopaminergic neurons described by Galliano and Korshunov at the border between the GL and the EPL layers (Galliano et al., 2018; Korshunov et al., 2020b).

Since dopaminergic neurons are believed to be the most important cells providing interglomerular connections (Aungst et al., 2003; Kosaka and Kosaka, 2008a; Kiyokage et al., 2010), sSA neurons were believed to be the only type of neuron expressing dopamine. However, a population of DA interneurons characterized by the absence of axons (Chand et al., 2015; Galliano et al., 2018) has been classified, based on the morphology of their dendritic arborization, as PG cells (Kosaka and Kosaka, 2009a, 2011, 2016; Korshunov et al., 2020a; Kosaka et al., 2020).

Thus, in the next chapters of this review, we will focus on the description of the properties characterizing PG cells, since they represent the most numerous types of neurons. Indeed, it has been calculated that they are almost the 60% of the total interneurons of the OB (Parrish-Aungst et al., 2007). Another characteristic of these neurons is related to the diameter of the cell body which was found to be in the range of 6–8 μm, thus making these cells the smallest among the different JGcs (Pinching and Powell, 1971a; Nagayama et al., 2014). In addition, in most cases, the dendrites departing from these neurons innervate only one glomerulus and less frequently more than one (Pinching and Powell, 1971b).

From this anatomical observation, PG interneurons surrounding the glomerulus are classified into two cell subtypes, type 1 and type 2, based on the nature of synaptic interaction they make with the axon terminals of the olfactory sensory neurons. Indeed, while both types of PG cells extend their dendritic processes in regions of the glomerulus devoid of olfactory nerves, only type 1 PG interneurons make synapses with olfactory nerves in ON zones (Kosaka et al., 1998). This observation was confirmed by electrophysiological studies performed in OB slices in which delays in response to the electric stimulation of olfactory nerve bundles in the olfactory nerve layer have been observed (Shao et al., 2009; Kiyokage et al., 2010).

Another characteristic that helps in classifying PG interneurons is their neurochemical nature, associated with the expression of neurotransmitters or calcium-binding proteins. PG cells can be divided into three main subtypes based on the immunoreactivity to tyrosine hydroxylase, calretinin, calbindin-28K (CB) (Kosaka et al., 1998; Kosaka and Kosaka, 2011).

Since the immunoreactivity for these compounds is largely mutually exclusive, these three cellular subtypes are virtually non-overlapping (Kosaka and Kosaka, 2007; Parrish-Aungst et al., 2007). The functional roles of each PG cells subtype in odor processing are still being the object of investigation. However, it has been reported that all PG interneurons synthesize γ-aminobutyric acid (GABA) and express at least one of the two glutamic acid decarboxylase (GAD) isoforms, GAD65 and GAD67, except for a small percentage of CR-positive neurons

(Kosaka, 2007). Therefore, they can be classified as inhibitory neurons. In more than half of the JG cells population, one or both isoforms are expressed (Parrish-Aungst et al., 2007; Whitman and Greer, 2007).

Several studies have also tried to calculate how many PG cells belong to the different groups. Results suggest that CR cells are the most abundant subtype, while the CB-positive cells are the fewest, but these proportions vary among the different studies, probably depending on the method employed in the analysis (Kosaka and Kosaka, 2007; Panzanelli et al., 2007; Parrish-Aungst et al., 2007; Whitman and Greer, 2007).

The different subtypes of interneurons present in the glomerulus also have different temporal patterns of neurogenesis throughout life. PG cells, together with granular cells, represent a neuronal population that is produced both during embryonic life and in adulthood (Altman, 1962, 1969; Hinds, 1968). PG cells expressing TH and CB are added mainly at embryonic days 12.5–15.5, while interneurons expressing CR increase in number during adulthood (Batista-Brito et al., 2008; Nagayama et al., 2014; Kim et al., 2020).

DA CELLS IN THE OLFACTORY BULB

Juxtaglomerular dopaminergic neurons of the olfactory bulb represent the most numerous endogenous dopamine-producing cells in the forebrain (Guyenet and Crane, 1981; Cave and Baker, 2009) and they are identified in the A16 group of neurons in the standard classification (Bjorklund and Dunnett, 2007).

Dopaminergic neurons are purposely located at the entrance of the bulbar circuitry, in this way they are directly in contact with the olfactory nerve terminals and sustain odor processing and adaptation processes of the bulbar network to external environments.

Mature DA neurons in OB have been almost exclusively described in the glomerular layer (Halasz et al., 1981), and there is consensus on the fact that they co-release dopamine and GABA from separate pools of vesicles (Maher and Westbrook, 2008; Borisovska et al., 2013).

Thanks to the use of TH as a marker of dopaminergic neurons, it has been estimated that 10–16% of the neurons in the glomerular layer of adult animals are indeed DA (McLean and Shipley, 1988; Panzanelli et al., 2007).

In the last decades, there has not been a unison agreement on the classification based on the morphology and nomenclature of the DA cells present in the glomerular layer. One classification distinguishes three types of cells: (1) PG-DA (Kosaka et al., 1985; Gall et al., 1987); (2) a subpopulation of external tufted cells which, differently from the ET neurons present in the EPL, are not projection neurons (Gall et al., 1987; Halász, 1990; Kosaka and Kosaka, 2011) and (3) a subpopulation of short axon cells (SA) (Kiyokage et al., 2010; Liu et al., 2013; Nagayama et al., 2014; Sanz Diez et al., 2019) with soma in the glomerular layer that has been called superficial (sSA) and are distinguished from those present in the granule cell layer which are called deep SA (dSA). Both subtypes are important for intrabulbar connections. Several subtypes of dSA cells have been reported to play the role of mediating GABAergic inhibition on interneurons PG and Gr (Eyre et al., 2008; Boyd et al., 2012; Burton, 2017). The superficial SA cells instead release both GABA and DA in other glomeruli and produce a temporally biphasic inhibition-excitation response in external tufted cells (Liu et al., 2013; Whitesell et al., 2013; Sanz Diez et al., 2019). A detailed analysis using the retrograde tracing technique showed that these cells possess long neuronal processes and are positive not only for the TH marker but also for the GAD67 isoform (Kiyokage et al., 2010).

The sSA $TH^+/GAD67^+$ cells differ from the classic sSA cell reported by Pinching and Powell previously (Pinching and Powell, 1971a,b) because they have an axon that extends for ∼1 mm, and its dendrites make contacts with up to 50 glomeruli, while sSA cell has classically been described to have a shorter axon extending only for one to two glomeruli while dendrites avoid glomeruli (Nagayama et al., 2014).

In the second type of classification, it appears that DA neurons present in the glomerulus layer fall into at least two subpopulations that are differentiated by a bimodal distribution of the size and diameter of the soma (Pignatelli et al., 2005; Kosaka et al., 2020) and last for the presence or absence of an axon (Chand et al., 2015; Galliano et al., 2018). Larger neurons probably might correspond to external tufted cells or sSAc (Kosaka et al., 2020) and the smallest to PG cells (Halasz et al., 1981; Davis and Macrides, 1983; Hoogland and Huisman, 1999; Pignatelli et al., 2005; Kosaka, 2007; Kosaka and Kosaka, 2008b; Liberia et al., 2012; Pignatelli and Belluzzi, 2017; Kosaka et al., 2020). External tufted neurons were initially thought to be excitatory neurons, and the small PG inhibitory neurons (Halasz et al., 1981; Davis and Macrides, 1983). However, subsequent studies have indicated that both large and small dopaminergic subgroups are GABAergic interneurons (Kosaka et al., 1985, 1987a; Gall et al., 1987).

Experimental analyses confirmed the classification of these two main subtypes in mice, as reported by Kosaka's laboratory. In a first paper, these authors showed that small DA neurons have an average diameter between 8.76 ± 1.58 μm and 10.69 ± 2.70 μm for the large one. In more recent publications the peak and half-width of the diameters measured of the smaller group were 9.9 ± 2.5 μm, and those of the larger group 13.8 ± 2.1 μm (Kosaka and Kosaka, 2008b; Kosaka et al., 2020). Measures performed in our lab confirmed these data, showing values of 5.67 ± 0.96 and 9.48 ± 2.39 μm respectively for small and large DA-PG neurons (Pignatelli et al., 2005). The existence of large and small PG neurons has been confirmed using electrophysiological analysis observing the difference of action potentials that originate in the soma and then propagate to the dendrites or action potentials that originate in the initial segment of the axon and propagate backward into the soma. In our electrophysiological analyses on the excitability of DA-PG cells (Pignatelli et al., 2005) we did not find significant differences between large and small subtypes, but more recent studies have shown greater excitability of the larger cells which could be correlated to differences in excitability parameters such as a lower threshold and rheobase current, faster action potentials rise phase, higher firing frequency and other electrophysiological peculiarities (Chand et al., 2015).

The presence of axons departing from PG interneurons has been for a long time a matter of debate. The analysis of the two cell types by Kosaka's group showed that the larger cell type of PG neurons projects axonal processes toward glomeruli distant from the glomerulus where the soma is located, becoming a neuron that plays a role in interglomerular association (Kosaka and Kosaka, 2008a, 2011, 2016). These data were confirmed using molecular markers of an initial axon segment (Chand et al., 2015), being this parameter useful for the discrimination of large and small DA neurons.

Axon segment markers are absent in most small DA neurons, as shown both *in vivo* (Kosaka and Kosaka, 2011, 2016) and *in vitro* neurons (Chand et al., 2015; Galliano and Grubb, 2016). However, in a recent review, Kosaka et al. reported the presence of rare small DA neurons characterized by thin axon-like processes positive for axon segment markers (Kosaka et al., 2020). Thus, it can be suggested that, although the proposed classification in large and small DA PG interneurons is one mostly used nowadays, large and short axon DA PG neurons might correspond to the short axon cells described in Nagayama et al. (2014).

ET cells (Halasz et al., 1981; Davis and Macrides, 1983), later recognized as GABAergic are glomerular interneurons that can coordinate long-range intrabulbar connections (Kosaka and Kosaka, 2007; Panzanelli et al., 2007; Parrish-Aungst et al., 2007). On one hand, large DA-PG neurons make synapses with granule cells on the opposite edge of the OB, establishing an association inhibitory circuit through which isofunctional odor columns are connected (Schoenfeld et al., 1985; Lodovichi et al., 2003; Kosaka and Kosaka, 2011). Another circuit is characterized by large type DA glomerular neurons which connect ipsilateral glomeruli (Kosaka and Kosaka, 2011).

Concerning small PG neurons, they represent about 85% of DA neurons in the OB (Pignatelli et al., 2005) and they were found to connect to one glomerulus or few glomeruli in their proximity (Kosaka and Kosaka, 2011, 2016; Kosaka et al., 2020).

To conclude, a recent work from the Kosaka group has further improved the classification of previously described bulbar DA cells by integrating them with three other DA cell subtypes (Kosaka et al., 2020), besides large and small DA-PG neurons, bringing to five subpopulations of DA-positive juxtaglomerular neurons. The first group is referred to as the transglomerular neurons which have a medium-sized cell body and dendritic processes that can reach up to 2–6 glomeruli. They are not only expressing TH but also secretagogin. The second group of juxtaglomerular TH neurons has been defined by Kosaka et al. as "incrusting" cell group which is characterized by dendritic branches running through the periphery of one or more glomeruli, decorating them (Kosaka et al., 2020). The last group of neurons include cells that have no axonal processes and are TH and secretagogin positive and are but that, from the morphological point of view, cannot be classified into the previously described groups. In their study, Kosaka et al. suggest naming them oligoglomerular neurons since they extend their dendrites in more glomeruli (Kosaka et al., 2020).

PHYSIOLOGICAL ROLE OF DOPAMINERGIC NEURONS

Dopaminergic cells play a dual role in controlling the local gain of transmitter release from the terminals of olfactory sensory neurons (Hsia et al., 1999; Ennis et al., 2001; McGann, 2013) and determine inhibition of lateral glomerular output (Liu et al., 2013). In this way, they can influence the basic characteristics of olfactory sensory behavior (Wei et al., 2006; Serguera et al., 2008). Those cells are also responsible for remarkable activity-dependent plasticity, controlling the release of TH and the synthesis of GAD67 in an activity-dependent manner (Baker et al., 1983; Cave et al., 2010; Parrish-Aungst et al., 2011; Banerjee et al., 2013).

In recent years, DA interneurons in the olfactory bulb have been studied because these cells have three interesting characteristics: first, they are extremely plastic (Baker et al., 1983; Bastien-Dionne et al., 2010), second, they are cells anatomically found at the entrance of the bulbar circuit, suggesting an important role in the odor processing process (Borisovska et al., 2013) and, finally, they are cells constantly generated throughout life (Altman, 1969; Betarbet et al., 1996; Baker et al., 2001; Winner et al., 2002; Mizrahi et al., 2006; Ventura and Goldman, 2007; Lazarini et al., 2014). The fact that they can be produced and replaced during the whole life makes them interesting for regenerative medicine studies as a source of new dopaminergic autologous cells to repair brain-damaged areas, such as in Parkinson's disease (Cave et al., 2014).

From the physiological point of view, the importance of DA interneurons in olfaction has been demonstrated in mice in which the knocking out of dopamine receptors or transporters leads to decreased ability to discriminate odors (Wilson and Sullivan, 1995; Tillerson et al., 2006; Taylor et al., 2009). A similar result was obtained when mice with genetically induced mitochondrial dysfunction were analyzed and found that the odor discrimination deficit was paralleled by a decrease in the number of small PG-DA neurons (Paß et al., 2020). Evidence of their role in humans comes from several studies in which it is shown that olfaction impairment in Parkinson's disease is one of the first signs of neurodegeneration, even prodromic to motor deficits (Doty, 2012).

DA-PG neurons are endowed with autorhythmicity which implies a tonic release of neurotransmitter in the synaptic cleft with ON the terminal. The role of this neurotransmitter in the bulbar circuits, as described in the literature, lends itself to an uncertain interpretation, also due to the presence of various dopamine receptors and their different distribution in the OB. The expression of these receptors within the OB has been analyzed using different techniques spanning from *in situ* hybridization, autoradiography, immunohistochemistry combined with electron microscopy. A first study by Meador-Woodruff detected D1 receptor mRNA in the olfactory bulb (Meador-Woodruff et al., 1991) which was then specifically identified to be the subtype D1A while D1B receptors were undetectable (Coronas et al., 1997). In the same study, *in situ* hybridization showed that D1A is localized in the glomerular

and granular layers of the OB, while autoradiography using the [^{125}I]SCH23982 ligand demonstrated the presence of D1A not only in the neuropil of the glomerular layer but also in EPL, mitral layer and IPL. D2 receptors were studied more extensively. They were found to be expressed in the neuropil of all olfactory glomeruli and specifically they were identified by electron microscopy on olfactory axons, dendrites of mitral and tufted neurons (Gutierrez-Mecinas et al., 2005). The presence of D2 receptors in the glomerular layer was also confirmed by autoradiography using the [H^3]quinpirole D2 agonist as a ligand (Levant et al., 1993). Interestingly, D2 receptors were also found to be expressed on type 1, GABAergic PG neurons (Gutierrez-Mecinas et al., 2005), the function of which remains to be discovered. Very few data are available on other DA receptor types. Faint radiolabelled D3 receptor was found in the olfactory nerve layer and the glomerular layer consistently with mRNA distribution (Sokoloff et al., 1990; Bouthenet et al., 1991; Levant et al., 1993; Coronas et al., 1997). D4 receptor mRNA was not found in the OB while D5 receptor was found in the neuropil of the glomerular, IPL, EPL and granular layers (Coronas et al., 1997; Ciliax et al., 2000).

However, despite this heterogeneity, it has been identified that an important functional role is played by D2 receptors. Indeed, DA can exert an inhibitory effect on olfactory sensory fibers after binding to D2 presynaptic receptors and the reduction of calcium influx via N-type calcium channels. This data is confirmed by the fact that antagonizing D2 receptor activity there is an almost 30% increase in levels of intracellular Ca^{2+} (Wachowiak and Cohen, 1999).

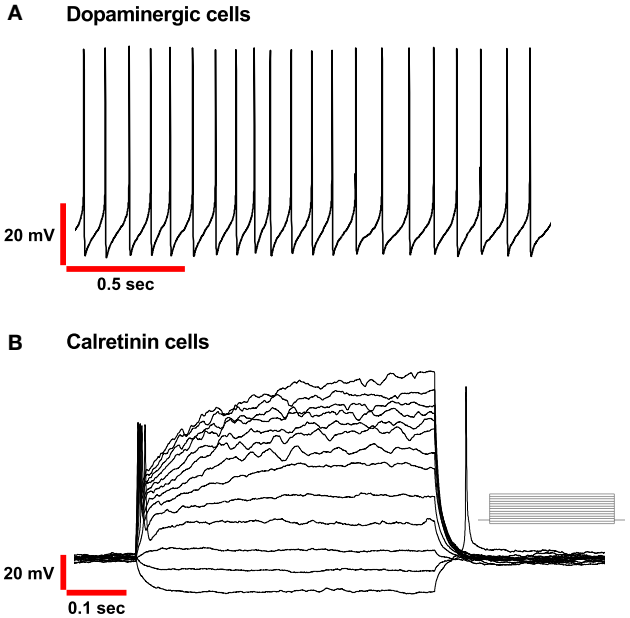

FIGURE 2 | Basic electrophysiological properties of PG Dopaminergic and Calretinin cells in OB. **(A)** Spontaneous autorhythmic action potentials in Dopaminergic cells recorded in current-clamp mode. Frequency range (4–12 Hz). **(B)** Voltage responses of Calretinin cells recorded in current-clamp mode. Only a single action potential was elicited to depolarizing injected current (from−15 pA, in increments of 10 pA as shown in the inset).

ELECTROPHYSIOLOGICAL CHARACTERISTICS OF THE DA CELLS OF THE OLFACTORY BULB

Autorhythmicity is a unique property common to many DA neurons in the Central Nervous System which allows generating rhythmic action potentials even in the absence of synaptic inputs (Grace and Onn, 1989; Hainsworth et al., 1991; Yung et al., 1991; Feigenspan et al., 1998; Neuhoff et al., 2002). The electrophysiological analysis confirmed that also DA cells present in the glomerular layer of the mouse olfactory bulb possess this pacemaker activity but it was not detected in dopaminergic cells of the rat olfactory bulb suggesting a possible species difference (Pignatelli et al., 2005; Puopolo et al., 2005; Korshunov et al., 2020b). Moreover, we can only hypothesize why in previous studies in mice the authorithmicity of these cells was not reported. One hypothesis is that in some electrophysiological experiments performed in tissue slices derived from wild type mice or, in any case, not from TH-EGFP mice it has not been possible to identify beyond any reasonable doubt the specific subtype of the cell recorded in glomerular layer of the OB slices. Since it has been estimated that only 10–16% of the neurons in the glomerular layer are DA and therefore the use of an unsafe preparation can lead to the lack of certainty of the registrations in the searched subtype.

To further strengthen this finding, we found that this autorhythmicity has similar characteristics to those recorded in midbrain dopamine neurons that are spontaneously active (Grace and Bunney, 1984) and where tonic firing is likely important for maintaining background dopamine levels.

Autorhythmicity in DA-PG neurons differs from that recorded previously in ET cells in the OB by other researchers (Hayar et al., 2004). DA-PG neurons are spontaneously active and fire in a regular, rhythmic pattern with interspike intervals rather constant in most of the cells (**Figure 2A**).

In ET cells, on the other hand, the most evident physiological feature is that they spontaneously generate rhythmic *bursts* of action potential that consisted of two or more action potentials on a slow depolarizing envelope.

To describe the ionic basis of rhythm generation in these cells our group used a transgenic mouse expressing an enhanced green fluorescent protein (eGFP) reporter construct under the promoter of TH. This animal model gave us the possibility to identify with absolute precision dopaminergic neurons (TH-GFP cells) in living slices and cultured cells during electrophysiological experiments (Sawamoto et al., 2001).

The complex pattern of voltage-dependent conductance of PG-DA cells that determines their excitability profile, including the pacemaker machinery, has been completely described in our laboratory (Pignatelli et al., 2005, 2012; Pignatelli and Belluzzi, 2017). The first electrophysiological feature of bulbar DA cells is that they have spontaneous activity, mainly within the theta frequency range (4–12 Hz). In all the papers of

our group reported here, only cells that showed spontaneous regular firing during electrophysiological recording were taken into consideration.

We used pharmacological approaches and ion substitution methods to describe two large and five small voltage-dependent conductances in these cells.

Following a kinetic characterization, these conductances were analyzed using a Hodgkin-Huxley computational model of DA-PG cells (Pignatelli et al., 2005). We found the two characterized by a large amplitude are a fast transient Na^+ current and a delayed rectifier current. They generate the action potential in DA-PG neurons.

Two of the small voltage-dependent conductance were identified in a persistent Na^+ current (INa_P) and a T-type Ca^{2+} current (ICa_T) and are responsible for the spontaneous activity of these interneurons (Pignatelli et al., 2012).

The electrophysiological analysis highlighted the presence of two other small conductances, activated by hyperpolarization: an h-current (Fried et al., 2010; Pignatelli et al., 2013) and an inward rectifier current of potassium (KIR) (Borin et al., 2014).

These two currents do not appear to be directly involved in the pacemaking mechanism but play an important role in controlling the excitability of these cells. Both currents are active at rest membrane potential but exert opposite effects on it: h-current leads to depolarization and vice versa the KIR hyperpolarizes it. This control of the membrane potential modulates the excitability of the cell.

Another aspect that should not be underestimated on the role of these currents activated by hyperpolarization is that both are effectively modulated by the mechanisms of the second messenger.

In particular, the two currents h and KIR rely on a cAMP pathway that can be modulated by the several neurotransmitters that are released by the numerous afferents making synapses on DA-PG interneurons.

In the past, it has been shown that afferents from the anterior olfactory nucleus (AON), the piriform cortex and the olfactory tubercle were all involved in odor processing. (Kiselycznyk et al., 2006; Matsutani, 2010; Markopoulos et al., 2012; Rothermel et al., 2014; Otazu et al., 2015; Zhang et al., 2017), although more recently the contribution of olfactory tubercle projections has been challenged by retrograde tracing based on adeno-associated viruses (In 't Zandt et al., 2019). Concerning the inputs to juxtaglomerular interneurons, it has been reported a glutamatergic innervation from the AON to PGCs which leads to their excitation and consequent inhibition of mitral cells (Markopoulos et al., 2012). Juxtaglomerular cells receive also serotoninergic innervation from dorsal and medial raphe nuclei (McLean and Shipley, 1987). Serotonin binds to 5-HT_{1A}, 5-HT_2 and 5-HT_{2C} (Wright et al., 1995). The consequences of this binding have been reported only for 5-HT_{2C} receptors. Indeed, electrophysiological studies showed that the activation of this receptor leads to depolarization of a subset of juxtaglomerular cells (Hardy et al., 2005; Petzold et al., 2009). However, the classification of these cells is unknown.

In the OB the afferents that could be involved with mechanisms regulating pacemaking are the serotonergic ones from the ventral and dorsal raphe nuclei (Araneda et al., 1980), noradrenergic fibers from the locus coeruleus (McLean et al., 1989), cholinergic afferents from the nucleus of the horizontal flap of the diagonal band (Zaborszky et al., 1986) and histaminergic projections from the hypothalamus (Panula et al., 1989).

We demonstrated that the amplitude of the KIR current can be increased when D2 receptors are activated or when DA-PG interneurons are exposed to muscarinic and GABA agonists. On the contrary, when these interneurons are incubated with α1, 5 -HT and histamine receptor agonists the KIR current decreases in amplitude (Borin et al., 2014). The h-current does not appear to be sensitive to 5-HT agonists by its amplitude is strongly reduced when the DA interneurons are exposed to noradrenaline (Pignatelli et al., 2013). Thus, based on the characterization of the h and KIR current it can be hypothesized their multiple and complex regulation can strongly contribute to the plasticity of the OB neuronal network.

Besides serotoninergic and noradrenergic innervation, there is solid evidence that OB is under a massive extrinsic cholinergic innervation, and that the main source of cholinergic afferents is represented by the nucleus of the horizontal limb of the diagonal band (Carson, 1984; Zaborszky et al., 1986).

Experimental observations report the presence of cholinergic innervation from the basal forebrain both in the mitral layer and in the glomerular layer (Ravel et al., 1990; Le Jeune and Jourdan, 1993; Nickell et al., 1994; Kasa et al., 1995; Crespo et al., 1999). The cholinergic terminals preferentially, though not exclusively, innervate the subpopulation of DA-PG interneurons through morphologically symmetric contacts, generally associated with inhibitory synaptic actions (Le Jeune and Jourdan, 1993). However, in contrast to this study, De Saint Jan identified a new subtype of type 2 PG neurons as a target of cholinergic innervation which are neither DA, neither CR nor calbindin immunopositive. These cells express M1 muscarinic receptors and they are characterized by a small cell body, apparent absence of axons and dendrites that innervate a single glomerulus. The activation of these cells by acetylcholine provokes inhibition of OB tufted cells (De Saint Jan, 2021).

Despite these contradictions, the cholinergic system appears to influence many basic functions of OB, including maturation (Halasz and Shepherd, 1983; Kratskin and Belluzzi, 2003), olfactory memory (Ravel et al., 1994; Levy et al., 1995) and odors processing (Nickell and Shipley, 1988; Elaagouby and Gervais, 1992; Linster and Hasselmo, 1997). These findings prompted us to study the effects of this innervation on the activity of dopaminergic neurons in the OB (Pignatelli and Belluzzi, 2008). It was shown that the effect of muscarinic agonists (M_2 agonist oxotremorine) leads to the reduction of DA periglomerular firing, because of membrane potential hyperpolarization. In this study, we hypothesized that a second messenger leads to the activation of potassium conductance, which is most likely represented by the previously described KIR current.

This muscarinic effect described on DA-PG cells can play a role in the modulation of the signal output from OB to central structures. It can be also relevant to understand the

perturbations of cholinergic inputs to the cerebral cortex that occur in Alzheimer's disease.

Glutamatergic projections that make direct synaptic contact on DA-PG cells are innervated by presynaptic terminals (Kosaka et al., 1997) and modulate the release of DA. Indeed, metabotropic glutamate receptors present in DA bulb cells were the subject of electrophysiological studies, which confirmed the presence in this area of two receptor subtypes: mGluR1 and mGluR5 (Martin et al., 1992; Shigemoto et al., 1993; Romano et al., 1995). First, the expression of these receptors was demonstrated by quantitative Real-Time PCR and then, using selective agonists and antagonists of mGluR different subtypes, different electrophysiological parameters were analyzed (Jian et al., 2010). The consequence of this glutamatergic innervation of DA-PG interneurons is an inhibition of neurotransmitter release from olfactory nerve terminals acting on presynaptic D2 receptors (Berkowicz and Trombley, 2000; Ennis et al., 2001; Davila et al., 2003).

Pharmacological activation in bulbar DA cells of mGluR1 receptors produces a depolarization which is presumed to lead to an increase of DA release from the cell, with a consequent reduction in the release of glutamate from the ON axon terminals. On the other hand, mGluR5 was seen to produce the opposite effect. Various hypotheses on the physiological significance of the opposite effects of mGluR1 and mGluR5 on DA can be formulated as suggested by our group (Jian et al., 2010), but in general, this differential regulation mechanism leads to fine regulation of DA excitability.

ADULT NEUROGENESIS OF DA CELLS

OB displays another interesting feature, namely, it is one of the two regions of the mammalian CNS that undergo continuous neuronal replacement during adulthood (Gross, 2000). In the subventricular zone (SVZ) of the lateral ventricles, new cells are generated and migrate in the rostral stream toward the OB (Pignatelli and Belluzzi, 2010; Cave and Baker, 2015; Lledo and Valley, 2016; Malvaut and Saghatelyan, 2016). Here they differentiate into diverse subtypes of interneurons that lead to the formation of new granules or periglomerular neurons (Belluzzi et al., 2003; Carleton et al., 2003; Yang, 2008) and finally integrate synaptically into the existing neural network (Belluzzi et al., 2003). The formation of new cells and their integration into the circuitry is essential for maintaining homeostasis in the olfactory bulb.

Interneurons increase in different proportion in the granular and glomerular layer of OB (Kosaka et al., 1987b; McLean and Shipley, 1988; Winner et al., 2002; De Marchis et al., 2007; Batista-Brito et al., 2008). Adult neurogenesis restores the subtypes belonging to the PG population, which express TH, calretinin and a fraction of calbindin glutamatergic interneurons (Lledo and Valley, 2016). In the work by De Marchis et al. (2007) data for adult regeneration of less studied PG subtype cells are also reported. These cells are positive for neurocalcin calcium-binding proteins. Example of BrdU labeled cells co-expressing parvalbumin have also been reported (Whitman and Greer, 2007). The rate of neurogenesis in these three subtypes of PG cells is different and is higher for the PGs expressing calretinin and the lowest in the PGs expressing calbindin indicating that each PG subtype has the unique substitution and/or addition modality (Sakamoto et al., 2014).

Indeed, it was observed that, after 2 months, adult neurogenesis provokes a complete turnover in the granular cell layer, with the cell number remaining stable, while in the glomerular layer the number of new neurons outnumbers about 30% the cell loss (Ninkovic et al., 2007). Intriguingly, the net increase in the number of cells resulting from the added and the lost, in the glomerular layer during adult neurogenesis in the OB, is subtype-specific, as it concerns only two subtypes of interneurons, i.e., calretinin and DA cells (Ninkovic et al., 2007; Adam and Mizrahi, 2011).

The dorsolateral region of SVZ (Fiorelli et al., 2015) is engaged in generating DA progenitor cells characterized by the expression of the transcription factor Pax6 (Merkle et al., 2007; Young et al., 2007; Brill et al., 2008; Fernandez et al., 2011) which is necessary for the development of the DA phenotype (Dellovade et al., 1998; Kohwi et al., 2005; Haba et al., 2009). Other markers for the DA phenotype are the transcription factors Dlx2 and Meis2 (Brill et al., 2008; de Chevigny et al., 2012; Agoston et al., 2014).

It is also important that these newly generated neurons can survive and integrate into the circuitry. The addition of new DA neurons in the olfactory bulb is a plastic, experience-dependent process, and occurs in response to sensory stimuli. Surprisingly, this phenomenon is only specific to DA cells and not to calretinin or calbindin PG cells (Bonzano et al., 2014; Galliano et al., 2021).

Survival and integration processes depend on the abundance of the olfactory input, being strongly enhanced by odor enrichment (Rochefort et al., 2002; Yamaguchi and Mori, 2005; Bonzano et al., 2014, 2016). The DA-PG cells, as commented before, are type 1 cells that make direct contact with the olfactory nerve at the beginning of the bulbar circuitry. Due to this direct connection with the olfactory nerve, DA-PG cells are therefore particularly sensitive to different degrees of olfactory inputs to which they are exposed (Kosaka and Kosaka, 2007). This leads to dynamic control of turnover in a spatial and neuronal subtype-specific manner (Sawada et al., 2011). In fact, in animals that are odor-deprived by either chemical or surgical deafferentation of the OB (Nadi et al., 1981; Kawano and Margolis, 1982; Baker et al., 1983) or naris occlusion (Brunjes et al., 1985) a large reduction in the number of DA cells is observed. This phenomenon can be reverted and affects both pre-existing and adult-generated neurons (Bovetti et al., 2009; Bastien-Dionne et al., 2010). It is not yet clear which mechanisms are involved in these events, but a role is presumed to be played by transcriptional and epigenetic regulators (Banerjee et al., 2013; Bovetti et al., 2013; Bonzano et al., 2016) and microglia (Grier et al., 2016).

ELECTROPHYSIOLOGY OF DA NEURONS DURING ADULT NEUROGENESIS

Immunohistochemical observations performed in the 80s' showed that mature DA neurons are strictly localized in the glomerular layer (Halasz et al., 1981). However, subsequent observations using a transgenic mice model, indicate that some

neurons expressing eGFP under the TH promoter can be also observed in other layers including EPL, MCL and GCL (Baker et al., 2001; Pignatelli et al., 2009; Korshunov et al., 2020a; Kosaka et al., 2020). For these cells, the transcription of the TH gene occurs in absence of significant translational activity (Jeong et al., 2003). For this reason, it has been proposed that these neurons express TH, but dopamine is not produced. Thus, these neurons could be newly neurons observed at different stages of maturation committed to becoming DA neurons (Saino-Saito et al., 2004). We tested this hypothesis with different methods (Pignatelli et al., 2009).

After the characterization of the mature DA cells present in the glomerular layer (Pignatelli et al., 2005, 2012), a comparative analysis of the cells presents in the other layers that are assumed to be immature was carried out (Pignatelli et al., 2009). Using TH-GFP transgenic mice (Sawamoto et al., 2001) in which the eGFP gene is located under the TH promoter, we were able to observe that TH^+ neurons present in the mitral and EPL layers have an eGFP fluorescence lower than that present in the cells of the glomerular layer, but still sufficient to allow the identification of these cells.

TH-GFP neurons recorded in EPL are autorhythmic cells, as they show a spontaneous firing almost indistinguishable from that of the mature DA neurons present in the GL. Autorhythmicity in these cells is due to the presence of the same voltage-dependent currents: Na^+ persistent (INa_P) and a T-type Ca^{2+}; as it occurs in the spontaneous activity of mature DA neurons (Pignatelli et al., 2009, 2012). Autorhythmicity instead is not observed in TH-GFP cells present in the mitral layer, where the T-type calcium current, which is one of the currents involved in the pacemaker mechanism, is absent. However, these cells can generate trains of action potentials in response to depolarizing pulses.

High intracellular Cl^- concentration is a marker for immature neurons (Ben-Ari et al., 2007). To demonstrate the hypothesis that the TH-GFP cells present in the three layers of the olfactory bulb (mitral, EPL and GL) are cells with an increasing degree of maturity, the intracellular concentration of Cl^- was measured (Pignatelli et al., 2009). The results showed that neurons in the EPL and mitral layer possess a higher intracellular Cl^- concentration than those within the GL, thus confirming this hypothesis.

One further observation supporting the hypothesis of maturation of glomerular DA neurons is based on experiments of TH-GFP cells stimulation from the olfactory nerve. Indeed, to complete their maturation they must establish an asymmetric connection with fibers derived from the olfactory epithelium (Brunjes et al., 1985; Stone et al., 1991; Wilson and Wood, 1992; Cho et al., 1996; Toida et al., 2000).

Our electrophysiological analysis showed that most (75%) of the EPL cells respond upon ON stimulation with a monosynaptic EPSP and that this response can be reverted by incubation with kynurenate (Pignatelli et al., 2009). On the other hand, the cells present in the mitral layer, which were supposed to be more immature, do not respond synaptically to ON stimulation. However, mitral TH-GFP neurons respond to the focal application of glutamate, which is the same neurotransmitter released by the ON on mature DA cells (Pignatelli et al., 2009). This suggests that these cells already have functional receptors for glutamate, but not a synaptic connection with the olfactory nerve.

All these observations suggest that the weakly fluorescent TH-GFP cells observed in the mitral layer represent newly generated DA cells that arrived in the OB which stopped their migration process at this level. To reach their destination in the glomerular layer, these immature cells require a consensus signal coming from the glomerular region and the passage across the EPL that brings to the end their differentiation toward the DA phenotype. The signal is still unknown, but previously data from our group suggests that the establishment of synaptic contacts with the olfactory nerve could be the trigger (Pignatelli et al., 2009).

CR-PG CELLS IN THE OLFACTORY BULB

Calretinin is a calcium-binding protein commonly used as a marker for several cellular populations in the nervous system (Jacobowitz and Winsky, 1991; Miettinen et al., 1992; Resibois and Rogers, 1992; Huberman et al., 2008; Barinka and Druga, 2010). Under this aspect, the olfactory bulb represents no exception, considering that most of the neurons in different OB layers are positive to CR staining. In the glomerular layer alone, studies have calculated that CR cells account for a percentage of all the juxtaglomerular cells ranging from 28 to 44% (Kosaka and Kosaka, 2007; Panzanelli et al., 2007; Parrish-Aungst et al., 2007; Whitman and Greer, 2007) representing the most abundant PG interneurons in the glomerular layer of the olfactory bulb. CR-PG cells are also the most abundant PG cells generated postnatally. These neurons are mostly generated after birth, in adulthood, from neural stem cells derived from the dorsal septal and subventricular areas and have homogeneous morphological and electrophysiological properties (Benito et al., 2018).

From the temporal point of view, the production of new CR-PG cells peaks around birth and continues throughout life. This differs from the other subtypes of PG cells (dopaminergic and calbindin immunoreactive) whose production is maximum during embryogenesis and decreases after birth (De Marchis et al., 2007; Ninkovic et al., 2007; Batista-Brito et al., 2008; Li et al., 2011; Weinandy et al., 2011).

A recent work by the De Saint Jan group showed that the newly generated CR-PG cells can be distinguished from the other generated neurons because they seem to maintain properties of immaturity. Other subtypes of neurons generated after birth are rapidly integrated into the pre-existing circuitry of olfactory bulbs, while these cells are not inserted into the activity of the local network, as if they never fully mature. The function of this reserve of immature cells in this bulbar area is still unclear (Benito et al., 2018).

The presence of calretinin-positive neurons has been described also in the accessory olfactory bulb of the mouse, where inhibitory interneurons play a role related to behavior following the exposition to social odors (Jacobowitz and Winsky, 1991; Maksimova et al., 2019).

CR neurons, together with calbindin-positive neurons, constitute the type 2 PG cells identified by the Kosaka

group (Kosaka, 2007; Kosaka and Kosaka, 2009b). As previously described, the processes of these PG cells create contact with other classes of OB neurons but do not receive direct synaptic connections from the olfactory nerve axons.

From the morphological point of view, CR-PG cells are described as axonless neurons characterized by compact round-shaped soma with dendrites. When compared to the other JG cells, their soma size results to be the smallest, with an average diameter varying from 6 to 8 μm (Batista-Brito et al., 2008; Fogli Iseppe et al., 2016). In addition, differently from the other JG neurons, the soma diameters of CR cells are unimodally and normally distributed, suggesting the existence of a quite homogeneous population.

Consistent with this classification, has recently been confirmed that CR-PG cells do not receive synaptic inputs from OSNs (Najac et al., 2011). They are not innervated by olfactory sensory neurons and receive few synaptic inputs from mitral or tufted cells at excitatory synapses where NMDA receptors predominate (Benito et al., 2018) but establish GABAergic type dendrodendritic synapses with mitral and tufted cells (Panzanelli et al., 2007).

In adult animals, CR-PG interneurons are considered to participate in the inhibitory glomerular circuitry via GABA release (Burton, 2017). In the murine olfactory bulb, the majority of CR-PG cells express indeed GABAergic markers, as shown both in knock-in animals (Panzanelli et al., 2007) and by immunohistochemistry (Kosaka, 2007; Parrish-Aungst et al., 2007). In addition, type 2 CR-PG cells have been associated with cholinergic immunoreactivity. Notably, CR staining does not colocalize with cholinergic cells, which characterizes instead the large majority of CB-positive PG neurons (Krosnowski et al., 2012). On the other side, CR cells in the glomerular region show a nontrivial expression of nitric acid synthase, while this biomarker is rarely associated with the calbindin-positive population of periglomerular cells (Kosaka and Kosaka, 2007).

CR-PG CELLS: ELECTROPHYSIOLOGICAL PROFILE

From the electrophysiological point of view, CR-PG neurons display several peculiar characteristics. First, CR cells in the glomerular region possess small membrane capacitance and elevated input resistance, calculated to be approximately 4 pF and 2 GΩ, respectively. Notably, the variance of these measurements across cells is low, in agreement with the idea of a unique neuronal population previously introduced. When CR-PG neurons are recorded with voltage-clamp protocols, the two mains ionic conductances that can be distinguished are a transient outward A-type K^+ and fast transient Na^+ current (Fogli Iseppe et al., 2016; Benito et al., 2018). It is interesting to notice that being both these two currents only transiently active, the electrical behaviour of the CR-PG cells become purely ohmic under prolonged depolarizing stimulation. An additional consequence, which clearly distinguishes the electrophysiological characteristics of this group of periglomerular cells from the other classes, can be observed in current-clamp conditions. When a depolarization is applied, the CR neurons can generate only one complete action potential, as opposed to the train of spikes that dopaminergic neurons can generate (**Figures 2A,B**) and remain silent for the remaining duration of the stimulus; this observation was also confirmed by De Saint Jan group (Benito et al., 2018).

However, the two transiently activated currents do not constitute the entire set of conductances that this group of periglomerular neurons expresses. Carefully dissecting the remaining current observable during long depolarizing steps in voltage clamp, it is indeed possible to pharmacologically isolate a small persistent L-type Ca^{2+} current (Fogli Iseppe et al., 2016). Lastly, CR-PG cells possess an h-current, as clearly indicated also by the time-dependent depolarizing sag produced in response to the injection of a hyperpolarizing current.

CR-PG CELLS: POSSIBLE ROLE IN BULBAR CIRCUITRY

Some studies have investigated the role of the CR-PG cells in the complex process of olfactory information processing (Fogli Iseppe et al., 2016; Benito et al., 2018; Sanz Diez et al., 2019). Despite a comprehensive understanding of the synaptic connectivity inside the glomerulus is still missing (Vaaga and Westbrook, 2016), recent findings can help in defining some hypotheses. Differently from dopaminergic PG cells, CR neurons are anaxonic (Kosaka and Kosaka, 2010). Thus, their action is confined to the intraglomerular region, where they could regulate their activity by self-inhibition or self-modulation processes (Gire and Schoppa, 2009; Kosaka and Kosaka, 2011).

In addition, CR cells have been shown to have weak connectivity with the rest of the glomerular network (Benito et al., 2018; Sanz Diez et al., 2019). Coherently with the histological investigations, these neurons show few EPSCs in response to ON stimulation. The same is generally true for inhibitory postsynaptic currents, which suggests that inputs received from interneurons nearby are rare as well. Conversely, the stimulation of centrifugal fibers originated in the basal forebrain has been described to elicit GABAergic responses in the CR-PG neurons (Sanz Diez et al., 2019).

Taken all together, the findings described above support the idea of an extremely focused role for the CR-PG population. In particular, considering their extremely peculiar electrophysiological profile, these neurons have been proposed to improve the signal-to-noise ratio, acting as a filter against randomly occurring ON-evoked excitatory stimuli (Fogli Iseppe et al., 2016).

What is the function of this neuronal population, which is very abundant and continuously renewed, is still difficult to identify. The work of Benito et al. proposes an additional hypothesis based on their evidence that indicates these CR-positive cells as immature. These cells could therefore constitute a reserve pool of latent and not completely differentiated interneurons that could be recruited on request. The authors also hypothesize that

these cells can mature because of sensory input but also convert into another cellular subtype of PG. This phenomenon would lead to greater recruitment of PG cells generated in the adult (Benito et al., 2018).

CONCLUDING REMARKS

In the CNS, interneurons play a fundamental role in modulating the transmission of nerve information. Depending on the brain areas and the different neuronal functions, interneurons develop in subtypes with different morphologically, molecularly, and electrophysiological properties.

The study of interneurons is important for at least two reasons: on one hand, it allows us to understand complex brain circuits (Maccaferri and Lacaille, 2003). On the other hand, it provides more information on neurodevelopmental disorders that are associated with interneuron malfunction (Fang et al., 2014), such as autism spectrum disorder and Tourette's syndrome (Ashwin et al., 2014).

The mammalian OB is a part of the brain where it is possible to identify a large percentage of diversified interneurons that are continuously generated in postnatal and adult periods (Batista-Brito and Fishell, 2009; Bartolini et al., 2013; Kepecs and Fishell, 2014).

The olfactory bulb interneurons have another peculiar characteristic: it has been observed that the proportion of inhibitory interneurons concerning excitatory neurons is extremely higher (100: 1 ratio, compared to other brain regions at a 1:5 ratio (Kim et al., 2020).

In this review, we focus on the description of dopaminergic and calretininergic cells, two populations of interneurons that play a role in olfactory information processing.

DA cells present in the olfactory bulb are the largest population of dopaminergic neurons in the brain and have been the object of many studies describing both the morphology and the electrophysiological properties of these cells. The functional role of these interneurons is still unclear, especially when we look at the DA cells that are generated in this area in adulthood.

These interneurons are supposed to play important roles in the control of glomerular output information in the OB (Banerjee et al., 2015; Liu et al., 2016; Burton, 2017; Pignatelli and Belluzzi, 2017; Vaaga et al., 2017; Shao et al., 2019). To understand how DA neurons contribute to signal processing, it is important to know their connections. A recent work (Kosaka et al., 2020) has shown a great heterogeneity of the DA cells in the olfactory bulb, and that still little is known about the synaptic connections of each cell type described and their role in the bulbar circuitry.

However, electrophysiological analyses of DA olfactory bulb neurons gave the possibility to understand important aspects of the voltage-conductance involved in the excitability profile and synaptic modulation of these cells (Pignatelli et al., 2005, 2013; Pignatelli and Belluzzi, 2008; Jian et al., 2010; Borin et al., 2014).

To answer the question of why DA neurons are continuously produced in the olfactory bulb, we need to consider the characteristics of the olfactory structure and how the adult neurogenesis process occurs. In mice, adult neurogenesis is a process in which new neurons are added and odor memory is improved. This cell increase is stimulated by enriched odor exposure, even if constrained to keep the number of neurons constant in time (Rochefort et al., 2002). This means that the new neurons are not added but replace the existing ones. The reason for this process could be that the olfactory bulb needs to adjust the circuitry following new olfactory experiences.

The data reported in this review can give a possible explanation of how this process occurs. DA cells are continuously generated over time and migrate in the OB until they reach the mitral cell layer. Here, they remain in a standby condition waiting to receive a consensus signal to finish their differentiation process and reaching the final position in the glomerular layer (Pignatelli et al., 2009). Then, we hypothesize that the differentiation and maturation will be completed when immature cells in the mitral layer will start making active synapses within the glomerular layer. However, many cells will not follow this path and will therefore undergo to apoptosis and death, as indicated by evidence that shows most of the newly generated cells arriving from the SVZ being eliminated before reaching the olfactory bulb.

All these data, together with the recent observation that DA cells undergo to adult neurogenesis also in humans (Inta et al., 2015) and their capacity to integrate into neuronal circuits make them an attractive tool for replacement strategies in cases of loss of dopaminergic neurons, such as Parkinson's disease (Lledo and Saghatelyan, 2005).

Another interesting aspect concerning DA cells was recently discussed in a review (Korshunov et al., 2020b), which describes how the two sensory systems, the retina and OB, are remarkably similar. Both areas have an anatomical structure made up of layers where sensory signals follow a precise sequence, and both areas utilize lateral inhibition. Moreover, the presence of interneurons that release DA is important to have a correct interpretation of both olfactory and visual signals.

We described that CR interneurons located in the glomerular layer are the most abundant neuronal population in the olfactory bulb. As in the case of DA cells, CR-PG cells are continuously produced in adulthood, but surprisingly in some cases, they do not integrate into pre-existing olfactory bulb networks for a long time (Benito et al., 2018).

Electrophysiological studies also reveal another unusual feature of these cells. CR-PG cells when stimulated by a train of excitatory inputs, sufficiently close to depolarize stably the membrane, respond with a single action potential (Fogli Iseppe et al., 2016). This behaviour is due to the inactivation of the two main voltage-dependent currents expressed by these cells, an A-type K^+ and a classic Na^+ current. Therefore, if a train of excitatory inputs arrives, the cell will fire only one complete spike before becoming completely unexcitable.

What could be the role of these cells in the olfactory bulb? They are inhibitory interneurons and are positioned at the entry of the bulbar network. It has been proposed that they could improve the signal-to-noise ratio of the network. If a random excitatory input, representing a meaningless signal (noise), arrives, CR-PG cells will activate and lead to

an inhibition of the projection neurons (Fogli Iseppe et al., 2016).

In conclusion, the information presented in this review gave some initial clues on the functions of these two populations of interneurons, but further studies are needed to completely define their role in the olfactory sensory process.

AUTHOR CONTRIBUTIONS

SC, AP, and AFI conceived the review and wrote the manuscript. SC, AP, and FC checked and revised the manuscript. All authors contributed to the article and approved the submitted version.

FUNDING

This research was supported by the Italian Ministry of University and Research (PRIN 2019-PRA.A-PA_001) and by local funds of the University of Ferrara (2020-FAR.L-PA_001).

ACKNOWLEDGMENTS

We thank Prof. Ottorino Belluzzi for his precious comments on the manuscript and Dr. Faride Pighin for his critical reading of the manuscript.

REFERENCES

Adam, Y., and Mizrahi, A. (2011). Long-term imaging reveals dynamic changes in the neuronal composition of the glomerular layer. *J. Neurosci.* 31, 7967–7973. doi: 10.1523/JNEUROSCI.0782-11.2011

Agoston, Z., Heine, P., Brill, M. S., Grebbin, B. M., Hau, A. C., Kallenborn-Gerhardt, W., et al. (2014). Meis2 is a Pax6 co-factor in neurogenesis and dopaminergic periglomerular fate specification in the adult olfactory bulb. *Development* 141, 28–38. doi: 10.1242/dev.097295

Altman, J. (1962). Are new neurons formed in the brains of adult mammals? *Science* 135, 1127–1128. doi: 10.1126/science.135.3509.1127

Altman, J. (1969). Autoradiographic and histological studies of postnatal neurogenesis. IV. Cell proliferation and migration in the anterior forebrain, with special reference to persisting neurogenesis in the olfactory bulb. *J. Comp. Neurol.* 137, 433–457. doi: 10.1002/cne.901370404

Araneda, S., Gamrani, H., Font, C., Calas, A., Pujol, J.-F., and Bobillier, P. (1980). Retrograde axonal transport following injection of [3H]-serotonin into the olfactory bulb. II. Radioautographic study. *Brain Res.* 196, 417–427. doi: 10.1016/0006-8993(80)90405-9

Ashwin, C., Chapman, E., Howells, J., Rhydderch, D., Walker, I., and Baron-Cohen, S. (2014). Enhanced olfactory sensitivity in autism spectrum conditions. *Mol. Autism.* 5:53. doi: 10.1186/2040-2392-5-53

Attems, J., Walker, L., and Jellinger, A. K. (2015). Olfaction and aging: a mini-review. *Gerontology* 61, 485–490. doi: 10.1159/000381619

Aungst, J. L., Heyward, P. M., Puche, A. C., Karnup, S. V., Hayar, A., Szabo, G., et al. (2003). Centre-surround inhibition among olfactory bulb glomeruli. *Nature* 426, 623–629. doi: 10.1038/nature02185

Baker, H., Kawano, T., Margolis, F. L., and Joh, H. T. (1983). Transneuronal regulation of tyrosine hydroxylase expression in olfactory bulb of mouse and rat. *J. Neurosci.* 3, 69–78. doi: 10.1523/jneurosci.03-01-00069.1983

Baker, H., Liu, N., Chun, H. S., Saino, S., Berlin, R., Volpe, B., et al. (2001). Phenotypic differentiation during migration of dopaminergic progenitor cells to the olfactory bulb. *J. Neurosci.* 21, 8505–8513. doi: 10.1523/jneurosci.21-21-08505.2001

Banerjee, A., Marbach, F., Anselmi, F., Koh, M. S., Davis, M. B., Garcia da Silva, P., et al. (2015). An interglomerular circuit gates glomerular output and implements gain control in the mouse olfactory bulb. *Neuron* 87, 193–207. doi: 10.1016/j.neuron.2015.06.019

Banerjee, K., Akiba, Y., Baker, H., and Cave, W. J. (2013). Epigenetic control of neurotransmitter expression in olfactory bulb interneurons. *Int. J. Dev. Neurosci.* 31, 415–423. doi: 10.1016/j.ijdevneu.2012.11.009

Barinka, F., and Druga, R. (2010). Calretinin expression in the mammalian neocortex: a review. *Physiol. Res.* 59, 665–677. doi: 10.33549/physiolres.931930

Bartolini, G., Ciceri, G., and Marin, O. (2013). Integration of GABAergic interneurons into cortical cell assemblies: lessons from embryos and adults. *Neuron* 79, 849–864. doi: 10.1016/j.neuron.2013.08.014

Bastien-Dionne, P. O., David, L. S., Parent, A., and Saghatelyan, A. (2010). Role of sensory activity on chemospecific populations of interneurons in the adult olfactory bulb. *J. Comp. Neurol.* 518, 1847–1861. doi: 10.1002/cne.22307

Batista-Brito, R., Close, J., Machold, R., and Fishell, G. (2008). The distinct temporal origins of olfactory bulb interneuron subtypes. *J. Neurosci.* 28, 3966–3975. doi: 10.1523/JNEUROSCI.5625-07.2008

Batista-Brito, R., and Fishell, G. (2009). Chapter 3 the developmental integration of cortical interneurons into a functional network. *Curr. Top. Dev. Biol.* 87, 81–118. doi: 10.1016/S0070-2153(09)01203-4

Bay, H. H., and Cavdar, S. (2013). Regional connections of the mediodorsal thalamic nucleus in the rat. *J. Integr. Neurosci.* 12, 201–219. doi: 10.1142/s021963521350012x

Bekkers, J. M., and Suzuki, N. (2013). Neurons and circuits for odor processing in the piriform cortex. *Trends Neurosci.* 36, 429–438. doi: 10.1016/j.tins.2013.04.005

Belluzzi, O., Benedusi, M., Ackman, J., and LoTurco, J. J. (2003). Electrophysiological differentiation of new neurons in the olfactory bulb. *J. Neurosci.* 23, 10411–10418. doi: 10.1523/jneurosci.23-32-10411.2003

Ben-Ari, Y., Gaiarsa, J. L., Tyzio, R., and Khazipov, R. (2007). GABA: a pioneer transmitter that excites immature neurons and generates primitive oscillations. *Physiol. Rev.* 87, 1215–1284. doi: 10.1152/physrev.00017.2006

Benito, N., Gaborieau, E., Sanz Diez, A., Kosar, S., Foucault, L., Raineteau, O., et al. (2018). A pool of postnatally generated interneurons persists in an immature stage in the olfactory bulb. *J. Neurosci.* 38, 9870–9882. doi: 10.1523/JNEUROSCI.1216-18.2018

Berkowicz, D. A., and Trombley, P. Q. (2000). Dopaminergic modulation at the olfactory nerve synapse. *Brain Res.* 855, 90–99. doi: 10.1016/s0006-8993(99)02342-2

Betarbet, R., Zigova, T., Bakay, R. A., and Luskin, B. M. (1996). Dopaminergic and GABAergic interneurons of the olfactory bulb are derived from the neonatal subventricular zone. *Int J Dev Neurosci.* 14, 921–930. doi: 10.1016/s0736-5748(96)00066-4

Bjorklund, A., and Dunnett, S. B. (2007). Dopamine neuron systems in the brain: an update. *Trends Neurosci.* 30, 194–202. doi: 10.1016/j.tins.2007.03.006

Blazing, R. M., and Franks, K. M. (2020). Odor coding in piriform cortex: mechanistic insights into distributed coding. *Curr. Opin. Neurobiol.* 64, 96–102. doi: 10.1016/j.conb.2020.03.001

Bonzano, S., Bovetti, S., Fasolo, A., Peretto, P., and De Marchis, S. (2014). Odour enrichment increases adult-born dopaminergic neurons in the mouse olfactory bulb. *Eur. J. Neurosci.* 40, 3450–3457. doi: 10.1111/ejn.12724

Bonzano, S., Bovetti, S., Gendusa, C., Peretto, P., and De Marchis, S. (2016). Adult born olfactory bulb dopaminergic interneurons: molecular determinants and experience-dependent plasticity. *Front. Neurosci.* 10:189. doi: 10.3389/fnins.2016.00189

Borin, M., Fogli Iseppe, A., Pignatelli, A., and Belluzzi, O. (2014). Inward rectifier potassium (Kir) current in dopaminergic periglomerular neurons of the mouse olfactory bulb. *Front. Cell. Neurosci.* 8, 223. doi: 10.3389/fncel.2014.00223

Borisovska, M., Bensen, A. L., Chong, G., and Westbrook, L. G. (2013). Distinct modes of dopamine and GABA release in a dual transmitter neuron. *J. Neurosci.* 33, 1790–1796. doi: 10.1523/JNEUROSCI.4342-12.2013

Bouthenet, M. L., Souil, E., Martres, M. P., Sokoloff, P., Giros, B., and Schwartz, C. J. (1991). Localization of dopamine D3 receptor mRNA in the rat brain using *in situ* hybridization histochemistry: comparison with dopamine D2 receptor mRNA. *Brain Res.* 564, 203–219. doi: 10.1016/0006-8993(91)91456-b

Bovetti, S., Bonzano, S., Garzotto, D., Giannelli, S. G., Iannielli, A., Armentano, M., et al. (2013). COUP-TFI controls activity-dependent tyrosine hydroxylase expression in adult dopaminergic olfactory bulb interneurons. *Development.* 140, 4850–4859. doi: 10.1242/dev.089961

Bovetti, S., Veyrac, A., Peretto, P., Fasolo, A., and De Marchis, S. (2009). Olfactory enrichment influences adult neurogenesis modulating GAD67 and plasticity-related molecules expression in newborn cells of the olfactory bulb. *PLoS ONE* 4:e6359. doi: 10.1371/journal.pone.0006359

Boyd, A. M., Sturgill, J. F., Poo, C., and Isaacson, S. J. (2012). Cortical feedback control of olfactory bulb circuits. *Neuron.* 76, 1161–1174. doi: 10.1016/j.neuron.2012.10.020

Brill, M. S., Snapyan, M., Wohlfrom, H., Ninkovic, J., Jawerka, M., Mastick, G. S., et al. (2008). A dlx2- and pax6-dependent transcriptional code for periglomerular neuron specification in the adult olfactory bulb. *J. Neurosci.* 28, 6439–6452. doi: 10.1523/JNEUROSCI.0700-08.2008

Brunjes, P. C., Smith-Crafts, L. K., and McCarty, R. (1985). Unilateral odor deprivation: effects on the development of olfactory bulb catecholamines and behavior. *Brain Res.* 354, 1–6. doi: 10.1016/0165-3806(85)90063-x

Burton, S. D. (2017). Inhibitory circuits of the mammalian main olfactory bulb. *J. Neurophysiol.* 118, 2034–2051. doi: 10.1152/jn.00109.2017

Bushdid, C., Magnasco, M. O., Vosshall, L. B., and Keller, A. (2014). Humans can discriminate more than 1 trillion olfactory stimuli. *Science* 343, 1370–1372. doi: 10.1126/science.1249168

Carleton, A., Petreanu, L. T., Lansford, R., Alvarez-Buylla, A., and Lledo, M. P. (2003). Becoming a new neuron in the adult olfactory bulb. *Nat. Neurosci.* 6, 507–518. doi: 10.1038/nn1048

Carson, K. A. (1984). Quantitative localization of neurons projecting to the mouse main olfactory bulb. *Brain Res. Bull.* 12, 629–634. doi: 10.1016/0361-9230(84)90143-6

Cave, J. W., Akiba, Y., Banerjee, K., Bhosle, S., Berlin, R., and Baker, H. (2010). Differential regulation of dopaminergic gene expression by Er81. *J. Neurosci.* 30, 4717–4724. doi: 10.1523/JNEUROSCI.0419-10.2010

Cave, J. W., and Baker, H. (2009). Dopamine systems in the forebrain. *Adv. Exp. Med. Biol.* 651, 15–35. doi: 10.1007/978-1-4419-0322-8_2

Cave, J. W., and Baker, H. (2015). "Adult neurogenesis in the subventricular zone and migration to the olfactory bulb," in *Handbook of Olfaction and Gustation*, ed R. L. Doty (WILEY Blackweel).

Cave, J. W., Wang, M., and Baker, H. (2014). Adult subventricular zone neural stem cells as a potential source of dopaminergic replacement neurons. *Front. Neurosci.* 8:16. doi: 10.3389/fnins.2014.00016

Chand, A. N., Galliano, E., Chesters, R. A., and Grubb, S. M. (2015). A distinct subtype of dopaminergic interneuron displays inverted structural plasticity at the axon initial segment. *J. Neurosci.* 35, 1573–1590. doi: 10.1523/JNEUROSCI.3515-14.2015

Cherry, J. A., and Baum, M. J. (2020). Sex differences in main olfactory system pathways involved in psychosexual function. *Genes Brain Behav.* 19:e12618. doi: 10.1111/gbb.12618

Cho, J. Y., Min, N., Franzen, L., and Baker, H. (1996). Rapid down-regulation of tyrosine hydroxylase expression in the olfactory bulb of naris-occluded adult rats. *J. Comp. Neurol.* 369, 264–276. doi: 10.1002/(SICI)1096-9861(19960527)369:2<264::AID-CNE7>3.0.CO;2-1

Ciliax, B. J., Nash, N., Heilman, C., Sunahara, R., Hartney, A., Tiberi, M., et al. (2000). Dopamine D(5) receptor immunolocalization in rat and monkey brain. *Synapse* 37, 125–145. doi: 10.1002/1098-2396(200008)37:2<125::AID-SYN7>3.0.CO;2-7

Coronas, V., Srivastava, L. K., Liang, J. J., Jourdan, F., and Moyse, E. (1997). Identification and localization of dopamine receptor subtypes in rat olfactory mucosa and bulb: a combined *in situ* hybridization and ligand binding radioautographic approach. *J. Chem. Neuroanat.* 12, 243–257. doi: 10.1016/s0891-0618(97)00215-9

Courtiol, E., and Wilson, D. A. (2015). The olfactory thalamus: unanswered questions about the role of the mediodorsal thalamic nucleus in olfaction. *Front. Neural Circuits* 9:49. doi: 10.3389/fncir.2015.00049

Crespo, C., Brinon, J. G., Porteros, A., Arevalo, R., Rico, B., Aijon, J., et al. (1999). Distribution of acetylcholinesterase and choline acetyltransferase in the main and accessory olfactory bulbs of the hedgehog (Erinaceus europaeus). *J. Comp. Neurol.* 403, 53–67. doi: 10.1002/(sici)1096-9861(19990105)403:1<53::aid-cne5>3.0.co;2-o

Davila, N. G., Blakemore, L. J., and Trombley, Q. P. (2003). Dopamine modulates synaptic transmission between rat olfactory bulb neurons in culture. *J. Neurophysiol.* 90, 395–404. doi: 10.1152/jn.01058.2002

Davis, B. J., and Macrides, F. (1983). Tyrosine hydroxylase immunoreactive neurons and fibers in the olfactory system of the hamster. *J. Comp. Neurol.* 214, 427–440. doi: 10.1002/cne.902140407

de Chevigny, A., Core, N., Follert, P., Wild, S., Bosio, A., Yoshikawa, K., et al. (2012). Dynamic expression of the pro-dopaminergic transcription factors Pax6 and Dlx2 during postnatal olfactory bulb neurogenesis. *Front. Cell. Neurosci.* 6:6. doi: 10.3389/fncel.2012.00006

De Marchis, S., Bovetti, S., Carletti, B., Hsieh, Y. C., Garzotto, D., Peretto, P., et al. (2007). Generation of distinct types of periglomerular olfactory bulb interneurons during development and in adult mice: implication for intrinsic properties of the subventricular zone progenitor population. *J. Neurosci.* 27, 657–664. doi: 10.1523/JNEUROSCI.2870-06.2007

De Saint Jan, D. (2021). Target-specific control of olfactory bulb periglomerular cells by GABAergic and cholinergic basal forebrain inputs. *bioRxiv [Preprint].* doi: 10.1101/2021.07.06.451255

Dellovade, T. L., Pfaff, D. W., and Schwanzel-Fukuda, M. (1998). Olfactory bulb development is altered in small-eye (Sey) mice. *J. Comp. Neurol.* 402, 402–418. doi: 10.1002/(sici)1096-9861(19981221)402:3<402::Aid-cne8>3.0.Co;2-0

Doty, R. L. (2012). Olfactory dysfunction in Parkinson disease. *Nat. Rev. Neurol.* 8, 329–339. doi: 10.1038/nrneurol.2012.80

Elaagouby, A., and Gervais, R. (1992). ACh-induced long-lasting enhancement in excitability of the olfactory bulb. *Neuroreport* 3, 10–12. doi: 10.1097/00001756-199201000-00002

Ennis, M., Zhou, F. M., Ciombor, K. J., Aroniadou-Anderjaska, V., Hayar, A., Borrelli, E., et al. (2001). Dopamine D2 receptor-mediated presynaptic inhibition of olfactory nerve terminals. *J. Neurophysiol.* 86, 2986–2997. doi: 10.1152/jn.2001.86.6.2986

Eyre, M. D., Antal, M., and Nusser, Z. (2008). Distinct deep short-axon cell subtypes of the main olfactory bulb provide novel intrabulbar and extrabulbar GABAergic connections. *J. Neurosci.* 28, 8217–8229. doi: 10.1523/JNEUROSCI.2490-08.2008

Fang, W. Q., Chen, W. W., Jiang, L., Liu, K., Yung, W. H., Fu, A. K. Y., et al. (2014). Overproduction of upper-layer neurons in the neocortex leads to autism-like features in mice. *Cell Rep.* 9, 1635–1643. doi: 10.1016/j.celrep.2014.11.003

Feigenspan, A., Gustincich, S., Bean, B. P., and Raviola, E. (1998). Spontaneous activity of solitary dopaminergic cells of the retina. *J. Neurosci.* 18, 6776–6789. doi: 10.1523/jneurosci.18-17-06776.1998

Fernandez, M. E., Croce, S., Boutin, C., Cremer, H., and Raineteau, O. (2011). Targeted electroporation of defined lateral ventricular walls: a novel and rapid method to study fate specification during postnatal forebrain neurogenesis. *Neural. Dev.* 6:13. doi: 10.1186/1749-8104-6-13

Ferris, C. F., Stolberg, T., Kulkarni, P., Murugavel, M., Blanchard, R., Blanchard, D. C., et al. (2008). Imaging the neural circuitry and chemical control of aggressive motivation. *BMC Neurosci.* 9:111. doi: 10.1186/1471-2202-9-111

Fine, L. G., and Riera, C. E. (2019). Sense of Smell as the Central Driver of Pavlovian Appetite Behavior in Mammals. *Front. Physiol.* 10:1151. doi: 10.3389/fphys.2019.01151

Fiorelli, R., Azim, K., Fischer, B., and Raineteau, O. (2015). Adding a spatial dimension to postnatal ventricular-subventricular zone neurogenesis. *Development* 142, 2109–2120. doi: 10.1242/dev.119966

Fogli Iseppe, A., Pignatelli, A., and Belluzzi, O. (2016). Calretinin-periglomerular interneurons in mice olfactory bulb: cells of few words. *Front. Cell. Neurosci.* 10:231. doi: 10.3389/fncel.2016.00231

Fried, H. U., Kaupp U. B., and Muller, F. (2010). Hyperpolarization-activated and cyclic nucleotide-gated channels are differentially expressed in juxtaglomerular cells in the olfactory bulb of mice. *Cell Tissue Res.* 339, 463–479. doi: 10.1007/s00441-009-0904-9

Gall, C. M., Hendry, S. H., Seroogy, K. B., Jones, E. G., and Haycock, W. J. (1987). Evidence for coexistence of GABA and dopamine in neurons of the rat olfactory bulb. *J. Comp. Neurol.* 266, 307–318. doi: 10.1002/cne.902660302

Galliano, E., Franzoni, E., Breton, M., Chand, A. N., Byrne, D. J., and Murthy, V. N. (2018). Embryonic and postnatal neurogenesis produce functionally distinct subclasses of dopaminergic neuron. *Elife.* 7:32373. doi: 10.7554/eLife.32373

Galliano, E., and Grubb, M. (2016). "Not all dopaminergic neurones are created equal," in: *Proceedings of the 10Th Federation of European Neuroscience Societies Meeting* (Copenhagen).

Galliano, E., Hahn, C., Browne, L. P., Tufo, C., and Crespo, A. (2021). Brief sensory deprivation triggers cell type-specific structural and functional plasticity in olfactory bulb neurons. *J. Neurosci.* 41, 2135–2151. doi: 10.1523/JNEUROSCI.1606-20.2020

Gire, D. H., and Schoppa, N. E. (2009). Control of on/off glomerular signaling by a local GABAergic microcircuit in the olfactory bulb. *J. Neurosci.* 29, 13454–13464. doi: 10.1523/JNEUROSCI.2368-09.2009

Glusman, G., Yanai, I., Rubin, I., and Lancet, D. (2001). The complete human olfactory subgenome. *Genome Res.* 11, 685–702. doi: 10.1101/gr.171001

Gottfried, J. A., and Dolan, R. J. (2003). The nose smells what the eye sees: crossmodal visual facilitation of human olfactory perception. *Neuron* 39, 375–386. doi: 10.1016/s0896-6273(03)00392-1

Grace, A. A., and Bunney, B. S. (1984). The control of firing pattern in nigral dopamine neurons: burst firing. *J. Neurosci.* 4, 2877–2890. doi: 10.1523/jneurosci.04-11-02877.1984

Grace, A. A., and Onn, S. P. (1989). Morphology and electrophysiological properties of immunocytochemically identified rat dopamine neurons recorded *in vitro*. *J. Neurosci.* 9, 3463–3481. doi: 10.1523/jneurosci.09-10-03463.1989

Grier, B. D., Belluscio, L., and Cheetham, E. C. (2016). Olfactory sensory activity modulates microglial-neuronal interactions during dopaminergic cell loss in the olfactory bulb. *Front. Cell. Neurosci.* 10:178. doi: 10.3389/fncel.2016.00178

Gross, C. G. (2000). Neurogenesis in the adult brain: death of a dogma. *Nat. Rev. Neurosci.* 1, 67–73. doi: 10.1038/35036235

Gutierrez-Mecinas, M., Crespo, C., Blasco-Ibanez, J. M., Gracia-Llanes, F. J., Marques-Mari, A. I., Nacher, J., et al. (2005). Distribution of D2 dopamine receptor in the olfactory glomeruli of the rat olfactory bulb. *Eur. J. Neurosci.* 22, 1357–1367. doi: 10.1111/j.1460-9568.2005.04328.x

Guyenet, P. G., and Crane, J. K. (1981). Non-dopaminergic nigrostriatal pathway. *Brain Res.* 213, 291–305. doi: 10.1016/0006-8993(81)90235-3

Haba, H., Nomura, T., Suto, F., and Osumi, N. (2009). Subtype-specific reduction of olfactory bulb interneurons in Pax6 heterozygous mutant mice. *Neurosci. Res.* 65, 116–121. doi: 10.1016/j.neures.2009.05.011

Hainsworth, A. H., Roper, J., Kapoor, R., and Ashcroft, M. F. (1991). Identification and electrophysiology of isolated pars compacta neurons from guinea-pig substantia nigra. *Neuroscience* 43, 81–93. doi: 10.1016/0306-4522(91)90419-o

Halász, N. (ed.). (1990). *The Vertebrate Olfactory System: Chemical Neuroanatomy, Function and Development*. Budapest: Akadémiai Kiadó.

Halasz, N., Johansson, O., Hokfelt, T., Ljungdahl, A., and Goldstein, M. (1981). Immunohistochemical identification of two types of dopamine neuron in the rat olfactory bulb as seen by serial sectioning. *J. Neurocytol.* 10, 251–259. doi: 10.1007/BF01257970

Halasz, N., and Shepherd, G. M. (1983). Neurochemistry of the vertebrate olfactory bulb. *Neuroscience* 10, 579–619. doi: 10.1016/0306-4522(83)90206-3

Hardy, A., Palouzier-Paulignan, B., Duchamp, A., Royet, J. P., and Duchamp-Viret, P. (2005). 5-Hydroxytryptamine action in the rat olfactory bulb: *in vitro* electrophysiological patch-clamp recordings of juxtaglomerular and mitral cells. *Neuroscience* 131, 717–731. doi: 10.1016/j.neuroscience.2004.10.034

Hatton, G. I., and Yang, Q. Z. (1989). Supraoptic nucleus afferents from the main olfactory bulb–II. Intracellularly recorded responses to lateral olfactory tract stimulation in rat brain slices. *Neuroscience* 31, 289–297. doi: 10.1016/0306-4522(89)90374-6

Hayar, A., Karnup, S., Shipley, M. T., and Ennis, M. (2004). Olfactory bulb glomeruli: external tufted cells intrinsically burst at theta frequency and are entrained by patterned olfactory input. *J. Neurosci.* 24, 1190–1199. doi: 10.1523/JNEUROSCI.4714-03.2004

Hinds, J. W. (1968). Autoradiographic study of histogenesis in the mouse olfactory bulb. I. Time of origin of neurons and neuroglia. *J. Comp. Neurol.* 134, 287–304. doi: 10.1002/cne.901340304

Hoogland, P. V., and Huisman, E. (1999). Tyrosine hydroxylase immunoreactive structures in the aged human olfactory bulb and olfactory peduncle. *J. Chem. Neuroanat.* 17, 153–161. doi: 10.1016/s0891-0618(99)00035-6

Hsia, A. Y., Vincent, J. D., and Lledo, M. P. (1999). Dopamine depresses synaptic inputs into the olfactory bulb. *J. Neurophysiol.* 82, 1082–1085. doi: 10.1152/jn.1999.82.2.1082

Huberman, A. D., Manu, M., Koch, S. M., Susman, M. W., Lutz, A. B., Ullian, E. M., et al. (2008). Architecture and activity-mediated refinement of axonal projections from a mosaic of genetically identified retinal ganglion cells. *Neuron.* 59, 425–438. doi: 10.1016/j.neuron.2008.07.018

In 't Zandt, E. E., Cansler, H. L., Denson, H. B., and Wesson, W. D. (2019). Centrifugal innervation of the olfactory bulb: a reappraisal. *eNeuro.* 6:2019. doi: 10.1523/ENEURO.0390-18.2019

Inta, D., Cameron, H. A., and Gass, P. (2015). New neurons in the adult striatum: from rodents to humans. *Trends Neurosci.* 38, 517–523. doi: 10.1016/j.tins.2015.07.005

Jacobowitz, D. M., and Winsky, L. (1991). Immunocytochemical localization of calretinin in the forebrain of the rat. *J. Comp. Neurol.* 304, 198–218. doi: 10.1002/cne.903040205

Jeong, Y. G., Lee, N. S., Lee, K. Y., Chung, S. H., Hwang, I. K., Suh, J. G., et al. (2003). Morphological characteristics of dopaminergic immunoreactive neurons in the olfactory bulb of the common marmoset monkey (Callithrix jacchus). *Ann. Anat.* 185, 543–547. doi: 10.1016/S0940-9602(03)80123-1

Jian, K., Cifelli, P., Pignatelli, A., Frigato, E., and Belluzzi, O. (2010). Metabotropic glutamate receptors 1 and 5 differentially regulate bulbar dopaminergic cell function. *Brain Res.* 1354, 47–63. doi: 10.1016/j.brainres.2010.07.104

Johnson, D. M., Illig, K. R., Behan, M., and Haberly, B. L. (2000). New features of connectivity in piriform cortex visualized by intracellular injection of pyramidal cells suggest that "primary" olfactory cortex functions like "association" cortex in other sensory systems. *J. Neurosci.* 20, 6974–6982. doi: 10.1523/JNEUROSCI.20-18-06974.2000

Kang, N., McCarthy, E. A., Cherry, J. A., and Baum, J. M. (2011). A sex comparison of the anatomy and function of the main olfactory bulb–medial amygdala projection in mice. *Neuroscience* 172, 196–204. doi: 10.1016/j.neuroscience.2010.11.003

Kasa, P., Hlavati, I., Dobo, E., Wolff, A., Joo, F., and Wolff, R. J. (1995). Synaptic and non-synaptic cholinergic innervation of the various types of neurons in the main olfactory bulb of adult rat: immunocytochemistry of choline acetyltransferase. *Neuroscience* 67, 667–677. doi: 10.1016/0306-4522(95)00031-d

Kawano, T., and Margolis, F. L. (1982). Transsynaptic regulation of olfactory bulb catecholamines in mice and rats. *J. Neurochem.* 39, 342–348. doi: 10.1111/j.1471-4159.1982.tb03953.x

Kepecs, A., and Fishell, G. (2014). Interneuron cell types are fit to function. *Nature* 505, 318–326. doi: 10.1038/nature12983

Kim, J. Y., Choe, J., and Moon, C. (2020). Distinct developmental features of olfactory bulb interneurons. *Mol. Cells* 43, 215–221. doi: 10.14348/molcells.2020.0033

Kiselycznyk, C. L., Zhang, S., and Linster, C. (2006). Role of centrifugal projections to the olfactory bulb in olfactory processing. *Learn. Mem.* 13, 575–579. doi: 10.1101/lm.285706

Kitamura, A., Torii, K., Uneyama, H., and Niijima, A. (2010). Role played by afferent signals from olfactory, gustatory and gastrointestinal sensors in regulation of autonomic nerve activity. *Biol. Pharm. Bull.* 33, 1778–1782. doi: 10.1248/bpb.33.1778

Kiyokage, E., Pan, Y. Z., Shao, Z., Kobayashi, K., Szabo, G., Yanagawa, Y., et al. (2010). Molecular identity of periglomerular and short axon cells. *J. Neurosci.* 30, 1185–1196. doi: 10.1523/JNEUROSCI.3497-09.2010

Kohwi, M., Osumi, N., Rubenstein, J. L., and Alvarez-Buylla, A. (2005). Pax6 is required for making specific subpopulations of granule and periglomerular neurons in the olfactory bulb. *J. Neurosci.* 25, 6997–7003. doi: 10.1523/JNEUROSCI.1435-05.2005

Korshunov, K. S., Blakemore, L. J., Bertram, R., and Trombley, Q. P. (2020b). Spiking and membrane properties of rat olfactory bulb dopamine neurons. *Front. Cell. Neurosci.* 14:60. doi: 10.3389/fncel.2020.00060

Korshunov, K. S., Blakemore, L. J., and Trombley, Q. P. (2020a). Illuminating and sniffing out the neuromodulatory roles of dopamine in the retina and olfactory bulb. *Front. Cell. Neurosci.* 14:275. doi: 10.3389/fncel.2020.00275

Kosaka, K. (2007). Two types of periglomerular cells (PG1 and PC2) in the main olfactory bulb of mice and other mammals. *Chem. Senses* 32, J21–J21. doi: 10.1093/chemse/bjl045

Kosaka, K., Hama, K., Nagatsu, I., Wu, J.-Y., Ottersen, O. P., Storm-Mathisen, J., et al. (1987a). Postnatal development of neurons containing both

catecholaminergic and GABAergic traits in the rat main olfactory bulb. *Brain Res.* 403, 355–360. doi: 10.1016/0006-8993(87)90075-8

Kosaka, K., and Kosaka, T. (2007). Chemical properties of type 1 and type 2 periglomerular cells in the mouse olfactory bulb are different from those in the rat olfactory bulb. *Brain Res.* 1167, 42–55. doi: 10.1016/j.brainres.2007.04.087

Kosaka, K., Toida, K., Aika, Y., and Kosaka, T. (1998). How simple is the organization of the olfactory glomerulus?: the heterogeneity of so-called periglomerular cells. *Neurosci. Res.* 30, 101–110. doi: 10.1016/s0168-0102(98)00002-9

Kosaka, K., Toida, K., Margolis, F. L., and Kosaka, T. (1997). Chemically defined neuron groups and their subpopulations in the glomerular layer of the rat main olfactory bulb–II. Prominent differences in the intraglomerular dendritic arborization and their relationship to olfactory nerve terminals. *Neuroscience* 76, 775–786. doi: 10.1016/s0306-4522(96)00308-9

Kosaka, T., Hataguchi, Y., Hama, K., Nagatsu, I., and Jang-Yen, W. (1985). Coexistence of immunoreactivities for glutamate decarylase and tyrosine hydroxylase in some neurons in the periglomerular region of the rat main olfactory bulb: possible coexistence of gamma-aminobutyric acid (GABA) and dopamine. *Brain Res.* 343, 166–171. doi: 10.1016/0006-8993(85)91172-2

Kosaka, T., and Kosaka, K. (2008a). Heterogeneity of parvalbumin-containing neurons in the mouse main olfactory bulb, with special reference to short-axon cells and betaIV-spectrin positive dendritic segments. *Neurosci. Res.* 60, 56–72. doi: 10.1016/j.neures.2007.09.008

Kosaka, T., and Kosaka, K. (2008b). Tyrosine hydroxylase-positive GABAergic juxtaglomerular neurons are the main source of the interglomerular connections in the mouse main olfactory bulb. *Neurosci. Res.* 60, 349–354. doi: 10.1016/j.neures.2007.11.012

Kosaka, T., and Kosaka, K. (2009a). Olfactory bulb anatomy. *Encyclop. Neurosci.* 26, 59–69. doi: 10.1016/b978-008045046-9.01686-7

Kosaka, T., and Kosaka, K. (2009b). Two types of tyrosine hydroxylase positive GABAergic juxtaglomerular neurons in the mouse main olfactory bulb are different in their time of origin. *Neurosci. Res.* 64, 436–441. doi: 10.1016/j.neures.2009.04.018

Kosaka, T., and Kosaka, K. (2010). Heterogeneity of calbindin-containing neurons in the mouse main olfactory bulb: I. General description. *Neurosci. Res.* 67, 275–292. doi: 10.1016/j.neures.2010.04.009

Kosaka, T., and Kosaka, K. (2011). "Interneurons" in the olfactory bulb revisited. *Neurosci. Res.* 69, 93–99. doi: 10.1016/j.neures.2010.10.002

Kosaka, T., and Kosaka, K. (2016). Neuronal organization of the main olfactory bulb revisited. *Anat. Sci. Int.* 91, 115–127. doi: 10.1007/s12565-015-0309-7

Kosaka, T., Kosaka, K., Hataguchi, Y., Nagatsu, I., Wu, J. Y., Ottersen, O. P., et al. (1987b). Catecholaminergic neurons containing GABA-like and/or glutamic acid decarboxylase-like immunoreactivities in various brain regions of the rat. *Exp. Brain Res.* 66, 191–210. doi: 10.1007/BF00236215

Kosaka, T., Pignatelli, A., and Kosaka, K. (2020). Heterogeneity of tyrosine hydroxylase expressing neurons in the main olfactory bulb of the mouse. *Neurosci. Res.* 157, 15–33. doi: 10.1016/j.neures.2019.10.004

Kratskin, I., and Belluzzi, O. (2003). "Anatomy and Neurochemistry of the Olfactory Bulb," in *Handbook of Olfaction and Gustation*, ed R. L. Doty (New York, NY: Marcel Dekker), 139–164.

Krettek, J. E., and Price, J. L. (1977). The cortical projections of the mediodorsal nucleus and adjacent thalamic nuclei in the rat. *J. Comp. Neurol.* 171, 157–191. doi: 10.1002/cne.901710204

Krosnowski, K., Ashby, S., Sathyanesan, A., Luo, W., Ogura, T., and Lin, W. (2012). Diverse populations of intrinsic cholinergic interneurons in the mouse olfactory bulb. *Neuroscience* 213, 161–178. doi: 10.1016/j.neuroscience.2012.04.024

Lazarini, F., Gabellec, M. M., Moigneu, C., de Chaumont, F., Olivo-Marin, J. C., and Lledo, M. P. (2014). Adult neurogenesis restores dopaminergic neuronal loss in the olfactory bulb. *J. Neurosci.* 34, 14430–14442. doi: 10.1523/JNEUROSCI.5366-13.2014

Le Jeune, H., and Jourdan, F. (1993). Cholinergic innervation of olfactory glomeruli in the rat: an ultrastructural immunocytochemical study. *J. Comp. Neurol.* 336, 279–292. doi: 10.1002/cne.903360209

Levant, B., Grigoriadis, D. E., and DeSouza, B. E. (1993). [3H]quinpirole binding to putative D2 and D3 dopamine receptors in rat brain and pituitary gland: a quantitative autoradiographic study. *J. Pharmacol. Exp. Ther.* 264, 991–1001.

Levy, F., Kendrick, K. M., Goode, J. A., Guevara-Guzman, R., and Keverne, B. E. (1995). Oxytocin and vasopressin release in the olfactory bulb of parturient ewes: changes with maternal experience and effects on acetylcholine, gamma-aminobutyric acid, glutamate and noradrenaline release. *Brain Res.* 669, 197–206. doi: 10.1016/0006-8993(94)01236-b

Li, Q., and Liberles, S. D. (2015). Aversion and attraction through olfaction. *Curr. Biol.* 25, R120–R129. doi: 10.1016/j.cub.2014.11.044

Li, X., Sun, C., Lin, C., Ma, T., Madhavan, M. C., Campbell, K., et al. (2011). The transcription factor Sp8 is required for the production of parvalbumin-expressing interneurons in the olfactory bulb. *J. Neurosci.* 31, 8450–8455. doi: 10.1523/JNEUROSCI.0939-11.2011

Liberia, T., Blasco-Ibanez, J. M., Nacher, J., Varea, E., Zwafink, V., and Crespo, C. (2012). Characterization of a population of tyrosine hydroxylase-containing interneurons in the external plexiform layer of the rat olfactory bulb. *Neuroscience.* 217, 140–153. doi: 10.1016/j.neuroscience.2012.05.007

Linster, C., and Hasselmo, M. (1997). Modulation of inhibition in a model of olfactory bulb reduces overlap in the neural representation of olfactory stimuli. *Behav. Brain Res.* 84, 117–127. doi: 10.1016/s0166-4328(97)83331-1

Liu, S., Plachez, C., Shao, Z., Puche, A., and Shipley, T. M. (2013). Olfactory bulb short axon cell release of GABA and dopamine produces a temporally biphasic inhibition-excitation response in external tufted cells. *J. Neurosci.* 33, 2916–2926. doi: 10.1523/JNEUROSCI.3607-12.2013

Liu, S., Puche, A. C., and Shipley, T. M. (2016). The interglomerular circuit potently inhibits olfactory bulb output neurons by both direct and indirect pathways. *J. Neurosci.* 36, 9604–9617. doi: 10.1523/JNEUROSCI.1763-16.2016

Lledo, P. M., and Saghatelyan, A. (2005). Integrating new neurons into the adult olfactory bulb: joining the network, life-death decisions, and the effects of sensory experience. *Trends Neurosci.* 28, 248–254. doi: 10.1016/j.tins.2005.03.005

Lledo, P. M., and Valley, M. (2016). Adult olfactory bulb neurogenesis. *Cold Spring Harb Perspect Biol.* 8:18945. doi: 10.1101/cshperspect.a018945

Lodovichi, C., Belluscio, L., and Katz, C. L. (2003). Functional topography of connections linking mirror-symmetric maps in the mouse olfactory bulb. *Neuron* 38, 265–276. doi: 10.1016/s0896-6273(03)00194-6

Maccaferri, G., and Lacaille, J. C. (2003). Interneuron Diversity series: Hippocampal interneuron classifications–making things as simple as possible, not simpler. *Trends Neurosci.* 26, 564–571. doi: 10.1016/j.tins.2003.08.002

Maher, B. J., and Westbrook, G. L. (2008). Co-transmission of dopamine and GABA in periglomerular cells. *J. Neurophysiol.* 99, 1559–1564. doi: 10.1152/jn.00636.2007

Maksimova, M. A., Cansler, H. L., Zuk, K. E., Torres, J. M., Roberts, D. J., and Meeks, P. J. (2019). Interneuron functional diversity in the mouse accessory olfactory bulb. *eNeuro* 6:2019. doi: 10.1523/ENEURO.0058-19.2019

Malvaut, S., and Saghatelyan, A. (2016). The role of adult-born neurons in the constantly changing olfactory bulb network. *Neural Plast.* 2016:1614329. doi: 10.1155/2016/1614329

Markopoulos, F., Rokni, D., Gire, D. H., and Murthy, N. V. (2012). Functional properties of cortical feedback projections to the olfactory bulb. *Neuron* 76, 1175–1188. doi: 10.1016/j.neuron.2012.10.028

Martin, L. J., Blackstone, C. D., Huganir, R. L., and Price, L. D. (1992). Cellular localization of a metabotropic glutamate receptor in rat brain. *Neuron* 9, 259–270. doi: 10.1016/0896-6273(92)90165-a

Matsutani, S. (2010). Trajectory and terminal distribution of single centrifugal axons from olfactory cortical areas in the rat olfactory bulb. *Neuroscience* 169, 436–448. doi: 10.1016/j.neuroscience.2010.05.001

McGann, J. P. (2013). Presynaptic inhibition of olfactory sensory neurons: new mechanisms and potential functions. *Chem. Senses.* 38, 459–474. doi: 10.1093/chemse/bjt018

McGann, J. P. (2017). Poor human olfaction is a 19th-century myth. *Science* 356:7263. doi: 10.1126/science.aam7263

McLean, J. H., and Shipley, M. T. (1987). Serotonergic afferents to the rat olfactory bulb: Origins I, and laminar specificity of serotonergic inputs in the adult rat. *J. Neurosci.* 7, 3016 −3028.

McLean, J. H., and Shipley, M. T. (1988). Postmitotic, postmigrational expression of tyrosine hydroxylase in olfactory bulb dopaminergic neurons. *J. Neurosci.* 8, 3658–3669. doi: 10.1523/jneurosci.08-10-03658.1988

McLean, J. H., Shipley, M. T., Nickell, W. T., Aston-Jones, G., and Reyher, K. C. (1989). Chemoanatomical organization of the noradrenergic input from locus

coeruleus to the olfactory bulb of the adult rat. *J. Comp. Neurol.* 285, 339–349. doi: 10.1002/cne.902850305

Meador-Woodruff, J. H., Mansour, A., Healy, D. J., Kuehn, R., Zhou, Q. Y., Bunzow, J. R., et al. (1991). Comparison of the distributions of D1 and D2 dopamine receptor mRNAs in rat brain. *Neuropsychopharmacology* 5, 231–242.

Merkle, F. T., Mirzadeh, Z., and Alvarez-Buylla, A. (2007). Mosaic organization of neural stem cells in the adult brain. *Science* 317, 381–384. doi: 10.1126/science.1144914

Miettinen, R., Gulyas, A. I., Baimbridge, K. G., Jacobowitz, D. M., and Freund, F. T. (1992). Calretinin is present in non-pyramidal cells of the rat hippocampus–II. Co-existence with other calcium binding proteins and GABA. *Neuroscience* 48, 29–43. doi: 10.1016/0306-4522(92)90335-y

Miura, K., Mainen, Z. F., and Uchida, N. (2012). Odor representations in olfactory cortex: distributed rate coding and decorrelated population activity. *Neuron* 74, 1087–1098. doi: 10.1016/j.neuron.2012.04.021

Mizrahi, A., Lu, J., Irving, R., Feng, G., and Katz, C. L. (2006). *In vivo* imaging of juxtaglomerular neuron turnover in the mouse olfactory bulb. *Proc. Natl. Acad. Sci. U.S.A.* 103, 1912–1917. doi: 10.1073/pnas.0506297103

Mori, K., and Sakano, H. (2011). How is the olfactory map formed and interpreted in the mammalian brain? *Annu. Rev. Neurosci.* 34, 467–499. doi: 10.1146/annurev-neuro-112210-112917

Mouly, A. M., and Sullivan, R. (2010). "Memory and plasticity in the olfactory system: from infancy to adulthood," in *The Neurobiology of Olfaction, Menini*, ed A. Menini (Boca Raton, FL: CRC Press/Taylor & Francis).

Nadi, N. S., Head, R., Grillo, M., Hempstead, J., Grannot-Reisfeld, N., and Margolis, L. F. (1981). Chemical deafferentation of the olfactory bulb: plasticity of the levels of tyrosine hydroxylase, dopamine and norepinephrine. *Brain Res.* 213, 365–377. doi: 10.1016/0006-8993(81)90241-9

Nagayama, S., Homma, R., and Imamura, F. (2014). Neuronal organization of olfactory bulb circuits. *Front. Neural Circuits* 8:98. doi: 10.3389/fncir.2014.00098

Najac, M., De Saint Jan, D., Reguero, L., Grandes, P., and Charpak, S. (2011). Monosynaptic and polysynaptic feed-forward inputs to mitral cells from olfactory sensory neurons. *J. Neurosci.* 31, 8722–8729. doi: 10.1523/JNEUROSCI.0527-11.2011

Neuhoff, H., Neu, A., Liss, B., and Roeper, J. (2002). IhChannels contribute to the different functional properties of identified dopaminergic subpopulations in the midbrain. *The J. Neurosci.* 22, 1290–1302. doi: 10.1523/jneurosci.22-04-01290.2002

Neville, K. R., and Haberly, L. B. (2004). "Olfactory cortex," in *The Synaptic Organization of the Brain*, ed G. M. Shepherd (Oxford: Oxford University Press).

Nickell, W. T., Behbehani, M. M., and Shipley, T. M. (1994). Evidence for GABAB-mediated inhibition of transmission from the olfactory nerve to mitral cells in the rat olfactory bulb. *Brain Res. Bull.* 35, 119–123. doi: 10.1016/0361-9230(94)90091-4

Nickell, W. T., and Shipley, M. T. (1988). Neurophysiology of magnocellular forebrain inputs to the olfactory bulb in the rat: frequency potentiation of field potentials and inhibition of output neurons. *J. Neurosci.* 8, 4492–4502.

Ninkovic, J., Mori, T., and Gotz, M. (2007). Distinct modes of neuron addition in adult mouse neurogenesis. *J. Neurosci.* 27, 10906–10911. doi: 10.1523/JNEUROSCI.2572-07.2007

Olender, T., Keydar, I., Pinto, J. M., Tatarskyy, P., Alkelai, A., Chien, M. S., et al. (2016). The human olfactory transcriptome. *BMC Genomics* 17:619. doi: 10.1186/s12864-016-2960-3

Otazu, G. H., Chae, H., Davis, M. B., and Albeanu, F. D. (2015). Cortical feedback decorrelates olfactory bulb output in awake mice. *Neuron* 86, 1461–1477. doi: 10.1016/j.neuron.2015.05.023

Panula, P., Pirvola, U., Auvinen, S., and Airaksinen, S. M. (1989). Histamine-immunoreactive nerve fibers in the rat brain. *Neuroscience* 28, 585–610. doi: 10.1016/0306-4522(89)90007-9

Panzanelli, P., Fritschy, J. M., Yanagawa, Y., Obata, K., and Sassoe-Pognetto, M. (2007). GABAergic phenotype of periglomerular cells in the rodent olfactory bulb. *J. Comp. Neurol.* 502, 990–1002. doi: 10.1002/cne.21356

Parrish-Aungst, S., Kiyokage, E., Szabo, G., Yanagawa, Y., Shipley, M. T., and Puche, C. A. (2011). Sensory experience selectively regulates transmitter synthesis enzymes in interglomerular circuits. *Brain Res.* 1382, 70–76. doi: 10.1016/j.brainres.2011.01.068

Parrish-Aungst, S., Shipley, M. T., Erdelyi, F., Szabo, G., and Puche, C. A. (2007). Quantitative analysis of neuronal diversity in the mouse olfactory bulb. *J. Comp. Neurol.* 501, 825–836. doi: 10.1002/cne.21205

Paß, T., Aßfalg, M., Tolve, M., Blaess, S., Rothermel, M., Wiesner, R. J., et al. (2020). The impact of mitochondrial dysfunction on dopaminergic neurons in the olfactory bulb and odor detection. *Mol. Neurobiol.* 57, 3646–3657. doi: 10.1007/s12035-020-01947-w

Petzold, G. C., Hagiwara, A., and Murthy, N. V. (2009). Serotonergic modulation of odor input to the mammalian olfactory bulb. *Nat. Neurosci.* 12, 784–791. doi: 10.1038/nn.2335

Pignatelli, A., Ackman, J. B., Vigetti, D., Beltrami, A. P., Zucchini, S., and Belluzzi, O. (2009). A potential reservoir of immature dopaminergic replacement neurons in the adult mammalian olfactory bulb. *Pflugers Arch.* 457, 899–915. doi: 10.1007/s00424-008-0535-0

Pignatelli, A., and Belluzzi, O. (2008). Cholinergic modulation of dopaminergic neurons in the mouse olfactory bulb. *Chem. Senses.* 33, 331–338. doi: 10.1093/chemse/bjm091

Pignatelli, A., and Belluzzi, O. (2010). "Neurogenesis in the adult olfactory bulb," in *The Neurobiology of Olfaction*, ed A. Menini (Boca Raton, FL: CRC Press/Taylor & Francis).

Pignatelli, A., and Belluzzi, O. (2017). Dopaminergic neurones in the main olfactory bulb: an overview from an electrophysiological perspective. *Front. Neuroanat.* 11:7. doi: 10.3389/fnana.2017.00007

Pignatelli, A., Borin, M., Fogli Iseppe, A., Gambardella, C., and Belluzzi, O. (2013). The h-current in periglomerular dopaminergic neurons of the mouse olfactory bulb. *PLoS ONE* 8:e56571. doi: 10.1371/journal.pone.0056571

Pignatelli, A., Fogli Iseppe, A., Gambardella, C., Borin, M., and Belluzzi, O. (2012). "Pacemaker currents in dopaminergic neurons of the mice olfactory bulb," in *Electrophysiology From Plants to Heart*, ed S. Orai (Einbeck: Intechopen).

Pignatelli, A., Kobayashi, K., Okano H, and Belluzzi, O. (2005). Functional properties of dopaminergic neurones in the mouse olfactory bulb. *J. Physiol.* 564, 501–514. doi: 10.1113/jphysiol.2005.084632

Pinching, A. J., and Powell, T. P. (1971a). The neuron types of the glomerular layer of the olfactory bulb. *J. Cell Sci.* 9, 305–345.

Pinching, A. J., and Powell, T. P. (1971b). The neuropil of the glomeruli of the olfactory bulb. *J. Cell Sci.* 9, 347–377.

Price, J. L. (1985). Beyond the primary olfactory cortex: olfactory-related areas in the neocortex, thalamus and hypothalamus. *Chem. Senses* 10, 239–258. doi: 10.1093/chemse/10.2.239

Price, J. L., and Slotnick, B. M. (1983). Dual olfactory representation in the rat thalamus: an anatomical and electrophysiological study. *J. Comp. Neurol.* 215, 63–77. doi: 10.1002/cne.902150106

Prieto-Godino, L. L., Rytz, R., Bargeton, B., Abuin, L., Arguello, J. R., Peraro, M. D., et al. (2016). Olfactory receptor pseudo-pseudogenes. *Nature* 539, 93–97. doi: 10.1038/nature19824

Puopolo, M., Bean, B. P., and Raviola, E. (2005). Spontaneous activity of isolated dopaminergic periglomerular cells of the main olfactory bulb. *J. Neurophysiol.* 94, 3618–3627. doi: 10.1152/jn.00225.2005

Ravel, N., Akaoka, H., Gervais, R., and Chouvet, G. (1990). The effect of acetylcholine on rat olfactory bulb unit activity. *Brain Res. Bull.* 24, 151–155. doi: 10.1016/0361-9230(90)90199-a

Ravel, N., Elaagouby, A., and Gervais, R. (1994). Scopolamine injection into the olfactory bulb impairs short-term olfactory memory in rats. *Behav. Neurosci.* 108, 317–324. doi: 10.1037//0735-7044.108.2.317

Resibois, A., and Rogers, J. H. (1992). Calretinin in rat brain: an immunohistochemical study. *Neuroscience* 46, 101–134. doi: 10.1016/0306-4522(92)90012-q

Rochefort, C., Gheusi, G., Vincent, J. D., and Lledo, M. P. (2002). Enriched odor exposure increases the number of newborn neurons in the adult olfactory bulb and improves odor memory. *J. Neurosci.* 22, 2679–2689. doi: 10.1523/JNEUROSCI.22-07-02679.2002

Rolls, E. T. (2019). Taste and smell processing in the brain. *Handb. Clin. Neurol.* 164, 97–118. doi: 10.1016/B978-0-444-63855-7.00007-1

Romano, C., Sesma, M. A., McDonald, C. T., O'Malley, K., Van den Pol, A. N., and Olney, J. W. (1995). Distribution of metabotropic glutamate receptor mGluR5 immunoreactivity in rat brain. *J. Comp. Neurol.* 355, 455–469. doi: 10.1002/cne.903550310

Rothermel, M., Carey, R. M., Puche, A., Shipley, M. T., and Wachowiak, M. (2014). Cholinergic inputs from Basal forebrain add an excitatory

bias to odor coding in the olfactory bulb. *J. Neurosci.* 34, 4654–4664. doi: 10.1523/JNEUROSCI.5026-13.2014

Saino-Saito, S., Sasaki, H., Volpe, B. T., Kobayashi, K., Berlin, R., and Baker, H. (2004). Differentiation of the dopaminergic phenotype in the olfactory system of neonatal and adult mice. *J. Comp. Neurol.* 479, 389–398. doi: 10.1002/cne.20320

Sakamoto, M., Ieki, N., Miyoshi, G., Mochimaru, D., Miyachi, H., Imura, T., et al. (2014). Continuous postnatal neurogenesis contributes to formation of the olfactory bulb neural circuits and flexible olfactory associative learning. *J. Neurosci.* 34, 5788–5799. doi: 10.1523/JNEUROSCI.0674-14.2014

Sanz Diez, A., Najac, M., and De Saint Jan, D. (2019). Basal forebrain GABAergic innervation of olfactory bulb periglomerular interneurons. *J. Physiol.* 597, 2547–2563. doi: 10.1113/JP277811

Sarafoleanu, C., Mella, C., Georgescu, M., and Perederco, C. (2009). The importance of the olfactory sense in the human behavior and evolution. *J. Med. Life.* 2, 196–198.

Sawada, M., Kaneko, N., Inada, H., Wake, H., Kato, Y., Yanagawa, Y., et al. (2011). Sensory input regulates spatial and subtype-specific patterns of neuronal turnover in the adult olfactory bulb. *J. Neurosci.* 31, 11587–11596. doi: 10.1523/JNEUROSCI.0614-11.2011

Sawamoto, K., Nakao, N., Kobayashi, K., Matsushita, N., Takahashi, H., Kakishita, K., et al. (2001). Visualization, direct isolation, and transplantation of midbrain dopaminergic neurons. *Proc. Natl. Acad. Sci. U.S.A.* 98, 6423–6428. doi: 10.1073/pnas.111152398

Schoenfeld, T. A., Marchand, J. E., and Macrides, F. (1985). Topographic organization of tufted cell axonal projections in the hamster main olfactory bulb: an intrabulbar associational system. *J. Comp. Neurol.* 235, 503–518. doi: 10.1002/cne.902350408

Scott, J. W., and Pfaffmann, C. (1967). Olfactory input to the hypothalamus: electrophysiological evidence. *Science* 158, 1592–1594. doi: 10.1126/science.158.3808.1592

Serguera, C., Triaca, V., Kelly-Barrett, J., Banchaabouchi, M. A., and Minichiello, L. (2008). Increased dopamine after mating impairs olfaction and prevents odor interference with pregnancy. *Nat. Neurosci.* 11, 949–956. doi: 10.1038/nn.2154

Shao, Z., Liu, S., Zhou, F., Puche, A. C., and Shipley, T. M. (2019). Reciprocal inhibitory glomerular circuits contribute to excitation-inhibition balance in the mouse olfactory bulb. *eNeuro* 6:2019. doi: 10.1523/ENEURO.0048-19.2019

Shao, Z., Puche, A. C., Kiyokage, E., Szabo, G., and Shipley, T. M. (2009). Two GABAergic intraglomerular circuits differentially regulate tonic and phasic presynaptic inhibition of olfactory nerve terminals. *J. Neurophysiol.* 101, 1988–2001. doi: 10.1152/jn.91116.2008

Shepherd, G. M., Chen, W. R., Willhite, D., Migliore, M., and Greer, A. C. (2007). The olfactory granule cell: from classical enigma to central role in olfactory processing. *Brain Res. Rev.* 55, 373–382. doi: 10.1016/j.brainresrev.2007.03.005

Shigemoto, R., Nomura, S., Ohishi, H., Sugihara, H., Nakanishi, S., and Mizuno, N. (1993). Immunohistochemical localization of a metabotropic glutamate receptor, mGluR5, in the rat brain. *Neurosci. Lett.* 163, 53–57. doi: 10.1016/0304-3940(93)90227-c

Shipley, M. T., and Ennis, M. (1996). Functional organization of olfactory system. *J. Neurobiol.* 30, 123–176. doi: 10.1002/(SICI)1097-4695(199605)30:1<123::AID-NEU11>3.0.CO;2-N

Sokoloff, P., Giros, B., Martres, M. P., Bouthenet, M. L., and Schwartz, C. J. (1990). Molecular cloning and characterization of a novel dopamine receptor (D3) as a target for neuroleptics. *Nature* 347, 146–151. doi: 10.1038/347146a0

Spinella, M. (2002). A relationship between smell identification and empathy. *Int. J. Neurosci.* 112, 605–612. doi: 10.1080/00207450290025680

Stettler, D. D., and Axel, R. (2009). Representations of odor in the piriform cortex. *Neuron.* 63, 854–864. doi: 10.1016/j.neuron.2009.09.005

Stone, D. M., Grillo, M., Margolis, F. L., Joh, T. H., and Baker, H. (1991). Differential effect of functional olfactory bulb deafferentation on tyrosine hydroxylase and glutamic acid decarboxylase messenger RNA levels in rodent juxtaglomerular neurons. *J. Comp. Neurol.* 311, 223–233. doi: 10.1002/cne.903110205

Takahashi, H., Yoshihara, S., and Tsuboi, A. (2018). The functional role of olfactory bulb granule cell subtypes derived from embryonic and postnatal neurogenesis. *Front. Mol. Neurosci.* 11:229. doi: 10.3389/fnmol.2018.00229

Taylor, T. N., Caudle, W. M., Shepherd, K. R., Noorian, A., Jackson, C. R., Iuvone, P. M., et al. (2009). Nonmotor symptoms of Parkinson's disease revealed in an animal model with reduced monoamine storage capacity. *J. Neurosci.* 29, 8103–8113. doi: 10.1523/JNEUROSCI.1495-09.2009

Tillerson, J. L., Caudle, W. M., Parent, J. M., Gong, C., Schallert, T., and Miller, W. G. (2006). Olfactory discrimination deficits in mice lacking the dopamine transporter or the D2 dopamine receptor. *Behav. Brain Res.* 172, 97–105. doi: 10.1016/j.bbr.2006.04.025

Toida, K., Kosaka, K., Aika, Y., and Kosaka, T. (2000). Chemically defined neuron groups and their subpopulations in the glomerular layer of the rat main olfactory bulb—IV. Intraglomerular synapses of tyrosine hydroxylase-immunoreactive neurons. *Neuroscience* 101, 11–17. doi: 10.1016/s0306-4522(00)00356-0

Vaaga, C. E., and Westbrook, G. L. (2016). Parallel processing of afferent olfactory sensory information. *J Physiol.* 594, 6715–6732. doi: 10.1113/JP272755

Vaaga, C. E., Yorgason, J. T., Williams, J. T., and Westbrook, L. G. (2017). Presynaptic gain control by endogenous cotransmission of dopamine and GABA in the olfactory bulb. *J. Neurophysiol.* 117, 1163–1170. doi: 10.1152/jn.00694.2016

Ventura, R. E., and Goldman, J. E. (2007). Dorsal radial glia generate olfactory bulb interneurons in the postnatal murine brain. *J. Neurosci.* 27, 4297–4302. doi: 10.1523/JNEUROSCI.0399-07.2007

Wachowiak, M., and Cohen, L. B. (1999). Presynaptic inhibition of primary olfactory afferents mediated by different mechanisms in lobster and turtle. *J. Neurosci.* 19, 8808–8817.

Wei, C. J., Linster, C., and Cleland, A. T. (2006). Dopamine D(2) receptor activation modulates perceived odor intensity. *Behav. Neurosci.* 120, 393–400. doi: 10.1037/0735-7044.120.2.393

Weinandy, F., Ninkovic, J., and Gotz, M. (2011). Restrictions in time and space–new insights into generation of specific neuronal subtypes in the adult mammalian brain. *Eur. J. Neurosci.* 33, 1045–1054. doi: 10.1111/j.1460-9568.2011.07602.x

Whitesell, J. D., Sorensen, K. A., Jarvie, B. C., Hentges, S. T., and Schoppa, E. N. (2013). Interglomerular lateral inhibition targeted on external tufted cells in the olfactory bulb. *J. Neurosci.* 33, 1552–1563. doi: 10.1523/JNEUROSCI.3410-12.2013

Whitman, M. C., and Greer, C. A. (2007). Adult-generated neurons exhibit diverse developmental fates. *Dev. Neurobiol.* 67, 1079–1093. doi: 10.1002/dneu.20389

Wilson, D. A., and Sullivan, R. M. (1995). The D2 antagonist spiperone mimics the effects of olfactory deprivation on mitral/tufted cell odor response patterns. *J. Neurosci.* 15, 5574–5581. doi: 10.1523/jneurosci.15-08-05574.1995

Wilson, D. A., and Wood, J. G. (1992). Functional consequences of unilateral olfactory deprivation: time-course and age sensitivity. *Neuroscience* 49, 183–192. doi: 10.1016/0306-4522(92)90086-h

Winner, B., Cooper-Kuhn, C. M., Aigner, R., Winkler, J., and Kuhn, G. H. (2002). Long-term survival and cell death of newly generated neurons in the adult rat olfactory bulb. *Eur. J. Neurosci.* 16, 1681–1689. doi: 10.1046/j.1460-9568.2002.02238.x

Wright, D. E., Seroogy, K. B., Lundgren, K. H., Davis, B. M., and Jennes, L. (1995). Comparative localization of serotonin1A, 1C, and 2 receptor subtype mRNAs in rat brain. *J. Comp. Neurol.* 351, 357–373. doi: 10.1002/cne.903510304

Yamaguchi, M., and Mori, K. (2005). Critical period for sensory experience-dependent survival of newly generated granule cells in the adult mouse olfactory bulb. *Proc. Natl. Acad. Sci. U.S.A.* 102, 9697–9702. doi: 10.1073/pnas.0406082102

Yang, Z. (2008). Postnatal subventricular zone progenitors give rise not only to granular and periglomerular interneurons but also to interneurons in the external plexiform layer of the rat olfactory bulb. *J. Comp. Neurol.* 506, 347–358. doi: 10.1002/cne.21557

Young, J. M., and Trask, B. J. (2002). The sense of smell: genomics of vertebrate odorant receptors. *Hum. Mol. Genet.* 11, 1153–1160. doi: 10.1093/hmg/11.10.1153

Young, K. M., Fogarty, M., Kessaris, N., and Richardson, D. W. (2007). Subventricular zone stem cells are heterogeneous with respect to their embryonic origins and neurogenic fates in the adult olfactory bulb. *J. Neurosci.* 27, 8286–8296. doi: 10.1523/JNEUROSCI.0476-07.2007

Yung, W. H., Hausser, M. A., and Jack, J. J. (1991). Electrophysiology of dopaminergic and non-dopaminergic neurones of the guinea-pig substantia nigra pars compacta *in vitro*. *J Physiol.* 436, 643–667. doi: 10.1113/jphysiol.1991.sp018571

Zaborszky, L., Carlsen, J., Brashear, H. R., and Heimer, L. (1986). Cholinergic and GABAergic afferents to the olfactory bulb in the rat with special emphasis on the projection neurons in the nucleus of the horizontal limb of the diagonal band. *J. Comp. Neurol.* 243, 488–509. doi: 10.1002/cne.902430405

Zhang, Z., Zhang, H., Wen, P., Zhu, X., Wang, L., Liu, Q., et al. (2017). Whole-brain mapping of the inputs and outputs of the medial part of the olfactory tubercle. *Front. Neural Circuits* 11:52. doi: 10.3389/fncir.2017.00052

Conflict of Interest: The authors declare that the research was conducted in the absence of any commercial or financial relationships that could be construed as a potential conflict of interest.

Advantages of publishing in Frontiers

OPEN ACCESS
Articles are free to read for greatest visibility and readership

FAST PUBLICATION
Around 90 days from submission to decision

HIGH QUALITY PEER-REVIEW
Rigorous, collaborative, and constructive peer-review

TRANSPARENT PEER-REVIEW
Editors and reviewers acknowledged by name on published articles

Frontiers
Avenue du Tribunal-Fédéral 34
1005 Lausanne | Switzerland

Visit us: www.frontiersin.org
Contact us: frontiersin.org/about/contact

REPRODUCIBILITY OF RESEARCH
Support open data and methods to enhance research reproducibility

DIGITAL PUBLISHING
Articles designed for optimal readership across devices

FOLLOW US
@frontiersin

IMPACT METRICS
Advanced article metrics track visibility across digital media

EXTENSIVE PROMOTION
Marketing and promotion of impactful research

LOOP RESEARCH NETWORK
Our network increases your article's readership